Elastohydrodynamic lubrication based on the Navier-Stokes equations

by
Christian Thomas Schäfer

A thesis submitted in partial fulfilment of the requirements of
Liverpool John Moores University
for the degree of
Doctor of Philosophy

in collaboration with
INA-Schaeffler KG,
Herzogenaurach (Germany)

December 2005

Abstract

The elastohydrodynamic lubrication (ehl) problem has hitherto been solved almost exclusively using a form of the Reynolds equation to describe the lubricant flow. This implies a constant pressure across the gap. The present investigation takes up the idea that consideration of the full Navier-Stokes equations leads to a broader understanding of the ehl regime. Pursuing a practical approach, the thesis evaluates the significance of the terms of the Navier-Stokes equations previously neglected in Reynolds equation, gives a new, simple but extended set of governing equations, and discusses the prospective influence of the extended set on the ehl regime including pressure variation across the gap.

In order to realise a numerical solution for the extended approach, a variety of new possible analysis schemes is derived from the established ehl solution concepts. Simultaneously, the introduction of computational fluid dynamics software (CFD) as a general purpose Navier-Stokes equations solver to the ehl problem is considered. Two variants of the derived schemes are selected for implementation since they were found to be most suitable. Both are based on the established Newton-Raphson technique for the ehl problem and allow the application of CFD software. Implementation is realised using CFD software in two steps. Initially, pressure is kept constant across the gap in order to detect, analyse and solve problems caused by the novel application of CFD software and to validate the new method. Later, the implementation is extended to allow variable pressure across the gap.

Results of the extended approach are presented for various velocity, pressure, viscosity and sliding ratio values. For sliding conditions, a change of the contact shape and the pressure distribution in comparison with established solutions can be observed as well as pressure variation across the gap. All results are discussed with respect to the established Reynolds equation, the presented extended set of equations and the technical relevance of the new approach. Finally, the extended approach is looked at in the context of arbitrary pressure-viscosity dependencies, thermal and non-Newtonian effects.

Zusammenfassung

Bei der Lösung des Problems elastohydrodynamischer (EHD) Schmierung wurden zur Beschreibung der Schmiermittelströmung in der Vergangenheit beinahe ausschließlich unterschiedliche Formen der Reynoldsgleichung angewandt. Dies bedeutet auch stets die Annahme eines konstanten Drucks über der Spalthöhe. Die vorliegende Arbeit greift den Gedanken auf, dass die Berücksichtigung der Navier-Stokes-Gleichungen das Verständnis des EHD-Kontaktes noch weiter verbessern kann. Dazu werden – im Bemühen um ein möglichst praktisches Verfahren – die einzelnen, bisher teilweise vernachlässigten Terme der Navier-Stokes-Gleichungen hinsichtlich ihrer Relevanz für das EHD-Problem untersucht und bewertet. Damit wird ein neuer, einfacher, aber dennoch erweiterter Satz an Grundgleichungen für das EHD-Problem erstellt und die daraus zu erwartenden Änderungen der typischen EHD-Ergebnisse diskutiert.

Für eine numerische Lösung des erweiterten Gleichungssatzes werden auf der Basis der für das EHD-Problem bekannten Berechnungsverfahren verschiedene neuartige Berechnungsverfahren für den erweiterten Gleichungssatz abgeleitet. Dabei wird die Anwendbarkeit verfügbarer numerischer Strömungssimulationsprogramme (CFD-Software) zur Berechnung der Strömung geprüft. Als am besten geeignet werden schließlich zwei Varianten eines Berechnungsverfahrens ausgewählt, welches auf der Newton-Raphson-Technik für das EHD-Problem beruht und die Anwendung von CFD-Software erlaubt. Die anschließende Implementierung erfolgt in zwei Schritten: Zunächst wird der Druck über der Spalthöhe noch konstant gehalten, um die Probleme, die aus der erstmaligen Anwendung der CFD-Software auf das EHD-Problem herrühren, eingrenzen und beheben zu können, aber auch, um das neue Verfahren zu validieren. In einem zweiten Schritt erfolgt dann eine Erweiterung, so dass auch eine Druckänderung über der Spalthöhe zulässig ist.

Ergebnisse für den neuen, erweiterten Ansatz werden für verschiedene Druck-, Geschwindigkeits- und Viskositätswerte sowie für unterschiedliche Roll-/Gleitverhältnisse vorgestellt. Für den Fall, dass im Kontakt ein relatives Gleiten der beiden Oberflächen auftritt, kann – im Vergleich zu bekannten Lösungen – eine Veränderung des Spalt- und Druckverlaufes im Kontakt beobachtet werden. Ebenso stellt sich ein über der Spalthöhe veränderlicher Druck ein. Alle Ergebnisse werden im Hinblick auf die üblicherweise verwendete Reynoldsgleichung, den vorgelegten Gleichungssatz und ihre technische Relevanz diskutiert. Abschließend erfolgt ein Ausblick auf den erweiterten Ansatz im Bezug auf beliebige Druck-Viskosität-Zusammenhänge sowie thermische und nicht-newtonische Aspekte.

Acknowledgements

Throughout the research, I met numerous people accompanying me and my research project for a shorter or longer period of time and I would like to use this opportunity to thank all of them for their contribution and support. To some of them, I want to express my special thanks:

First of all I would like to thank Dr.-Ing. Peter Giese, who initiated the research project, introduced me to INA-Schaeffler's motto "thinking outside the box", and acted as industrial supervisor for the project.

I am most indebted to Dr. Neil H. Woolley, my director of studies, for extensive and patient discussion and advice in so many aspects of all fields of the research project undertaken.

I am very grateful to Professor W. Brian Rowe, second supervisor, for many valuable discussions, advice and an outlook on the project from a different point of view.

I would like to thank Dipl.-Ing. Jochen Sarfert, Dr.-Ing. Jörg Weber and all other colleagues of INA-Schaeffler KG, who provided minor or major support to my research.

Finally, I would like to thank INA-Schaeffler KG in Herzogenaurach (Germany) for providing funding and resources for the research.

Table of contents

List of appendices

List of figures

Thesis

Appendices

List of tables

Thesis

Appendices

Nomenclature

symbol	description	dimension [*]
a	coefficient in the pressure-density dependency description	$M^{-1} \cdot L \cdot T^2$
$\tilde{a}$	coefficient in the dimensionless pressure definition by Mohrenstein-Ertel	—
b	coefficient in the pressure-density dependency description	$M^{-1} \cdot L \cdot T^2$
b_{hz}	Hertzian width	L
e	specific energy	$L^2 \cdot T^{-2}$
f	x-momentum residual	$M \cdot L \cdot T^{-2}$
f_{Re}	Reynolds equation residual	$M \cdot L^{-2} \cdot T^{-2}$
f_{sum}	sum of x-momentum residuals	$M \cdot L \cdot T^{-2}$
$f_{x\text{-}mom,sum}$	minimum sum of x-momentum residuals	$M \cdot L \cdot T^{-2}$
h	height of the gap	L
h_0	height of gap at contact centreline, where pressure gradient along the contact is zero	L
$h_{0,ext}$	height of the gap at contact centreline determined with the extended approach	L
$h_{0,Re}$	height of the gap at contact centreline determined with Reynolds equation based approach	L
$h_{max}{}'$	maximum height of the gap between additional and established ehl constriction	L
h_{min}	minimum height of the gap at established ehl constriction	L
$h_{min}{}'$	minimum height of the gap at additional constriction	L

[*] L represents length dimension, M mass dimension, T time dimension and T temperature dimension.

symbol	description	dimension
h_r	height of the gap due to curvature of the contact partners	L
h_{r1}	height of the gap due to curvature of the lower surface	L
h_{r2}	height of the gap due to curvature of the upper surface	L
h^*	height at the position of film rupture at outlet, where the pressure gradient is zero at ambient conditions.	L
i	number of an individual finite volume in x-direction	—
j	number of an individual finite volume in y-direction	—
k	thermal conductivity	$M \cdot L \cdot T^{-3} \cdot T$
k_1	coefficient for discretisation error	—
k_2	coefficient for discretisation error	—
k_c	dimensionless factor	—
k_p	dimensionless sliding influence factor	—
$\tilde{k}_p$	dimensionless sliding influence factor for Roelands' approach	—
$\hat{k}_p$	dimensionless sliding influence factor for thermal Roelands' approach	—
k_r	dimensionless pressure gradient ratio	—
$\tilde{k}_r$	dimensionless pressure gradient ratio for Roelands' approach	—
$\hat{k}_r$	dimensionless pressure gradient ratio for thermal Roelands' approach	—
k_η	viscosity ratio	—
l	number of finite volumes in z-direction	—
l_c	length of the contact in z-direction	L
m	total number of finite volumes in y-direction	—
$\dot{m}$	mass flow	$M \cdot T^{-1}$
m'_L	mass flow per unit length	$M \cdot L^{-1} \cdot T^{-1}$
$m'_{L,Re}$	mass flow per unit length determined with Reynolds equation based approach	$M \cdot L^{-1} \cdot T^{-1}$
n	total number of finite volumes in x-direction	—
n_n	normal direction	—
p	pressure	$M \cdot L^{-1} \cdot T^{-2}$
p_0	pressure at ambient conditions	$M \cdot L^{-1} \cdot T^{-2}$

symbol	*description*	*dimension*
p_1	pressure on the lower surface	$M \cdot L^{-1} \cdot T^{-2}$
p_2	pressure on the upper surface	$M \cdot L^{-1} \cdot T^{-2}$
p_{cl}	pressure at the centreline along the contact	$M \cdot L^{-1} \cdot T^{-2}$
p_{fast}	pressure on the faster surface	$M \cdot L^{-1} \cdot T^{-2}$
p_{hz}	Hertzian pressure	$M \cdot L^{-1} \cdot T^{-2}$
p_{mean}	mean pressure	$M \cdot L^{-1} \cdot T^{-2}$
	$p_{mean} = \dfrac{p_1 + p_2}{2} = \dfrac{p_{slow} + p_{fast}}{2}$	
p_{prev}	pressure of previous time step or iteration loop	$M \cdot L^{-1} \cdot T^{-2}$
p_{Re}	pressure determined with Reynolds equation based approach	$M \cdot L^{-1} \cdot T^{-2}$
p_{slow}	pressure at the slower surface	$M \cdot L^{-1} \cdot T^{-2}$
$\tilde{p}$	order of the discretisation error	—
$\hat{p}$	smoothed pressure	$M \cdot L^{-1} \cdot T^{-2}$
q	reduced pressure	—
q^*	reduced pressure	—
$\tilde{q}$	reduced pressure (alternative definition)	$M \cdot L^{-1} \cdot T^{-2}$
r_1	radius of lower surface	L
r_2	radius of upper surface	L
r_{red}	reduced radius of the contact	L
	$\dfrac{1}{r_{red}} = \dfrac{1}{r_1} + \dfrac{1}{r_2}$	
t	time	T
t_1	function in thermal Reynolds equation	—
t_2	function in thermal Reynolds equation	—
u	velocity component in x-direction (along the gap)	$L \cdot T^{-1}$
u_1	velocity of lower surface	$L \cdot T^{-1}$
u_2	velocity of upper surface	$L \cdot T^{-1}$
u_h	hydrodynamic speed $u_h = \frac{1}{2} \cdot (u_1 + u_2)$	$L \cdot T^{-1}$
u_{Re}	velocity component in x-direction (along the gap) determined with Reynolds equation based solution	$L \cdot T^{-1}$
v	velocity component in y-direction (across the gap)	$L \cdot T^{-1}$
v_d	elastic deflection	L
v_{d1}	elastic deflection of the lower surface	L

symbol	description	dimension
V_{d2}	elastic deflection of the upper surface	L
V_{ges}	value of velocity $$V_{ges} = \sqrt{u^2 + v^2 + w^2}$$	$L \cdot T^{-1}$
$V_{ges,Re}$	value of velocity determined with Reynolds equation based approach	$L \cdot T^{-1}$
V_m	reference velocity in y-direction	$L \cdot T^{-1}$
V_{normal}	velocity component perpendicular to a wall in CFD software	$L \cdot T^{-1}$
V_t	tangential velocity	$L \cdot T^{-1}$
$V_{tangential}$	velocity component parallel to the wall in CFD software	$L \cdot T^{-1}$
w	velocity component in z-direction	$L \cdot T^{-1}$
$\vec{w}$	velocity vector $$\vec{w} = \begin{pmatrix} u & v & w \end{pmatrix}^T$$	$L \cdot T^{-1}$
w'	load per unit length in z-direction	$M \cdot T^{-2}$
x	axis of the Cartesian co-ordinate system along the gap	L
$\vec{x}_u$	unknown variable vector $$\vec{x}_u = \begin{pmatrix} x_{u1}, x_{u2} \dots x_{ui} \dots x_{un} \end{pmatrix}^T$$	—
x_{cross}	position of agreement of height of extended approach and Reynolds equation based approach $$x_{cross} = x(h = h_{0,Re})$$	L
x_{hmax}	position of maximum height of the gap between additional and established ehl constriction $$x_{hmax} = x(h = h_{max}')$$	L
x_{hmin}	position of additional ehl constriction $$x_{hmin} = x(h = h_{min}')$$	L
x_{inlet}	position of the inlet of the contact	L
x_{outlet}	position of the outlet of the contact	L
x_{pfast}	position of maximum pressure on the faster surface $$x_{pfast} = x(P_{fast} = P_{fast,max})$$	L
x_{pslow}	position of maximum pressure on the slower surface $$x_{pslow} = x(P_{slow} = P_{slow,max})$$	L
x_{pmean}	position of maximum mean pressure $$x_{pmean} = x(P_{mean} = P_{mean,max})$$	L

symbol	description	dimension
x_{ref}	reference position for determination of the deflection	L
$x_{\Delta Pmax}$	position of maximum pressure difference $x_{\Delta Pmax} = x(\Delta P = \Delta P_{max})$	L
$x_{\Delta Pmin}$	position of minimum pressure difference $x_{\Delta Pmin} = x(\Delta P = \Delta P_{min})$	L
y	axis of the Cartesian co-ordinate system perpendicular to the gap	L
$y_{I,max}$	position of the upper surface in y-direction	L
$y_{I,min}$	position of the lower surface in y-direction	L
z	axis of the Cartesian co-ordinate system along the axis of the rolling elements	L
A	surface area	L^2
D	factor of dominance for constant pressure across gap	—
D_{ext}	factor of dominance for the extended approach and variable pressure across the gap	—
E_1	Young's modulus of lower solid body	$M \cdot L^{-1} \cdot T^{-2}$
E_2	Young's modulus of upper solid body	$M \cdot L^{-1} \cdot T^{-2}$
$E_{computational}$	error due to limited resolution of numbers	—
E_{trunc}	truncation error	—
E'	reduced Young's modulus $\frac{1}{E'} = \frac{1}{2} \cdot \left(\frac{1+v_1^2}{E_1} + \frac{1+v_2^2}{E_2} \right)$	$M \cdot L^{-1} \cdot T^{-2}$
F	load on contact	$M \cdot L \cdot T^{-2}$
$\vec{F}$	vector of functions $\vec{F} = (F_1, F_2 \dots F_i \dots F_n)^T$	—
F_0	function in thermal Reynolds equation	—
F_2	function in thermal Reynolds equation	—
F_3	function in thermal Reynolds equation	—
F_n	normal force per unit width	$M \cdot T^{-2}$
F_t	tangential force per unit width	$M \cdot T^{-2}$
G	dimensionless material parameter $G = E' \cdot \alpha$	—
G_1	function in thermal Reynolds equation	—
G_2	function in thermal Reynolds equation	—
G_3	function in thermal Reynolds equation	—

symbol	*description*	*dimension*
H	dimensionless height of the gap in numerical results $H = \overline{H} = h/h_{0,Re}$	—
$\overline{H}$	dimensionless height of the gap in theoretical considerations $H = \overline{H} = h/h_{0,Re}$	—
$H_{0,ext}$	dimensionless height of the gap at contact centreline $H_0 = h_{0,ext}'/h_{0,Re}$	—
H_{max}'	dimensionless maximum height of the gap between additional and established ehl constriction $H_{max}' = h_{max}'/h_{0,Re}$	—
H_{median}	median of height of three configurations	—
H_{min}	dimensionless minimum height of the gap at established ehl constriction $H_{min} = h_{min}/r_{red}$	—
H_{min}'	dimensionless minimum height of the gap at additional constriction $H_{min}' = h_{min}'/h_{0,Re}$	—
H_{Re}	dimensionless height of the gap determined with Reynolds equation based approach	—
I	number of the corner or edge of an individual finite volume in x-direction	—
J	number of the corner or edge of an individual finite volume in y-direction	—
$\overline{J}$	Jacobian matrix	—
K_{Re}	dimensionless factor for determination of Reynolds number	—
M	total number of corners or edges of finite volumes in y-direction	—
N	total number of corners or edges of finite volumes in x-direction	—
P	dimensionless pressure in numerical results $P = \overline{P} = p/p_{hz}$	—
$\overline{P}$	dimensionless pressure in theoretical considerations $P = \overline{P} = p/p_{hz}$	—
$P_0, \overline{P}_0$	dimensionless pressure $P_0 = \overline{P}_0 = p/p_0$	—

symbol	description	dimension
P_1	dimensionless pressure at the lower surface $P_1 = p_1/p_{Hz}$	—
P_2	dimensionless pressure at the upper surface $P_1 = p_1/p_{Hz}$	—
P_{fast}	dimensionless pressure at the faster surface $P_{fast} = p_{fast}/p_{Hz}$	—
P_{mean}	dimensionless mean pressure $P_{mean} = \dfrac{P_1 + P_2}{2} = \dfrac{P_{slow} + P_{fast}}{2}$	—
P_{median}	median of pressure of three configurations	—
P_{Re}	dimensionless pressure determined with Reynolds equation based approach	—
P_{slow}	dimensionless pressure at the slower surface $P_{slow} = p_{slow}/p_{Hz}$	—
Q_L	flow rate along the gap per unit width	$L^2 \cdot T^{-1}$
S	sliding ratio $S = \dfrac{(u_1 - u_2)}{(u_1 + u_2)} = \dfrac{(U_1 - U_2)}{(U_1 + U_2)}$	—
$S_{N\text{-}R}$	accuracy required for Newton-Raphson technique	—
$S_{residual}$	ratio of applied and theoretical x-momentum residual	—
S_ϕ	source term in the transport equation	T^{-1} [*]
$\hat{S}$	source term	$M \cdot L^{-2} \cdot T^{-2}$
U	dimensionless velocity parameter $U = \dfrac{u_h \cdot \eta_0}{E' \cdot r_{red}}$	—
$\overline{U}$	dimensionless velocity in x-direction $\overline{U} = u/u_h$	—
$\overline{V}$	dimensionless velocity in y-direction $\overline{V} = \gamma \cdot (v/u_h)$	—
W	dimensionless load parameter $W = \dfrac{w'}{E' \cdot r_{red}} = \dfrac{\frac{1}{2} \cdot b_{Hz} \cdot p_{Hz} \cdot \pi}{E' \cdot r_{red}}$	—

---

[*] The transport variable is a variable which can take on any dimension.

symbol	*description*	*dimension*
X	dimensionless variable of length along the gap in numerical results $$X = \overline{X} = x/b_{hz}$$	—
$\overline{X}$	dimensionless variable of length along the gap in theoretical considerations $$X = \overline{X} = x/b_{hz}$$	—
X_{cross}	dimensionless position of agreement of height of extended approach and Reynolds equation based approach $$X_{cross} = \frac{x_{cross}}{b_{Hz}} = X(H=1)$$	—
X_{hmax}	dimensionless position of maximum height of the gap between additional and established ehl constriction $$X_{hmax} = \frac{x_{hmax}}{b_{Hz}} = X(H = H_{max}')$$	—
X_{hmin}	dimensionless position of additional ehl constriction $$X_{hmin} = \frac{x_{hmin}}{b_{Hz}} = X(H = H_{min}')$$	—
X_{pfast}	dimensionless position of maximum pressure on the faster surface $$X_{pfast} = \frac{x_{pfast}}{b_{Hz}} = X(P_{fast} = P_{fast,max})$$	—
X_{pslow}	dimensionless position of maximum pressure on the slower surface $$X_{pslow} = \frac{x_{pslow}}{b_{Hz}} = X(P_{slow} = P_{slow,max})$$	—
X_{pmean}	dimensionless position of maximum mean pressure $$X_{pmean} = \frac{x_{pmean}}{b_{Hz}} = X(P_{mean} = P_{mean,max})$$	—
$X_{\Delta Pmax}$	dimensionless position of maximum pressure difference $$X_{\Delta P max} = \frac{x_{\Delta P max}}{b_{Hz}} = X(\Delta P = \Delta P_{max})$$	—
$X_{\Delta Pmin}$	dimensionless position of minimum pressure difference $$X_{\Delta P min} = \frac{x_{\Delta P min}}{b_{Hz}} = X(\Delta P = \Delta P_{min})$$	—

symbol	description	dimension
Y	dimensionless variable of length perpendicular to the gap in numerical results $Y = \overline{Y} = y/h_0$	—
$\overline{Y}$	dimensionless variable of length perpendicular to the gap in theoretical considerations $Y = \overline{Y} = y/h_0$	—
Y^*	dimensionless normalised variable of length perpendicular to the gap $Y^* = \dfrac{y}{h} = \dfrac{Y}{H}$	—
Z_i	dimensionless pressure viscosity index	—
α	pressure-viscosity coefficient	$M^{-1} \cdot L \cdot T^2$
$\overline{\alpha}$	dimensionless pressure-viscosity coefficient $\overline{\alpha} = \alpha \cdot p_{hz}$	—
γ	geometrical ratio $\gamma = h_0 / b_{hz}$	—
$\delta\vec{x}_u$	solution correction vector $\delta\vec{x}_u = \left(\delta x_{u1}, \delta x_{u2} \ldots \delta x_{ui} \ldots \delta x_{un}\right)^T$	—
γ_R	temperature coefficient for Roelands pressure-temperature-viscosity description	T^{-1}
ε_{disc}	discretisation error	—
ε_H	relative deviation of height from median value $\varepsilon_H = \dfrac{H - H_{median}}{H_{median}}$	—
$\varepsilon_{H,Re}$	relative deviation of height from Reynolds equation based solution $\varepsilon_{H,Re} = \dfrac{H - H_{Re}}{H_{Re}}$	—
$\varepsilon_{m,Re}$	relative deviation of mass flow from Reynolds equation based solution $\varepsilon_{m,Re} = \dfrac{m'_L - m'_{L,Re}}{m'_{L,Re}}$	—
ε_P	relative deviation of pressure from median value $\varepsilon_P = \dfrac{P - P_{median}}{P_{median}}$	—

symbol	*description*	*dimension*
$\varepsilon_{p,abs}$	absolute deviation of pressure from centreline pressure $$\varepsilon_{p,abs} = p - p_{cl}$$	$M \cdot L^{-1} \cdot T^{-2}$
$\varepsilon_{Pfast,Re}$	relative deviation of pressure on faster surface from Reynolds equation based solution $$\varepsilon_{Pfast,Re} = \frac{P_{fast} - P_{Re}}{P_{Re}}$$	—
$\varepsilon_{Pmean,Re}$	relative deviation of mean pressure from Reynolds equation based solution $$\varepsilon_{Pmean,Re} = \frac{P_{mean} - P_{Re}}{P_{Re}}$$	—
$\varepsilon_{Pslow,Re}$	relative deviation of pressure on slower surface from Reynolds equation based solution $$\varepsilon_{Pslow,Re} = \frac{P_{slow} - P_{Re}}{P_{Re}}$$	—
$\varepsilon_{u,Re}$	relative deviation of velocity component in x direction from Reynolds equation based solution $$\varepsilon_{u,Re} = \frac{u - u_{Re}}{u_h}$$	—
$\varepsilon_{v,Re}$	relative deviation of value of speed from Reynolds equation based solution $$\varepsilon_{V,Re} = \frac{V_{ges} - V_{ges,Re}}{u_h}$$	—
$\varepsilon_{\eta,abs}$	absolute deviation of viscosity from viscosity for mean pressure $$\varepsilon_{\eta,abs} = \eta - \eta(p = p_{mean})$$	$M \cdot L^{-1} \cdot T^{-1}$
$\varepsilon_{\eta fast,Re}$	relative deviation of viscosity near the faster surface from Reynolds equation based solution $$\varepsilon_{\eta fast,Re} = \frac{\eta_{fast} - \eta_{Re}}{\eta_{Re}}$$	—
$\varepsilon_{\eta slow,Re}$	relative deviation of viscosity near the slower surface from Reynolds equation based solution $$\varepsilon_{\eta slow,Re} = \frac{\eta_{slow} - \eta_{Re}}{\eta_{Re}}$$	—
$\varepsilon_{\Delta\eta}$	relative deviation of viscosity across the height of the gap $$\varepsilon_{\Delta\eta} = \frac{\eta_{slow} - \eta_{fast}}{\frac{1}{2} \cdot (\eta_{slow} + \eta_{fast})}$$	—

symbol	description	dimension
$\varepsilon_{\mu T,Re}$	relative deviation of traction coefficient from Reynolds equation based solution $$\varepsilon_{\mu T,Re} = \frac{\mu_T - \mu_{T,Re}}{\mu_{T,Re}}$$	—
$\varepsilon_{Tfast,Re}$	relative deviation of shear stress at the faster surface from Reynolds equation based solution $$\varepsilon_{Tfast,Re} = \frac{T_{slow} - T_{Re,fast}}{T_{Re,fast}}$$	—
$\varepsilon_{Tslow,Re}$	relative deviation of shear stress at the faster surface from Reynolds equation based solution $$\varepsilon_{Tslow,Re} = \frac{T_{slow} - T_{Re,slow}}{T_{Re,slow}}$$	—
η	dynamic viscosity	$M \cdot L^{-1} \cdot T^{-1}$
η_0	dynamic viscosity at ambient conditions	$M \cdot L^{-1} \cdot T^{-1}$
η_e	effective dynamic viscosity for thermal Reynolds equation	$M \cdot L^{-1} \cdot T^{-1}$
η_{fast}	dynamic viscosity near the faster surface	$M \cdot L^{-1} \cdot T^{-1}$
η_{hz}	dynamic viscosity at Hertzian pressure	$M \cdot L^{-1} \cdot T^{-1}$
η_m	mean dynamic viscosity	$M \cdot L^{-1} \cdot T^{-1}$
η_{max}	maximum dynamic viscosity to obtain realistic traction coefficient values	$M \cdot L^{-1} \cdot T^{-1}$
η_{Re}	dynamic viscosity determined with Reynolds equation based approach	$M \cdot L^{-1} \cdot T^{-1}$
η_{slow}	dynamic viscosity near the slower surface	$M \cdot L^{-1} \cdot T^{-1}$
ϑ	temperature	T
λ	second viscosity coefficient	$M \cdot L^{-1} \cdot T^{-1}$
μ_T	traction coefficient $$\mu_T = \int (-T_{slow}) \cdot dX$$	—
ν_1	Poisson's ratio of lower solid body	—
ν_2	Poisson's ratio of upper solid body	—
$\tilde{\pi}$	pressure function	—
ρ	oil density	$M \cdot L^{-3}$
ρ_0	oil density at ambient conditions	$M \cdot L^{-3}$
σ	stress (normal and tangential)	$M \cdot L^{-1} \cdot T^{-2}$
τ	shear stress $$\tau = \eta \cdot \frac{\partial v_t}{\partial n_n} \approx \eta \cdot \frac{\partial u}{\partial y}$$	$M \cdot L^{-1} \cdot T^{-2}$

symbol	*description*	*dimension*
τ_{fast}	shear stress on the lubricant at the faster surface	$M \cdot L^{-1} \cdot T^{-2}$
τ_{slow}	shear stress on the lubricant at the slower surface	$M \cdot L^{-1} \cdot T^{-2}$
τ_{xy}	shear stress in x-momentum equation	$M \cdot L^{-1} \cdot T^{-2}$
ϕ	transport variable	—[*]
ϕ_1	transport variable on sample grid	—
ϕ_2	transport variable on alternative sample grid	—
ϕ_{2h}	transport variable on a grid of half resolution	—
ϕ_{4h}	transport variable on a grid of quarter the resolution	—
ϕ_h	transport variable on a grid of original resolution	—
ϕ_q	reduced pressure variable	—
ψ	stream function	$L \cdot T^{-1}$
ω	vorticity	T^{-1}
Γ	diffusion coefficient for transport equation	$M \cdot L^{-1} \cdot T^{-1}$
ΔH	dimensionless height difference $\Delta H = H_{max}' - H_{min}'$	—
ΔP	dimensionless pressure difference between faster and slower surface $\Delta P = P_{slow} - P_{fast}$	—
ΔV	volume of finite volume	L^3
Δx	dimensional finite volume width in x-direction	L
ΔX	dimensionless finite volume width in x-direction	—
Δy	dimensional finite volume width in y-direction	L
ΔY	dimensionless finite volume width in y-direction	—
Δz	dimensional finite volume width in z-direction	L
ΔZ	dimensionless finite volume width in z-direction	—
ΔT	dimensionless shear stress difference $\Delta T = T_{slow} - (-T_{fast})$	—
$\Delta \vartheta$	temperature difference to ambient conditions	T
$\Delta \vartheta_{max}$	maximum temperature difference to ambient conditions	T

[*] The transport variable is a variable which can take on any dimension.

symbol	*description*	*dimension*
$\overline{\Delta\vartheta}$	dimensionless temperature $$\overline{\Delta\vartheta} = \frac{\Delta\vartheta}{\Delta\vartheta_{max}}$$	—
T	dimensionless shear stress $$T = \frac{\tau}{p_{Hz}}$$	—
T_{fast}	dimensionless shear stress on the lubricant at the faster surface	—
T_{Re}	dimensionless shear stress determined with Reynolds equation based approach	—
T_{slow}	dimensionless shear stress on the lubricant at the slower surface	—
Φ	dissipation function $$\Phi = 2 \cdot \left[\left(\frac{\partial u}{\partial x}\right)^2 + \left(\frac{\partial v}{\partial y}\right)^2 + \left(\frac{\partial w}{\partial z}\right)^2 \right]$$ $$+ \left(\frac{\partial v}{\partial x} + \frac{\partial u}{\partial y}\right)^2 + \left(\frac{\partial w}{\partial y} + \frac{\partial v}{\partial z}\right)^2 + \left(\frac{\partial u}{\partial z} + \frac{\partial w}{\partial x}\right)^2$$ $$- \frac{2}{3} \cdot \left(\frac{\partial u}{\partial x} + \frac{\partial v}{\partial y} + \frac{\partial w}{\partial z}\right)^2$$	T^{-2}
Φ'	variable for Reynolds equation modification $$\Phi' = q \cdot h^{\frac{3}{2}}$$	$L^{\frac{3}{2}}$
Φ^*	variable for Reynolds equation modification $$\Phi^* = p \cdot h^{\frac{3}{2}}$$	$M \cdot L^{\frac{1}{2}} \cdot T^{-2}$

Part I

Background
for introducing the
Navier-Stokes equations

Chapter 1

Introduction

1.1 The theory of elastohydrodynamic lubrication

In many machine elements, contact forces are transmitted across curved surfaces of low geometrical conformity which are also in relative motion. Such contacts may be highly loaded and occur, for example, in roller bearings, gear-tooth systems, and cam-tappet devices. Most of these machine elements operate with very low wear as they are lubricated. This phenomenon and the detailed conditions in the contact area are explained by the theory of elastohydrodynamic lubrication (ehl).

The two surfaces are separated by a hydrodynamically generated fluid film. The principle of hydrodynamic fluid flow is described in the differential equation given by Reynolds [1] in 1886. However, the application of Reynolds theory to non-conformal contacts shows that the load carrying zone is far smaller and the pressure is considerably higher than in conformal contacts. It thus becomes necessary to take additional phenomena into account. The most essential are:

♦ The relatively high pressure leads to an elastic deformation of the surfaces.

♦ The viscosity of the lubricant varies significantly due to the wide range of pressure occurring in the contact.

The first analytical solution to take the above phenomena into account was given by both Mohrenstein-Ertel [2] and Grubin and Vinogradova [3] in 1949. A decade later a numerical solution was presented by Dowson and Higginson [4]. A typical result incorporating these phenomena is given in figure 1.1. Essentially, the typical ehl pressure distribution follows the pressure distribution occurring in a dry, Hertzian contact without relative motion but with two significant differences: In the inlet zone of the contact, where the lubricant enters, a smooth transition occurs and, near the outlet of the gap, a sudden pressure spike is present. As the Hertzian pressure distribution suggests, the shape of the gap is nearly parallel but with a sudden constriction at the end corresponding to the pressure spike.
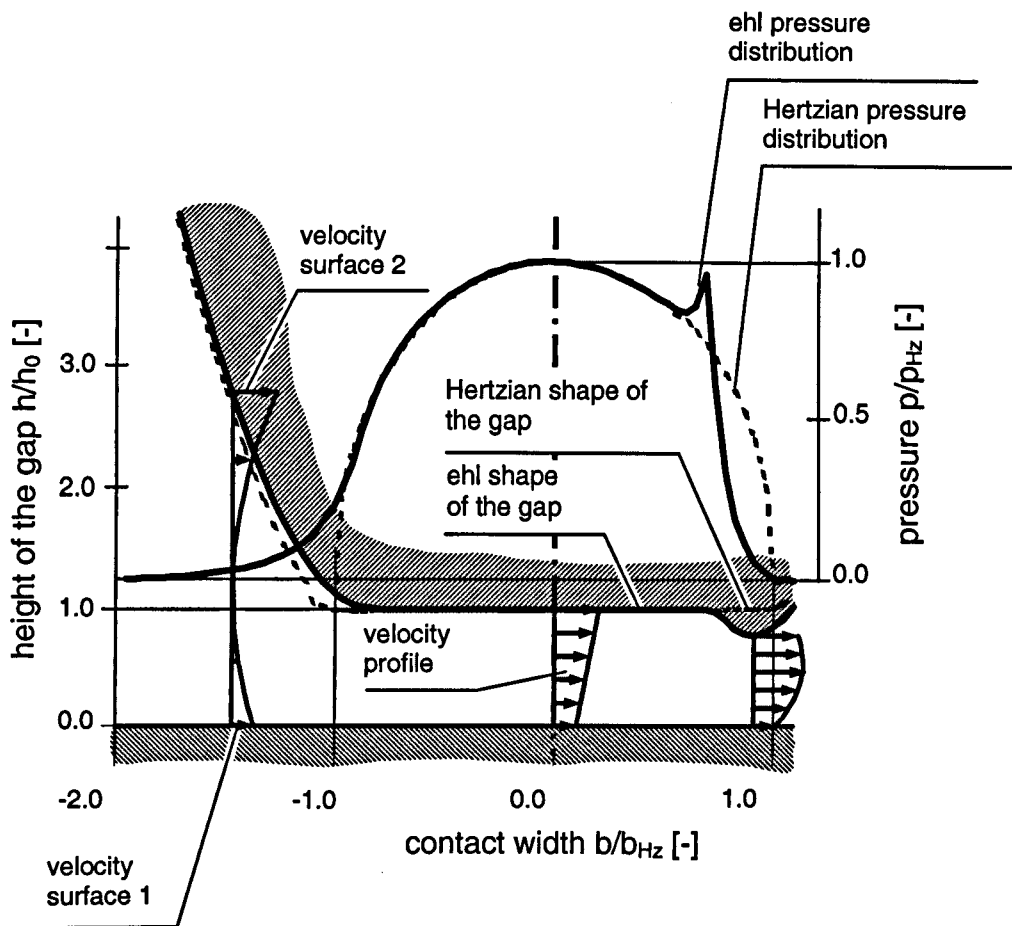
Figure 1.1:   *Typical shape, pressure distribution and velocity profiles in an elastohydrodynamically lubricated line contact (different surface velocities).*

1.2   Developments in ehl calculations

Continuing from the early investigations, further phenomena have been investigated during the last four decades in order to achieve improved results.

- ◆ The lubricant increases in temperature due to shear forces. The generation of heat and its transport in the lubricant and through the surfaces have been introduced into the calculation. The influence of the temperature on the viscosity has also been considered.

- ◆ The lubricant in the gap undergoes severe changes of condition when passing through the contact. In particular, the pressure in the lubricant changes significantly and this has a marked effect on the viscosity. Because of sliding, the shear stress can reach high values. It is widely believed that the lubricant loses its Newtonian character under such severe conditions. A variety of different approaches have been suggested to take these non-Newtonian effects into account.

- ◆ The contact surfaces are not ideally smooth. The influence of the roughness of the surfaces has been investigated.

As a result, the analysis of the elastohydrodynamic contact problem has reached a standard [5], such that the results exhibit the quality required for the simulation of dynamic systems such as dynamic bearing analysis. However, all such analyses are still based on the assumption of a Reynolds equation for the lubricant flow with a constant pressure across the gap in the contact. Application of the more general full Navier-Stokes equations to ehl analysis has hardly been investigated yet, but promises a potential contribution to a further understanding of the ehl contact.

1.3   Aim and objectives

1.3.1   Aim

The aim of the work presented in this thesis is to achieve improved results for ehl calculations by incorporating the Navier-Stokes equations in the solution procedure.

1.3.2   Objectives

The objectives of this investigation are:

(i)   to investigate the influence of the individual terms in the Navier-Stokes equations and to select those terms which are important for the solution of the ehl problem,

(ii) to develop a suitable numerical method to solve the Navier-Stokes equations within the ehl regime, and

(iii) to evaluate the benefit of the new approach by numerical results and to compare it with experimental or theoretical data.

Practical application of elastohydrodynamic lubrication requires a system approach taking as many effects into account as possible [6]. However, since the Navier-Stokes equations for the ehl problem have hardly been investigated, the present investigation tries to reduce the problem to its principal effects. Following such a measure the investigation is restricted to the line contact problem, i.e. the contact between two infinitely wide rollers. This assumption of a line contact problem includes physical phenomena but allows a reduction of the problem to two dimensions. However, a further consideration is that an extension of the proposed method to three dimensions should be possible. In addition, the contact is assumed to be ideally smooth.

1.4   Scope of the work

The thesis is structured into three parts.

The first part comprises chapters 1 to 4 and considers the theoretical background of the work. Following the introduction of the present chapter, chapter 2 surveys the phenomena modelled in ehl analysis showing that, practically always, Reynolds equation has been used to describe fluid flow, although questioned occasionally. Consequently, in chapter 3, the relevance of the individual terms of the Navier-Stokes equations for the ehl problem is determined and the influence of any additional relevant terms on the typical ehl result is considered. Chapter 4 closes the part on the theoretical background by summarizing the needs for and the requirements of a new solution of the ehl problem.

The second part of the thesis concentrates on the numerical method for the solution of the ehl problem using the Navier-Stokes equations and covers chapters 5 to 9. Chapter 5 gives an introduction to numerical methods. Chapter 6 provides a detailed overview of numerical methods used for the ehl problem to date and for the solution of the Navier-Stokes equations including fluid-structure interaction. Chapter 7 considers how the numerical methods available can be combined into a new numerical method, including the selection of the most suitable method. Chapter 8 shows the implementation of the selected method such that an ehl analysis with constant pressure across the height of the gap can be undertaken. Chapter 9 gives details of the implementation of further aspects so that the full Navier-Stokes equations can be solved.

The third and last part of the thesis, chapters 10 to 14, considers the results of the extended approach. Chapter 10 presents the results of the approach. In chapter 11 these results are considered, discussed and evaluated with regards to their technical relevance. In chapter 12 the discussion is broadened to include further aspects, such as validation and the influence of earlier assumptions.

Finally, chapters 13 and 14 draw conclusions and propose future work.

Chapter 2

Flow description in elastohydrodynamic lubrication

As mentioned in the introduction, the basic solution of the elastohydrodynamic lubrication problem requires consideration of three phenomena: Firstly the description of the lubricant fluid flow in the gap, secondly a description of the pressure-viscosity dependency, and thirdly a description of the deflection of the solids. Starting from these considerations, a lot of research has been done in this field to date. Various aspects of the basic solution have been considered and extended models proposed and introduced which improve those aspects regarding lubricant properties and flow in the contact.

The present chapter aims to overview both the aspects covered and the range of models proposed concerning the ehl problem. In parallel, an attempt is made at understanding the role of the Navier-Stokes equations for these models.

2.1   Basic solutions

2.1.1   Flow description and derivation

A first solution of the ehl contact was given by both Mohrenstein-Ertel [2] and Grubin and Vinogradova [3]. To describe the flow, they used a one-dimensional, incompressible Reynolds equation, as obtained from a

simplified x-momentum Navier-Stokes equation, and an exponential pressure-viscosity dependency. This is briefly described in the following:

For a line contact such as that of figure 1.1*, Reynolds' derivation [1] for the equation named after him, which was frequently repeated e.g. by Eller [7], or Lubrecht [8], is based on two equations. The first is a momentum equation along the contact, obtained from the Navier-Stokes equations in the corresponding direction with most terms neglected. Also the assumption of constant viscosity across the height of the gap is made, so the momentum equation is

$$\frac{\partial p}{\partial x} = \eta \cdot \frac{\partial^2 u}{\partial y^2}$$

(2.1),

where   p   is the pressure,
         u   is the velocity along a line contact,
         x   is the coordinate along the contact,
         y   is the coordinate across the contact, and
         η is the viscosity, as stated constant across the gap.

Equation 2.1 represents the force equilibrium of pressure forces and shear forces along the gap. Hence occasionally [9], the term *"force equilibrium equation"* is used instead of *"momentum equation"*.

The second governing equation is a continuity equation, written in a steady-state, integral form as

$$\frac{dQ_L}{dx} = \frac{d\left[\int_{y=0}^{y=h} u \cdot dy\right]}{dx} = 0$$

(2.2),

where   h   the height of the gap,
         u, x, y are as above, and
         Q_L is the flow rate along the contact per unit width.

---

*   In the present chapter, all derivations and equations will be discussed and shown for the infinitely wide line contact problem, even if the underlying literature discussed contacts of finite width, i.e. point contacts or elliptical contacts. This is because this procedure allows a clearer presentation of the issues discussed without a loss of information.

The momentum equation in the y-direction is assumed to be irrelevant so that the pressure gradient across the gap is zero

$$\frac{\partial p}{\partial y} = 0 \qquad (2.3),$$

where   p, y   are as above.

The momentum equation in the z-direction disappears due to the line contact assumption.

With twofold integration of equation 2.1 with respect to y, incorporation of the result in equation 2.2 and determination of the integration constants Reynolds equation can be written as

$$\frac{d}{dx}\left(\frac{h^3}{\eta} \cdot \frac{dp}{dx}\right) = 6 \cdot (u_1 + u_2) \cdot \frac{dh}{dx} \qquad (2.4),$$

where   h, p, x, η are as above and
          u_1, u_2 are the surface velocities of the two solid contact partners.

This equation 2.4 can be modified to a so-called integral form of Reynolds equation, which is preferred in the present section, where possible,

$$\frac{dp}{dx} = 6 \cdot \eta \cdot (u_1 + u_2) \cdot \frac{h - h_0}{h^3} \qquad (2.5),$$

where   h, p, u_1, u_2, x , η are as above and
          h_0 is the height of gap at the contact centreline, where pressure gradient along the contact is zero.

Because equation 2.5 is that for the basic ehl situation, it will be referred to with regard to the underlying assumptions as the isothermal and/or incompressible Reynolds equation.

This Reynolds equation was also used by Dowson and Higginson [4] and Archard, Gair and Hirst [10] for their first numerical solutions of the problem. However, the pressure-viscosity descriptions which they applied were different but of similar, exponential form.

All three early authors [2, 4, 10] obtained the Reynolds equation by transferring the flow equation developed for (rigid) hydrodynamic load cases to the ehl case: Mohrenstein-Ertel refers to his own earlier, hydrodynamic work [11]. There he mentions the *"Navier-Stokes-Gleichung der Hydrodynamik"*, i.e. "the Navier-Stokes equation of hydrodynamic" [*], as the basic equation, which is apparently a simplified x-momentum equation like equation 2.1. Archard, Gair and Hirst [10] refer to the derivations of Mohrenstein-Ertel [2]. Dowson and Higginson [4] derive the equation from a two-dimensional, so-called *"general form of Reynolds equation"*, also developed for the hydrodynamic lubrication problem, and hence obtain the same Reynolds equation. The equations can be traced back to the hydrodynamic problem, hence it is likely that the equations were obtained with Reynolds' original simplifications [1] to the Navier-Stokes equations for the rigid hydrodynamic problem.

Later, Dowson [12] gave a new full derivation of Reynolds equation from the complete three-dimensional Navier-Stokes equations focusing on the elasto-hydrodynamic problem, using non-dimensionalisation and order-of-magnitude considerations. Inertia effects and body forces are considered irrelevant with viscous and pressure terms predominant. Using ambient viscosity for the non-dimensionalisation, Dowson shows that, due to the small magnitude of the height of the gap, in comparison with the length of the contact, various terms, including pressure variation across the gap, are negligible and that the fluid flow description for the ehl problem is given by Reynolds equation 2.5, when constant viscosity across the gap is considered.[†] This derivation is used if justification for application of the derived simplified momentum equation 2.5, e.g. by Gohar [9] and Welsch [13], is given. However, the non-dimensionalisation using ambient viscosity was later questioned by Bair, Winer and Konshari [5]. This is considered in some more detail at the end of the present chapter in subsection 2.4.4.

---

[*]   Indeed the singular form *"Navier-Stokes-Gleichung"* – Navier-Stokes <u>equation</u> – is used by Mohrenstein-Ertel [2].

[†]   The aim of the derivation was the development of a thermal Reynolds equation, section 2.3.2.2, but the aspects can also be applied to the present isothermal consideration.

2.1.2   Self-critical remarks on basic solutions

By the time the above authors [2], [4] and [10] published their results, they already understood that the lubricant property and the flow description from the set of equations which they used cannot determine correct contact traction* coefficients for sliding conditions. While Mohrenstein-Ertel [2] defines them rather generally as *"still unknown effects"*, Dowson and Higginson [4] already give some estimation of the possible temperature rise along and across an elastohydrodynamic gap, which is relevant for sliding conditions. On the other hand, Archard, Gair and Hirst [10] mention compressibility, thermal effects and *"viscosity [...] been regarded as Newtonian"* as possible areas for model improvement, and give estimations of the compressibility influence. Together with the implicit fact that there was not yet general agreement on pressure-viscosity dependency, compressibility, thermal effects and Newtonian versus non-Newtonian flow behaviour, already marked the four important fields for future model refinements in the context of these first ehl solutions. The use of Reynolds equation, however, seems to be uncontested in the context of these works.

The influence of the above-mentioned areas of model refinement on the flow and lubricant property description, also with a view to the full Navier-Stokes equations, is discussed in the following sections.

Notwithstanding these extensions, the above described set of equations is still recognized as the minimum set of equations to be solved in order to obtain a principal ehl solution as it is used for the implementation and test of new numerical methods, e.g. Okamura [14], Lubrecht [8] and Hamrock and Jacobson [15].

---

* The traction coefficient is defined as the ratio of shear forces along a contact surface to the load.

2.2   Modifications to the assumption of incompressibility

The relevance of lubricant compressibility to the ehl regime has already been mentioned and considered in the work of Mohrenstein-Ertel [2] and first taken into account in a numerical solution by Cheng and Sternlicht [16]. The consideration of the compressible ehl regime required a twofold change of the approach sketched above [4, 10]. The fluid flow description by Reynolds equation required modification and a description of the pressure-density dependency had to be provided.

For the latter, Cheng and Sternlicht [16] initially applied an exponential pressure-density approach. The widely established approach is now that proposed by Dowson and Higginson [17],

$$\rho = \rho_0 \cdot \left(\frac{1 + a \cdot p}{b \cdot p} \right)$$ (2.6),

where p is as above,
         a, b are constants,
         ρ is the density, and
         ρ_0 is the density at ambient conditions.

This equation is shown to agree with experimental results [9, 17], reducing the increase in density at high pressure. The approach is frequently presented in literature [9, 13, 18], and used by Hamrock, Pan and Lee [19] for their detailed comparative investigation of the compressible with the incompressible ehl regime. A further enhanced pressure-density correlation is given by Jacobson and Vinet [20], which is later solved by Venner and Bos [21].

Regarding the fluid flow description, a modified Reynolds equation taking the compressibility into account is given by Cheng and Sternlicht [16] as

$$\frac{dp}{dx} = 6 \cdot \eta \cdot (u_1 + u_2) \cdot \frac{h - h^* \cdot \frac{\rho_0}{\rho}}{h^3}$$ (2.7),

where   h, p, u_1, u_2, x , η, ρ, ρ_0 are as above and

                h^* is the height at the position of film rupture at the outlet, where the pressure gradient is zero at ambient conditions.

This equation differs from the previous, incompressible equation with regards to the characteristic height of the gap terms, h_0 and h^* respectively, and the density ratio (ρ/ρ_0); it is subsequently referred to as the compressible Reynolds equation. The derivation of such a Reynolds equation is contained in the derivation of a general Reynolds equation by Dowson [12], or in the derivations by Welsch [13]:

Of the two governing equations 2.1 and 2.2 of the basic solution, the continuity equation 2.2 must be written as a conservation of mass equation and cannot be simplified by the assumption of constant density to a volumetric continuity equation. Hence it changes in its integral, steady state form to

$$\frac{dm'_L}{dx} = \frac{d\left[\int_{y=0}^{y=h} \rho \cdot u \cdot dy\right]}{dx} = 0 \tag{2.8},$$

where   u, x, y, ρ are as above and

           m'_L is the mass flow along the contact per unit width.

On the other hand, in the derivation of the momentum equation 2.1, the assumption of a compressible or an incompressible lubricant neither required nor influenced the momentum equation used for the Reynolds equation, at least as long as thermal effects are not considered. Due to that, the compressibility effect can be regarded as independent of the Navier-Stokes equations, but it relies on the correctness of a momentum equation such as equation 2.1.

2.3   Modifications to the viscosity description

In contrast to the above-mentioned influence of variable density on the Reynolds equation via the mass conservation equation, derivations [12] and [13] show that viscosity is that lubricant parameter which is present in the momentum equation, such as in equation 2.1. The majority of further

modifications of the ehl problem can be considered as modifications of the viscosity and viscosity distribution in the ehl regime. Two methods of modification to the viscosity can be observed: Firstly improving the originally applied pressure-viscosity dependency descriptions and secondly taking into consideration further aspects influencing viscosity. Part of the latter is the consideration of thermal effects, but also in some sense the effects of non-Newtonian fluid properties. Although both ways described are not independent from each other, they are treated rather independently in the following.

2.3.1   Modification to the pressure-viscosity dependency

Originally, exponential descriptions for the pressure-viscosity dependency were applied to solve the ehl problem [2, 4, 10]. These models can be understood as variations of Barus' law [22]

$$\eta = \eta_0 \cdot e^{\alpha \cdot p} \tag{2.9},$$

where   p, η are as above,

η_0 is the dynamic viscosity at ambient conditions, and

α is a pressure-viscosity coefficient,

which many authors referred to as a suitable and convenient pressure-viscosity description [8, 9, 15, 18].

However, when extrapolating results of experiments of modest pressure of up to 0.1 GPa to higher pressure values, the Barus' law omits some reduction of the pressure-viscosity gradient appearing at pressures much higher than 0.1 GPa. Hence it is recognized to overestimate viscosity. Since traction coefficient is determined by the shear strain rate at the wall and the viscosity, overestimation of the viscosity means an overestimated traction coefficient. Thus, Barus' law is regarded as inaccurate above 0.5 GPa, particularly when traction coefficient is considered [9].

Various approaches considering the reduction of the pressure-viscosity coefficient at high pressure have been proposed. The most well-known probably is that by Roelands [23]. Other descriptions have been presented e.g. by Rodermund [24], or Chu and Cameron [25], and a list of further

approaches is given by Welsch [13]. Most approaches agree with Barus' approach at ambient pressure but show a smaller value of pressure-viscosity gradient at higher pressures. A comparison of various of the mentioned approaches by Welsch [13] shows that for a selected reference oil, Barus' approach represents a kind of upper limit and Roelands' approach some kind of lower limit[*]. Similarly, Wolff et al. [26] propose a variety of three pressure-viscosity laws and compare them.

As long as the pressure-viscosity descriptions exclusively consider an influence of the pressure on the viscosity and no other properties, none of the conditions assumed when developing the relevant momentum equation will change, and hence the momentum equation in the form 2.1 and the Reynolds equation 2.5 remain the same, independent of the pressure-viscosity description. This can be seen in the theory by Houpert and Hamrock [27].

2.3.2   Viscosity changes due to thermal effects

Real lubricants change their viscosity not only due to pressure but also due to temperature. Hence, as initially proposed by Mohrenstein-Ertel [2], Dowson and Higginson [4] or Archard, Gair and Hirst [10], the consideration of thermal effects in the ehl problem facilitates viscous heating of the lubricant and the resulting viscosity modification can be used to improve result quality and realistic traction coefficients can be achieved. For their early solution of the thermal ehl problem, Sternlicht, Lewis and Flynn [28] proposed that an energy equation and the respective boundary conditions must be introduced, a description of the viscosity due to pressure and temperature found, and the thermally modified viscosity also applied in the fluid flow description. Considering the latter aspect, three groups of treatment, discussed in the following three subsections, can be observed.

---

[*]   Welsch's comparison covered isothermal and thermal descriptions of viscosity. The findings are also valid for the thermal case which is discussed below.

2.3.2.1   Thermal solutions using isothermal Reynolds equation

A first solution of the thermal problem by Sternlicht, Lewis and Flynn [28] assumed only viscous heating and convective heat transfer along the gap, in other words there was no conduction in the lubricant. This applied form of energy equation gave a temperature distribution along the gap and implied constant temperature across the gap. With an exponential extension of Barus' law incorporating the temperature influence, viscosity values were obtained which were used in a Reynolds equation of form 2.3. Sternlicht, Lewis and Flynn also state that, due to the one-dimensional energy equation, Reynolds equation of form 2.5 and the underlying x-momentum equation of form 2.1 are valid.

Cheng and Sternlicht [16] soon realised that beside the convection along the gap, conductive heat transport across the gap is also relevant, particularly at the slower surface of a sliding contact. Such a solution meant the introduction of a two-dimensional energy equation for the lubricant providing a temperature variation across and along the contact as well as the introduction of a temperature distribution in the conducting solids such as that of Carslaw and Jaeger [29]. They understood that a pressure variation across the gap means a variable viscosity across the gap. Hence a momentum equation in the form 2.1

$$\frac{\partial p}{\partial x} = \eta \cdot \frac{\partial^2 u}{\partial y^2} \qquad (2.10)$$

is not valid, but must be replaced by a form considering variable viscosity across the gap:

$$\frac{\partial p}{\partial x} = \frac{\partial}{\partial y}\left(\eta \cdot \frac{\partial u}{\partial y}\right) \qquad (2.11).$$

However, to be able to use a Reynolds equation of the established form, in the presented case equation 2.7, because of the considered compressibility, a mean viscosity

$$\eta_m = \frac{1}{h} \cdot \int_{y=0}^{h} \eta \cdot dy \qquad (2.12),$$

where   h, y, η are as above and

          η_m is the mean dynamic viscosity

had to be determined for the fluid flow description and analysis.

Although soon Reynolds equations which are consistent with equation 2.11 were available, Reynolds equations using the mean viscosity approach were still applied. Eller [7] proposed a method with a two-dimensional energy equation which reduces numerically to a one-dimensional energy equation along the gap by incorporating an analytical solution across the gap with the assumption of a parabolic temperature profile. Since the model results in a mean viscosity, an isothermal Reynolds equation, in the present case equation 2.3 because the case is incompressible, can be used. Lee and Hsu [30] based their analysis on a similar reduction to a one-dimensional energy equation. Lin, Lin and Jang [31] used an energy equation based on a mean temperature and hence an isothermal Reynolds equation.

2.3.2.2   Thermal solutions using thermal Reynolds equation

To overcome the limitations of Reynolds equation 2.3 and 2.5 and to fulfil the thermal x-momentum equation 2.11, Cheng [32] used a purpose made compressible Reynolds equation of the form

$$\frac{dp}{dx} = 6 \cdot \eta_e \cdot (u_1 + u_2) \cdot \frac{t_2 \cdot h - h^* \cdot \frac{\rho_0}{\rho}}{t_1 \cdot h^3} \tag{2.13},$$

where   h, h*, u_1, u_2, ρ, ρ_0 are as above,

          η_e is an effective viscosity, and

          t_1, t_2 are functions considering the viscosity variation across the height of the gap.

Determination of the variables η_e, t_1 and t_2 requires the solution of an integral across the height of the gap similar to equation 2.12.

An expansion of Reynolds equation was also the intention of Dowson's investigation [12][*]. He provided a Reynolds equation for thermal problems with variable viscosity and density across the gap. The admissible simplifications of the momentum equation are the same as those mentioned above, i.e. irrelevance of inertia and body force effects. Constant pressure across the gap is hence the same as for the isothermal analysis. However, the derivation requires variable viscosity across the gap so that Dowson's governing momentum equation for Reynolds equation is the same as equation 2.11 and the applied continuity equation is compressible. With these assumptions, a thermal Reynolds equation in the non-integral form is

$$\frac{d}{dx}\left[\left(F_2 + G_1\right) \cdot \frac{dp}{dx}\right]$$

$$= h \cdot \frac{d}{dx}\left(\rho \cdot u\right)_2 - \frac{d}{dx} \cdot \left[\frac{\left(u_2 - u_1\right) \cdot \left(F_3 + G_2\right)}{F_0} + u_1 \cdot G_3\right] + \left(\rho \cdot v\right)_2 - \left(\rho \cdot v\right)_1 \tag{2.14},$$

where p, x, y, u_1, u_2, ρ are as above,
            v is the speed perpendicular to the gap,
            F_0, F_2, F_3 are functions considering the variable viscosity across the gap which require fourfold the determination of an integral,
            G_1, G_2, G_3 are functions considering the variable density across the gap which require also the determination of an integral, and
            1 and 2   are subscripts marking the lower and upper surface respectively.

Fowles [33] proposed slightly different functions for the thermal Reynolds equation in order to reduce the numerical effort for solution. He developed his form directly from Dowson's thermal equation. This equation was frequently used for thermal analysis of the ehl regime, e.g. by Sui and Sadeghi [34], Sadeghi and Dow [35] and Welsch [13]. Due to the history of development, all these equations are based on an x-momentum equation of the form 2.11 and a negligible pressure variation across the gap, equation 2.3.

---

[*]   Dowson's fundamental derivation was cited earlier in the discussion of the isothermal Reynolds equation in section 2.1.

2.3.2.3   Thermal solutions without Reynolds equation

Occasionally, solutions of the ehl problem were proposed which are characterised by a renunciation of any Reynolds equation. Liesegang [36] and Brüggemann and Kollmann [37] followed the frequently reported opinion that viscous heating and heat transport in the gap lead to variable viscosity across the height of the gap. They concluded, like e.g. Dowson [12], that the momentum equation of the form 2.1 must not be applied, and the traditional way of developing Reynolds equation, such as sketched in section 2.1, cannot be followed. Despite that, a full set of momentum equations – and continuity equation – must be solved, including discretisation of the equations across the gap. Brüggemann and Kollmann [37] even state that the *"Navier-Stokes equations"* are to be solved. However, Liesegang [36] as well as Brüggemann and Kollmann propose and introduce simplifications to the Navier-Stokes equations which reduce them exactly to the form of momentum equation 2.11 which is used for the derivation of the thermal Reynolds equations. The derivation also excludes a pressure variation across the gap by assuming the pressure gradient in the y-momentum equation to be zero. Hence their approach is rather more a different numerical method than a different description of fluid flow.

2.4   Non-Newtonian effects

2.4.1   Available non-Newtonian models

Thermal effects were also insufficient to obtain realistic traction coefficient values and lubricant was hence assumed to exhibit non-Newtonian behaviour, i.e. Newton's approach that the local shear stress τ is linear to the shear strain rate γ_S is invalid, but the shear stress depends on further parameters [32, 38]. Various models were proposed to describe the non-Newtonian behaviour:

♦ **Pseudoplastic:**
The lubricant is assumed to show a purely viscous behaviour, but the higher the shear strain rate rises, the smaller is the correlated rise of the shear stress. In other words, the absolute viscosity appears to be

smaller the higher the shear strain rate rises. For infinite shear strain rate the shear stress rises also to infinity, i.e. the absolute viscosity never reaches a zero value. Eyring' hyperbolic sine model [39] represents such a behaviour and Houpert and Hamrock [40] applied the model to the ehl problem.

Also a so-called power law model, where the shear stress is proportional to the shear strain rate raised to the power of a constant, represents a pseudoplastic behaviour when the exponent is less then unity. Such a model found application and solution for the ehl problem by Wang, Hua and Zhang [41]. Lin and Lin [42] show pseudoplastic behaviour results when their exponent of the power law falls below unity.

◆ **Limiting shear stress**

Similar to the above Eyring model, the limiting shear stress assumes a reduced rise of the shear stress with an increasing shear strain rate. However, for high shear strain rates, the shear stress does not continue to rise, but approaches a finite asymptotic limiting shear stress value. Correspondingly, absolute viscosity asymptotically approaches zero with increasing shear strain rate.

For the mathematical description a variety of shear strain rate-shear stress dependencies have been proposed, such as a logarithmic, a hyperbolic tangent, an exponential and, as special case of the exponential, the circular. An overview and comparison of the above descriptions is given by Elsharkawy and Hamrock [43].

◆ **Visco-elastic**

The visco-elastic model means that a fluid does not behave exclusively as viscous, but as a mixture of viscous and elastic behaviour, whereas the influence of the two effects depends on the time the lubricant stays in the contact.

This model was proposed by Johnson and Tevaarwerk [44] for the ehl regime, assuming an Eyring-type viscous behaviour. Bair and Winer [45] proposed a model combining the elastic behaviour with a viscous limiting shear stress model.

♦ **Visco-plastic**

Like the limiting shear stress model, the visco-plastic model assumes a shear stress which does not exceed a limiting shear stress value independent of the shear strain rate. However, in contrast to the limiting shear stress models, it is assumed that this shear stress can be reached, and that the liquid is showing a plastic behaviour once the value is reached.

Iivonen and Hamrock [46] proposed and solved a model for such a behaviour in which they assumed a Newtonian fluid behaviour for shear strain rates leading to a shear stress below the limiting value.

2.4.2   Flow description for non-Newtonian models

To solve the ehl regime for a non-Newtonian lubricant, a revised equation to describe the flow is required. The procedure is similar for the various non-Newtonian models, such as the Eyring model by Conry, Wang and Cusano [47] or Houpert and Hamrock [40], the circular by Lee and Hamrock [48], the power law by Wang, Hua and Zhang [41], the visco-plastic by Iivonen and Hamrock [46] or a generally valid model by Hughes and Bush [49]. Since the x-momentum equation 2.5 and 2.11 respectively incorporates Newton's law, it is written in the generally valid manner as

$$\frac{\partial p}{\partial x} = \frac{\partial \tau_{xy}}{\partial y}$$

(2.15),

where   p, x ,y   are as above and
τ_{xy} is the shear stress component directed along the gap.

Hence at the start of the development of a non-Newtonian flow equation with equation 2.15, the validity of the assumptions applied to obtain the respective equation for the Newtonian Reynolds equation is implied. Using the above momentum equation 2.15, a respective description of shear strain-shear stress dependency, continuity equation, assumptions regarding the shear rate distribution across the gap and of the constant pressure across the gap, and a procedure as that for a Newtonian Reynolds equation, non-Newtonian Reynolds equations are obtained, which differ from the Newtonian Reynolds

equation 2.7 by some additional terms taking the described additional effects into account.

2.4.3   Combination of non-Newtonian and thermal analysis

As Crook [38] concluded from thermal results, that there is a need to consider non-Newtonian lubricant properties, Hamrock [18] recognizes from his non-Newtonain results vice versa that there is a need for consideration of thermal effects in order to obtain realistic results.

The two approaches observed for Newtonian, thermal ehl analysis, i.e. a solution using average viscosity across the gap and another using a thermal equation with numerical integration across the gap, are also observed for the non-Newtonian problem.

For the first method Salehizadeh and Saka [50] start the development of a suitable flow equation from an x-momentum equation not representing the full Navier-Stokes equation, but a more extensive form than equation 2.15. However, like Dowson [12] they conclude that the pressure variation across the gap is negligible and that the momentum equation can be reduced to the form of 2.15. Others, like Wang, Cusano and Conry [51], start directly from the x-momentum equation 2.15. Due to the mean viscosity, both [50] and [51] obtain Reynolds equations with the structure of an isothermal, non-Newtonian Reynolds equation.

Peiran and Shizhu [52] developed a generalized Reynolds equation for non-Newtonian thermal and compressible elastohydrodynamic lubrication. Formally, the Reynolds equation looks like the thermal Newtonian Reynolds equation of Dowson [12] and Fowles [33], equation 2.14. However, the contained factors are not based on the viscosity, but on an equivalent viscosity, which itself must be determined numerically for each position across the gap. The derivation of the equation follows the procedure of Dowson [12] and is hence again based on the x-momentum equation 2.15.

Thus, from the basic solutions of section 2.1 to the most advanced models of the ehl regime with compressible, thermal and non-Newtonian effects, all solutions are based on a simplified x-momentum equation and a negligible y-

momentum equation, meaning that there is no pressure variation across the gap.

2.4.4   Overcoming constant pressure across the gap and simplified x-momentum equation

The above observation of exclusive application of Reynolds equation and assumption of constant pressure across the gap is confirmed by Bair, Khonsari and Winer [5], who quote the determination of the pressure in the ehl regime is *"almost exclusively performed with a form of the classical Reynolds equation"*.

However, when performing experiments and considering Navier-Stokes equations to understand non-Newtonian behaviour, Bair, Khonsari and Winer show that pressure variation across the gap has some relevance. Hence Navier-Stokes equations should be used instead of Reynolds equation. They further show that for pressure dependent viscosity such as in the elastohydrodynamic contact problem, the Navier-Stokes equations can develop a singularity, where the characteristic of the Navier-Stokes equations will change. They link this singularity with the appearance of shear bands and the reaching of limiting shear stress. Bair, Khonsari and Winer conclude that for a full understanding of the ehl contact there is need for a numerical solution of the Navier-Stokes equations, not just for the reason mentioned, but also for consideration of rough surfaces.

A solution of an approach using the full Navier-Stokes equations was given by Almqvist and Larsson for isothermal [53] and thermal contacts [54]. Their analysis parameters were limited so that the singularity of the Navier-Stokes equations was approached but not exceeded. Their results show no qualitative and minor quantitative differences in comparison to Reynolds equation based solutions.

2.5   Summary and conclusion

Since the first solution of the elastohydrodynamic contact problem by Mohrenstein-Ertel [2], Reynolds equation has been used as the usual description for the lubricant flow. This fluid flow description allows variable

density, viscosity and various shear rate-shear stress dependencies, but remains an equation based on a simplified x-momentum equation

$$\frac{\partial p}{\partial x} = \frac{\partial \tau_{xy}}{\partial y} \qquad (2.16)$$

and the assumption of a constant pressure across the gap

$$\frac{\partial p}{\partial y} = 0 \qquad (2.17)$$

for the elastohydrodynamic contact problem. Although widely accepted, this assumption of a constant pressure across the gap is now questioned, proposing the application of Navier-Stokes equations instead of Reynolds equation. However, this proposal has hardly been investigated numerically and hence requires further exploration.

Chapter 3

Significance of the individual terms in the Navier-Stokes equations

As shown in the previous chapter, almost all existing solutions of the ehl line contact problem use various forms of the Reynolds equation to describe the lubricant flow. Almost all available solutions agree with respect to some fundamental assumptions, e.g. the neglect of inertia forces and the assumption of a constant pressure across the gap. On the other hand, recommendations to apply the full Navier-Stokes equations are made.

In this chapter, the basic derivation of the relevant equations for the fluid flow description is repeated with the aim of understanding the significance of the individual terms of the Navier-Stokes equations. For this, simplifications will be introduced during the derivation, which are discussed and evaluated in detail. A need for the consideration of additional terms of the Navier-Stokes equations is confirmed and sets of equations restricted to the relevant terms are given. These sets of equations reduce the complexity of the Navier-Stokes equations and allow a practical understanding and handling of the extended approach.

3.1   Governing equations

3.1.1   Fluid flow equations

The basis for the derivation of the momentum equation is the application of Newton's second law to an infinitesimal fluid element as shown, e.g. in

Schlichting [55], [56]. The inertia forces on a fluid element are balanced by pressure, viscous, and body forces, figure 3.1:

$$\left.\begin{array}{l}\dfrac{Du}{Dt}=\dfrac{1}{\rho}\cdot f_x-\dfrac{1}{\rho}\cdot\dfrac{\partial p}{\partial x}+\dfrac{1}{\rho}\cdot\left(\dfrac{\partial \sigma_{xx}}{\partial x}+\dfrac{\partial \sigma_{yx}}{\partial y}+\dfrac{\partial \sigma_{zx}}{\partial z}\right)\\[3mm]\dfrac{Dv}{Dt}=\dfrac{1}{\rho}\cdot f_y-\dfrac{1}{\rho}\cdot\dfrac{\partial p}{\partial y}+\dfrac{1}{\rho}\cdot\left(\dfrac{\partial \sigma_{yy}}{\partial y}+\dfrac{\partial \sigma_{xy}}{\partial x}+\dfrac{\partial \sigma_{zy}}{\partial z}\right)\\[3mm]\dfrac{Dw}{Dt}=\dfrac{1}{\rho}\cdot f_z-\dfrac{1}{\rho}\cdot\dfrac{\partial p}{\partial z}+\dfrac{1}{\rho}\cdot\left(\dfrac{\partial \sigma_{zz}}{\partial z}+\dfrac{\partial \sigma_{xz}}{\partial x}+\dfrac{\partial \sigma_{yz}}{\partial y}\right)\end{array}\right\}\qquad(3.1).$$
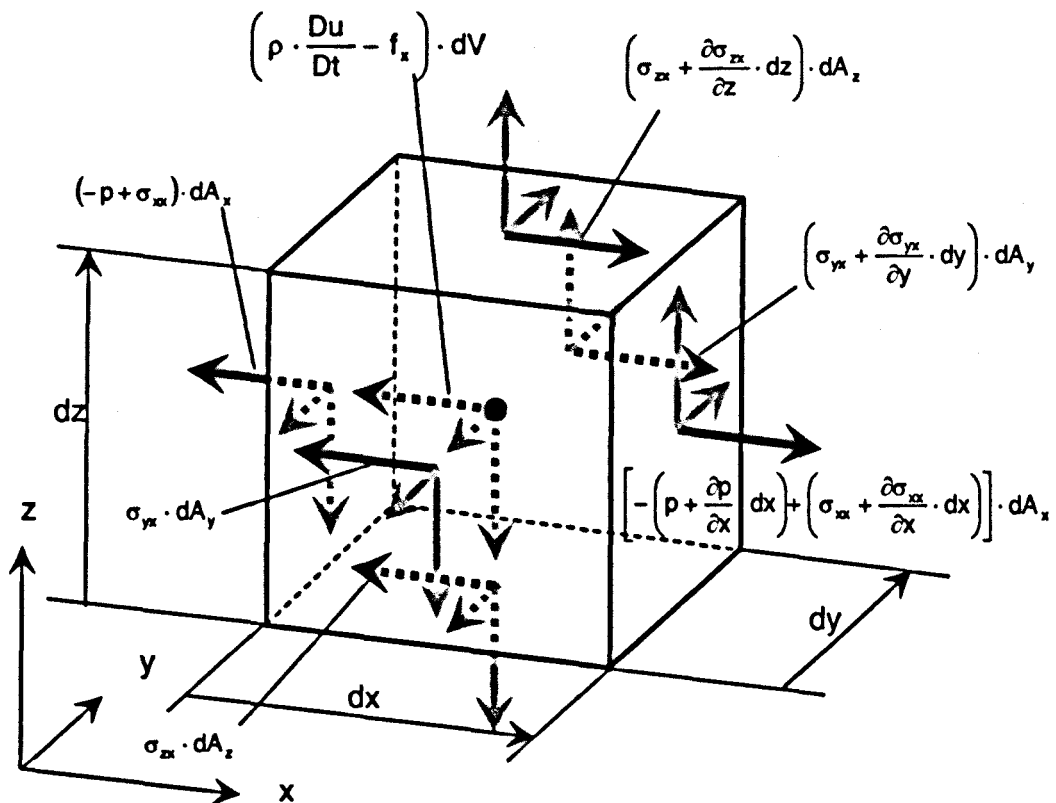
Figure 3.1:   *Equilibrium of forces on a fluid element by inertia, body, pressure, and viscous components.*

Fulfilling the requirement of equilibrium of momentum for all surfaces of the fluid element leads to the result of symmetry for the tangential stress components:

$$\sigma_{xy}=\sigma_{yx}\,,\ \sigma_{xz}=\sigma_{zx}\,,\ \sigma_{yz}=\sigma_{zy}\qquad(3.2).$$

There still remain six independent terms describing the stress. Further simplification of the momentum equation requires that these stress terms are rewritten in terms of other dependent variables. The approach used for this investigation is Stokes' approach, the three-dimensional extension of Newton's approach that shear stress and velocity gradient are proportional. In the x-direction the stresses can be written as:

$$
\left.
\begin{aligned}
\sigma_{xx} &= 2 \cdot \eta \cdot \frac{\partial u}{\partial x} + \lambda \cdot \left(\frac{\partial u}{\partial x} + \frac{\partial v}{\partial y} + \frac{\partial w}{\partial z} \right) \\
\sigma_{xy} &= \eta \cdot \left(\frac{\partial u}{\partial y} + \frac{\partial v}{\partial x} \right) \\
\sigma_{xz} &= \eta \cdot \left(\frac{\partial u}{\partial z} + \frac{\partial w}{\partial x} \right)
\end{aligned}
\right\}
\qquad (3.3).
$$

The stress components in the y- and z-directions can be obtained by cyclic transposition.

In the set of equations 3.3 the first equation represents normal stress except for the pressure while the second and third represent shear stress in the respective directions. The variable η is the dynamic viscosity and λ is a second viscosity coefficient. For gases, a good working approximation for the second viscosity coefficient can be obtained by using Stokes' hypothesis [55, 56], where

$$
\lambda = -\frac{2}{3} \cdot \eta
\qquad (3.4).
$$

In the case of liquids, the same hypothesis is used for the value of the second viscosity coefficient λ. However, the variable is increasingly irrelevant for weakly compressible and fully irrelevant for incompressible liquids. This is because the term $\left(\partial u/\partial x + \partial v/\partial y + \partial w/\partial z \right)$ represents the mass continuity for an incompressible flow as shown below [57].

Introducing equations 3.3 into 3.1 results in the Navier-Stokes equations:

$$\rho \cdot \frac{Du}{Dt} = f_x - \frac{\partial p}{\partial x} + 2 \cdot \frac{\partial}{\partial x}\left[\eta \cdot \frac{\partial u}{\partial x}\right] + \frac{\partial}{\partial x}\left[\lambda \cdot \left(\frac{\partial u}{\partial x} + \frac{\partial v}{\partial y} + \frac{\partial w}{\partial z}\right)\right]$$

$$+ \frac{\partial}{\partial y}\left[\eta \cdot \left(\frac{\partial u}{\partial y} + \frac{\partial v}{\partial x}\right)\right] + \frac{\partial}{\partial z}\left[\eta \cdot \left(\frac{\partial u}{\partial z} + \frac{\partial w}{\partial x}\right)\right]$$

$$\rho \cdot \frac{Dv}{Dt} = f_y - \frac{\partial p}{\partial y} + 2 \cdot \frac{\partial}{\partial y}\left[\eta \cdot \frac{\partial v}{\partial y}\right] + \frac{\partial}{\partial y}\left[\lambda \cdot \left(\frac{\partial u}{\partial x} + \frac{\partial v}{\partial y} + \frac{\partial w}{\partial z}\right)\right]$$

$$+ \frac{\partial}{\partial x}\left[\eta \cdot \left(\frac{\partial u}{\partial y} + \frac{\partial v}{\partial x}\right)\right] + \frac{\partial}{\partial z}\left[\eta \cdot \left(\frac{\partial v}{\partial z} + \frac{\partial w}{\partial y}\right)\right]$$

$$\rho \cdot \frac{Dw}{Dt} = f_z - \frac{\partial p}{\partial z} + 2 \cdot \frac{\partial}{\partial z}\left[\eta \cdot \frac{\partial w}{\partial z}\right] + \frac{\partial}{\partial z}\left[\lambda \cdot \left(\frac{\partial u}{\partial x} + \frac{\partial v}{\partial y} + \frac{\partial w}{\partial z}\right)\right]$$

$$+ \frac{\partial}{\partial x}\left[\eta \cdot \left(\frac{\partial u}{\partial z} + \frac{\partial w}{\partial x}\right)\right] + \frac{\partial}{\partial y}\left[\eta \cdot \left(\frac{\partial v}{\partial z} + \frac{\partial w}{\partial y}\right)\right]$$

$$(3.5).$$

As discussed in section 2.4, many authors suggest that the lubricant does not exhibit Newtonian behaviour under the severe conditions of the contact. However, the Navier-Stokes equations assume a Newtonian fluid. Therefore, the use of the Navier-Stokes equations as a basis for the following investigation is a major assumption. It is clear that any results obtained using the assumption of a Newtonian fluid must be considered with respect to possible non-Newtonian influences. These will be discussed in section 12.4.

All body force terms are set to zero. These could be, for example, electrical, magnetic, or gravitational forces[*]. Electrical and magnetic forces do not affect the lubricant. Gravitational effects might be non-zero in certain applications but they are usually relatively small in fully flooded situations and always dependent on the position and orientation of the application. Body force terms are often used to introduce appropriate models for effects beyond the assumption of a continuum, e.g. intermolecular forces at the interface to other fluids such as surface tension and capillarity. These phenomena might

---

[*]   Occasionally, centrifugal and Coriolis forces are considered as body forces, but this is only the case when the reference system is moving or rotating. When considering a stationary system, any centrifugal or Coriolis effects are represented by the momentum terms.

have an influence on the contact because the height of the gap at the outlet, where the film ruptures, is very small. In the following investigations only fully flooded areas of the contact are considered allowing surface tension effects to be neglected.

If the fluid properties, i.e. density, viscosity, and the second viscosity parameter, are known, four unknown variables, i.e. pressure and three velocity components, remain in the three Navier-Stokes equations. A fourth equation is necessary to allow the system of equations to be solved. This equation is the continuity equation describing the conservation of mass:

$$\frac{\partial \rho}{\partial t} + \frac{\partial(\rho \cdot u)}{\partial x} + \frac{\partial(\rho \cdot v)}{\partial y} + \frac{\partial(\rho \cdot w)}{\partial z} = 0 \qquad (3.6).$$

3.1.2   Fluid properties

To solve the Navier-Stokes equations, the fluid properties must be prescribed.

3.1.2.1   Density

The influence of variable density was assumed to be negligible for the main part of the present investigation. As mentioned in chapter 2.1, the principal solutions and typical phenomena of an ehl contact can be shown without variable density and the influence of variable density is relatively small. On the other hand, variable density spoils the parallel shape of the gap, which results in a more difficult understanding of further phenomena such as thermal or Non-Newtonian effects.

The assumption of incompressibility can be written as

$$\frac{\partial \rho}{\partial x} = \frac{\partial \rho}{\partial y} = \frac{\partial \rho}{\partial z} = \frac{\partial \rho}{\partial t} = 0 \qquad (3.7),$$

which reduces the continuity equation to

$$\frac{\partial u}{\partial x} + \frac{\partial v}{\partial y} + \frac{\partial w}{\partial z} = 0 \qquad (3.8).$$

A combination of the incompressible continuity equation with the Navier-Stokes equations leads to the disappearance of those terms of the Navier-Stokes equations which contain the second viscosity coefficient λ. It is obvious that, for exact solutions, a detailed investigation of compressible influences is necessary.

3.1.2.2   Viscosity

The lubricant was assumed to follow Barus' pressure-viscosity dependency [22]

$$\eta = \eta_0 \cdot e^{\alpha \cdot p} \qquad (3.9),$$

where η_0 is the viscosity at ambient conditions,
          α is a pressure-viscosity coefficient, and
          p is the relative pressure.

Although Barus' approach leads to traction coefficients which are much higher than reality, subsection 2.3.1 and [9], the principal behaviour of the ehl contact can still be modelled with the advantage that the equation is easy to handle. In case a more exact description is required, Roelands' approach [23] is used in its isothermal form:

$$\eta = \eta_0 \cdot \exp\left[\left(\ln(\eta_0) + 9.67\right) \cdot \left[-1 + \left(1 + 5.1 \cdot 10^{-9} \cdot p\right)^{z}\right]\right] \qquad (3.10)$$

with

$$Z = \frac{\alpha}{5.1 \cdot 10^{-9} \cdot \left(\ln(\eta_0) + 9.67\right)}.$$

The restriction to an isothermal case is chosen in order to restrict the scope of the principal investigation of the individual terms. It was realised that the reduction to the isothermal case causes the elimination of some important effects. These effects have already been discussed in detail as reviewed in subsection 2.3.2. Care is taken that any new findings for the isothermal case will be discussed with respect to thermal effects, e.g. in section 12.5.

3.1.3   Description of the elastic behaviour

For the description of the contact deformation, Boussinesq's approach is used as described in Szabó [58]. The approach assumes an infinitely wide half-space. Due to this assumption, the deflections can only be calculated relative to another point. Details can be seen from figure 3.2, where the deformation at a location x is given by

$$v_d(x) = -\frac{2 \cdot (1-v^2)}{\pi \cdot E} \cdot \int_{-\infty}^{+\infty} p(s) \cdot \ln\left|\frac{x-s}{x_{ref}-s}\right| \cdot ds \qquad (3.11).$$
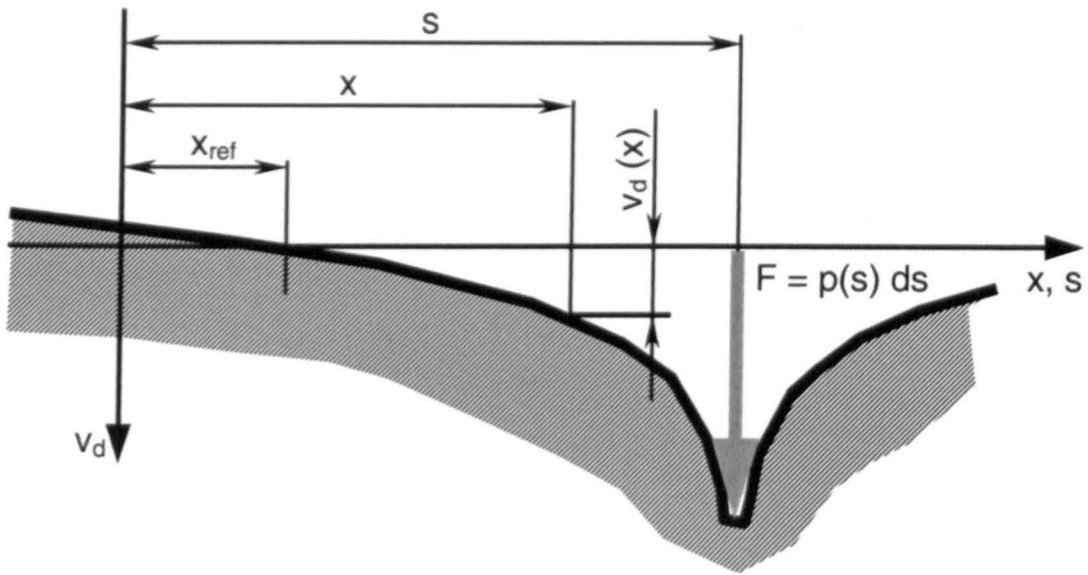
Figure 3.2:   *Deflection of an infinitely wide half-space due to local pressure p. Definition of the variables for the Boussinesq equation.*

3.1.4   Reduction to two-dimensional, steady-state conditions

The premise, made in section 1.3, that a steady state line contact problem should be considered, reduces the number of independent variables. Using the axis orientation as defined in figure 3.3, an infinitely wide line contact has the consequence that

$$\frac{\partial}{\partial z} = 0 \text{ and } w = 0 \qquad (3.12a).$$

The above condition, together with the steady state condition,

$$\frac{\partial}{\partial t} = 0 \tag{3.12b},$$

leads to the simplified form of the Navier-Stokes equations

$$\left.\begin{array}{l} \rho \cdot \left(u \cdot \dfrac{\partial u}{\partial x} + v \cdot \dfrac{\partial u}{\partial y} \right) = -\dfrac{\partial p}{\partial x} + 2 \cdot \dfrac{\partial}{\partial x}\left[\eta \cdot \dfrac{\partial u}{\partial x} \right] + \dfrac{\partial}{\partial y}\left[\eta \cdot \left(\dfrac{\partial u}{\partial y} + \dfrac{\partial v}{\partial x} \right) \right] \\[4mm] \rho \cdot \left(u \cdot \dfrac{\partial v}{\partial x} + v \cdot \dfrac{\partial v}{\partial y} \right) = -\dfrac{\partial p}{\partial y} + 2 \cdot \dfrac{\partial}{\partial y}\left[\eta \cdot \dfrac{\partial v}{\partial y} \right] + \dfrac{\partial}{\partial x}\left[\eta \cdot \left(\dfrac{\partial u}{\partial y} + \dfrac{\partial v}{\partial x} \right) \right] \end{array}\right\} \tag{3.13}$$

and the continuity equation reduces to

$$\frac{\partial u}{\partial x} + \frac{\partial v}{\partial y} = 0 \tag{3.14}.$$

The Boussinesq equation and the fluid property descriptions remain unchanged.
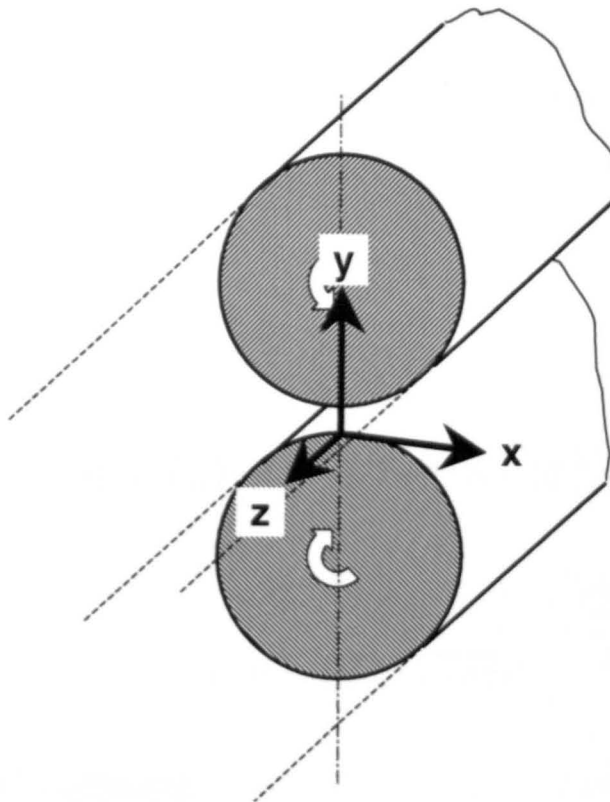
Figure 3.3:   Orientation of the system of co-ordinates for the ehl line contact.

3.1.5   Final set of equations

The set of equations developed above and used in the rest of the present study is summarised below:

♦ Two-dimensional, incompressible Navier-Stokes equations:

$$\left.\begin{aligned} \rho\cdot\left(u\cdot\frac{\partial u}{\partial x}+v\cdot\frac{\partial u}{\partial y}\right) &= -\frac{\partial p}{\partial x}+2\cdot\frac{\partial}{\partial x}\left[\eta\cdot\frac{\partial u}{\partial x}\right]+\frac{\partial}{\partial y}\left[\eta\cdot\left(\frac{\partial u}{\partial y}+\frac{\partial v}{\partial x}\right)\right] \\ \rho\cdot\left(u\cdot\frac{\partial v}{\partial x}+v\cdot\frac{\partial v}{\partial y}\right) &= -\frac{\partial p}{\partial y}+2\cdot\frac{\partial}{\partial y}\left[\eta\cdot\frac{\partial v}{\partial y}\right]+\frac{\partial}{\partial x}\left[\eta\cdot\left(\frac{\partial u}{\partial y}+\frac{\partial v}{\partial x}\right)\right] \end{aligned}\right\} \quad (3.15).$$

♦ Two-dimensional, incompressible continuity equation:

$$\frac{\partial u}{\partial x}+\frac{\partial v}{\partial y}=0 \qquad (3.16).$$

♦ Boussinesq's equation describing the elastic deformation:

$$v_d(x)=-\frac{2\cdot\left(1-\nu^2\right)}{\pi\cdot E}\cdot\int_{-\infty}^{+\infty}p(s)\cdot\ln\left|\frac{x-s}{x_{ref}-s}\right|\cdot ds \qquad (3.17).$$

♦ Barus' and Roelands' equations describing the pressure-viscosity dependency:

Barus' equation

$$\eta=\eta_0\cdot e^{\alpha p} \qquad (3.18a),$$

Roelands' equation

$$\eta=\eta_0\cdot\exp\left[\left(\ln(\eta_0)+9.67\right)\cdot\left[-1+\left(1+5.1\cdot10^{-9}\cdot p\right)^z\right]\right] \qquad (3.18b)$$

with

$$Z=\frac{\alpha}{5.1\cdot10^{-9}\cdot\left(\ln(\eta_0)+9.67\right)}.$$

3.2   Inertia effects

In the following, the relative importance of the inertia terms in comparison with the viscous terms in the ehl regime is considered. Inertia effects are expected to appear in regions of significant geometry change and also in

areas of low viscosity. Both these conditions are fulfilled in the inlet zone of the ehl contact. The present section thus concentrates on this inlet zone.

3.2.1   Non-dimensional form of the Navier-Stokes equations

In order to investigate the influence of inertia forces, the Navier-Stokes equations are written in non-dimensional form. All variables are normalised by relating each variable to a characteristic value so that the dimensionless variables range approximately between zero and unity. The characteristic values are specific constants for any ehl line contact configuration and illustrated in figure 3.4.
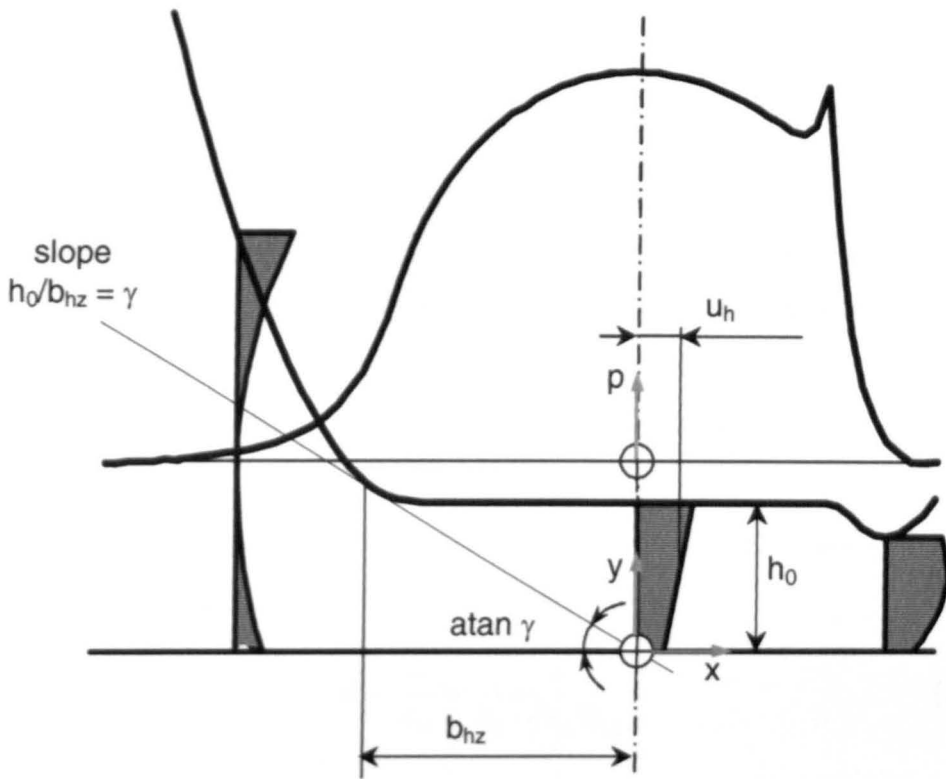
height of the gap vs. length of the gap
100 times magnified

Figure 3.4:   Characteristic values in the ehl contact as reference values for normalising the Navier-Stokes equations for the investigation of inertia effects.

The distance along the gap x is non-dimensionalised with respect to the Hertzian width b_{hz}:

$$\overline{X} = \frac{x}{b_{hz}}$$ (3.19a).

The distance across the gap y is non-dimensionalised with respect to the height of the parallel section of the gap h_0, although, particularly for heavy loaded cases such as illustrated in figure 3.4, the height of the gap at the start of the inlet zone might be up to one order of magnitude higher,

$$\overline{Y} = \frac{y}{h_0}$$ (3.19b).

The velocity component parallel to the gap u is non-dimensionalised with respect to the mean of the two contact surface speeds, the hydrodynamic speed u_h,

$$\overline{U} = \frac{u}{u_h} = \frac{u}{\frac{1}{2} \cdot (u_1 + u_2)}$$ (3.19c).

The velocity component across the gap v is non-dimensionalised with respect to an assumed mean perpendicular speed $v_m{}^{\bullet}$. Since there is no obvious predefined characteristic speed across the gap, such a component has to be defined by a characteristic speed along the contact, i.e. the hydrodynamic speed, and a characteristic geometrical ratio comparing the dimensions along and across the gap, i.e. a characteristic slope. With Hertzian width b_{hz} and the centreline height h_0 defining such a characteristic slope[t], the definition of dimensionless speed across the gap is

$$\overline{V} = \frac{v}{v_m} = \frac{v}{u_h \cdot (h_0/b_{hz})}$$ (3.19d).

Similar to the dimensionless height of the gap, the dimensionless velocity $\overline{V}$ might exceed unity by up to one order of magnitude.

---

[*]   Contrary to the practice of introducing only a single dimensionless speed, e.g. Schlichting [55, 56], in the present study a dimensionless speed value is introduced for each direction to obtain unity dimensionless speeds in both co-ordinate directions.

[t]   An alternative definition could be the slope of the curved surface near the edge of a dry Hertzian contact. Such a method might represent a better approximation of the contact situation but would be independent of the characteristic length across the gap.

The characteristic pressure was taken as ambient p_0 rather than the Hertzian pressure p_{hz} because any inertia effects were expected in the inlet zone, where viscosity and pressure will be approximately ambient. This definition tends to emphasize the influence of the inertia terms in comparison with the pressure and viscous terms of the Navier-Stokes equations. Thus

$$\overline{P}_0 = \frac{p}{p_0} \quad^{\bullet}$$ (3.19e).

For approximately ambient conditions, Barus' approach delivers very small changes to the viscosity so that for the viscosity η

$$\eta = \eta_0 = \text{constant}$$ (3.19f).

Incompressible fluid behaviour was assumed as discussed in section 3.1

$$\rho = \rho_0 = \text{constant}$$ (3.19g).

Introducing the above definitions, the Navier-Stokes equations in dimensionless form are obtained:

$$
\left.
\begin{aligned}
\frac{\rho_0 \cdot u_h^2}{b_{hz}} \cdot \left(\overline{U} \cdot \frac{\partial \overline{U}}{\partial \overline{X}} + \overline{V} \cdot \frac{\partial \overline{U}}{\partial \overline{Y}} \right) &= -\frac{p_0}{b_{hz}} \cdot \frac{\partial \overline{P}_0}{\partial \overline{X}} + \frac{2 \cdot \eta_0 \cdot u_h}{b_{hz}^2} \cdot \frac{\partial^2 \overline{U}}{\partial \overline{X}^2} \\
&\quad + \frac{\eta_0 \cdot u_h}{h_0^2} \cdot \frac{\partial^2 \overline{U}}{\partial \overline{Y}^2} + \frac{\eta_0 \cdot u_h}{b_{hz}^2} \cdot \frac{\partial^2 \overline{V}}{\partial \overline{Y} \partial \overline{X}} \\
\frac{\rho_0 \cdot u_h^2 \cdot h_0}{b_{hz}^2} \cdot \left(\overline{U} \cdot \frac{\partial \overline{V}}{\partial \overline{X}} + \overline{V} \cdot \frac{\partial \overline{V}}{\partial \overline{Y}} \right) &= -\frac{p_0}{h_0} \cdot \frac{\partial \overline{P}_0}{\partial \overline{Y}} + \frac{2 \cdot \eta_0 \cdot u_h}{h_0 \cdot b_{hz}} \cdot \frac{\partial^2 \overline{V}}{\partial \overline{Y}^2} \\
&\quad + \frac{\eta_0 \cdot u_h}{h_0 \cdot b_{hz}} \cdot \frac{\partial^2 \overline{U}}{\partial \overline{Y} \partial \overline{X}} + \frac{\eta_0 \cdot u_h \cdot h_0}{b_{hz}^3} \cdot \frac{\partial^2 \overline{V}}{\partial \overline{X}^2}
\end{aligned}
\right\}
$$ (3.20).

Introducing the geometry ratio γ

$$\gamma = \frac{h_0}{b_{hz}}$$ (3.21),

replacing the Hertzian width b_{hz} in the velocity gradient terms, and re-ordering the terms, equations 3.20 become:

$^{\bullet}$ $\overline{P}_0$ was used rather than $\overline{P}$ as symbol for the dimensionless pressure related to ambient pressure because the latter symbol will be required for an alternative definition of the dimensionless pressure in section 3.3.

$$\gamma \cdot \frac{p_0 \cdot u_h{}^2}{h_0} \cdot \left(\overline{U} \cdot \frac{\partial \overline{U}}{\partial \overline{X}} + \overline{V} \cdot \frac{\partial \overline{U}}{\partial \overline{Y}} \right) = -\frac{p_0}{b_{hz}} \cdot \frac{\partial \overline{P}_0}{\partial \overline{X}}$$

$$+ \frac{\eta_0 \cdot u_h}{h_0^2} \cdot \left(2 \cdot \gamma^2 \cdot \frac{\partial^2 \overline{U}}{\partial \overline{X}^2} + \frac{\partial^2 \overline{U}}{\partial \overline{Y}^2} + \gamma^2 \cdot \frac{\partial^2 \overline{V}}{\partial \overline{Y} \partial \overline{X}} \right)$$

$$\gamma^2 \cdot \frac{p_0 \cdot u_h{}^2}{h_0} \cdot \left(\overline{U} \cdot \frac{\partial \overline{V}}{\partial \overline{X}} + \overline{V} \cdot \frac{\partial \overline{V}}{\partial \overline{Y}} \right) = -\frac{p_0}{h_0} \cdot \frac{\partial \overline{P}_0}{\partial \overline{Y}}$$

$$+ \gamma \cdot \frac{\eta_0 \cdot u_h}{h_0^2} \cdot \left(2 \cdot \frac{\partial^2 \overline{V}}{\partial \overline{Y}^2} + \frac{\partial^2 \overline{U}}{\partial \overline{Y} \partial \overline{X}} + \gamma^2 \cdot \frac{\partial^2 \overline{V}}{\partial \overline{X}^2} \right)$$

$$(3.22).$$

3.2.2   Determining Reynolds number

The geometry ratio γ is obviously very small, hence the sum of the viscous terms in the brackets terms remain in the normalised range. Reynolds number is the ratio of inertia forces to viscous forces and therefore can be calculated by dividing the multiplying factors outside the brackets. The Navier-Stokes equations written with Reynolds number become:

$$\text{Re} \cdot \left(\overline{U} \cdot \frac{\partial \overline{U}}{\partial \overline{X}} + \overline{V} \cdot \frac{\partial \overline{U}}{\partial \overline{Y}} \right) = -\gamma^2 \cdot \frac{p_0 \cdot b_{hz}}{\eta_0 \cdot u_H} \cdot \frac{\partial \overline{P}_0}{\partial \overline{X}}$$

$$+ \left(2 \cdot \gamma^2 \cdot \frac{\partial^2 \overline{U}}{\partial \overline{X}^2} + \frac{\partial^2 \overline{U}}{\partial \overline{Y}^2} + \gamma^2 \cdot \frac{\partial^2 \overline{V}}{\partial \overline{Y} \partial \overline{X}} \right)$$

$$\text{Re} \cdot \left(\overline{U} \cdot \frac{\partial \overline{V}}{\partial \overline{X}} + \overline{V} \cdot \frac{\partial \overline{V}}{\partial \overline{Y}} \right) = -\frac{p_0 \cdot b_{hz}}{\eta_0 \cdot u_H} \cdot \frac{\partial \overline{P}_0}{\partial \overline{Y}}$$

$$+ \left(2 \cdot \frac{\partial^2 \overline{V}}{\partial \overline{Y}^2} + \frac{\partial^2 \overline{U}}{\partial \overline{Y} \partial \overline{X}} + \gamma^2 \cdot \frac{\partial^2 \overline{V}}{\partial \overline{X}^2} \right)$$

$$(3.23a, b),$$

where Re is Reynolds number

$$\text{Re} = \gamma \cdot \frac{p_0 \cdot u_h \cdot h_0}{\eta_0} \qquad (3.23c),$$

which is identical for both the Navier-Stokes equations.*

---

* The presented definition of the Reynolds number differs from the form used for most applications by the geometrical ratio γ.

To calculate values of Reynolds number, the Hertzian width b_{hz}, the height of the gap at the contact centreline h_0, the hydrodynamic speed u_h, as well as viscosity η_0 and density ρ_0 at ambient conditions must be known. However, for normal ehl contacts only the viscosity, density, and hydrodynamic velocity are specifically known. The Hertzian width and the central height of the gap must be evaluated from other parameters normally available for the contact such as the Hertzian pressure or distributed load, the radii of both contact partners and the material properties.

The Hertzian width can be easily determined by re-arranging Hertz's basic formula as given in [59]. For a particular Hertzian pressure, the Hertzian width of the contact is

$$b_{hz} = 4 \cdot p_{hz} \cdot \frac{r_{red}}{E'} \qquad (3.24a),$$

where p_{hz} is the Hertzian pressure,

   r_{red} is the reduced radius, calculated from both the surface radii,

$$\frac{1}{r_{red}} = \left[\frac{1}{r_1} + \frac{1}{r_2} \right],$$

   and

   E' is the reduced Young's modulus, calculated from Young's modulus and Poisson's ratio for each surface

$$\frac{1}{E'} = \frac{1}{2} \cdot \left[\frac{1-v_1^2}{E_1} + \frac{1-v_2^2}{E_2} \right].$$

For a particular distributed load F/l_c, the Hertzian width of the contact is obtained from

$$\frac{F}{l_c} = \frac{1}{2} \cdot b_{hz} \cdot p_{hz} \cdot \pi \qquad (3.24b),$$

as

$$b_{hz} = \sqrt{\frac{8}{\pi} \cdot \frac{F}{l_c} \cdot \frac{r_{red}}{E'}} \qquad (3.24c),$$

where parameters are as above.

The height of the gap can be obtained from empirical formulae. A number of film thickness formulae are available as summarised by Wilson [60]. Many of the formulae are based on three dimensionless parameters and the dimensional reduced radius. The minimum film thickness h_{min} according to Dowson and Higginson [17] is

$$h_{min} = 1.6 \cdot G^{0.6} \cdot U^{0.7} \cdot W^{-0.13} \cdot r_{red} \qquad (3.25),$$

where   W   is the dimensionless load parameter,

$$W = \frac{F}{l_c \cdot E' \cdot r_{red}} = 2 \cdot \pi \cdot \left(\frac{p_{hz}}{E'}\right)^2,$$

U   is the dimensionless speed parameter,

$$U = \frac{\eta_0 \cdot u_h}{E' \cdot r_{red}},$$

G   is the dimensionless material parameter,

$$G = E' \cdot \alpha,$$

and

E', r_{red} are as above.

For the present consideration, the minimum film thickness was assumed to be about 80 per cent of the centreline film thickness h_0 which is an approximate value, for example given by Gohar [9],

$$h_0 = 1.9 \cdot G^{0.6} \cdot U^{0.7} \cdot W^{-0.13} \cdot r_{red} \qquad (3.26).$$

The above formula for the film thickness is only reasonably valid for the elastohydrodynamic lubrication regime and not for hydrodynamic lubrication with rigid surfaces. A limiting condition ensuring that the formula is reasonably valid can be determined from the map of film thickness as given in Dowson and Higginson [17] by

$$W \geq 0.017 \cdot U^{0.325} \qquad (3.27)$$

for

$$G = 5000.$$

Introducing the above formulations 3.21, 3.24c, and 3.26 and definitions of the dimensionless ehl parameters 3.25 into the definition of Reynolds number, equation 3.23,

$$Re = \gamma \cdot \frac{\rho_0 \cdot u_h \cdot h_0}{\eta_0} \qquad (3.28a),$$

the Reynolds number can be written, as shown in detail in appendix A, as

$$Re = 0.56 \cdot p_{hz}^{-1.52} \cdot r_{red}^{-0.4} \cdot u_h^{2.4} \cdot E'^{1.32} \cdot \alpha^{1.2} \cdot \eta_0^{0.4} \cdot \rho_0 \qquad (3.28b).$$

Using the dimensionless parameters defined in equation 3.25, Reynolds number can be written in various forms, but an additional dimensionless variable K_{Re} is always required, e.g.

$$Re = 2.26 \cdot K_{Re} \cdot G^{1.2} \cdot W^{-0.76} \cdot U^{0.4} \qquad (3.28c)$$

with the dimensionless constant

$$K_{Re} = \frac{\rho_0 \cdot u_h^2}{E'}.$$

3.2.3   Values of Reynolds number

Altogether, Reynolds number depends on seven variables. Typical parameters appearing in practical line contact applications are given in table 3.1. For the present consideration, a fixed value was assumed for the reduced Young's modulus, the pressure-viscosity coefficient and the density of the lubricant.

Hertzian pressure	$p_{hz} = 0.1...4.0$ GPa
reduced radius	$r_{red} = 0.0002...0.1$ m
hydrodynamic speed	$u_h = (0.0)...0.2...20$ $m \cdot s^{-1}$
reduced Young's modulus	$E' = 2.27 \cdot 10^5$ $N \cdot mm^{-2}$
pressure-viscosity coefficient	$\alpha = 2.18 \cdot 10^{-8}$ Pa^{-1}
viscosity	$\eta_0 = 0.002...0.5$ $Pa \cdot s$
density	$\rho = 870$ $kg \cdot m^{-3}$

Table 3.1:   Range of parameters appearing in practical ehl line contact applications for the determination of Reynolds number.

Figure 3.5 shows results for Reynolds number as a function of the dimensionless parameters U and W with G = 5000. For the additional parameter K_{Re} the maximum possible value is chosen by assuming a maximum hydrodynamic speed of 20 m/s. This choice maximises the Reynolds number. Results are shown in figure 3.5 within a limited range of parameters only. The borders are defined by maximum and minimum values for the dimensionless parameters U and W and by the transition to the rigid hydrodynamic lubrication regime. The maximum Reynolds number is Re = 0.2 approximately. This number can be confirmed analytically as shown in appendix B.
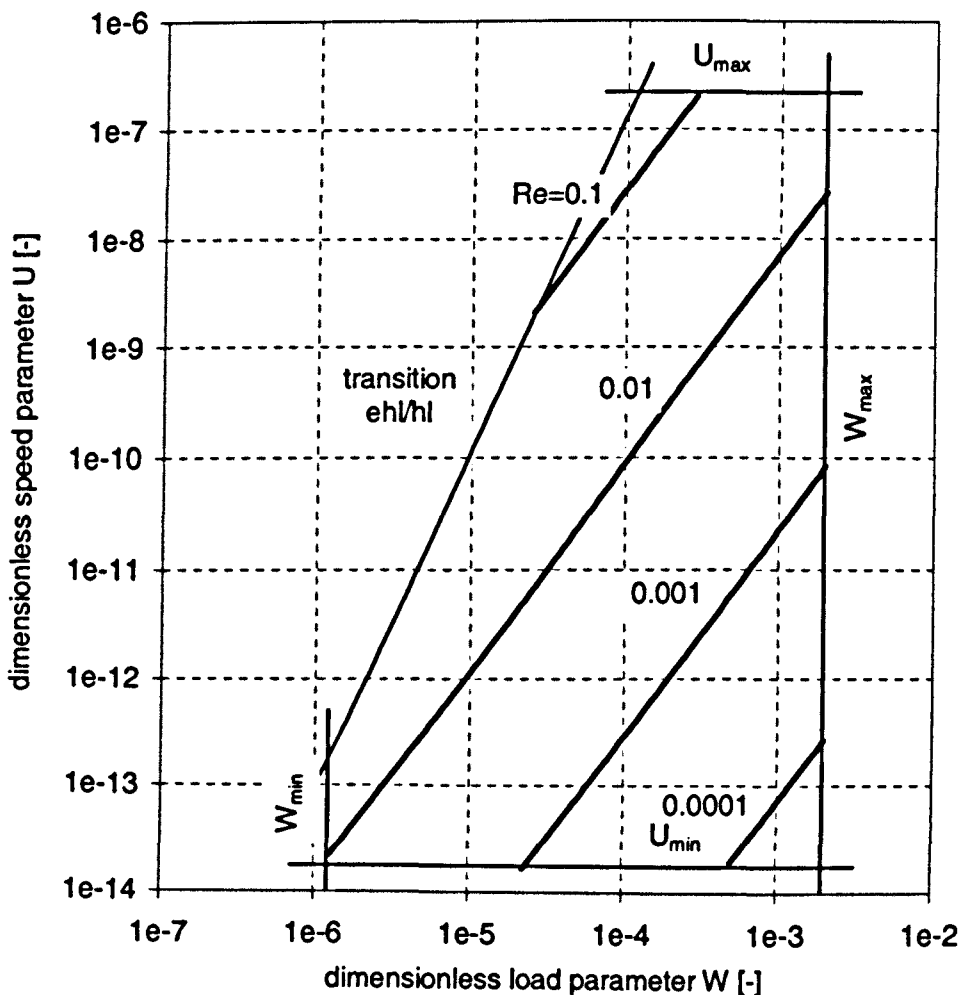
Figure 3.5:   Reynolds number for the ehl line contact problem assuming maximum hydrodynamic speed $u_h = 20$ m/s; G = 5000.

3.2.4   Discussion and conclusions

The results show generally very low Reynolds numbers ranging from about 0.2 to less than 10^{-4}. These values were obtained for the maximum value of K_{Re} assuming maximum hydrodynamic speed. For practically more common values of the parameters, e.g. the radius, the Reynolds number is at least two orders of magnitude smaller. It thus may be concluded that inertia effects do not have to be taken into account for ehl calculations. The result confirms the findings by Dowson [12] and justifies the respective assumptions made by Dowson and Higginson [4, 17], Archard, Gair and Hirst [10] and others to date.

When non-dimensionalising the variables, it was mentioned that the dimensionless height of the gap at the start of the inlet zone might be considerably higher than unity. Consequently, that would mean an underestimation of Reynolds number. However, for the case of maximum Reynolds number, the Hertzian width is small and the height of the gap is large. In consequence, the geometry ratio γ is relatively large and this tends to compensate for any underestimation of Reynolds number.

A consideration of the general simplifying assumptions made earlier in the investigation of the governing equations and Reynolds number retains the conclusion that inertia terms need not be taken into account: Because non-Newtonian effects are rather significant in the heavily loaded zone, Non-Newtonian effects do not influence Reynolds number in the inlet zone. Consideration of thermal effects in the inlet zone results in a reduced height of the gap, as shown by Greenwood and Kauzlarich [61] or Murch and Wilson [62], which reduces Reynolds number, and a slight decrease of the viscosity, which causes an increased Reynolds number. However, considerable temperature rises would be required to reduce the viscosity to a value which provides significant Reynolds number values.

Since the inertia terms are indeed negligible, further investigations concentrate on the viscous terms of the Navier-Stokes equations and their importance in relation to the pressure terms.

3.3   Viscous effects

3.3.1   Non-dimensional form of the Navier-Stokes equations

For an investigation of the significance of the individual viscous terms of the Navier-Stokes equations, an analysis of the normalised form of those equations is performed, similar to that of the previous section. In contrast to the inertia effects, viscous effects appear in both the inlet and the heavily loaded zone of the contact. This requires a revision of the non-dimensionalising procedure previously discussed, which is illustrated in figure 3.6.

Distances and velocities are non-dimensionalised in the same manner as for the investigation of inertia effects, equations 3.19a–d. It should be noted that the normalised velocity $\overline{V}$ is much smaller than unity when the gap is parallel in the heavily loaded zone of the contact. This is because the parallel shape does not induce a perpendicular velocity component due to the hydrodynamic speed as assumed in the definition of $\overline{V}$.

The Hertzian pressure of a dry contact is selected as the characteristic pressure

$$\overline{P} = \frac{p}{p_{hz}} \qquad (3.29a).$$

The viscosity is normalised by introducing Barus' exponential pressure-viscosity dependency of equation 3.18a and using the non-dimensional description of the pressure, equation 3.29a:

$$\eta = \eta_0 \cdot e^{(\alpha \cdot p_{hz} \cdot \overline{P})} \qquad (3.29b).$$

As shown in detail in appendix C, neglecting all inertia terms, performing differentiation of the products, introducing the above conventions 3.19a–d and 3.29a–b, and using the geometry ratio γ leads to the following non-dimensionalised form of the Navier-Stokes equations:
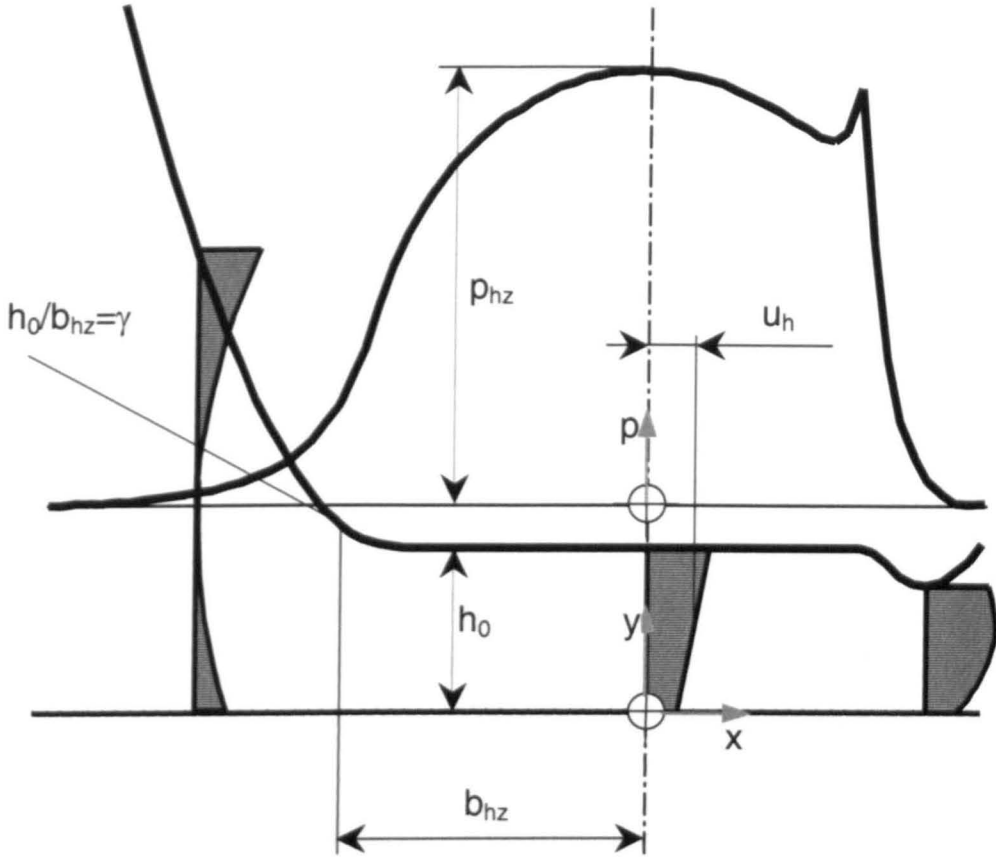
height of the gap vs. length of the gap
100 times magnified

Figure 3.6:   Characteristic values in the ehl contact as reference values for normalising the Navier-Stokes equations for the investigation of the significance of the various viscous terms.

$$
\begin{aligned}
0 = & -\frac{p_{hz}}{b_{hz}}\cdot\frac{\partial\overline{P}}{\partial\overline{X}} + 2\cdot\gamma^2\cdot\kappa\cdot\frac{\partial^2\overline{U}}{\partial\overline{X}^2} + 2\cdot\gamma^2\cdot\kappa\cdot\overline{\alpha}\cdot\frac{\partial\overline{P}}{\partial\overline{X}}\cdot\frac{\partial\overline{U}}{\partial\overline{X}} \\
& + \kappa\cdot\frac{\partial^2\overline{U}}{\partial\overline{Y}^2} + \kappa\cdot\overline{\alpha}\cdot\frac{\partial\overline{P}}{\partial\overline{Y}}\cdot\frac{\partial\overline{U}}{\partial\overline{Y}} \\
& + \gamma^2\cdot\kappa\cdot\frac{\partial^2\overline{V}}{\partial\overline{Y}\partial\overline{X}} + \gamma^2\cdot\kappa\cdot\overline{\alpha}\cdot\frac{\partial\overline{P}}{\partial\overline{Y}}\cdot\frac{\partial\overline{V}}{\partial\overline{X}} \\
\\
0 = & -\frac{p_{hz}}{h_0}\cdot\frac{\partial\overline{P}}{\partial\overline{Y}} + 2\cdot\gamma\cdot\kappa\cdot\frac{\partial^2\overline{V}}{\partial\overline{Y}^2} + 2\cdot\gamma\cdot\kappa\cdot\overline{\alpha}\cdot\frac{\partial\overline{P}}{\partial\overline{Y}}\cdot\frac{\partial\overline{V}}{\partial\overline{Y}} \\
& + \gamma\cdot\kappa\cdot\frac{\partial^2\overline{U}}{\partial\overline{Y}\partial\overline{X}} + \gamma\cdot\kappa\cdot\overline{\alpha}\cdot\frac{\partial\overline{P}}{\partial\overline{X}}\cdot\frac{\partial\overline{U}}{\partial\overline{Y}} \\
& + \gamma^3\cdot\kappa\cdot\frac{\partial^2\overline{V}}{\partial\overline{X}^2} + \gamma^3\cdot\kappa\cdot\overline{\alpha}\cdot\frac{\partial\overline{P}}{\partial\overline{X}}\cdot\frac{\partial\overline{V}}{\partial\overline{X}}
\end{aligned}
\qquad (3.30)
$$

with

$$\overline{\alpha} = \alpha \cdot p_{hz} \qquad (3.31a),$$

$$\gamma = \frac{h_0}{b_{hz}} \qquad (3.31b),$$

and

$$\kappa = \frac{\eta_0 \cdot e^{\overline{\alpha} \cdot \overline{P}} \cdot u_h}{h_0^{\,2}} \qquad (3.31c).$$

The conversion of the Navier-Stokes equations leads to the circumstance that the original meaning of the individual terms of the equation 3.30 is no longer obvious. The first term of each equation 3.30 represents the pressure term, the second and third the normal stress and the last four the shear stress on an infinitesimal small volume. In order to make the further steps of the derivation straightforward, the meanings of individual terms will be moved into the background and recalled again in subsection 3.3.4.7.

3.3.2   Simplifying the equations

The normalised equations are re-arranged. Employing the continuity equation in its dimensionless form,

$$\frac{\partial \overline{U}}{\partial \overline{X}} + \frac{\partial \overline{V}}{\partial \overline{Y}} = 0 \qquad (3.32),$$

the Navier-Stokes equations become

$$
\left.
\begin{aligned}
0 &= \frac{\partial \overline{P}}{\partial \overline{X}} \cdot \left[-\frac{p_{hz}}{b_{hz}} + 2 \cdot \kappa \cdot \gamma^2 \cdot \overline{\alpha} \cdot \frac{\partial \overline{U}}{\partial \overline{X}} \right] + \\
&\quad \frac{\partial \overline{P}}{\partial \overline{Y}} \cdot \left[\kappa \cdot \overline{\alpha} \cdot \left(\frac{\partial \overline{U}}{\partial \overline{Y}} + \gamma^2 \cdot \frac{\partial \overline{V}}{\partial \overline{X}} \right) \right] + \left[\kappa \cdot \left(\gamma^2 \cdot \frac{\partial^2 \overline{U}}{\partial \overline{X}^2} + \frac{\partial^2 \overline{U}}{\partial \overline{Y}^2} \right) \right] \\[2mm]
0 &= \frac{\partial \overline{P}}{\partial \overline{Y}} \cdot \left[-\frac{p_{hz}}{h_0} + 2 \cdot \kappa \cdot \gamma \cdot \overline{\alpha} \cdot \frac{\partial \overline{V}}{\partial \overline{Y}} \right] + \\
&\quad \frac{\partial \overline{P}}{\partial \overline{X}} \cdot \left[\kappa \cdot \gamma \cdot \overline{\alpha} \cdot \left(\frac{\partial \overline{U}}{\partial \overline{Y}} + \gamma^2 \cdot \frac{\partial \overline{V}}{\partial \overline{X}} \right) \right] + \left[\kappa \cdot \gamma \cdot \left(\frac{\partial^2 \overline{V}}{\partial \overline{Y}^2} + \gamma^2 \cdot \frac{\partial^2 \overline{V}}{\partial \overline{X}^2} \right) \right]
\end{aligned}
\right\} \quad (3.33).
$$

Due to the selected method of non-dimensionalisation, the differentials have principally a similar order of magnitude. On the other hand, γ is very small, and hence γ^2 is negligible when compared with unity. This allows the neglecting of the terms multiplied by γ^2 in the second and third term of each equation of set 3.33. However, neglection in the first term is not permitted, because the term containing γ^2 is multiplied by further terms different from unity and compared with terms also different from unity. Omitting the negligible terms, equation 3.33 reduces to

$$\left. \begin{array}{l} 0 = \dfrac{\partial \overline{P}}{\partial \overline{X}} \cdot \left[-\dfrac{p_{hz}}{b_{hz}} + 2 \cdot \kappa \cdot \gamma^2 \cdot \overline{\alpha} \cdot \dfrac{\partial \overline{U}}{\partial \overline{X}} \right] + \dfrac{\partial \overline{P}}{\partial \overline{Y}} \cdot \left[\kappa \cdot \overline{\alpha} \cdot \dfrac{\partial \overline{U}}{\partial \overline{Y}} \right] + \left[\kappa \cdot \dfrac{\partial^2 \overline{U}}{\partial \overline{Y}^2} \right] \\[4mm] 0 = \dfrac{\partial \overline{P}}{\partial \overline{Y}} \cdot \left[-\dfrac{p_{hz}}{h_0} + 2 \cdot \kappa \cdot \gamma \cdot \overline{\alpha} \cdot \dfrac{\partial \overline{V}}{\partial \overline{Y}} \right] + \dfrac{\partial \overline{P}}{\partial \overline{X}} \cdot \left[\kappa \cdot \gamma \cdot \overline{\alpha} \cdot \dfrac{\partial \overline{U}}{\partial \overline{Y}} \right] + \left[\kappa \cdot \gamma \cdot \dfrac{\partial^2 \overline{V}}{\partial \overline{Y}^2} \right] \end{array} \right\} \quad (3.34).$$

3.3.3   Zone of maximum influence of viscous forces

The influence of the viscous forces is dependent on the strength of the factor κ in comparison with the factor accompanying the pressure terms p_{hz}/b_{hz} and p_{hz}/h_0 respectively. Since κ contains the dimensionless pressure as an exponential index, κ varies along a contact, while p_{hz}/b_{hz} and p_{hz}/h_0 remain constant. Figure 3.7 shows the variation of a normalised κ with dimensionless pressure. For a modest pressure of $p_{hz} = 0.5$ GPa, the value of κ is seen to have fallen by an order of magnitude if the pressure reduces to 80 per cent of the Hertzian pressure. The maximum influence of the viscous forces in comparison with pressure forces is obtained for high pressure values and is therefore in the heavily loaded zone of the contact. In the inlet zone, pressure is smaller, and the factor κ decreases rapidly. Consequently, it was decided to concentrate on the heavily loaded zone of the contact.
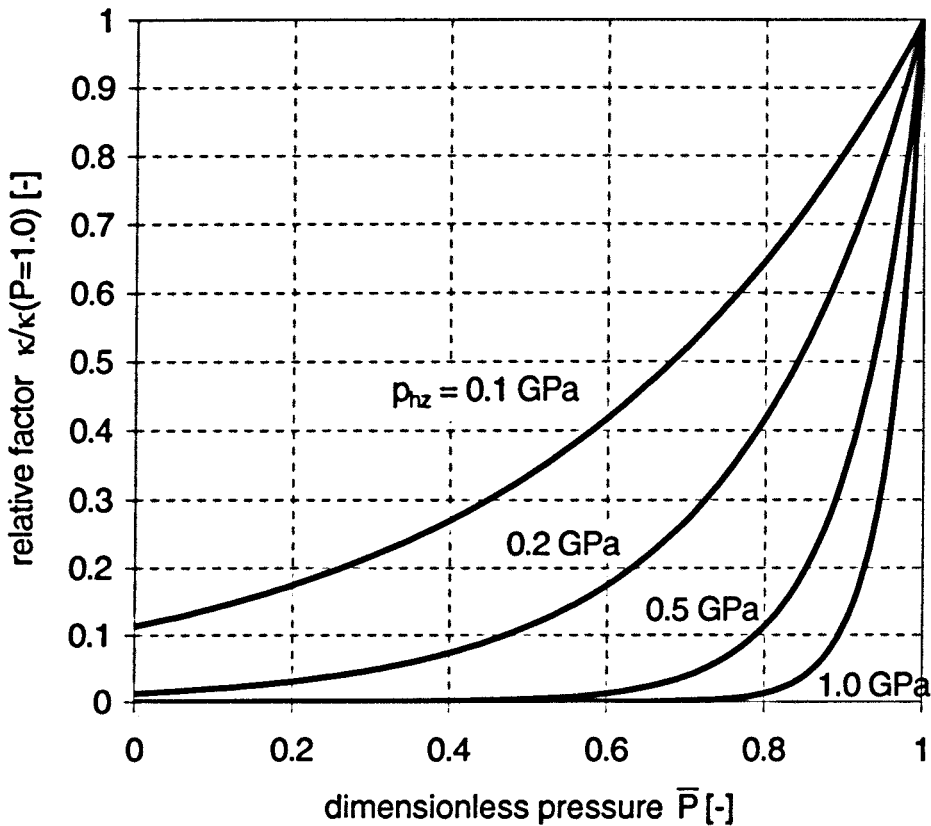
Figure 3.7:   *Normalised variation of factor κ with dimensionless pressure*
             $\overline{P}$.

3.3.4   Consideration of a parallel gap for the contact

3.3.4.1   Introduction

For isothermal and incompressible conditions, the gap between the solid surfaces is practically parallel in the heavily loaded zone of the contact. This implies that in this zone the dimensionless velocity $\overline{V}$ is zero at both surfaces and considerably smaller than unity in the area between both the solid surfaces. For further simplification, the dimensionless velocity $\overline{V}$ was assumed to be zero everywhere in the contact:

$$\overline{V} \equiv 0 \qquad\qquad (3.35).$$

Incorporating the above assumption and employing the continuity equation, which is also explained in detail in appendix C, section C.3, the Navier-Stokes equations simplify to

$$0 = -\frac{p_{hz}}{b_{hz}} \cdot \frac{\partial \overline{P}}{\partial \overline{X}} + \kappa \cdot \overline{\alpha} \cdot \frac{\partial \overline{U}}{\partial \overline{Y}} \cdot \frac{\partial \overline{P}}{\partial \overline{Y}} + \kappa \cdot \frac{\partial^2 \overline{U}}{\partial \overline{Y}^2}$$

$$0 = -\frac{p_{hz}}{h_0} \cdot \frac{\partial \overline{P}}{\partial \overline{Y}} + \kappa \cdot \gamma \cdot \overline{\alpha} \cdot \frac{\partial \overline{U}}{\partial \overline{Y}} \cdot \frac{\partial \overline{P}}{\partial \overline{X}}$$

$$(3.36).$$

Substituting each equation into the other in order to obtain equations containing only a single pressure gradient, either along or across the contact, gives

$$0 = -\frac{p_{hz}}{b_{hz}} \cdot \frac{\partial \overline{P}}{\partial \overline{X}} \left[1 - \left(\frac{h_0 \cdot \kappa \cdot \overline{\alpha}}{p_{hz}} \cdot \frac{\partial \overline{U}}{\partial \overline{Y}}\right)^2\right] + \kappa \cdot \frac{\partial^2 \overline{U}}{\partial \overline{Y}^2}$$

$$0 = -\frac{p_{hz}}{h_0} \cdot \frac{\partial \overline{P}}{\partial \overline{Y}} \left[1 - \left(\frac{h_0 \cdot \kappa \cdot \overline{\alpha}}{p_{hz}} \cdot \frac{\partial \overline{U}}{\partial \overline{Y}}\right)^2\right] + \frac{\kappa^2 \cdot \gamma \cdot \overline{\alpha} \cdot b_{hz}}{p_{hz}} \cdot \frac{\partial \overline{U}}{\partial \overline{Y}} \cdot \frac{\partial^2 \overline{U}}{\partial \overline{Y}^2}$$

$$(3.37).$$

In the above sets of equations, 3.36 and 3.37, most of the dimensional factors are constant but, as shown above, factors κ varies considerably with dimensionless pressure $\overline{P}$. In order to make an order of magnitude comparison, the dimensionless pressure $\overline{P}$ was assumed unity in this term. Due to the exponential form of the term, this assumption tends to overestimate the factor κ.

For a better understanding and presentation of the results, the dimensionless parameters for speed, load and material, U, W, and G, equation 3.25, were introduced. The procedure was similar to that used for determination of the Reynolds number and is given in detail in appendix D. The second equation of set 3.36 and the first of set 3.37 become

$$\frac{\partial \overline{P}}{\partial \overline{Y}} \bigg/ \frac{\partial \overline{P}}{\partial \overline{X}} = k_r \cdot \frac{\partial \overline{U}}{\partial \overline{Y}} \qquad (3.38)$$

with k_r as a pressure gradient ratio

$$k_r = 0.63 \cdot U \cdot G \cdot W^{-0.5} \cdot e^{0.4 \cdot G \cdot W^{0.5}}$$

and

$$\frac{\partial \overline{P}}{\partial \overline{X}} \cdot \left[1 - \left(k_p \cdot \frac{\partial \overline{U}}{\partial \overline{Y}} \right)^2 \right] = k_c \cdot \frac{\partial^2 \overline{U}}{\partial \overline{Y}^2} \tag{3.39}$$

with k_p subsequently called sliding influence factor

$$k_p = 0.53 \cdot U^{0.3} \cdot G^{0.4} \cdot W^{0.13} \cdot e^{0.4 \cdot G \cdot W^{0.5}}$$

and

$$k_c = 1.11 \cdot U^{-0.4} \cdot G^{-1.2} \cdot W^{0.26} \cdot e^{0.4 \cdot G \cdot W^{0.5}}$$

respectively. Details of the determination of the factors k_c, k_p, and k_r in their dimensionless form are given in appendix D. If the factors k_r and k_p are small, the pressure variation across the gap in equation 3.38 is negligible. i.e. the assumption of a constant pressure across the gap, equation 2.3, is correct. Correspondingly, equation 3.39 reduces to the x-momentum equation 2.1 widely used to derive Reynolds equation.

3.3.4.2   Results for the significance of terms

All results are shown for the same range of speed and load parameters for which the ASME map of film thickness [17] is available, and which covers a wide field of engineering problems. For all results a material parameter of $G = 5000$ was assumed. Results for the pressure gradient ratio k_r, according to equation 3.38, are given in figure 3.8. Figure 3.9 shows values for the sliding influence factor k_p of equation 3.39. Figure 3.10 summarises the major result of figure 3.8 and 3.9 and plots load cases analysed in the literature against k_p and k_r.
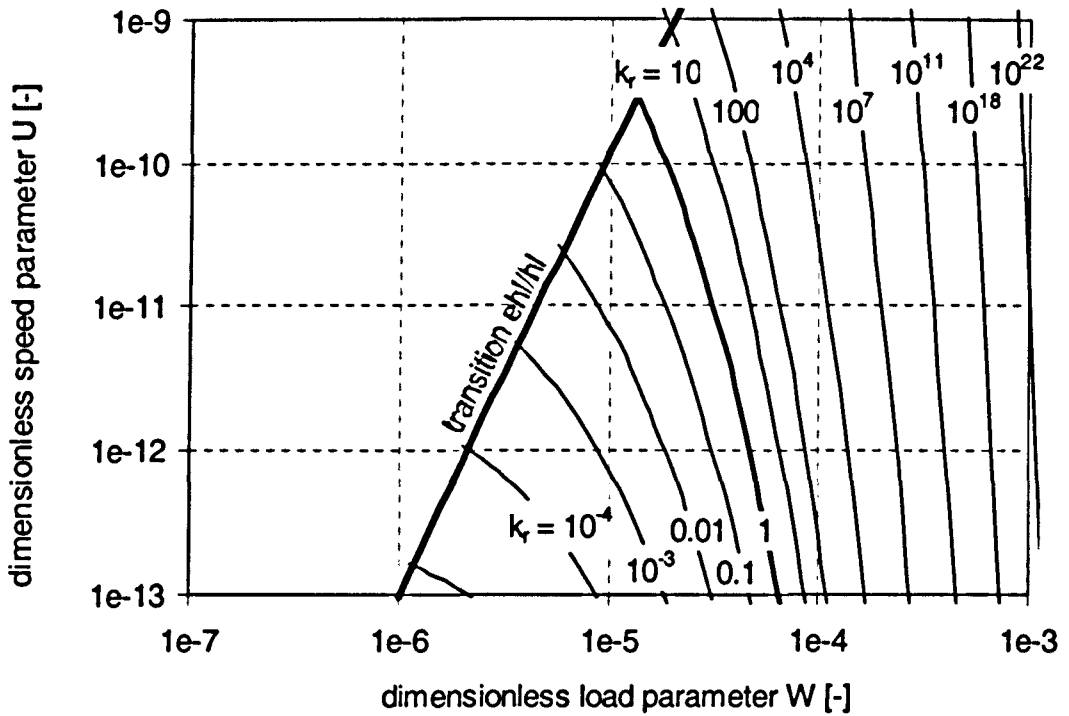
Figure 3.8:   Dimensionless pressure gradient ratio k_r for various speed and load parameter values at constant material parameter $G = 5000$.
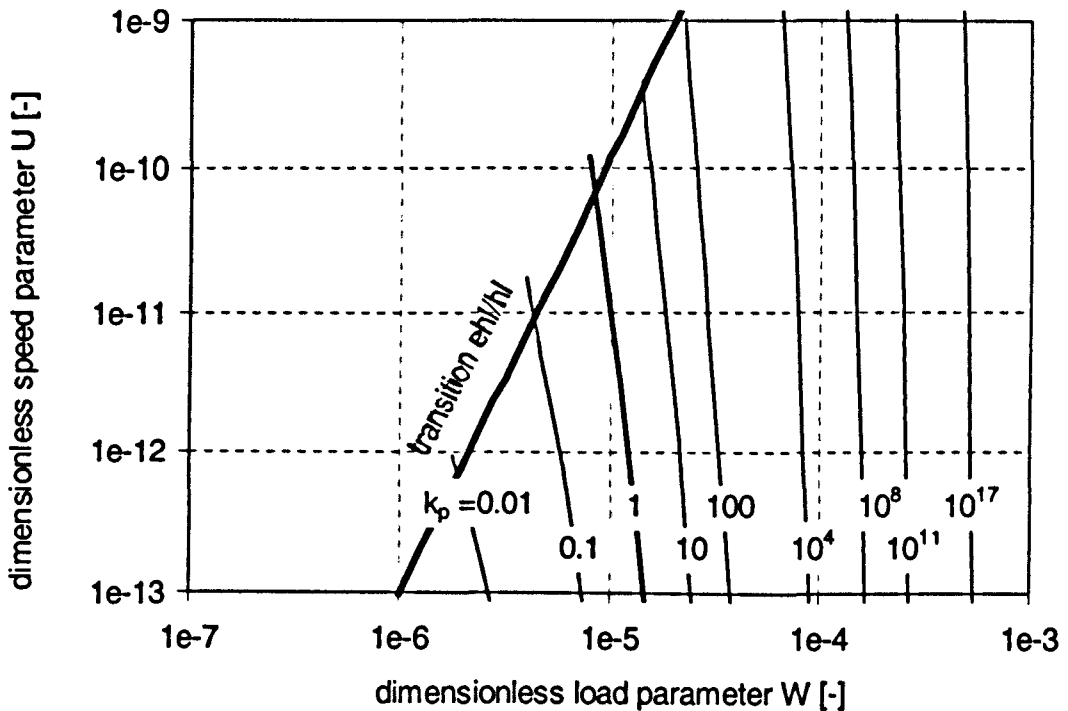
Figure 3.9:   Dimensionless siding influence factor k_p for various speed and load parameter values at constant material parameter $G = 5000$.
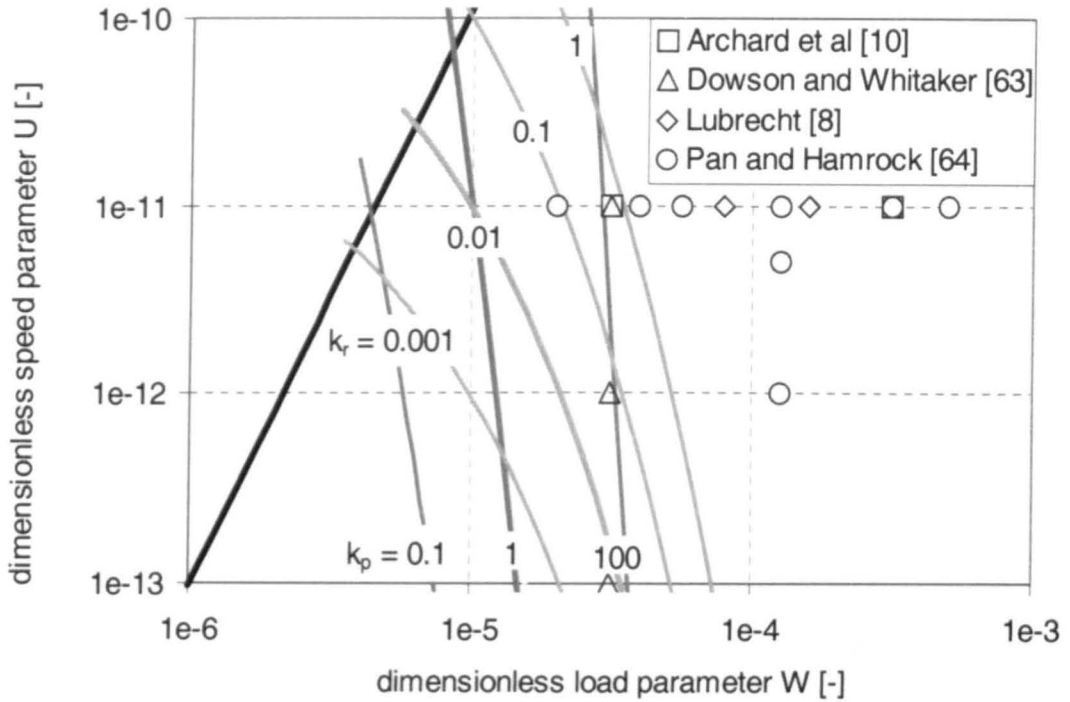
Figure 3.10: Dimensionless pressure gradient ratio k_r and dimensionless siding influence factor k_p at a material parameter $G = 5000$ in comparison with published results for $G = 5000$ (for results by Lubrecht $G = 4000$).

3.3.4.3   Limited validity of Reynolds equation

Over the investigated range of parameters, both factors k_p and k_r have small values corresponding to low velocity and load parameters but range up to almost infinity. Both factors vary particularly with the load parameter but little with velocity parameter, principally due to the appearance of the load parameter in the exponent.

As previously stated, the governing equations to determine Reynolds equation are obtained when the terms including the factors k_p and k_r are neglected. This is justified for low values of k_p or k_r. However, it can be seen from figures 3.8 and 3.9 that k_p or k_r can take quite considerable values for a wide range of parameters. The conclusion is that, instead of Reynolds equation, an extended set of equations of equation 3.38 and 3.39 with additional terms must be solved. A more detailed discussion of the values of factors k_p and k_r which require consideration of the full set of equations is in the subsections below.

The significance of the additional terms as shown on the maps, figures 3.8 to 3.10, is based on the assumption that the velocity gradient $\partial \overline{U}/\partial \overline{Y}$ is unity. Approximating the velocity gradient by a difference quotient

$$\frac{\partial \overline{U}}{\partial \overline{Y}} = \frac{\Delta \overline{U}}{\Delta \overline{Y}}$$
(3.40),

where $\Delta \overline{Y}$ is the dimensionless height of the gap which is according to its definition, equation 3.19b, unity in a parallel gap, and

$\Delta \overline{U}$ is the dimensionless difference of the two surfaces velocities $\Delta \overline{U} = (u_1 - u_2)/u_h$,

the range of values for the velocity gradient can be discussed:

♦ When both surfaces have identical speed, i.e. pure rolling, the surface velocity difference and hence the velocity gradient becomes zero.[*]

♦ When one surface is stationary and the other is in motion, which means pure sliding, the velocity gradient takes on the value of two.[†]

♦ When the motion between the two surfaces is a mixture of pure rolling and pure sliding, and one surface has triple the speed of the other, then the velocity gradient takes on the assumed unity.[‡]

Hence, the relevance of the extended set of equations is dependent on the degree of sliding between the contact partners, which is defined as

$$S = \frac{u_1 - u_2}{u_1 + u_2}$$
(3.41),

so that it ranges from zero to unity for pure rolling to pure sliding and becomes 0.5 for the conditions causing unity velocity gradient.

---

[*]   With $u_1 = u_2$ and $\frac{u_1 + u_2}{2} = u_h$ follows $\Delta \overline{U} = \frac{u_1 - u_1}{\frac{1}{2} \cdot (u_1 + u_1)} = 0 \cdot$

[†]   With $u_2 = 0$ and $\frac{u_1 + u_2}{2} = u_h$ follows $\Delta \overline{U} = \frac{u_1 - 0}{\frac{1}{2} \cdot (u_1 + 0)} = 2 \cdot$

[‡]   With $u_1 = 3 \cdot u_2$ and $\frac{u_1 + u_2}{2} = u_h$ follows $\Delta \overline{U} = \frac{u_1 - \frac{1}{3} \cdot u_1}{\frac{1}{2} \cdot (u_1 + \frac{1}{3} \cdot u_1)} = 1 \cdot$

Hence, with sliding ratios S falling below 0.5, the influence of the terms containing the factors k_p and k_r decreases accordingly. Consequently, the range of parameters where Reynolds equation is valid increases. For the pure rolling case, where the velocity gradient $\partial \overline{U}/\partial \overline{Y}$ is zero in the parallel gap, Reynolds equation is basically valid for all parameters. Effects due to the additional viscous terms can only appear near the pressure spike. On the other hand, with sliding/rolling ratios S above 0.5 and up to unity, the influence of terms containing the factors k_p and k_r increases and the range of parameters, for which the extended approach has to be used, increases accordingly.

The above results are based on the assumption that the dimensionless pressure in the exponential function always equals unity, resulting in an overestimation of the factors k_p and k_r. Hence, the zone where Reynolds equation can be used might be slightly wider. As discussed in section 3.3.3 and illustrated in figure 3.7, the overestimation appears for all load parameters but is more significant at higher loads. However, here the dominance of k_p and k_r is so significant that even strong overestimation of k_p and k_r does not reduce the influence of the additional viscous terms.

Plotting the curves showing the values of factors k_p and k_r against published analyses, as presented in figure 3.10, makes it obvious that factors k_p and k_r would take on very high values for analyses previously undertaken with Reynolds equation. Hence, the application of additional terms is not only of theoretical but also of practical relevance.

3.3.4.4   Extended x-momentum equation

In comparison with the governing equation leading to Reynolds equation, the extended equation 3.39 contains the additional term $\left(k_p \cdot \partial \overline{U}/\partial \overline{Y}\right)^2$.

If this term is small, e.g. $\left|k_p \cdot \partial \overline{U}/\partial \overline{Y}\right| \leq 0.1$, its influence can generally be neglected.

For $0.1 < \left| k_p \cdot \partial \overline{U} / \partial \overline{Y} \right| < 1.0$ the characteristic of the equation remains much the same as for Reynolds equation. In comparison with Reynolds equation, the dominance of the second derivative of speed $\partial^2 \overline{U} / \partial \overline{Y}^2$ increases. However, since k_c is already dominant itself, it was concluded that the further increase in dominance hardly influences the qualitative shape of the gap and pressure distribution.

When the value of the term $k_p \cdot \partial \overline{U} / \partial \overline{Y}$ is unity, the sum the pressure gradient is multiplied with becomes zero and equation 3.39 seems to develop a singularity. This singularity correlates with the same phenomena described by Bair, Winer and Khonsari [5], for the general Navier-Stokes equations. The authors conclude the development of infinitely high pressure. Since this is unrealistic, non-Newtonian fluid properties must be occurring. However, equation 3.30 can be solved when the second derivative of velocity, which represents the presence and direction of the Poiseuille part of the lubricant flow, becomes zero and changes sign. This means an identical height of the gap at the position of any singularity to that at the position of zero pressure gradient along the gap. This is possible due to the fact that the shape of the gap is not rigid and fixed but a result of elastic deformation of the solid surfaces. However, an analysis with a fixed geometry would not allow the fulfilment of the required condition and hence lead to infinitely high pressure.

As the Poiseuille contribution is negative in the inlet zone, it must be positive in the region between the point of singularity and the centreline. Since the lubricant was assumed to be incompressible, the height of the gap must converge at the point where the singularity appears. The same considerations made for the zone of decreasing pressure lead to corresponding results. Figure 3.11 illustrates the expected deformation of the gap due to the singularity.

For higher speed and load parameters, the value of the term $k_p \cdot \partial \overline{U} / \partial \overline{Y}$ becomes increasingly dominant ($>> 1$). The Poiseuille contribution to the flow is more and more important and therefore the velocity gradient no longer remains constant across the gap. Then the above considerations based on a

one-dimensional solution are no longer valid and a numerical solution is necessary.

The effect of the velocity profile across the gap will also affect the tangential stress acting on the surface and hence the traction coefficient. However with the above assumption, the considerable contribution to the traction produced at the centreline of the contact will be unaffected as pure Couette flow is still present at this location.
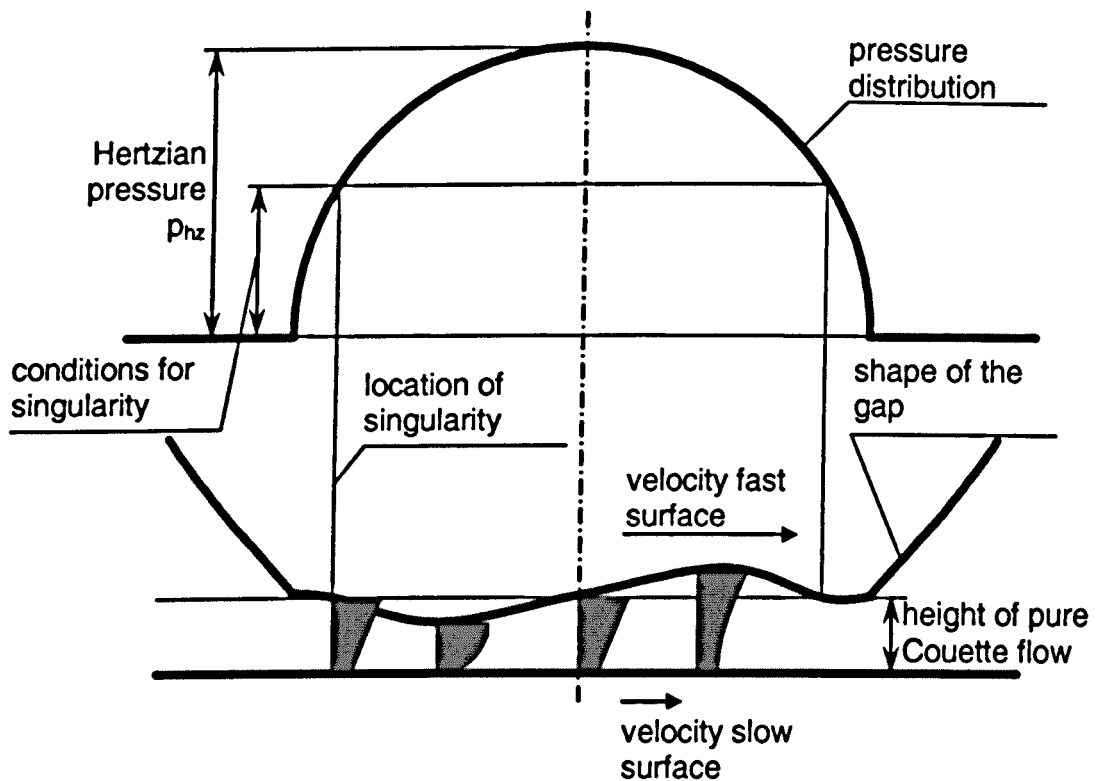
Figure 3.11:   Expected shape of the gap considering additional viscous effects.

3.3.4.5   Pressure variation across the height of the gap

Along the lines previously discussed for equation 3.39, it should be expected that a limit could also be determined when the pressure variation across the gap $\partial p / \partial y$, equation 3.38, can be neglected. However, a much smaller value, for which the additional term can be neglected, should be selected than for k_p, e.g. $k_r < 0.01$ or 10^{-3}. This is due to two reasons. Firstly, the term is not used in its squared form and secondly, the variation of pressure implies

also a variation of viscosity which is more significant due to the exponential nature of the pressure-viscosity dependency.

The effects of a pressure variation across the gap are now to be considered, which is also illustrated in figure 3.11. Again the elliptic pressure distribution was assumed to be a good approximation and the following conclusions were drawn:

If the pressure along the gap is rising, the viscosity near the slow surface is lower than that near the fast surface. Consequently the velocity gradient at the slow surface is higher than at the fast surface. Thus the flow must have a Poiseuille-like contribution in the same direction as the Couette contribution of the flow. To maintain continuity of mass, the height of the gap must be smaller than for a pure Couette flow.

For the second half of the contact, where the pressure gradient is negative, the situation reverses:

The viscosity near the fast surface is lower and the velocity gradient is higher than at the slow surface. The Poiseuille contribution has the opposite direction to the Couette component, implying that the gap height must be greater than for pure Couette flow.

In comparison with a Reynolds equation based solution, velocity gradients and viscosities are different at the solid surfaces. This also implies differences in tangential forces and friction coefficients on the two surfaces.

3.3.4.6   Interaction of perpendicular and longitudinal effects

The consideration of both equations 3.38 and 3.39 leads to qualitatively identical results. This must be expected, since both the equations describe the same physical effect, are derived from the same governing equations and are not independent.

Consideration of figure 3.11 describing the expected development of the flow profiles and of the shape of the gap show, however, an inconsistency between the shape of the gap and the Hertzian pressure profile, which is still unchanged. To balance this inconsistency, a pressure reduction in the first

half of the contact causing less deflection and a pressure increase in the second half of the contact with increased deflection is required, such as sketched in figure 3.12. This change of the original assumption will affect the above ideas which will have to be determined numerically.
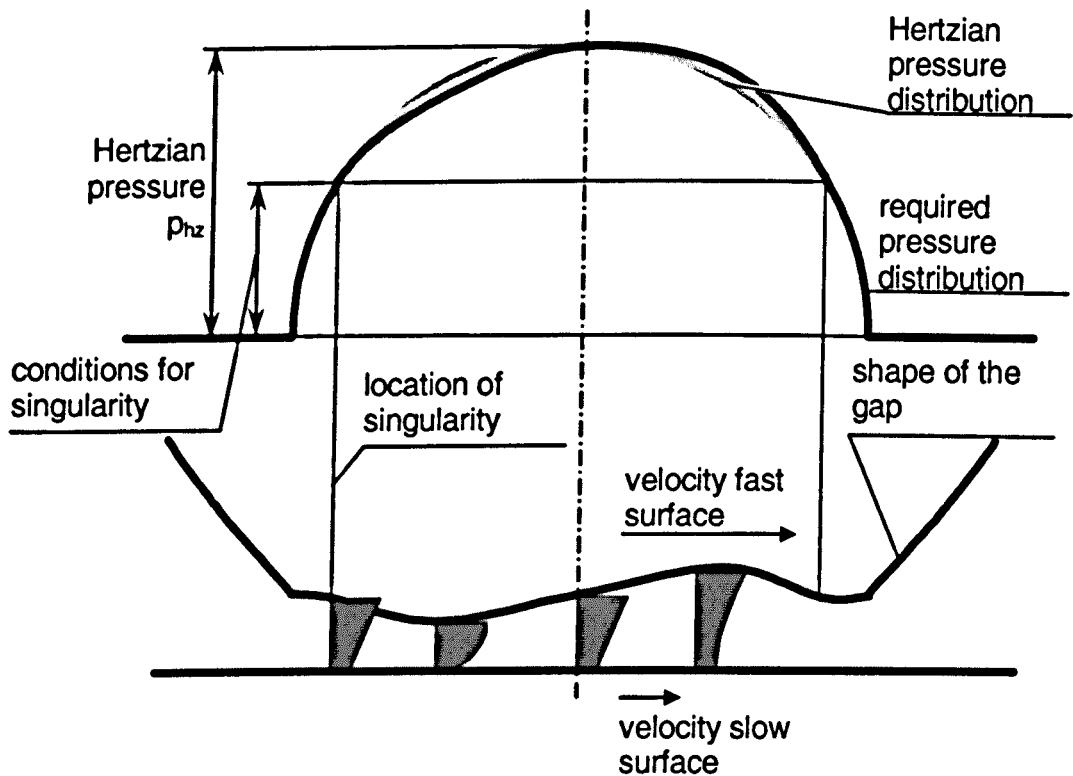
Figure 3.12: Expected shape of the gap and required pressure distribution for respective deformation considering additional viscous effects.

A consideration of both equations also shows that many terms, i.e. pressure, viscosity and velocity gradients vary across the gap. Therefore the above analysis, where the whole system was assumed to remain basically one-dimensional, is only valid for modest values of the factors k_p and k_r. For the range of parameters where these factors are large, the expected variation across the gap will also require a fully two-dimensional solution for the ehl line contact problem.

Equations 3.38 and 3.39 also suggest a variation of the height of the gap so that the assumed condition that there is no velocity component in the perpendicular direction is not fulfilled. The required revision of this assumption is undertaken in section 3.3.5.

3.3.4.7   Physical interpretation of the extended set of equations

The derivations of the present section 3.3 concentrated mainly on the mathematical treatment of the governing equations. Tracking the physical meaning of the individual terms was arduous and moved to the background. Reverse tracking of the remaining relevant terms back to the governing equations proved to be an easier way. This procedure leads to figure 3.13, showing the significant forces on an infinitely small fluid volume for the highly loaded line contact.

$$\left(p + \frac{\partial p}{\partial y} \cdot dy\right) \cdot dx$$

$$\left(\eta \cdot \frac{\partial u}{\partial y} + \frac{\partial}{\partial y}\left(\eta \cdot \frac{\partial u}{\partial y}\right) \cdot dy\right) \cdot dx$$

$$\left(\eta \cdot \frac{\partial u}{\partial y} + \frac{\partial \eta}{\partial x} \cdot \frac{\partial u}{\partial y} \cdot dx\right) \cdot dy$$

$$(p) \cdot dy$$

$$\left(p + \frac{\partial p}{\partial x} \cdot dx\right) \cdot dy$$

$$\left(\eta \cdot \frac{\partial u}{\partial y}\right) \cdot dy$$

$$\left(\eta \cdot \frac{\partial u}{\partial y}\right) \cdot dx$$

$$(p) \cdot dx$$
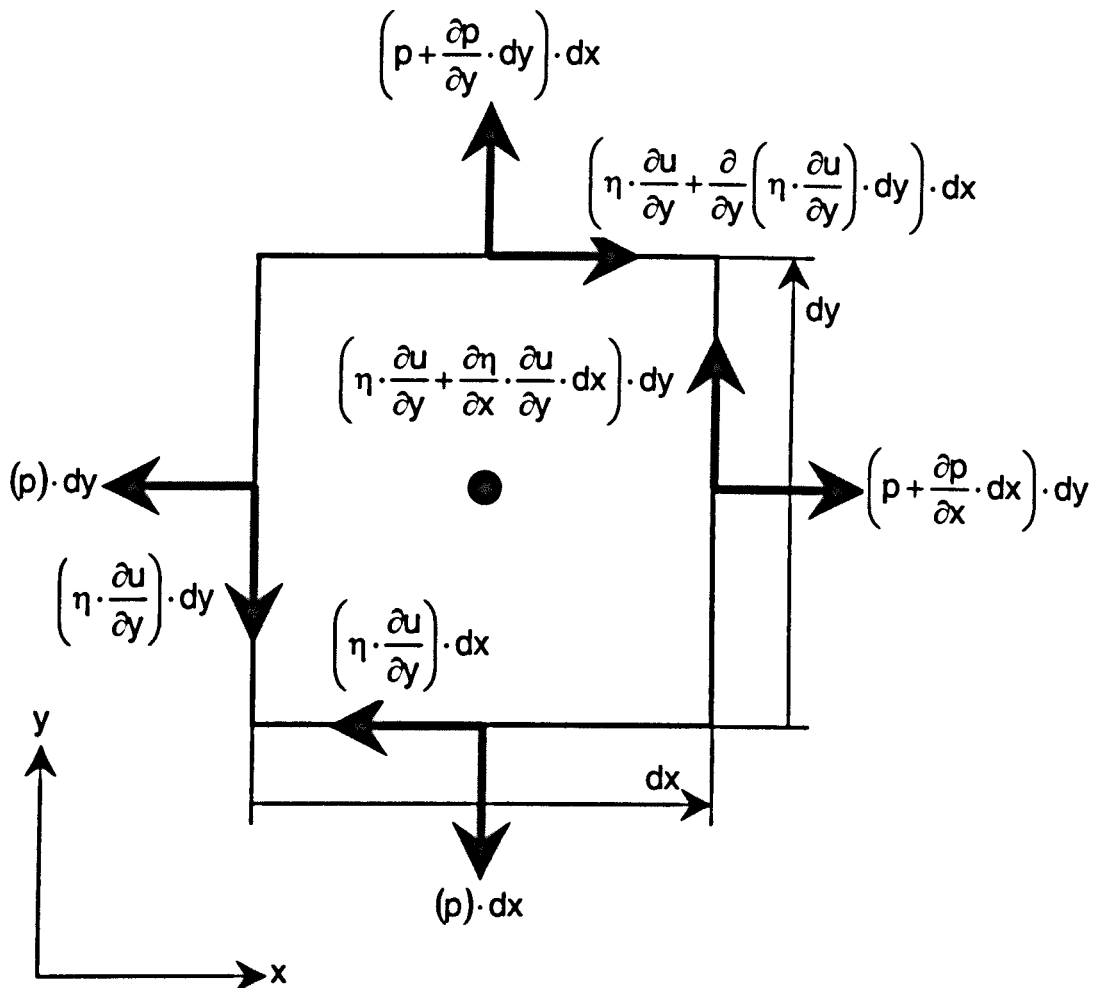
Figure 3.13:   *Relevant forces on an infinitely small fluid volume in the highly loaded zone of an ehl line contact.*

Viscosity variation along the gap due to the strong pressure variation along the contact and the strong pressure-viscosity dependency leads to a shear force component of the magnitude $\frac{\partial \eta}{\partial x} \cdot \frac{\partial u}{\partial y} \cdot dx \cdot dy$ across the gap, which is

neglected in Reynolds equation. This component must be balanced by a pressure variation across the gap, i.e. a pressure force variation of $\frac{\partial p}{\partial y} \cdot dx \cdot dy$. The pressure variation across the gap influences due to the pressure-viscosity dependency the viscosity variation across the gap, which finally means that the shear force variation along the gap must consider variable viscosity $\frac{\partial}{\partial y}\left(\eta \cdot \frac{\partial u}{\partial y} \right) \cdot dx \cdot dy$ even for an isothermal contact.

3.3.4.8   Prospect for the extended approach

The extended approach is expected to lead to changes in the shape of the gap and the flow profile and consequently a variation of the traction coefficient might be expected. These effects are expected to be stronger the higher the sliding ratio S and the dimensionless speed and load parameters U and W rise, i.e. the effects are significant for those conditions, for which non-Newtonian fluid behaviour is important to obtain realistic conditions for a Reynolds equation based approach, cf. section 2.4.

The described correlation between the significance of the extended approach terms and the need for non-Newtonian behaviour hence raises the question whether some of the lubricant behaviour, understood as non-Newtonian behaviour in Reynolds equation based solutions, can be explained by the extended approach in its current form based on the assumption of a Newtonian fluid behaviour.

3.3.5   Arbitrary shape of the gap

3.3.5.1   Governing equations

As discussed, the extended approach leads to a non-parallel gap, at least for the isothermal case with heavy loading. The perpendicular velocity $\overline{V}$ can no longer be assumed zero. The governing equations are as previously given equation 3.34:

$$0 = \frac{\partial \overline{P}}{\partial \overline{X}} \cdot \left[-\frac{p_{hz}}{b_{hz}} + 2 \cdot \kappa \cdot \gamma^2 \cdot \overline{\alpha} \cdot \frac{\partial \overline{U}}{\partial \overline{X}} \right] + \frac{\partial \overline{P}}{\partial \overline{Y}} \cdot \left[\kappa \cdot \overline{\alpha} \cdot \frac{\partial \overline{U}}{\partial \overline{Y}} \right] + \left[\kappa \cdot \frac{\partial^2 \overline{U}}{\partial \overline{Y}^2} \right]$$

$$0 = \frac{\partial \overline{P}}{\partial \overline{Y}} \cdot \left[-\frac{p_{hz}}{h_0} + 2 \cdot \kappa \cdot \gamma \cdot \overline{\alpha} \cdot \frac{\partial \overline{V}}{\partial \overline{Y}} \right] + \frac{\partial \overline{P}}{\partial \overline{X}} \cdot \left[\kappa \cdot \gamma \cdot \overline{\alpha} \cdot \frac{\partial \overline{U}}{\partial \overline{Y}} \right] + \left[\kappa \cdot \gamma \cdot \frac{\partial^2 \overline{V}}{\partial \overline{Y}^2} \right]$$

$$\left. \right\} \quad (3.42).$$

Substituting each equation into the other and neglecting terms in summands multiplied by γ^2, equations with only one pressure gradient were obtained, which is shown in detail in the last section of appendix C:

$$\frac{\partial \overline{P}}{\partial \overline{X}} \cdot \left[\left(\frac{p_{hz}}{b_{hz}} \right)^2 - \left(\kappa \cdot \overline{\alpha} \cdot \gamma \cdot \frac{\partial \overline{U}}{\partial \overline{Y}} \right)^2 \right] =$$

$$\kappa \cdot \left[\frac{p_{hz}}{b_{hz}} \cdot \frac{\partial^2 \overline{U}}{\partial \overline{Y}^2} + \kappa \cdot \gamma^2 \cdot \overline{\alpha} \cdot \left(\frac{\partial \overline{U}}{\partial \overline{Y}} \cdot \frac{\partial^2 \overline{V}}{\partial \overline{Y}^2} - 2 \cdot \frac{\partial \overline{V}}{\partial \overline{Y}} \cdot \frac{\partial^2 \overline{U}}{\partial \overline{Y}^2} \right) \right]$$

$$\frac{\partial \overline{P}}{\partial \overline{Y}} \cdot \left[\left(\frac{p_{hz}}{b_{hz}} \right)^2 - \left(\kappa \cdot \overline{\alpha} \cdot \gamma \cdot \frac{\partial \overline{U}}{\partial \overline{Y}} \right)^2 \right] =$$

$$\kappa \cdot \gamma^2 \left[\frac{p_{hz}}{b_{hz}} \cdot \frac{\partial^2 \overline{V}}{\partial \overline{Y}^2} + \kappa \cdot \overline{\alpha} \cdot \left(\frac{\partial \overline{U}}{\partial \overline{Y}} \cdot \frac{\partial^2 \overline{U}}{\partial \overline{Y}^2} \right) \right]$$

$$\left. \right\} \quad (3.43)$$

Since it might be of some use in later sections, the equations are also given with the abbreviating terms κ, γ and $\overline{\alpha}$, equation 3.31, resolved to the original characteristic values; equations 3.43 become

$$\frac{p_{hz}}{b_{hz}} \cdot \frac{\partial \overline{P}}{\partial \overline{X}} \cdot \left[1 - \left(\frac{\eta_0 \cdot u_h \cdot \alpha}{h_0} \cdot e^{\alpha \cdot p_{hz} \cdot \overline{P}} \cdot \frac{\partial \overline{U}}{\partial \overline{Y}} \right)^2 \right] =$$

$$\frac{\eta_0 \cdot u_h}{h_0^2} \cdot e^{\alpha \cdot p_{hz} \cdot \overline{P}}$$

$$\left[\left(\frac{\partial^2 \overline{U}}{\partial \overline{Y}^2} \right) + \gamma \cdot \frac{\eta_0 \cdot u_h \cdot \alpha}{h_0} \cdot e^{\alpha \cdot p_{hz} \cdot \overline{P}} \cdot \left(\frac{\partial \overline{U}}{\partial \overline{Y}} \cdot \frac{\partial^2 \overline{V}}{\partial \overline{Y}^2} - 2 \cdot \frac{\partial \overline{V}}{\partial \overline{Y}} \cdot \frac{\partial^2 \overline{U}}{\partial \overline{Y}^2} \right) \right]$$

$$\frac{p_{hz}}{b_{hz}} \cdot \frac{\partial \overline{P}}{\partial \overline{Y}} \cdot \left[1 - \left(\frac{\eta_0 \cdot u_h \cdot \alpha}{h_0} \cdot e^{\alpha \cdot p_{hz} \cdot \overline{P}} \cdot \frac{\partial \overline{U}}{\partial \overline{Y}} \right)^2 \right] =$$

$$\frac{\eta_0 \cdot u_h}{b_{hz}^2} \cdot e^{\alpha \cdot p_{hz} \cdot \overline{P}} \cdot \left[\left(\frac{\partial^2 \overline{V}}{\partial \overline{Y}^2} \right) + \frac{\eta_0 \cdot u_h \cdot \alpha}{h_0 \cdot \gamma} \cdot e^{\alpha \cdot p_{hz} \cdot \overline{P}} \cdot \left(\frac{\partial \overline{U}}{\partial \overline{Y}} \cdot \frac{\partial^2 \overline{U}}{\partial \overline{Y}^2} \right) \right]$$

$$\left. \right\} \quad (3.44).$$

3.3.5.2   Discussion

Rejection of the assumption of a parallel gap leads to a more complex set of equations.

Consideration of the first equation of set 3.43 shows that those velocity gradients, which were previously neglected due to the assumption of zero perpendicular velocity, i.e. $\kappa \cdot \gamma^2 \cdot \overline{\alpha} \cdot \left(\partial \overline{U}/\partial \overline{Y} \cdot \partial^2 \overline{V}/\partial \overline{Y}^2 - 2 \cdot \partial \overline{V}/\partial \overline{Y} \cdot \partial^2 \overline{U}/\partial \overline{Y}^2 \right)$, are multiplied by parameters which are the factor γ smaller than the parameters of the pressure term $\left(\kappa \cdot \overline{\alpha} \cdot \gamma \cdot \partial \overline{U}/\partial \overline{Y} \right)^2$. However, the dominance of this term against the other summand p_{hz}/b_{hz} is represented by the factor k_p in equation 3.39. As explained in appendix E, the geometrical ratio γ cannot fall below 10^{-5}. Since k_p took on values much higher than 10^5 in figure 3.9, the term $\kappa \cdot \gamma^2 \cdot \overline{\alpha}$ can well exceed p_{hz}/b_{hz}. Hence, other terms than those discussed for a parallel gap might become predominant.

In conclusion, the predictions of subsection 3.3.3 regarding the development of the shape of the gap due to the extended approach might be combined with effects due to the variation of the perpendicular velocity across the gap. However, due to the complex form of equations, qualitative prediction of the development of the further modifications of the shape of the gap was not attempted for the governing equations 3.43 and 3.44.

As for the set of equations obtained for a parallel gap, the set of equations 3.43 and 3.44 contain singularities, which occur simultaneously for the equations describing the pressure gradient along and across the gap. For the equations obtained with the assumption of a parallel gap, a condition was described for which the singularity will not lead to infinite pressure gradients. It is assumed that also for the extended set of equations 3.43 and 3.44 such a condition can be found and that the singularities will not spoil the solution if the gap is allowed to vary its height.

3.3.5.3   Wall forces

Finally, the force terms on the wall are considered in order to see whether the extended approach influences the forces on the wall. The derivation for the forces acting on a solid surface element is given in appendix F. For an infinitely small fluid volume, tangential force is

$$dF_t = \left(\frac{\eta_0 \cdot u_h}{h_0} \cdot e^{\alpha \cdot p_{hz} \cdot \overline{P}} \cdot \frac{\partial \overline{U}}{\partial \overline{Y}} \right) \cdot dx \qquad (3.45a),$$

and the normal force is

$$dF_n = \left(-p_{hz} \cdot \overline{P} + 2 \cdot \frac{\eta_0 \cdot u_h}{b_{hz}} \cdot e^{\alpha p_{hz} \overline{P}} \cdot \frac{\partial \overline{V}}{\partial \overline{Y}} \right) \cdot dA_y \qquad (3.45b).$$

The forces by the wall on the fluid are of the same absolute value but of opposite sign.

The tangential force is defined in the same way as e.g. Dowson and Higginson [17]. The normal force component contains an additional tensile stress component. Appendix F shows that this term can have, in comparison to the pressure term, some significance if the gap is non-parallel, and it should be incorporated in a solution of the extended approach of the ehl problem.

3.3.6   Summary

The investigation of the Navier-Stokes equation for the ehl problem showed, that in addition to the terms used for Reynolds equation, additional viscous terms are relevant for the ehl problem. These represent additional shear forces due to the strong viscosity variation along the contact resulting from the pressure variation along an ehl contact. The additional shear forces appear in the y-direction, and mean that, for the y-momentum equation across the gap, pressure varies rather than being constant. This varying pressure across the gap, however, means a viscosity variation across the gap to be considered in the x-momentum equation.

For the developed set of two equations, a singularity appears in the governing equations, as it does in the Navier-Stokes equations. The

singularity can disappear when the flow profile takes on a particular distribution. Because the boundaries for the ehl problem are elastic, it is believed that a solution of the Navier-Stokes equations rectifying the singularity can be found. Such a solution is expected to differ from the parallel shape of the gap and the Hertzian pressure distribution.

Chapter 4

Methodology for further treatment of the extended approach

4.1   The need for using the extended approach

In the previous chapters it was shown that many refinements of the original model to describe the behaviour of elastohydrodynamic contacts have been undertaken and that all were based on the assumption of a constant pressure across the gap and modelled with one or other forms of a Reynolds equation. However, it was also shown that, due to additional viscous forces for isothermal conditions and the assumption of Newtonian fluid behaviour, an extended approach, with a set of equations allowing pressure variation across the height of the gap, has to be taken into account. The proposed extended approach is increasingly relevant as soon as both load and hydrodynamic speed increase and sliding appears in the contact. It is hence relevant for those conditions for which non-Newtonian fluid behaviour is considered in established, Reynolds equation based solutions. For the extended approach some qualitative considerations have been proposed for the development of the ehl contact results, but neither evidence nor numerical values are available at this stage of the study.

4.2   Proposed method of development

Implementation, discussion and evaluation of a full numerical solution using the extended approach would offer some advantages. A full numerical method could give evidence for the theoretical predictions. In addition, the

influence of the facts that the gap will not remain parallel and that the theoretical predictions were made with considerations based on the one-dimensional solution of Reynolds equation, could be considered. Numerical results could be compared to results based on the Reynolds equation, and contributions of the extended approach to effects modelled in Reynolds equation based solutions with a non-Newtonian fluid description could be discussed. In summary, a much broader understanding of the contact could be achieved.

On the other hand, contributions would also be provided by further theoretical work on correlations between the extended approach and other phenomena such as thermal or non-Newtonian effects. These are effects which have been assumed negligible in the development of the extended approach theory so far and have yet to be discussed in more detail. However, further theoretical work would rely on the predictions and assumptions of section 3.3, which are limited and not yet proven. Additionally the question whether a non-Newtonian fluid behaviour can be explained by the extended, Newtonian approach has not yet been answered.

Hence, it was decided at this stage to concentrate on the numerical solution with the development of a suitable method before undertaking further theoretical considerations.

4.3   Specification for the numerical method and its implementation

A specification for the numerical method and its implementation is now to be defined. It was generally considered that not only the current project should be able to be handled, but also extensions in order to accommodate future industrial research.

Principal influences

The basic influence of the pressure variation across the height of the gap can be investigated ignoring, for example, thermal and compressible effects. In order to achieve more precise results, these effects would have to be considered. However, for the present investigation it was decided to

concentrate initially on the basic influence, keeping further solution refinement in mind.

Flexibility

The method implemented should obviously be able to cope with the present configuration of the problem. However, it was also considered desirable that the method could be easily and quickly adapted to include any additional effects.

Implementation effort

It was desired that the effort required to implement the method of solution into a computational program should be as small as possible. The implementation was therefore expected to comprise the discretisation of the governing equations, the generation of an appropriate grid and the solution of the resulting system of linear equations. It was anticipated that the requirement could be fulfilled by the employment of commercially available software packages and software components.

Performance

The above requirements for a flexible and easily implementable computational code are estimated to lead to programs consuming more time and system resources than special purpose programs optimised for one particular problem. It was decided that throughout the present research programme, high priority would be given to flexibility, efficient implementation, a wide range of practical application and robust performance of the program. Less priority was given to solution speed, ultimate accuracy, and optimisation over a limited range of parameters.

Part II

Numerical method for the extended set of equations

Chapter 5

Introduction to the development of the new numerical method

5.1　Methods to solve the ehl problem

The solution of the ehl problem basically means the solution of Reynolds equation, a pressure-viscosity relationship and an equation describing the deformation of the elastic surfaces. Various methods were applied throughout the development from the outset such as Grubin's [2, 3], utilising so-called direct, indirect and hybrid methods, leading to Newton-Raphson based and multi-grid techniques. Thereby, the development was driven by a desire to understand more of the ehl contact and the availability of increased computer power, both resulting in model refinements. However, despite all these developments, the fluid flow description used in these methods is still a Reynolds equation.

5.2　Solution of the Navier-Stokes equations

On the other hand, the Navier-Stokes equations together with the continuity equation are the generally valid description for any flow problem. Correspondingly, the number of solution approaches and techniques to solve the equations for particular flow problems is very high, among them, solution techniques which can solve the Navier-Stokes equations as required for the extended approach. Available as general purpose software, such solution techniques can be applied without having a deep knowledge of the details;

moreover, even some form of realisation of fluid-structure interaction is possible.

Available Navier-Stokes solvers and established solution techniques for the ehl problem form two groups of approaches. The solution of the ehl problem with the extended equations is likely to be a combination of both. Possible strategies of combination will either be the application of general purpose Navier-Stokes solver software with its coupling capability to the ehl problem or the incorporation of Navier-Stokes solving approaches into existing ehl solution techniques. Both strategies will deliver the desired numerical data for the extended approach.

5.3   Aim of the method development

Consequently, the aim of the present part II is to define and test a method, which is able to solve the ehl problem using the Navier-Stokes equations. This should be achieved while applying general purpose software as much as possible. In order to achieve this aim, the following objectives were defined:

5.4   Objectives and scope of the method development

In its first section 6.1, the subsequent chapter 6 provides a survey of numerical techniques applied to solve the ehl problem as well as their features and behaviour. Section 6.2 then repeats the process for the numerical techniques available to solve the Navier-Stokes equations. In both sections, these techniques are considered independently. A systematic definition of possible methods combining both ehl and Navier-Stokes techniques to obtain a solution method for the ehl problem while using the extended approach is given in chapter 7. An evaluation of the various methods used is provided and finally the most suitable method is selected. Chapter 8 considers the implementation of the selected method to the degree that pressure variation across the gap is not yet allowed, but validation of the new method in comparison with existing methods is permitted. Finally, chapter 9 presents the extension of the implementation towards the extended approach.

Chapter 6

Established numerical techniques

6.1   Numerical methods for the ehl problem

6.1.1   Introductory remarks

Beginning with the first analysis of the ehl problem by Mohrenstein-Ertel [2], several analysis methods have been proposed for the ehl problem. Their development was (and is) driven by the permanent interest in further explanation of the ehl problem and by the increasing computational options provided by the development of hardware as well as general numerical techniques.

As a result of that, a variety of numerical techniques is now available, and various authors, such as Hamrock and Tripp [65], Lubrecht [8] or Welsch [13], have surveyed and categorized them. The present section also reviews the numerical techniques available, however, with some focus on those features, which will be of relevance for the development of a numerical method for the solution of the ehl problem using the Navier-Stokes equations. Hence, the survey follows mainly the categories established [8, 13, 65], but shows in detail sometimes an unconventional link, sequence or accentuation.

In addition, in the course of the survey, some aspects of the solution of contacts showing features previously defined as irrelevant or unimportant for the present study, such as elliptical contacts or thermal problems, are occasionally referred to. They are nevertheless shown when they are of relevance for the development and discussion of the solution.

6.1.2   Grubin style methods

6.1.2.1   Mohrenstein-Ertel's principal approach

The first analytical method successfully solving the ehl problem for highly loaded contacts, taking the deflection and the variable viscosity into account, is that given by Mohrenstein-Ertel [2], also published by Grubin and Vinogradova [3]. A key feature of Mohrenstein-Ertel's approach is the split of the whole contact and hence the ehl problem into several sections. Each section allows or at least undergoes some simplifications such that the problem can be solved. Mohrenstein-Ertel splits the total system into three zones, the inlet zone, the highly loaded zone, and the outlet zone.

The **inlet zone** ranges from infinity before the contact to the beginning of the Hertzian contact. The pressure is assumed to be rather small in this zone. Hence an influence of the pressure onto the deflection of the solids is hardly expected and consequently neglected. On the other hand, Reynolds equation is rewritten using a normalised pressure Π considering the pressure-viscosity dependency

$$\Pi = \frac{1 - \tilde{a}^{-p}}{\ln(\tilde{a})} \qquad (6.1).$$

This flow equation is solved with a boundary condition which means that an infinite pressure boundary appears for the transition to the heavily loaded zone. With the condition of a pure Couette flow at this boundary, the analysis also returns the height of the ehl gap at the transition to the heavily loaded zone.

For the **heavily loaded zone**, it has been discussed, using the normalised Reynolds equation, that the shape of the gap must be very similar to that for the dry contact, i.e. the gap remains parallel with the height as determined at the end of the inlet zone. The pressure distribution follows that of Hertz. Reynolds equation is not solved for this zone, consequently, correction of the pressure distribution due to the flow, as opposed to that causing the deformation, is not carried out.

For the **outlet zone,** it is assumed that, as for the inlet zone, the pressure has no influence on the deflection. It is further shown that there must be a constriction to the gap, i.e. that the transition from the heavily loaded zone is earlier than the end of a Hertzian pressure zone. Such a shape of the gap can be obtained if an elastic curved surface is loaded with a rigid stamp which has a segment cut off at the outlet. This is another key element of Mohrenstein-Ertel's considerations. With the modified Reynolds equation as used for the inlet, assuming infinite pressure and Couette flow at the transition from the heavily loaded zone, the location of the edge of the stamp and the pressure distribution in the outlet zone is obtained.

The above solution with the infinite pressure at the end of the inlet zone and the start of a Hertzian pressure distribution at the beginning of the heavily loaded zone still delivers a discontinuous pressure distribution. Consequently, as for the beginning of the outlet zone, the location of the transition from the inlet to the heavily loaded zone must be corrected by shifting the transition so that a continuous pressure distribution is obtained.

With the above procedure, Mohrenstein-Ertel is able to get a solution for the ehl problem which is mainly analytical and with rather few numerical operations.

6.1.2.2   Evaluation of Mohrenstein-Ertel's method

Mohrenstein-Ertel [2] judges his method to be best for highly loaded contacts, where the assumption for the highly loaded zone fits best, with increasing inaccuracy the higher the contact speed rises and the lower the load falls. Christensen [66] specifies that the approach *"is excellent"* for the shape of the pressure distribution and the central film thickness of the contact. Hence Mohrenstein-Ertel's method is very suitable for film thickness determinations such as those of Greenwood and Kauzlarich [61] or Murch and Wilson [62]. On the other hand Christensen claims that features such as the pressure spike, the constriction of the film at the exit and the inlet zone are *"not so well represented".*

In addition, Christensen [66] and particularly Wallinger [67] outline the simplicity of Mohrenstein-Ertel's approach in comparison to other methods. The authors claim that the computational effort of such a style of solution is much lower than that of the other methods below. This reduced effort is a particular advantage for the solution of complex ehl problems, such as thermal, transient, or rough contacts. However, the solution of the complex problem of a point contact remains unmentioned.

6.1.2.3   Modification of Mohrenstein-Ertel's approach

Christensen [66] presents a more detailed procedure for the treatment of the idea that the deformation can be represented by a rigid stamp with a cut-off segment deforming an elastic cylinder. This method was further developed by Wallinger [67]. The author presents a method with multiple refinements using Mohrenstein-Ertel's ideas but overcoming many of the assumptions. Wallinger takes the deflection due to the pressure in the inlet and outlet zone into account, ensures exact continuity of the pressure distribution at the transition between the three sections, and takes thermal effects accurately into account. In order to achieve this, many more iterative procedures have to be introduced: Iterative solution of Reynolds equation with adaptation of the shape of the gap, as discussed in detail for the direct methods in subsection 6.1.3, are introduced to the inlet and outlet zone, the transitions between inlet, outlet and the heavily loaded zone are iterated and also the thermal effects. However, the method concentrates on the assumption of a perfectly parallel gap in the heavily loaded zone, which is extended with a quantitative determination of the error of this assumption. This error is found to be approximately one per cent on average and is not corrected.

Other authors' attempts to eliminate this error, which mean an elimination of the assumption of a perfectly parallel gap and perfect Hertzian pressure distribution in the heavily loaded zone, yet stay with the split into three sections, result in the hybrid methods discussed in subsection 6.1.5.

6.1.2.4   Summarizing definition of Grubin style methods

All the above authors of subsection 6.1.2 define their methods as Grubin style methods. However, they give different reasons. Greenwood and Kauzlarich [61] and Murch and Wilson [62] name their analysis *"Grubin style"* in the context of the assumption that the pressure in the inlet zone does not influence the deflection. Christensen [66] and Wallinger [67] state it because of the application of the idea that the deflection in the highly loaded zone can be modelled by a stamp with a cut-off segment. For the present work, all methods applying the split of the contact into three sections *and* assuming the cut-off stamp model for the highly loaded zone are considered as Grubin style methods.

6.1.3   Direct methods

6.1.3.1   The pure form

Generally speaking, a direct method means that Reynolds equation, as for example presented in equation 2.4*,

$$\frac{d}{dx}\left(\frac{h^3}{\eta}\cdot\frac{dp}{dx}\right) = 6\cdot(u_1 + u_2)\cdot\frac{dh}{dx} \qquad (6.2),$$

is solved for the pressure p with a given height distribution h. The obtained pressure distribution is then used to modify the shape of the gap [8]. This procedure is repeated until convergence is reached. In other words, Reynolds equation is understood as a second order differential equation of pressure p, with height and viscosity given and subsequently corrected. This type of method is also considered by Lubrecht as the *"'natural' way"* [8] or for example by Potthoff as the *"naheliegend"*, which means obvious, method [68], and hence frequently attempted.

Possibly the purest form of this solution procedure is that presented in the work of Weber and Saalfeld [69] and by Potthoff [68]. Both solve Reynolds

---

*   For the explanation of the numerical methods the dimensional form of Reynolds equation for the isothermal line contact problem was used throughout the present section, even if the original form is different.

equation for the pressure p as visible in equation 6.2. Weber and Saalfeld used the method in the 1950s, where the iterations were manually performed using characteristic graphs. Potthoff attempts the computational solution with strong under-relaxation because of the fact that tri-diagonal algorithms can be used for the fast solution of Reynolds equation. However both methods have been judged to be unsuitable for intermediately and highly loaded contacts since they fail to converge.

6.1.3.2   Modified forms

Hamrock and Dowson [70] modified the direct method for point contact problems by introducing a new variable

$$\Phi^* = p \cdot h^{\frac{3}{2}}$$

(6.3)

into the (dimensional) Reynolds equation considering pressure and height of the gap. Reynolds equation changes to

$$h^{\frac{3}{2}} \cdot \left[\frac{d}{dx}\left(\frac{1}{\eta} \cdot \frac{d\Phi^*}{dx} \right) \right] - \frac{3}{2} \cdot \Phi^* \cdot \left[\frac{d}{dx}\left(\frac{h^{\frac{1}{2}}}{\eta} \cdot \frac{dh}{dx} \right) \right] = 6 \cdot (u_1 + u_2) \cdot \frac{dh}{dx}$$

(6.4).

In the solution, Reynolds equation is understood as linear and solved with respect to Φ^*. Once a solution is obtained for the variable Φ^*, viscosity (and density) are corrected and later also the shape of the gap and the total load balance in superimposed loops. The arrangement and control of these loops was later modified, e.g. by Chittenden et al. [71]. The modified method shows also convergence problems for highly loaded contacts. However, its convergence behaviour is better than that of the above described pure form. This is because the new variable Φ^* contains at least some of the height information in the variable Φ^*, which is assumed to be known in the pure form.

A similar effect can be observed when a reduced pressure, such as described by Lubrecht [8], derived with Barus' approach

$$q = e^{-\alpha \cdot p}$$

(6.5),

is introduced to Reynolds equation, which can then be re-written in the form

$$\frac{1}{\alpha} \cdot \frac{d}{dx}\left(h^3 \cdot \frac{dq}{dx}\right) = 6 \cdot (u_1 + u_2) \cdot \frac{dh}{dx}$$

(6.6).

Evans and Snidle [72] present a more general reduced pressure definition, which is applicable for any pressure-viscosity description,

$$q^* = \eta_0 \cdot \int_0^p \frac{1}{\eta(\tilde{\pi})} \cdot d\tilde{\pi}$$

(6.7).

This definition leads also to a Reynolds equation with the structure of equation 6.6*. This Reynolds equation is then solved for the reduced pressure q or q* respectively. The convergence behaviour is again better than that of the pure form because the reduced pressure contains the information of the pressure-viscosity dependency which is assumed to be known in the pure form.

A combination of the two pressure modification methods discussed above is used, for example, by Hamrock and Jacobson [15] or Seabra and Berthe [73]. They modify the definition of the variable Φ^* in the way that they introduce a reduced pressure q rather than the pressure p, so that the definition is now

$$\Phi' = q \cdot h^{\frac{3}{2}}$$

(6.8),

leading to a Reynolds equation of the form

$$h^{\frac{3}{2}} \cdot \frac{d^2\Phi'}{dx^2} - \frac{3}{2} \cdot \Phi' \cdot \left[\frac{d}{dx}\left(h^{\frac{1}{2}} \cdot \frac{dh}{dx}\right)\right] = \alpha \cdot 6 \cdot (u_1 + u_2) \cdot \frac{dh}{dx}$$

(6.9).

The combination of the two pressure modification methods means that information of the height of the gap and also of the pressure-viscosity

---

* Applying Barus' pressure-viscosity description leads to a reduced pressure definition of

$$q^* = -\frac{1}{\alpha} \cdot \left(e^{-\alpha \cdot p} - 1\right),$$

which slightly differs from that by Lubrecht, equation 6.5, i.e.

$$q^* = -\frac{q-1}{\alpha},$$

but is very similar to that by Mohrenstein-Ertel, equation 6.1.

dependency is contained. This means a further extension of the range of converged solutions towards highly loaded contacts, however without the ability to solve heavily loaded contacts.

All the above approaches assume the more or less modified Reynolds equations to be linear with respect to the unknown variable p, q, q^*, Φ^* or Φ' at the moment of solution. All non-linearity is introduced in subsequent iteration loops; therefore the methods are also categorized as *"iterative"* direct methods [8].

In contrast to the above, there are also approaches where Reynolds equation is understood as a non-linear differential equation but still solved for the pressure. Then Newton's method is used to linearise Reynolds equation. These methods can still be categorized as "direct" because they still solve Reynolds equation for the pressure and later the elasticity equation for the height of the gap. Various forms of these direct methods are discussed below, in subsections 6.1.6 and 6.1.7.

6.1.4   Inverse methods

6.1.4.1   Fields of application

The inverse method was used as part of the first full numerical solutions using the hybrid method, which is discussed in the below subsection 6.1.5, e.g. by Dowson and Higginson [17], and Archard, Gair and Hirst [10]. However, it was also used in its pure form, for example by Potthoff [68] and Eller [7], and the present subsection concentrates, for the moment, on this pure form.

6.1.4.2   Principal approach

The inverse approach understands Reynolds equation 2.4,

$$\frac{d}{dx}\left(\frac{h^3}{\eta}\cdot\frac{dp}{dx}\right) = 6\cdot(u_1+u_2)\cdot\frac{dh}{dx} \qquad (6.10),$$

not as a second order differential equation in the pressure p but as a first order differential equation in the height of the gap h, for which the pressure

distribution and consequently the viscosity is given. Applying the integrated form 2.5,

$$\frac{dp}{dx} = 6 \cdot \eta \cdot (u_1 + u_2) \cdot \frac{h - h_0}{h^3} \qquad (6.11),$$

the differential equation reduces to an algebraic cubic equation

$$h^3 - \frac{6 \cdot \eta \cdot (u_1 + u_2)}{\frac{dp}{dx}} \cdot h + \frac{6 \cdot \eta \cdot (u_1 + u_2) \cdot h_0}{\frac{dp}{dx}} = 0 \qquad (6.12).$$

With the Cardanian formulae, equation 6.12 can be solved for the height of the gap h if the central height of the gap h_0 is known. This value h_0 can be derived from conditions that the solution must deliver a continuous gap with some convergence at the beginning and divergence at the end.

In parallel, the "elastic" shape of the gap is obtained from the Boussinesq equation. For an initial guess of the pressure, the hydraulic shape differs from the elastic, and hence requires a correction of the pressure distribution.

For this correction, different methods are proposed.

Archard, Gair and Hirst [10] developed the Boussinesq equation in a manner that a correlation between the difference between the two gaps and the change of the deforming pressure necessary to close this difference at each discretised point along the contact is described. The solution of this set of equations returns the pressure correction at all locations along the contact.

Eller [7] uses two methods; one for the inlet zone which is based on the assumption that the inlet pressure hardly influences the deflection and is thus very similar to a direct method. For the heavily loaded zone, the deformation equation, as by Archard, Gair and Hirst [10] *and* the flow equation are written in such a manner that a set of equations is obtained describing a correlation between the current differences in the height of the gaps and a pressure correction necessary so that the gap difference diminishes. This set of equations is solved numerically for the pressure corrections.

Once pressure corrections are obtained with one or the other method, they are applied and the procedure is repeated until convergence is reached.

Potthoff [68] uses two different methods which do not require the simultaneous solution of a set of equations. The first method expands or compresses the pressure distribution along an initially long, later shorter portion of the contact until the quadratic deviations of the two gaps reach a minimum. Since this procedure cannot create pressure spikes, the second method increases and decreases single pressure values also to minimise the quadratic deviation of the two shapes. Both methods are used alternately until a sufficient overall agreement of the two shapes is reached.

6.1.4.3   Evaluation

The extended approach is evaluated to show good convergence for highly loaded contacts [7], but is reported to become inaccurate in the inlet zone, which Eller overcomes by his description of the pressure corrections for this zone, and others, as Dowson and Higginson [4] or Archard, Gair and Hirst [10] by applying the below hybrid method. The suitability for high loads is confirmed by Lubrecht [8], but the author also states bad convergence for intermediately loaded contacts.

6.1.4.4   Modifications

As a further drawback of the inverse method, it is mentioned that a straightforward application of the inverse method to point contacts is not possible [70].

Evans and Snidle [74] overcome this problem. As can be seen from the work of these authors, an integrated form of Reynolds equation, such as equation 6.11, is not available for two-dimensional regimes but one of second order form 6.10*. The authors show that with rewriting and discretisation of the equation along and perpendicular to the contact, the two-dimensional Reynolds equation can also be reduced to a cubic equation in h, which however requires some information of the height h in the neighbourhood.

---

* The two-dimensional, isothermal, incompressible Reynolds equation is

$$\frac{\partial}{\partial x}\left(\frac{h^3}{\eta}\cdot\frac{\partial p}{\partial x}\right)+\frac{\partial}{\partial x}\left(\frac{h^3}{\eta}\cdot\frac{\partial p}{\partial z}\right)=6\cdot(u_1+u_2)\cdot\frac{\partial h}{\partial x}.$$

Since this information is not exactly known at the outset, some iterative loops are required for the determination of the correct height h. Complementary to the determination of the central height h_0 for the line contact problem the point contact problem requires boundary conditions or locations of known height[*]. At the centreline along the contact, the gradient perpendicular to the contact, $\partial/\partial z$, diminishes and Reynolds equation reduces to its one-dimensional form. Here, Evans and Snidle obtain a first location of known height and the respective height value at the inlet of the contact in the manner as used for line contact problems. Then further locations perpendicular to the contact are determined on a curve through the initial boundary location, which fulfil the same definition of the respective height values as at the centreline.

Hou, Zhu and Wen [75] give details for the pressure modification in an inverse point contact solution. They use the method proposed by Archard, Gair and Hirst [10], that the Boussinesq equation is used to describe a set of equations giving the correlation between the differences in the height of the gap and the necessary pressure corrections so that they diminish. To reduce the enormous numerical effort of solving this set of equations, it is assumed that a pressure correction influences the deflections only in its near neighbourhood.

6.1.5   Hybrid methods

Hybrid methods are a development of the Mohrenstein-Ertel approach of subsection 6.1.2.1, and are a combination of Grubin style methods, direct methods and inverse methods. The idea of splitting the contact into several regions is maintained from Mohrenstein-Ertel. In the section in which Mohrenstein-Ertel assumes a perfectly parallel gap a modification is applied: In this region, the above inverse method is applied. In the sections, in which Mohrenstein-Ertel solves the Reynolds equation, the direct solution is used,

---

[*] The expression "boundary values" can be confusing at this place, because any location can be the boundary of a section of the ehl contact, even those lying inside the analysis domain.

but also with the deflection caused by the inlet or outlet pressure distribution being considered.

The method was used for example by Dowson and Higginson [17] or Evans and Snidle [74], who split the contact into two sections[*], or Archard, Gair and Hirst [10], who used four sections[†].

All authors obtained results for highly loaded contacts without convergence problems worth mentioning. However, due to the split in several sections, all methods required algorithms to locate the transition between the zones in a way that a continuous pressure distribution is obtained as observed for Grubin style methods.

6.1.6   Newton-Raphson techniques

6.1.6.1   Principal approach

The (multi-dimensional) Newton-Raphson technique, as described by Press et al. [76], enables the solution of a set of n non-linear equations F_i of the form

$$F_i(\bar{x}_u) = 0 \quad \text{with} \quad i = 1, 2 \ldots n \tag{6.13}$$

for the vector of n unknown $\bar{x}_u = (x_{u1}, x_{u2} \ldots x_{un})$.

In the neighbourhood of $\bar{x}_u$, every single equation F_i can be considered as a truncated Taylor series

$$F_i(\bar{x}_u + \delta\bar{x}_u) = F_i(\bar{x}_{uj}) + \sum_j \frac{\partial F_i}{\partial x_{uj}} \cdot \delta x_{uj} + \ldots \tag{6.14}.$$

With a reasonable, but not perfect solution, available for $\bar{x}_u$ and with the objective, that the equation is perfectly satisfied for $\bar{x}_u + \delta\bar{x}_u$, means that

---

[*]   (i) inlet zone: direct method, (ii) combined heavily loaded and outlet zone: inverse method.

[†]   (i) inlet zone: direct method, (ii) heavily loaded zone until contact centreline: inverse method, (iii) heavily loaded zone after centreline: inverse method, (iv) outlet zone: direct method.

$$F_i(x_{uj} + \delta x_{uj}) = 0 \qquad (6.15),$$

equation 6.14 reduces to

$$0 = F_i(x_{uj}) + \sum_{j=1}^{n} \frac{\partial F_i}{\partial x_{uj}} \cdot \delta x_{uj} \qquad (6.16).$$

Putting all terms F_i in a vector $\vec{F}$ and introducing Jacobian matrix $\bar{J}$ with the derivatives $\partial F_i / \partial x_{uj}$ as elements $J_{i,j}$, equation 6.16 becomes

$$0 = -\vec{F} + \bar{J} \cdot \delta \vec{x}_u \qquad (6.17).$$

By inversion of the Jacobian matrix, the vector giving the necessary modifications $\delta \vec{x}_u$ to the previous guess of the solution $\vec{x}_u$

$$\delta \vec{x}_u = \bar{J}^{-1} \cdot (-\vec{F}) \qquad (6.18)$$

is obtained. The procedure is repeated with the corrected solution vector $\vec{x}_u$ until convergence is reached.

6.1.6.2   Principal application

Application of the Newton-Raphson technique to the elastohydrodynamic problem was first presented by Okamura [14]. The author uses the Reynolds equation in the form of equation 2.5

$$f_{Re} = \frac{dp}{dx} - 6 \cdot \eta \cdot (u_1 + u_2) \cdot \frac{h - h_0}{h^3} = 0 \qquad (6.19)$$

and understands it as non-linear with respect to pressure because of the pressure dependencies of viscosity and height. Consequently, the above described Newton-Raphson technique is applied with equation 6.19 discretised at n locations along the contact as a set of equations $\vec{F}$ and the pressure at these locations as unknowns $\vec{x}_u$ *.

---

*   Strictly speaking, discretisation at n locations leads to n-1 unknown pressure values with the unknown constant h_0 being the nth unknown value.

For the derivatives of the Jacobian matrix, Okamura considered not only the pressure itself but also the pressure dependencies of viscosity and the height of the gap:

$$\frac{\partial f_{Re\,i}}{\partial p_j} = \frac{\partial f_{Re\,i}}{\partial p_j} + \frac{\partial f_{Re\,i}}{\partial \eta} \cdot \frac{\partial \eta}{\partial p_j} + \frac{\partial f_{Re\,i}}{\partial h} \cdot \frac{\partial h}{\partial p_j} \cdot \qquad (6.20)$$

For the solution procedure, Hertzian pressure distribution is selected as the initial pressure distribution for the first Newton-Raphson step and for the determination of viscosity and the shape of the gap. For the subsequent Newton-Raphson steps, height of the gap and viscosity is calculated from the pressure distribution at the beginning of that step. Hence, the Newton-Raphson method can be understood as a direct method as defined in subsection 6.1.3.

The method is reported to converge rapidly in several iterations and for a wide range of load cases including highly loaded contacts [8]. However this is only the case, when first order backward approximation is used for the pressure gradient dp/dx of Reynolds equation 6.19. In the case of second order central approximation of the pressure gradient dp/dx, oscillations and non-unique results were observed.

An additional advantageous aspect of Okamura's approach is that the author understands the equation describing the equilibrium of pressure on the contact surface and applied load, as a further, n+1th equation and the distance between the two un-deformed contact partners as the n+1th unknown variable. Hence with this little extension, the superimposed loop necessary in other methods to adjust that load equilibrium can be spared.

6.1.6.3   Modifications

Many modifications of Okamura's approach were proposed or can be observed for the Newton-Raphson technique.

---

* Viscosity η and height of the gap h is written without an index i or j because discretisation leads to the fact that the variables at more than one locations, for example at i and i+1 must be considered.

♦ **Governing equations**

Many authors of the above mentioned, for example Hamrock, Pan and Lee [19], Wolff et al. [26] and Houpert and Hamrock [27], stay with the Reynolds equation which was used by Okamura, equation 6.19,

$$\frac{dp}{dx} - 6 \cdot \eta \cdot (u_1 + u_2) \cdot \frac{h - h_0}{h^3} = 0 \qquad (6.21).$$

On the other hand, as for the direct methods of subsection 6.1.3, also equations containing the reduced pressure q, equation 6.6,

$$\frac{1}{\alpha} \cdot \frac{d}{dx}\left(h^3 \cdot \frac{dq}{dx}\right) = 6 \cdot (u_1 + u_2) \cdot \frac{dh}{dx} \qquad (6.22)$$

were used, for example by Lubrecht [8]. Other authors such as Welsch [13], Lee and Hsu [30] or Chang, Conry and Cusano [77] stayed with the Reynolds equation with the pressure p, but preferred the second order differential form of equation 2.4

$$\frac{d}{dx}\left(\frac{h^3}{\eta} \cdot \frac{dp}{dx}\right) = 6 \cdot (u_1 + u_2) \cdot \frac{dh}{dx} \qquad (6.23)$$

in contrast to the first order differential form of Okamura and the others.

None of the two above modifications seems to have a substantial impact on the quality of the solution.

♦ **Discretisation**

Okamura stated that first order discretisation of the first order derivatives dp/dx is necessary to get non-oscillating, unique solutions of the ehl problem.

For the application of the second order Reynolds equation 6.23, the problem that second order central approximation for first order derivatives spoils the numerical method, moves from the pressure gradient term dp/dx for the first order Reynolds equation 2.5 to the height gradient term dh/dx. For example Kostreva [78] detected regions of parameters for which the solution was unstable while

applying a second order central approximation the to the height gradient term dh/dx. Lubrecht, ten Napel and Bosma [79] claimed that central approximation is the reason for the instabilities and recommended first order backward approximation as a remedy.

For the second order form of Reynolds equation 2.4, Čermák, [80] and [81], proposed a non-symmetric discretisation formula to minimise the discretisation error of the first order approximation. Non-symmetric discretisation means that the grid for the pressure gradient d^2p/dx^2 is shifted by a quarter grid cell width in comparison to that for the height gradient dh/dx. Under these circumstances, second order central approximation can be used for the height gradient.

Another procedure to improve numerical accuracy of the second order form of Reynolds equation 2.4 was proposed by Chang, Conry and Cusano [77] and used by Lee and Hsu [30]. The authors showed with their study that a second order central approximation can be used for the height gradient term in the determination of the residuals of Reynolds equation if first order backward approximation is used for the determination of the Jacobian matrix.

♦ **Nested loops**

Most authors, such as Lubrecht [8] or Welsch [13], follow Okamura's [14] proposal to incorporate the load equilibrium equation into the overall set of equations. However, for example Hamrock and Tripp [65] show also the possibility, well known from other methods, to treat the load equilibrium in a superimposed loop.

♦ **Jacobian matrix**

According to Press et al. [76], in the original Newton-Raphson technique, the full matrix of derivatives is determined analytically from the governing equations, e.g. Okamura [14].

Alternatively, Welsch [13], or Čermák [80] determined the derivatives numerically instead of analytically to reduce implementation effort,

which means that they changed from a tangent to a secant method. Čermák outlines the reduced effort of analytical work using numerical derivatives but an increased CPU effort, which makes such a procedure efficient when testing, for example, discretisation schemes. However neither of the two authors discusses changes in performance or range of convergence.

A different modification in the determination of the Jacobian matrix is proposed by Chang, Conry and Cusano [77]. In order to accelerate analysis, the authors assume that the relevance of elements of the Jacobian matrix decreases as the distance of the element from the matrix's main diagonal increases. Since the Gaussian tri-diagonal algorithm provides a fast solution method, the authors reduce the Jacobian matrix to a tri-diagonal form. In addition, they start with a coarse grid and refine the grid, as often as a solution is obtained for the coarser grid. They claim a speed-up factor of two for this last feature.

6.1.6.4   Disadvantages

Some points are found to be disadvantageous for the Newton-Raphson approaches. Lubrecht [8] claims a cubic increase of the necessary computational resources, such as memory space and analysis time, for a linear increase of the number of discretised points. This might be acceptable for one-dimensional steady state analysis but is a particular problem for two-dimensional flow and transient problems. Lubrecht also reports that, for an increasingly parallel gap as appears with increasing load, the diagonal dominance of the Jacobian matrix disappears, leading to difficulty in matrix inversion. However, Houpert and Hamrock [27] overcame the problem with non-equidistant grid application.

6.1.7   The multigrid method

6.1.7.1   Principal approach

As the latest major step in development of the solution of the elastohydrodynamic problem, Lubrecht [8] introduced the application of the full multigrid technique to ehl problems to overcome the problems observed

for the Newton-Raphson technique. The basic ideas of multigrid are explained in Press et al. [76]. The authors define convergence speed as the number of iterations required for a Jacobi or Gauss-Seidel iterative scheme to sufficiently minimise the deviation of the actual solution of a problem from its perfect solution. This convergence speed is dependent on the width of a deviation on the grid which should be reduced in comparison to the grid size. With solutions on grids of different resolutions, with a particular sequence of solutions on those different grids and respective interpolation between the various grids, fast solutions are obtained. This is because for every extension of a deviation the ideal grid, leading to maximum convergence speed, is used sooner or later in the solution procedure. In the case where a loop is superimposed on the above method which stepwise refines the original grid, the method is named *"full multigrid"*.

In order to deal with the non-linearity as it appears in the ehl problem, a (one-dimensional) Newton iteration must be introduced to the Gauss-Seidel relaxation scheme [76]. Similar to the Newton-Raphson scheme, the improved value for an unknown variable x_i^{new} is obtained with a previous guess x_i^{old}, the function F_i, which should be zero for the final solution, and its derivative with respect to the variable x_i

$$x_{u_i}^{new} = x_{u_i}^{old} - \frac{F_i}{\frac{\partial F_i}{\partial x_{u_i}}}$$
(6.24).

6.1.7.2   Principal application

For the solution of the ehl problem, Lubrecht uses the second order differential form of Reynolds equation 2.4

$$f_{Re} = 0 = -\frac{d}{dx}\left(\frac{h^3}{\eta} \cdot \frac{dp}{dx}\right) + 6 \cdot (u_1 + u_2) \cdot \frac{dh}{dx}$$
(6.25)

and states that for the derivatives the pressure dependency of the viscosity and the height of the gap must be considered:

$$\frac{df_{Re\,i}}{dp_i} = \frac{\partial f_{Re\,i}}{\partial p_i} + \frac{\partial f_{Re\,i}}{\partial \eta} \cdot \frac{\partial \eta}{\partial p_i} + \frac{\partial f_{Re\,i}}{\partial h} \cdot \frac{\partial h}{\partial p_i}$$
(6.26).

However, the height of the gap cubed, h_i^3, can be seen as a separate variable in comparison with the height of the gap h and need not be considered.

On the other hand, he claims that derivatives taking viscosity as the only pressure dependent variable, i.e.

$$\frac{df_{Re\,i}}{dp_i} = \frac{\partial f_{Re\,i}}{\partial p_i} + \frac{\partial f_{Re\,i}}{\partial \eta} \cdot \frac{\partial \eta}{\partial p_i}$$ (6.27),

lead to the same poor convergence as the direct iterative methods of subsection 6.1.3.

Using the derivative formulation 6.26, the multigrid method converges for the same parameters as the Newton-Raphson method does but with a much lower computational time, particularly for fine grids. Hence it can be concluded that the fact of understanding Reynolds equation as non-linear due to the pressure dependency of viscosity and height of the gap is important for the convergence of direct methods. Vice versa, omitting some dependency, as it cannot be avoided for the direct iterative methods of section 6.1.3, spoils convergence, independent of whether a direct iterative, a multigrid or a Newton-Raphson technique is used.

The technique is refined by Venner, ten Napel and Bosma [82], who partially replaced the Gauss-Seidel method by Jacobi's dipole method to get improved convergence, obtaining converging results for Hertzian pressures at and above those technically relevant.

6.1.7.3   Modifications and similarity with Newton-Raphson techniques

By applying the Jacobi method rather than the Gauss-Seidel method, the method will deliver the same results as a Newton-Raphson method with the Jacobian matrix truncated to its main diagonal. Hence the multi-grid technique can also be understood as a particular modification of the Newton-Raphson technique with peculiarities with respect to matrix truncation. In addition the derivative determination is of relevance for multigrid and Newton-Raphson techniques. Hence in the further development of a solution method

for the proposed extended approach, multigrid will not be treated as a separate category but with the Newton-Raphson technique.

6.1.8   Treatment of thermal and non-Newtonian problems

The subsequent overview briefly covers the treatment of thermal and non-Newtonian aspects in ehl analysis, in order to see whether these aspects require substantial alterations of the previously discussed methods, which would not allow a later extension of the intended Newtonian, isothermal solution of the ehl problem.

For thermal solutions, three principal methods seem to be available; all of them are modifications of isothermal methods

(i)   The thermal analysis is treated in a superimposed loop:

After a full solution of the ehl problem is obtained, the energy equation is solved for a temperature distribution in the contact and at the contact surfaces. With that temperature field correcting the viscosity field, a new solution for the pressure and height distribution is obtained. This procedure is repeated until convergence of the temperature field is reached.

This method can be observed for the iterative direct method by Ghosh and Hamrock [83] and for the Newton-Raphson technique, for example by Sadeghi and Sui [84] or Welsch [13]. In these cases the thermal solution requires a CPU time many times that of the isothermal case, but convergence of the temperature is independent of the convergence of the ehl problem for a given temperature field.

(ii)   The thermal effects are considered during the analysis as soon as possible, meaning additional steps and eventually nested loops during the established isothermal method. This method can be observed in all styles of solution:

In the Grubin style method of Murch and Wilson [62], thermal effects are already considered in the innermost solution of Reynolds equation in the inlet zone. In the thermal solution by Wallinger [67], the

temperature field is determined in a loop inside the outermost loop ensuring the equilibrium of integrated pressure along the contact and applied load.

Liesegang [36] uses this method for his direct method, where thermal effects are considered before the pressure distribution is updated.

For the hybrid solution, for example Cheng and Sternlicht [16], and for the inverse solution, for example Eller [7], the temperature effects are calculated before the procedure of updating the pressure distribution is carried out.

Wolff et al. [26] avoided the superimposed loop in the Newton-Raphson technique, by solving the energy equation and updating the temperature distribution after every single Newton-Raphson step.

In summary, the above methods seem to aim to incorporate the thermal effects as soon as possible into the ehl analysis. However numerical advantages in terms of convergence behaviour or solution speed are hardly discussed.

(iii) A fully simultaneous treatment of thermal effects is shown by Lee and Hsu [30]. The authors use the Newton-Raphson method in a manner such that the pressure along the contact *and* the temperature along the contact form together the vector of unknowns $\bar{x}_u$, and Reynolds equation *and* the energy equation form together the vector of equations which have to be fulfilled $\bar{F}$.

For the treatment of non-Newtonian lubricants, often non-Newtonian Reynolds equations are derived. Of the above mentioned, for example Houpert and Hamrock [40], Lin and Lin [42], Iivonen and Hamrock [46], and Conry, Wang and Cusano [47] followed that procedure. For the solution of the ehl problem, all these authors use exclusively the Newton-Raphson technique and treat the non-Newtonian Reynolds equation in the same manner as the Newtonian Reynolds equation is treated in a Newton-Raphson technique.

Sui and Sadeghi [34] use, instead of a non-Newtonian Reynolds equation, the generalised Reynolds equation, such as equation 2.14, which allows consideration of any non-linear viscosity behaviour of the lubricant and solve Reynolds equation also with the Newton-Raphson technique.

In summary, the observed treatment of thermal or non-Newtonian methods mean that all solution concepts were derived from adaptation or extension of procedures applied for Newtonian or isothermal cases.

6.1.9   Concluding remarks

The above survey covered several numerical solution techniques, each of them showing variations. For the subsequent development of a method for the solution of the ehl problem using the Navier-Stokes equations, they are briefly characterized as following:

(i)   **Grubin style methods** mean methods in which the contact is split into three sections, the assumption of Hertzian pressure and a parallel gap being assumed for the heavily loaded central section of the contact. The error of this assumption can be checked and evaluated but will, a-priori, not be corrected.

(ii) **Direct methods** mean iterative methods in which initially Reynolds equation is solved for the pressure, or any modified variable instead of pressure, with subsequent modification of height and viscosity. The loop is repeated until convergence is reached. Any application of Newton's method is considered in the category Newton-Raphson techniques.

(iii) **Inverse methods** mean methods in which, for a given pressure distribution, the flow equations and the deformation equations are solved for the shape of the gap. If both results disagree, the pressure distribution is adapted until convergence is reached

(iv) **Hybrid methods** mean methods in which the inverse method is used for the highly loaded zone of the contact and a direct method is used for the inlet and outlet region.

(v) **Newton-Raphson techniques** mean a direct method, in which Reynolds equation is solved for the pressure applying Newton's method for non-linear equations. Due to the fact that the method comprises various truncations of the Jacobian matrices and various methods of the matrix inversion, Newton-Raphson techniques includes also the one-dimensional Newton's method and thus the multigrid method for the subsequent chapters of this study.

6.2   Numerical techniques for solving the Navier-Stokes equations

6.2.1   General remarks

According to Schlichting [55, 56], the Navier-Stokes equations, the continuity equation and an equation of state for the density behaviour, give a general description of fluid flow behaviour. The solution of this set of equations is difficult due to the number and complexity of the equations. The traditional strategy to solve the equations is the introduction of assumptions or simplifications to reduce the equations to an extent that they can be solved analytically or with simple numerical techniques [57]. For example, the determination of Reynolds equation follows this strategy and hence, strictly speaking, Reynolds equation is a solution of the Navier-Stokes equations.

Hence for the present study the expression *"numerical techniques for solving the Navier-Stokes equations"* can be stated more precisely as follows: Numerical techniques for solving the incompressible, two-dimensional Navier-Stokes equations neglecting the inertia terms but with highly variable viscosity. Any development of the proposed method should involve an extension to weakly compressible fluid behaviour, three dimensions, and thermal or non-Newtonian considerations.

Two general approaches were found fulfilling this requirement:

6.2.2   The vorticity-stream function approach

Roache [85] discusses the vorticity-stream function approach, which aims for the solution of the Navier-Stokes equations and the continuity equation by

converting the equations into a different form for which treatment is easier. For the two-dimensional case, the two Navier-Stokes equations are converted into a single transport equation* for vorticity ω which is generally defined according to Schlichting, [55, 56], as

$$\omega = \frac{\partial v}{\partial x} - \frac{\partial u}{\partial y} \qquad (6.28)$$

and the continuity equation is converted with the help of the stream function ψ, where [57]

$$u = \frac{\partial \psi}{\partial y} \text{ and } v = -\frac{\partial \psi}{\partial x} \qquad (6.29)$$

into a Poisson partial differential equation.

To obtain a solution, the vorticity transport equation, the stream function Poisson equation and the velocity equations 6.29 are solved successively and this is repeated until convergence is reached. Variations of this principal sequence, various methods to solve the single equations and settings for control parameters of the analysis have been reported, which might represent an optimum for one application but could fail for another [85, 86, 87].

Pressure determination, which is necessary for a variable viscosity approach, is carried out at the end of the above sequence after convergence has been reached. Any parameters dependent on pressure mean a re-run of the complete iterative procedure, a reason why Roache [85] considers the approach as less suitable for applications requiring pressure data.

---

* The transport equation is a partial differential equation consisting of convective, diffusive, and source terms of the general form

$$\frac{\partial(\rho \cdot \phi)}{\partial t} + \text{div}(\rho \cdot \phi \cdot \vec{w}) = \text{div}(\Gamma \cdot \text{grad}\phi) + S_\phi \cdot$$

Navier-Stokes equations can be understood as transport equations for the velocity component of that direction, for which they describe the equilibrium of momentum, i.e. $\phi \doteq u$ for the x-momentum equation, and $\phi \doteq v$ for the y-momentum equation.

The above method, given in [85] for incompressible flow, implies iso-viscous flow. The equations for variable viscosity would be much more complex than the above-mentioned case. Extension to the three-dimensional case would be even less straightforward, since the stream function expands to a three component vector, with the number of equations and difficulties in solution rising [85].

6.2.3   SIMPLE based methods

6.2.3.1   Principal method

A more popular alternative than the vorticity-stream function approach is the solution of the so-called primitive variables, which means the velocity components and the pressure are directly sought. Basically, for the solution of the primitive variables, the solution of each Navier-Stokes equation for its corresponding velocity component would be obvious. However this implies that the continuity equation must be used for pressure determination. However, its original form, equation 3.6, contains only velocity gradient terms.

Patankar and Spalding [88] proposed the so-called SIMPLE method to convert the continuity equation into a pressure correction equation overcoming the above problem. The pressure correction equation is derived for the discretised equations. Each variable sought, i.e. pressure and velocity components, is split into a known* and unknown portion, the latter being the difference between the known values and the final result, i.e. representing the necessary correction of the known value to the final result, which is of course still unknown. Substituting these split descriptions into the momentum equations gives new transport equations describing the correlation of the pressure corrections and the velocity corrections. Some terms are omitted from these velocity correction equations as they are condensed to a simpler form. Incorporation of this simplified form into the continuity equation, for which the split of the velocities into a known and a correction portion is also

---

*   The known portion can be the initial values or any actual value of the iterative solution process.

applied, finally leading to a transport equation containing pressure corrections as the unknown term.

With the above described equations, the solution procedure for pressure and velocity components is again successive and iterative: each loop starts with a given pressure distribution and the velocities from the momentum equations are determined. Subsequently the pressure corrections from the respective transport equation and finally the velocity corrections from the simplified velocity correction equations are calculated and applied to the original values. This loop is repeated until convergence is reached.

This procedure was later revised by Patankar [89] to the SIMPLER, SIMPLE-revised, algorithm with improved robustness and computational speed. With SIMPLEC, SIMPLE-consistent, a further modification of the SIMPLE-algorithm is available [90].

The SIMPLE based algorithm and its derivatives are robust and widely applicable, which is proved by the fact that all commercially available major CFD codes to solve the Navier-Stokes equations, such as CFX-4 [91] and CFX-5 [92], Fluent [93] or Star CD [94], are based on the SIMPLE approach or its derivatives and have been successfully applied to a wide range of applications.

6.2.3.2   Further aspects of SIMPLE based approaches

In commercial packages other aspects are also taken into account, which must be kept in mind for the application of CFD software to ehl or when considering a special purpose adaptation of a SIMPLE based code to the ehl problem.

Viscosity variation is considered at the beginning of each iterative loop, where all coefficients could be updated before the re-calculation of the variables [90, 91]. This means that the determination of pressure and viscosity is a successive process. Arbitrary descriptions for viscosity can also be used in commercial packages, since either Fortran routines [91, 93] or special command language expressions [92] can be added to describe the fluid properties. Even a major variation of viscosity in a domain, as relevant

for ehl, is a common case for commercial packages, since the influence of turbulence is modelled via changes in viscosity. The above location of viscosity modification can also be used to take other influences on the fluid into account, such as temperature or non-Newtonian behaviour, for which in commercial software packages often predefined models are available.

Thermal effects in SIMPLE based solution algorithms are realised by adding the solution of the heat transportation equation to the end of the successive solution of velocity components and pressure correction [90].

Discretisation is also an essential issue for the implementation of SIMPLE based approaches. Versteeg and Malalasekera [90] show that a staggered grid, where the grid for the momentum equations is shifted half a cell width in the direction of force equilibrium, must be used to get a proper solution. Alternatively, if a single grid for all variables is desired, particular algorithms must be used, such as that by Rich and Chow [95] , e.g. in CFX-4 [91], which do not allow the use of the calculated velocity components for further analysis, but that of pressure gradients in the discretised cell and flow rates at the faces of the discretised cell.

6.2.4   Fluid-structure interaction for CFD software

For commercial CFD software, all three types of coupling proposed by Gärtner, Rettweiler, and van de Sand [96], for coupling some structural analysis to the fluid flow analysis, can be observed.

The concept of *"program coupling"* (co-simulation) means that one software, e.g. CFD software, delivers data relevant for another software, e.g. a pressure distribution. These are subsequently taken and used by the other software, e.g. a structural analysis code, which itself returns some modified data back to the first code, e.g. deflection data. This is repeated until convergence is reached. The method was used in the field of CFD, for example, by Ramos [97].

The concepts *"model coupling"* and *"solver coupling"* both mean the incorporation of one procedure, e.g. structural analysis, into the other, e.g.

the CFD software, which has to allow the change of the flow domain within an analysis.

The major CFD codes allow the change of the flow domain as long as the topology* is not changed and offer Fortran interfaces and subroutines to allow the implementation of structural analysis *and* its solver (*"solver coupling"*). However, flow domain adaptation is located prior to the loop determining velocity, pressure, viscosity, and, eventually, temperature. It is hence less frequently visited than the other modifications and requires the generation of a superimposed loop as with a transient analysis [90, 93]. The coupling of pressure and temperature is successive as when coupling pressure with the other variables, but since the geometry determination is undertaken less frequently in the superimposed loop, the coupling is weaker. The method and the problem of the coupling are dealt with, for example, by Cabrera [98].

"Model coupling" is similar to *"solver coupling"*, the main difference being that the former method uses the solver of the CFD code to solve the structural analysis model. Such results are available for CFX [99], but they require access to the software source code. The quality of the coupling is identical to that for *"solver coupling"*.

6.2.5   Concluding remark

For the solution of the Navier-Stokes equations, SIMPLE based approaches are the most developed and also available in commercial software packages. They provide the capability to fulfil all requirements and can be coupled with structural analysis. With the vorticity-stream function, a second suitable method is available; however, the approach seems to be more cumbersome and less suitable for extension.

---

*   The topology means the number of discretised elements of cells and the qualitative position to each other.

Chapter 7

Development of numerical method

7.1   Introductory remarks

Although both groups of methods shown in the previous chapter, i.e. the special purpose ehl solution methods and the general Navier-Stokes equations solvers, can handle fluid flow problems with variable viscosity and elastic boundaries, they concentrate on different details.

It can be seen from section 6.1 that the coupling of the fluid flow equations to the viscosity and deformation description is the essential problem when solving the ehl problem. Some five different categories of coupling schemes were specified for the realisation of this interaction. It should be noted that all the schemes are based on forms of the Reynolds equation and apparently have not been used for the extended approach. Similar considerations can be made for the solution methods for the Navier-Stokes equations, section 6.2. Two principal methods are suggested for the coupling of the momentum equation to the continuity equation. However, for fluid-structure interactions, only the approach of successive coupling is established.

Hence, a successive method of coupling appears to be the obvious approach to solve the ehl problem with the extended fluid flow description. However, this method of ehl coupling is only one out of a range of five methods. It has the disadvantage of suffering from relatively bad numerical performance as discussed in detail in subsection 6.1.3 and 7.2.1. Therefore, it was decided to attempt the combination of other coupling schemes with the Navier-Stokes

solvers. The five different methods of fluid-structure coupling and the further two methods of techniques to solve the Navier-Stokes equations, lead to a matrix of ten numerical schemes. For the investigation of these schemes, a method to realise the fluid-structure-viscosity interaction was prescribed and the incorporation of each of the various momentum-continuity coupling methods was then attempted. This method was preferred to the reverse procedure, because

♦   the field of ehl solution methods is small in comparison to the field of the solvers of the complete Navier-Stokes equations with the enormous variety of applications, and

♦   solution techniques for the Navier-Stokes equations also cover problems which are of minor relevance for the ehl problem, such as the determination of a converged solution without a good initial value or inertia flow.

Consideration of the performance of a proposed numerical method was always made immediately after its introduction. This technique of development and appraisal allowed the recognition of problems at a very early stage and hence allowed for possible improvements to be made without any expensive computations.

A final and summarizing overall comparison and evaluation of all discussed methods leading to the selection of a suitable method is given in section 7.3. Section 7.4 checks the applicability of commercially available software for the selected methods and finally section 7.5 reduces it to a single suitable CFD code.

7.2   Calculation schemes

7.2.1   Direct methods of coupling

7.2.1.1   Schemes using real pressure p

In the established methods for the direct method of coupling, subsection 6.1.3, the three equations, describing fluid flow, viscosity and deformation, are coupled successively. This means that each equation is solved for a specified unknown variable while all others were assumed to be known. This sequence of solutions is repeated until convergence is reached. The equality of applied load and resulting pressure is determined within an additional superimposed iteration scheme.

The fluid flow equation requires geometry and viscosity as input and provides the pressure as output. These inputs and outputs are exactly the same as they are required by all established solvers of the Navier-Stokes equations based either on the SIMPLE algorithm or on the vorticity-stream function approach. Hence, the extended set of equations can be introduced simply by replacing the Reynolds equation solver by a Navier-Stokes solver. Calculation of viscosity and deformation would remain unchanged. The respective calculation scheme is given in figure 7.1. The figure also illustrates which parts of the algorithm originate from established ehl calculation schemes and which from established Navier-Stokes equations solvers.

The application of the fluid-structure interaction method proposed for the SIMPLE based codes, subsection 6.2.4, leads to a similar calculation scheme. In comparison with the scheme in figure 7.1, a SIMPLE based calculation allows the pressure-dependent variation of the viscosity be made within the fluid flow calculation. This feature reduces the previous loop coupling three equations to a pure fluid-structure coupling loop. This variant is illustrated in figure 7.2.
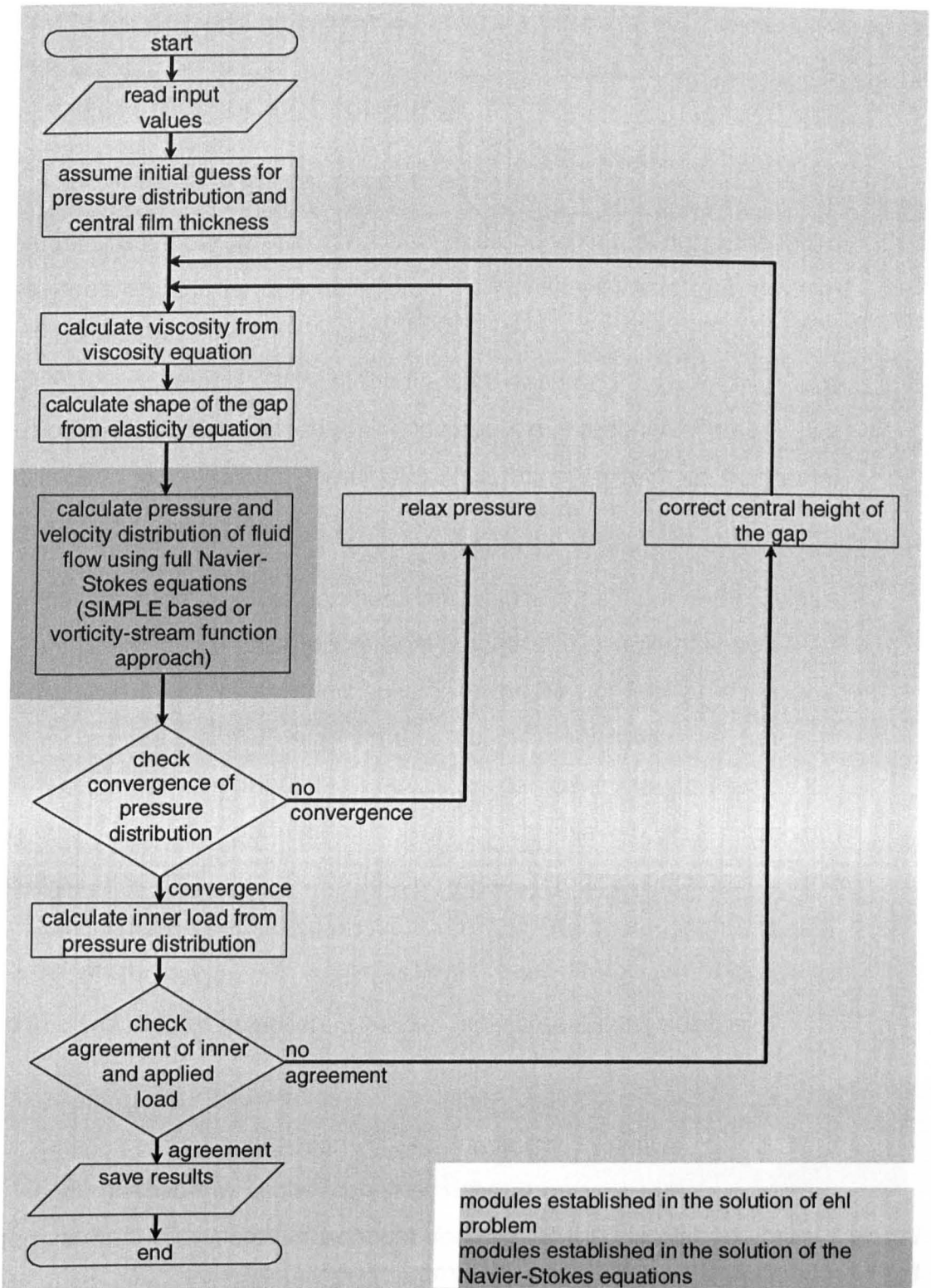
Figure 7.1:   Calculation scheme for the direct method to solve the ehl problem using the complete Navier-Stokes equations.
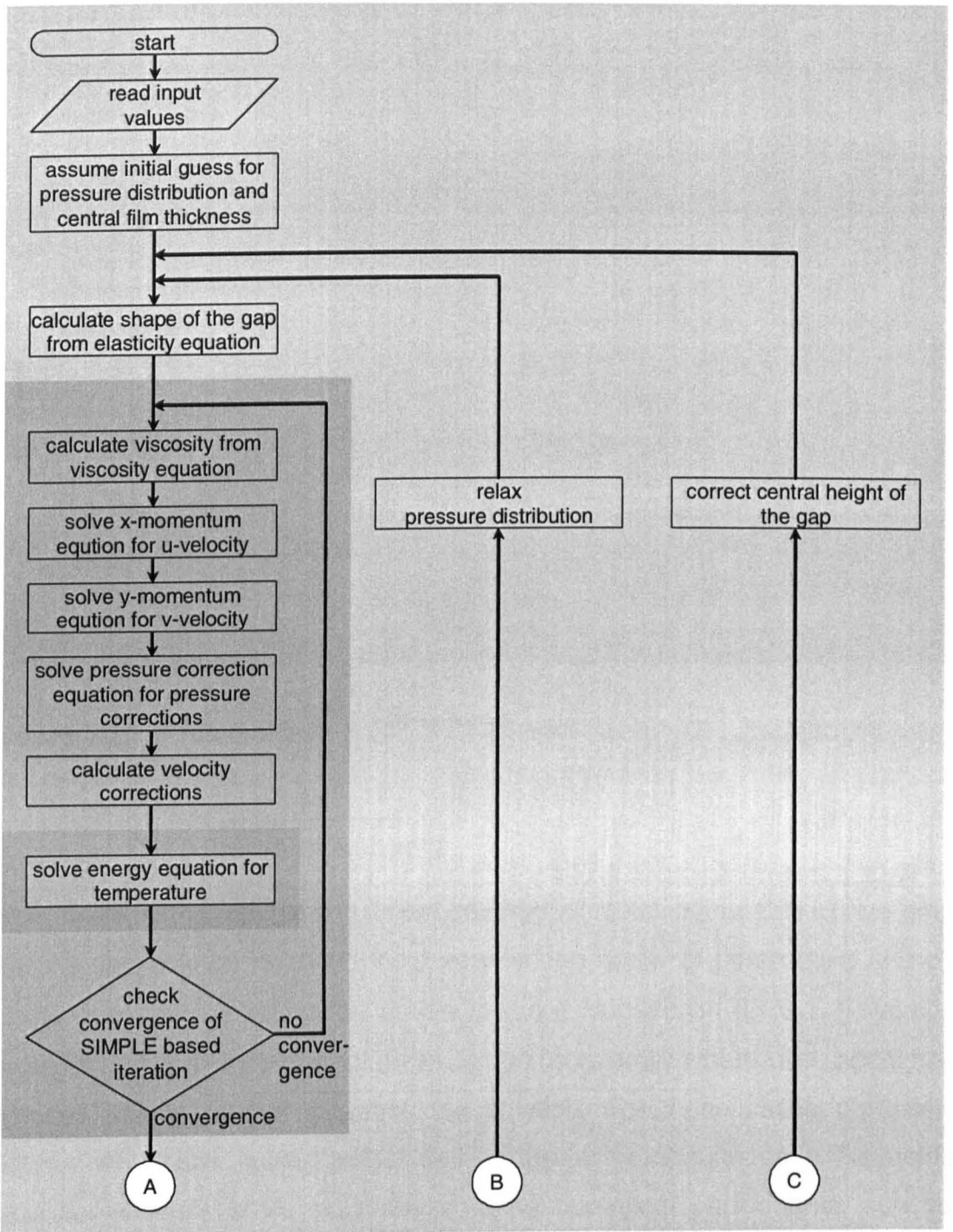
Figure 7.2:   Calculation scheme for the direct method to solve the ehl problem using the complete Navier-Stokes equations and full capabilities of SIMPLE based algorithms for thermal effects (continued).
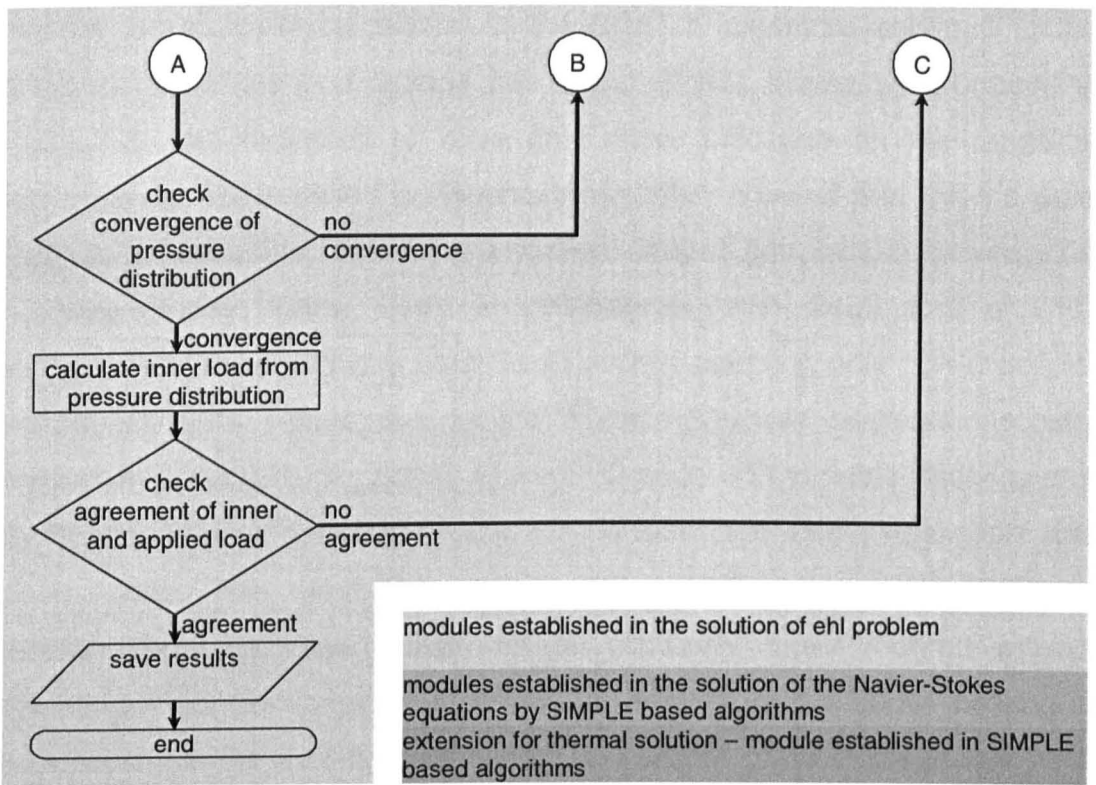
Figure 7.2:   *(concluded).*

7.2.1.2   Discussion of scheme

The major drawback of the direct method of coupling is that converging results can only be obtained for a very limited range of parameters and by using considerable relaxation as discussed in subsection 6.1.3.1. Reynolds equation based solutions already fail to converge where the additional viscous effects do not influence the solution. For these cases a Navier-Stokes equations solver would deliver the same results as a Reynolds equation solver. Hence no change in the numerical performance can be expected at the edge of convergence. Similarly, no converging results can be expected for high load and speed parameters in the case of pure rolling, since here Reynolds equation is expected to provide a correct solution as well. Therefore it was concluded that it is unlikely that the method delivers converging results for the case where additional viscous effects have a major influence.

Nesting the viscosity calculation in the SIMPLE algorithm and putting the fluid-structure interaction outside the Navier-Stokes solver, as proposed in figure 7.2, was expected to have only minor influence on the range of convergence. Tests based on Reynolds equation showed that even a pure fluid-viscosity coupling, assuming a rigid ehl shaped gap, fails to converge for relatively modest loads. Tests in collaboration with distributors of CFD software also showed that a pure fluid-viscosity coupling only converges for modest pressure values due to the highly non-linear pressure viscosity dependency. Accordingly, a test with a CFD code with variable viscosity and elastic boundaries converged only for considerable under-relaxation and modest load. This result, however, contrasts with that of Almqvist and Larsson [54] who show results for an obviously direct method without indicating major convergence problems. In addition to the above nesting of the viscosity in the fluid-flow calculation, a number of other measures were tested to try and improve the range of convergence for the method of direct coupling. Relaxation of the gap shape, stepwise application of the load, smoothing of the pressure distribution, smoothing of the height of the gap, normalising the load for viscosity and elasticity calculations, introducing artificial time steps in the Reynolds equation solver, and changing of the nesting of the different iteration loops were tested. None of these measures led to a reasonable improvement of the numerical behaviour.

All the above schemes would require little implementation effort, since all the modules employ methods which are well established. Since SIMPLE based codes can be used without any major changes, even the application of commercially available codes is possible.

7.2.1.3   Extension to thermal problems

Two methods are possible to extend the above schemes to thermal calculations. The method of superimposing another loop outside the total calculation is widely established and was mentioned in subsection 6.1.8. This method is basically independent of the method of fluid-structure coupling and can therefore be used with all types of Navier-Stokes equation solvers.

The second method can be applied when using SIMPLE based methods for the solution of the Navier-Stokes equations. In SIMPLE based algorithms the fluid flow-heat transfer interaction is realised by incorporating the energy equation into the SIMPLE sequence as presented in subsection 6.2.3.2. This method is also shown in figure 7.2.

7.2.1.4   Schemes for modified direct methods

The introduction of reduced pressure parameters, such as q, q^*, Φ^*, or Φ', equations 6.3, 6.5, and 6.8 in subsection 6.1.3.2, into ehl solution schemes ensures a closer coupling of the three equations describing fluid-flow, viscosity and deformation. The well-established methods for solving the Navier-Stokes equations do not provide such a close coupling. Hence, the application of this closer method of coupling means the introduction of an appropriate variable into the Navier-Stokes equation, which has not yet been suggested.

When introducing the parameters q or q^* into the Navier-Stokes equations, the original form of the equation would still look like a momentum equation with *variable* viscosity dependent of the reduced pressure and with a *nonlinear* pressure source term*. However, in the original SIMPLE method the linear source term $\partial p/\partial x$ is substantial for the development of the pressure and velocity corrections. Hence introduction of the parameters q or q^* would require at least a careful revision of the derivation of pressure and velocity coupling for a SIMPLE-similar scheme. Nevertheless a momentum

---

*   For example, considering the simplified x-momentum equation 2.11

$$\frac{\partial p}{\partial x} = \frac{\partial}{\partial y}\left(\eta \cdot \frac{\partial u}{\partial y}\right)$$

and applying the reduced pressure definition equation 6.5

$$q = e^{-\alpha \cdot p},$$

x-momentum equation becomes

$$-\frac{1}{\alpha} \cdot \frac{1}{q} \cdot \frac{\partial q}{\partial x} = \frac{\partial}{\partial y}\left(\frac{\eta_0}{q} \cdot \frac{\partial u}{\partial y}\right).$$

equation in q or q* would remain non-linear, in contrast to the reduction of Reynolds equation to linearity with respect to the pressure and viscosity.

To reduce or overcome the non-linearity in the governing equations another variable description has to be found. It is not known whether there is any. Such a variable would give a new, different set of momentum and continuity equations requiring a new method of solution.

When a parameter contains additional information about the geometry, such as the parameter Φ^* or Φ', it cannot be introduced into the Cartesian form of the Navier-Stokes equations as no geometry information is incorporated in the equations. This information is normally introduced by discretisation or by transformation of the equations to body fitted co-ordinates. If it were possible to introduce a similar parameter into these transformed or discretised equations, again a new system of equations would have to be solved.

In conclusion, any introduction of variables would require the development, implementation and testing of new equations and a method of coupling the developed momentum to the developed continuity equation. It would be expected that the development of such a method of coupling would be of similar complexity to the development of SIMPLE-algorithms or the vorticity-stream function approach. Hence, the implementation of this method could be expected to require a major effort.

Regarding the quality, it is expected, due to observations described in subsection 6.1.3.2, that the described effort could result in converging results for a wider range of parameters than the pure form of the direct method of coupling, but could not be as successful as e.g. a Newton-Raphson or inverse technique.

7.2.2   Inverse methods

7.2.2.1   Inverse solution of the flow equations

The inverse method of subsection 6.1.4 is characterised by the solution of the Reynolds equation for the height of the gap while the pressure is prescribed and a superimposed correction of this pressure. Regarding the first, the established calculation schemes to solve the Navier-Stokes equations and the continuity equation are designed for the converse, the determination of the pressure for a given geometry. In the Cartesian form of the Navier-Stokes equations the height geometry is not included. This information is brought into the equations either by discretisation or by the transformation of the equations to body-fitted co-ordinates. Additionally, in these equations, the pressure is only known at the boundaries of the flow, and unknown in the domain. A special purpose method of coupling the discretised momentum and continuity equations to solve the transformed equations for the height with given pressure boundaries would be necessary. As stated for the direct methods, the implementation of such a new method is expected to be a major effort.

Alternatively, an iterative method searching for the correct shape of the gap for given pressure distributions can be considered.

One proposal is that an initial shape of the gap is guessed. For this shape of the gap the pressure distribution can be calculated using the Navier-Stokes solver with the boundary conditions assuming tangentially moving walls. The calculated pressure is then compared with the given pressure distribution. If there are differences, the shape of the gap is changed and the calculation repeated until convergence is obtained. The correction of the shape could be realised for example by a Newton-Raphson scheme with the height as the unknown value $\bar{x}_u{}^*$ and the difference between the desired and the given pressure as the residual $\bar{F}$ which should diminish. However this method would suffer from the fact that the determination of the pressure has to

---

*   cf. subsection 6.1.6.1

consider the pressure-viscosity dependency. As mentioned in subsection 7.2.1.2 for direct methods, this innermost loop will fail to converge.

Alternatively, for a given shape of the gap also the pressure distribution – or a combination of tangential velocity and pressure – at the walls can be prescribed as boundary conditions. Then the Navier-Stokes solver returns the normal flow through the surfaces which means that the non-fulfilment of the obvious velocity boundary condition of no entrainment through the wall is quantified. Again with a Newton-Raphson method, the shape of the gap could then be determined by minimising the entrainment flow through the wall. For such an approach, neither the numerical performance of the Navier-Stokes solver nor of the Newton-Raphson scheme is known.

7.2.2.2   Correction of the pressure distribution

Once a hydrodynamic shape of the gap is found with a new algorithm or an iterative search, the pressure correction must be undertaken. This uncovers another problem. The method such as proposed by Archard, Gair and Hirst [10], in which the correction is determined from the deflection equation, will suffer from the circumstance that it returns only a single pressure adaptation, but no information as to how the pressure varies between the two surfaces. This problem can be overcome by adopting Eller's idea [7] to consider also the flow description. However with the set of flow equations 3.38 and 3.39, the flow description is not available in a self contained form as it is with Reynolds equation for Eller.

An alternate idea to overcome the problem is to start with identical pressure distributions for both surfaces, but to treat them separately for the determination of the hydrodynamic and elastic shape determination and for the pressure corrections due to the contour differences on both surfaces.

7.2.2.3   Discussion of scheme

An inverse method seems to be desirable due to the fact that it shows a good convergence behaviour for Reynolds equation.

However the iterative search contained in the method leads to some drawbacks. The convergence behaviour of a Newton-Raphson technique leading to the final shape of the gap has not yet been investigated. The solution of the Navier-Stokes equations within the innermost loop makes the calculation delicate to convergence problems and is likely to be extremely time-consuming, or, if other boundary conditions are considered, unpredictable. However, it allows the scheme to employ established solution methods for the Navier-Stokes equations contributing to easy implementation and allowing the use of commercially available CFD software packages.

Also the fact that the pressure distribution at both surfaces must be treated separately makes the method cumbersome and its performance unpredictable.

As for all methods the algorithm can be easily extended to thermal problems by a superimposed loop. Alternatively, the Navier-Stokes equations could be solved taking thermal effects into account. Due to the iterative determination of the shape of the gap even an extension of the calculation method to the point contact problem would be possible but again cumbersome.

7.2.3   Hybrid methods

Hybrid methods combine elements of the direct and the inverse solution schemes. Since both schemes can be implemented with a solver for the Navier-Stokes equations, the hybrid method can also be implemented. The problems and drawbacks discussed for the inverse solution will occur similarly for hybrid methods. In addition, the effort to iterate the various sections would appear.

7.2.4   Grubin style methods

In the Grubin style methods the coupling problem is solved by assuming a rigid stamp-elastic cylinder model, subsection 6.1.2.1. The fluid flow equation is solved in the inlet and outlet zones but not in the central high pressure region where the gap is always assumed to be parallel. In the zones where the fluid flow is calculated, a direct method of coupling is used. This allows the easy application of any of the established solvers for the Navier-Stokes

equations. The algorithm requires a frequent solution of the Navier-Stokes equations which might cause considerable calculation times. The major drawback of the method lies in the assumption of a parallel gap in the heavily loaded zone. This assumption is reasonable for an isothermal and incompressible Reynolds equation based solution, but hides information when considering thermal or compressible effects. Accordingly, expected changes due to the additional viscous effects in the highly loaded zone on the shape of the gap cannot be investigated. However, as for Reynolds equation based solutions, where the error due to the assumption of the parallel gap can be determined, a detailed error consideration and further evidence for the need for the extended approach could be obtained.

7.2.5   Newton-Raphson techniques

7.2.5.1   Basic considerations

Fully simultaneous coupling of the three equations describing the ehl problem can be realised by the Newton-Raphson technique: All three variables, pressure, viscosity and height of the gap, are assumed to be unknown in Reynolds equation at the same time. Thus Reynolds equation is understood as highly non-linear. For the solution, a pressure distribution is prescribed and the non-fulfilment, i.e. the residual vector, of Reynolds equation is quantified. With the knowledge of the residual change due to a pressure change, i.e. the Jacobian matrix, the non-fulfilment is then minimised. Since the Reynolds equation is, as shown in section 2.1, the integral continuity equation, into which the x-momentum equation has been incorporated, the residuals to be reduced are the mass continuity residuals.

SIMPLE based, and vorticity-stream function based, Navier-Stokes equation solvers modify the pressure, rather than keeping it prescribed, and aim to iteratively minimise the continuity residuals. Consequently, they do not return the desired residuals and hence cannot be used for a Newton-Raphson method without being adapted.

The realisation of the Newton-Raphson technique for the extended approach must rather attempt the solution of both momentum equations with a

prescribed pressure, so that the non-fulfilment, i.e. the residual vector, of the continuity equation is returned, even if that is likely to require an iterative procedure. For the general considerations of fluid flow, two forms of the continuity equation are available. Normally, the differential form of the continuity equation

$$\frac{\partial u}{\partial x} + \frac{\partial v}{\partial y} = 0 \qquad (7.1)$$

is used, but when considering, for example, fluid flow in a gap, often the integral form can be employed

$$\frac{d\left(\int_{y=lower\,surface}^{y=upper\,surface} u \cdot dy\right)}{dx} = 0 \qquad (7.2).$$

Consequently, schemes for both forms of the continuity equation are considered in the following.

7.2.5.2   Fully simultaneous method

The fully simultaneous method is based on the differential continuity equation 7.1. In order to obtain the residual vector for a given pressure distribution, the shape of the gap and the viscosity distribution are first calculated for this pressure distribution. Then the velocity components in the x- and y-direction are calculated from the respective momentum equations. Since both momentum equations include velocity components in both directions, an iterative solution of these two equations is necessary. After the determination of the velocity components, all information is available to calculate the residuals. The derivative terms of the Jacobian matrix for the Newton-Raphson method can be numerically determined: One point of the pressure vector is slightly varied and the residual vector is recalculated in the same way as for the original pressure vector. The complete Jacobian matrix is then inverted and pressure corrections can be determined and applied. This loop is repeated until convergence is reached. The central height of the gap can be determined by considering the overall load within the Jacobian matrix as mentioned in subsection 6.1.6.2 or by adding a superimposed loop, as

discussed in subsection 6.1.6.3. The algorithm with this latter scheme is shown in figure 7.3.
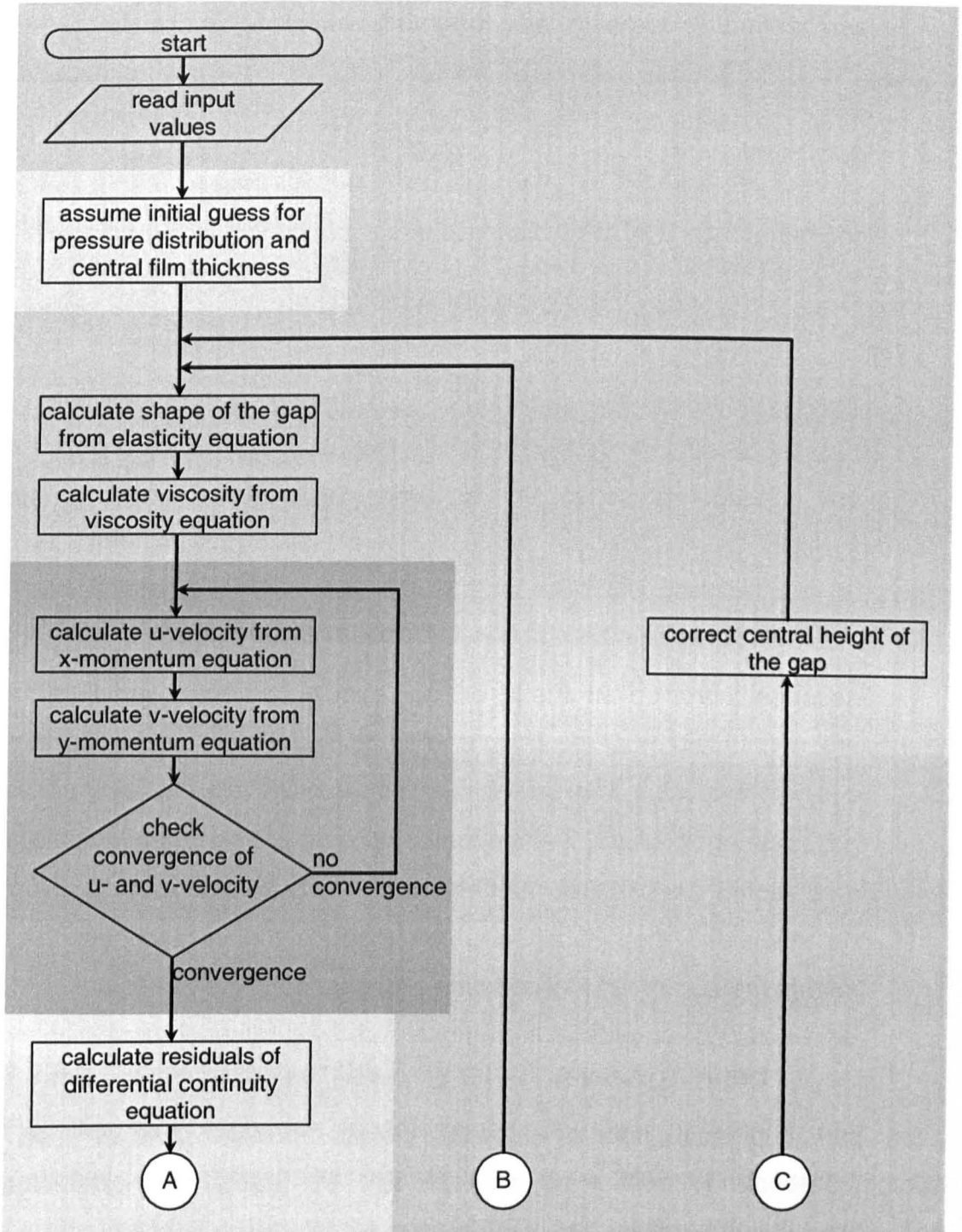
Figure 7.3:   Calculation scheme for the fully simultaneous Newton-Raphson method to solve the ehl problem using the complete Navier-Stokes equations
(continued).
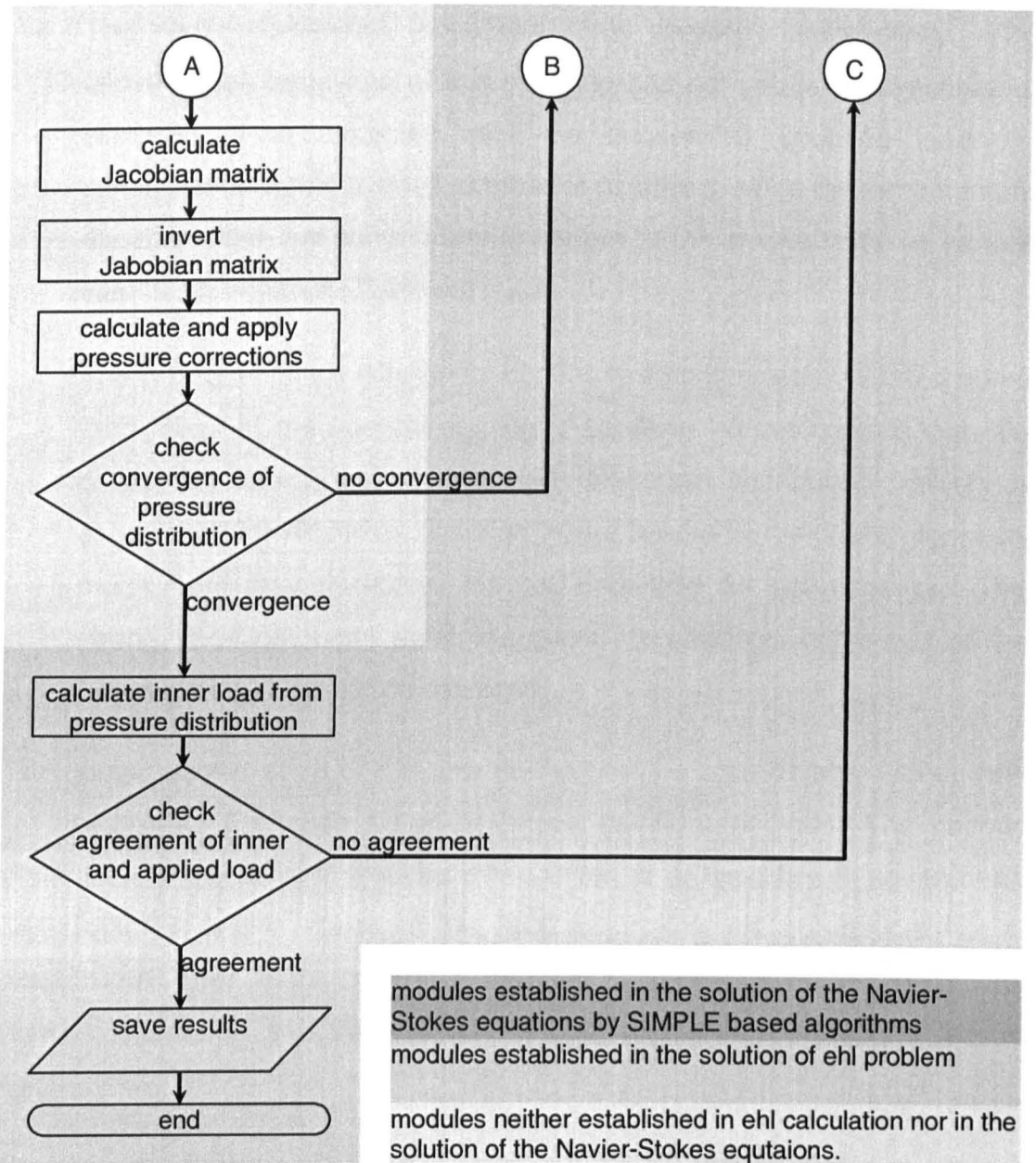
Figure 7.3:   (concluded).

7.2.5.3   Discussion of the fully simultaneous method

The Reynolds equation based Newton-Raphson technique has been established throughout the last decades as a form of standard method because of its balance between robustness and range of convergence. The proposed method is expected to show similar performance. However, two details differ from the established scheme and hinder the prediction of the performance of the method.

- ◆ The two momentum equations are coupled successively. The convergence behaviour of this coupling has not yet been investigated. However, it is expected that the successive coupling leads to convergence within a small number of iterations, since the x-momentum equation does not contain any important terms of v-velocity, as can be seen from equations 3.36 and 3.42.

- ◆ The residuals of the differential continuity equation are evaluated rather than those of the integral continuity equation. In comparison with the perpendicularly constant Hertzian pressure distribution, which is established for Reynolds equation based solutions, residuals might vary much more strongly across the gap than they do along the gap. This strong variation might spoil the good convergence behaviour of the Reynolds equation based solutions.

The computational effort of the new method will be considerably higher than for established Reynolds equation based solution methods. The second dimension in the contact requires a resolution of at least five to seven cells. Determination and inversion of the Jacobian matrix rise quadratically or at least more than linear with the number of elements. Additionally, the numerical solution and the iteration of both momentum equations require further time.

When comparing the calculation method with the SIMPLE based solution schemes it can be seen that many components appear in both techniques. This means that experience gained in SIMPLE based methods can be used. Eventually even the adaptation of SIMPLE based commercially available software codes can be considered.

Vorticity stream-function based solutions of the Navier-Stokes equations solve pressure field implicitly and are hence not suitable for the Newton-Raphson technique applied in this manner.

7.2.5.4   Combined successive-simultaneous method

In order to reduce the numerical effort and to overcome the problems with the uncertain numerical behaviour due to the perpendicular pressure variation, a method was developed employing the integral continuity equation as established for Reynolds equation based solutions. The proposed method is illustrated in figure 7.4.

When returning to the evaluation of the integral continuity equation, only a one-dimensional pressure variation along one line of the gap can be determined within the Newton-Raphson process. The definition of this line is arbitrary, for example one of the surfaces or the centreline between. The pressure corrections perpendicular to the gap must be determined separately. This is realised by solving the y-momentum equation for the pressure and not for v-velocity. Any necessary v-velocity components can be determined from the continuity equation in its differential form. Since the pressure variation across the height of the gap influences its height, the viscosity distribution, and hence the u-velocity profile, the above loop must be repeated until convergence is reached for the pressure distribution across the height of the gap. The residuals for the Jacobian matrix to determine the longitudinal pressure corrections at the selected line can then be calculated numerically by again using the previously mentioned algorithm. Determination and application of the longitudinal pressure corrections is repeated in the usual manner until convergence is reached. The determination of the central height of the gap representing the equilibrium of applied load and pressure is realised by an additional superimposed loop, but could also be realised fully simultaneously within the fluid flow equations, as mentioned in subsections 6.1.6.3 and 7.2.5.2.
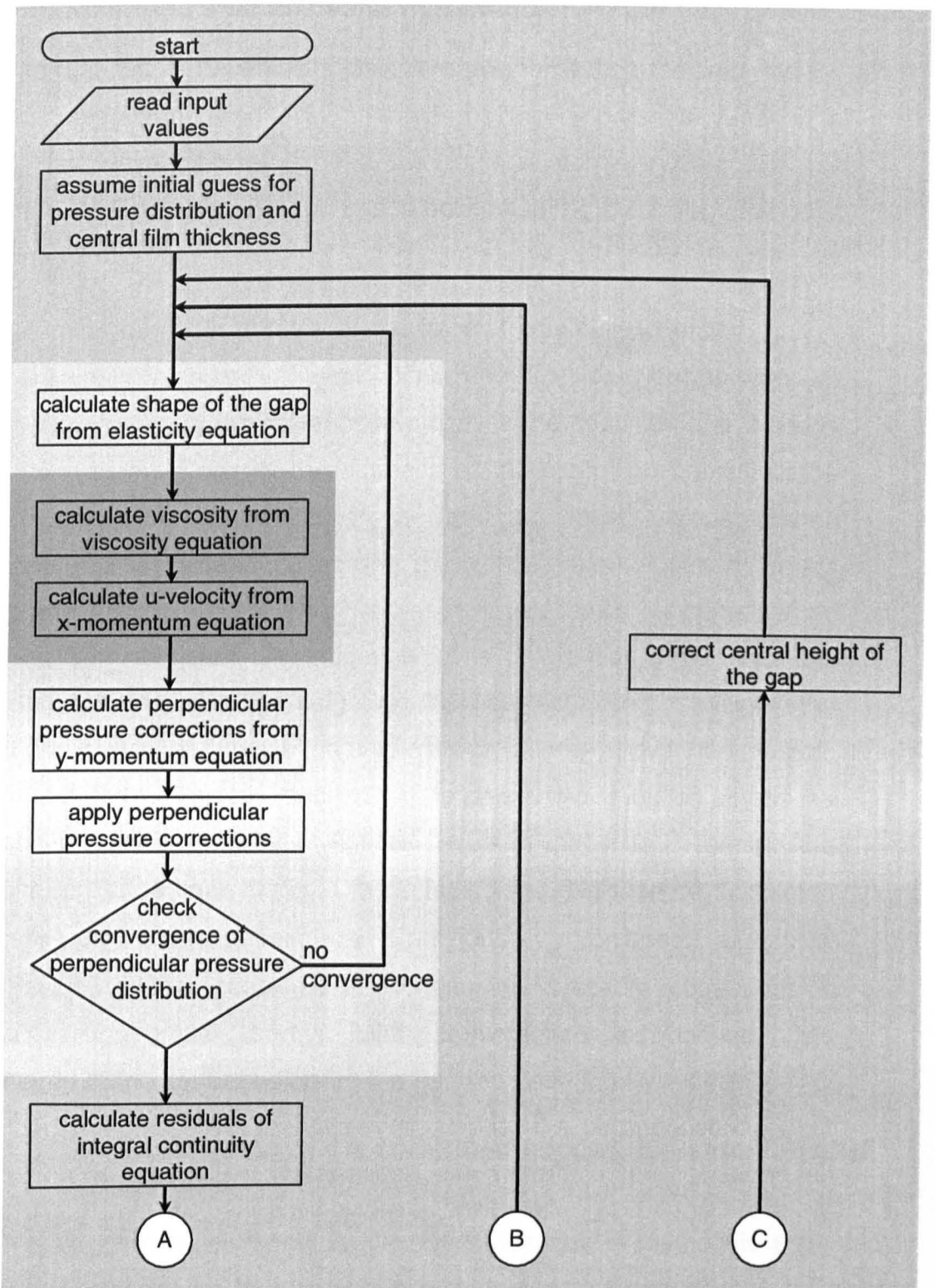
Figure 7.4:   Calculation   scheme   for   the   combined   successive-
simultaneous   Newton-Raphson   method   to   solve   the   ehl
problem using the complete Navier-Stokes equations
(continued).
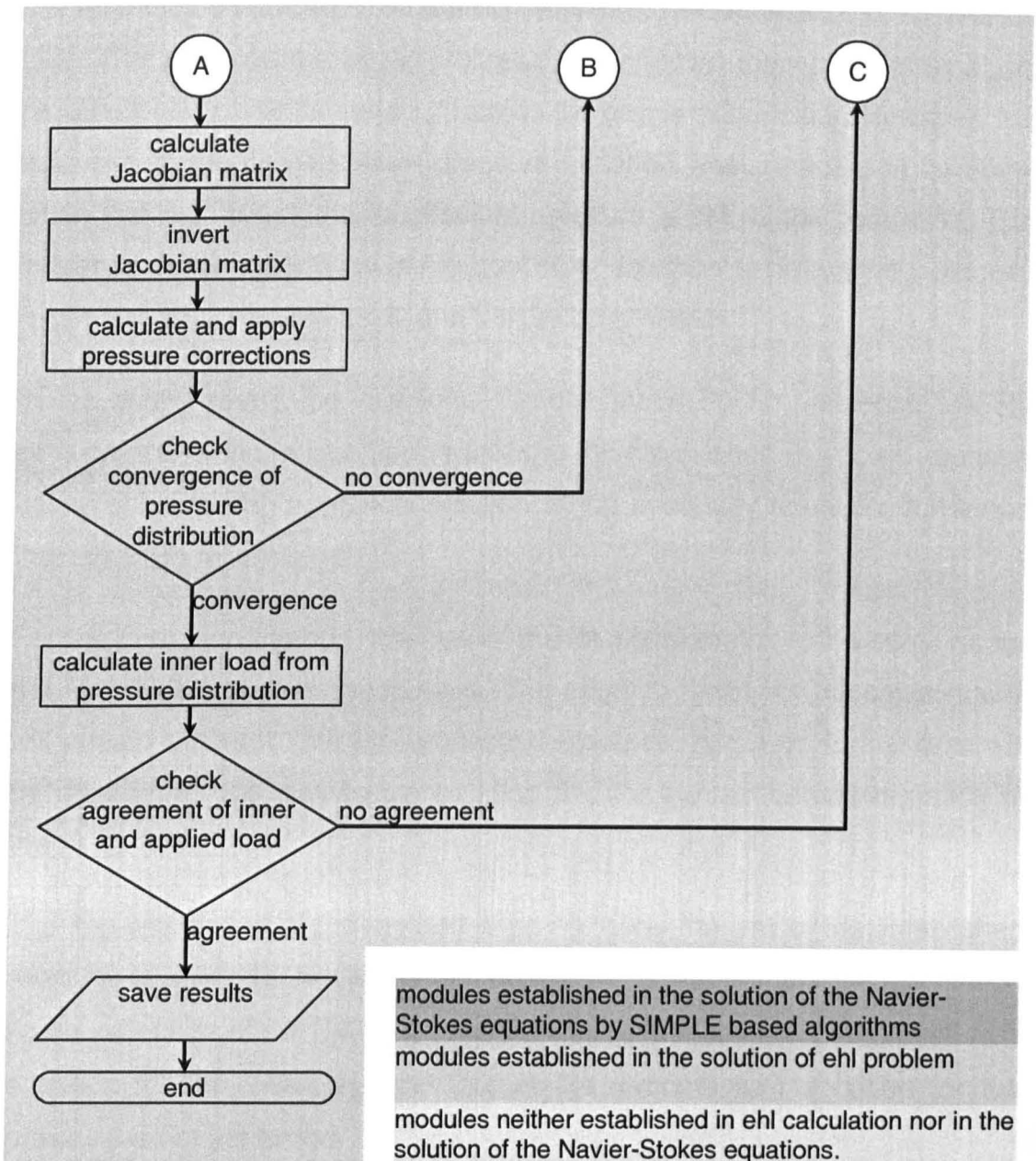
Figure 7.4:   (concluded).

7.2.5.5   Discussion of the combined successive-simultaneous method

The suggested combined successive-simultaneous method is expected to follow basically the behaviour of Reynolds equation based Newton-Raphson methods. However, some details differ from the established Newton-Raphson technique and were expected to influence the performance. The integration of the continuity equation is carried out analytically in the isothermal Reynolds equation based solutions. In the present case, the mass flow must be integrated numerically. The numerical method is expected to require exact methods since exact numerical methods are also essential in

the Reynolds equation based thermal solutions as discussed e.g. by Welsch [13]. The performance of the successively coupled loop to determine the perpendicular pressure variation across the gap is still unclear. However, the influence of the perpendicular pressure variation was expected to be small when the line, where the longitudinal pressure is set, is the centreline. The influence of the application of the continuity equation to determine v-velocity might also influence residuals and the Jacobian matrix.

In the cases where the additional viscous terms do not influence the ehl solution, the proposed method reduces to the established Reynolds equation based solution with numerical solution of the continuity equation, a method that is known to converge.

For the proposed method, the size of the Jacobian matrix is the same as for the Reynolds equation based case. The effort to invert the Jacobian matrix will remain similar to that for established solutions. However, further time will be required for the successive coupling and for the numerical integration of the mass flow.

The implementation of the method does not allow the use of the established methods to solve the Navier-Stokes equations. Some parts of the calculation agree with parts of the SIMPLE based code, but the solution of the continuity equation for the v-velocity and that of the y-momentum equation for the pressure is not yet tested.

For the same reason as for the fully simultaneous method, the combined successive-simultaneous method cannot be combined with a vorticity-stream function approach.

7.2.5.6   Extension of methods

Both methods can be extended to thermal problems. As for all methods, this can be done by introducing a superimposed loop as discussed in section 6.1.8. However, similar to other methods, the extension can also be incorporated in the iteration of the two momentum equations, similar as in the SIMPLE scheme. The extension to non-Newtonian fluid behaviour is possible using the methods established for SIMPLE algorithms, subsection 6.2.3.

Both methods can also be extended to three-dimensional problems. However, particularly for the fully simultaneous method, the calculation would require enormous computational resources.

7.2.5.7   Truncated Jacobian matrices

Both proposed methods, the fully simultaneous and the successive-simultaneous method, require iterative procedures to determine the mass continuity residuals in comparison to non-iterative solutions of equations for the Reynolds equation based solution. This means, in comparison with a Reynolds equation based solution, the contribution of the mass continuity residual determination to the total computational time will rise in comparison to the time required for the inversion of Jacobian matrix. In addition, one converged iterative procedure delivers residual data for all locations of the analysed domain. Hence opposite to the Reynolds equation based Newton-Raphson technique, the effort to determine one or all residual values at a time is identical. Hence a method using as many residuals as possible at one time is advantageous.

Additionally, since the residual analysis causes the most significant increase in analysis time, the method with a minimum number of residual evaluations should be chosen. The number of evaluations is the number of elements n plus one per Newton-Raphson step independent of the width of the Jacobian matrix but also per sweep of the multigrid technique of subsection 6.1.7 if simply the determination of the residuals is changed and the rest of the method remains unchanged. Since the Newton-Raphson method with the inversion of a full Jacobian matrix needs the minimum number of steps or sweeps, it is preferable.

A substantial advantage might be a multigrid method which can deal with a full sequence of equations, however, this is outside the capabilities of the methods proposed and discussed for Reynolds equation based ehl problems in Lubrecht [8] or Press et al. [76].

7.3   General comparison and selection of method

In section 7.2, a number of different methods were presented and discussed. In the present section, a brief comparison and evaluation of the methods with a view to the specification of section 4.3 is given, in order to select the most suitable method. The results of this evaluation are summarised in table 7.1.

♦ **Principal influences**

All methods with exception for the Grubin-type methods can be used for the principal investigation of the isothermal line contact problem with the additional viscous terms. Due to the assumption of a parallel gap, Grubin-type methods are unsuitable for the investigation.

♦ **Flexibility**

Basically all methods allow the extension to investigate further effects such as compressible, thermal or transient flow. An extension to three dimensions is not possible with the vorticity-stream function approach. However, a replacement of the vorticity-stream function approach by a SIMPLE based method is always possible.

♦ **Implementation effort**

Two aspects are considered when evaluating the implementation effort: Firstly, it is evaluated to what degree components of the respective scheme have been already employed elsewhere, so that the behaviour, any problems and respective solutions can be transposed. The second aspect is the extent of the scheme itself and the number of different operations and iterations which have to be implemented and tested.

Concerning the former point, the direct method of coupling using a modified pressure parameter and non-iterative forms of the inverse method are the most difficult methods to implement since neither suitable equations nor methods of coupling are available for them. The iterative forms of the inverse method require an iterative search for the hydrodynamic shape and a revised pressure correction strategy, both not yet tested. A corresponding implementation effort is necessary for the hybrid methods. Both Newton-Raphson methods mainly contain

well-known algorithms but contain one iteration loop for which the convergence behaviour cannot be predicted. In the direct method employing the real pressure and the Grubin style method, the Navier-Stokes equations solvers can replace the Reynolds equation solvers without any further changes in the scheme. This means that the implementation only consists of the combination of well established modules and is therefore straightforward.

With regard to the latter aspect, the complexity of the method itself, the iterative inverse method needs one more loop of iteration and correction and is therefore evaluated to require more implementation effort than the Newton Raphson technique.

♦ **Performance**

The main requirement is for a robust solver capable of dealing with a wide range of load and speed parameters. The direct method of coupling using the real pressure is expected to converge only for a very limited range of parameters and is therefore evaluated to be unsuitable for the present extended ehl problem. A slightly wider, but nevertheless insufficient range of parameters, is expected when employing the direct method with any modified pressure variables. Good numerical performance is expected for a range of four methods, the inverse, the hybrid and the two Newton-Raphson techniques. The Grubin-type method is expected to maintain its excellent numerical behaviour.

Summarising the above details, it becomes clear that Grubin-type methods and direct methods cannot be employed due to essential drawbacks which would not allow a successful investigation. The direct method was evaluated to be the worst of acceptable methods. Of the remaining methods, the Newton-Raphson techniques seem to have advantages in comparison with inverse and hybrid methods. The two Newton-Raphson methods are relatively similar in structure and neither of the methods show significant advantages. Hence it was decided to implement and test both the fully simultaneous and the combined successive-simultaneous Newton-Raphson method.

7.4   Application of commercially available software

After selection of suitable methods of solution the implementation of the scheme is to be realised. According to the specification, section 4.3, maximum flexibility, maximum robustness and minimum implementation effort was desired. In order to fulfil the specification, it was anticipated to consider the application of commercially available software tools and components. Three types of software were found which could possibly be used for the solution of the ehl problem with the extended set of equations: structural analysis packages, mathematical libraries and SIMPLE based CFD packages to solve the Navier-Stokes equations. It is discussed in the following whether the application of commercial software will lead to expected fulfilment of the specification.

Structural analysis software can be used as a tool to calculate the matrix of influence numbers to determine the deflection of the solid surfaces and hence the shape of the gap. However, since application and implementation of the Boussinesq equation are expected to be both simple and fast, the application of structural analysis software was rejected.

Mathematical libraries, such as NAG [100] or IMSL [101], can be used, as for example by Welsch [13], for the efficient solution of the discretised equations or inversion of the Jacobian matrix. However, other effects, such as discretisation of equations and the generation of an appropriate grid, are not supported. The employment of appropriate tools is therefore desired.

CFD software offers a much wider range of support. These codes provide many of the features which have to be implemented for the solution of the ehl problem. Such components are, for example,

♦   use of the exact governing equations,

♦   interfaces to introduce user-defined description of the fluid properties such as viscosity and density,

♦   discretisation and grid-generation for the geometry,

Method \ Criteria	Direct method employing real pressure	Direct method employing modified pressure parameter	Inverse method	Hybrid method	Grubin-type method	Full simultaneous Newton-Raphson method	Combined successive –simultaneous Newton-Raphson method
Description see section	7.2.1.1	7.2.1.3	7.2.2	7.2.3	7.2.4	7.2.5.2	7.2.5.4
Principal influences	++	++	++	++	--	++	++
Flexibility	++	-	++	++	++	++	++
Implementation effort	++	o	o	o	++	+	+
Performance	--	-	o	o	++	+	+
Overall evaluation	--	-	o	o	--	+	+

Table 7.1:   Evaluation of calculation schemes for the ehl calculation taking additional viscous effects into account;

++   means specification criterion is perfectly fulfilled,

+   means specification criterion is fulfilled with some minor problems,

o   means specification criteria is reasonably fulfilled,

-    means specification criterion is not fulfilled,

--   means specification criteria is not fulfilled and the complete method is not suitable for the investigation.

♦ correct, grid-independent coupling of the Navier-Stokes and the continuity equation,

♦ advanced and efficient numerical solvers adapted to the purpose, and

♦ possible extension to thermal calculations.

However, the complete SIMPLE-based algorithm cannot be used unchanged by the promising calculation schemes. The following problems must be solved:

♦ the pressure corrections and the velocity corrections of the SIMPLE sequence must be switched off, other equations must be added,

♦ the variation of the geometry during calculation, and

♦ the implementation of the Newton Raphson scheme.

These requirements are discussed in the following.

7.4.1   Switching off particular equations

A number of different methods are available to realise the switching off of certain equations in the SIMPLE algorithm. The most obvious and most convenient is simply to delete the appropriate components in the source code of the CFD program. That would require full access to the code, which is very unusual for such commercial packages. Other possibilities are, for example, to reset the appropriate values to zero in a later and accessible program module, to suppress them by extreme under-relaxation, or to manipulate the equation matrices in an appropriate way.

7.4.2   Adding modules

Similar to the switching off of particular modules of the SIMPLE code, the addition of modules can be realised: The most straightforward way would be the adding of appropriate subroutines to the source code of the program which would again require access to the source code. Alternatively, user-defined subroutines within the program can be used to introduce additional data code.

7.4.3   Variation of geometry

Variation of geometry is essential for all calculation schemes and can be realised either by coupling outside the code, i.e. program coupling, or inside the code, i.e. solver coupling, both introduced in section 6.2.4 and illustrated

in figure 7.5. In the former method, geometry calculation is carried out outside the CFD code by user-defined code. Each time results from the modified SIMPLE algorithm are required, the CFD code must be started. The method is expected to require a great deal of file handling to transfer the respective geometry data into the CFD code and to return the pressure results. In addition, each time the CFD code is started, its time consuming initialisation sequence must be carried out. Hence, a variation of the geometry inside the CFD code is perceived as being a more efficient method. This can be realised using the capabilities of a transient calculation. Each new solution of the modified SIMPLE algorithm is considered to be a new time step with a new geometry. Hence, the method requires that the code allows a change of geometry between time steps. With the suggested procedure being the solution of a steady state problem by a transient calculation, it must be ensured that transient terms do not influence the result. However, since Reynolds number is small, the influence is expected to be small, and can be influenced by adopting large time steps. Nevertheless, a switching off of the transient terms would be desirable.

(a) outer coupling

user defined code

modified steady state CFD code

(b) inner coupling

user defined code

modified transient CFD code
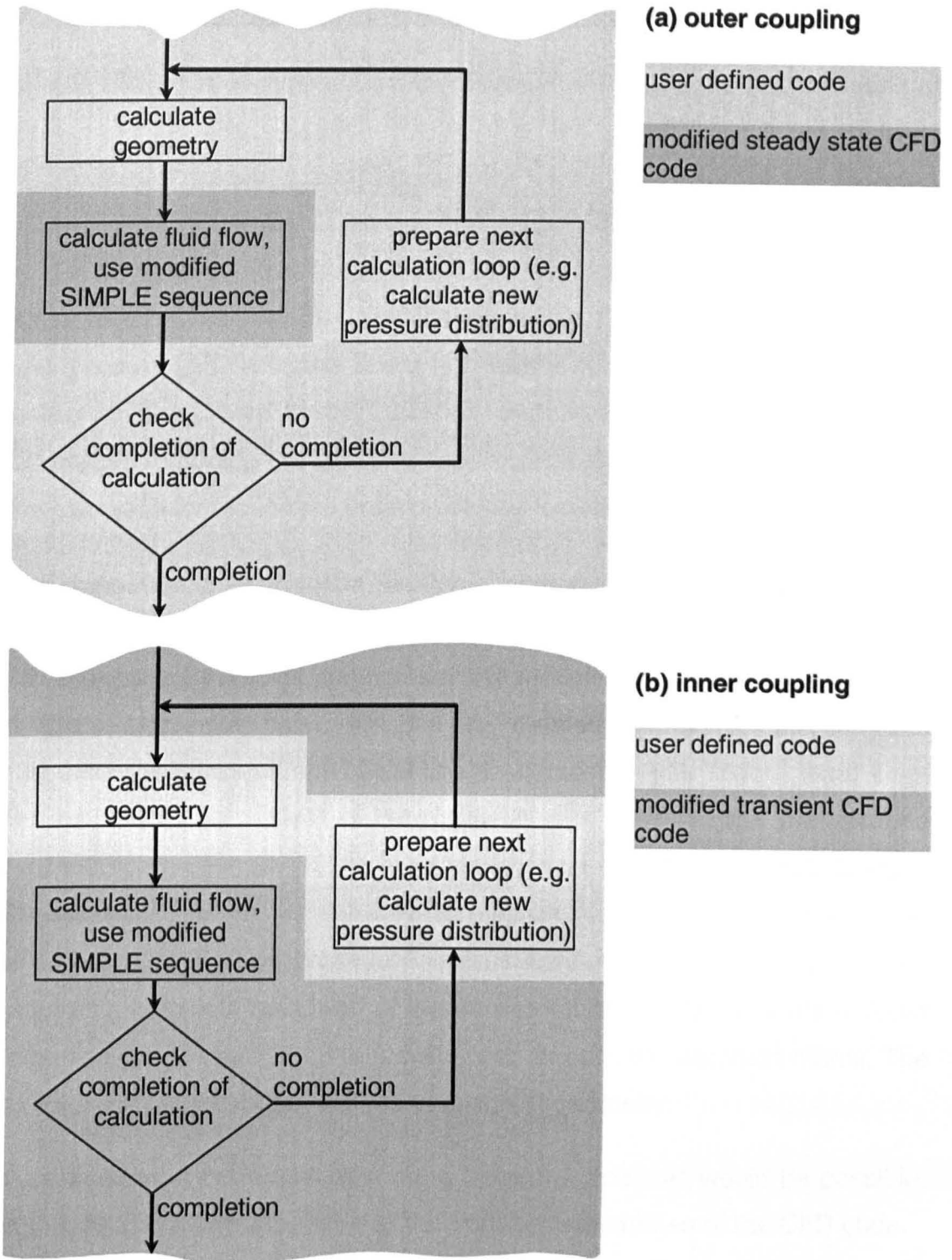
Figure 7.5:   Coupling of the modified CFD code and variable geometry by coupling (a) outside the code, i.e. program coupling, and (b) inside the code, i.e. solver coupling.

7.4.4   Implementation of the Newton-Raphson technique

Newton-Raphson techniques normally require the analytical determination of derivatives for the Jacobian matrix. For the present case, numerically approximated gradients must be used for the determination of the Jacobian matrix. The calculation scheme and the necessary extensions for the numerical determination of the Jacobian matrix are shown in figure 7.6. This figure also shows that the combination of the Newton-Raphson technique and modified CFD software is easily possible by coupling outside the code, similar to that shown for the geometry variation above. Consequently, the drawbacks regarding file handling and frequent initialisation of the CFD code are also valid for the implementation of Newton-Raphson techniques.

The realisation of the Newton-Raphson scheme within a CFD code requires a rearrangement of the calculation scheme for outer coupling shown in figure 7.6. Using the CFD code, the residual calculation is called at one point in the program sequence only. As for the variable geometry, the transient calculation feature of the CFD code is used. After each time step, represented by calculation of the residuals, it is decided, in a user-defined subroutine, at which part of the Newton-Raphson scheme the calculation is at the moment. The results are then treated appropriately and the next time-step is prepared. The procedure is illustrated in figure 7.7. The method requires a complete switch-off of the transient terms of the calculation. Even large time steps would lead to a systematic error in the Jacobian matrix. The method can be combined with the variation of geometry.

An extension of the above method to transient problems would be possible, but would require manipulation of the transient capabilities of the CFD code.

```
  ( start )
      │
      ▼
assume initial guess          alter first element of
for unknown vector            vector of unknowns
      │                            │
      ▼                            ▼
calculate residual            calculate residuals
vector                        for altered vector of        alter next element of
                              unknowns                     vector of unknowns
      │                            │                            ▲
      ▼                            ▼                       reset altered element
calculate                     calculate and store              of the
Jacobian matrix               line of Jacobian            vector of unknowns
      │                            │                       to original value
      ▼                            ▼
invert Jacobian                  check
matrix                         whether          Jacobian matrix
                              Jacobian matrix    not completed
      │                        completed
      ▼                            │
calculate and apply           Jacobian matrix completed
correction for vector              │
of unknowns                        ▼
      │                       reset last element of
      ▼                       vector of unknowns
     check              no    to original value
  convergence        convergence
      │
 convergence
      ▼
   ( end )
```

modified steady state CFD code

user developed code

Figure 7.6:   *Calculation scheme for the Newton-Raphson method approximating the derivatives numerically. Realisation of the method using a modified CFD code using outer coupling, i.e. program coupling.*

The above considerations show that the application of CFD software to the ehl problem requires a CFD program that can be adapted by the user. If available, such a code can reduce much of the implementation effort, but any adaptation will require a detailed knowledge of the code. It is understood that any adaptation may influence the performance of the code, e.g. for the combined successive-simultaneous method, where the y-momentum equation must be solved for the pressure gradient in the perpendicular direction, discretisation by the user is necessary. Care must be taken to

maintain consistency of the original with any implemented equations. Although there are some problems which appear when adapting commercially available CFD codes, it was expected that the advantages dominate the drawbacks. Therefore, the adaptation was pursued.
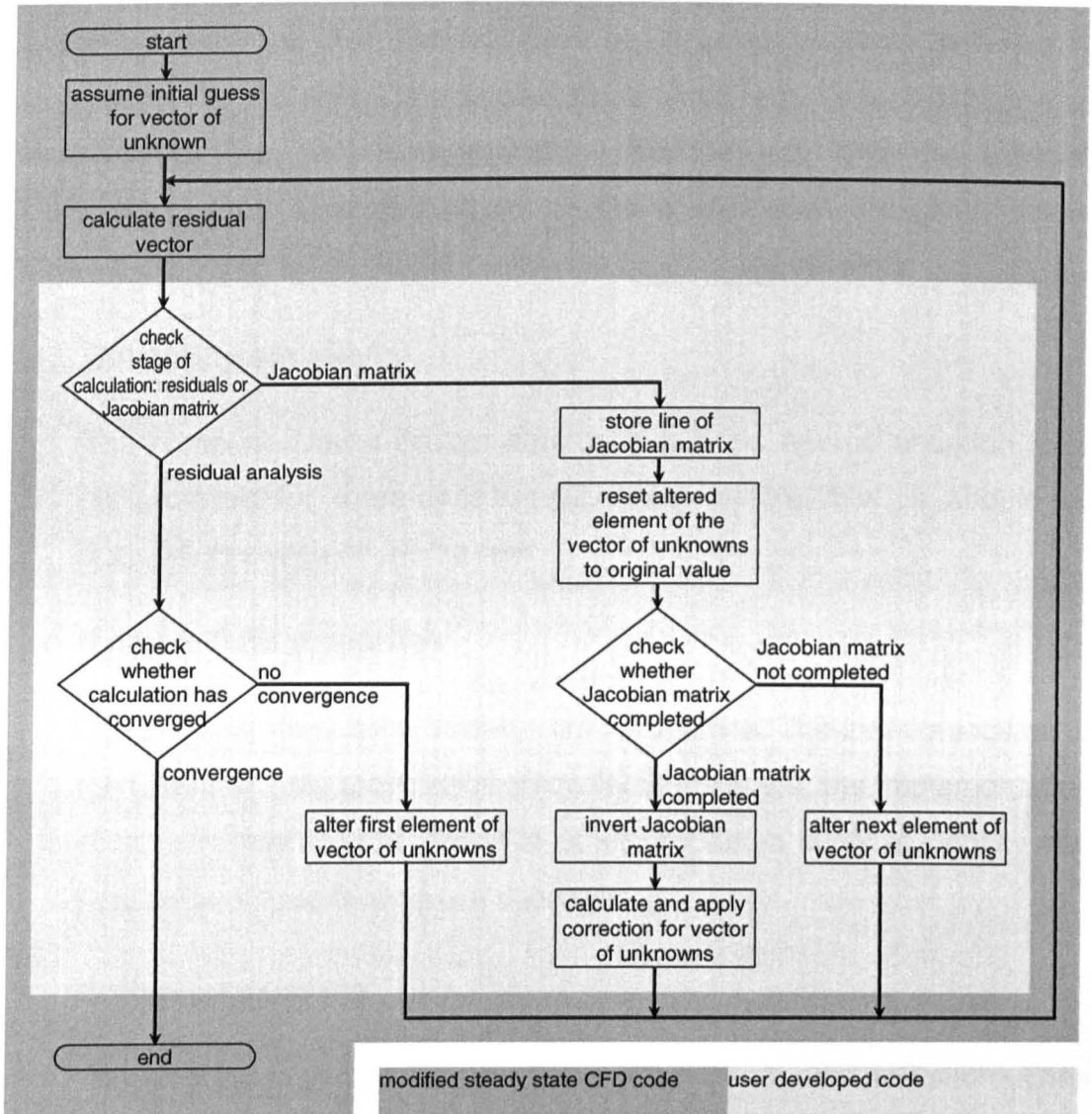
Figure 7.7:   *Calculation scheme for the Newton-Raphson method approximating the derivatives numerically. Realisation of the method within a CFD code.*

7.5   Selection of suitable CFD software

7.5.1   Specification for CFD software

It was concluded that the application of commercially available CFD software makes implementation easier. However, the code must allow for adaptation to the ehl problem. For the selection of the most suitable software, a specification for the software was developed using requirements which were derived from the general specification, section 4.3, and the selected numerical method. Essential details of the specification are given below, however the exact list of requirements was much more detailed.

◆ **Governing equations**

   The complete Navier-Stokes equations and the energy equation must be provided for three-dimensional, compressible flow. It should be possible to switch off inertia terms.

◆ **Variable fluid properties**

   The program must allow variable fluid properties. The implementation of user-defined laws to describe viscosity is essential, the implementation of user-defined laws to describe other properties such as density and heat capacity coefficients are desirable.

◆ **Method of coupling**

   The program must allow the implementation of user defined subroutines to enable the calculation of pressure corrections using the Newton-Raphson method. The program must also allow the change of geometry during the calculation procedure. It must be possible to switch off certain modules of the code. It should be possible to change all the variables at arbitrary positions in the code.

Rating of priority was assigned to all requirements to indicate whether the requirement was essential, necessary or desirable.

7.5.2   Survey of available software

Advertisements in journals and the internet were searched for available CFD codes. A list of codes is given in table 7.2. Only commercial software products were considered to ensure maximum state of the art regarding physical models, numerical techniques and user support.

Name of the code	Developer of the code	Internet address
ADINA-F	ADINA R & D, Inc.	www.adina.com
CFDesign	Blue Ridge Numerics	www.cfdesign.com
CFD-ACE	CFDRC	www.cfdrc.com
CFX-4.2	AEA Technology	www.ansys.com
FASTEST	INVENT computing GmbH	*
FIDAP	Fluid Dynamics International *	www.fluent.com
FIRE	AVL List GmbH	www.avl.com
FLOW-3D	Flow Science, Inc.	www.flow3d.com
FLOWPLUS	Blue Ridge Numerics	www.cfdesign.com
FLOTRAN	ANSYS, Inc.	www.ansys.com
FLUENT	Fluent, Inc.	www.fluent.com
P3/CFD[†]	PDA Engineering	www.mscsoftware.com
PAMFLOW	PSI	www.esi-group.com
PHOENICS	CHAM	www.cham.co.uk
STAR CD	Computational Dynamics	www.cd-adapco.com

Table 7.2:   Available commercial CFD software, code developer (state August 1995), and homepage (state December 2004).

---

[*]   Provider is out of business (state December 2004).
      Former internet address: www.invent-computing.de.

[†]   Program name is now MSc Nastran for Windows CFD (state December 2004).

7.5.3   Selection of CFD software

All the above software was analysed to establish whether the requirements could be fulfilled by the particular code. The information was obtained from technical brochures for the programs and from personal discussion with the distributors. A detailed evaluation scheme was used to take the rating of priority as well as the degree of fulfilment into account. A survey of all the results is given in table 7.3. CFX-4.2 was found to be most suitable for the calculation. Other programs such as PHOENICS, FIRE and STAR CD are also assessed to be basically adaptable to ehl calculations.

Specification criteria / Program	Governing equations	Fluid properties	Numerical method
ADINA-F	-	-	
CFDesign	-		
CFD-ACE	o	o	-
CFX-4	+	+	+
FASTEST	+	+	-
FIDAP	+	+	-
FIRE	o	+	o
FLOW-3D	+	-	
FLOWPLUS	o	o	-
FLOTRAN	o	-	
FLUENT	+	+	o
P3/CFD	-		
PAM FLOW	-		
PHOENICS	+	+	o
STAR CD	+	o	o

Table 7.3:   Evaluation of available commercial CFD software;

+   means all requirements are fulfilled;

o   means essential requirements are fulfilled, but some necessary or desirable requirements are not or only partially fulfilled; investigation of the ehl problem would still be possible;

-      means essential requirements are not fulfilled; investigation of the ehl problem could not be carried out using this code; this assessment means that further requirements may not be evaluated, because the code could not be used.

Chapter 8

Implementation assuming constant pressure across the height of the gap

As a first step, a calculation method was implemented assuming constant pressure across the gap. The extension to variable pressure across the gap is described and discussed in chapter 9. This stepwise approach contains some advantages. The physical model for this simplified method is based on Reynolds equation and hence is well established. However, the adaptation of CFD software is novel. This enabled attention to be concentrated on the analysis and evaluation of the numerical method. On the other hand, this simplified method represents a special case of both proposed numerical schemes. Hence, the method implemented can easily be extended to allow variable pressure across the gap.

8.1   Implementation details

The implementation comprises the practical application of the ideas presented in sections 7.2 to 7.4 to the selected CFD code, CFX-4.2. The implementation required an exact knowledge of the calculation scheme of the CFD code. The scheme was analysed from the code manuals [91] and from tests with the software. The program structure, which was determined, is given in figure 8.1. It shows particularly the interfaces for user-defined adaptations. The following subsections widely refer to figure 8.1. A complete calculation scheme showing all the implementations is given at the end of the present section in figure 8.6.

(a)

* **transport equations:**
  - x-momentum equation
  - y-momentum equation
  - z-momentum equation
  - pressure correction equation
  - energy equation
  - user defined equations
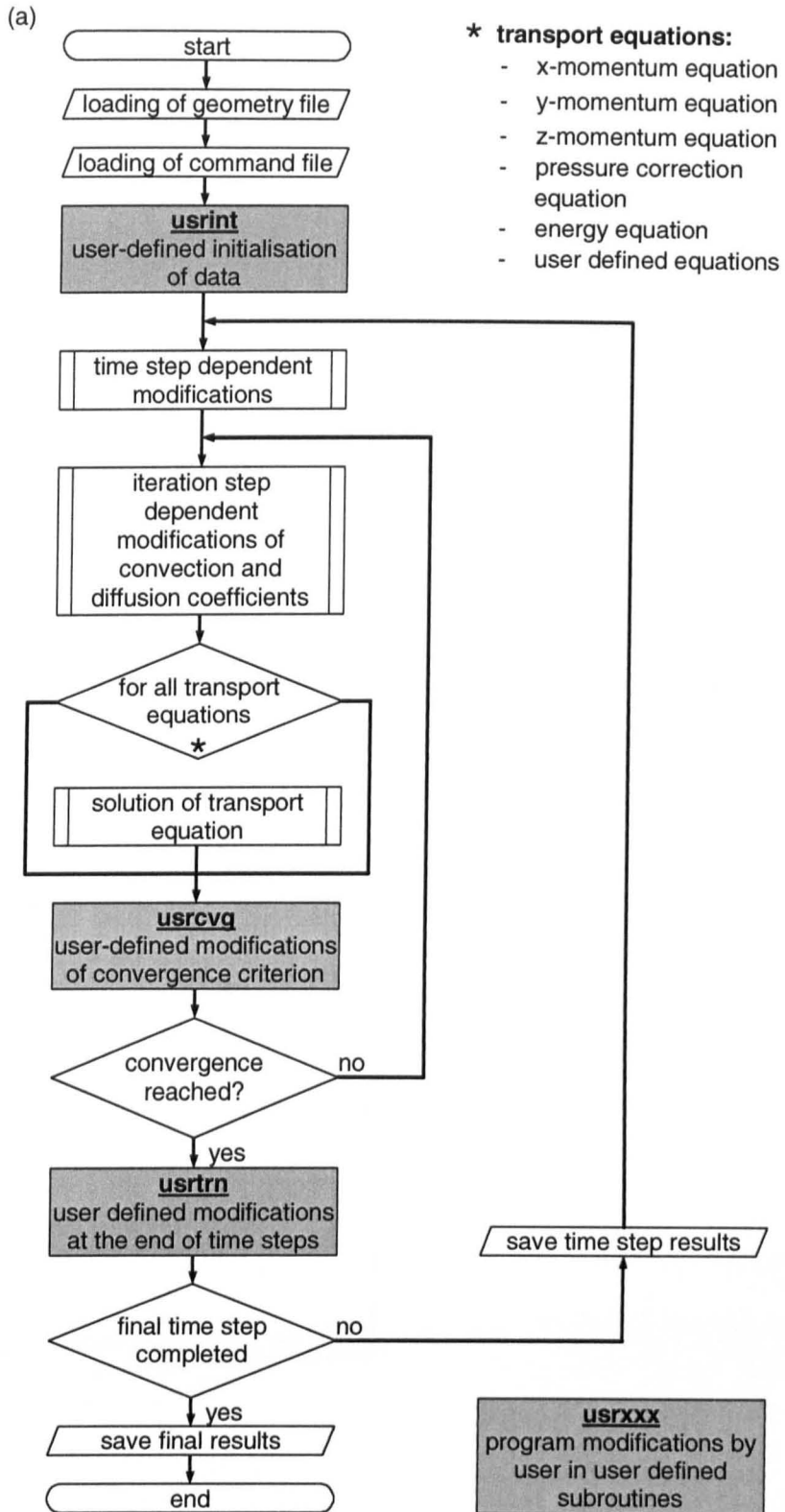
Figure 8.1:   *Relevant parts of calculation scheme of the CFD software CFX-4 for solution of the ehl problem:*
(a) main calculation scheme,
(b) time step dependent modifications,
(c) iteration step dependent modifications,
(d) solution of transport equation
(continued).

(b)   time step dependent modifications

(c)   iteration step dependent modifications
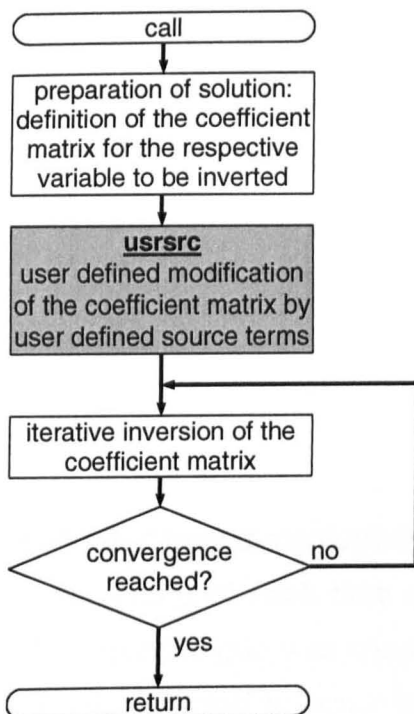
Figure 8.1:   *(concluded).*

8.1.1   Switching off modules

The calculation method requires the switching off of the pressure and velocity corrections. A complete deletion of the pressure correcting subroutines was not possible. Therefore the coefficients of the matrix for the determination of pressure corrections for all points along and across the gap were manipulated within the subroutine USRSRC so that all values became zero:

$$\Delta p_{i,j} = 0 \qquad\qquad (8.1).$$

The zero pressure correction values lead automatically to zero velocity corrections. This procedure was preferred to strong relaxation of the pressure correction results, because pressure correction relaxation does not lead to zero velocity corrections. These corrected velocities can falsify the residuals of the continuity equation and hence spoil the Newton-Raphson scheme. Details of the residual calculation are given in subsection 8.3.3.

8.1.2   Viscosity variation

Barus' description was implemented in the user-defined subroutine USRVIS, dedicated by the code for the introduction of a user-defined viscosity prescription,

$$\eta_{i,j} = \eta_0 \cdot e^{\alpha \cdot p_{i,j}} \qquad\qquad (8.2).$$

8.1.3   Grid calculation

Grid variation during the calculation was realised by the subroutine USRGRD which is dedicated to grid manipulation and is called during code initialisation and at the beginning of each time step. A uniform grid was used in the x-direction. This uniform grid was chosen since influences due to the extended approach were expected to occur all along the heavily loaded zone of the contact and zones of particular interest could not be predicted in advance.

In the y-direction, two different approaches were implemented: firstly the established method as nearly always used e.g. by [8, 13, 17], where all deformations and curvatures are applied to one surface as illustrated in figure 8.2(a). Secondly the rather more correct method, illustrated in figure 8.2(b), in which the deformations and curvatures are applied to the corresponding

surfaces. The first method was applied in the present chapter aiming at the reproduction of established Reynolds equation based results. The benefit of the latter is considered in chapter 10.3.

The calculation of the deformation of the solid differs slightly from the established approaches because the CFD code is based on a finite volume method (FVM) where the pressure is calculated and is available at the centre of the volumes but the geometry is described at the corners of the volume. Two approaches were applied, a zeroth order and a first order approximation. The zeroth order approximation is fully consistent with the calculation of surface forces of the CFD code, while the first order approach is more accurate. More details of the grid calculation are given in appendix G.

(a)

(b)
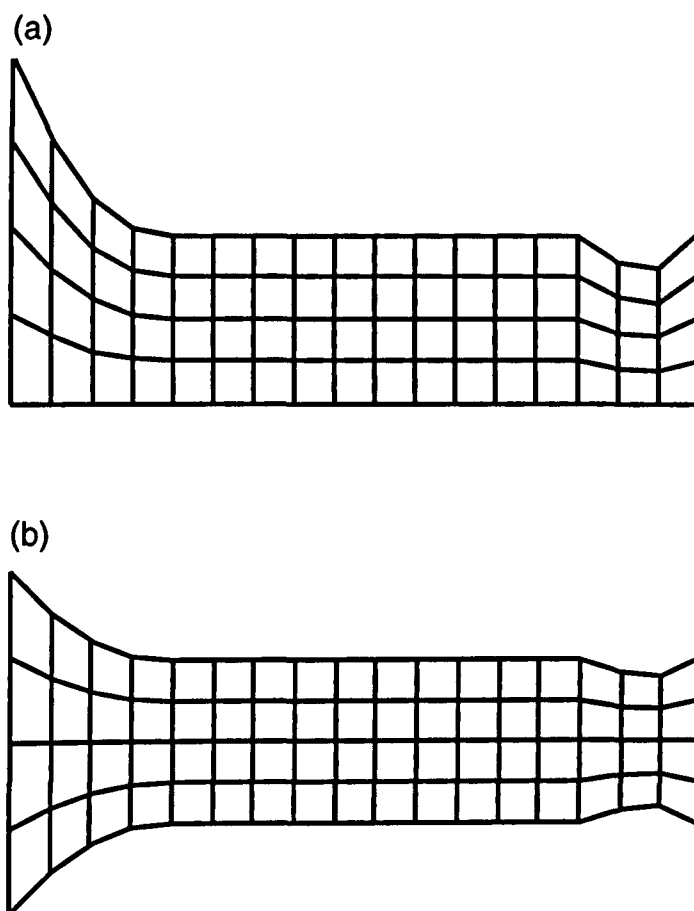
Figure 8.2:   *Established geometry distribution assuming all contributions to one surface (a) and real geometry distribution assuming identical surface curvatures and material properties (b).*

The fact that, in the finite volume discretisation of the CFD code, some values are determined and available for the centre of the finite volumes but others at the corners, edges or faces of the volumes requires some particular treatment of the indexing of variables. A small letter represents a position at the centre of a finite volume, and a capital letter a position at its surface. This is not only relevant for the grid determination but also for other aspects discussed in the following.

8.1.4   Fluid flow boundary conditions

The same boundary conditions as used in Reynolds equation based solutions were applied and are shown in figure 8.3. The code only requires the input of keywords. The software allows the input of tangential and normal velocity components, not necessitating the Cartesian components.[*]

♦ At both solid surfaces the tangential velocity and the velocity perpendicular to the wall were set to the surface velocities and zero respectively

$$V_{tangential\ i,1} = u_1 \qquad V_{tangential\ i,M} = u_2$$
$$V_{normal\ i,1} = 0.0 \left[\tfrac{m}{s}\right] \quad \text{and} \quad V_{normal\ i,M} = 0.0 \left[\tfrac{m}{s}\right] \qquad \text{(8.3a, b).}$$

♦ At the inlet the pressure was assumed to be zero:

$$p_{1,j} = 0.0 \ [Pa] \qquad\qquad \text{(8.3c).}$$

♦ At the outlet the pressure was assumed to be zero:

$$p_{N,j} = 0.0 \ [Pa] \qquad\qquad \text{(8.3d).}$$

---

[*]   The boundary conditions obtain the mixed indexing with one capital and one small letters because the values are defined at the centre (small letter) of the edge (capital letter) of the adjoining finite volume.

Upper surface: J = M
wall boundary condition

$$V_{tangential \ i,M} = U_2$$

$$V_{normal \ i,M} = 0.0 \left[\frac{m}{s}\right]$$

Inlet: I = 1
pressure boundary condition
$$p_{1,j} = 0.0 \ [Pa]$$

Outlet: I = N
pressure boundary condition
$$p_{N,j} = 0.0 \ [Pa]$$

Lower surface: J = 1
wall boundary condition

$$V_{tangential \ i,1} = U_1$$

$$V_{normal \ i,1} = 0.0 \left[\frac{m}{s}\right]$$
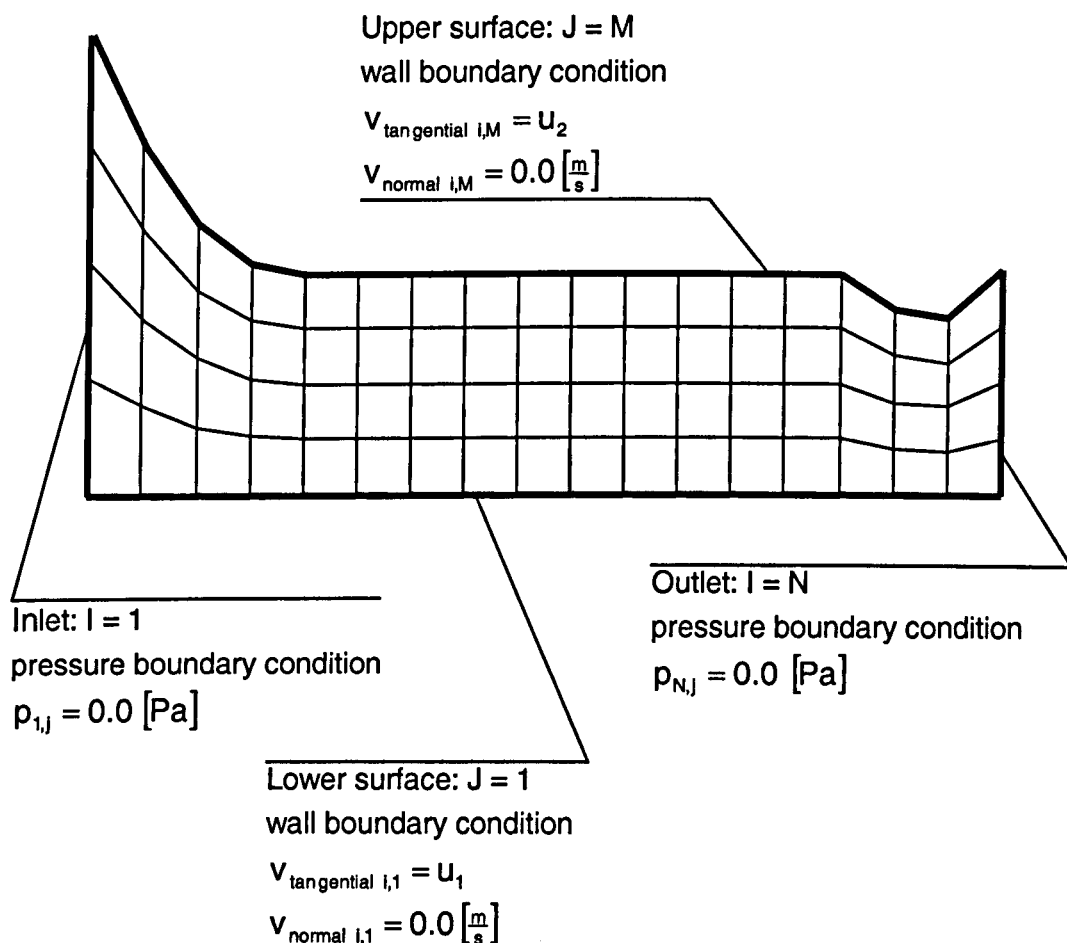
Figure 8.3:   Boundary conditions for the ehl problem using CFD software.

When the location of the outlet boundary is chosen correctly, the above Dirichlet boundary condition automatically fulfils the widely used cavitation boundary condition described e.g. by Dowson and Higginson [17]

$$p = 0.0 \ [Pa] \quad \text{and} \quad \frac{\partial p}{\partial x} = 0.0 \left[\tfrac{Pa}{m}\right] \qquad (8.4).$$

The correct choice of the outlet boundary condition can be automated in a superimposed loop [8]. Tests using a Reynolds equation based solution scheme showed that the exact iterative calculation for the outlet position is time consuming. Therefore, for the principal test of the program the location of the outlet boundary was set to be fixed.

8.1.5   Convergence criteria of fluid flow calculation

The CFD calculation scheme requires the fulfilment of convergence criteria to complete a time step. Within the SIMPLE algorithm the pressure correction or the continuity equation are normally used for the check of overall convergence. However, since the pressure corrections were set to zero, the calculation cannot be controlled by this default convergence criterion; the residuals of the continuity equation are required for the Newton-Raphson scheme. Instead of the continuity equation the x- and y-momentum equations must be evaluated. This can be realised by two methods. The more general one is to use the subroutine USRCVG where user-defined convergence criteria can be calculated from the actual values of the variables. The second method is to use the capabilities of the code, which are provided when using the so-called advanced time stepping transient analysis: with this feature of the applied code, any variable can be evaluated without any user-defined programming.

8.1.6   Newton-Raphson method

The Newton-Raphson method was implemented as suggested in section 7.4 by solver coupling. The transient calculation capabilities of the CFD code were adapted using the user-defined subroutine USRTRN after each time step. Depending on the progress at the end of the different time steps, three options were available:

(i)   The current time step had the purpose of determining the residuals for a given pressure distribution, and, if convergence is not yet reached, a new Jacobian matrix has to be generated. This is carried out from the next time step, and, as preparation for this time step, the pressure in the first column of finite volumes is modified.

(ii)   The current time step had the purpose of determining a row of elements of the Jacobian matrix and these values are determined now. If the Jacobian matrix is not yet completed, the currently still modified pressure to determine the gradients is reset for the treated column of finite volumes, and, as preparation for the following time step, the pressure in the next column of finite volumes is modified.

(iii) The current time step had the purpose of determining a row of elements of the Jacobian matrix and these values are determined now. Because the Jacobian matrix is now complete, pressure corrections can now be determined by inversion of the Jacobian matrix. The corrected pressure is applied as preparation for the following residual determination.

Since analytical derivatives could not be obtained from the code, the Jacobian matrix elements were determined numerically. The selection of the numerical parameters for the Newton-Raphson method is discussed in subsection 8.3.3.

For the determination of the residuals of the continuity equation, the mass flow through the finite volume faces was considered rather than the velocity components. The mass flow values are much more accurate than the velocity at the cell centres. This is due to the Rhie and Chow method of avoiding numerical oscillations [95] when solving the Navier-Stokes equations. It is to be expected that the use of these accurate values also avoids the convergence problems which appear when numerical integration across the height of the gap is necessary for the thermal Reynolds equation solutions. These problems are reported e.g. by Welsch [13] or Liesegang [36].

Using the above mass flow values, the calculation of residuals for the differential and integral continuity equations is very similar. Calculation of the differential residuals is carried out by summing the fluid flow over all the (four) faces of the volume. Calculation of the integral residuals means only adding the differential residuals over a column of volumes. Thus, the flow through inner surfaces cancels out, again resulting in the integral residual of the continuity equation, which is illustrated in figure 8.4.

Although the flow rates through the inner surfaces cancel out, some accuracy for these values is required to avoid the residuals being spoiled by these values. This requires some knowledge of the v-velocity field, and hence a solution for the y-momentum equation is required but it does not have to be perfectly converged. Hence a solution for the v-velocity field, obtained with the minimum number of iterations, is considered in the calculation scheme.

Inversion of the Jacobian matrix was carried out by employment of the routine library IMSL and its inversion routine DLINGR [101].

(a)   (b)
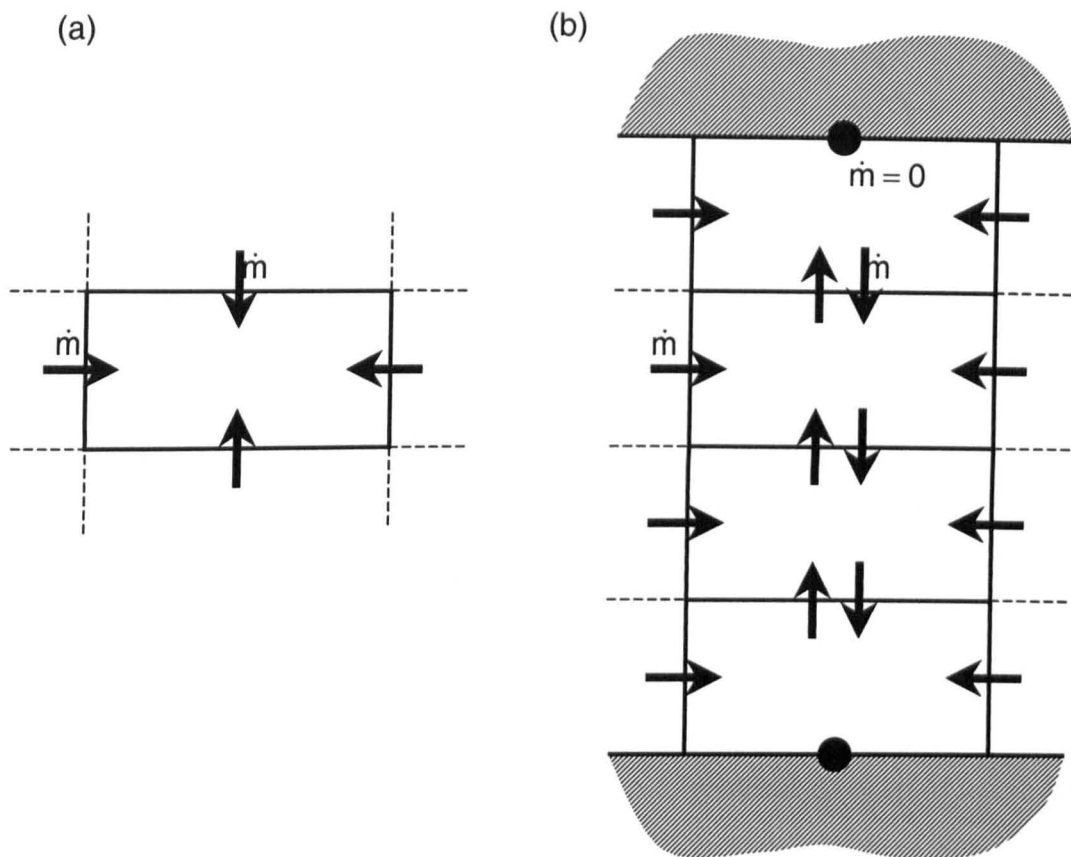
Figure 8.4:   Residual calculations for the continuity equation;
               (a) the differential continuity equation,
               (b) the integral continuity equation.

8.1.7   Initial values

As an initial value for the pressure distribution, the Hertzian pressure distribution was assumed within the Hertzian pressure zone with zero pressure being assumed everywhere else

$$p = p_{hz} \cdot \sqrt{x^2 - b_{hz}^2} \quad \text{for} \quad |x| \le b_{hz}$$
$$p = 0 \quad \text{for} \quad |x| > b_{hz}$$

(8.5).

Figure 8.5 illustrates the initial pressure distribution and the resulting shape of the gap.
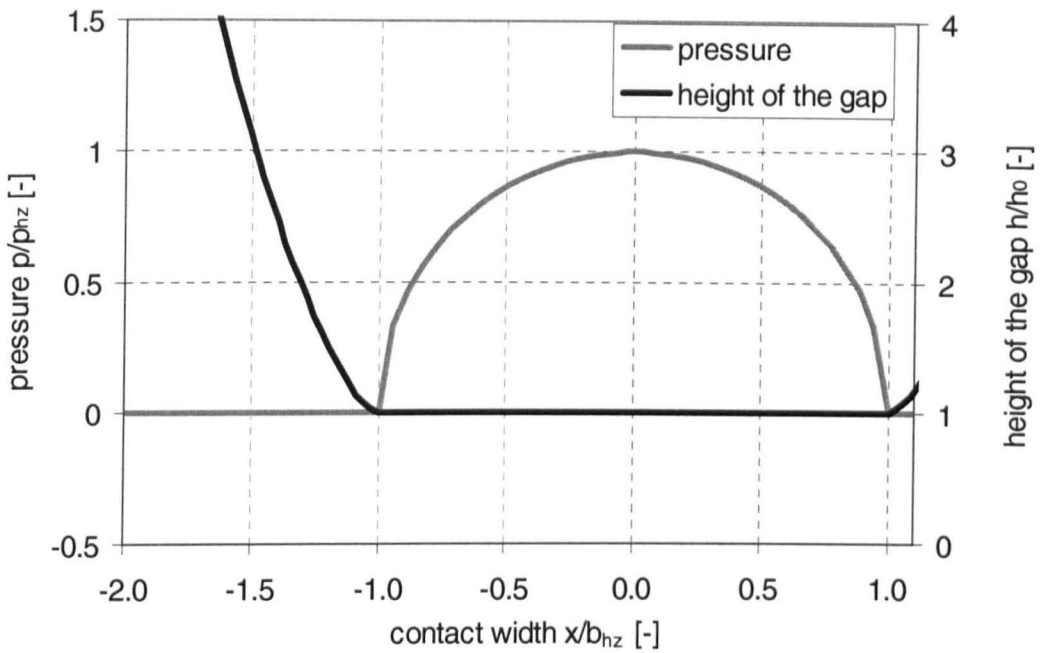
Figure 8.5:   *Initial pressure distribution for ehl problem using CFD software and resulting shape of the gap.*

8.1.8   Height correction

The correction of the central height of the gap to give equilibrium of inner and applied load was realised, as suggested in subsection 7.2.5, by a superimposed loop. As for the control of the Newton-Raphson scheme, the user subroutine USRTRN was used at the end of each time step to undertake the necessary actions.

For the central height of the gap h_0 the approximation of equation 3.26 was used:

$$h_0 = 1.9 \cdot G^{0.6} \cdot U^{0.7} \cdot W^{-0.13} \cdot r_{red} \tag{8.6}$$

The initialisation of the values was realised within the user-defined subroutine USRINT.

(a)

```
                        ╭──────────────────────────╮
                        │          start           │
                        ╰──────────────────────────╯
                                    │
                          ╱─────────────────────────╱
                         ╱   loading of command file╱
                        ╱─────────────────────────╱
                                    │
                        ╱──────────────────────────────────╱
                       ╱  loading of rectangular geometry file╱
                      ╱──────────────────────────────────╱
                                    │
    ┌──────┬────────────────────────────────────────┐
    │usrint│                                         │
    │      │     initial pressure distribution       │
    │      │                                         │
    └──────┴────────────────────────────────────────┘
                                    │
                                    ▼◄──────────────────────┐
    ┌──────┬────────────────────────────────────────┐      │
    │usrgrd│    modification of grid using pressure   │      │
    │      │  distribution and Bousinessq's equation  │      │
    └──────┴────────────────────────────────────────┘      │
                                    │                       │
                                    ▼◄──────────────┐       │
    ┌──────┬────────────────────────────────────────┐      │
    │usrvis│ modification of viscosity distribution using │  │
    │      │     Barus' or Roelands' description      │      │
    └──────┴────────────────────────────────────────┘      │
                                    │                       │
        ┌────────────────────────────────────────┐          │
        │  solution of x-momentum equation for u- │          │
        │                velocity                 │          │
        └────────────────────────────────────────┘          │
                                    │                       │
        ┌────────────────────────────────────────┐          │
        │   pro-forma solution of y-momentum      │          │
        │       equation for v-velcoity           │          │
        └────────────────────────────────────────┘          │
                                    │                       │
    ┌──────┬────────────────────────────────────────┐      │
    │usrsrc│ modification of source terms for pressure │     │
    │      │   correction equation that Δp = 0        │      │
    └──────┴────────────────────────────────────────┘      │
                                    │                       │
        ┌────────────────────────────────────────┐          │
        │ pro-forma solution of pressure correction│         │
        │          equation with Δp = 0           │          │
        └────────────────────────────────────────┘          │
                                    │                       │
                               ╱◇╲                          │
                          u-momentum                        │
                    ◇ equation: convergence ◇── no ─────────┘
                          reached ?
                               ╲◇╱
                                    │ yes
    ┌──────┬────────────────────────────────────────┐
    │usrtrn│   Newton-Raphson technique handling      │
    └──────┴────────────────────────────────────────┘
                                    │
                               ╱◇╲
                             solution
                    ◇      completed?      ◇── no ──────────┐
                               ╲◇╱                          │
                                    │ yes                    │
                          ╱─────────────────╱
                         ╱ saving of results╱
                        ╱─────────────────╱
                                    │
                        ╭──────────────────────────╮
                        │           end            │
                        ╰──────────────────────────╯
```

Figure 8.6:   *Complete calculation scheme for the ehl calculation using CFD software showing all details*
(a) main program,
(b) details of Newton-Raphson technique handling
(continued).

(b)   Newton-Raphson technique handling
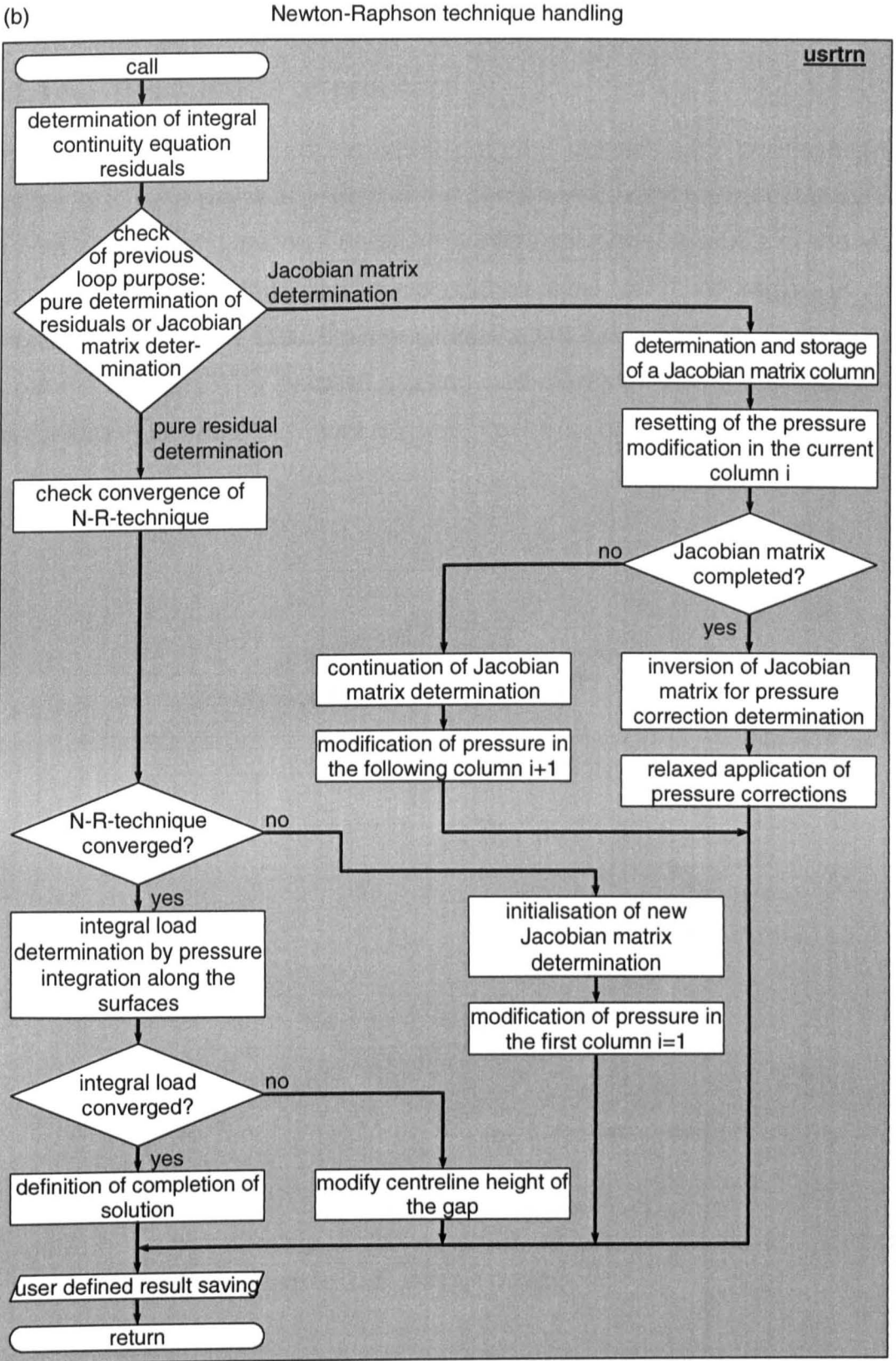
Figure 8.6:   *(concluded).*

8.2 Stabilising the solution method

8.2.1 Description of problem

The first tests with the implemented program did not lead to converging results for a wide range of values of the parameters, even where established methods based on Reynolds equation provide solutions. Analysis of the test calculations showed that oscillations start to build up in the region of the pressure spike, grow over the complete loaded zone and finally spoil the complete solution. The process starting and development of the pressure oscillations is illustrated in figure 8.7.
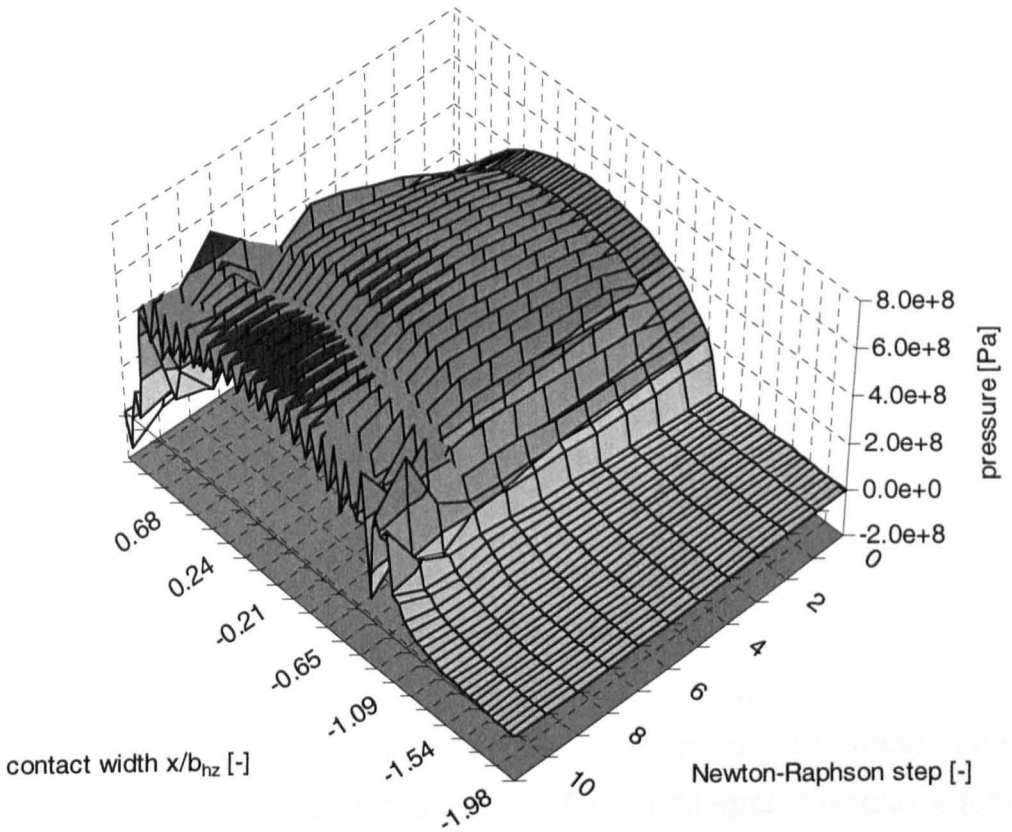
Figure 8.7: Development of the pressure distribution in the ehl contact during Newton-Raphson process.

8.2.2 Discussion of problem

To overcome the above problem various obvious measures were considered such as

- ◆ varying the numerical parameters of the calculation, as discussed in section 8.3,

- ◆ smoothing the pressure distribution after each Newton-Raphson step, or filtering high frequency oscillations out of pressure distribution, or

- ◆ refining the grid.

None of the above methods led to the necessary improvements.

Result graphs showing oscillating ehl problem results are presented, e.g. by Chang, Conry and Cusano [77] and Okamura [14]. Both show oscillating results due to coarse grid resolution, Chang, Conry and Cusano as an intermediate result subsequently refined on a finer grid of a multi-level analysis.

Additionally, Okamura [14] shows that oscillations could appear if the convergence of the gap is very small, i.e. the load is high and the Jacobian matrix is weakly conditioned. However, it was found that the initial oscillations were not due to insufficient accuracy of the Jacobian matrix inversion by the library routine, which was indicated by returned characteristic values from the inversion.

Another reason for the appearance of oscillations is the application of a second order, central approximation for the *first* order gradients in the governing Reynolds equation. As discussed in section 6.1.6.3, non-oscillating, converging results are obtained for a first order upwind discretisation of the pressure term $\partial p/\partial x$ for the integral Reynolds equation 2.5 and for first order upwind discretisation of the height gradient $\partial h/\partial x$ for the differential Reynolds equation 2.4.

The development and origin of the oscillations in the CFD code show a similar behaviour to those observed for a second order, central difference approximation of the first order gradient in Reynolds equation solution by Okamura [14]. The hypothesis that both phenomena might be the same is supported by the fact that, in the implemented CFD software based method, the height of the gap is determined for the corners of the finite volumes half

way between the volume centres, as discussed in subsection 8.1.3, independent of the flow direction. That means that, with respect to a finite volume, the corresponding height gradient is a central approximation from the two edges of a volume. Such central approximation of height terms causes oscillations for the differential Reynolds equation 2.4. Hence, it was concluded that the geometry determination in the CFD code based method must be adapted to introduce some effective upwinding to the ehl problem.

8.2.3   Solution approach

Changing the discretisation details of the CFD code was rejected as the code was not accessible in the necessary detail and an adaptation would mean a complete re-writing of the code.

Consequently it was decided to consider the practical differences between both discretisation schemes. If a function is curved convexly, central approximation means smaller gradients than the negative approximation and vice versa for a concavely curved function. This is clear from geometrical considerations, as in figure 8.8 or by mathematical means. For the second order central approximation of a first order differential

$$\frac{\partial f}{\partial x} = \frac{f_{i+1} - f_{i-1}}{2 \cdot \Delta x} + E_{trunc} \qquad (8.7)$$

the truncation error is according to Bronstein [102]

$$E_{trunc} = -\frac{1}{6} \cdot (\Delta x)^2 \cdot \frac{\partial^3 f}{\partial x^3} + \dots \qquad (8.8)$$

while for the first order negative approximation

$$\frac{\partial f}{\partial x} = \frac{f_i - f_{i-1}}{\Delta x} + E_{trunc} \qquad (8.9)$$

it is

$$E_{trunc} = +\frac{1}{2} \cdot \Delta x \cdot \frac{\partial^2 f}{\partial x^2} + \dots \qquad (8.10).$$

Since the truncation error of the first order negative approximation is greater than that of the second order central approximation, the difference between both approximations is

$$\frac{f_{i+1} - f_{i-1}}{2 \cdot \Delta x} - \frac{f_i - f_{i-1}}{\Delta x} = +\frac{1}{2} \cdot \Delta x \cdot \frac{\partial^2 f}{\partial x^2} \qquad (8.11).$$

convex curvature of function: $\dfrac{\partial^2 f}{\partial x^2} < 0$ concave curvature of function: $\dfrac{\partial^2 f}{\partial x^2} > 0$

$$\frac{f_i - f_{i-1}}{\Delta x} > \frac{f_{i+1} - f_{i-1}}{2 \cdot \Delta x} \qquad\qquad \frac{f_i - f_{i-1}}{\Delta x} < \frac{f_{i+1} - f_{i-1}}{2 \cdot \Delta x}$$
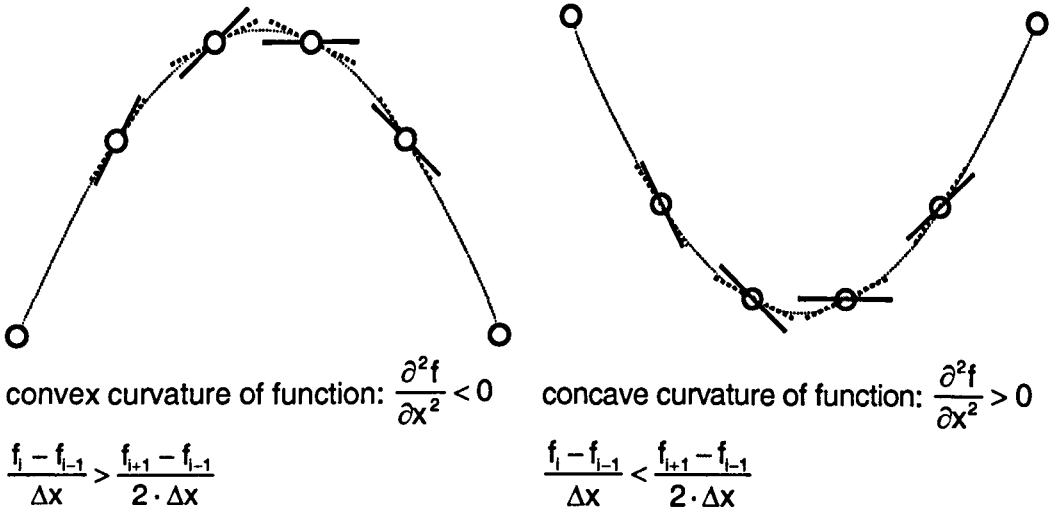
—— gradient assuming first order negative approximation $\dfrac{f_i - f_{i-1}}{\Delta x}$

······ gradient assuming second order central approximation $\dfrac{f_{i+1} - f_{i-1}}{2 \cdot \Delta x}$

Figure 8.8:   *Differences in gradients for first order negative and second order central approximation.*

The wish to obtain gradients as in the negative discretisation scheme would require the reduction of the gradients in the concavely and the increase of the gradients in the convexly curved sections of the function. At least qualitatively, these effects can be attained by moving the function half a grid-width to the right and retaining the use of central approximations. However, the shifting of the function leads to a change in the actual value of the function. The results from grid shifting are illustrated in figure 8.9.

convex curvature of function: $\dfrac{\partial^2 f}{\partial x^2} < 0$ concave curvature of function: $\dfrac{\partial^2 f}{\partial x^2} > 0$

$$\left.\frac{f_i - f_{i-1}}{\Delta x}\right|_{shifted} > \left.\frac{f_i - f_{i-1}}{\Delta x}\right|_{original} \qquad \left.\frac{f_i - f_{i-1}}{\Delta x}\right|_{shifted} < \left.\frac{f_i - f_{i-1}}{\Delta x}\right|_{original}$$

—— gradient assuming second order central approximation for the original grid

$$\left.\frac{f_i - f_{i-1}}{\Delta x}\right|_{original}$$

·········· gradient assuming second order central approximation for the shifted grid

$$\left.\frac{f_{i+1} - f_{i-1}}{2 \cdot \Delta x}\right|_{shifted}$$

O   original function $f|_{original}$

◌   shifted function $f|_{shifted}$

Figure 8.9:   *Change of second order central approximated gradients of pressure due to grid-shifting.*

Application of the above ideas to the ehl problem signifies a shifting of the geometry of the gap in relation to the pressure. The height of the gap is now described by

$$h_l = h_0 + h_{r,l-1/2} + V_{d,l-1/2} \tag{8.12}$$

and is shown in figure 8.10.

Since the Couette part of Reynolds equation is dominant in comparison with the Poiseuille contribution, the influence of the incorrect grid height due to grid shifting is expected to be small. Since, in this chapter, the assumption of constant pressure across the gap is made and the governing equations are the same, any improvements in numerical performance are also expected for

the solvers of the Navier-Stokes equations with variable pressure across the gap.

······· original grid
——— shifted grid
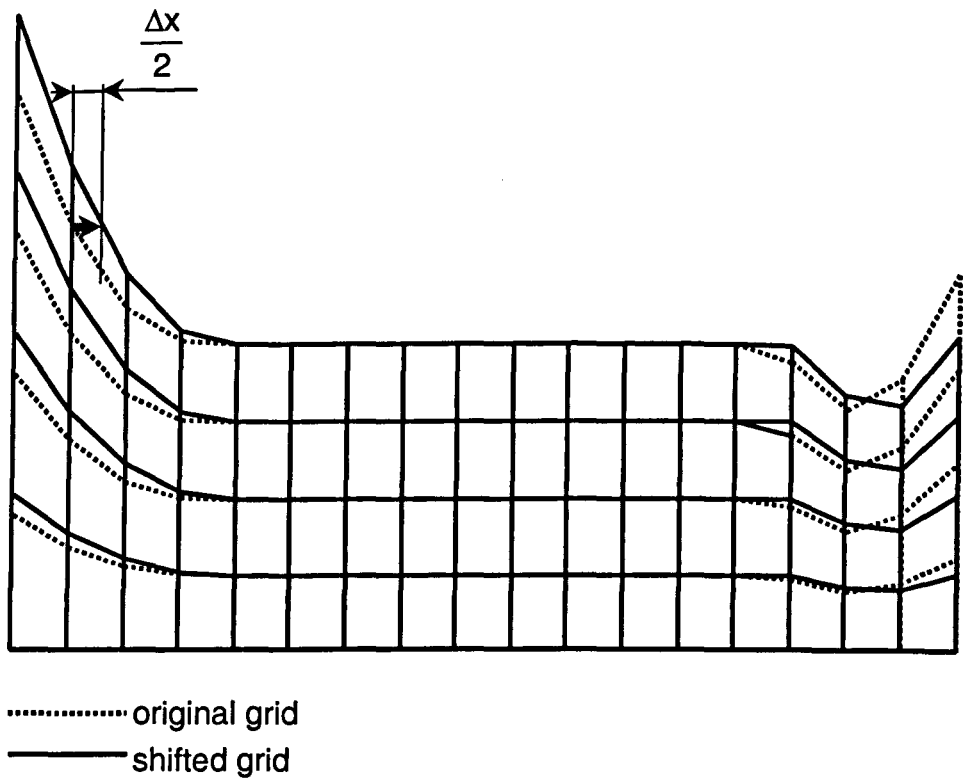
Figure 8.10:   Shifted and original grid for identical pressure distribution.

8.2.4   Results

The proposed method of grid-shifting leads to converging and non-oscillating results for the ehl problem when using CFD software. A sample result for the parameters listed in table 8.1 is given in figure 8.11. Variation of the shifting from half to a whole grid-width leads to an increasingly lower pressure spike, the rest of the results hardly changing. It is understood that, particularly for coarse grids, the method introduces a systematic error which decreases for finer grids. Comparison of calculated with published results is given below in subsection 8.4.5.

Application of the above ideas to a Reynolds equation with a centrally approximated Couette term leads to improvements of numerical performance. Hence it can be concluded that grid-shifting is a generally applicable method to improve numerical behaviour for a wider range of ehl calculations.

input parameters	
Hertzian pressure	$p_{hz} = 0.5 \cdot 10^9$ Pa
hydrodynamic speed	$u_h = 0.5$ m·s^{-1}
sliding ratio	$S = 0.5$
viscosity	$\eta_0 = 0.050$ Pa·s
pressure viscosity coefficient	$\alpha = 2.18 \cdot 10^{-8}$ Pa^{-1}
reduced Young's modulus	$E_{red} = 2.27 \cdot 10^{11}$ N·m^{-2}
reduced radius	$r_{red} = 0.025$ m
density	$\rho = 870$ kg·m^{-3}

Table 8.1:   Input parameters of sample ehl calculation of figure 8.11.
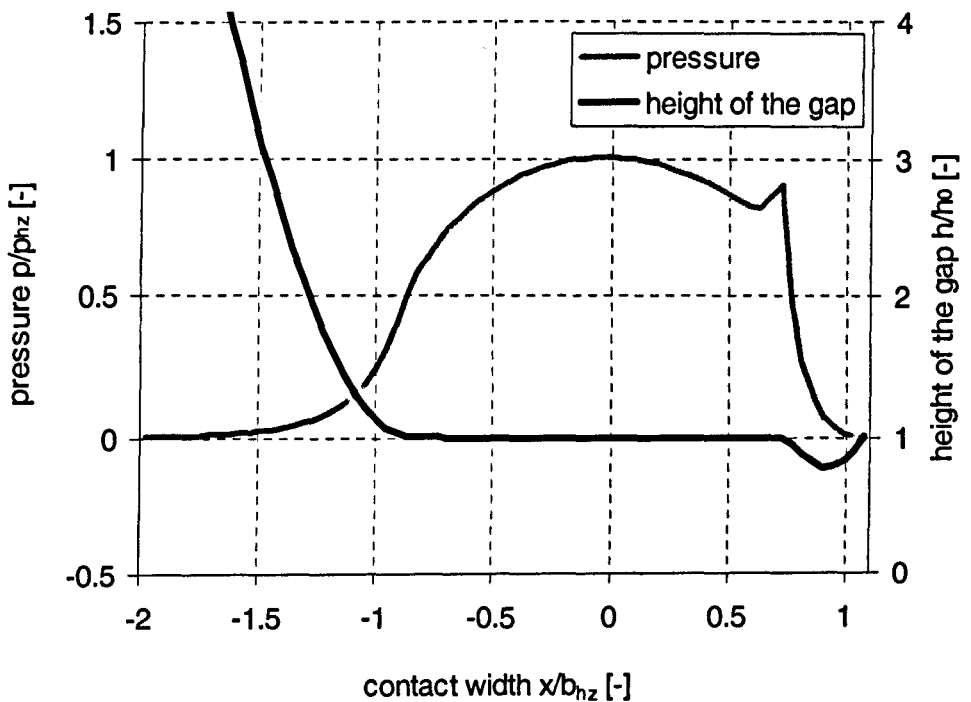
Figure 8.11:   Sample result for ehl calculation assuming constant pressure across the height of the gap and using CFD software. For input parameters see table 8.1.

8.3   Numerical parameters

8.3.1   Numerical parameters appearing in ehl calculation

Numerical analysis requires the setting of numerical parameters and for the present ehl investigation altogether five parameters must be set.

In the basic Newton-Raphson method using Reynolds equation two numerical parameters appear: firstly the number of volumes or grid-points and secondly the residual vector of the Reynolds equation. The number of cells must be set for the calculation. This number ranges from about 40 [7, 8, 36], where reasonable results are obtained, up to 1000 and more for detailed solutions [8]. The residuals of the Reynolds equation are returned from the solution procedure. The ratio of initial and current values can be used to evaluate the convergence of the solution.

When, as in the present study, the Jacobian matrix is determined numerically, a third value defining the length of the section of abscissa must be set by the user to approximate the tangent by a secant. General text books on numerical methods recommend a change of the original input value, i.e. in ehl calculations the pressure, by the square root of the computation precision, i.e. 10^{-16} for double precision calculations [76]

$$\frac{\Delta p}{p} = \sqrt{E_{computation}} = \sqrt{10^{-16}} = 10^{-8} \qquad (8.13)$$

For the particular case of ehl calculations, no details on the change of the original value for the numerical Jacobian matrix determination could be found. Detailed discussion on this issue is given in subsection 8.3.3.2.

The introduction of CFD software assuming constant pressure across the height of the gap means the introduction of the fourth and fifth numerical parameters: Since the calculation is two-dimensional, the number of volumes of grid points in the y-direction must be set; the calculation of the u-velocity distribution is carried out numerically and hence a criterion to define convergence of this inner loop iteration must be defined.

For the present considerations, usually a grid of 70 x 7 volumes was used. This combination enabled reasonable calculation times when employing the CFD code, a reasonable discretisation of the domain and a reasonable resolution of the results to show the principal effects of the new method.

Contrary to most Reynolds equation based solutions, the CFD code takes account of the dimensional problem. That means that residuals are dimensional and hence must be set individually for each particular calculation, even if dimensionless parameters might agree.

8.3.2   Ranges of converging and non-converging parameters

The interaction of the remaining three numerical parameters is now analysed with a defined grid of 70 x 7 volumes and for the set of parameters of table 8.1. This constitutes a basis for the selection of these parameters in subsection 8.3.3. The relative variation of the input value to approximate the Jacobian matrix and the reduction of the residuals for the x-momentum equation as convergence criteria for the inner iteration was varied over some orders of magnitude. The development of the residuals of the integral continuity equation was analysed for a high number of Newton-Raphson steps.

The results of this investigation are shown in figure 8.12. A triangular zone was found were the calculation method converges. In most of the zone the continuity residuals fall more than eight orders of magnitude below their initial values and then oscillate at this very low level. At one edge, the residuals of the continuity equation do not fall as much as eight orders of magnitude but remain at a low level. The triangular range of convergence is limited by three types of failure:

(i)   For low residual values for the x-momentum equation, the calculation fails because the x-momentum equation fails to converge to the desired residual.

(ii) For relatively large pressure variations the method fails initially due to strong oscillations of the pressure corrections based on the Newton-

Raphson technique. These oscillations lead to convergence problems for the x-momentum equation. For higher, relatively large pressure corrections, a negative height of the gap is obtained during calculation.

(iii) At a particular ratio of relatively inaccurate residuals, represented by high residual values and small pressure variations, the calculation fails due to increasing oscillations after initial convergence.

Furthermore, it was observed that calculation time increases with increasing pressure ratios and by decreasing the required residual for the x-momentum equation.
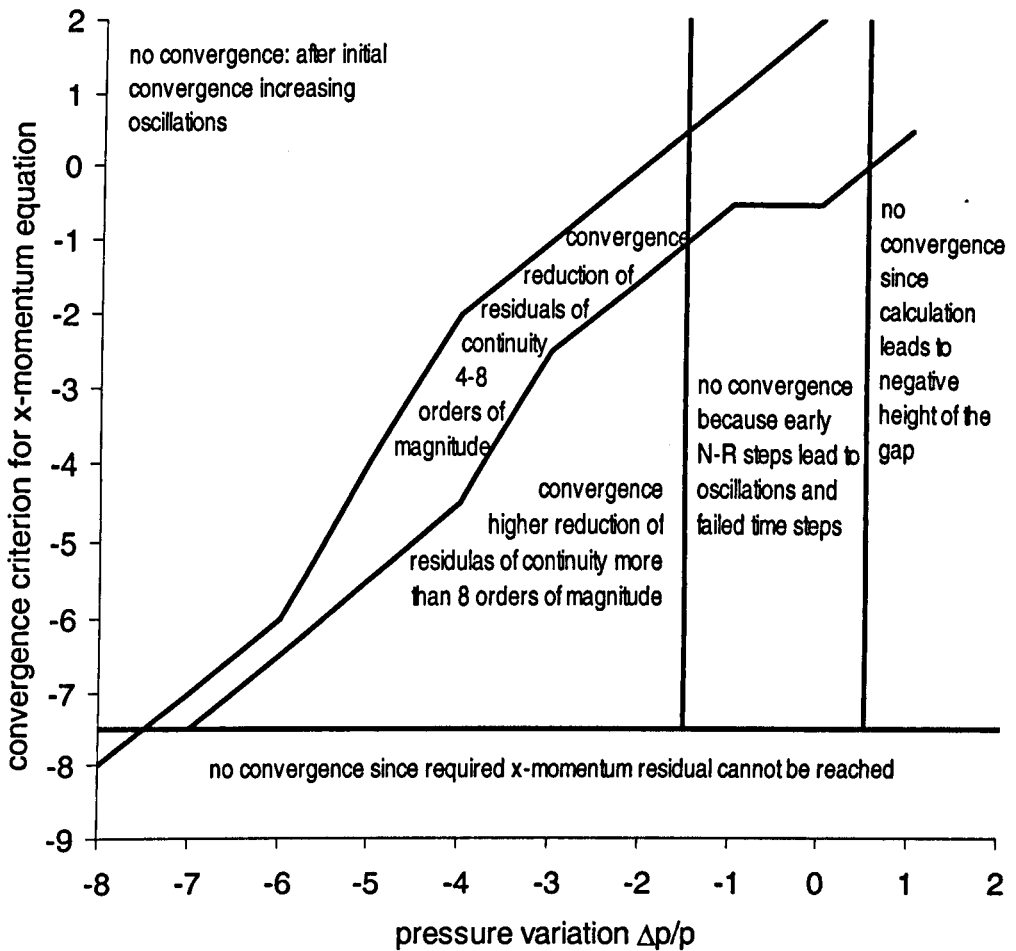
Figure 8.12:   Ranges of convergence and divergence for the ehl problem, parameters as in table 8.1.

8.3.3   Selection of parameters

8.3.3.1   Residual for the x-momentum equation

Figure 8.12 showed that the x-momentum equation fails to converge when the required norm of the residuals falls below a particular level. It is essential not to fall below this value, because otherwise the calculation procedure would be interrupted. On the other hand, the minimum residual should be as close as possible to the minimum possible value in order to attain maximum precision. The present subsection estimates an optimum value for the dimensional value of the residual vector of the x-momentum equation.

For this, the simplified Navier-Stokes equation in the x-direction assuming constant pressure across the gap and leading to Reynolds equation is considered, equation 2.1,

$$\frac{\partial p}{\partial x} = \eta \cdot \frac{\partial^2 u}{\partial y^2} \tag{8.14}.$$

When pressure and hence viscosity is variable across the gap, equation 8.14 is equal to the more general form, equation 2.11,

$$\frac{\partial p}{\partial x} = \frac{\partial}{\partial y}\left(\eta \cdot \frac{\partial u}{\partial y}\right) \tag{8.15}.$$

In this equation u velocity is now assumed to be the unknown variable and the pressure gradient a known source term. Application of the finite volume discretisation, figure 8.13, means integration over a discrete volume ΔV. Details are e.g. given by Patankar and Spalding [88] or by Versteeg and Malalasekera [90]. Equation 8.15 becomes

$$\int_{\Delta V}\frac{d}{dy}\left(\eta \cdot \frac{du}{dy}\right)\cdot dV - \int_{\Delta V}\left(\frac{dp}{dx}\right)\cdot dV = \left(\eta \cdot A \cdot \frac{du}{dy}\right)_{J+1} - \left(\eta \cdot A \cdot \frac{du}{dy}\right)_{J} - \hat{S}\cdot\Delta V = 0 \tag{8.16}$$

where

$$\int_{\Delta V}\left(\frac{dp}{dx}\right)\cdot dV = \hat{S}\cdot\Delta V.$$
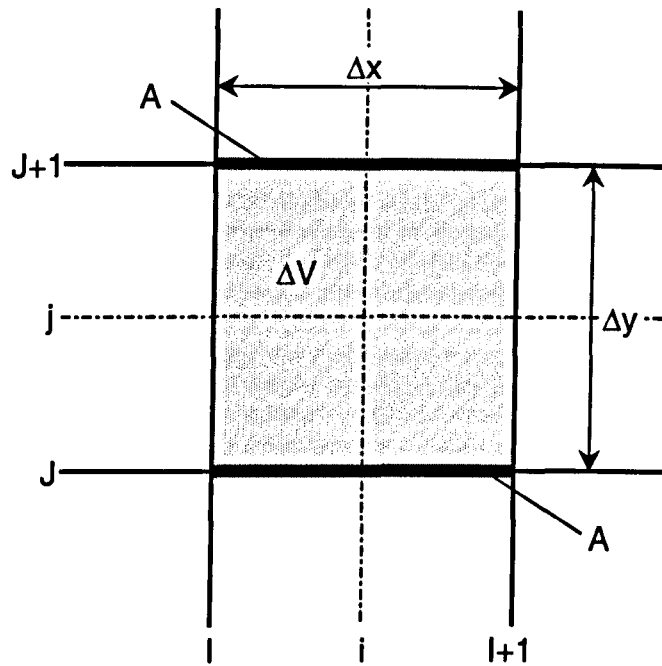
Figure 8.13:   Finite volume and description of indices.

Approximation of the velocity gradients by a second order central approximation leads to the discretised equation, and taking into account that cell surface and viscosity do not change across the height of the gap, equation 8.16 becomes

$$\frac{\eta \cdot A}{\Delta y} \cdot \left(u_{i,j+1} - 2 \cdot u_{i,j} + u_{i,j-1}\right) - \hat{S} \cdot \Delta V = 0 \qquad (8.17),$$

where Δy is the dimensional finite volume width across the gap and
        ΔV is the volume of the finite volume.

Introducing non-dimensionalisation, as in section 3.3, and Barus' equation 3.9 gives

$$\frac{\eta_0 \cdot e^{\alpha \cdot p_{hz} \cdot \overline{P}_{i,j}} \cdot u_h \cdot b_{hz} \cdot l_c \cdot \Delta X \cdot \Delta Z}{h_0 \cdot \Delta Y} \cdot \left(\overline{U}_{i,j+1} - 2 \cdot \overline{U}_{i,j} + \overline{U}_{i,j-1}\right) - \hat{S} \cdot \Delta V = 0 \qquad (8.18)$$

where l_c is the width of the system, which must be finite in the CFD code and

   ΔX, ΔY, and ΔZ are the dimensionless volume dimensions in x-, y-, and z-direction.

When computing, the above equation cannot be fulfilled exactly, a small algebraic error can remain due to the restrictions of digital calculations. When

computing in a double precision mode, the resolution of numbers is 16 digits, where the last digit is inaccurate. A change of the last digit of the central velocity value hence causes a residual for the cell of

$$f_{i,j} = 2 \cdot \frac{\eta_0 \cdot e^{\alpha \cdot p_{hz} \cdot \overline{P}_{i,j}} \cdot u_h \cdot b_{hz} \cdot l_c \cdot m}{h_0 \cdot n \cdot l} \cdot E_{computation} \tag{8.19}$$

where $E_{computation}$ is the error due to the limited resolution of numbers, which is 10^{-16} for double precision and

n, m, and l   are the number of cells in x, y and z direction respectively, with

$$\Delta X = \frac{1}{n}, \ \Delta Y = \frac{1}{m}, \ \Delta Z = \frac{1}{l};$$

The sum of all the residuals, as is used in the CFD software, is obtained by summing the residuals of all cells

$$f_{sum} = \sum_{\substack{i=1 \\ j=1}}^{\substack{i=n \\ j=m}} f_{i,j} \tag{8.20}.$$

With the assumptions that the residuals of all individual volumes are of the same value of $f_{i,j}$ and that for all residuals the dimensionless pressure is unity, the minimum sum residual become:

$$f_{x-mom,sum} = f_{i,j} \cdot n \cdot m \cdot l = 2 \cdot \frac{\eta_0 \cdot e^{\alpha \cdot p_{hz}} \cdot u_h \cdot b_{hz} \cdot l_c \cdot m^2}{h_0} \cdot E_{computation} \tag{8.21}.$$

This assumption overestimates the real situation since the pressure and hence the residuals outside the heavily loaded zone are much smaller than the proposed value.

Tests with the CFD software showed that setting the residual value of the CFD code to a value slightly higher than $f_{x-mom,sum}$ normally ensures convergence for the x-momentum equation and delivers accurate results for the u velocity field. However, when the pressure spike is considerably higher than the Hertzian pressure, convergence cannot be reached due to the residuals near the pressure spike. This normally happens for relatively high values of the hydrodynamic speed, which causes the spike to be relatively close to the centreline of the contact.

8.3.3.2 Pressure variations for numerical determination of the Jacobian matrix

Convergence of the Newton-Raphson method is only obtained when, for the numerical determination of the Jacobian matrix, certain values for the pressure variation are used. Figure 8.12 has illustrated, that the maximum admissible value is constant and the minimum is dependent on the selected x-momentum residual.

When the maximum admissible value is exceeded, strong oscillations develop near the vertex of the Hertzian pressure distribution. They lead normally to failure of convergence of the x-momentum equation. The appearance of the problem can be delayed but not avoided by under-relaxation of the calculated pressure corrections of the Newton-Raphson scheme. It is assumed that the reason for this behaviour is the following: The higher the value of the pressure variation to obtain a secant, the less accurate this secant approximates the tangent of the original Newton-Raphson technique. For the described case of oscillations, the two values describing the secant differ by so much that the secant represents an insufficient approximation of the tangent.

On the other hand, minimum admissible values are dependent on the selected residual for the x-momentum equation. The generally recommended value of input variable variation of 10^{-8} for double precision represents, for the present case, the minimum value for which converging results are obtained when the optimum x-momentum residual was chosen.

As, for example, discussed by Lubrecht [8], the velocity terms are dominant in comparison with the pressure terms. The non-dimensionalised and re-arranged Navier-Stokes equation in the x-direction with Barus' relation is

$$\frac{\partial \overline{P}}{\partial \overline{X}} - \frac{b_{hz} \cdot \eta_0 \cdot e^{\alpha \cdot p_{hz} \cdot \overline{P}_{i,j}} \cdot u_h}{h_0^2 \cdot p_{hz}} \cdot \frac{\partial^2 \overline{U}}{\partial \overline{Y}^2} = 0 \qquad (8.22).$$

Discretising the equation using a simple finite difference formula,

$$\left(\overline{P}_{i+1,j} - \overline{P}_{i,j}\right) = D \cdot \left(\overline{U}_{i,j+1} - 2 \cdot \overline{U}_{i,j} + \overline{U}_{i,j-1}\right) \qquad (8.23),$$

where D is the factor which causes the velocity terms to dominate the pressure terms, gives

$$D = \frac{b_{hz} \cdot \eta_0 \cdot e^{\alpha \cdot p_{hz} \cdot \bar{R}_{i,j}} \cdot u_h \cdot m^2}{h_0^2 \cdot p_{hz} \cdot n} \qquad (8.24).$$

When considering again the limited accuracy of the computation, the dominance factor D means that a change in the nth digit of one velocity value requires a change in that digit of one of the pressure terms, which is the order of the dominance factor D left of the nth digit, i.e. the $(n - \log D)^{th}$ digit. That means, for the discussed sample result, that a relative change of the pressure values of less than 10^{-12} would not cause any changes in the velocity profile. On the other hand, for the residuals of the continuity equation, the Newton-Raphson technique needs exact values, which are calculated from the u-velocity field. The difference of both the residuals, i.e. the original residual and the residual due to the change of the input value, should have as many correct digits as possible to keep algebraic errors small. Four to five digits were found to be the minimum number of correct digits necessary to obtain a converging solution. Therefore, the relative pressure variation can be calculated from the following formula:

$$\frac{\Delta p}{p} \geq E_{computation} \cdot S_{N-R} \cdot S_{residual} \cdot D \qquad (8.25),$$

where $E_{computation}$ is the numerical accuracy of the computation, 10^{-16} for the employed double precision mode,

            S_{N-R} is the accuracy required for the Newton-Raphson technique, at least four digits, 10^4,

            $S_{residual}$ is the difference between the theoretical minimum residual due to the computation and the selected minimum residual which should be as small as possible, and was, with the above criteria, $10^2...10^3$ and

            D   is the factor by which the velocity terms are dominant in comparison with the pressure terms, for the discussed sample result, 4×10^3.

Since the oscillations leading to the failure of convergence appear for increasing pressure variations, they should be chosen as small as possible.

It is clear from the above formula 8.24 that the dominance factor D grows rapidly with increasing Hertzian pressure. That means that the triangular range of convergence in figure 8.12 decreases for more severe conditions and that there will be a set of maximum values of parameters for which a successful calculation can be carried out. This limit is shown in section 8.5.

8.3.3.3   Convergence and relaxation of Newton-Raphson technique

Overall convergence of the analysis was defined to be obtained when the sum of the value of the continuity equation residuals decreased more than five orders of magnitude.

For the Newton-Raphson technique, a constant relaxation factor of 0.3 was found to cause sufficient under-relaxation at the beginning of the analysis while keeping the convergence speed at an acceptable level

8.4   Errors

8.4.1   Types of error

Errors appearing in numerical solutions can have a number of different origins. Normally, four groups of errors are distinguished; see e.g. Peric [103]:

♦   model errors,

♦   discretisation errors,

♦   iteration errors,

♦   implementation errors.

These errors and the influence on the numerical method are discussed in the following.

8.4.2   Model errors

Model errors cause the difference between the exact solution of the selected mathematical model described by differential equations and the real solution. In the present investigation, some model errors were intentionally admitted,

such as isothermal, incompressible and Newtonian conditions, as well as, in the present section, constant pressure across the gap. On the other hand it is the aim of the present investigation to improve the solution of the ehl problem. It is hoped that this is achieved by an improvement of the mathematical model, i.e. by reducing the model error.

8.4.3   Discretisation errors

Discretisation errors are the difference between the exact solution of the differential equation and the exact solution of the discretised system of algebraic equations.

According to Peric [103], the discretisation error can be estimated from two solutions of the problem on grids of different resolution and the order of the method.

$$\varepsilon_{disc} = \frac{\phi_h - \phi_{2h}}{2^{\tilde{p}} - 1} \tag{8.26}$$

where ϕ_h is the result on the originally coarse grid,

ϕ_{2h} is the result at the same point from a grid with half the number of finite volumes or grid points in each direction, and

$\tilde{p}$ is the order of the discretisation error.

The order of a method can be determined from three solutions on different fine grids by

$$\tilde{p} = \frac{\log\left(\frac{\phi_{2h} - \phi_{4h}}{\phi_h - \phi_{2h}}\right)}{\log 2} \tag{8.27}$$

where ϕ_h, ϕ_{2h} are as above and

ϕ_{4h} is the value for the function assuming quarter the resolution of the grid

Thereby, the order of the method must be determined only once for the calculation scheme.

The calculation of the order requires the iteration error, see below, to be as small as possible. Hence the calculation time is relatively long even for

coarse grids, and, as also applied, by considering only one superimposed loop of applied load equilibrium. In the present case, the first reasonable non-oscillating results were obtained for a grid of 50 x 5 volumes. The calculation time was found to increase quadratically with the number of cells, as shown in figure 8.14. Extrapolation showed that the finest necessary grid of 200 x 20 volumes would require a CPU time of more than 30 hours on a SGI R8000 processor.
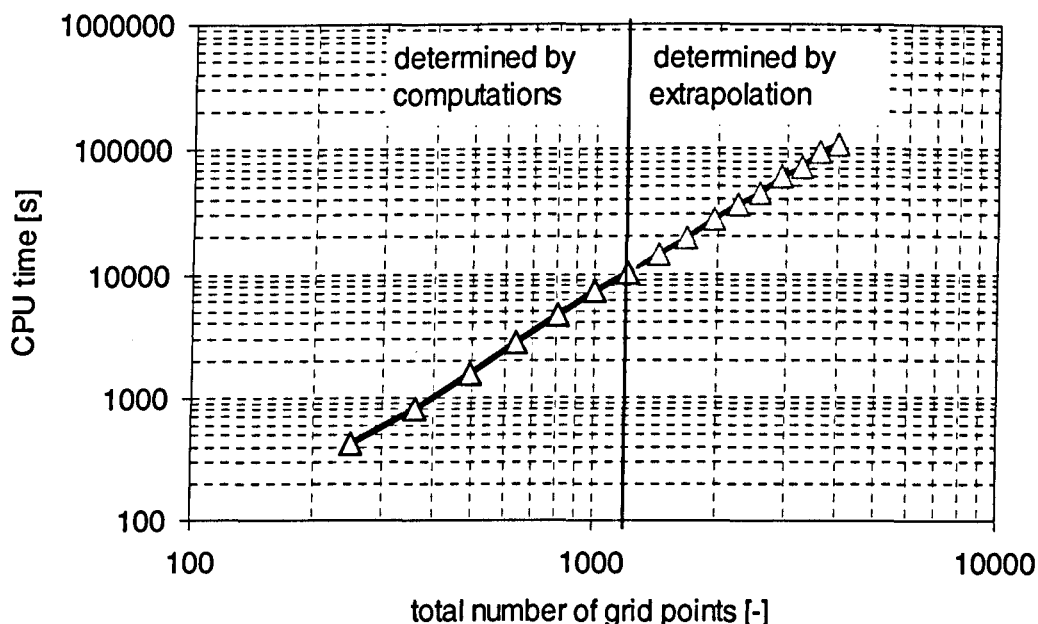
Figure 8.14: *CPU times for various total number of finite volume or grid points.*

Hence it was decided to test the order of the method using another method. When the order of a method is quadratic, function ϕ varies with the grid size as follows

$$\phi = \frac{k_1}{n^2} + k_2 \tag{8.28}$$

where n is the number of grid-points in one direction, e.g. the x-direction and

k_1, k_2 are coefficients which can be calculated from two pairs of function value and respective grid size,

$$k_1 = \frac{\phi_1 - \phi_2}{1/n_1^2 - 1/n_2^2} \text{ and } k_2 = \phi_1 - \frac{1}{n_1^2} \cdot \frac{\phi_1 - \phi_2}{1/n_1^2 - 1/n_2^2}$$

The order of the method implemented was checked by comparing the theoretical development of the central height of the gap for first and second order methods with calculated results. Results are shown in figure 8.15. The central height of the gap was chosen since comparison of pressure values would require interpolation which might influence the order.

Figure 8.15 shows that particularly for grids finer than 80 x 8 volumes, the method follows the second order method. This agrees with the expectation of section 8.1 because the CFD code is of second order and for the user defined features second order approximation was also chosen.
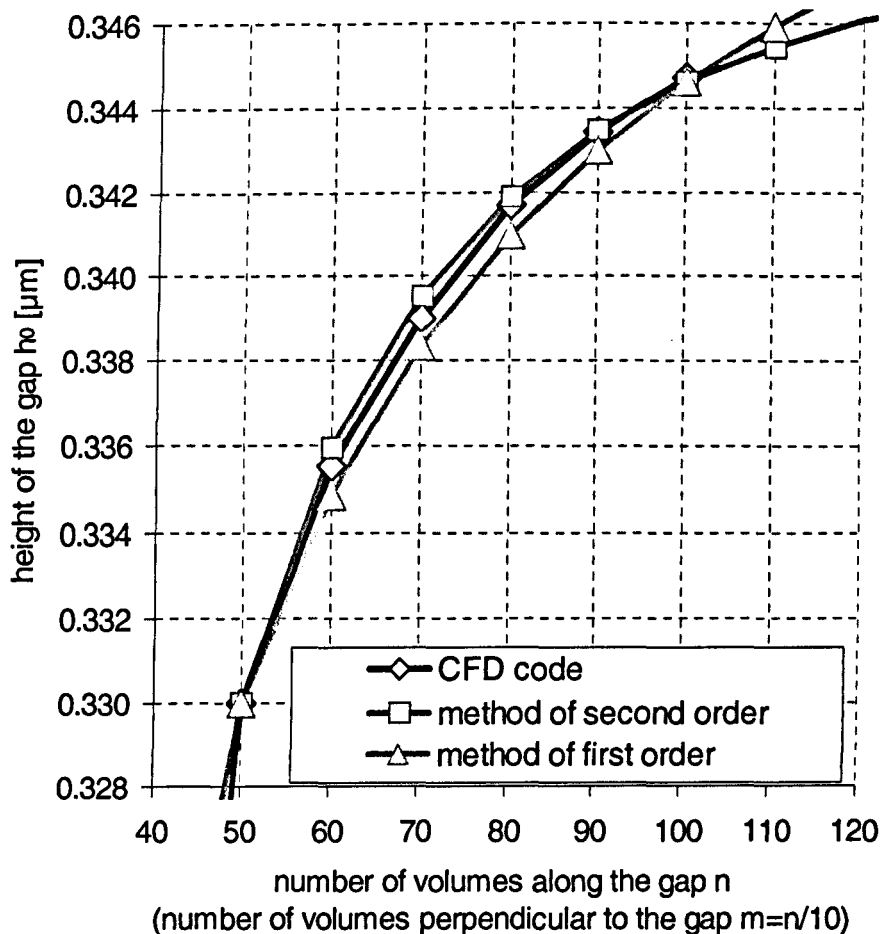
Figure 8.15:   Variation of the height of the gap h_0 depending on grid resolution.

8.4.4   Iteration errors

Iteration errors are the difference between the exact solution and the calculated result of the system of discretised, algebraic equations. Iteration errors appear due to both the limited accuracy of the computational calculation and the termination of iterative solution loops.

In the present investigation, problems due to the termination of the iterative solution loops appear at three levels, firstly for the iteration of the x-momentum equation, secondly for the Newton-Raphson scheme during iteration of the continuity equation and thirdly for the iteration for the exact height of the gap.

In subsection 8.3.3.1 a method was discussed to calculate the convergence criteria for the x-momentum equation as exactly as possible to keep the iteration error of the same order as the error due to the limited accuracy of the calculation. The reduction of the iteration error at this level is essential since the iteration error has a strong influence on the calculation of the residuals of the continuity equation and hence on the generation of the Jacobian matrix. Hence the iteration error can significantly influence the numerical performance of the calculation. The error due to the limited accuracy of the computational operation leads to the same problems, and it was expected that the iteration error would lead to failure of the calculation method if certain values of parameters are exceeded.

In contrast to the above iteration, a truncation of the Newton-Raphson iteration is less sensitive. Depending on the desired accuracy for the central height of the gap in the superimposed iteration loop, the reduction of the residuals of the continuity equation by four to five orders of magnitudes was found to be sufficient.

8.4.5   Implementation errors

Implementation errors appear due to incorrect implementation of the discretised equations and their solution into the computational program. Implementation errors can be detected by comparing results from one code with results obtained with another, independent code. However, it must be

ensured that other types of errors are as small as possible or that their magnitude is known.

For the detection of any implementation error of the present method, the sample result, figure 8.11, was compared with a result for the same parameters by Bakolas and Poulios [104]. Results are shown in figure 8.16. For both calculations identical models, i.e. isothermal, incompressible conditions using Barus' equation, and parameters, i.e. those of table 8.1, were used. Nevertheless minor differences between both approaches and hence of the model error must be expected from details such as the usage of the Hertzian pressure in the definition of the applied load.

Discretisation error must be expected to be different because of several differences between the two compared methods. The solution by Bakolas and Poulios [104] is based on finite differences, while the present study is based on the finite volume method. The approximation of the derivatives differs for both methods, with the present method using grid shifting to stabilise the solution. Additionally, Bakolas and Poulios use a finer grid; i.e. 32 finite differences per Hertzian width vs. 23 finite volumes for the present study.

Regarding the iteration error, differences between methods must be expected, because there are several differences in the analysis scheme. Nevertheless, it was attempted, in the present study, to keep iteration error as small as possible.

The comparison of figure 8.16 show very good qualitative agreement between the results of Bakolas and Poulios and those of the present study, e.g. when considering the position and the shape of the pressure spike and the ehl constriction.

On the other hand, some minor quantitative differences, such as a slightly higher central height of the gap, a slightly higher pressure in the inlet zone and a slightly lower pressure at the contact centreline, each for Bakolas and Poulios' result, can be observed.

Due to the good qualitative agreement of both results, and due to the fact that minor model, discretisation and iteration errors must be expected, it is concluded from figure 8.16 that implementation errors are most unlikely.

Further checks of the present method lead always to results qualitatively consistent with established observations, such as reduction of the central height of the gap with increasing load and movement of the pressure spike to the end of the contact with decreasing hydrodynamic speed.
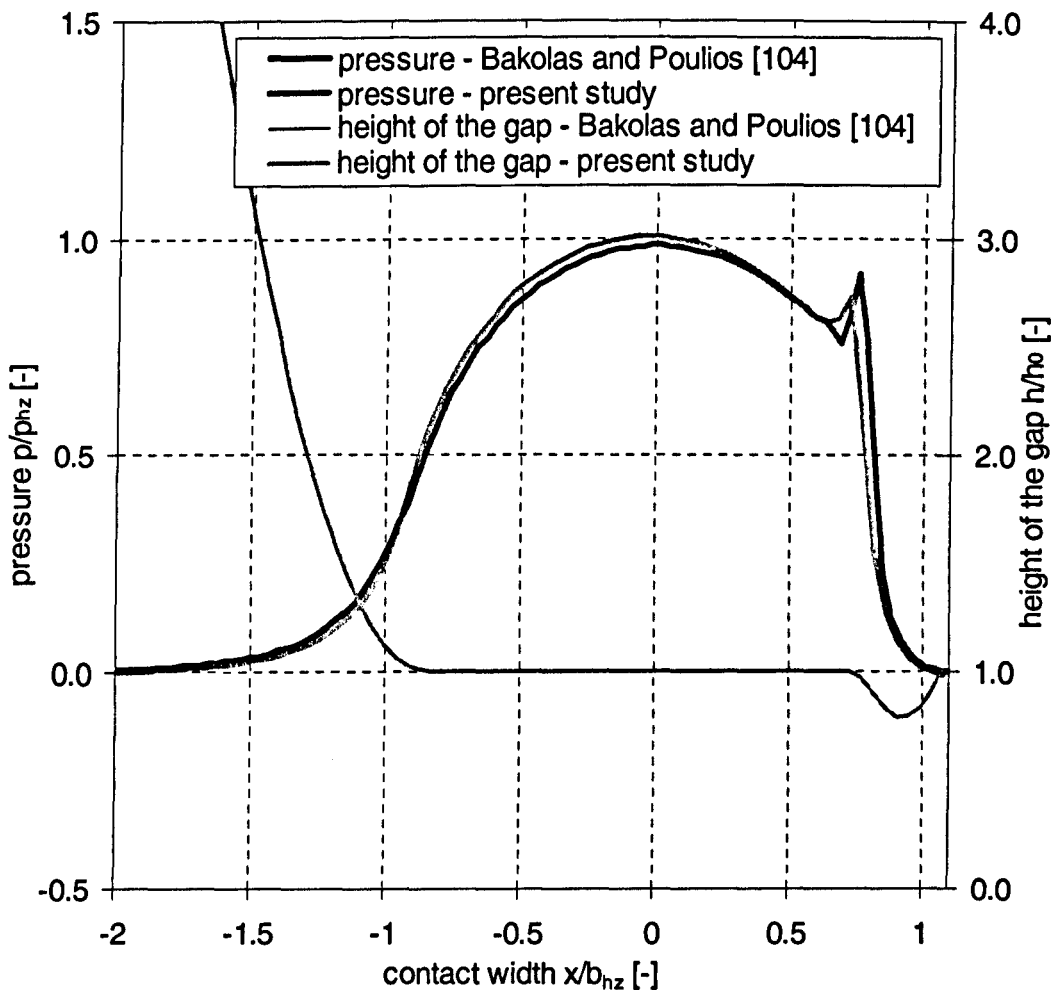
Figure 8.16:   Comparison of the sample of the present method with data from the method by Bakolas and Poulios [104].

8.5 Limits of the method

8.5.1 Sample calculation of limits

Limits of the method were determined empirically by sample calculations varying load, speed and viscosity. Young's modulus, radii of the surfaces and pressure-viscosity coefficient were kept constant. Barus' pressure viscosity approach was assumed for all calculations. Figure 8.17 illustrates for which sets of dimensionless load parameter W and dimensionless speed parameter U converging results were obtained. However it was also found that when keeping the dimensionless parameters U and W constant, sometimes converging results were obtained, while for higher speed and lower viscosity no converging results were obtained. It was found that the limits of figure 8.17 are only valid if the pressure spike is relatively close to the end of the contact and the absolute height of the spike is not higher than the Hertzian pressure.

8.5.2 Numerical description

Subsection 8.3.3.2 showed that selection of numerical parameters of the calculation method is dependent on the ratio of dominance in the Reynolds equation as defined in equation 8.24,

$$D = \frac{b_{Hz} \cdot \eta_0 \cdot e^{\alpha \cdot p_{Hz} \cdot P} \cdot u_h \cdot m^2}{h_0{}^2 \cdot p_{hz} \cdot n} \tag{8.29},$$

and that this value might limit the range of application of the presented numerical method.

Introduction of the dimensionless parameters for speed, load and material as well as the formula for the height of the gap, as discussed in chapter 3.3 and described in detail in appendix H, allows rewriting of the factor of dominance as

$$D = 1.11 \cdot \frac{m^2}{n} \cdot G^{-1.2} \cdot U^{-0.4} \cdot W^{0.26} \cdot e^{0.4 \cdot G \cdot W^{0.5}} \tag{8.30}.$$

This description enables the presentation of lines of constant factor of dominance in figure 8.17.

These lines show that converging results were only obtained if the factor of dominance was smaller than 10^5.

This is consistent with equation 8.25

$$\frac{\Delta p}{p} \geq E_{computation} \cdot S_{N-R} \cdot S_{residual} \cdot D \qquad (8.31).$$

For the factor $D = 10^5$, a pressure modification of $\Delta p/p = 10^{-4}$, double precision computation, i.e. $E_{computation} = 10^{-16}$, and a loss in accuracy due to numerical techniques of three orders of magnitude $S_{residual} = 10^3$, leads to an accuracy of the Newton-Raphson technique of $S_{N-R} = 10^4$, which is the empirically determined minimum. Hence a factor of dominance of $D = 10^5$ defines some limit of the presented method. This limit can be reduced by the previously described fact that a developing, high pressure spike spoils the convergence of the x-momentum equation and hence the analysis. The range of convergence can be slightly expanded by allowing coarser values for the pressure modification $\Delta p/p$ and attempting a reduction of the loss of accuracy due to the numerical technique $S_{residual}$, but both methods can easily lead to non-convergence as shown in subsection 8.3.2.

8.5.3   Comparison with other calculation methods

Beside sample analyses for the present study and lines of constant factors of dominance, figure 8.17 shows also those load cases for which Pan and Hamrock [64] presented numerical results. These cases were also shown in figure 3.10 of the present study to outline the practical relevance of the extended approach. Pan and Hamrock's load cases exceed clearly those parameters which mark the border of the numerical method of the present study. These might be due to the following reasons:

♦ The extended approach of the present study also requires discretisation across the gap. The number of volumes across the gap is part of the definition of the factor of dominance, equation 8.30, and leads to increase of this factor.
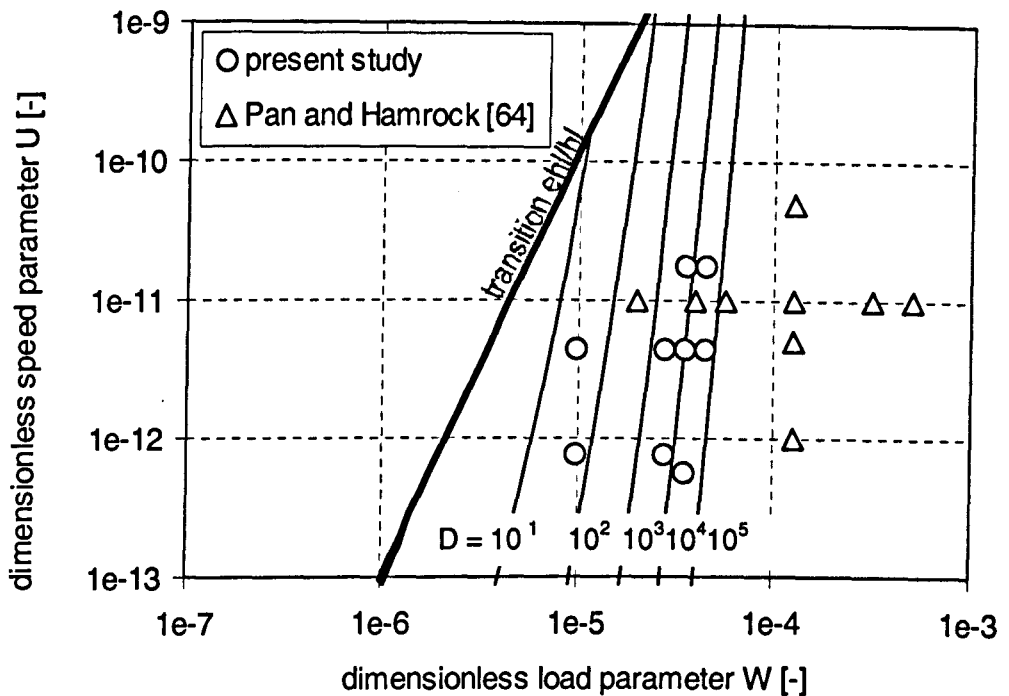
Figure 8.17: Load cases of converged solutions for the ehl regime with constant pressure across the gap, load cases of converged solutions by Pan and Hamrock [64] and lines of constant factor of dominance D.

♦ The numerical solution of the u-velocity field in the x-momentum equation requires a convergence criterion, subsection 8.3.3.1. Since this convergence criterion must be coarser than the numerical accuracy of the equation solver, the number of valid digits in the continuity equation is smaller, as discussed in section 8.3.3.1.

♦ The numerical determination of the elements of the Jacobian matrix implies a reduction of accuracy in comparison to analytically determined values.

In conclusion, the presented numerical method can only cope with a smaller range of dimensionless parameters U and W than established Newton-Raphson solutions of the ehl problem such as that presented by Pan and Hamrock [64].

Chapter 9

Implementation allowing variable pressure across the height of the gap

In the present chapter the calculation method is extended to allow variable pressure across the height of the gap. The two proposed methods which are derived from the Newton-Raphson technique, i.e. the fully simultaneous method of section 7.2.5.2 and the combined successive-simultaneous method of section 7.2.5.4, are implemented. Both methods are considered in a manner similar to that applied in chapter 8 for constant pressure across the gap. In the last section 9.3, both methods are compared, and the approach to get results for a wider range of parameters is selected.

9.1 The fully simultaneous method

9.1.1 Implementation details

The fully simultaneous method was realised by introducing some minor modifications to the calculation scheme for constant pressure across the gap discussed in section 8.1 and illustrated in figure 8.6. The modifications are discussed in the following and illustrated in figure 9.1.

(a)
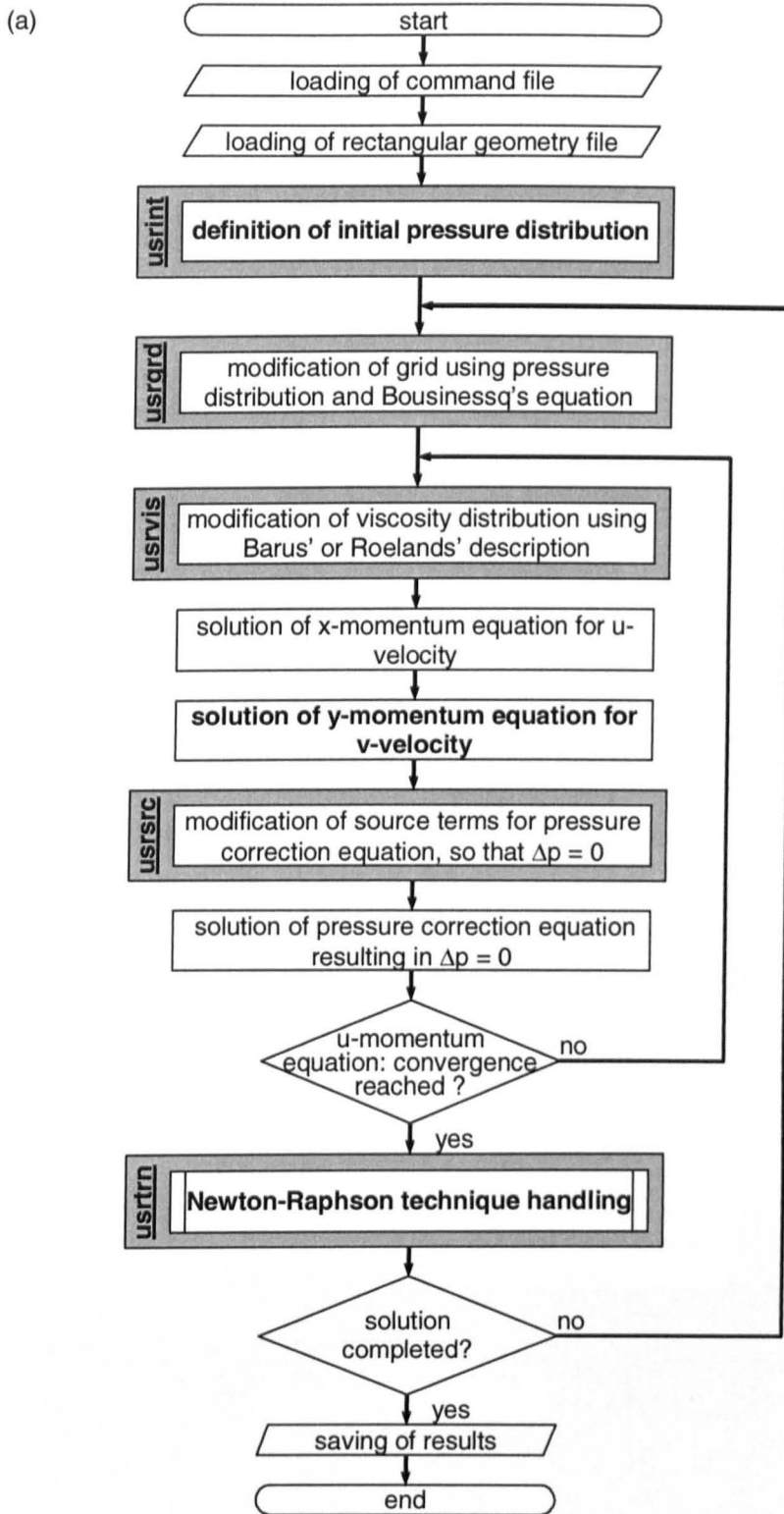
Figure 9.1:   Complete calculation scheme for the ehl calculation allowing pressure variation across the gap employing the fully simultaneous method of coupling and CFD software,

(a)   main program,

(b)   details of Newton-Raphson technique handling;

N.B. **bold text** *indicates differences to the method assuming constant pressure across the gap, figure 8.6*

(continued).

(b)   Newton-Raphson technique handling
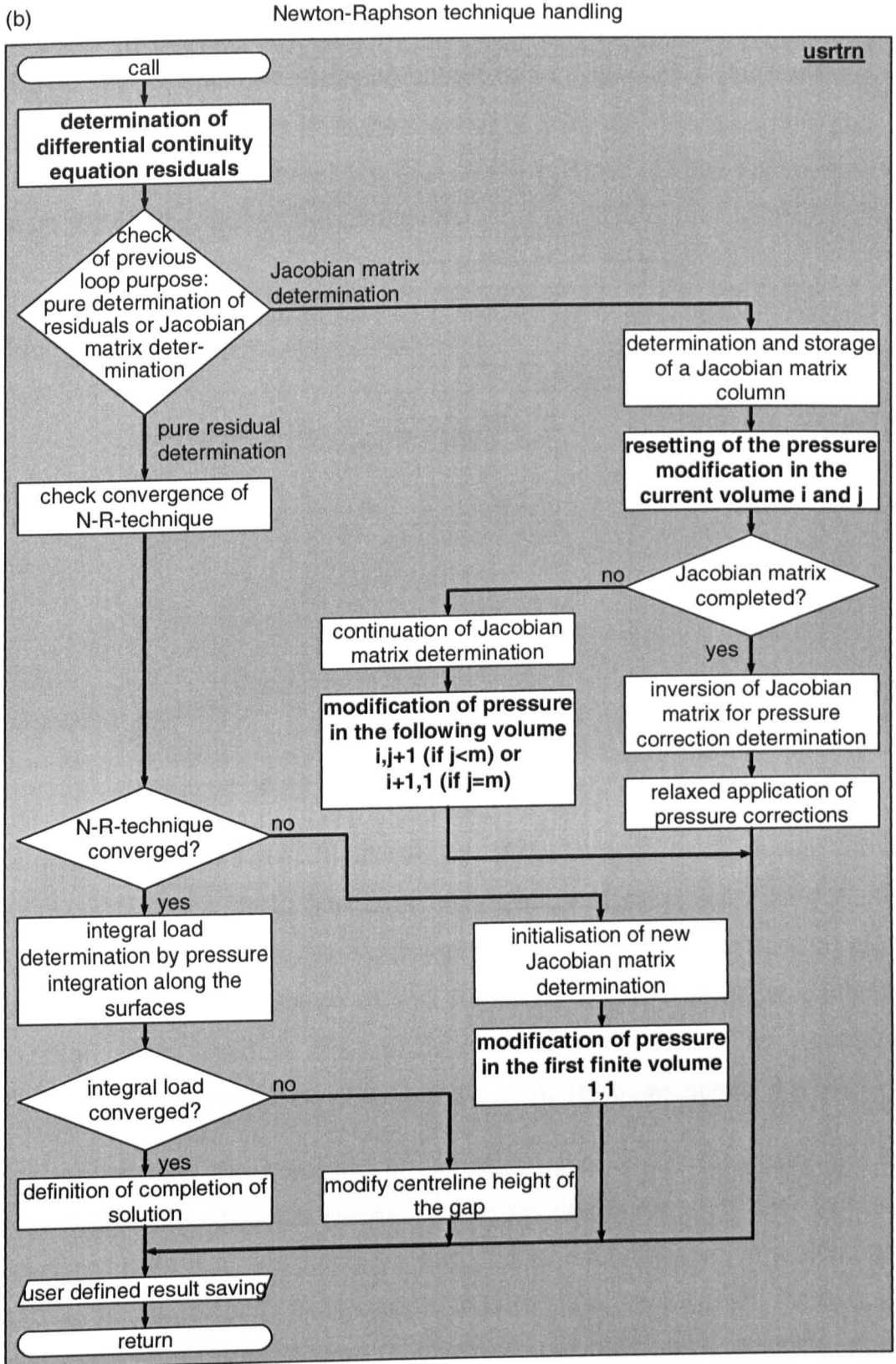
Figure 9.1:   (concluded).

9.1.1.1   Newton-Raphson technique

The number of unknown pressure values to be determined with the Newton-Raphson technique rises from the number of finite volumes along the gap, n, for constant pressure across the gap, to the number of finite volumes along times the number across the gap, n x m.

This means that for the fully simultaneous method the residuals of the differential continuity equation, equation 7.1,

$$\frac{\partial u}{\partial x} + \frac{\partial v}{\partial y} = 0 \qquad (9.1)$$

must be evaluated rather than the residuals of the integral continuity equation 7.2

$$\frac{d\left(\int_0^h u \cdot dy\right)}{dx} = 0 \qquad (9.2)$$

used for constant pressure across the gap.

As described in section 8.1.6, calculation of the integral residuals was carried out by adding the mass flow over all surfaces of each finite volume, and subsequent adding of all the residuals of one column, i.e. one position along the gap. Hence, calculation of the residuals of the differential continuity equation is included in the constant pressure method. The necessary modification is the omission of the adding of the residuals across the gap.

Correspondingly, the influence of pressure variation on the residuals, i.e. gradients of the Jacobian matrix, has to be determined not only for each column of finite volumes along the gap, but for each finite volume along and across the gap. Hence the procedure to determine the Jacobian matrix must be changed from column wise modification, evaluation and resetting of the pressure to individual treatment of each finite volume.

9.1.1.2   The y-momentum equation

For the determination of the differential continuity equation residuals, the v-velocity components across the gap must be known. These v-velocity components were also calculated and used in the method with constant pressure across the gap but their result cancelled out in the continuity equation residual determination and did not influence the calculation procedure. Hence, no adaptations are necessary.

Boundary conditions for the y-momentum equation are calculated by the CFD software automatically from the given tangential and normal speed components. Aspects of the convergence criteria for the y-momentum equation are discussed in section 9.1.3.1.

9.1.1.3   Initial values

As initial values two sets, illustrated in figure 9.2, were considered:

(i)   Hertzian pressure distribution with constant pressure across the height of the gap, as established for solutions assuming constant pressure across the height of the gap, or

(ii)   the converged ehl pressure distribution assuming a constant pressure across the height of the gap, i.e. a calculation with constant pressure across the height of the gap preceded the fully two-dimensional solution.

For the extended approach, the first approach is not only an approximation along but also across the gap, i.e. a "worse" initial value distribution than for the constant pressure. This could be the reason why no converging results could be obtained in numerical tests with this initial pressure distribution. In contrast, the latter approach might cause problems because it predefines the position of the pressure spike. However, the latter method did deliver converging sample results. Hence the latter method was used.

(a)

(b)
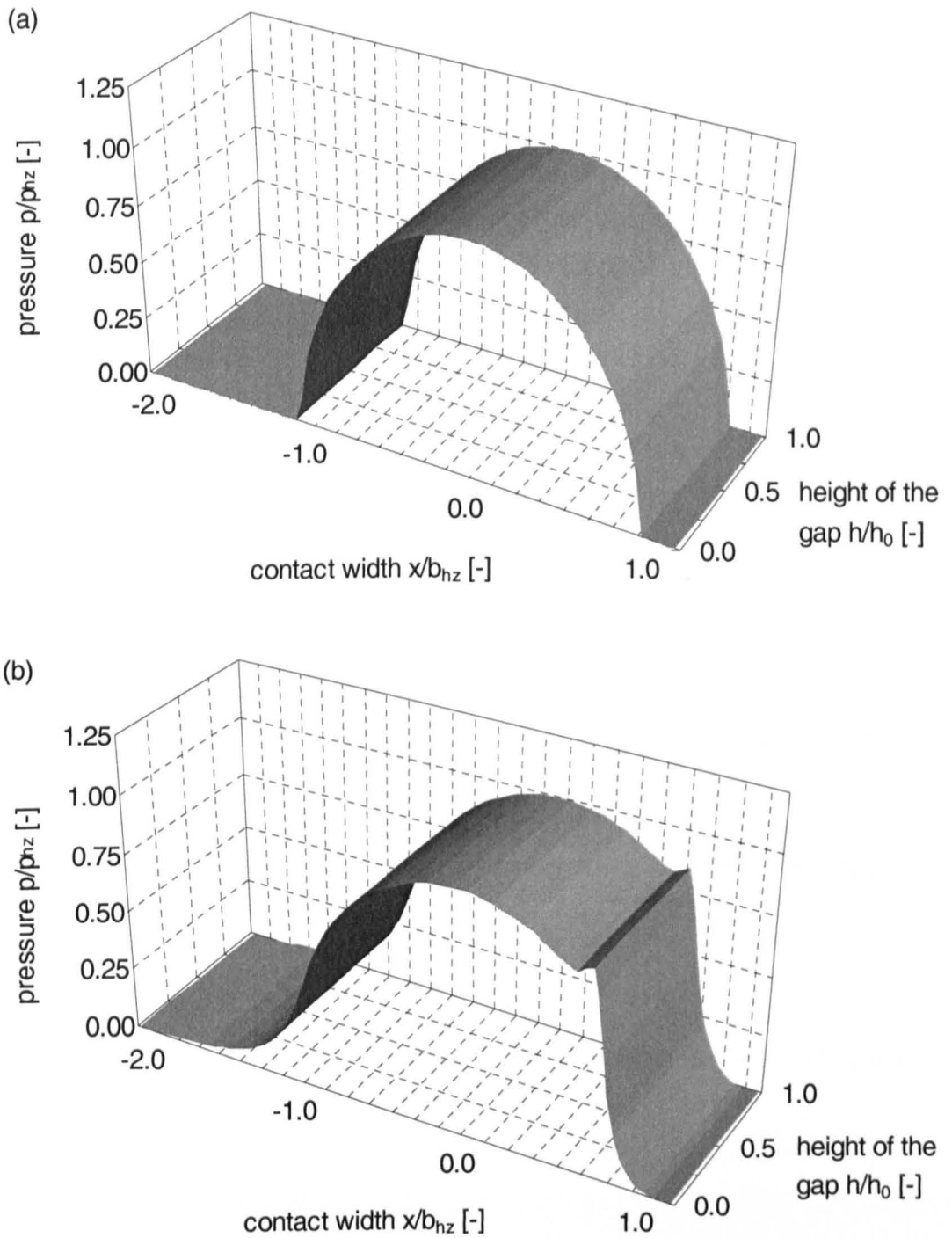
Figure 9.2:   *Possible initial pressure distributions for the ehl line contact problem allowing variable pressure across the height of the gap and using the fully simultaneous method of coupling:*

(a)   *Hertzian pressure distribution along the gap, constant pressure perpendicular to the gap,*

(b)   *ehl pressure distribution along the gap, constant pressure perpendicular to the gap.*

9.1.2   Sample result

A sample result of the extended method for the parameters also used for the sample in chapter 8, table 8.1 is given in figure 9.3. It is already obvious at this level that the sample results differ from those for the solution with the constant pressure across the height of the gap, figure 8.11. Detailed investigation is given in part III of the present study.
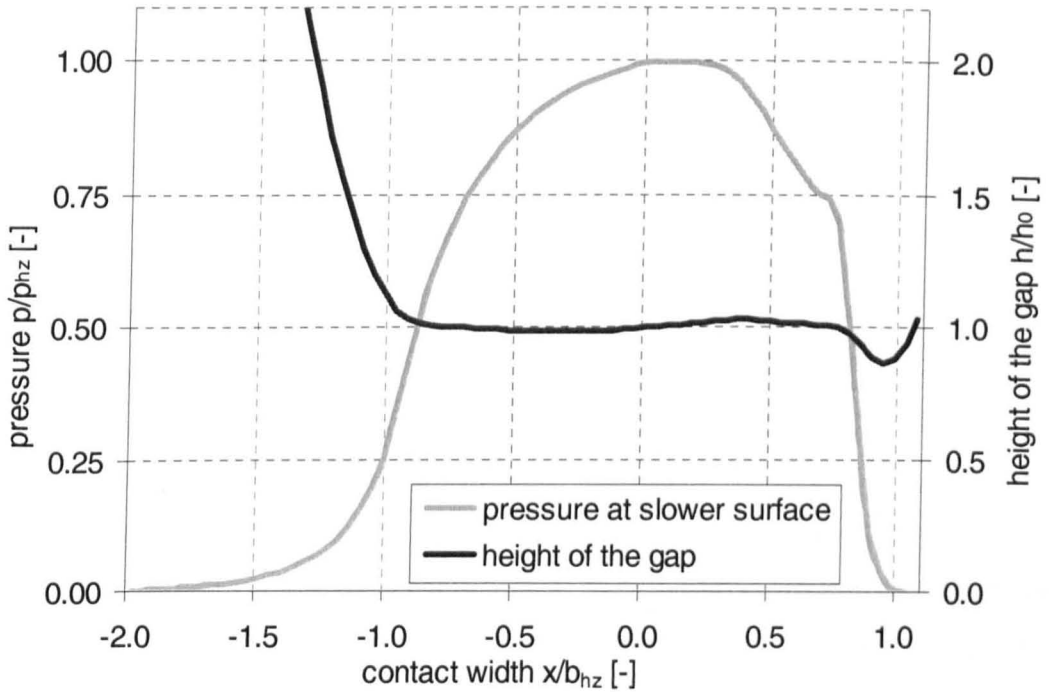
Figure 9.3:   Sample result for the ehl line contact problem allowing pressure variation across the gap using the fully simultaneous method of coupling.

9.1.3   Numerical parameters

9.1.3.1   The y-momentum equation residuals

The introduction of the y-momentum equation requires a revision of the convergence criteria for the inner, modified SIMPLE iteration loop. The x-momentum equation residuals were the only residuals relevant for constant pressure across the height of the gap and hence were used. With the extended approach, x- and y-momentum equations are solved and both deliver residuals which can be used to check convergence. However, the employed CFD code only allows the check of *one* of the variables of the loop, which means either the x-momentum or the y-momentum equation. This problem can be overcome by the use of a user defined Fortran routine.

Test showed that the y-momentum equation converges slightly faster than the x-momentum equation. When considering the residuals, the y-momentum equation already oscillated at a low level due to the limited accuracy of the computation before the x-momentum equation reached the required convergence criterion. Figure 9.4 illustrates the development of x- and y-momentum residuals during computation. Since the x-momentum residuals are the stronger convergence criterion than the y-momentum residuals, the x-momentum residual was used also used in the extended approach to check convergence.

The selection of the necessary numerical parameters, that are the residual of the x-momentum equation and the length of the abscissa for the approximation of the tangents for the Jacobian matrix, follows the methods proposed in section 8.3.

9.1.3.2   The x-momentum equation residuals

The residual value for the x-momentum equation is derived in appendix I. The value agrees with that for the solution assuming constant pressure across the gap and is

$$f_{x-mom,sum} = f_{i,j} \cdot n \cdot m \cdot l = \frac{\eta_0 \cdot e^{\alpha \cdot p_{hz} \cdot \overline{P}} \cdot u_h \cdot b_{hz} \cdot l_c \cdot m^2}{h_0} \cdot E_{computational} \qquad (9.3).$$
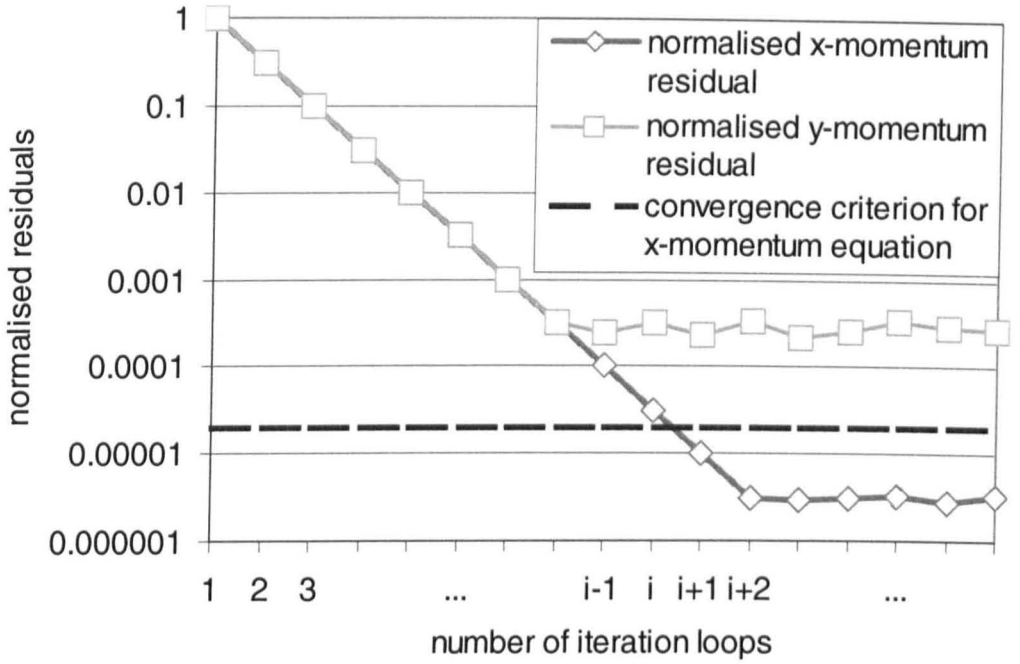
Figure 9.4:   Qualitative development of x- and y-momentum residuals during the modified SIMPLE iteration loops.

9.1.3.3   Pressure variation for Newton-Raphson technique

As discussed in 8.3.3.2, for the pressure variation to approximate the derivatives for the Jacobian matrix, the relative dominance of the different terms is helpful. When considering the set of equations 3.42, where Barus' equation is incorporated,

$$\left. \begin{aligned} 0 &= \frac{\partial \overline{P}}{\partial \overline{X}} \cdot \left[-\frac{p_{hz}}{b_{hz}} + 2 \cdot \kappa \cdot \gamma^2 \cdot \overline{\alpha} \cdot \frac{\partial \overline{U}}{\partial \overline{X}} \right] + \frac{\partial \overline{P}}{\partial \overline{Y}} \cdot \left[\kappa \cdot \overline{\alpha} \cdot \frac{\partial \overline{U}}{\partial \overline{Y}} \right] + \left[\kappa \cdot \frac{\partial^2 \overline{U}}{\partial \overline{Y}^2} \right] \\ 0 &= \frac{\partial \overline{P}}{\partial \overline{Y}} \cdot \left[-\frac{p_{hz}}{h_o} + 2 \cdot \kappa \cdot \gamma \cdot \overline{\alpha} \cdot \frac{\partial \overline{V}}{\partial \overline{Y}} \right] + \frac{\partial \overline{P}}{\partial \overline{X}} \cdot \left[\kappa \cdot \gamma \cdot \overline{\alpha} \cdot \frac{\partial \overline{U}}{\partial \overline{Y}} \right] + \left[\kappa \cdot \gamma \cdot \frac{\partial^2 \overline{V}}{\partial \overline{Y}^2} \right] \end{aligned} \right\}$$

(9.4),

an analysis is quite difficult due to the number of terms and the coupling between the equations. A more simple consideration is possible when using the equations where both momentum equations are combined, either equation 3.39 or, more detailed 3.44. The easiest consideration is possible with equation 3.39

$$\frac{\partial \overline{P}}{\partial \overline{X}} \cdot \left[1 - \left(k_p \cdot \frac{\partial \overline{U}}{\partial \overline{Y}} \right)^2 \right] = k_c \cdot \frac{\partial^2 \overline{U}}{\partial \overline{Y}^2}$$

(9.5)

with

$$k_c = \frac{\eta_0 \cdot u_h \cdot e^{\alpha \cdot p_{hz} \cdot \overline{P}}}{h_0^2} \cdot \frac{b_{hz}}{p_{hz}} \tag{9.6a}$$

and

$$k_p = \frac{\eta_0 \cdot u_h \cdot \alpha}{h_0} \cdot e^{\alpha \cdot p_{hz} \cdot \overline{P}} \tag{9.6b}.$$

Discretised, equation 9.5 becomes

$$\left(\overline{P}_{i+1,j} - \overline{P}_{i,j}\right) = D_{ext} \cdot \left(\overline{U}_{i,j+1} - 2 \cdot \overline{U}_{i,j} + \overline{U}_{i,j-1}\right) \tag{9.7}$$

with the factor D_{ext} describing how the velocity terms dominate the pressure term for the extended approach

$$D_{ext} = \frac{k_c \cdot m^2}{\left[1 - \left[\frac{1}{2} \cdot k_p \cdot m \cdot \left(\overline{U}_{i,j+1} - \overline{U}_{i,j-1}\right)\right]^2\right] \cdot n} \tag{9.8}.$$

Contrary to the Reynolds equation based case assuming constant pressure across the height of the gap, the ratio of dominance is dependent on the velocity gradient across the gap, discretised as $\frac{1}{2} \cdot m \cdot \left(\overline{U}_{i,j+1} - \overline{U}_{i,j-1}\right)$, and the factor k_p. Comparison of the factor describing the dominance for constant pressure across the gap, equation 8.24[*]

$$D = \frac{k_c \cdot m^2}{n} \tag{9.9},$$

with that factor for the extended approach D_{ext} is given in figure 9.4. The absolute value of the ratio $|D_{ext}/D|$ is shown versus the term $\frac{1}{2} \cdot k_p \cdot m \cdot \left(\overline{U}_{i,j+1} - \overline{U}_{i,j-1}\right)$. The figure shows that the ratio of dominance is unity as long as factor k_p or the sliding ratio is small, i.e. the numerical behaviour of the extended approach is identical to the solution with constant pressure across the gap.

---

[*]   The definition of factor k_c, e.g. equation 9.6a, was introduced to equation 8.24 to simplify comparison.

If the product $\frac{1}{2} \cdot k_p \cdot m \cdot \left(\overline{U}_{i,j+1} - \overline{U}_{i,j-1} \right)$ approaches unity, the dominance ratio reaches infinite values for the singularity of the governing equations. This means that near the location of the singularity, a variation of the pressure gradient would not lead to any change in velocity and consequently to no changes in the mass continuity residuals, which might spoil the condition of the Jacobian matrix or cause, at least, a numerically more sensitive analysis.

To overcome the problem, some measures can be employed.

◆ The pressure variation to determine the Jacobian matrix is selected as large as possible to maintain as much accuracy as possible,

◆ Obviously large pressure corrections caused by inaccurate Jacobian matrices are more strongly relaxed than obviously correct values. Care has to be taken not to extinguish the pressure spike by such procedures. Due to this problem a smoothing of the pressure corrections cannot be applied, as discussed by Okamura [14].
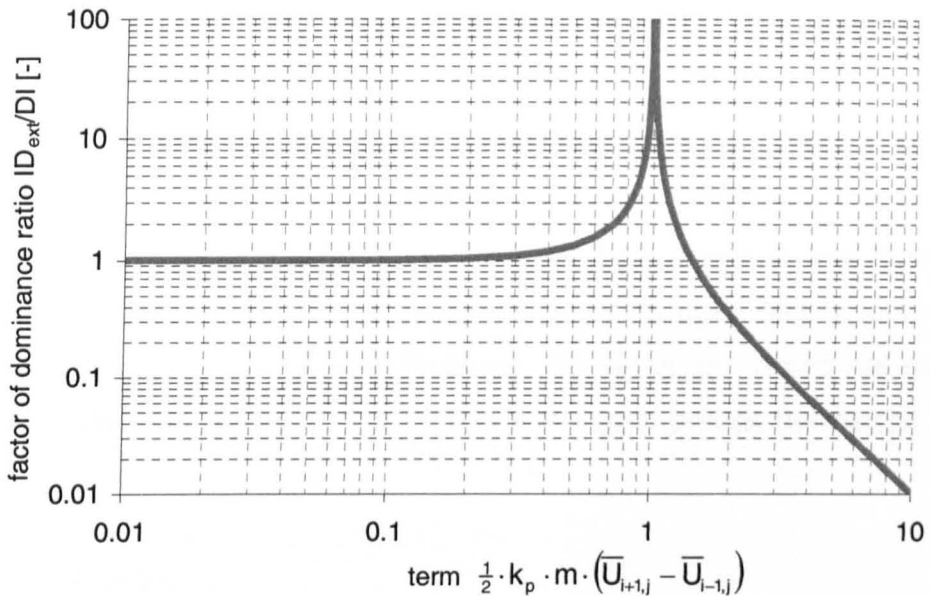
Figure 9.5:   *Value of factor of dominance ratio $|D_{ext}/D|$ versus term $\frac{1}{2} \cdot k_p \cdot m \cdot \left(\overline{U}_{i+1,j} - \overline{U}_{i-1,j} \right)$.*

◆ The quality of residuals is checked by calculating the approximated tangents of the Jacobian matrix not only from two but from more points. Using this method, accuracy of the Jacobian matrix could also be improved since the truncation error of the approximation can be reduced by one order.

◆ For fully user-implemented solutions, the ratio of dominance could be calculated at all grid-points and, if necessary, manipulated.

The first and the second measures were found to be sufficient for the present tests. All pressure corrections were restricted to 10 per cent of the Hertzian pressure and the pressure variation to determine the Jacobian matrix was set to 10^{-3}.

Beyond the point of the singularity, the ratio of dominance falls well below values for the case of constant pressure across the gap, determination of the Jacobian matrix elements is less sensitive than for the constant pressure case.

9.1.3.4   Relaxation and convergence criteria for the Newton-Raphson technique

For the Newton-Raphson scheme a relaxation factor of 0.15 was introduced; the relaxation factor of 0.3, which was used when analysing the constant pressure across the gap, was found to cause oscillations in test runs. With the above parameters mass continuity residuals reduced nearly four orders of magnitude during the Newton-Raphson iterations, but could not achieve the eight orders observed for the constant viscosity across the height of the gap.

9.1.4   Errors

9.1.4.1   Discretisation error

For the fully simultaneous method discretisation error is of second order as for the method assuming constant pressure across the height of the gap. This is due to the fact that the discretisation of all modules of the CFD software is of second order and all user added modules are of second order,

as proved in subsection 8.4.3. Consequently the complete discretisation scheme is expected to be of second order. Numerical analysis of the code was not carried out since the calculation times were already considerable for a grid of 70 x 7 volumes, and were expected to rise by an order higher than for the calculation assuming constant pressure across the height of the gap.

9.1.4.2   Iteration error

Iteration errors are attempted to be minimized by appropriate selection of the convergence criterion for the inner loop. However, it is clear that, due to a sometimes more critical ratio of dominance, the iteration error due to the limited accuracy of the computational calculation might be considerable.

9.1.4.3   Implementation error

The implementation error is more difficult to detect than for the assumption of constant pressure across the height of the gap, since no other calculation results are available for the extended approach. The following measures to exclude implementation errors were considered:

♦ Comparison with results from the second calculation method considered, the combined successive-simultaneous method discussed in the following section 9.2. If the results of the two different added modules for the pressure variation across the height of the gap agree, and the basis, i.e. the calculation assuming constant pressure perpendicular to the gap, is free of errors, it is likely that there are no implementation errors.

♦ Qualitative comparison of calculated results with the theoretical considerations of section 3.3. When calculated results and theoretical considerations are consistent, errors are unlikely.

♦ Check of particular case of pure rolling, where no changes are expected in comparison with results assuming constant pressure across the height of the gap.

The first point is discussed in section 9.2, the latter two are considered in chapter 11.

9.1.5   Performance

In comparison with the method assuming constant pressure across the height of the gap the extended approach requires for the grid of 70 x 7 volumes 17 times the calculation time. Using a Silicon Graphics R 8000 processor a calculation time of approximately 17000 seconds is required, without modification of the height of the gap. The Newton-Raphson technique for the differential continuity equation converges within approximately 20 steps. The rise in the calculation time results from the larger Jacobian matrix and the increased number of time iteration steps until the Newton-Raphson scheme converged.

The higher ratio of dominance leads to a smaller range of values of parameters as the method converges. Additionally, due to the described problems with the singularity, the method fails for particular cases. For small changes of input or numerical values of parameters the method converges again. Therefore, no map of convergence was produced. For future application of the method, the application of the other methods of section 9.1.3.3 to overcome the singularity problem should be considered.

9.2   The combined successive simultaneous method

9.2.1   Implementation details

The combined successive-simultaneous method requires slightly more effort of implementation than the fully simultaneous method, because the y-momentum equation must be implemented and coupled by the user. However, it is a pure extension of the method for constant pressure across the gap, i.e. nothing of the method of chapter 8 has to be altered or switched off. The necessary adaptations are discussed in the following and illustrated in figure 9.6.

(a)
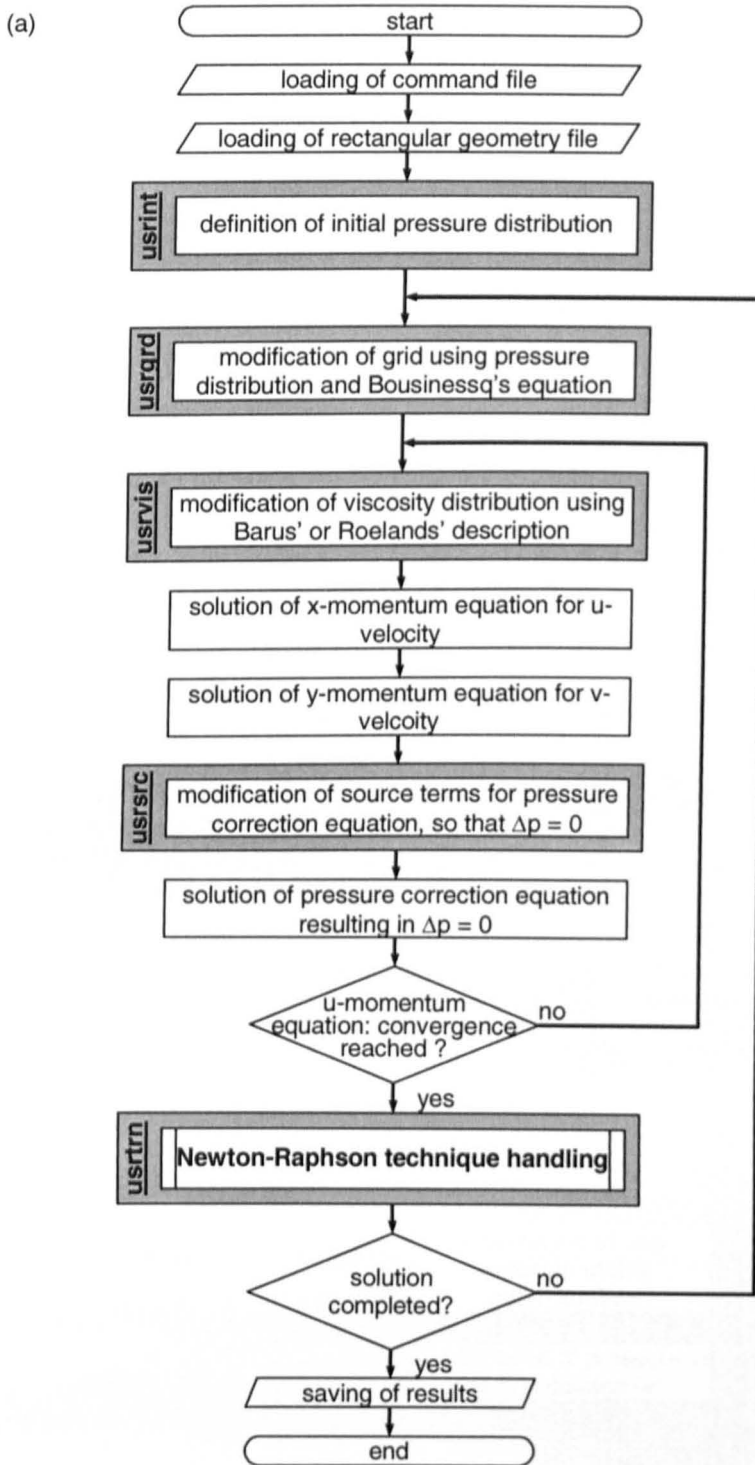
Figure 9.6:   *Complete calculation scheme for the ehl calculation allowing pressure variation across the gap employing the combined successive-simultaneous method of coupling and CFD software,*

(a)   main program,

(b)   details of Newton-Raphson technique handling,

N.B. **bold text** *indicates differences to the method for constant pressure across the gap, figure 8.6.*

(continued).

(b)   Newton-Raphson technique handling   **usrtrn**
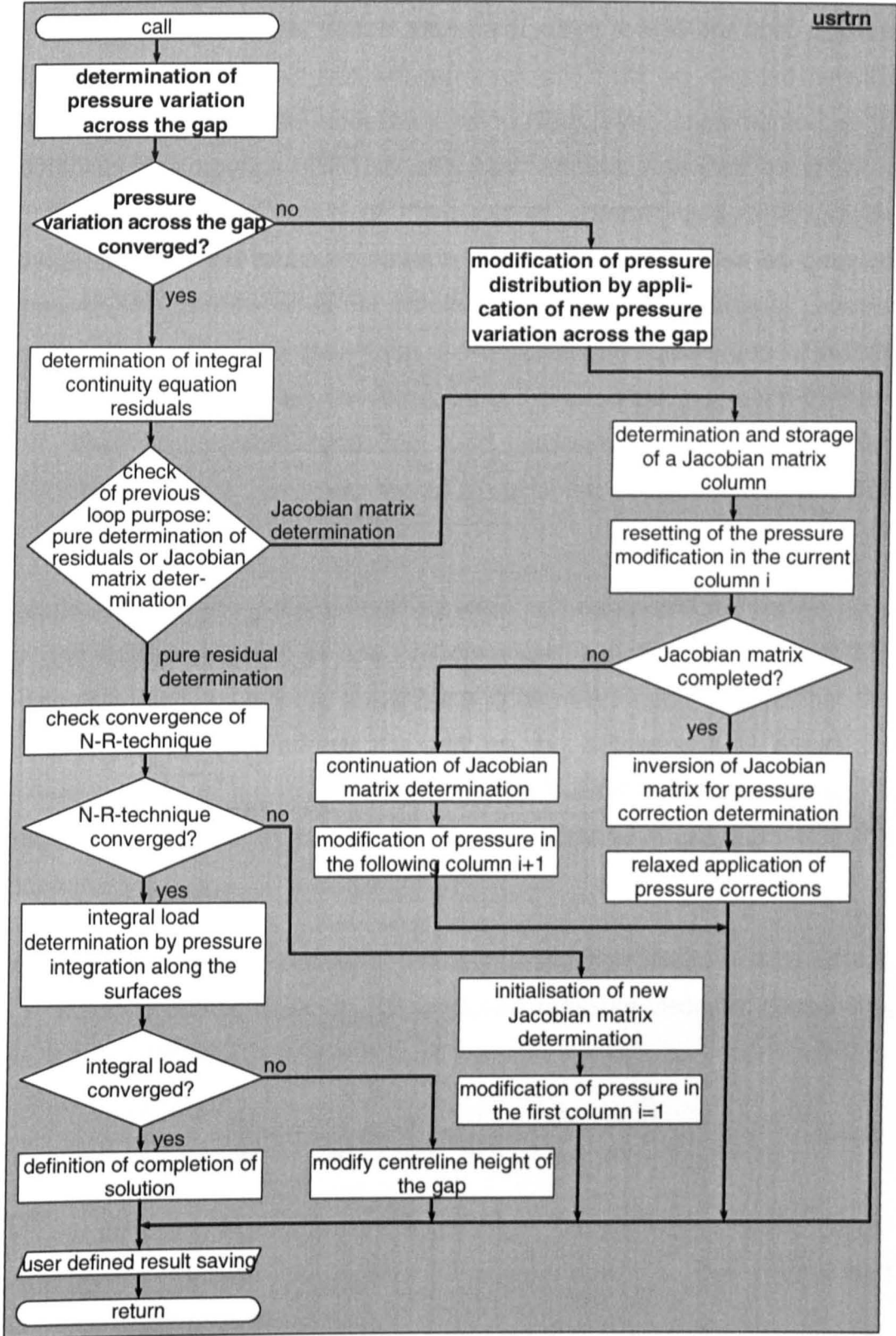
Figure 9.6:   *(concluded).*

9.2.1.1   The y-momentum equation

The introduction of the y-momentum equation solved for the pressure variation across the gap and not for v-velocity must be realised by user-defined subroutines. The necessary calculations were implemented at the beginning of subroutine USRTRN after each artificial time step, as shown in figure 9.6. An incorporation of the pressure corrections by manipulating source terms of the pressure correction equations would also be possible. However, this could lead to the problem that the determination of pressure corrections across the gap from an insufficiently converged u-velocity distribution might spoil the convergence of the successive solution of the x- and the y-momentum equation and pressure correction equation. Additionally, such a procedure would exclude the consideration of surface deflection from the innermost loop.

Various forms of the y-momentum equation can be considered as the basis for the implementation of the y-momentum equation as proposed in subsection 7.2.5.4. All these forms have to be re-arranged in a manner that the pressure gradient across the gap on the left hand side marks the unknowns, while all terms on the right hand side represent the source terms, which are assumed to be known at the moment of solution. Possible equations are, e.g.,

♦   the original Navier-Stokes equation in y-direction without inertia effects, which is independent of the employed pressure-viscosity description, i.e. equation 3.15,

$$\frac{\partial p}{\partial y} = 2 \cdot \frac{\partial}{\partial y}\left[\eta \cdot \frac{\partial v}{\partial y}\right] + \frac{\partial}{\partial x}\left[\eta \cdot \left(\frac{\partial u}{\partial y} + \frac{\partial v}{\partial x}\right)\right] \qquad (9.10),$$

♦   the simplified Navier-Stokes equation in the y-direction where Barus' pressure-viscosity description is incorporated, i.e. the re-arranged second equation of set 3.42,

$$\frac{\partial \overline{P}}{\partial \overline{Y}} = \frac{h_0}{p_{hz}} \cdot \left(1 - 2 \cdot \frac{\eta_0 \cdot u_h \cdot \alpha}{b_{Hz}} \cdot e^{\alpha \cdot p_{hz} \cdot \overline{P}} \cdot \frac{\partial \overline{V}}{\partial \overline{Y}}\right)^{-1} \cdot$$

$$\left[\frac{\partial \overline{P}}{\partial \overline{X}} \cdot \left(\gamma \cdot \frac{\eta_0 \cdot u_h \cdot \alpha \cdot p_{hz}}{h_0^{\,2}} \cdot e^{\alpha \cdot p_{hz} \cdot \overline{P}} \cdot \frac{\partial \overline{U}}{\partial \overline{Y}}\right) + \left(\gamma \cdot \frac{\eta_0 \cdot u_h}{h_0^{\,2}} \cdot e^{\alpha \cdot p_{hz} \cdot \overline{P}} \cdot \frac{\partial^2 \overline{V}}{\partial \overline{Y}^2}\right)\right]$$

$$(9.11),$$

or

♦ the simplified Navier-Stokes equation in the y-direction into which the simplified Navier-Stokes equation in the x-direction and Barus' pressure-viscosity description are incorporated, i.e. the rearranged second equation of set 3.44,

$$\frac{\partial \overline{P}}{\partial \overline{Y}} = \frac{b_{hz}}{p_{hz}} \cdot \left[1 - \left(\frac{\eta_0 \cdot u_h \cdot \alpha}{h_0} \cdot e^{\alpha \cdot p_{hz} \cdot \overline{P}} \cdot \frac{\partial \overline{U}}{\partial \overline{Y}}\right)^2\right]^{-1} \cdot$$

$$\left\{\frac{\eta_0 \cdot u_h}{b_{hz}^{\,2}} \cdot e^{\alpha \cdot p_{hz} \cdot \overline{P}} \cdot \left[\frac{\partial^2 \overline{V}}{\partial \overline{Y}^2} + \frac{\eta_0 \cdot u_h \cdot \alpha}{h_0 \cdot \gamma} \cdot e^{\alpha \cdot p_{hz} \cdot \overline{P}} \cdot \left(\frac{\partial \overline{U}}{\partial \overline{Y}} \cdot \frac{\partial^2 \overline{U}}{\partial \overline{Y}^2}\right)\right]\right\}$$

$$(9.12).$$

Selection of the most suitable equation is influenced by different aspects.

Firstly, the two equations 9.11 and 9.12 show a singularity while the first equation 9.10 does not. Accordingly, equations 9.11 and 9.12 require some treatment to avoid failure of the program.

Secondly, when considering the treatment of the viscosity gradients in the y-momentum equations, the equation shows different behaviour: equations 9.11 and 9.12 provide a closer coupling than equation 9.10. This is because in equation 9.10 all viscosity gradient terms are on the right hand side, i.e viscosity gradients from the previous iteration loop are considered. In equation 9.11, the pressure gradient and hence the viscosity gradient in the x-direction is on the right hand side, i.e. the values from the previous loop are considered, while the pressure gradient representing the viscosity gradient in the y-direction has been moved to the left hand side and is hence considered simultaneously. In equation 9.12, all pressure gradients and hence viscosity gradients are on the left hand side. Because the viscosity gradient along the gap was found to be significant, section 3.3, equation 9.12 appears to be preferable and it was selected for implementation.

The implementation of the equation requires re-transformation of the selected equation into its dimensional form, because the applied CFD software is based on the dimensional equations. The re-transformation is given in detail in appendix J. Equation 9.12 becomes

$$\frac{\partial p}{\partial y} = \left[1 - \left(\eta \cdot \alpha \cdot \frac{\partial u}{\partial y}\right)^2\right]^{-1} \cdot \left\{\eta \cdot \frac{\partial^2 v}{\partial y^2} + \eta^2 \cdot \alpha \cdot \left(\frac{\partial u}{\partial y} \cdot \frac{\partial^2 u}{\partial y^2}\right)\right\}$$

(9.13)

Replacing the perpendicular v-velocity component using the continuity equation makes the equation independent of this velocity component,

$$\frac{\partial p}{\partial y} = \left[1 - \left(\eta \cdot \alpha \cdot \frac{\partial u}{\partial y}\right)^2\right]^{-1} \cdot \left\{-\eta \cdot \frac{\partial^2 u}{\partial x \, \partial y} + \eta^2 \cdot \alpha \cdot \left(\frac{\partial u}{\partial y} \cdot \frac{\partial^2 u}{\partial y^2}\right)\right\}$$

(9.14).

The replacement of v-velocity means also that the result of the y-momentum equation solution in the CFD code is irrelevant.

Discretisation of equation 9.14 should maintain the second order accuracy of the method and take into account the peculiarities due to the algorithm by Rhie and Chow to avoid numerical oscillations, as mentioned in section 6.2.3.2.

The pressure gradient across the gap is discretised using the finite volume approach as used in the CFD code

$$\int_{\Delta V} \left(\frac{\partial p}{\partial y}\right) dV_{i,j} \approx \left(p_{i,J+1} - p_{i,J}\right) \cdot \Delta x \cdot l_c$$

(9.15).

with the pressure values $p_{i,J+1}$ and $p_{i,J}$ at the border of a finite volumes i,j as illustrated in figure 9.7.

The right hand side terms of equation 9.15, i.e. the source terms, are discretised with the velocity gradients provided by the CFD code for the first order and mixed second order derivatives, since they are most accurate. The remaining derivatives are approximated with second order discretisation:

$$\int_{\Delta V}\left[1-\left(\eta\cdot\alpha\cdot\frac{\partial u}{\partial y}\right)^2\right]^{-1}\cdot\left\{-\eta\cdot\frac{\partial^2 u}{\partial x\,\partial y}+\eta^2\cdot\alpha\cdot\left(\frac{\partial u}{\partial y}\cdot\frac{\partial^2 u}{\partial y^2}\right)\right\}\cdot dV_{i,j}\approx$$

$$\left[1-\left(\eta_{i,j}\cdot\alpha\cdot\left.\frac{\partial u}{\partial y}\right|_{i,j}\right)\right]^{-1}\cdot$$

$$\left\{-\eta_{i,j}\cdot\frac{\left.\frac{\partial u}{\partial x}\right|_{i,j+1}-\left.\frac{\partial u}{\partial x}\right|_{i,j-1}}{2\cdot\Delta y}+\eta_{i,j}{}^2\cdot\alpha\cdot\left.\frac{\partial u}{\partial y}\right|_{i,j}\cdot\frac{u_{i,j+1}-2\cdot u_{i,j}+u_{i,j-1}}{\Delta y^2}\right\}\cdot\Delta x\cdot\Delta y\cdot l_c$$

$$(9.16).$$
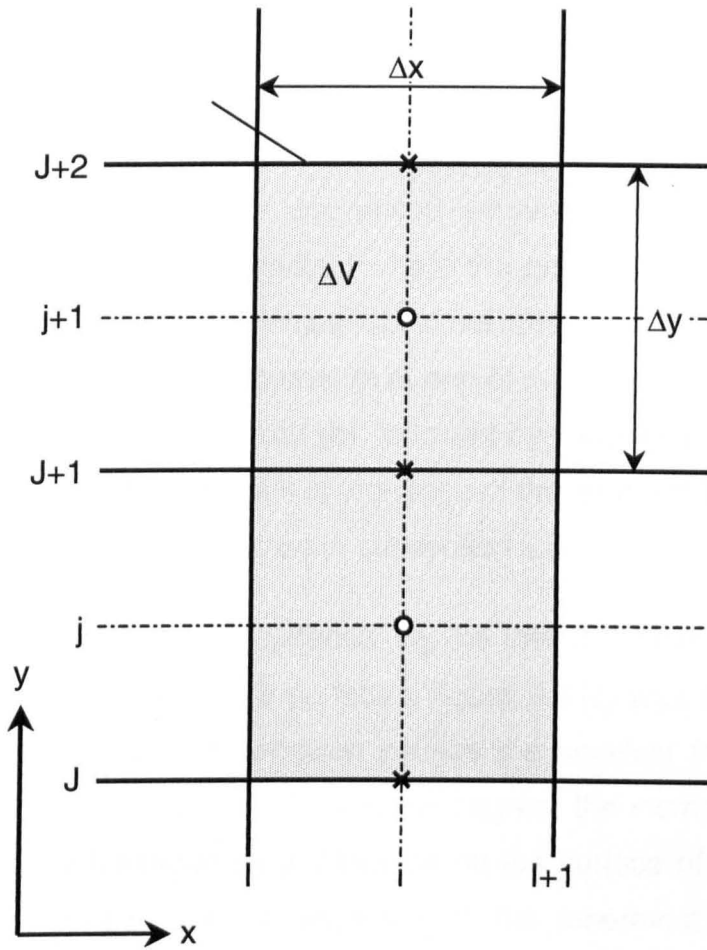
x location of pressure at volume face
o location of pressure at volume centre

Figure 9.7:   Nomenclature for discretisation of pressure terms of y-momentum equations.

Near the surfaces, for the finite volumes i,1 and i,m, the applied central approximation could not be used and respective negative or positive second order approximations were applied.

Integration from one volume centre i,j to the next i,j+1 was realised by using the pressure gradient of volume i,j and i,j+1 to determine the pressure increase between the volume centres and the common volume edge

$$p_{i,j+1} = p_{i,j} + \left(\left. \frac{\partial p}{\partial y} \right|_{i,j} + \left. \frac{\partial p}{\partial y} \right|_{i,j+1} \right) \cdot \frac{\Delta y}{2}$$
   (9.17).

For the extrapolation of the pressure value of the finite volume centres to the boundary surfaces centres, which is required for the determination of the surface deflection, the built in extrapolation of the CFD code was used.

Finally, the boundary for the discretised y-momentum equation must be defined, i.e. a line along the contact where the pressure distribution defined by the Newton-Raphson technique does not change due to the pressure variation across the gap. The pressure at one of the two surfaces may be set, as illustrated in figure 9.8 (a) and (b), followed by integration to the opposite surface. Such a setting will result in a change of the shape of the gap, in case (a) even opposite to that expected in subsection 3.3.4.

The centre line between both surfaces, i.e. the row of the centres of the finite volumes half way between the surfaces, figure 9.8 (c) was found to be the most suitable because this condition causes the smallest influence on the total deflection at a location x_i. To a major degree, the increase of pressure on one surface is balanced by a decrease on the surface of the other. This procedure accelerates the convergence of the innermost iteration loop. Additionally, with this approach the extrapolation of the pressure at the volume centres to the walls, which is implemented in the CFD code, can be used.
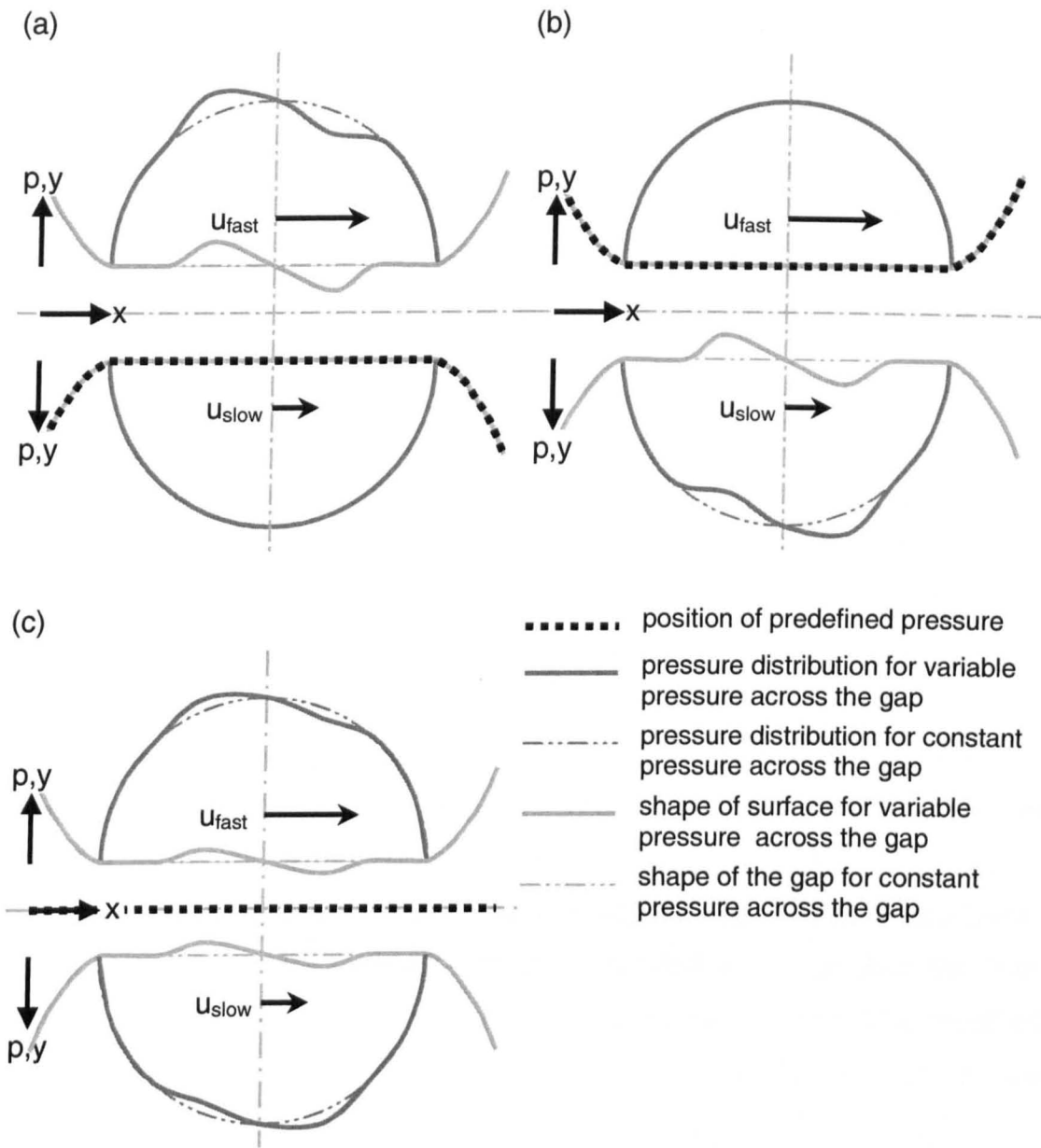
Figure 9.8:   Possible position for the boundary values for the y-momentum equation and resulting qualitative shape of the gap, (a) position of boundary values at the slower surface, (b) position of boundary values at the faster surface, (c) position of boundary values at the contact centreline.

9.2.1.2   Newton-Raphson technique and continuity equation residuals

For the combined successive-simultaneous method, the residuals of the integral continuity equation are evaluated. Hence the method proposed in section 8.1.6 for the method assuming constant pressure across the height of the gap, could be used unchanged.

9.2.1.3   Initial values

The same two initial pressure distributions, as used for the fully simultaneous method, can also be employed for the present method: The Hertzian pressure distribution or a converged pressure distribution assuming constant pressure across the height of the gap. However in the present case pressure corrections across the height of the gap are already calculated and employed before the continuity equation residuals are calculated for the first time. That means that the true pressure distribution, from which the Newton-Raphson technique starts, is already two-dimensional. Figure 9.9 illustrates the set Hertzian pressure distribution (a) and the real initial pressure distribution calculated by considering the y-momentum equation (b). The latter is a better initial value to the ehl problem with the extended approach than the first, which was also attempted for the fully simultaneous method. The modified Hertzian pressure distribution leads to converging results and was hence applied.

In contrast, the application of a converged ehl result as an initial pressure distribution leads to a strongly distorted initial pressure distribution near the pressure spike, which leads to convergence problems at the beginning of the calculations.

(a)

(b)
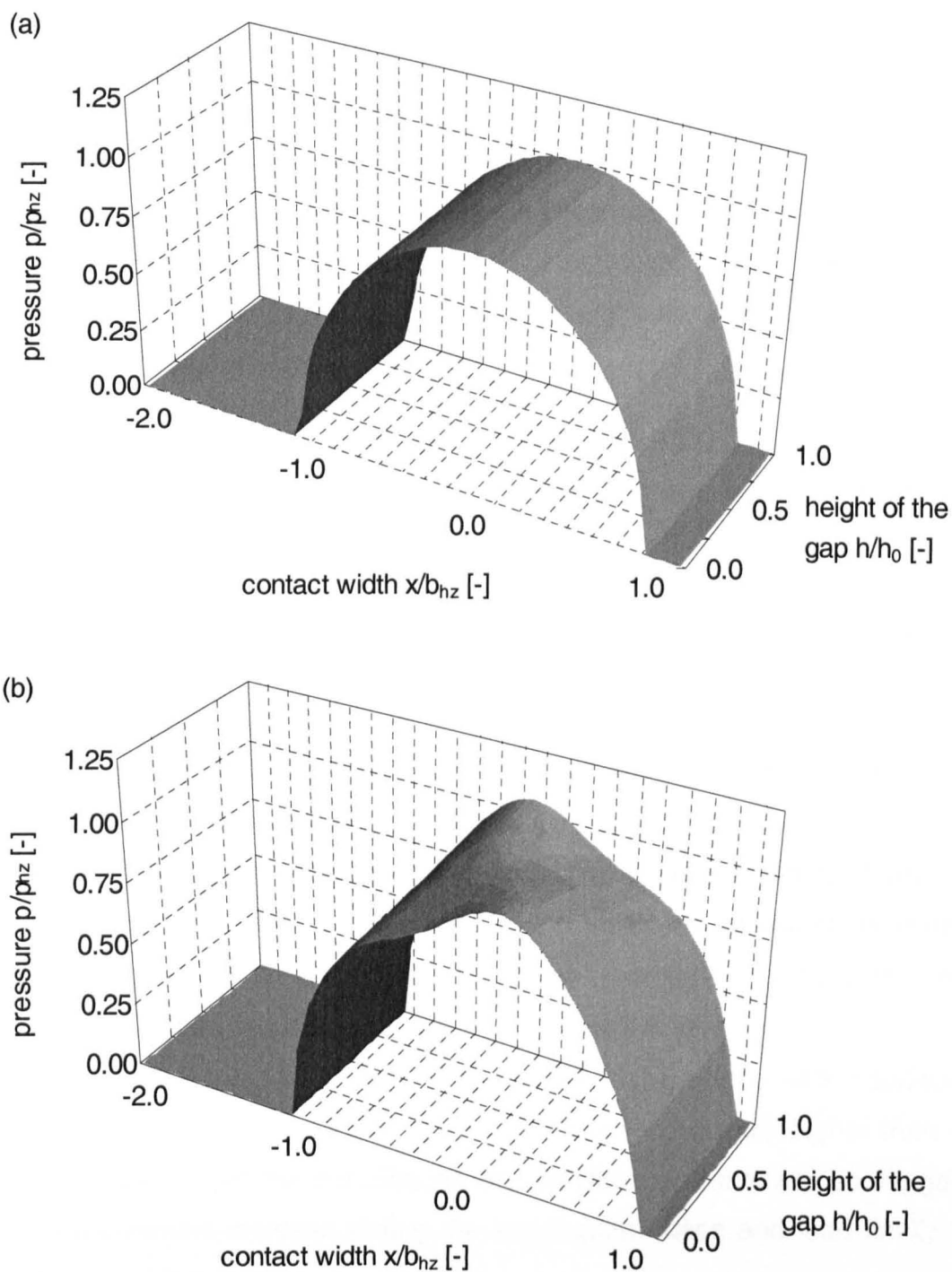
Figure 9.9:   Set (a) and real (b) initial values for the Newton-Raphson technique when employing combined successive-simultaneous method,
N.B. pressure variation across the gap is magnified in comparison to along the gap.

9.2.2   Stabilising the solution

9.2.2.1   Description of problem

Initial test of the program led to converging solutions only for modest values of load and speed parameters, where the influence of the additional viscous terms was expected to be small. For higher loads, the program failed to converge after increasing oscillations of the pressure corrections of the Newton-Raphson method.

It was observed for the calculation method assuming constant pressure across the gap, section 8.2.1, that the Newton-Raphson technique started to oscillate and failed to converge due to the central differencing scheme implied in the application of CFD software. This problem was cured by some grid shifting, which reduced the initial oscillations to a measure that they finally disappeared again.

The first Newton-Raphson step of the combined successive-simultaneous method, as with the method with constant pressure across the gap, also leads to a slightly oscillating pressure distribution along the gap, such as that shown in figure 8.7. These oscillations cause the pressure variations across the gap, i.e. the deviation from the pressure on the centreline along the gap, to change from the smooth distribution for the initial value, figure 9.10 (a) to the strongly oscillating shape shown in figure 9.10 (b). Hence, at the surfaces the oscillations for the successive-simultaneous method are higher than at the centreline and for the calculations with constant pressure across the gap. These oscillations increase during the subsequent steps and lead finally to divergence of the solution.

(a)

deviation from
centreline
pressure
$(p-p_{cl})/p_{hz}$ [-]

contact width x/b_{hz} [-]

height of the
gap y/h [-]

(b)

deviation from
centreline
pressure
$(p-p_{cl})/p_{hz}$ [-]

contact width x/bhz [-]

height of the
gap y/h [-]
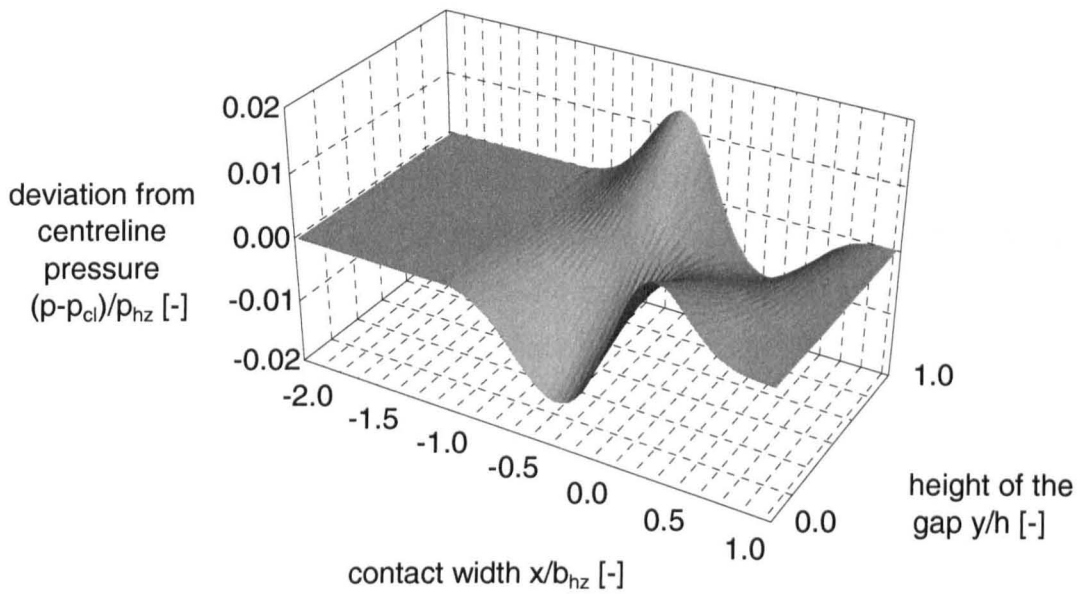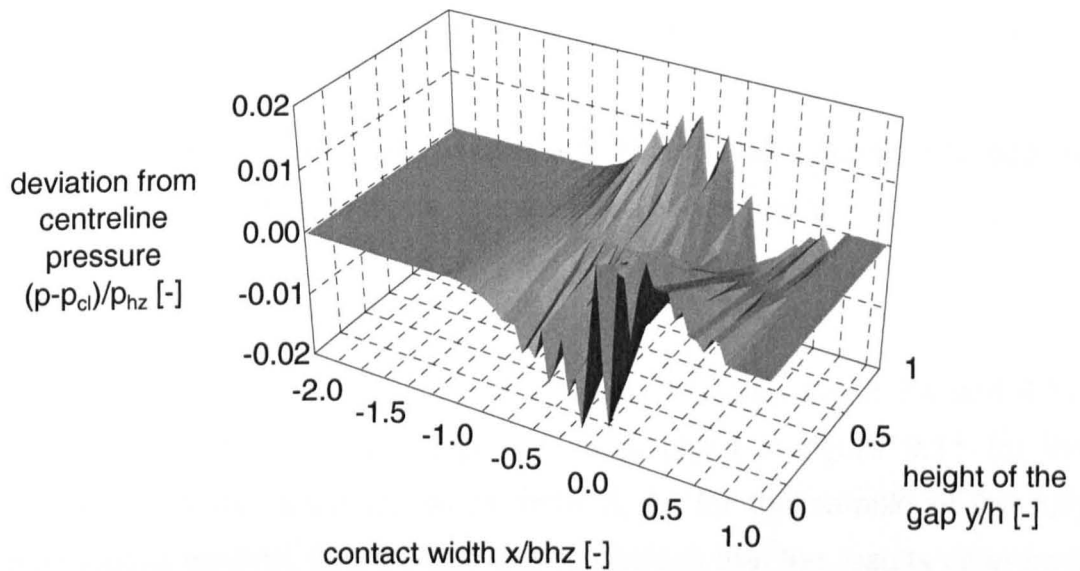
*Figure 9.10: Pressure variation across the gap resulting from smooth (a)
and oscillating (b) pressure corrections of the Newton-
Raphson technique,*
*N.B. pressure variation across the gap is magnified in
comparison to along the gap.*

9.2.2.2   Solution approach

Various methods to overcome oscillation problems were discussed in subsection 8.2.2. Although smoothing of the pressure was recognized as spoiling the solution near the pressure spike [14], it was the only method leading to converging results for the present approach. The smoothing was applied to the pressure distribution along the gap after the pressure corrections from the Newton-Raphson technique were applied, to which relaxation had already been applied. The smoothing was realised by calculating an average value of three or five values,

$$\hat{p}_{i,j} = \tfrac{1}{4} \cdot p_{i-1,j} + \tfrac{1}{2} \cdot p_{i,j} + \tfrac{1}{4} \cdot p_{i+1,j} \tag{9.18a}$$

and

$$\hat{p}_{i,j} = \tfrac{1}{16} \cdot p_{i-2,j} + \tfrac{1}{4} \cdot p_{i-1,j} + \tfrac{6}{16} \cdot p_{i,j} + \tfrac{1}{4} \cdot p_{i+1,j} + \tfrac{1}{16} \cdot p_{i+2,j} \tag{9.18b}.$$

In order to reduce the spoiling of any pressure spike, the application of the latter equation for the first three Newton-Raphson iterations and the subsequent application of the first equation in the case of a pressure maximum in the first half of the contact was found to be a practical smoothing scheme leading to converged results and was hence used.

9.2.3   Sample result

For the same parameters as previously used in subsection 8.2.4 and 9.1.2 and given in table 8.1, a sample result is given in figure 9.11 for the combined successive-simultaneous method. As for the sample of the fully simultaneous method, figure 9.3, it is also obvious that the results differ from those for the analysis assuming a constant pressure across the gap.
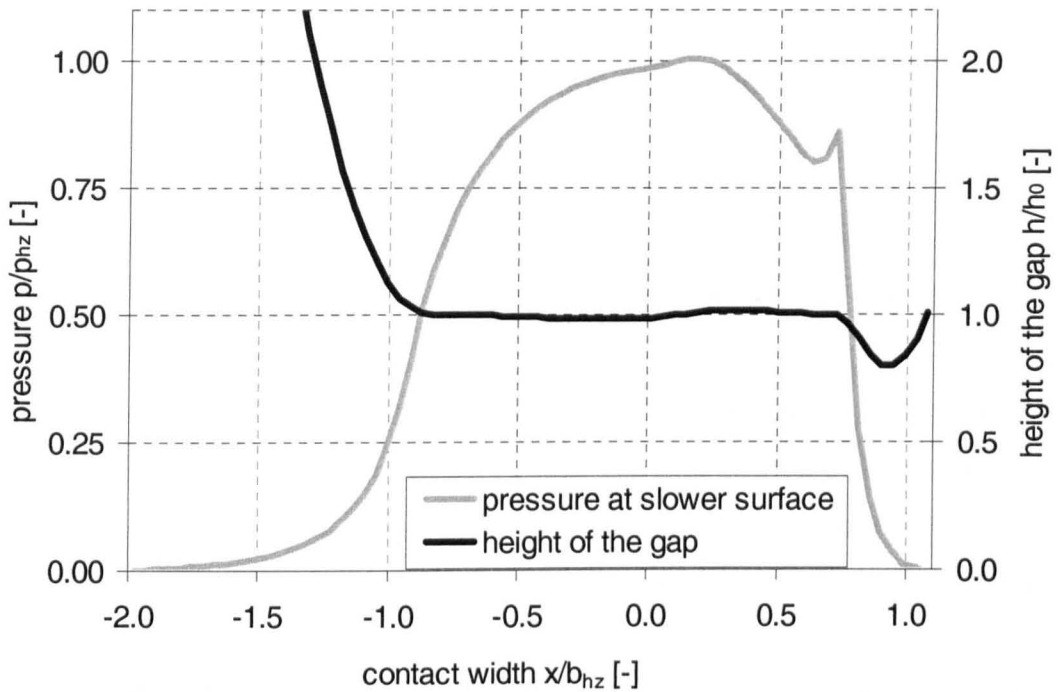
Figure 9.11:   Sample result for the ehl line contact problem allowing pressure variation across the gap using the combined successive-simultaneous method of coupling. Input parameters according to table 8.1 agree with those of the sample for the fully simultaneous method, figure 9.3.

9.2.4   Numerical parameters

The introduction of the additional iteration loop requires the introduction of an additional convergence criterion for the convergence of the y-momentum equation beside those parameters also used for the method with constant pressure across the gap.

9.2.4.1   The x-momentum equation

The criterion of convergence for the x-momentum equation remains unchanged as for the method assuming constant pressure across the gap and the fully simultaneous method.

$$f_{x-mom,sum} = f_{x-mom,i,j} \cdot n \cdot m \cdot l = \frac{\eta_0 \cdot e^{\alpha \cdot p_{Hz} \cdot P} \cdot u_H \cdot b_{hz} \cdot m^2 \cdot l_c}{h_0} \cdot E_{computational} \qquad (9.19).$$

9.2.4.2   The y-momentum equation

Because of the form of equations 9.15 to 9.17 and the resulting fact that the determination of the new pressure distribution across the gap is explicit and *non*-iterative, a residual for the y-momentum equation is not necessary.

9.2.4.3.   The coupling of x- and y-momentum and elasticity equations

However, it is necessary to establish a criterion, when the successive iteration of the x- and y-momentum equations and the deformation equation has converged. This means that the source term approximations for the y-momentum equation, equation 9.16, and also for the x-momentum equation, change their values only due to numerical truncation and round-off effects. The prediction of the number of valid digits in the source terms is difficult because of the variable, possibly infinite, factor of dominance discussed in subsection 9.1.3.3 and because of the successive treatment of the x- and y-momentum equations and deformation equation.

Hence a different consideration is attempted. It was found for the method with constant pressure across the gap that a pressure variation of $\Delta p/p = 10^{-4}$ was a good working approximation to obtain changes in the velocity field resulting in residual changes which are sufficiently accurate to provide a Jacobian matrix for a converging solution.

On the other hand, four valid digits for the u-velocity gradients were found necessary to obtain a Jacobian matrix for converging results. This means that changes of the pressure below $10^{-4} \times 10^{-4} = 10^{-8}$ are small enough that they do not have an arbitrary influence on the Jacobian matrix to secure convergence, as for the method with constant pressure across the gap.

Hence, the convergence criterion of the x-momentum and y-momentum iteration should be ideally set so that the change of the pressure from one iteration loop to the next should be smaller than 10^{-8},

$$\frac{p - p_{prev}}{p} \leq 10^{-8} \qquad (9.20).$$

However, practical tests showed that this convergence criterion is too tight to be fulfilled by the successive coupling of grid adaptation, and the x- and the y-momentum equation. A value of

$$\frac{p - p_{prev}}{p} \leq 10^{-6} \tag{9.21}$$

was found to be a reliably working convergence criterion.

9.2.4.4   Newton-Raphson technique

For the modification of pressure to approximate the Jacobian matrix the considerations for the ratio of dominance of the fully simultaneous method of subsection 9.1.3.3 are valid as well, because both solutions are based on the same differential equations. The measures mentioned there can also be applied to the present numerical method. However, the present method is expected to be slightly less sensitive than the fully simultaneous method, due to the evaluation of the residuals of the integral continuity equation. The integrated residuals are calculated from a sum of cell residuals. If the residual of one cell is inaccurate because of a high ratio of dominance, the summing can reduce the error.

Additionally, finer pressure modifications to determine the Jacobian matrix make the convergence criterion for the x-momentum-y-momentum coupling even tighter, although this value could not even be set to the desired value for pressure modifications of 10^{-4}, as discussed in the previous subsection.

Nevertheless, pressure modifications of $\Delta p/p = 10^{-4}$ were selected for the Newton-Raphson technique as a value previously used successfully.

The relaxation factor for the pressure corrections obtained from the Newton-Raphson method was set to 0.3. The described settings led to a reduction of the continuity equation residuals of about five orders of magnitude, i.e. values slightly better than that for the fully simultaneous method.

9.2.5   Errors

9.2.5.1   Discretisation errors

Discretisation error was investigated using the same method as for the method assuming constant pressure across the height of the gap of subsection 8.4.3. Again, not a full set of single, double and quadruple fine grids was used because of the expected calculation times. Similar to figure 8.15, figure 9.12 shows the development of the height of the gap depending on the grid size, for the implemented program and for the assumption of first and second order approximation.

The discretisation error figure 9.12 principally confirms the second order accuracy of the implemented method for the combined successive-simultaneous method, in particular when the grid size is finer than 80×8 volumes.

9.2.5.2   Iteration errors

The additional iteration loop leads to a further iteration. The iteration error of the x-momentum equation is minimized by making the residuals defining convergence as small as possible. However, the convergence criterion for the loop iterating the x-momentum equation, the modified y-momentum equation, and the elasticity equation could not be set as tight as possible. Although iteration errors are restricted to a minimum, an influence of these cannot be excluded for the combined successive-simultaneous method of coupling.

9.2.5.3   Implementation errors

The methods to detect implementation errors are the same as for the fully simultaneous method, i.e. comparison of the fully simultaneous method with the combined successive-simultaneous method, qualitative comparison with theory and evaluation for load cases where Reynolds equation based approach and extended approach are expected to agree. The latest approach investigates exclusively the extension to variable viscosity across the gap, because those parts of the method, which were already

implemented for a constant pressure across the gap, remained completely unaltered during the extension.

Any differences in results between both methods can also result from iteration errors.
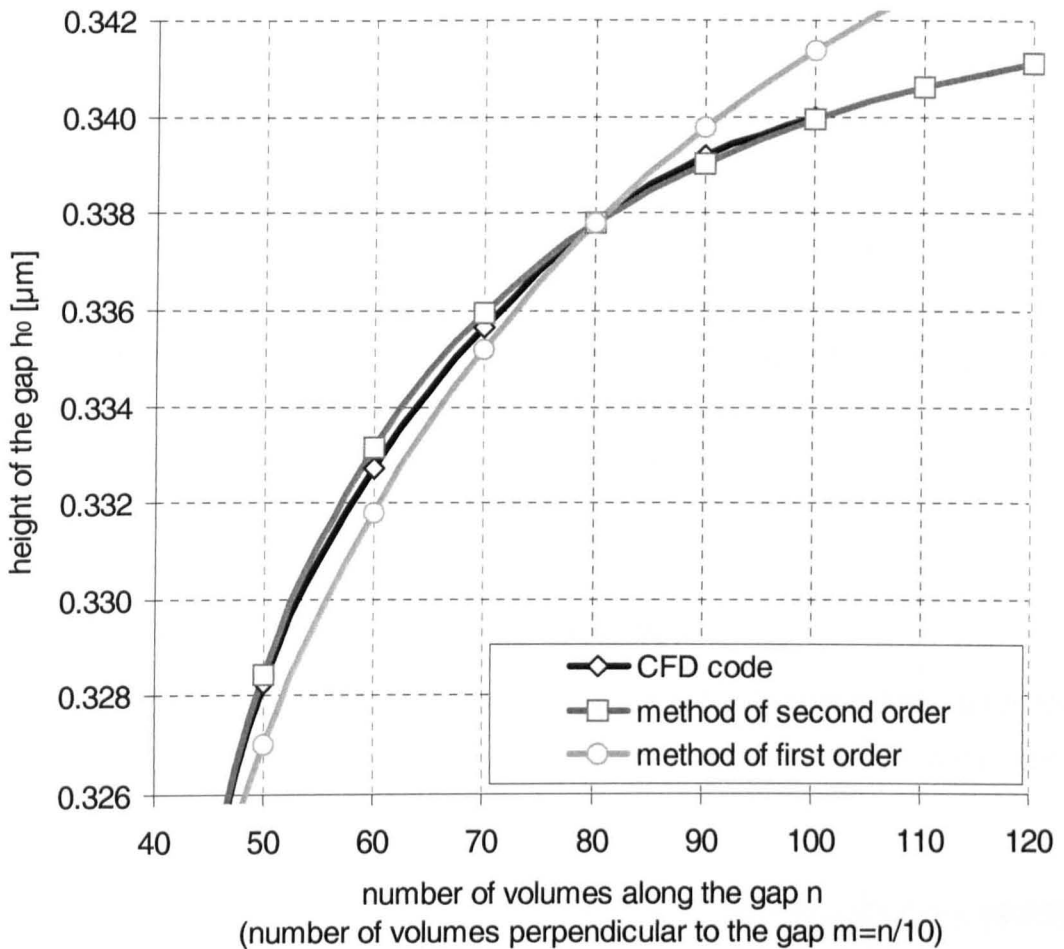
Figure 9.12:   Variation of height of the gap depending on grid resolution for the combined successive-simultaneous method of coupling.

9.2.6   Performance

The combined successive-simultaneous method proved to be 50 per cent slower than the calculation scheme with constant pressure of chapter 8.

For the limits of the method, the same aspects, as discussed for the method with the constant pressure across the height of the gap in section 8.5 and for the fully simultaneous method in subsection 9.1.5, are valid. If the influence

of the extended approach is small, the limits are as for the method with a constant pressure across the height of the gap. If influence of the extended approach is high, the very high factor of dominance near the singularity might cause bad conditioning of the Jacobian matrix and hence spoil the solution. A determination of the range of parameters, for which the combined successive-simultaneous method can be applied, is covered in part III of the present study, where a wider field of parameters is investigated.

9.3   Preliminary evaluation of the numerical methods

For preliminary evaluation of the two numerical methods for the extended approach, i.e. the fully simultaneous and the combined successive-simultaneous method, the sample results for these two methods are compared and features distinguishing the two methods are summarized. With this information, conclusions are drawn which define the further procedure of evaluation and discussion.

9.3.1   Comparison of sample results

Figure 9.13 compares the two numerical methods by showing results for the sample given in table 8.1. Part (a) of figure 9.13 gives the dimensionless pressure distribution at the lower, slower surface,

$$P_{slow} = \frac{p_{slow}}{p_{hz}} \qquad (9.22),$$

for a Reynolds equation based solution assuming constant pressure across the gap as presented in chapter 8, for the extended approach allowing pressure variation across the gap and using both the fully simultaneous method, section 9.1, and the combined successive-simultaneous method, section 9.2. The pressure distribution principally agrees for the two methods solving the extended approach except for the pressure spike area. Here, the combined successive-simultaneous method shows a pressure spike similar to that for the Reynolds equation based solution, while the pressure spike disappears for the solution from the fully simultaneous method.

Part (b) of figure 9.13 gives the height of the gap, non-dimensionalised by the height of the gap at the contact centreline for the Reynolds equation based solution,

$$H = \frac{h}{h_{0,Re}}$$ (9.23),

for the same three analysis methods. The shape of the gap is similar with an additional constriction in the first half of the contact and a widening in the second half of the contact. Some differences appear for the first half of the contact. Corresponding to the pressure distribution, significant differences between the methods are present for the traditional ehl constriction where the combined successive-simultaneous method agrees again with the Reynolds equation based solution, whereas the constriction appears later and is smaller for the fully simultaneous approach.

9.3.2   Further differences

In addition to the above sample result differences, the following major differences can be summarized for the two implemented methods:

9.3.2.1   Model aspects

♦ The forms of the governing equations are different for the fully simultaneous approach in comparison with the combined successive-simultaneous method. The former takes the genuine momentum equations into account, while the latter uses the genuine x-momentum equation and an equation derived from both the x- and y-momentum equations. The latter equation is, in comparison with the full Navier-Stokes equations, simplified by omitting negligible terms.

(a)

(b)
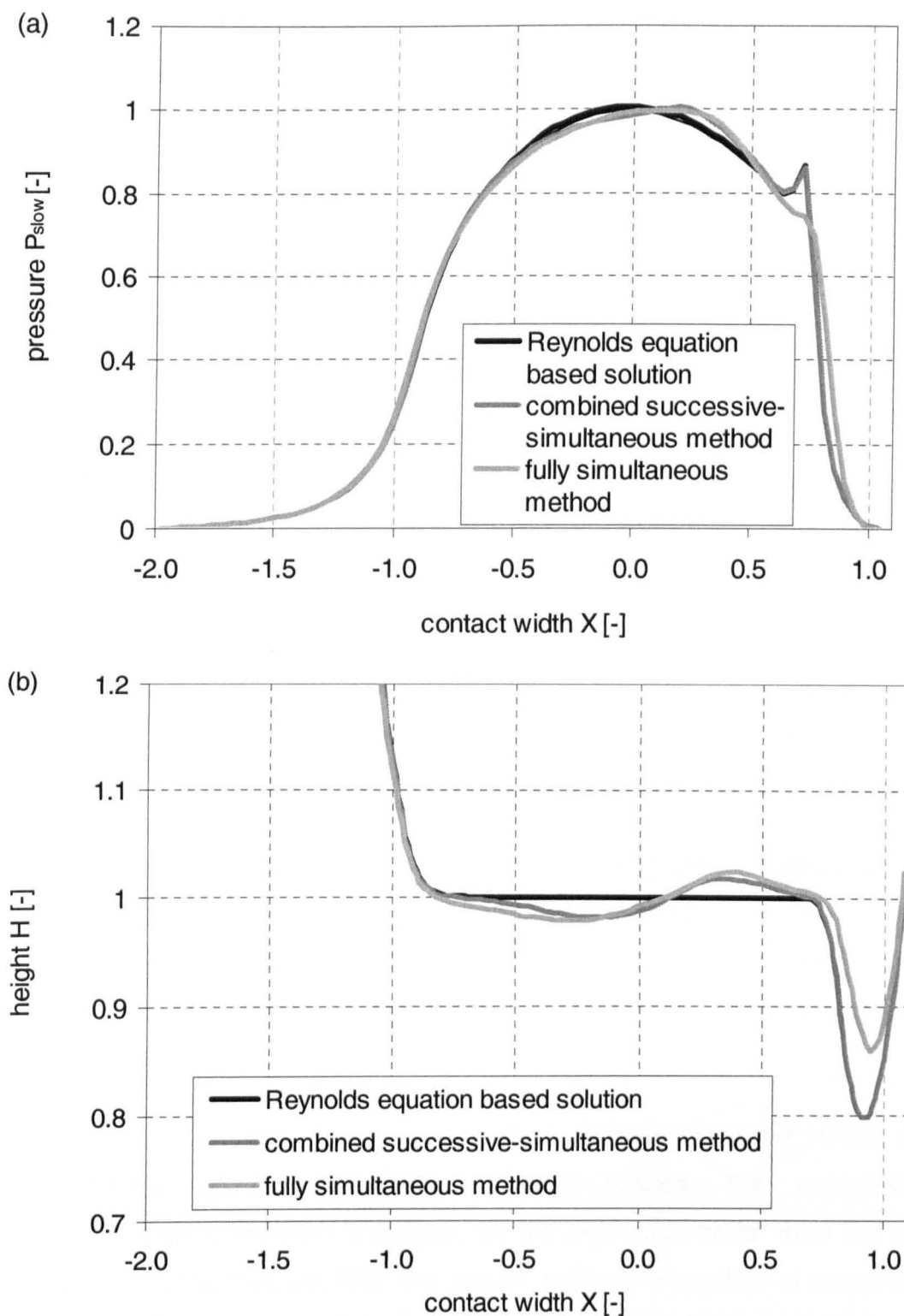
Figure 9.13:   Comparison of the sample result for the fully simultaneous and the combined successive-simultaneous method,
(a) pressure distribution at the lower, slower surface,
(b) height distribution.

9.3.2.2   Governing equations

♦   The combined successive-simultaneous method evaluates the integral conservation of mass residual values, equation 9.2, whilst the fully simultaneous method evaluates the differential values, equation 9.1.

♦   The fully simultaneous method requires the determination of the velocity component across the gap, while the combined successive-simultaneous method in the selected form does not evaluate any v-velocity values.

9.3.2.3   Numerical parameters

♦   The fully simultaneous method requires a converged Reynolds equation based solution as an initial guess to achieve convergence whilst the combined successive-simultaneous method can also cope with a Hertzian pressure distribution as initial values. This means, that during the run of the fully simultaneous method the pressure spike disappears while it develops for the combined successive-simultaneous method.

♦   The fully simultaneous method requires stronger relaxation of the pressure corrections proposed by the Newton-Raphson method than is required for the combined successive-simultaneous method. Hence more Newton-Raphson iterations are required until the same degree of convergence is reached.

♦   Described by the numbers of orders of magnitude by which the residuals of the continuity equation reduce, the successive-simultaneous method converges, for the test case, better than the fully simultaneous method. With the former method, five orders of magnitude were achieved compared with less than four for the latter method.

♦   Treatment of the numerical problems due to the singularity is easier for the combined successive-simultaneous method than it is for the fully simultaneous method.

♦   Results of the combined successive-simultaneous method might be influenced by some iteration error.

9.3.2.4   Computational effort

♦ The computational effort for a single Newton-Raphson step is higher for the fully simultaneous method due to the larger Jacobian matrix, so that the total computational time for the fully simultaneous exceeds that for the successive-simultaneous method by one order of magnitude.

♦ The total required number of Newton-Raphson steps to reach a particular convergence is higher for the fully simultaneous method than for the combined successive-simultaneous, which leads to an additional increase in the total computational time.

9.3.3   Conclusion

The above described similarity of the sample results for the fully simultaneous and the combined successive-simultaneous methods suggest at this stage that both methods seem to be suitable for the solution of the ehl problem using the extended approach. However, both methods show differences in the zone where Reynolds equation based solutions show the ehl pressure spike. For a full understanding and evaluation of the methods and its differences, detailed consideration and discussion of the results with reference to the governing equations is required.

The limits of the presented extended methods could not be predicted exactly, so determination of the limits by the application of the new numerical techniques to a wider range of parameters is desirable. Such an application would contribute considerably to the objective of the present study, to understand whether the extended approach can lead to a more realistic contact description.

For such a generation of multiple results as well as for any practical application, the combined successive-simultaneous solution with computational times measured in hours is much preferable to the fully simultaneous method with computational times of almost one day.

Hence, in the succeeding part III, results for a variety of parameters are presented, all of which were obtained with the combined successive-

simultaneous numerical method. Afterwards, these results are discussed with view to numerical and physical aspects, referring to the fully simultaneous method and sample results where necessary.

Part III

Application of the extended approach

and

General evaluation

Chapter 10

Results from the extended approach

10.1   Introduction

After the development, preliminary evaluation and selection of a numerical method for the extended approach in part II of this study, part III fulfils a twin function. On the one hand, it deals with those numerical method issues which could not be answered in part II. Simultaneously, it reverts to the consideration of physical phenomena due to the application of Navier-Stokes equations as discussed in part I. For a detailed understanding of numerical and physical phenomena, results for a range of parameters are considered. Chapter 10 defines this range and presents the results, while chapters 11 and 12 provide detailed discussion from different points of view for both numerical and physical aspects.

The present chapter initially introduces the parameters for which results are available and gives reasons why these parameters were chosen. The subsequent section 10.2 delivers results to answer the question as to whether traditional methods of data presentation are also suitable for the extended approach of the present study. From section 10.3 onwards, results for the various unknown variables of the ehl problem and comparison with Reynolds equation based solutions are given, starting with the shape of the gap as a one-dimensional variable. Subsequently, results for the two-dimensional variables, velocity and pressure, are given in sections 10.4 and

10.5 respectively. Finally, results for the shear stress and the traction coefficient are presented.

Two types of data presentation were chosen throughout this chapter:

♦ For selected operating conditions the full field distribution of a variable is presented at all positions of the contact.

♦ Where differences with Reynolds equation based solutions are significant, characteristic values describing these differences were defined. These values are then displayed for all investigated parameters in summarizing figures.

For the cases, where the full two-dimensional data fields were used, they were obtained from the default output files of the CFD software, showing results in a four digit format $x.xxx \times 10^{xx}$. This leads to the fact that, in some cases, effects due to the extended approach have the same order of magnitude as the accuracy of the numerical data used.

10.2   Investigated parameters

The selection of the parameters for this results chapter was guided by a number of aspects: The parameters were chosen so that the factors k_p and k_r, defined in equation 3.38 and 3.39, subsection 3.3.4.1, range up to values which require an extended solution approach instead of a Reynolds equation based solution. Similar parameters as used in the development of the numerical method and in other published work were desired. An attempt was made to cover some variety in result features by variation of the pressure spike position and central film thickness and by variation of the factors k_p and k_r.

Furthermore the parameters were chosen so that converging results were obtained for any sliding ratio value without alteration to the numerical settings defined in chapter 9. Hence, the cases considered define some zone where the proposed combined successive-simultaneous method can be applied. Solution of the extended approach with somewhat higher values for the

factors k_p and k_r may be possible with some purpose made alterations to numerical settings.

Taking the above-mentioned into consideration, results for the extended approach are presented for a sample configuration defined by the reduced radius of the contact, the oil density and the material parameters Young's modulus and Poisson's ratio for the solid surfaces. For this configuration two hydrodynamic speed-viscosity combinations and two applied load values were selected and the four possible combinations, subsequently named load cases, were considered. For all load cases, the sliding ratio was varied in eleven steps from pure rolling, $S = 0$ to pure sliding $S = 1$, while hydrodynamic speed was kept constant. The values for the load cases are given in table 10.1.

All cases were investigated with a grid of 70 x 7 finite volumes and, in terms of Hertzian width, fixed boundaries of $X = -2.0$ and $X = +1.08$ were defined, in order to get comparable resolution in the Hertzian pressure zone. [*]

For familiarisation, results based on a Reynolds equation based approach for the four load cases are given in figure 10.1[t]. Dimensional axes were used to emphasize the differences between the load cases. Load is smaller for load cases i and ii than for load cases iii and iv. Hence the length and height of the Hertzian pressure distribution is smaller for load cases i and ii. However, the height of the gap is hardly influenced by load increase[‡]. Velocity and viscosity are higher for load cases ii and iv than for load cases i and iii and therefore the height of the gap is larger for load cases ii and iv. Velocity and

---

[*]   In the present chapter the dimensionless values are still characterised by capital letters, however, since these are numerical data with some inherent inaccuracy, the bar was not applied. The bar indicates non-dimensional values in theoretical considerations.

[t]   The results shown were obtained assuming pure rolling conditions. However, since the results have been based on an isothermal Reynolds equation based approach, they would be identical for partial or pure sliding.

[‡]   The results shown were obtained with fixed, predefined boundaries at $X = -2.0$ and $X = +1.08$. At the outlet, $X = 1.08$, this leads to the fact that the cavitation boundary condition, pressure and pressure gradient are both zero, is not always perfectly fulfilled. At the inlet the distance $X = -2.0$ leads to a non-zero pressure gradient for load case ii, representing so-called starved conditions. This is the reason why the height of the gap increases as the load increases towards load case iv.

viscosity have a significant influence on the location of the pressure spike, which moves towards the contact centre with increasing velocity and viscosity, as shown by a comparison of load case i with load case ii and of load case iii with load case iv. Influence of the load on the pressure spike and constriction position is less significant, with lower load causing a movement of the pressure spike towards the contact centreline.
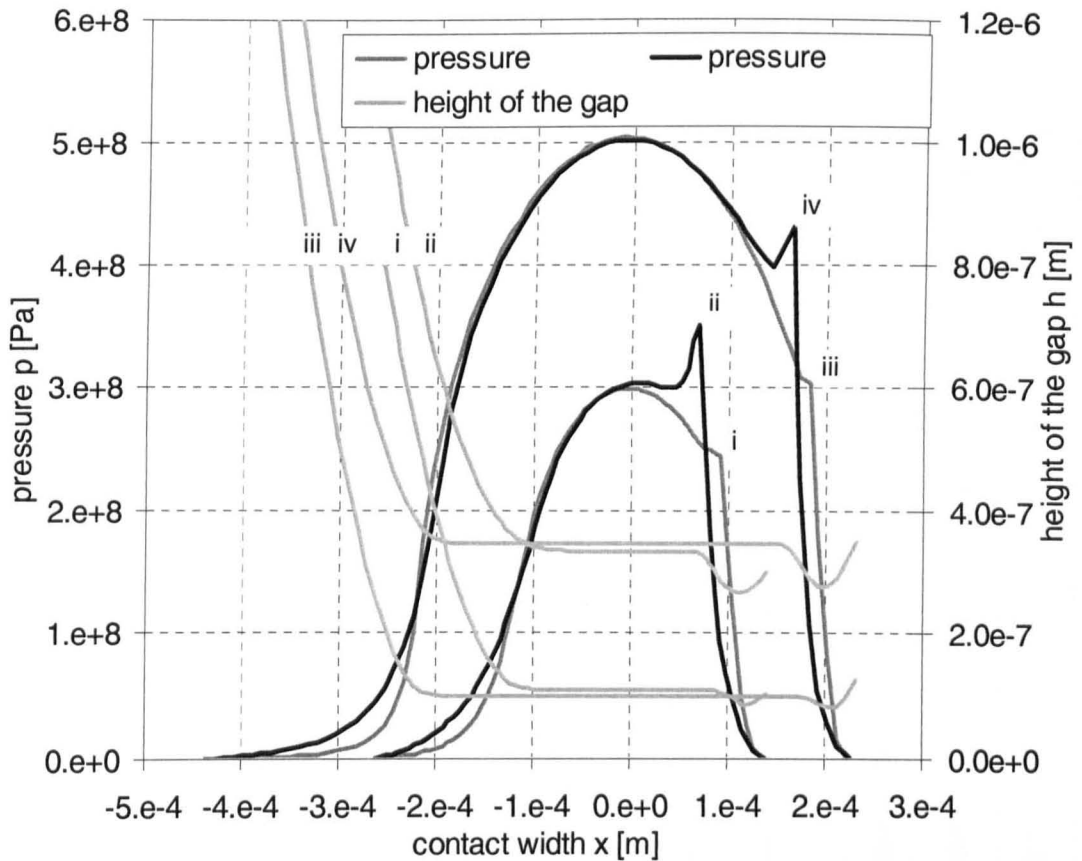
Figure 10.1:   Shape and pressure distribution along the gap obtained with a Reynolds equation based approach for the four investigated load cases (table 10.1),

load case i: $p_{Hz} = 0.3\,GPa$, $u_H = 0.2\,m\,s^{-1}$, $\eta_0 = 0.02\,Pa\,s$,
load case ii: $p_{Hz} = 0.3\,GPa$, $u_H = 0.5\,m\,s^{-1}$, $\eta_0 = 0.05\,Pa\,s$,
load case iii: $p_{Hz} = 0.5\,GPa$, $u_H = 0.2\,m\,s^{-1}$, $\eta_0 = 0.02\,Pa\,s$,
load case iv: $p_{Hz} = 0.5\,GPa$, $u_H = 0.5\,m\,s^{-1}$, $\eta_0 = 0.05\,Pa\,s$.

Table 10.1: Parameters for the load cases investigated.

load case number			i	ii	iii	iv
			input parameters			
Hertzian pressure	p_{Hz}	GPa	0.3		0.5	
hydrodynamic velocity	u_H	m s^{-1}	0.2	0.5	0.2	0.5
viscosity at ambient conditions	η_0	Pa s	0.020	0.050	0.020	0.050
pressure-viscosity coefficient	α	m^2 N^{-1}	$2.18 \cdot 10^{-8}$			
Young's modulus	E	GPa	206			
Poisson's ratio	ν	—	0.3			
reduced radius	r_{red}	m	0.025			
oil density	ρ	kg m^{-3}	870			
			calculated parameters			
dimensionless material parameter	G	—	5000			
dimensionless load parameter	W	—	$1.01 \cdot 10^{-5}$		$3.06 \cdot 10^{-5}$	
dimensionless speed parameter	U	—	$7.07 \cdot 10^{-13}$	$4.42 \cdot 10^{-12}$	$7.07 \cdot 10^{-13}$	$4.42 \cdot 10^{-12}$

Except for the pressure spike and constriction position details, the above is summarized in figure 10.2(a). A small change of the height of the gap is shown for dimensionless load parameter W variation with significant changes in gap height being obtained for dimensionless speed parameter U variation. Figures 10.2(b) and (c) show that the sliding influence factor k_p defined in equation 3.39 and discussed in subsections 3.3.4.4 to 3.3.4.6, takes on values from below 1 to approximately 100 and factor k_r, the pressure gradient ratio factor, defined in equation 3.38 and discussed in the same subsections takes on values from 10^{-3} to nearly unity.
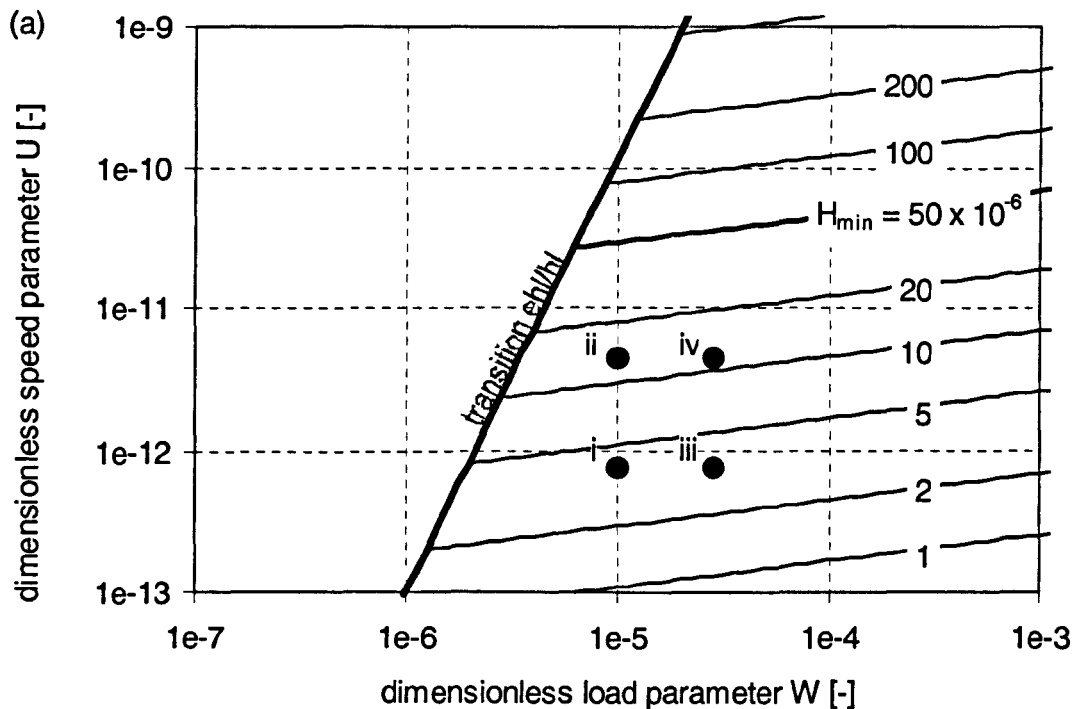
Figure 10.2:   Investigated load cases in the U-W-diagram with view to
            (a)   dimensionless minimum height of the gap H_{min},
            (b)   sliding influence factor k_p,
            (c)   pressure gradient ratio k_r,
            (continued).
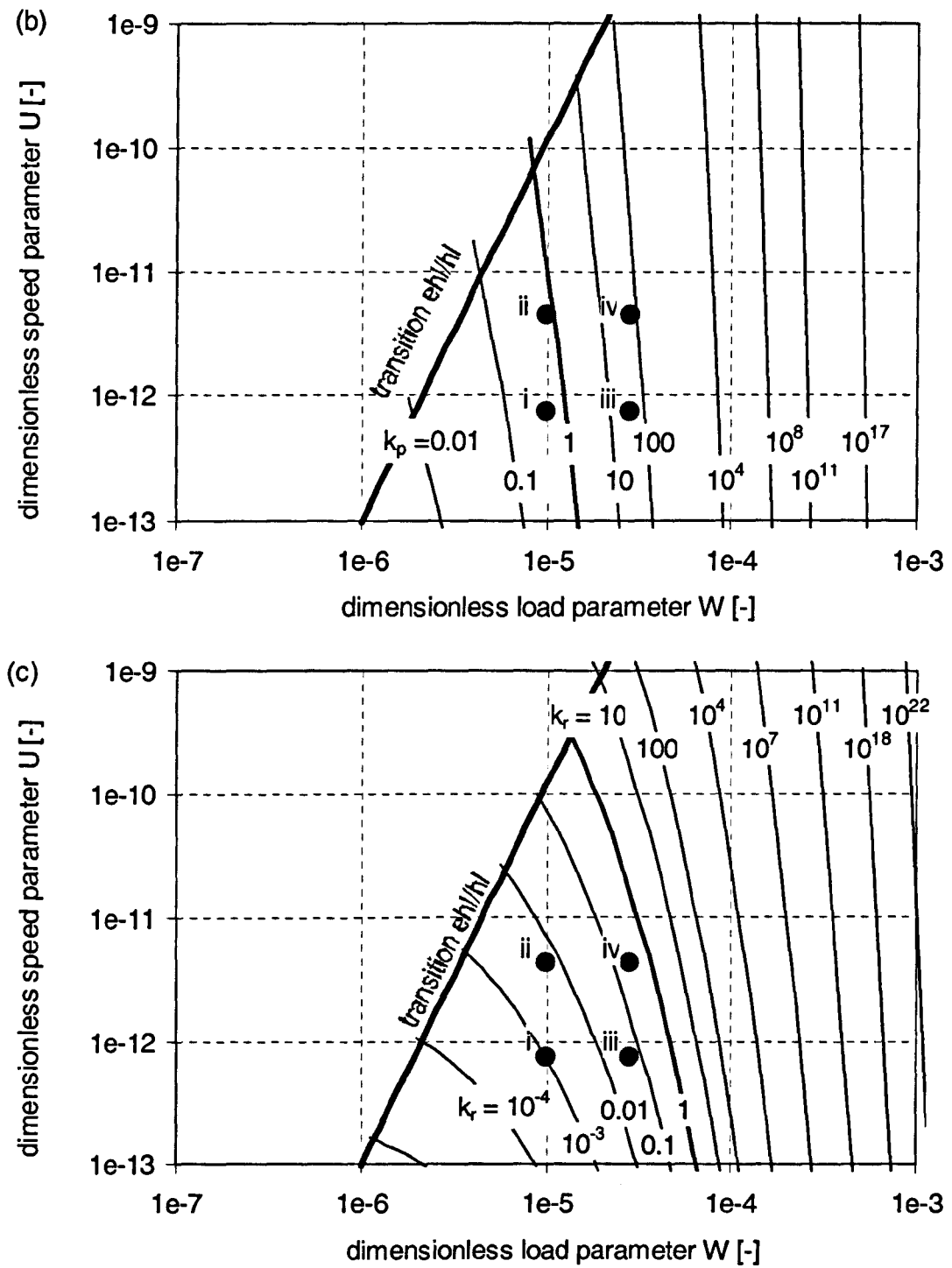
Figure 10.2:   (concluded).

10.3   Influence of the different load distribution on each contact surface

As mentioned in section 8.1.3, in the established Reynolds equation based solutions only the height of the gap and its gradients are taken into account but not the shape of the gap centreline of the contact. That means that the reduction of both curvatures of the surfaces to one reduced radius and the application of a mean reduced Young's modulus do not influence the results of the calculation. Consequently, Reynolds equation based results can be displayed with one straight and un-deformed and one curved and deformed surface without loss of information. This form of display is illustrated in figure 10.3(a) and is used in probably all publications on ehl.

With the new extended approach, not only the above mentioned effects of curvature and elasticity but also the expected different pressure distributions on each surface can cause a curved centreline of the contact, even if curvature and elasticity of both surfaces are identical. On the other hand, the new applied numerical method allows the investigation of such curved centreline effects.

The results in the present section concentrate on an investigation of the effect of the new method wherein the pressure distributions on each surface are different. Results are given for the following three configurations:

♦   All deflections and curvatures are applied to the upper, in this case faster, surface, as normally displayed and illustrated in figure 10.3(a).

♦   Each deflection and curvature is applied to the individual surface as in reality. This situation is illustrated in figure 10.3(b).

♦   All deflections and the curvatures are applied to the lower, in this case slower, surface as shown in figure 10.3(c).

For all results load case iv of table 10.1 and 50 per cent sliding, $S = 0.5$, was assumed.

Figure 10.4 shows results for the height of the gap. The upper part shows dimensionless height H along the dimensionless contact width X for the three

configurations. The lower section compares these values. The relative deviation from a median value ε_H, where

$$\varepsilon_H = \frac{H - H_{median}}{H_{median}} \qquad (10.1),$$

was locally determined from the three available values.

All data obtained using the extended approach and CFD software packages were stored in a scientific format with a four digit mantissa, $x.xxx \times 10^{xx}$. A change of the last digit can be caused by rounding-off effects on this four digit format. Depending whether the mantissa takes on its smallest value, 1.000, or its largest possible value, 9.999, the deviation caused by changing the last digit by one ranges from

$$\varepsilon = \left| \frac{1.001 - 1.000}{1.000} \right| = 10^{-3} \text{ to } \varepsilon = \left| \frac{9.999 - 9.998}{9.999} \right| \approx 10^{-4} \qquad (10.2).$$

In figure 10.4 additional lines have been introduced, indicating how much of the deviation could be caused by round-off errors. At the positions where the exponent of the height changes values, these lines develop a saw tooth like shape.

Figure 10.5 shows the dimensionless pressure P distribution and its relative deviation from the median value, ε_P, for the faster (a) and the slower (b) surface, where

$$\varepsilon_P = \frac{P - P_{median}}{P_{median}} \qquad (10.3).$$

A detailed discussion and conclusions of the results are given in chapter 11. However, it may be stated at this stage that applying all curvatures and deflections on one surface does not lead to a substantial loss of information. Hence the traditional from of displaying data was applied in the following sections of the present chapter.
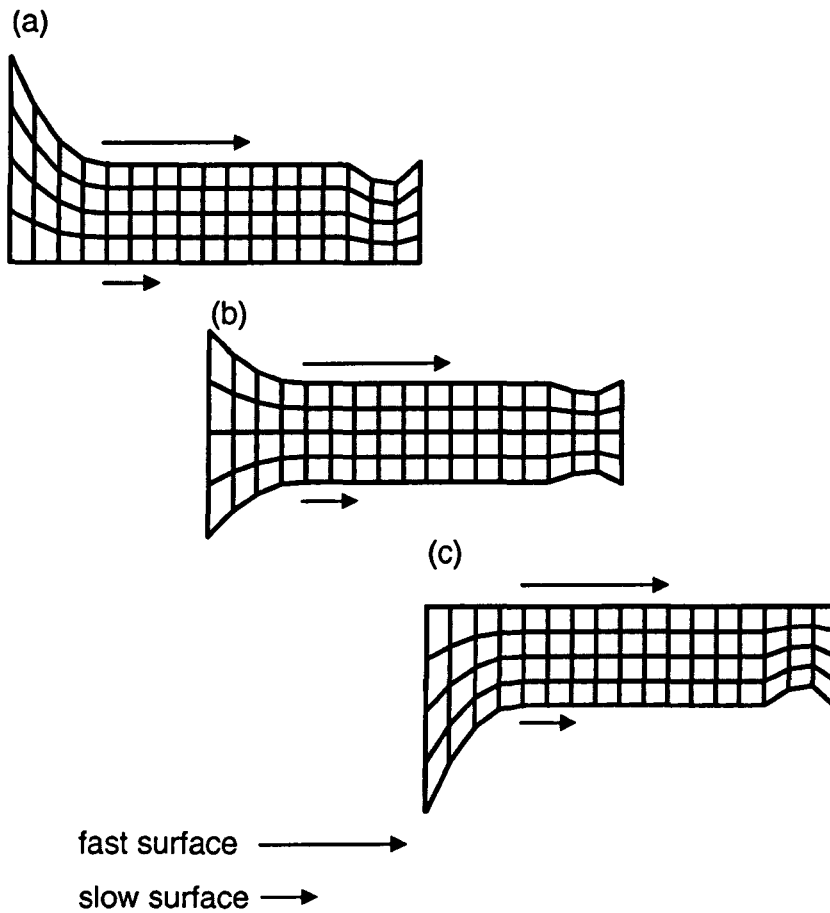
Figure 10.3:   *Possible distribution of curvature and deflections of the surfaces for ehl calculation and display of results:*
(a)   *all curvatures and deflections applied to and displayed on the upper (faster) surface,*
(b)   *curvatures and deflections applied to and displayed on the individual surfaces as in reality,*
(c)   *all curvatures and deflections applied to and displayed on the lower (slower) surface.*
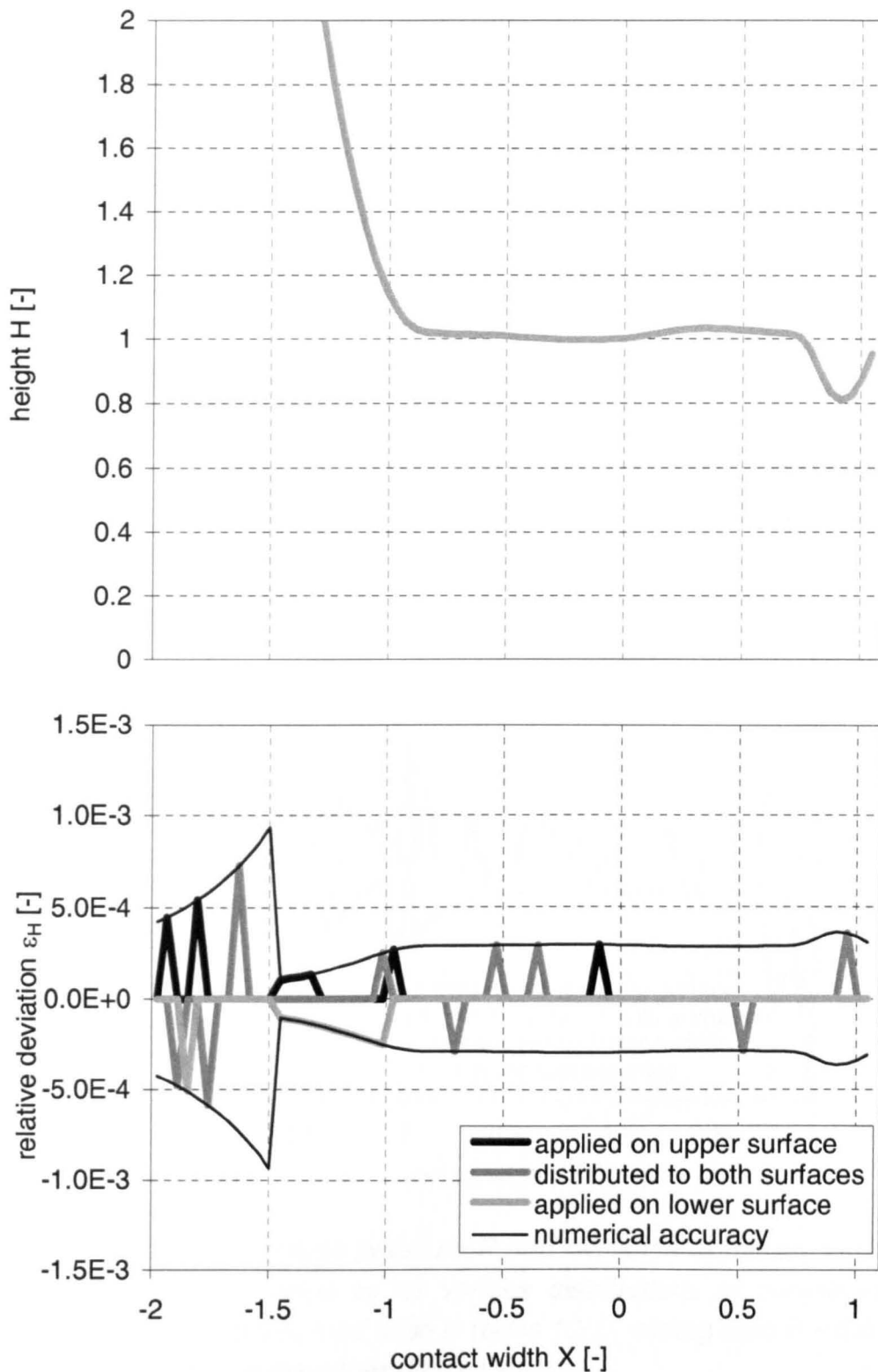
Figure 10.4:   Dimensionless height of the gap H and deviation of the height
               from median value ε_H for various distributions of curvatures
               and deflections; load case iv (table 10.1), sliding ratio $S = 0.5$.
               N.B. In the upper part, the line "applied on lower surface"
               hides the lines describing "applied on upper surface" and
               "distributed to both surfaces".
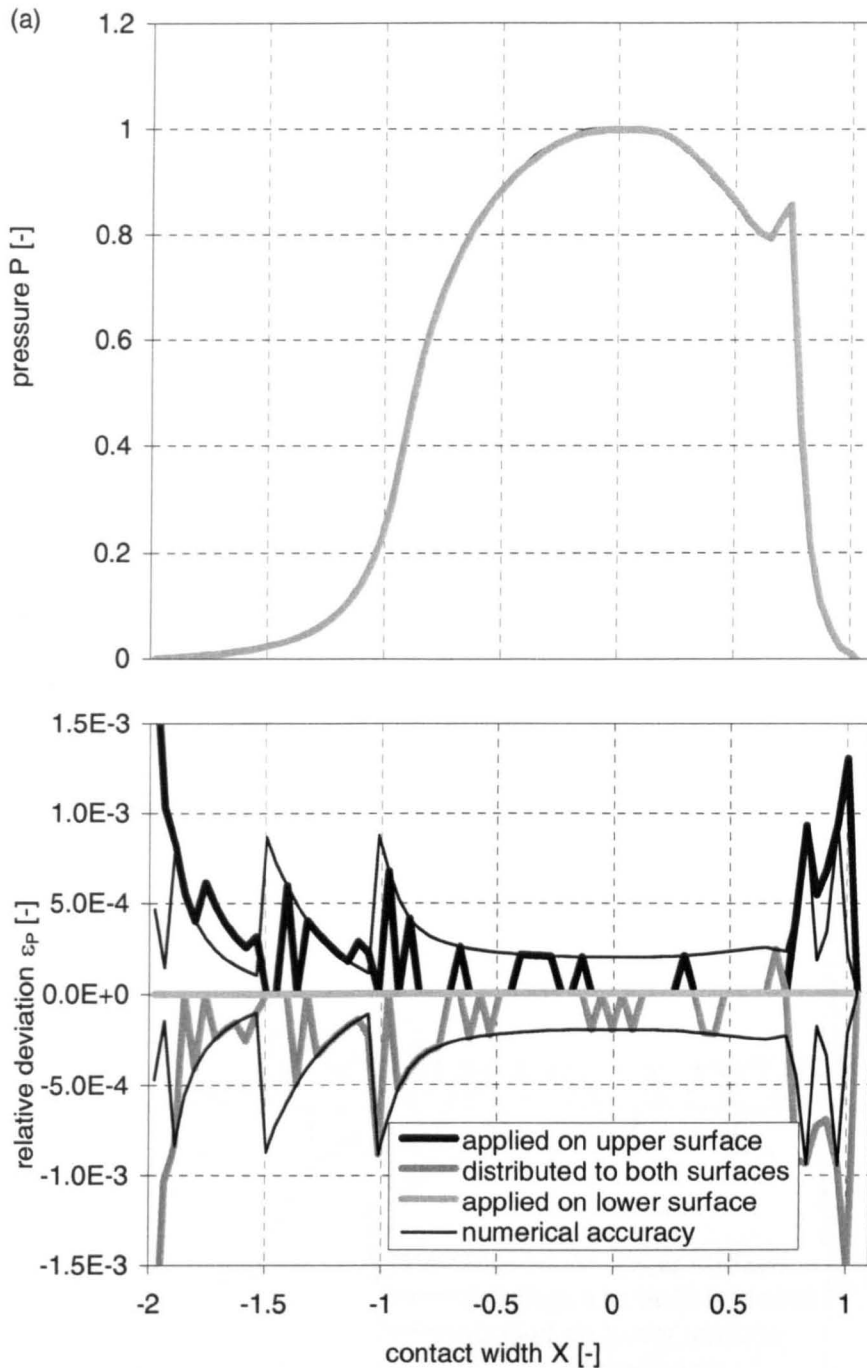
Figure 10.5: Dimensionless pressure P and deviation of the pressure from median value ε_P for various distributions of curvatures and deflections; load case iv (table 10.1), sliding ratio S = 0.5,
(a) on the upper (faster) surface,
(b) on the lower (slower) surface,
N.B. In the upper part of the figures (a) and (b), the line "applied on lower surface" hides the lines describing "applied on upper surface" and "distributed to both surfaces"
(continued).
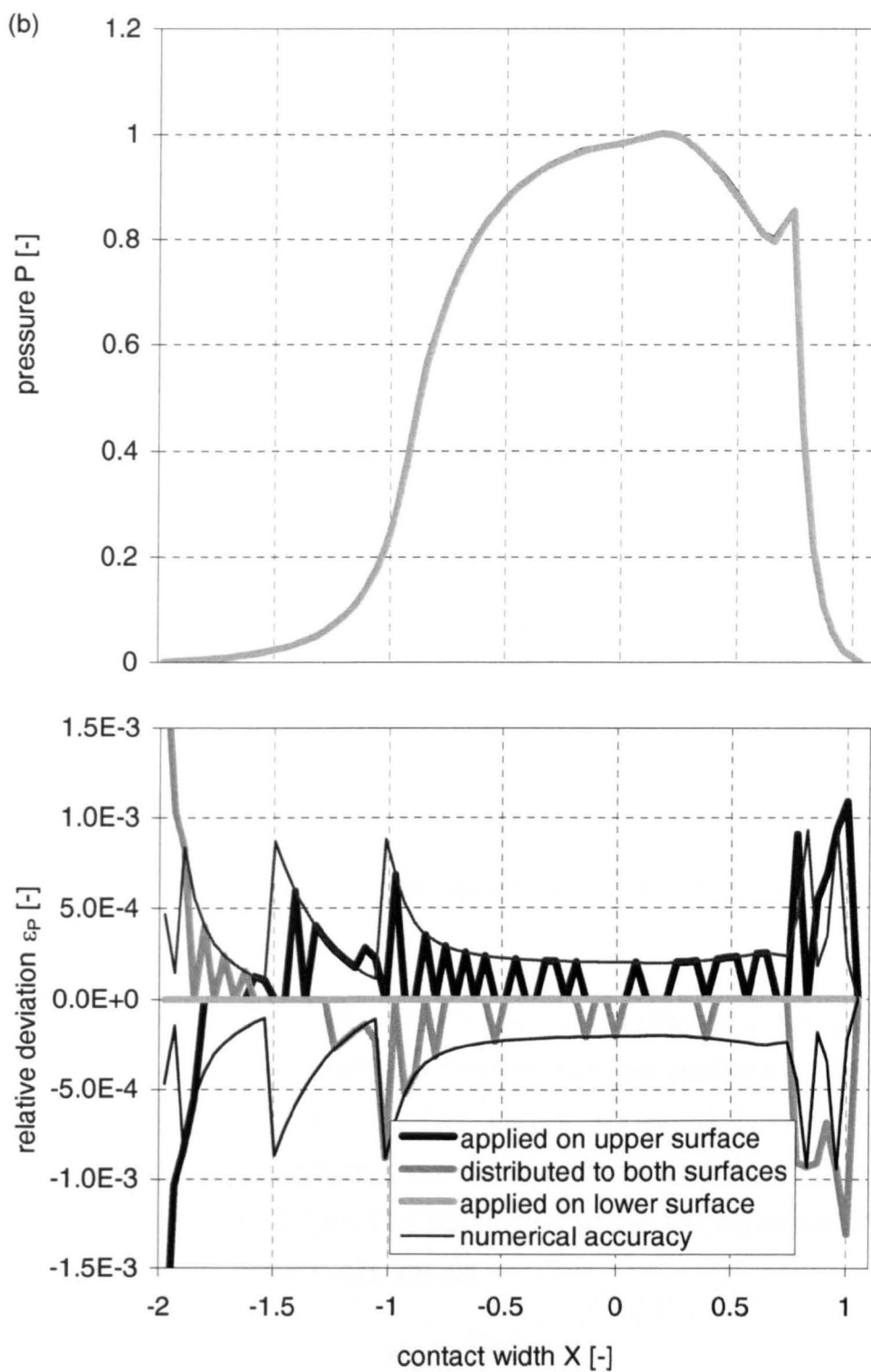
Figure 10.5:   (concluded).

10.4   Geometry of the gap

Results for the shape of the gap for the new extended approach are given in the present section. Figure 10.6 shows the shape of the gap for pure rolling, 50 per cent sliding and pure sliding for load case iv (table 10.1) and also compares these cases with a Reynolds equation based solution. The upper part of the figure shows the height of the gap H, which is normalized by dividing by the contact centreline height of a Reynolds equation based solution for the same load case:

$$H = \frac{h}{h_{0,Re}}$$
(10.4).

The relative deviation from the Reynolds equation based solution, $\varepsilon_{H,Re}$, where

$$\varepsilon_{H,Re} = \frac{H - H_{Re}}{H_{Re}}$$
(10.5)

is shown in the lower part of the figure.

The equivalent results for the load cases i to iii are given in appendix K, figures K.1 to K.3.

Figure 10.6 shows that the gap is not parallel when using the new approach. In addition to the well-known ehl constriction, the gap contains a constriction before the centreline of the contact and a subsequent widening. The minimum height at this additional constriction for all load cases and sliding ratios is given in figure 10.7(a). The upper part shows the dimensional height h_{min}', the lower the dimensionless values

$$H_{min}' = \frac{h_{min}'}{h_{0,Re}}$$
(10.6),

where again the central film thickness of a Reynolds equation based solution $h_{0,Re}$ was used as reference. Maximum film thickness between the additional and the well-known constriction is given in part (b) of figure 10.7. As for the minimum film thickness, the figure shows the dimensional height h_{max}' and dimensionless values H_{max}' with

$$H_{max}' = \frac{h_{max}'}{h_{0,Re}}$$ (10.7).

Figure 10.7(c) gives the height of the gap at the contact centreline in dimensional $h_{0,ext}$, and non-dimensional

$$H_{0,ext} = \frac{h_{0,ext}}{h_{0,Re}}$$ (10.8)

form.

Information on the dimensionless position of the minimum height H_{min}' and the maximum height H_{max}' is compiled in figure 10.8. Part (a) shows the dimensionless position of the minimum height

$$X_{hmin} = \frac{x_{hmin}}{b_{Hz}} = X(H = H_{min}')$$ (10.9),

part (b) that of the maximum height

$$X_{hmax} = \frac{x_{hmax}}{b_{Hz}} = X(H = H_{max}')$$ (10.10).

Apart from the well-known constriction, the height of the gap calculated with the new extended approach agrees at one point with that from Reynolds equation based solutions. The position of this point

$$X_{cross} = \frac{x_{cross}}{b_{Hz}} = X(H = 1)$$ (10.11)

is displayed in figure 10.8(c). For some load case-sliding ratio combinations minimum and maximum heights cannot be determined within the bounds of numerical accuracy of the result files. Hence positions for such combinations cannot be determined. Therefore results in figure 10.8 are only printed for those load case-sliding ratio combinations for which they could be determined.
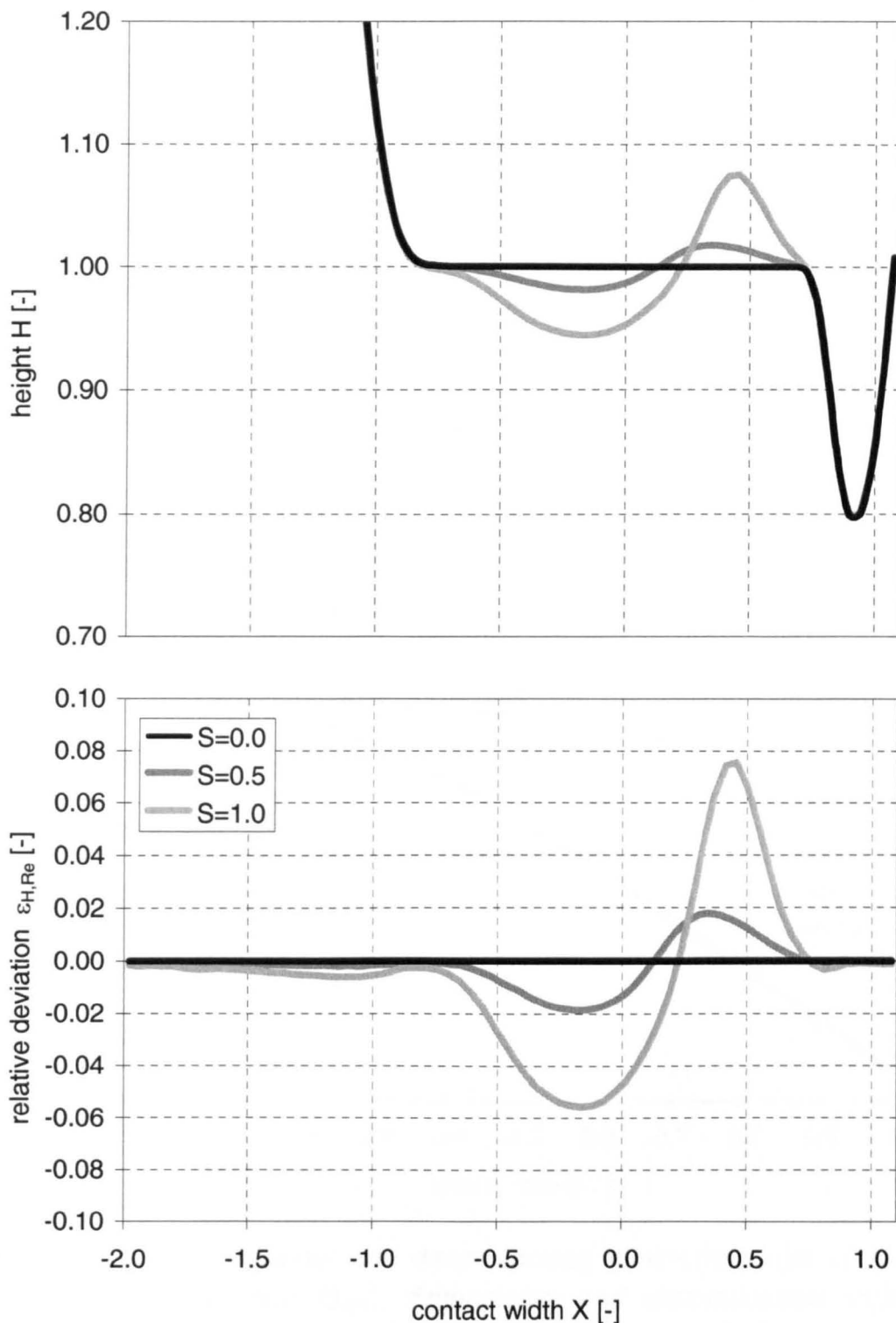
Figure 10.6:   Height of the gap H and relative deviation from Reynolds
               equation based solution $\varepsilon_{H,Re}$ for various sliding ratios; load
               case iv (table 10.1), sliding ratios S = 0.0, 0.5, and 1.0.
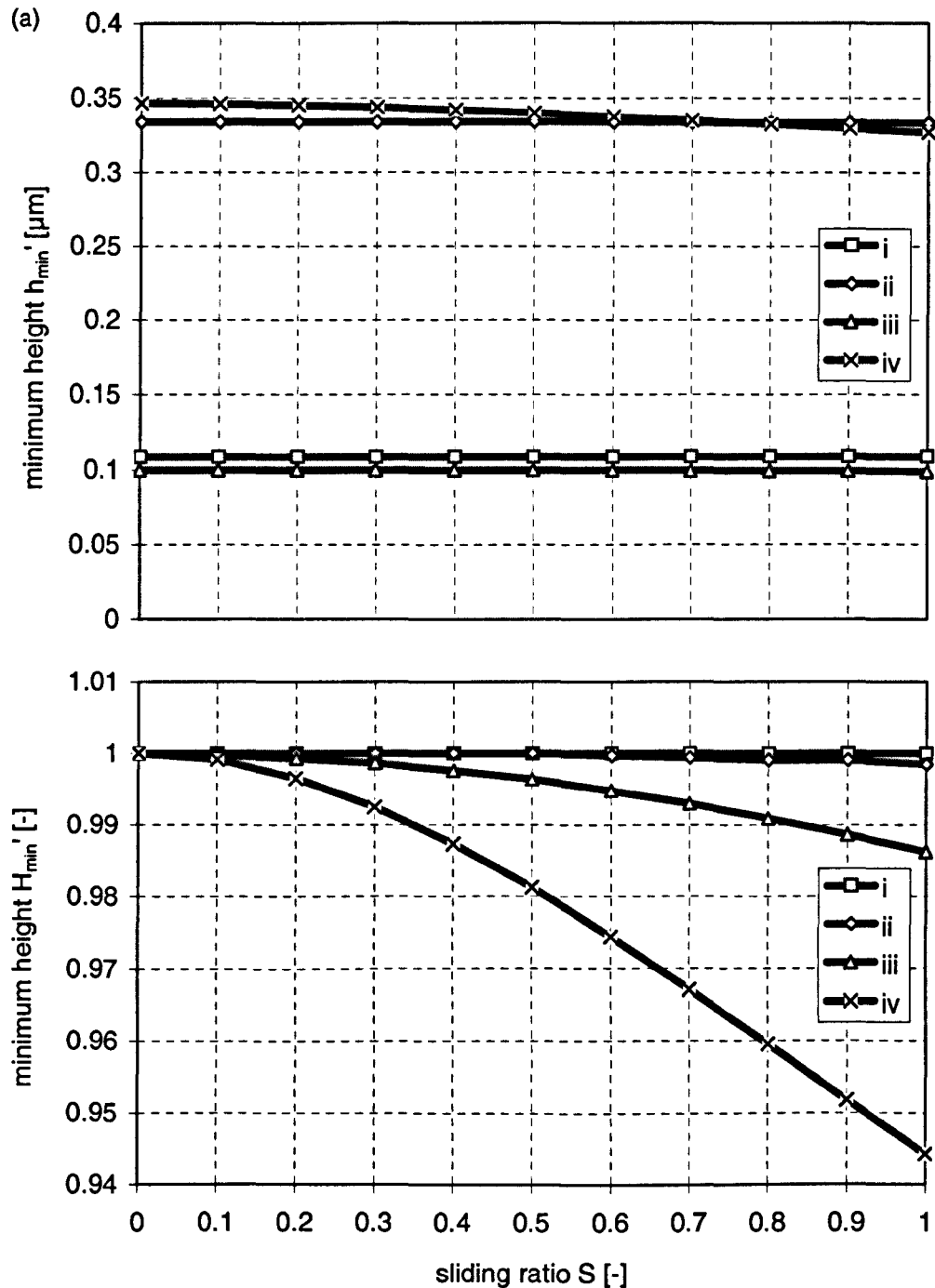
Figure 10.7: *Dimensional and dimensionless minimum height of the gap h_{min}' and H_{min}', dimensional and dimensionless maximum height of the gap h_{max}' and H_{max}' and dimensional and dimensionless height of the gap at the contact centreline $h_{0,ext}$ and $H_{0,ext}$ for load cases i to iv (table 10.1) and various sliding ratios S,*

(a) minimum height of the gap h_{min}' and H_{min}',

(b) maximum height of the gap h_{max}' and H_{max}',

(c) height at the contact centreline $h_{0,ext}$ and $H_{0,ext}$

(continued).
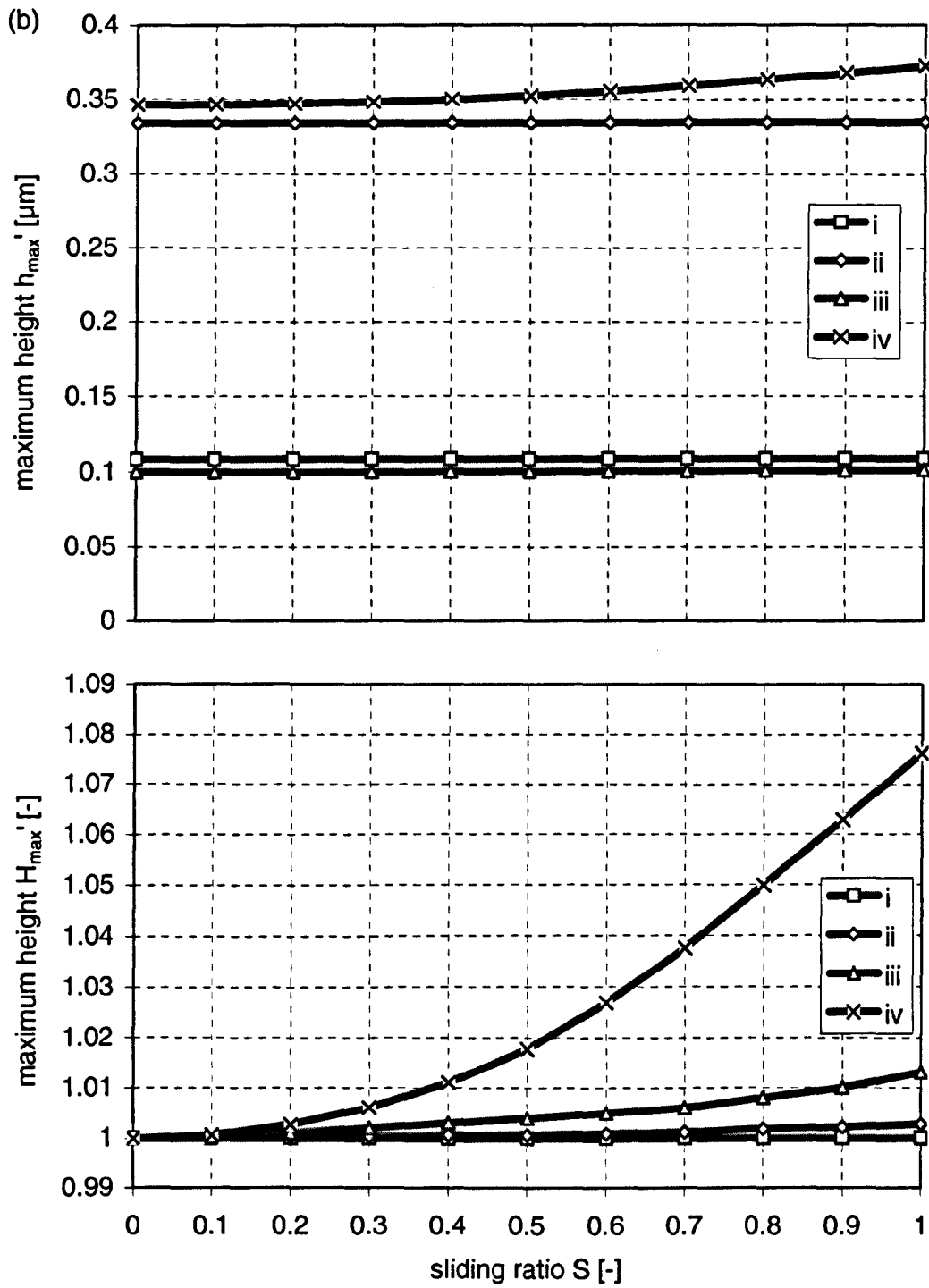
Figure 10.7:   (continued).
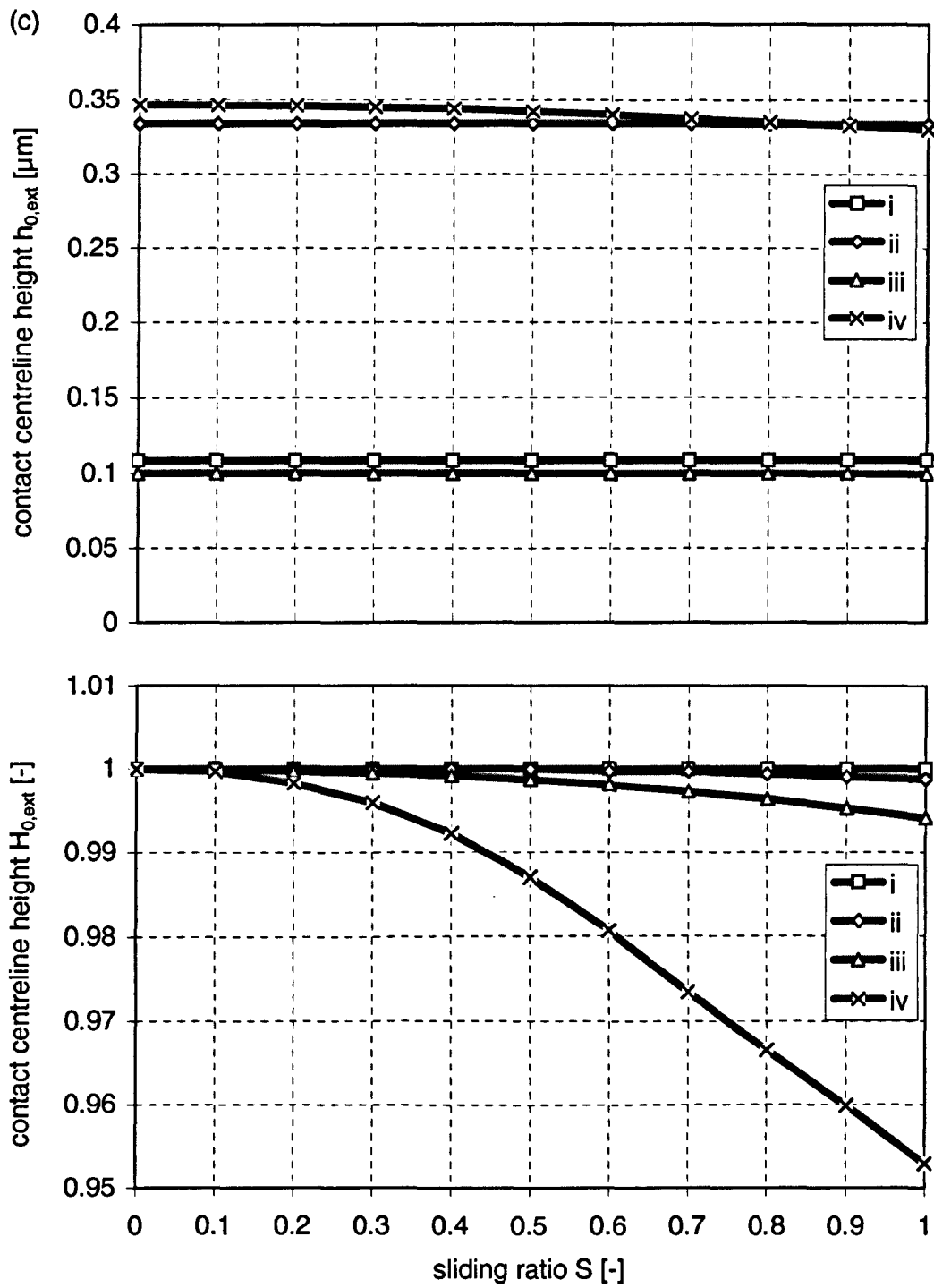
Figure 10.7:   (concluded).
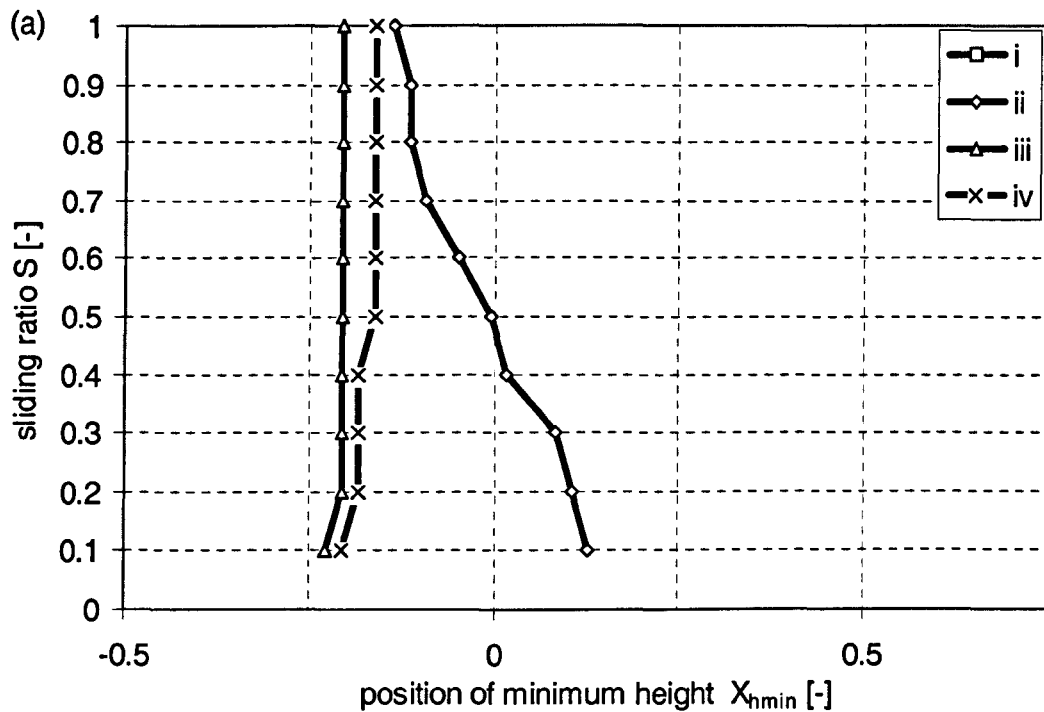
Figure 10.8: Dimensionless position of the minimum height X_{hmin} and maximum height of the gap X_{hmax} and dimensionless position of point of agreement of the extended approach with a Reynolds equation based approach X_{cross} for load cases i to iv (table 10.1) and various sliding ratios S,

(a) position of the minimum height of the gap X_{hmin},

(b) position of the maximum height of the gap X_{hmax},

(c) position of the intersection point with a Reynolds equation based solution X_{cross}.

N.B. Values are not displayed for all load cases and sliding ratio combinations

(continued).
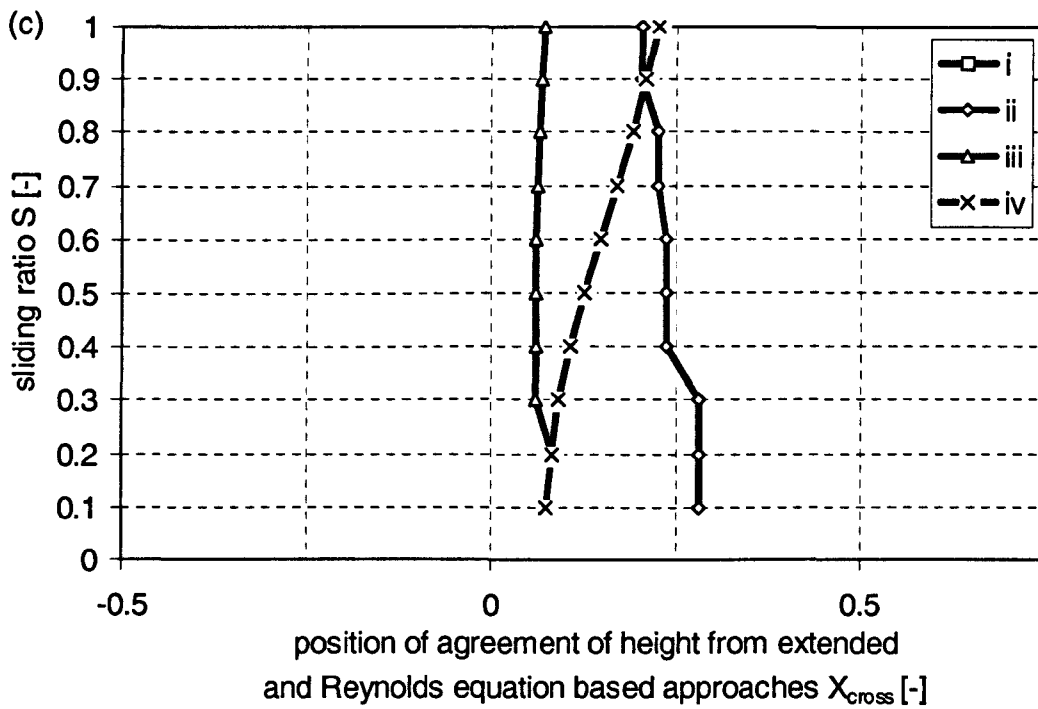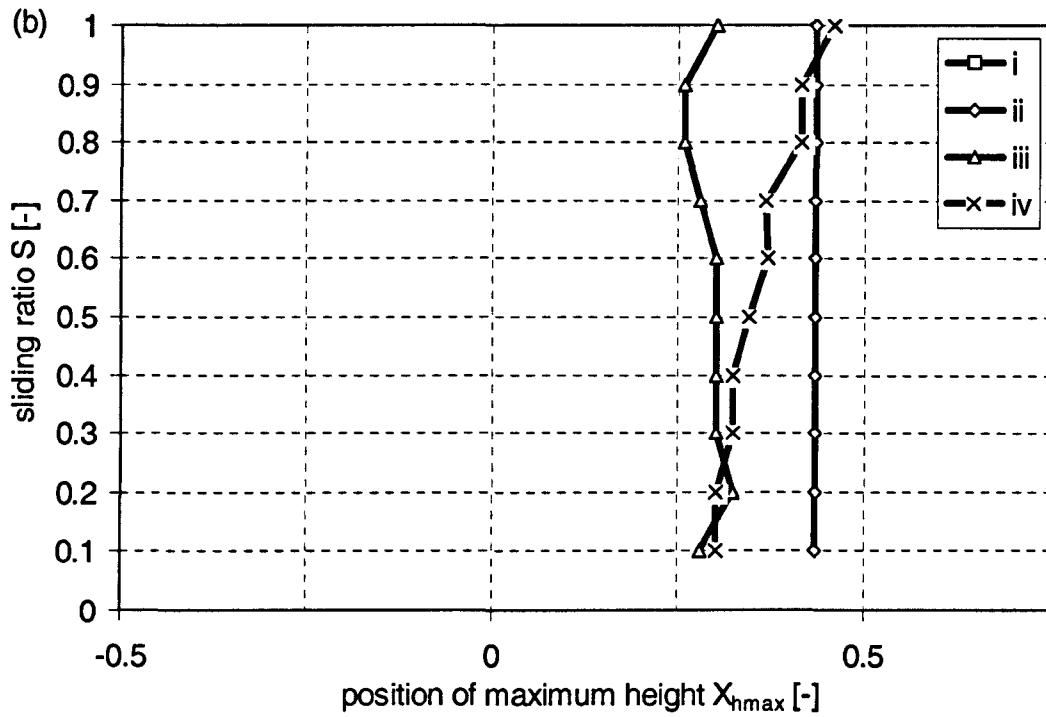
Figure 10.8:   (concluded).

10.5   Velocity

The present section contains results showing and discussing the velocity field in the gap.

10.5.1   Velocity fields

Contour plots provide a good qualitative impression of the velocity distribution when, as in the present case, one flow direction is dominant. Figure 10.9 shows contour plots of u-velocity for load case iv (table 10.1) and for pure rolling (a), 50 per cent sliding (b) and pure sliding (c). For each sliding ratio (a) to (c), two contour plots are given. The upper plot shows results determined with the new extended approach, the lower one showing results obtained from a Reynolds equation based solution for reference and comparison. Further results for load cases i to iii (table 10.1), can be found in appendix K, figures K.4 to K.6.

Quantitative comparison of the velocity fields from each approach is difficult, since the shape of the gap and hence the domain considered differ. With the introduction of a normalised co-ordinate perpendicular to the gap

$$Y^* = \frac{y}{h} = \frac{Y}{H}$$ (10.12),

all gaps appear parallel with unit height and thus plots can be compared. In figure 10.10, comparison of the two approaches is given by displaying the relative deviation of the u-velocity of the new extended from the Reynolds equation based solution

$$\varepsilon_{u,Re} = \frac{u - u_{Re}}{u_H}$$ (10.13)

as a contour plot.

Results are given for load case iv (table 10.1) and three sliding ratios 0.0, 0.5, and 1.0, results for load cases i to iii (table 10.1) can be found in appendix K, figures K.7 to K.9.

(a)

velocity u [m/s]

A	−2.00E−001
B	−1.00E−001
C	−4.97E−009
D	1.00E−001
E	2.00E−001
F	3.00E−001
G	4.00E−001
H	5.00E−001
I	6.00E−001
J	7.00E−001

velocity u [m/s]

A	−2.00E−001
B	−1.00E−001
C	−4.97E−009
D	1.00E−001
E	2.00E−001
F	3.00E−001
G	4.00E−001
H	5.00E−001
I	6.00E−001
J	7.00E−001
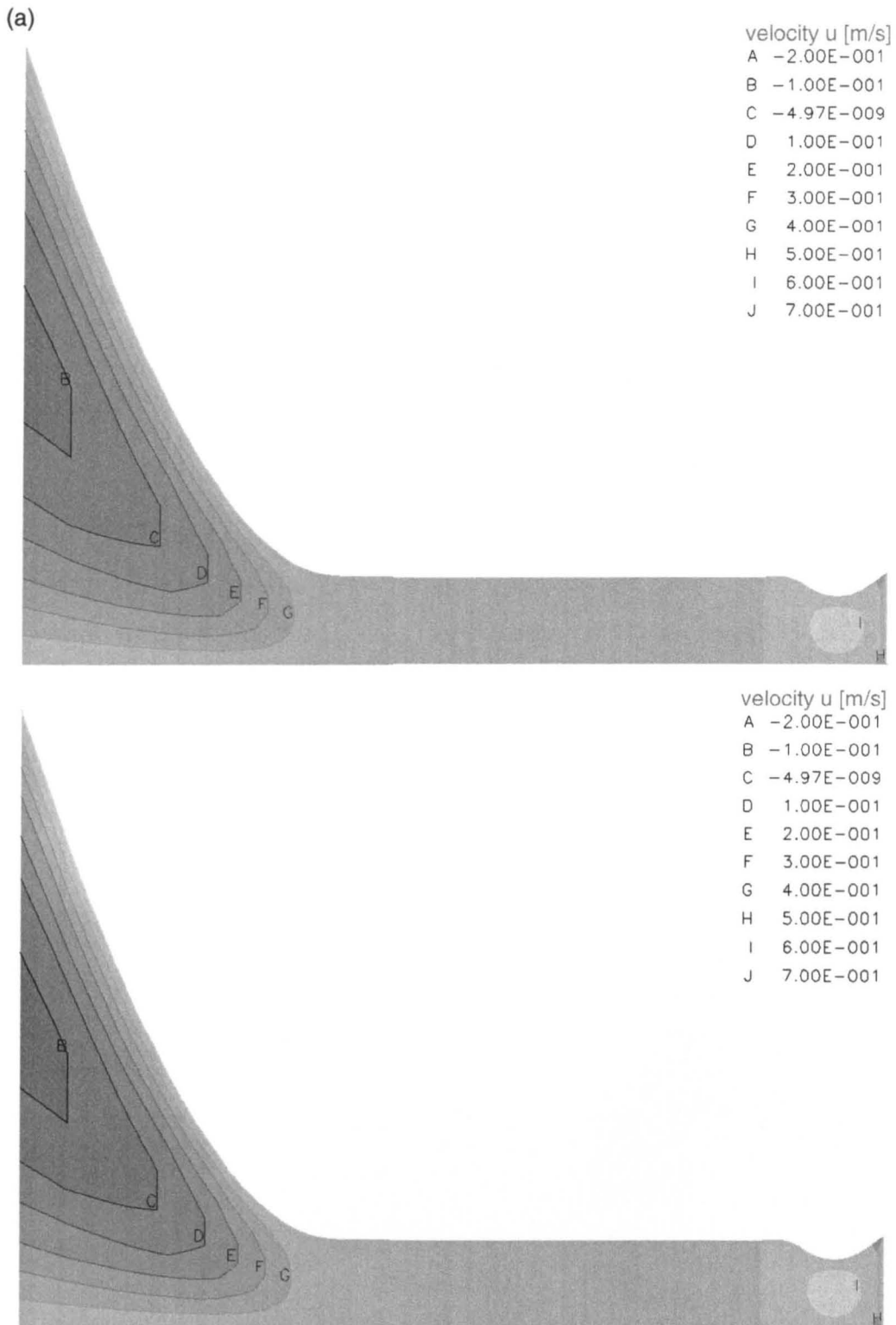
Figure 10.9:   Contour plots of velocity in x-direction u distribution in the gap
for extended (upper part) and Reynolds equation based (lower
part) approach; load case iv (table 10.1), sliding ratios S = 0.0,
0.5, and 1.0,
(a) sliding ratio S = 0.0,
(b) sliding ratio S = 0.5,
(c) sliding ratio S = 1.0
(continued).

(b)

velocity u [m/s]
A −2.50E−001
B −1.25E−001
C   0.00E+000
D   1.25E−001
E   2.50E−001
F   3.75E−001
G   5.00E−001
H   6.25E−001
I   7.50E−001

velocity u [m/s]
A −2.50E−001
B −1.25E−001
C   0.00E+000
D   1.25E−001
E   2.50E−001
F   3.75E−001
G   5.00E−001
H   6.25E−001
I   7.50E−001

Figure 10.9:   (continued).

(c)

velocity u [m/s]
A   −2.50E−001
B   0.00E+000
C   2.50E−001
D   5.00E−001
E   7.50E−001
F   1.00E+000

velocity u [m/s]
A   −2.50E−001
B   0.00E+000
C   2.50E−001
D   5.00E−001
E   7.50E−001
F   1.00E+000

Figure 10.9:   (concluded).

(a)

$\varepsilon_{u,Re}$ = ■ -0.0025-0.0025

(b)

contact width X [-]

$\varepsilon_{u,Re}$ = □ -0.04--0.02   ▨ -0.02-0   ▤ 0-0.02   ■ 0.02-0.04
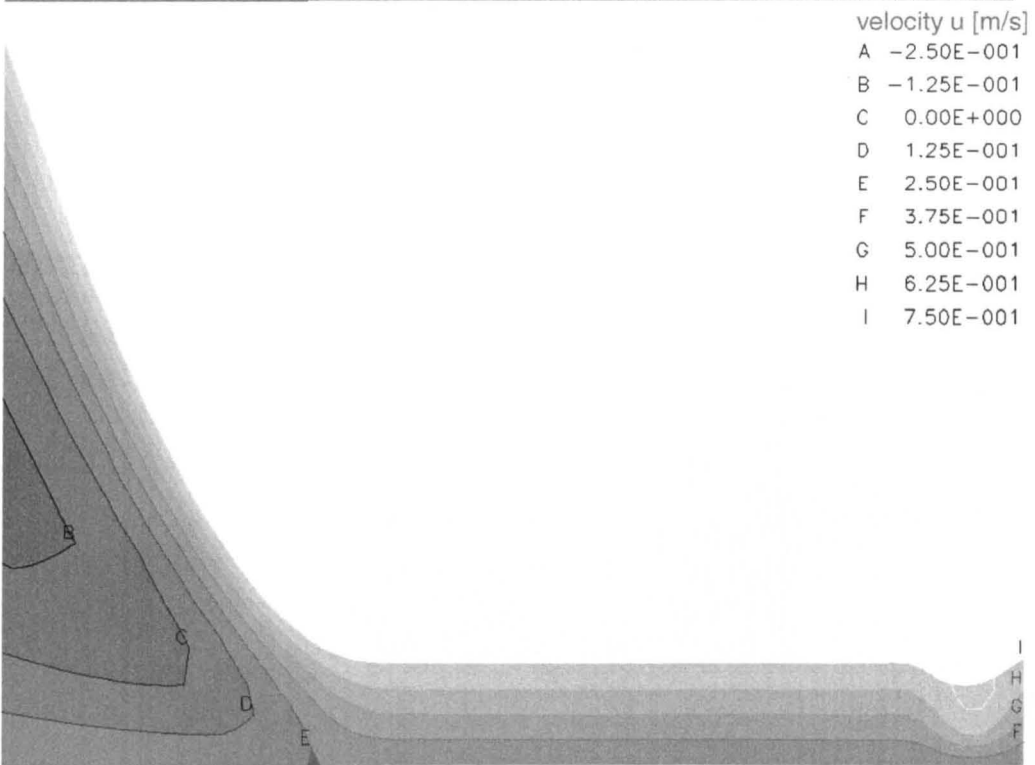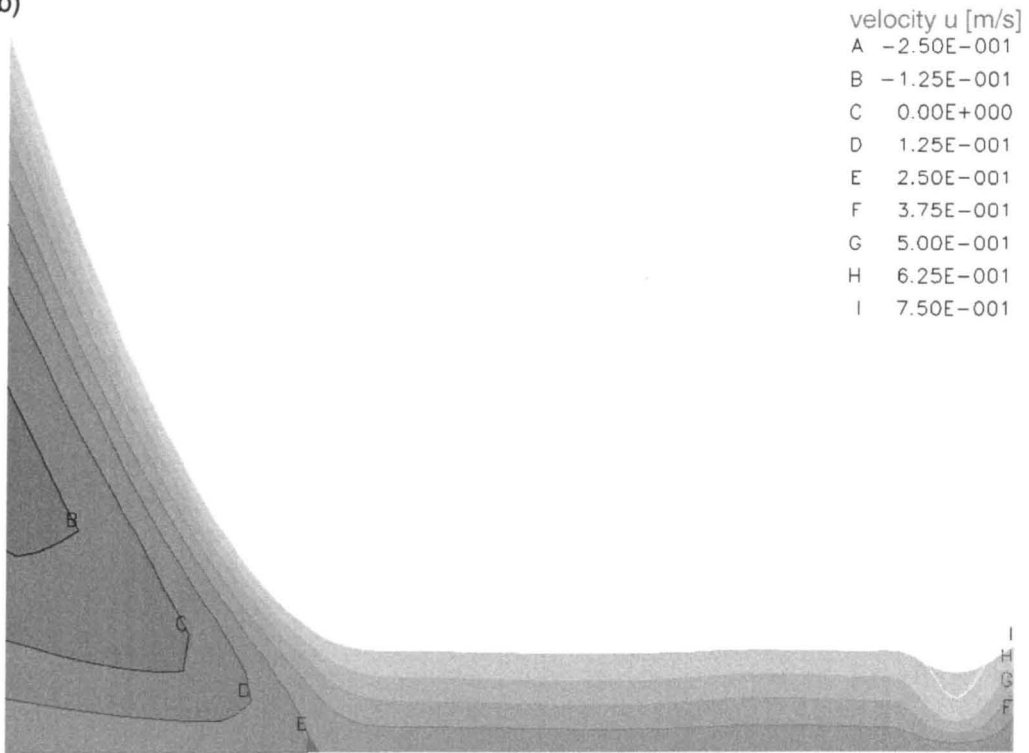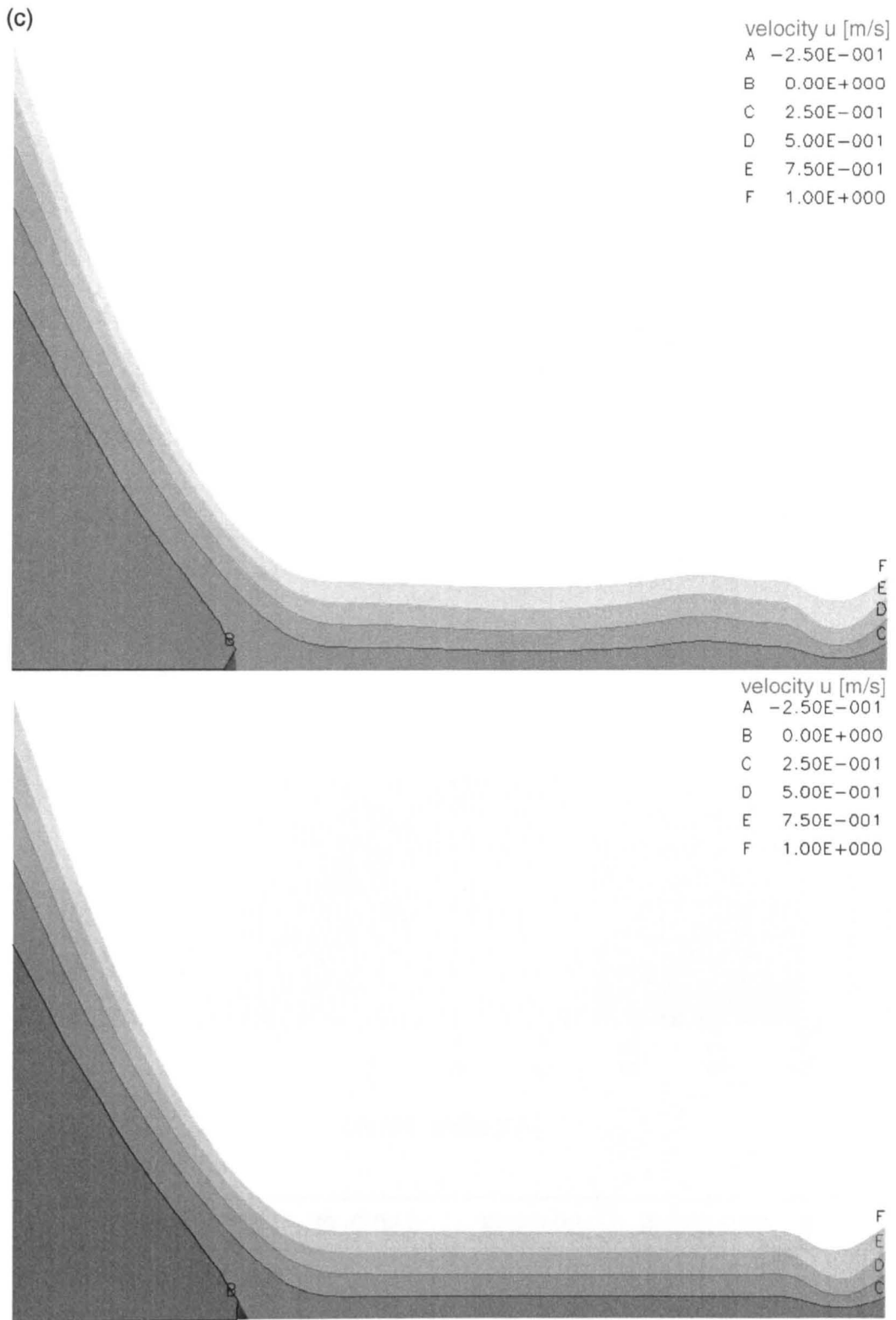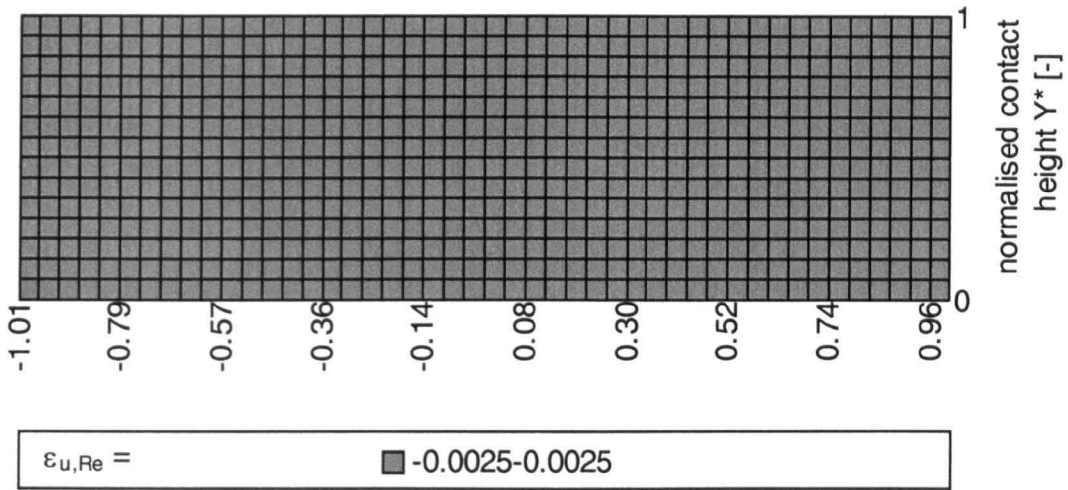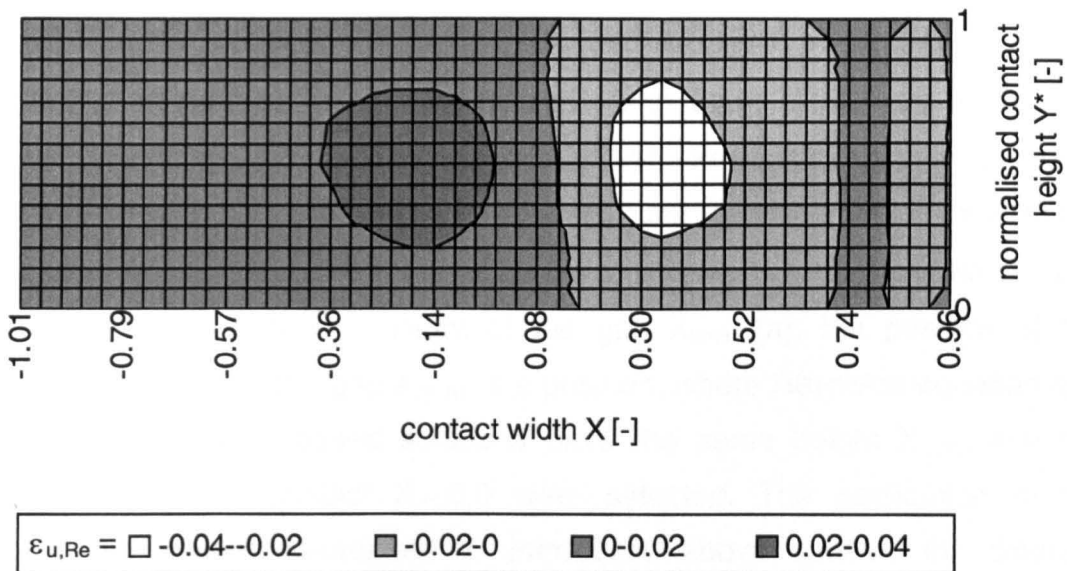
Figure 10.10: *Relative deviation of velocity in x-direction u of extended from Reynolds equation based approach $\varepsilon_{u,Re}$; load case iv (table 10.1), sliding ratios S = 0.0, 0.5, and 1.0,*
(a) sliding ratio S = 0.0,
(b) sliding ratio S = 0.5,
(c) sliding ratio S = 1.0
(continued).

(c)

$\varepsilon_{u,Re}$ =	□ -0.12--0.08	□ -0.08--0.04	■ -0.04-0
	■ 0-0.04	■ 0.04-0.08	■ 0.08-0.12
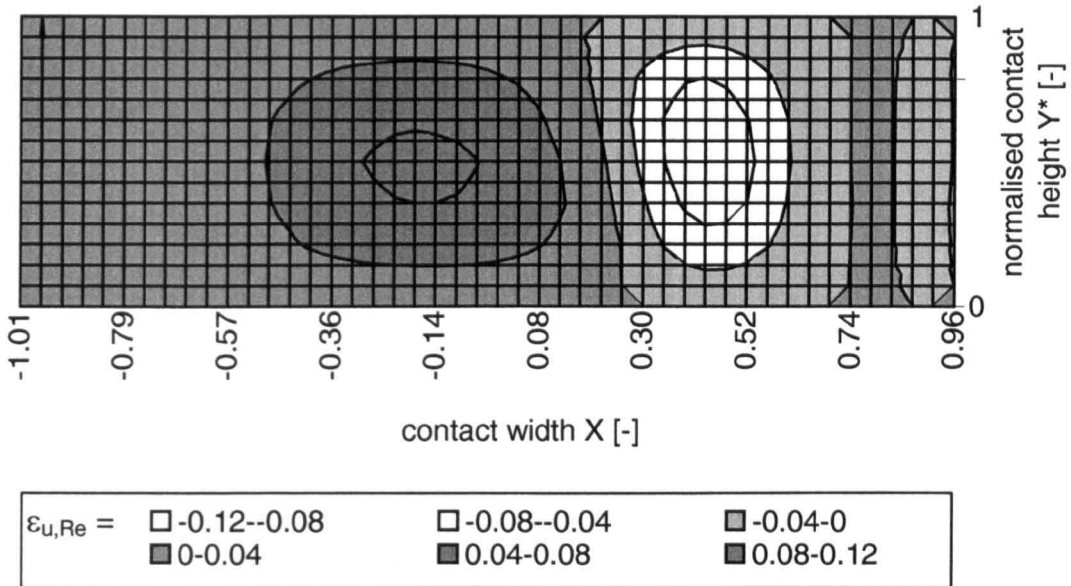
Figure 10.10: (concluded).

10.5.2 Velocity profiles

Detailed quantitative consideration and comparison of velocity fields from both approaches is provided in figure 10.11. For load case iv and three sliding ratios, $S = 0.0$, 0.5 and 1.0, profiles of the velocity component in the x-direction perpendicular to the gap are given for various positions. The position of the minimum height of the gap X_{hmin} (a), the position of the maximum height of the gap X_{hmax}, the position, where Reynolds equation and extended approach based solutions have the same height X_{cross} and the centreline of the contact $X = 0.0$ were selected. The application of the normalised height co-ordinate Y^* introduced above enabled the different sliding ratios and Reynolds equation and extended approach based solutions to be displayed in one diagram. The graphs also give comparison of both approaches by displaying the relative deviation of the extended approach from Reynolds equation based solutions as introduced for the velocity fields, equation 10.13.

For load cases i to iii, corresponding figures can be found in appendix K.
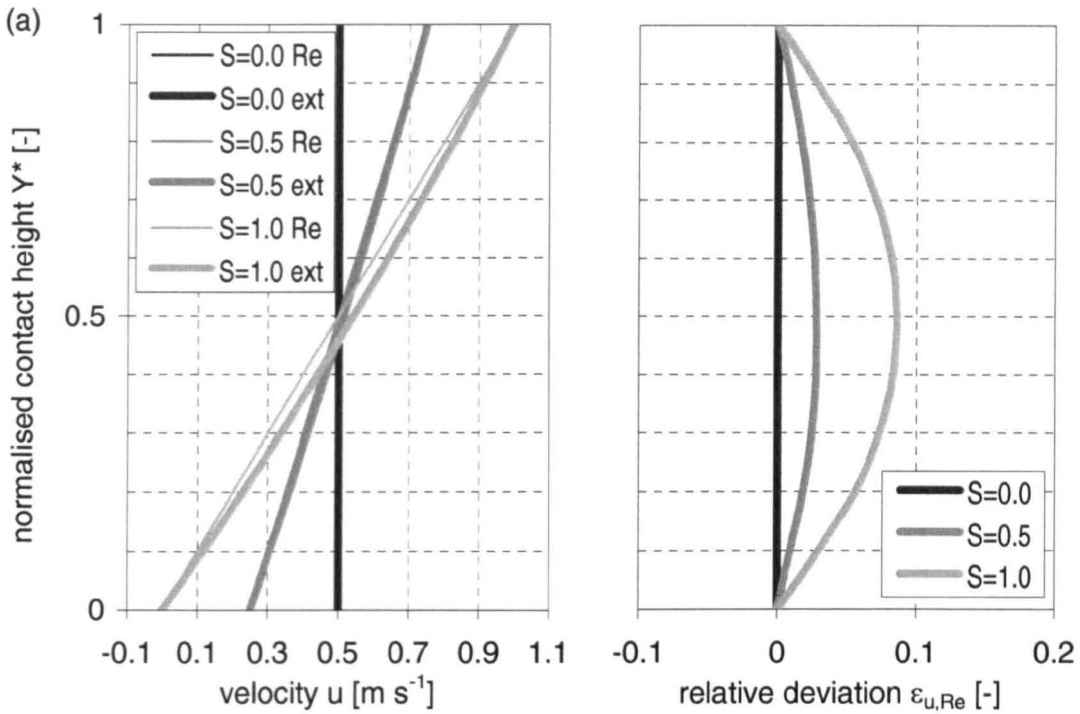
Figure 10.11: *Velocity in x-direction u and relative deviation from Reynolds equation based solution $\varepsilon_{u,Re}$ at selected positions X for various sliding ratios; load case iv (table 10.1), sliding ratios S = 0.0, 0.5, and 1.0,*
(a) at the position of minimum height of the gap X_{hmin},
(b) at the position of maximum height of the gap X_{hmax},
(c) at the position of agreement of Reynolds equation and extended approach based solution X_{cross},
(d) at the contact centreline X = 0.0
(continued).
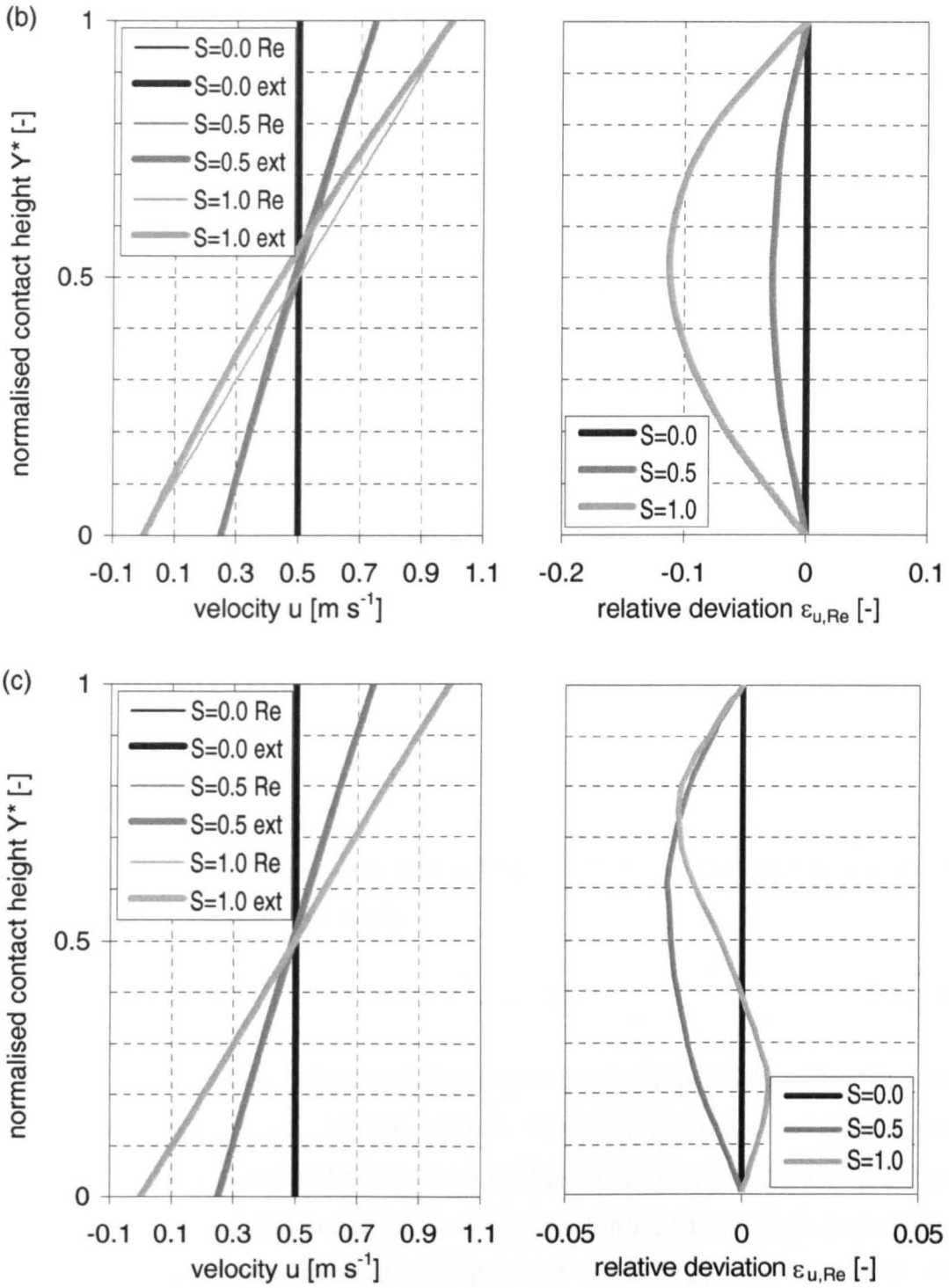
Figure 10.11 (continued).
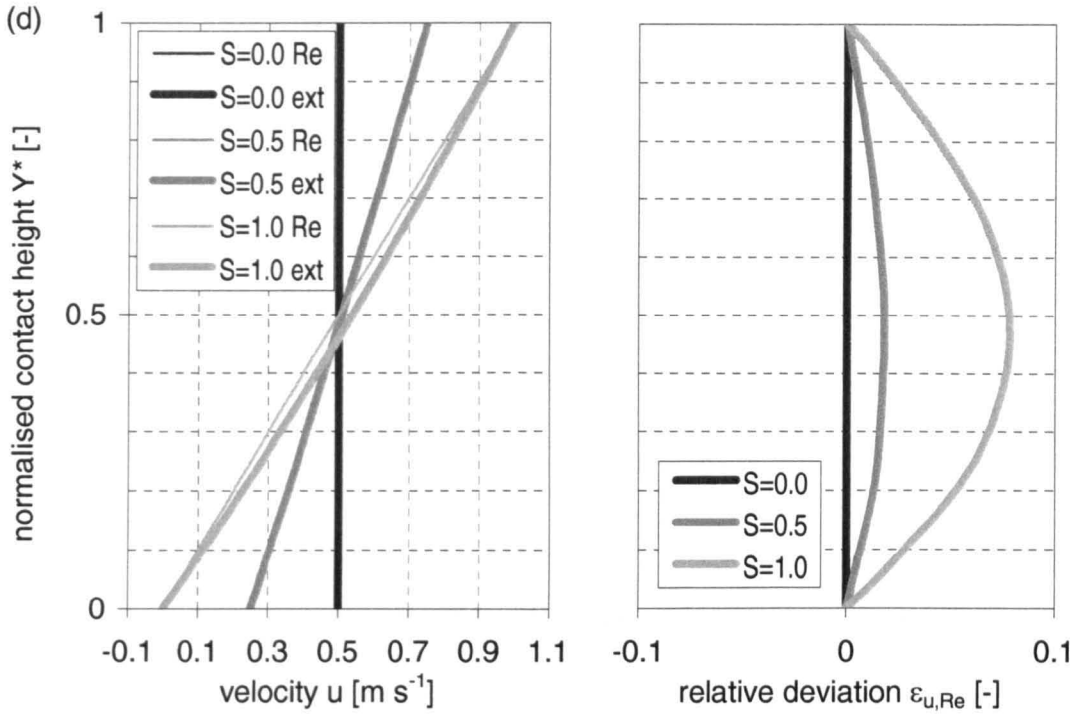
Figure 10.11 (concluded).

10.5.3 Flow rate

Integration of mass flux across the gap at an arbitrary position leads to the gap mass flow per unit flow width

$$m'_L = \int_0^h \rho \cdot u \cdot dy \qquad (10.14).$$

Mass flow m'_L reduces the velocity field information to a single value per load case and sliding ratio. Hence, mass flow m'_L enables a quantitative comparison of various load cases and sliding ratios independent of position. Figure 10.12 shows the mass flow m'_L for all load cases i to iv and sliding ratios and shows the relative deviation of mass flow m'_L between the extended and the Reynolds equation based solutions

$$\varepsilon_{m,Re} = \frac{m'_L - m'_{L,Re}}{m'_{L,Re}} \qquad (10.15).$$
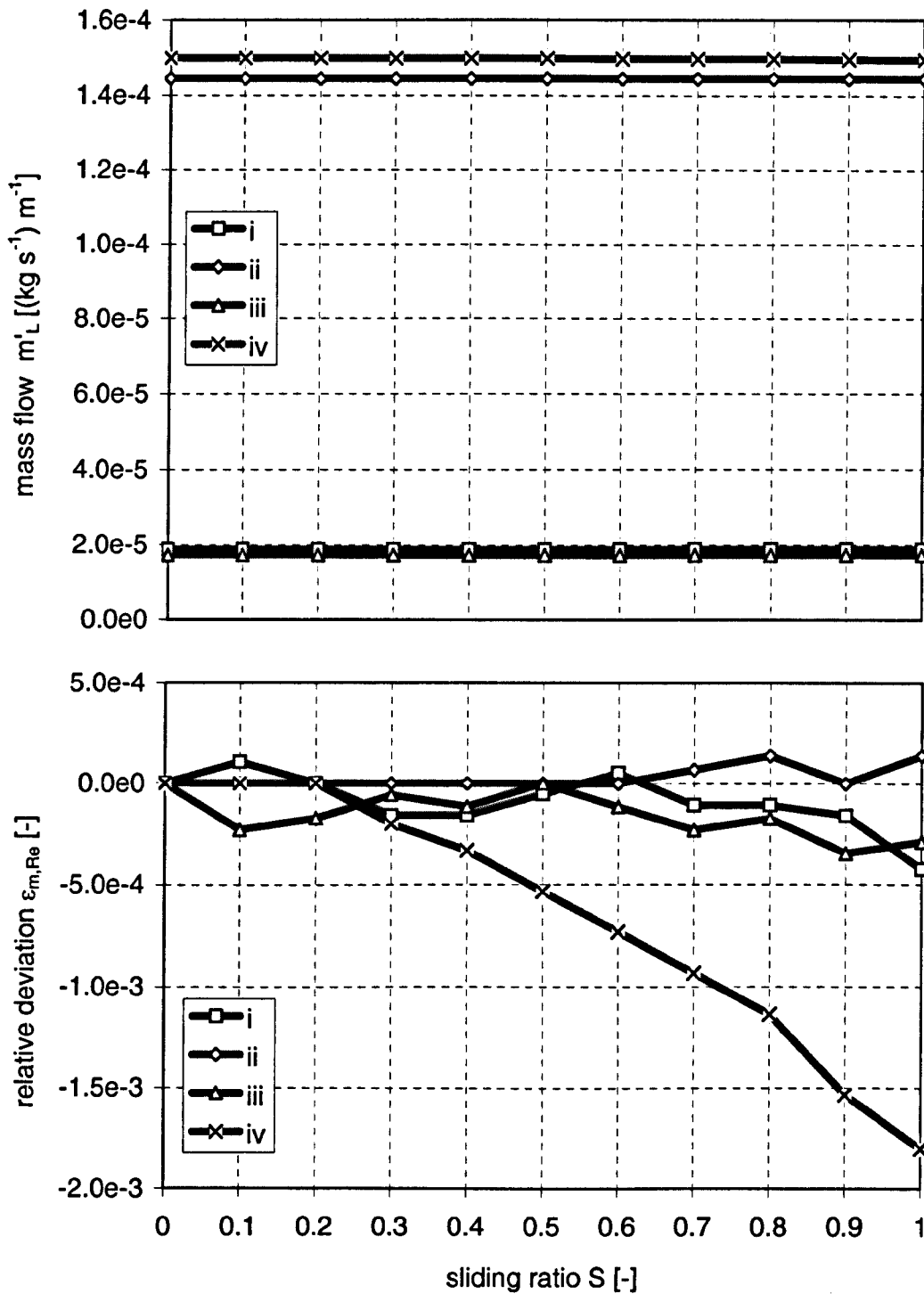
Figure 10.12: Mass flow per unit flow width m'_L and relative deviation of mass flow from Reynolds equation based solution $\varepsilon_{m,Re}$, for load case i to iv (table 10.1) and various sliding ratios S.

10.6   Pressure and pressure dependent variables

The new approach proposed within this thesis allows pressure variation across the height of the gap. Hence computations with the new approach lead to two-dimensional pressure fields instead of one-dimensional pressure results normally delivered by Reynolds equation based solutions. The following subsections present various types of graphs showing the pressure distribution in the gap and giving comparison with Reynolds equation based solutions.

10.6.1   Pressure fields

An overall impression of the pressure distribution in the contact is given in the contour plots of figure 10.13. The pressure distribution is given for load case iv and pure rolling (a), 50 per cent sliding (b) and pure sliding (c). In part (d), the pressure distribution of a Reynolds equation based solution is given for reference and comparison. Results for load cases i to iii can be found in appendix K, figures K.13 to K.15. In these plots, pressure variation along the gap dominates over pressure variation across the gap. However pressure variation across the gap is of particular interest in this work. The contour plots of figure 10.14 focus on the pressure variation across the gap by displaying the absolute pressure deviation across the gap

$$\varepsilon_{p,abs} = p - p_{cl} \qquad (10.16)$$

for load case iv and sliding ratios for pure rolling (a), 50 per cent sliding (b) and pure sliding (c). In equation 10.16 p_{cl} represents the centreline pressure, which is the pressure half way between the two surfaces actually at the position along the contact of a corresponding pressure value, i.e.

$$p_{cl} = p\left(y = \frac{h}{2}\right) \qquad (10.17).$$

The respective results for load cases i to iii are presented in figures K.16 to K.18 of appendix K. Comparison of the results of the extended approach with Reynolds equation based solutions for load case iv is given in figure 10.15. The contour plots show the relative deviation of pressure between the two approaches.

$$\varepsilon_{P,Re} = \frac{p - p_{Re}}{p_{Hz}} \qquad (10.18).$$

As for the comparison of velocity data, the normalised height Y^* was used for this figure. For the relative deviation of pressure, results for load cases i to iii are given in figures K.19 to K.21 of appendix K.

(a)
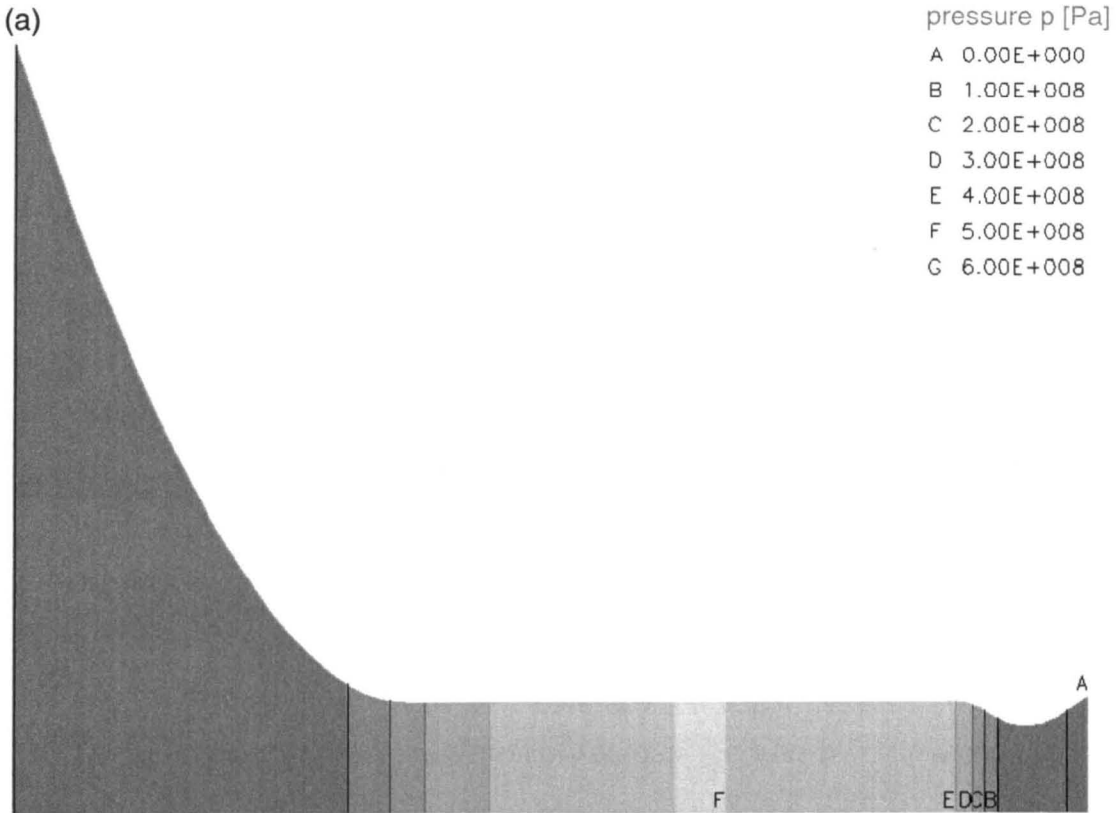
Figure 10.13: Contour plots of pressure distribution p in the gap for extended and Reynolds equation based approaches; load case iv (table 10.1), sliding ratios S = 0.0, 0.5, and 1.0,
(a) sliding ratio S = 0.0,
(b) sliding ratio S = 0.5,
(c) sliding ratio S = 1.0,
(d) Reynolds equation based solution
(continued).

(b)

pressure p [Pa]

A 0.00E+000
B 1.00E+008
C 2.00E+008
D 3.00E+008
E 4.00E+008
F 5.00E+008
G 6.00E+008

(c)

pressure p [Pa]

A 0.00E+000
B 1.00E+008
C 2.00E+008
D 3.00E+008
E 4.00E+008
F 5.00E+008
G 6.00E+008
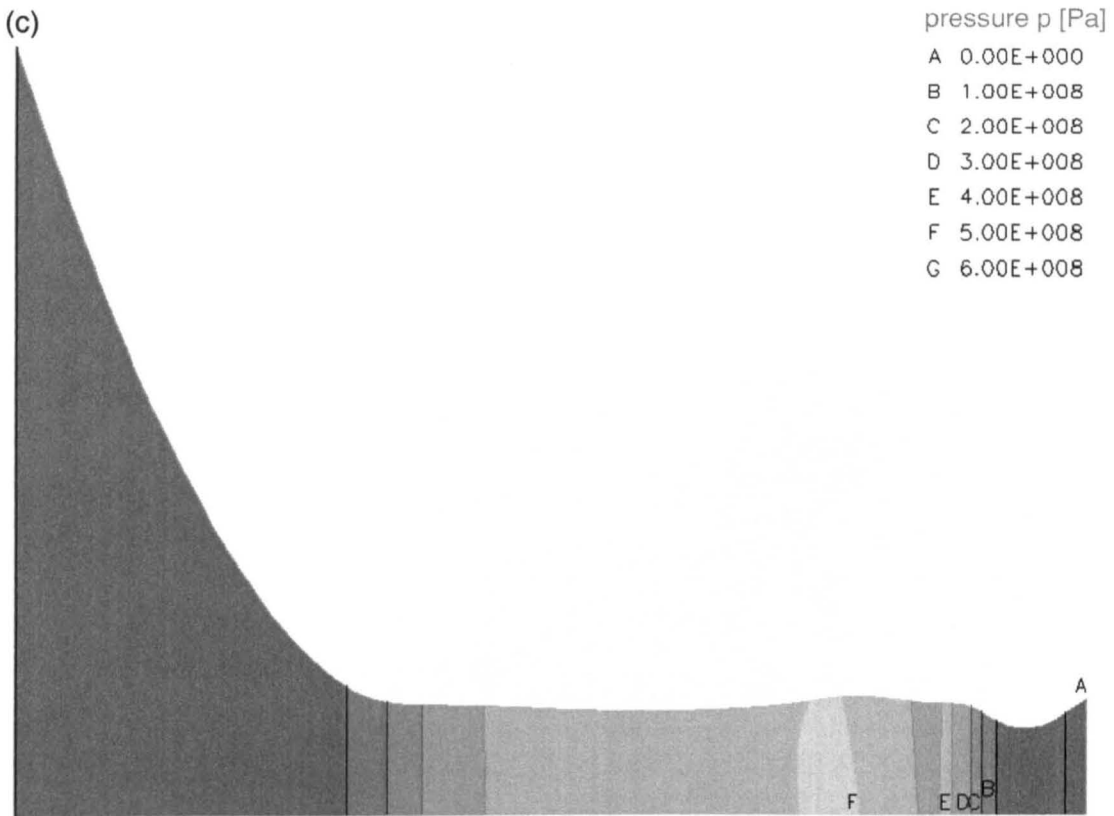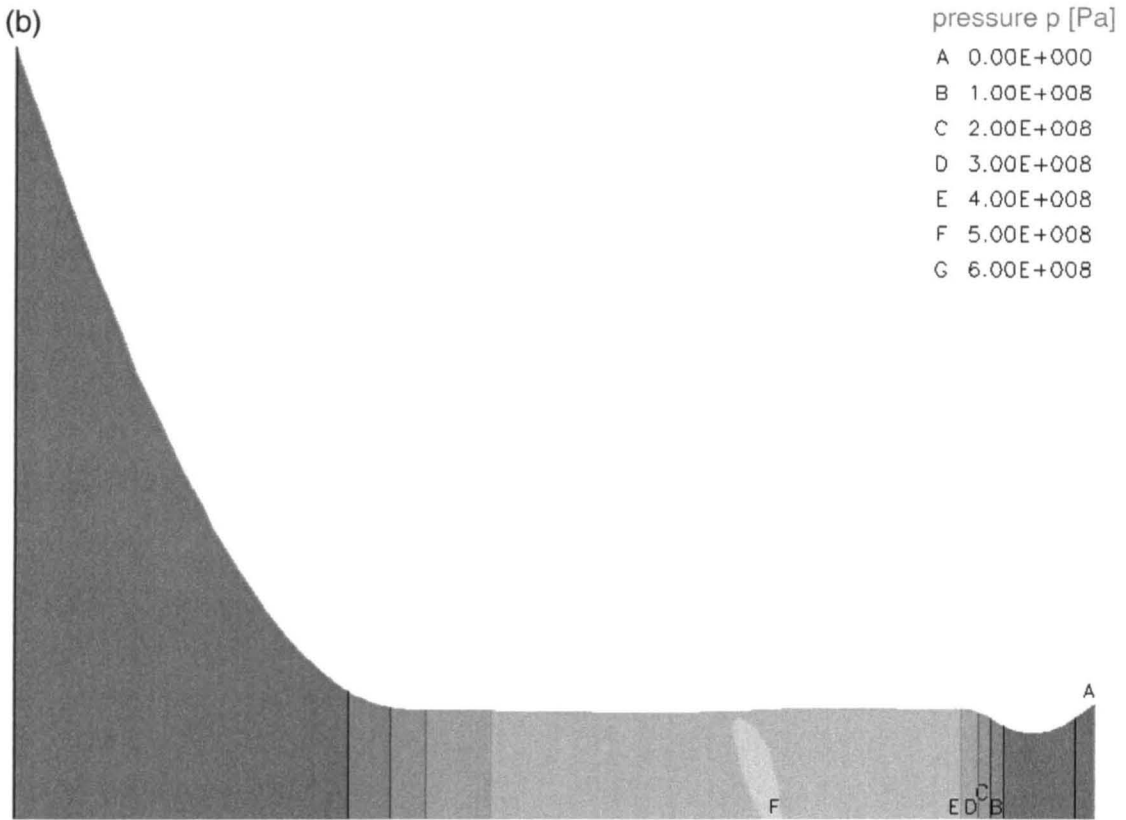
Figure 10.13: (continued).

(d)

Figure 10.13: (concluded).

(a)

absolute pressure deviation $\varepsilon_{p,abs}$ [Pa]

A $-2.00E+006$

B $2.00E+006$
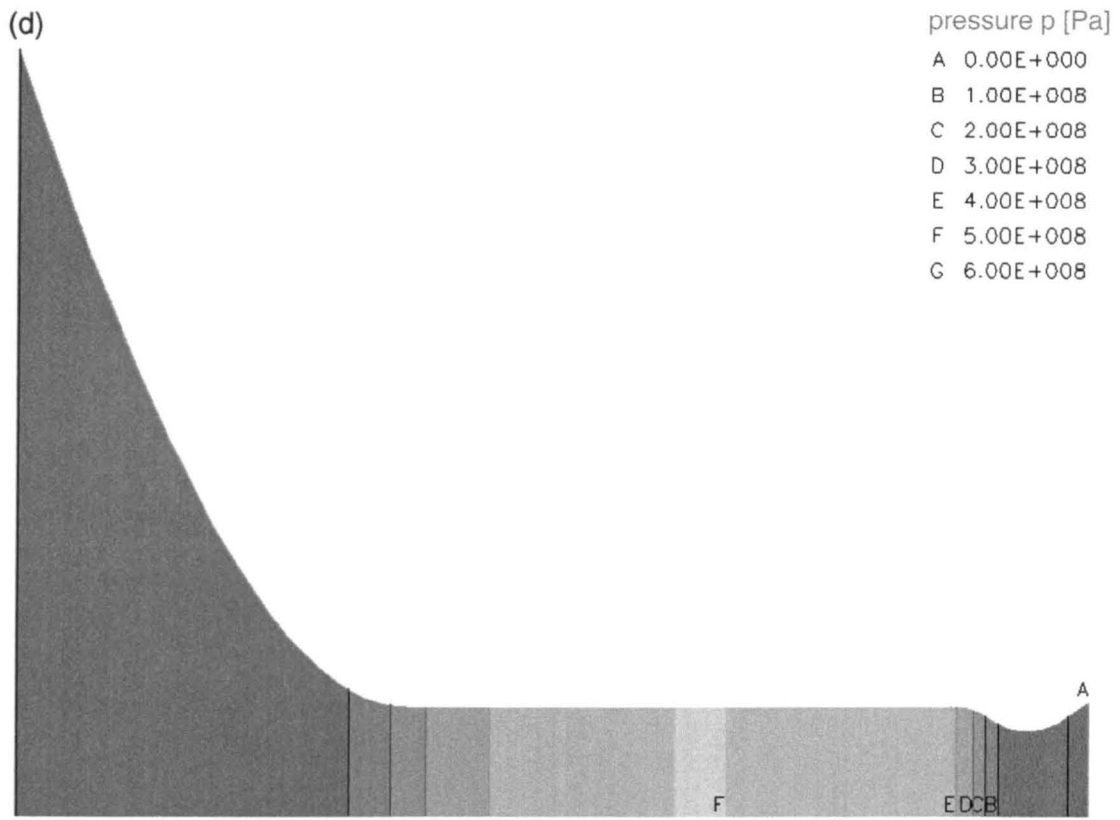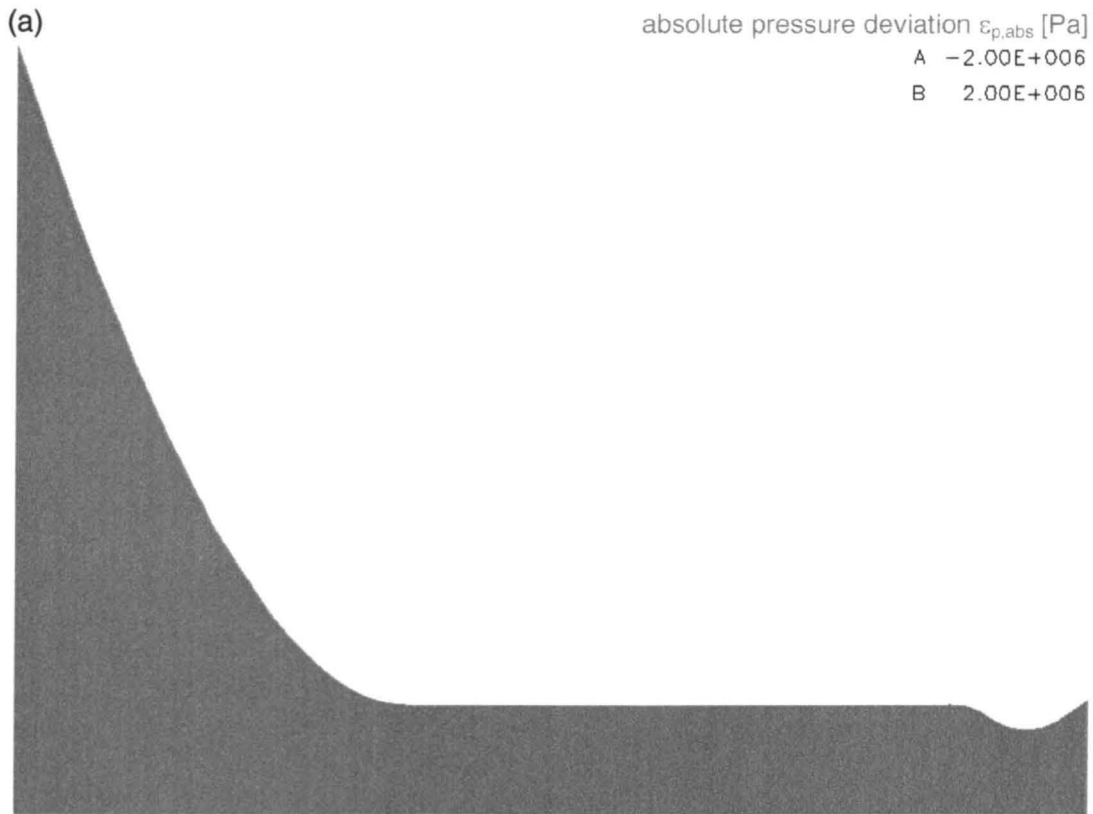
Figure 10.14: Contour plots of absolute pressure deviation from the centreline pressure $\varepsilon_{p,abs}$ in the gap for extended approach; load case iv (table 10.1), sliding ratios $S = 0.0$, 0.5, and 1.0,

(a) $S = 0.0$,

(b) $S = 0.5$,

(c) $S = 1.0$,

N.B. the absolute pressure deviation lies entirely between the two limits A and B

(continued).

(b)

absolute pressure deviation $\varepsilon_{p.abs}$ [Pa]

A	−6.00E+006
B	−2.00E+006
C	2.00E+006
D	6.00E+006

(c)

absolute pressure deviation $\varepsilon_{p,abs}$ [Pa]

A	−1.40E+007
B	−1.00E+007
C	−6.00E+006
D	−2.00E+006
E	2.00E+006
F	6.00E+006
G	1.00E+007
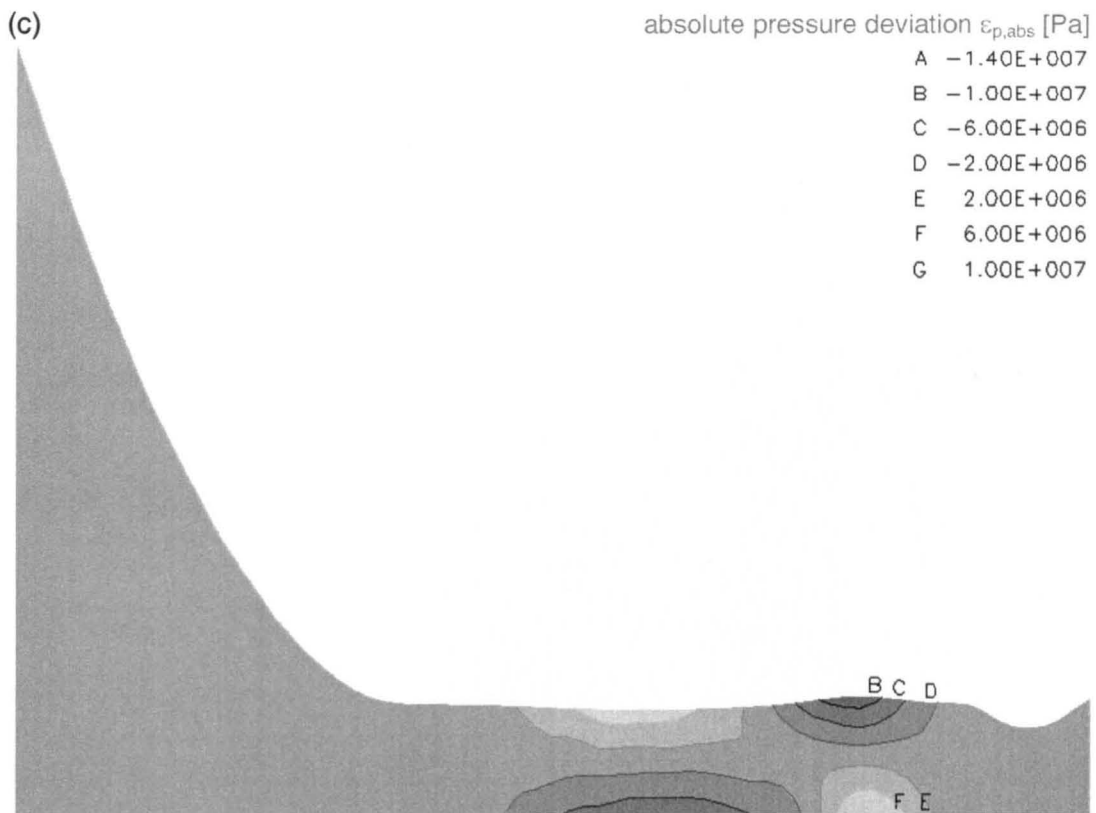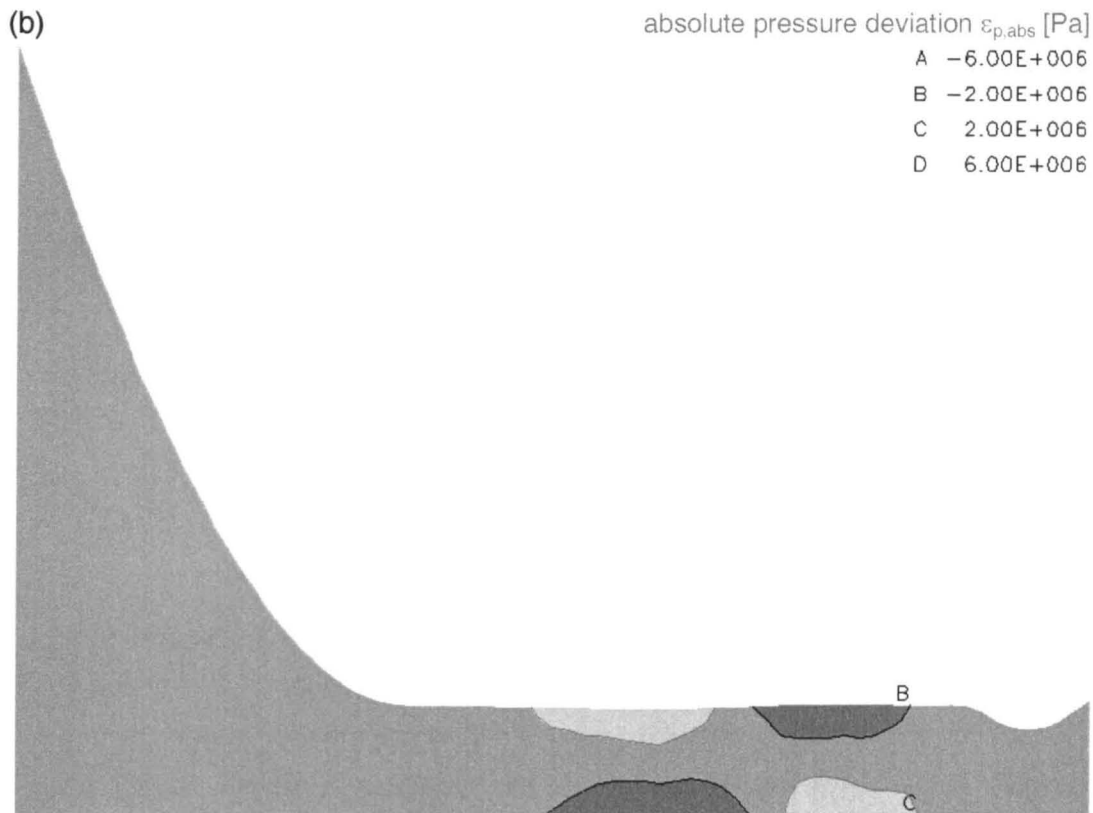
Figure 10.14: (concluded).

(a)

(a)

$\varepsilon_{P,Re}$ =   □ -0.002-0   ▨ 0-0.002
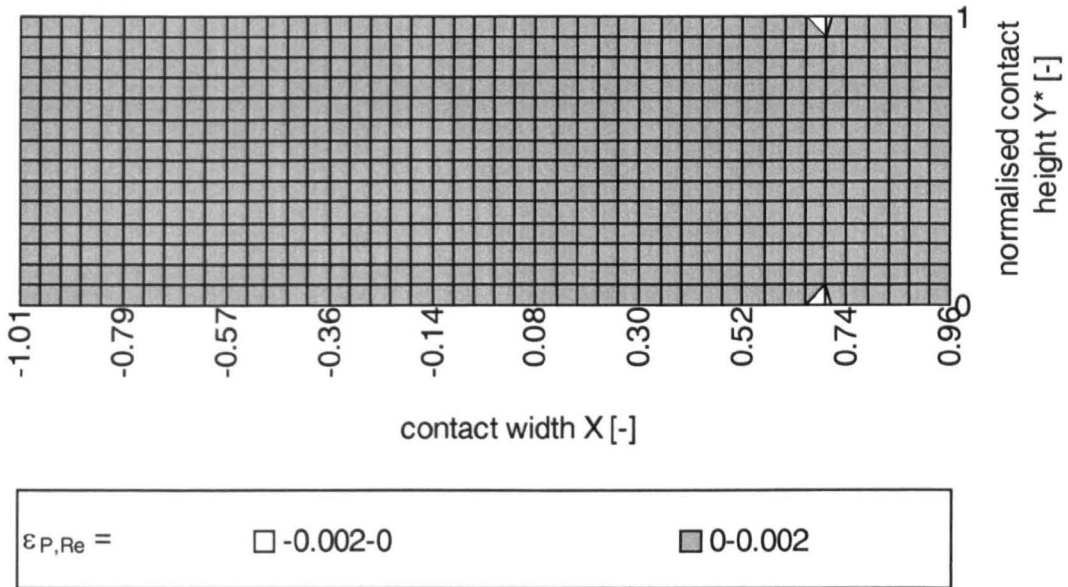
Figure 10.15: Relative deviation of pressure of extended from Reynolds equation based approach $\varepsilon_{P,Re}$; load case iv (table 10.1), sliding ratios S = 0.0, 0.5, and 1.0,
(a) S = 0.0,
(b) S = 0.5,
(c) S = 1.0
(continued).

(b)
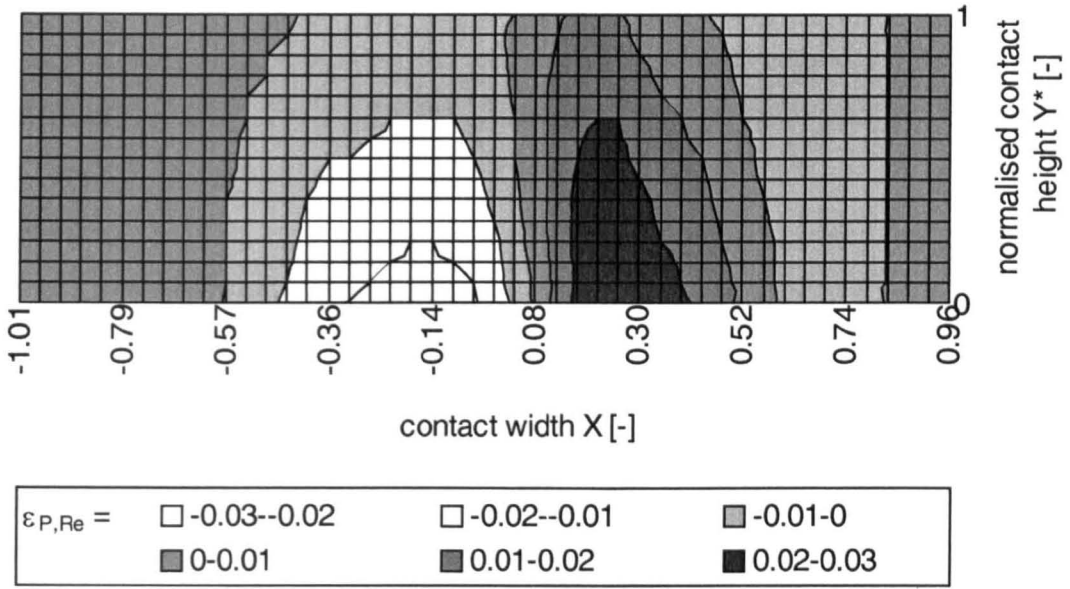
(c)
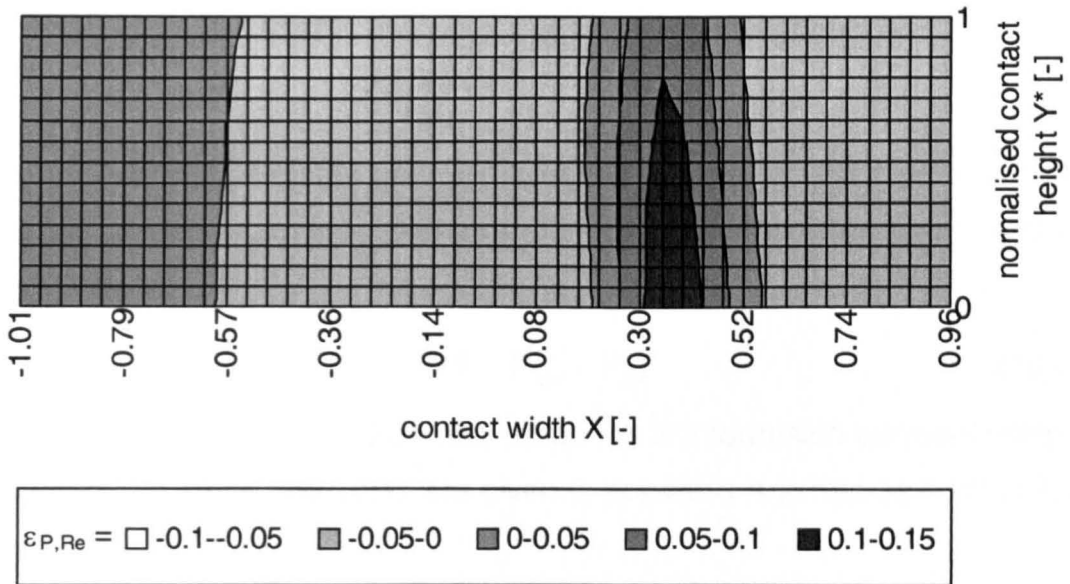
Figure 10.15: (concluded).

10.6.2   Pressure profiles

The plots of figure 10.14 and 10.15 show that the largest differences between the extended and Reynolds equation based solutions appear on the surfaces. Figure 10.16 gives the dimensionless pressure distribution for the slower surface (a) and the faster surface (b) for load case iv. Part (c) of figure 10.16 gives the mean value of both pressure distributions

$$P_{mean} = \tfrac{1}{2}\cdot(P_1 + P_2) = \tfrac{1}{2}\cdot(P_{slow} + P_{fast}) \tag{10.19},$$

which is relevant for the deformation of the solid surfaces. For all three pressure distributions, the relative deviation from a Reynolds equation based solution is shown for comparison together with the respective pressure distribution, where

$$\varepsilon_{Pslow,Re} = \frac{P_{slow} - P_{Re}}{P_{Re}} \tag{10.20},$$

$$\varepsilon_{Pfast,Re} = \frac{P_{fast} - P_{Re}}{P_{Re}} \tag{10.21},$$

and
$$\varepsilon_{Pmean,Re} = \frac{P_{mean} - P_{Re}}{P_{Re}} \tag{10.22}.$$

Further information on the pressure variation across the gap is given in figure 10.17. The dimensionless pressure difference between the slower and the faster surface

$$\Delta P = P_{slow} - P_{fast} \tag{10.23}$$

is shown for load case iv. For load cases i to iii information corresponding to that of figure 10.16 and 10.17 are given in appendix K in figures K.22 to K.24 and K.25 to K.27.
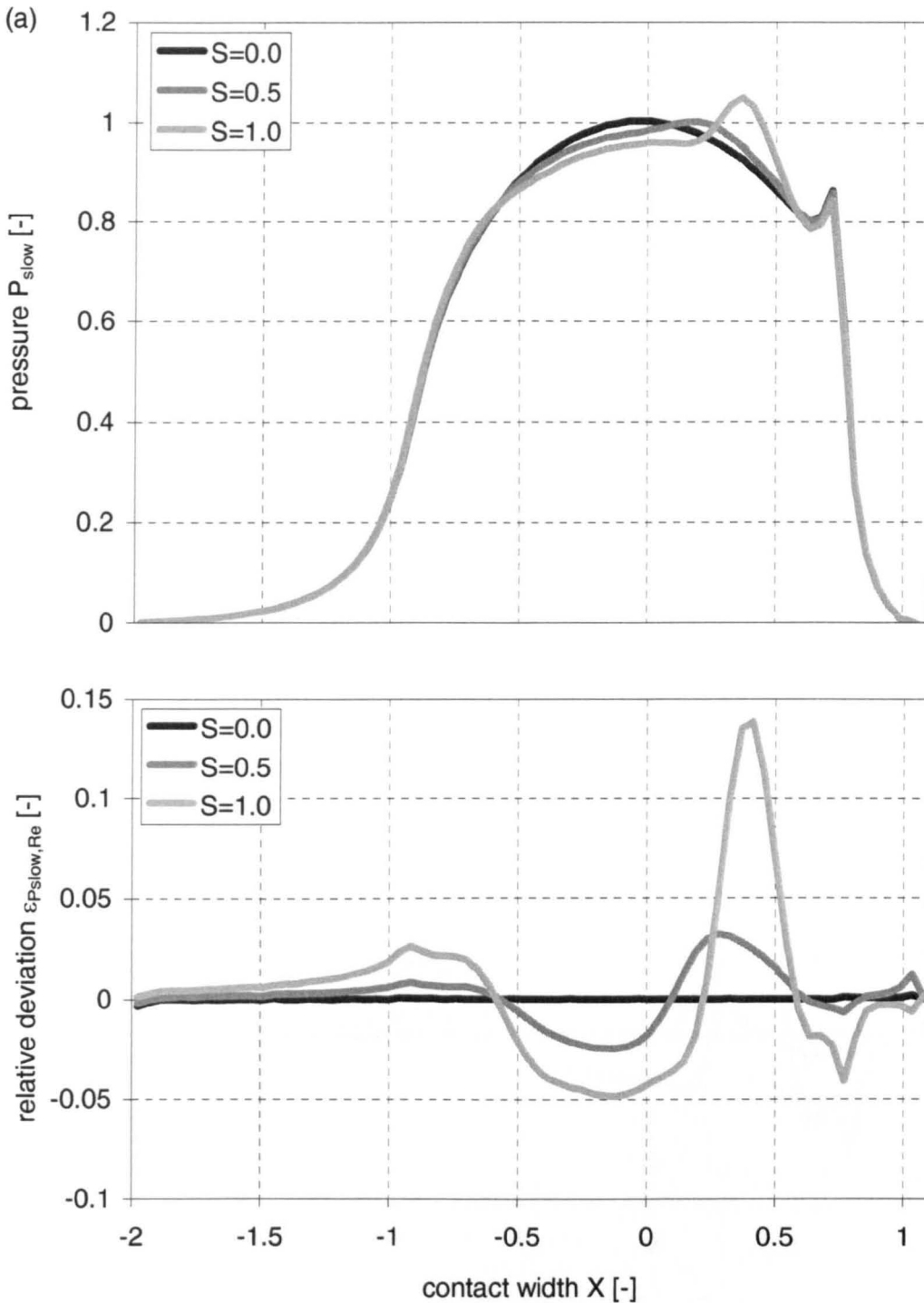
Figure 10.16: Pressure on the slower surface P_{slow} and the faster surface P_{fast} and mean pressure P_{mean} and relative deviation of these values from Reynolds equation based solution $\varepsilon_{Pslow,Re}$, $\varepsilon_{Pfast,Re}$, and $\varepsilon_{Pmean,Re}$ for various sliding ratios; load case iv (table 10.1), sliding ratios $S = 0.0$, 0.5, and 1.0,
(a) pressure on slower surface P_{slow} and relative deviation $\varepsilon_{Pslow,Re}$,
(b) pressure on faster surface P_{fast} and relative deviation $\varepsilon_{Pfast,Re}$,
(c) mean pressure P_{mean} and relative deviation $\varepsilon_{Pmean,Re}$
(continued).
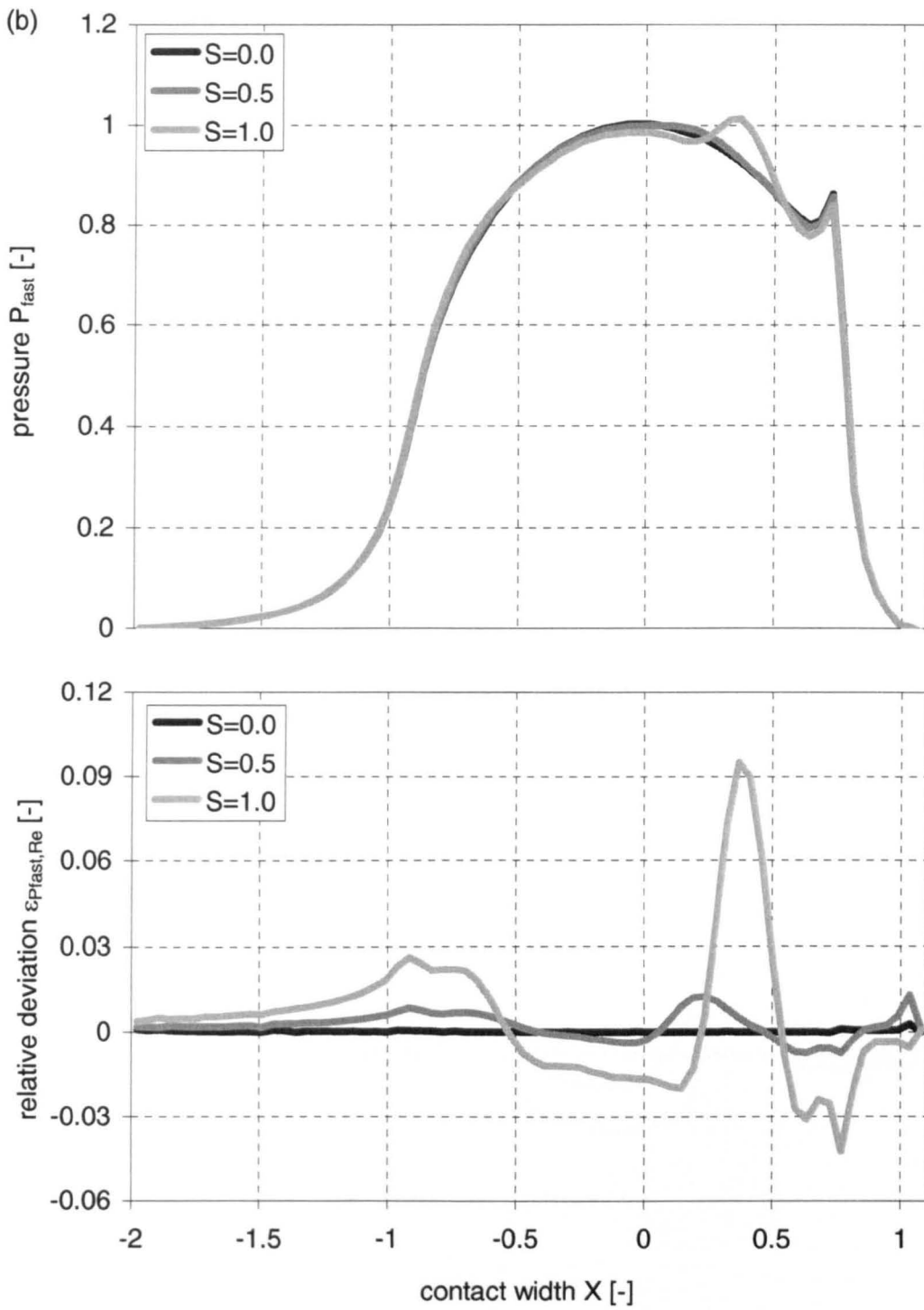
Figure 10.16: (continued).
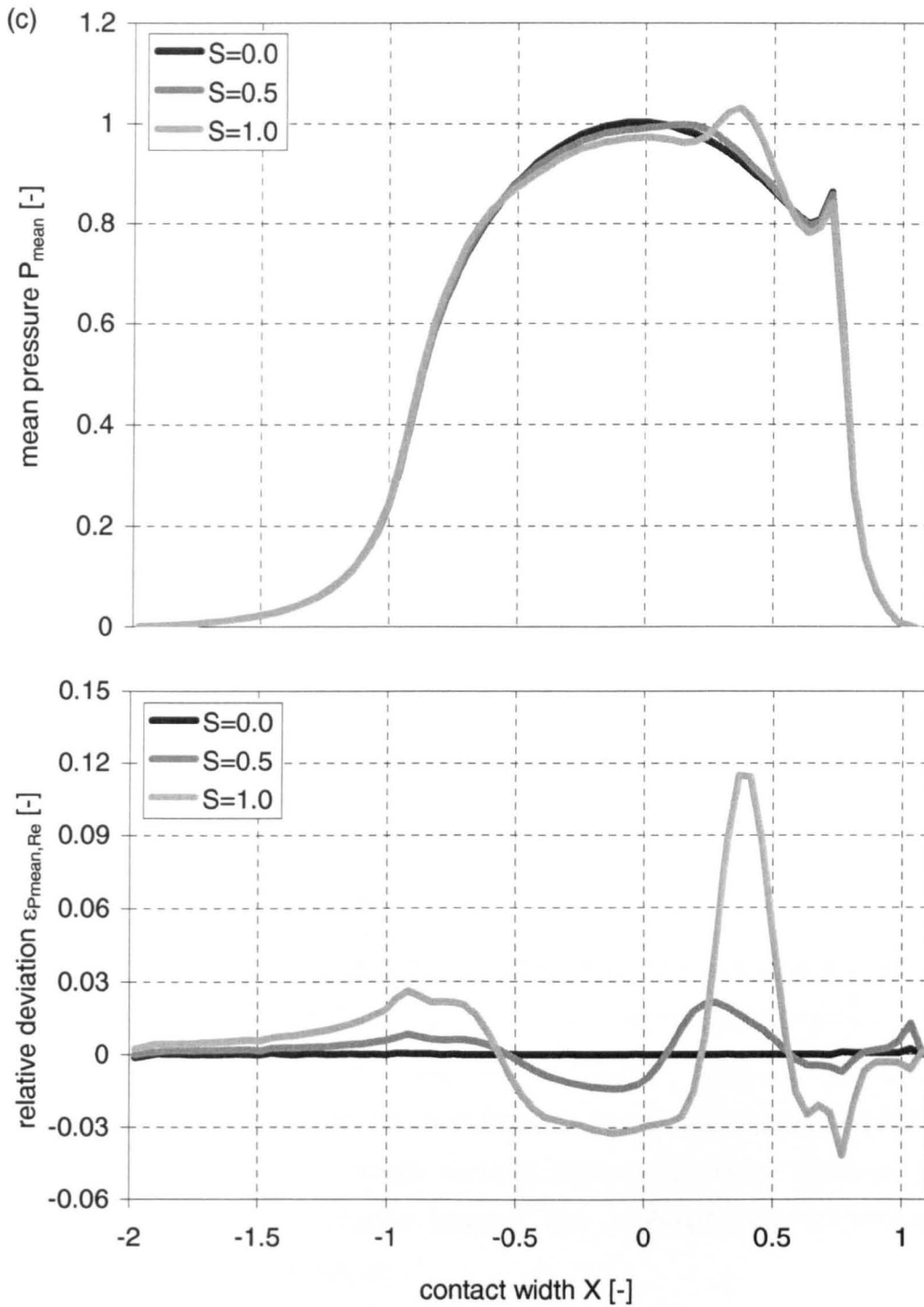
Figure 10.16: (concluded).
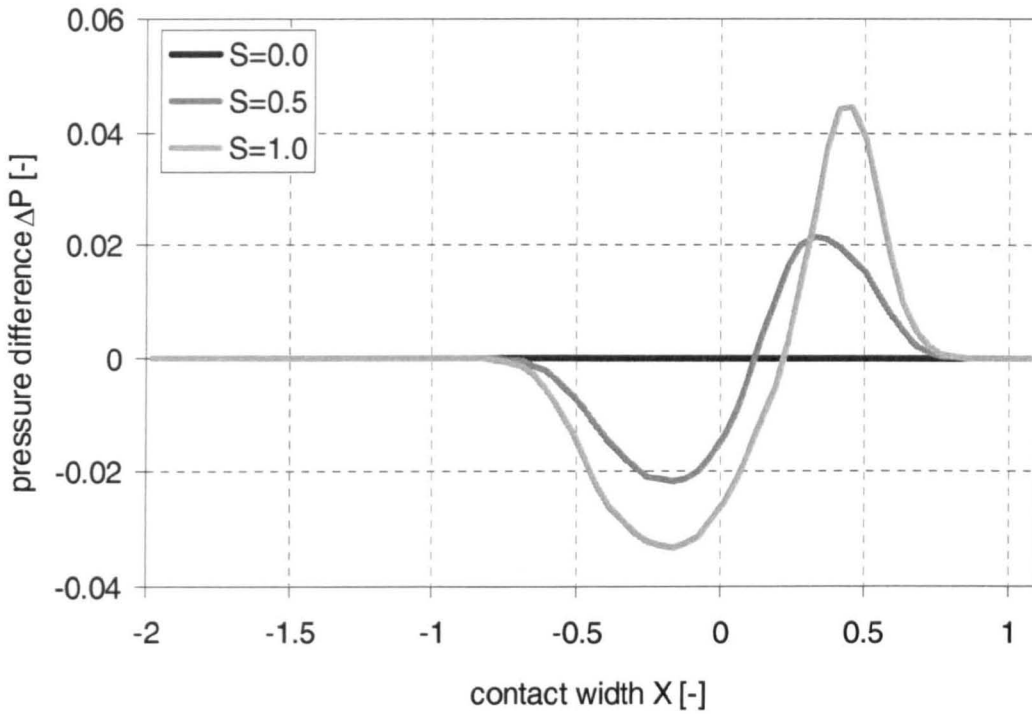
Figure 10.17: Dimensionless pressure difference between faster and slower surface ΔP for various sliding ratios; load case iv (table 10.1), sliding ratios S = 0.0, 0.5, and 1.0.

10.6.3   Pressure values

The above figures 10.16 and 10.17 show that the value and position of maximum pressure, apart from the ehl pressure spike, differ from the contact centreline for the extended approach. Figure 10.18 summarizes the maximum pressure value for all investigated load cases and sliding ratios for the slower surface (a), the faster surface (b) and the mean pressure (c) as dimensional and dimensionless values. The corresponding dimensionless positions of maximum pressure

$$X_{pslow} = \frac{x_{pslow}}{b_{Hz}} = X(P_{slow} = P_{slow,max}) \qquad (10.24),$$

$$X_{pfast} = \frac{x_{pfast}}{b_{Hz}} = X(P_{fast} = P_{fast,max}) \qquad (10.25),$$

and $$X_{pmean} = \frac{x_{pmean}}{b_{Hz}} = X(P_{mean} = P_{mean,max}) \qquad (10.26)$$

are given in figure 10.20 (a) to (c).

The figure 10.17 shows the difference between the slower and the faster surface. The curves contain two extreme values, a minimum where the pressure on the faster surface exceeds the pressure on the slow surface by a maximum amount and a maximum where the pressure on the slow surface exceeds the pressure on the fast surface by a maximum amount. The values of these extreme values for all load cases and sliding ratios are given in figure 10.19(a) and (b). The position of these extreme values

$$X_{\Delta P\,min} = \frac{x_{\Delta P\,min}}{b_{Hz}} = X(\Delta P = \Delta P_{min}) \qquad (10.27)$$

and
$$X_{\Delta P\,max} = \frac{x_{\Delta P\,max}}{b_{Hz}} = X(\Delta P = \Delta P_{max}) \qquad (10.28)$$

are given in part (d) and (e) of figure 10.20.
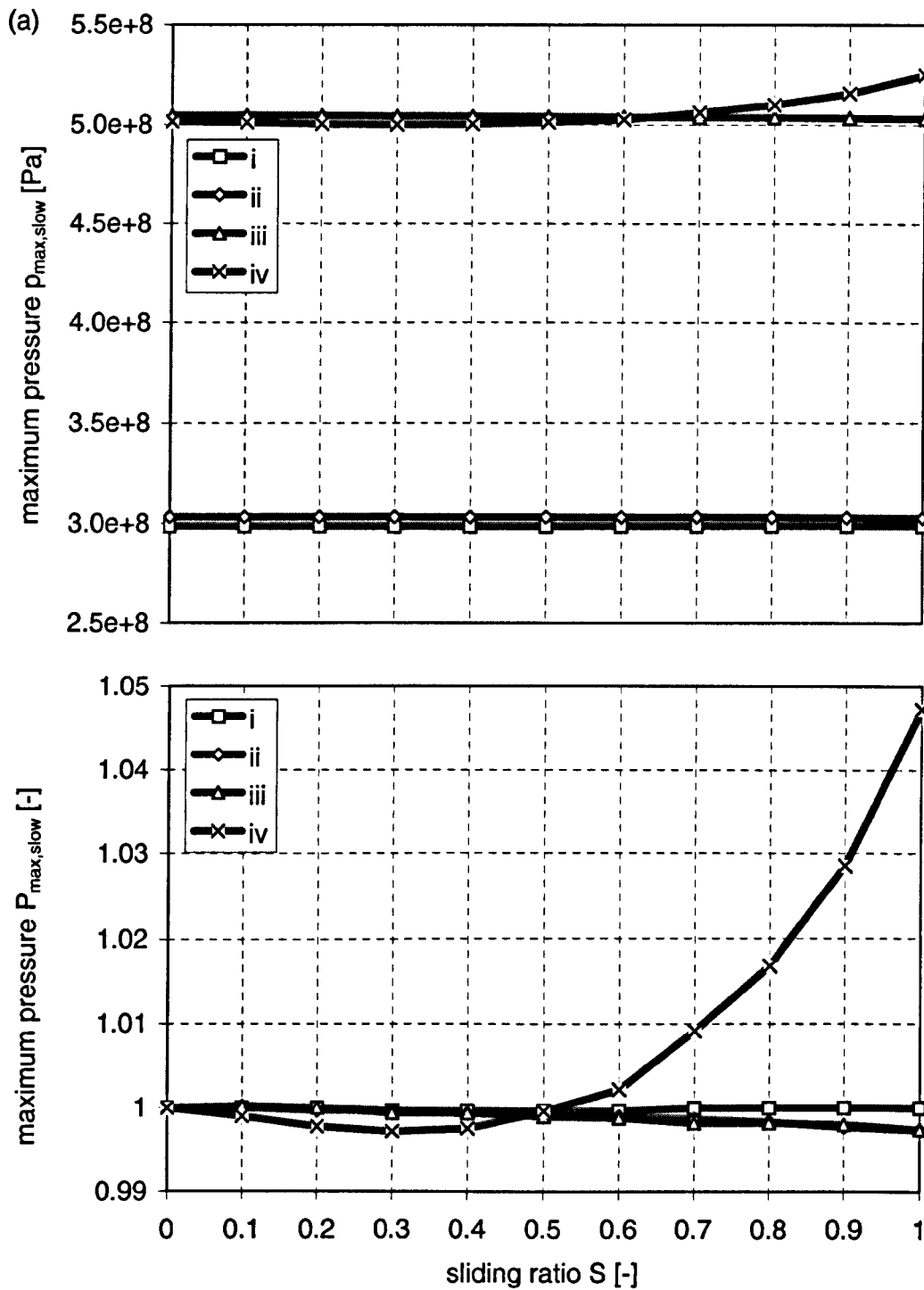
Figure 10.18: Dimensional and dimensionless maximum pressure on the slower surface $p_{slow,max}$ and $P_{slow,max}$, and on the faster surface $p_{fast,max}$ and $P_{fast,max}$ and dimensional and dimensionless maximum mean pressure $p_{mean,max}$ and $P_{mean,max}$ for load cases i to iv (table 10.1) and various sliding ratios S,
(a) maximum pressure at slower surface $p_{slow,max}$ and $P_{slow,max}$,
(b) maximum pressure at faster surface $p_{fast,max}$ and $P_{fast,max}$,
(c) maximum mean pressure $p_{mean,max}$ and $P_{mean,max}$
(continued).
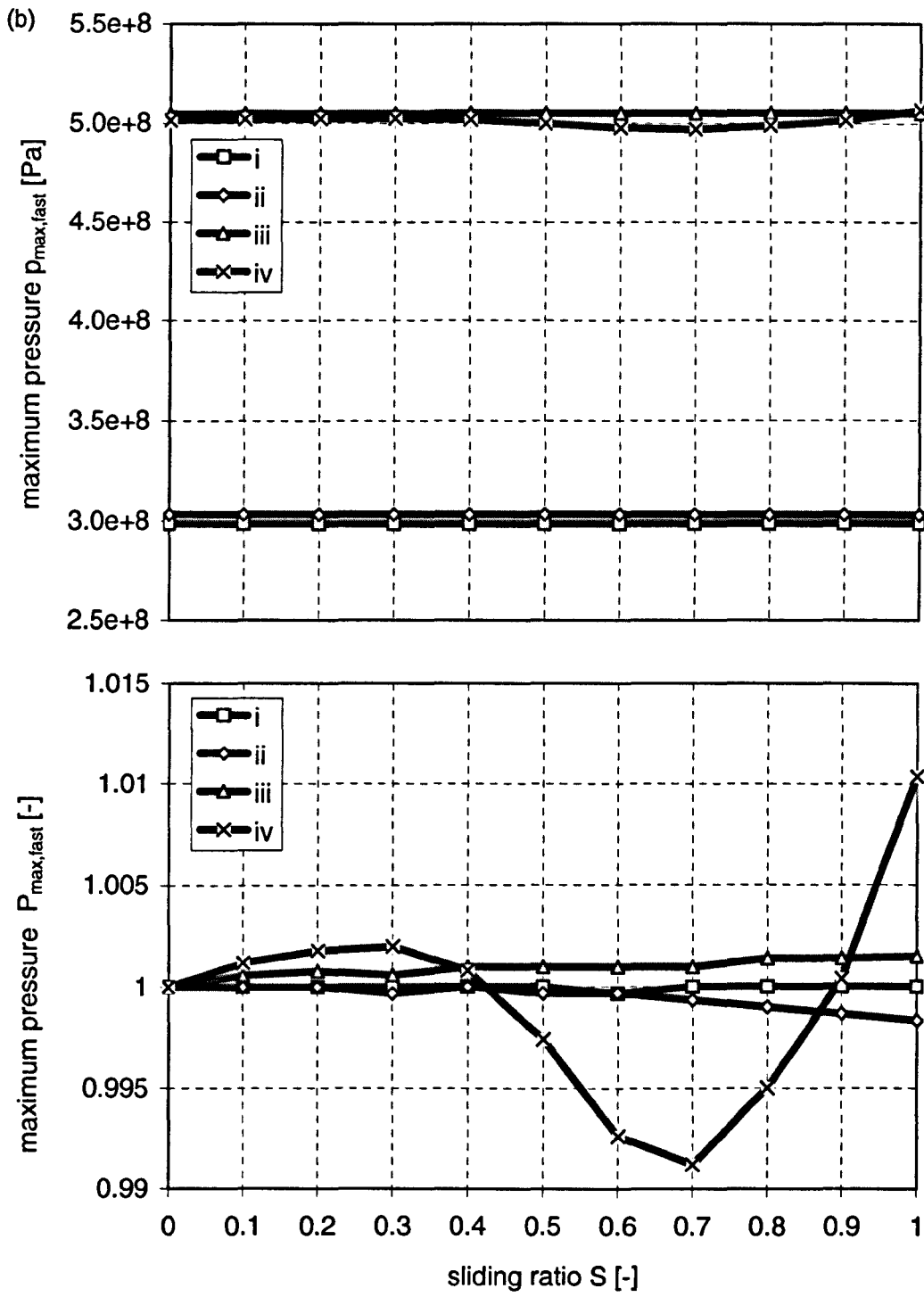
Figure 10.18: (continued).
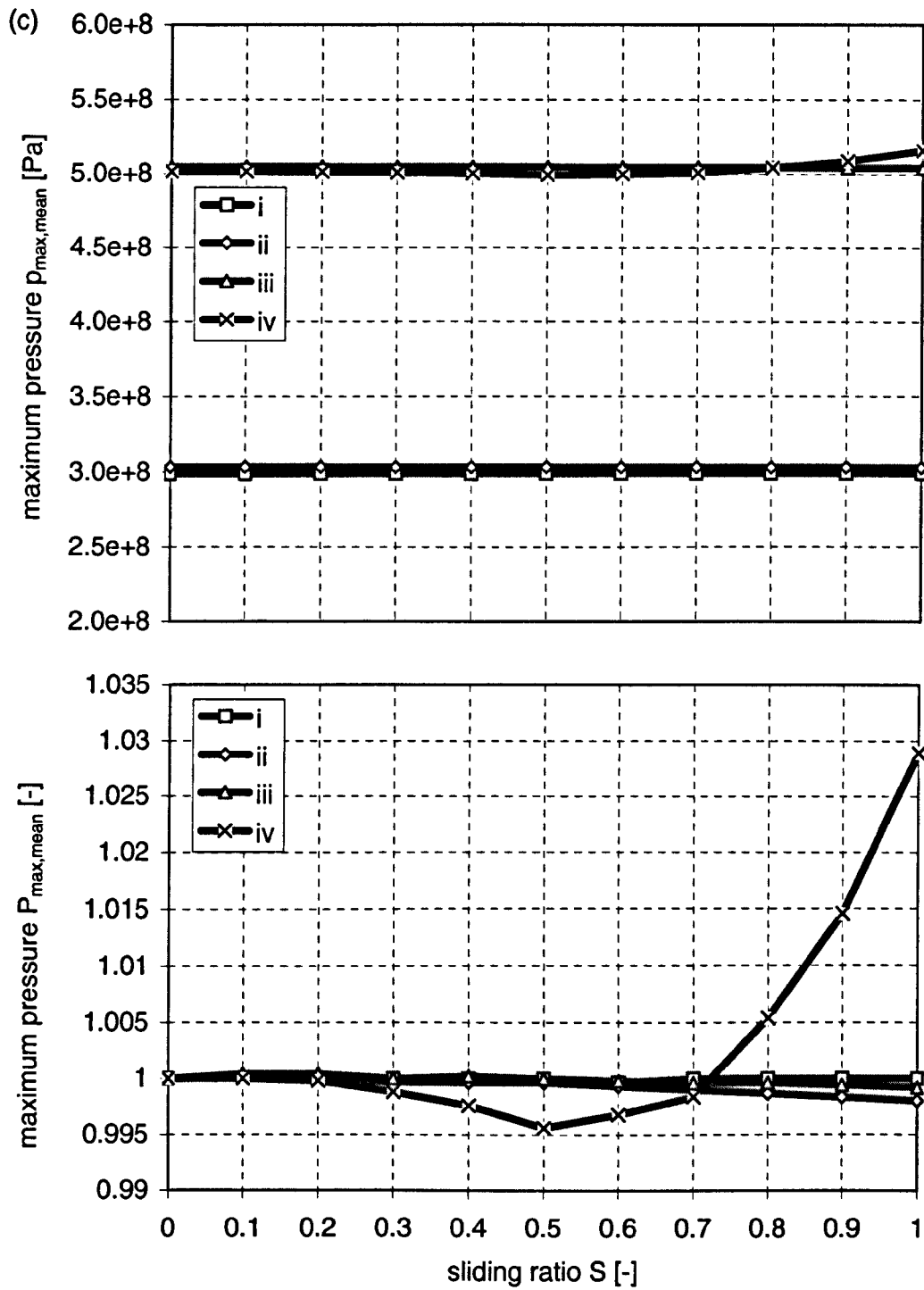
Figure 10.18: (concluded).
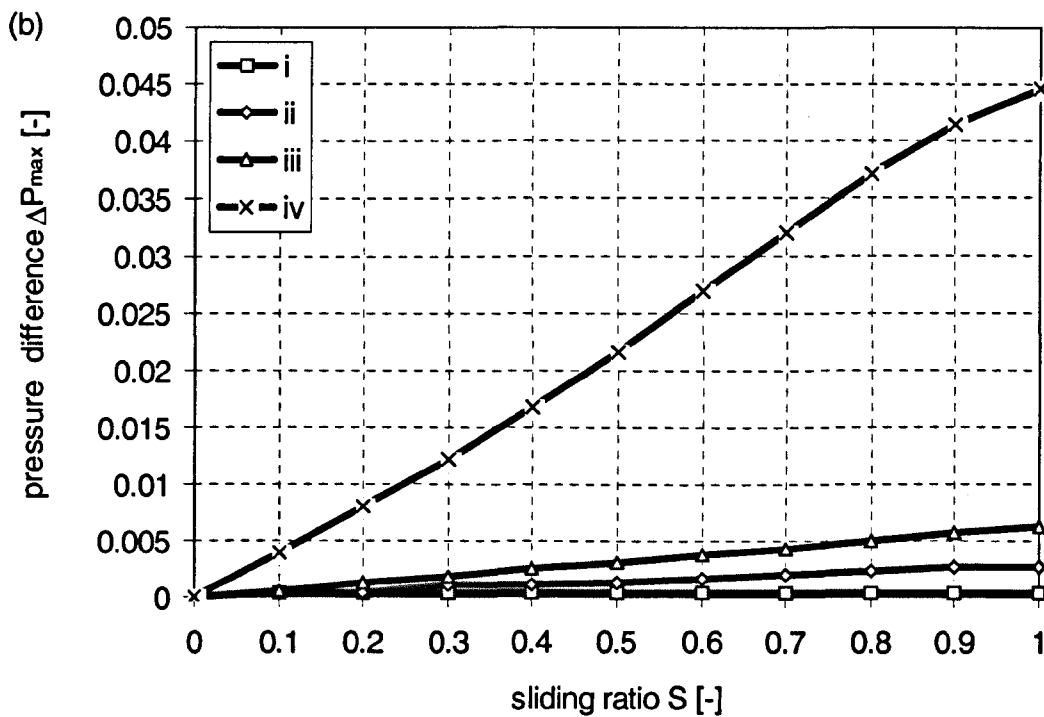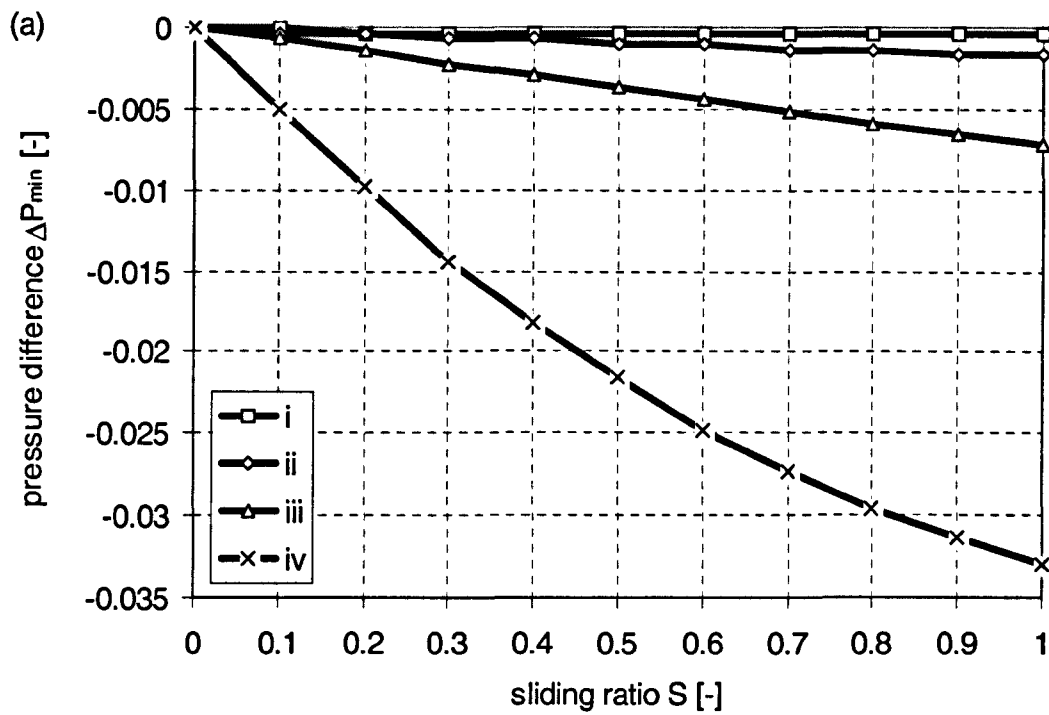
Figure 10.19: Dimensionless minimum and maximum pressure difference
ΔP_{min} and ΔP_{max} for load cases i to iv (table 10.1) and various
sliding ratios S,
(a) minimum pressure difference ΔP_{min},
(b) maximum pressure difference ΔP_{max}.
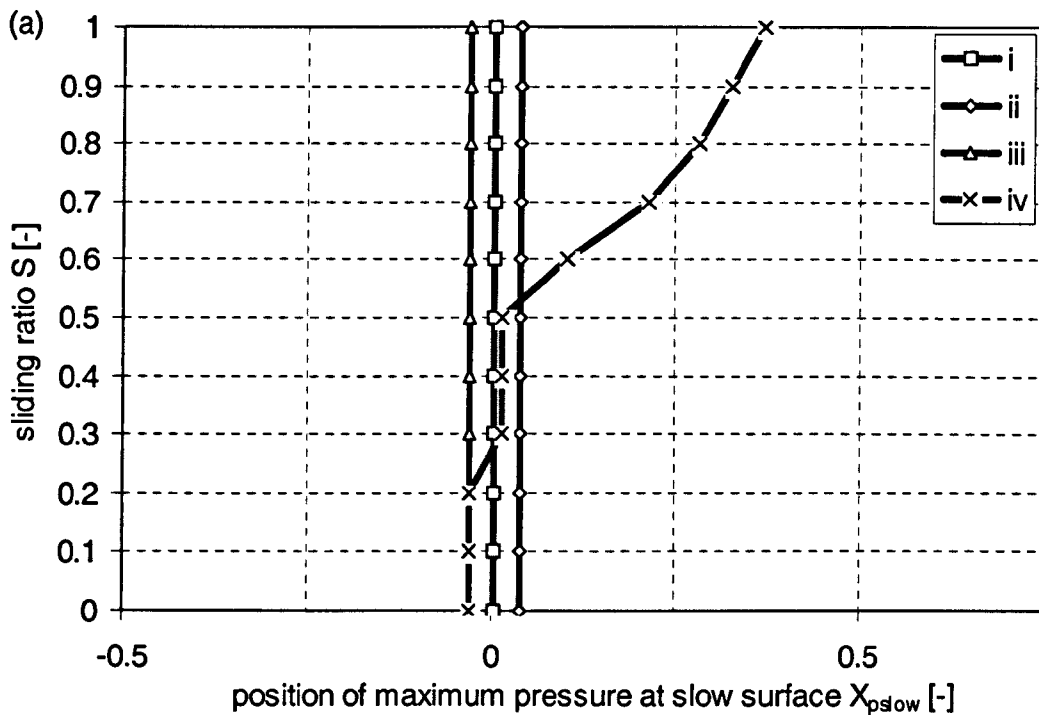
Figure 10.20: Dimensionless position of the maximum pressure on the slower and faster surface X_{pslow} and X_{pfast}, dimensionless position of maximum mean pressure X_{pmean}, and dimensionless position of minimum and maximum pressure difference $X_{\Delta Pmin}$ and $X_{\Delta Pmax}$ for load cases i to iv (table 10.1) and various sliding ratios S,

(a)   position of maximum pressure on slower surface X_{pslow},

(b)   position of maximum pressure on faster surface X_{pfast},

(c)   position of maximum mean pressure X_{pmean},

(d)   position of minimum pressure difference $X_{\Delta Pmin}$,

(e)   position of maximum pressure difference $X_{\Delta Pmax}$.

N.B.   Values are not displayed for all load case-sliding ratio combinations

(continued).

(b)

position of maximum pressure at fast surface X_{pfast} [-]

(c)

position of maximum mean pressure X_{pmean} [-]

Figure 10.20: (continued).

(d) position of minimum pressure difference $X_{\Delta Pmin}$ [-]

(e) position of maximum pressure difference $X_{\Delta Pmax}$ [-]
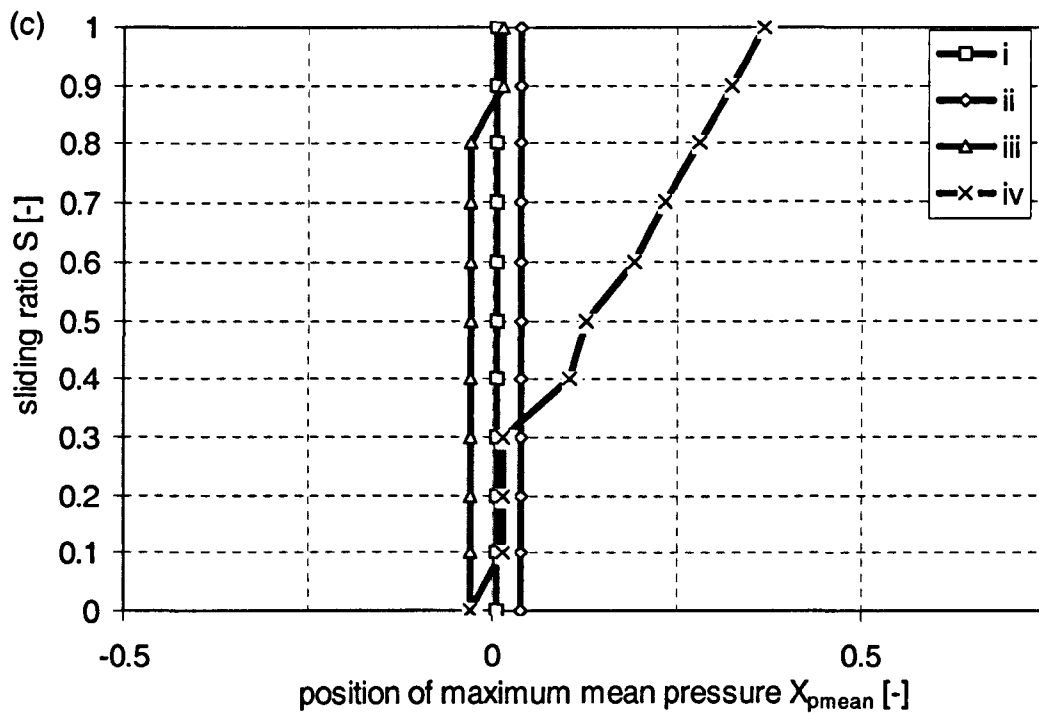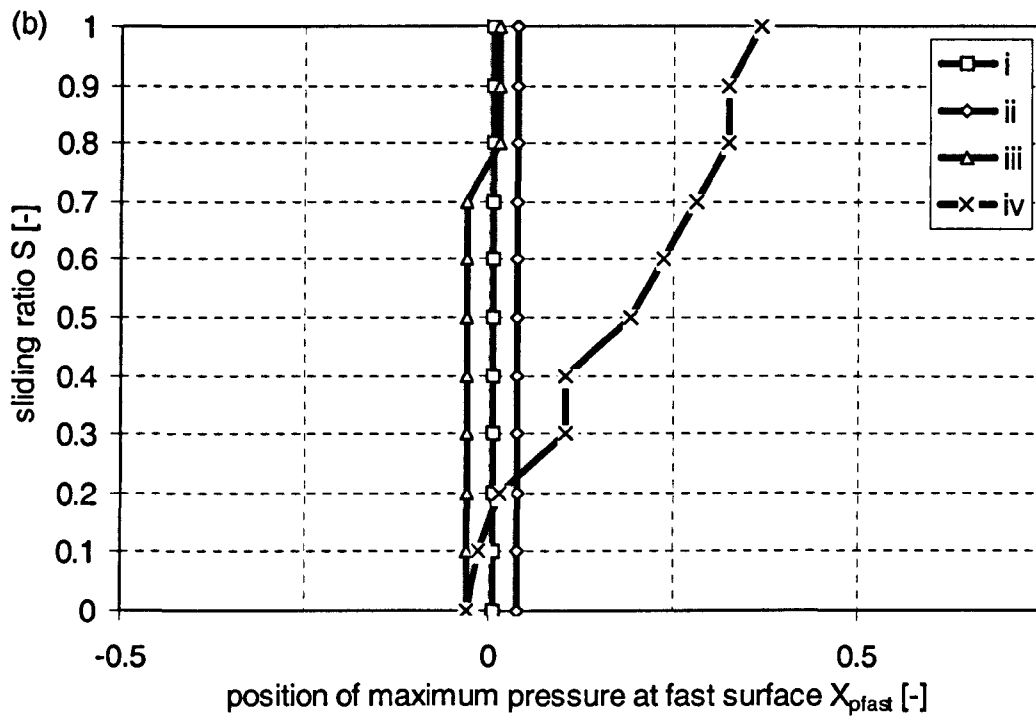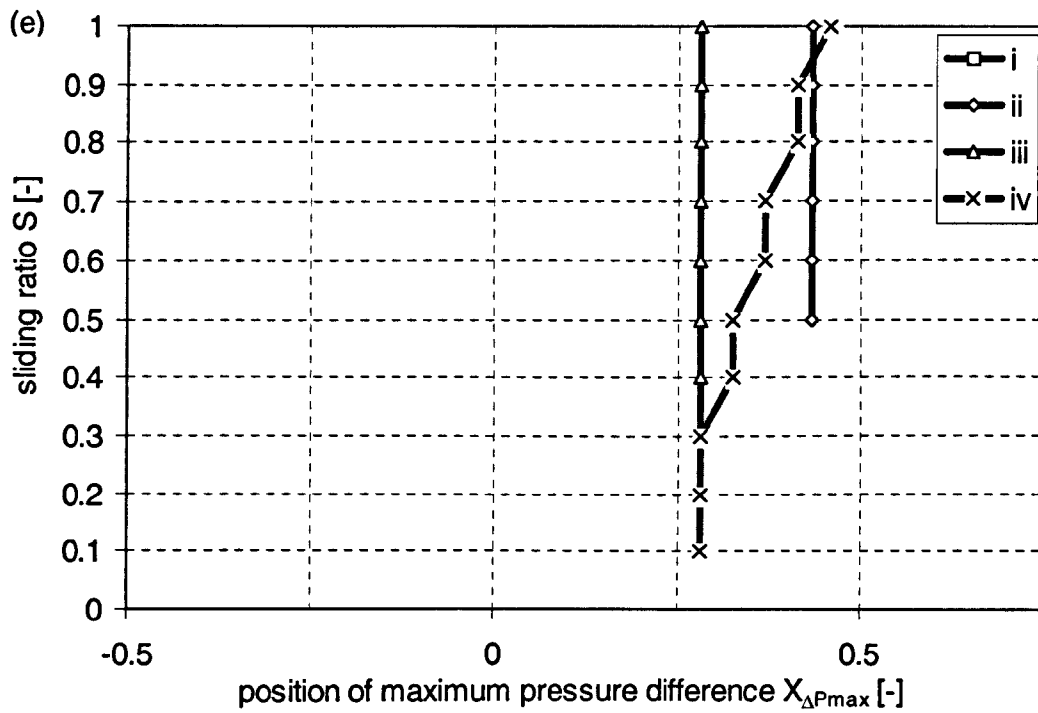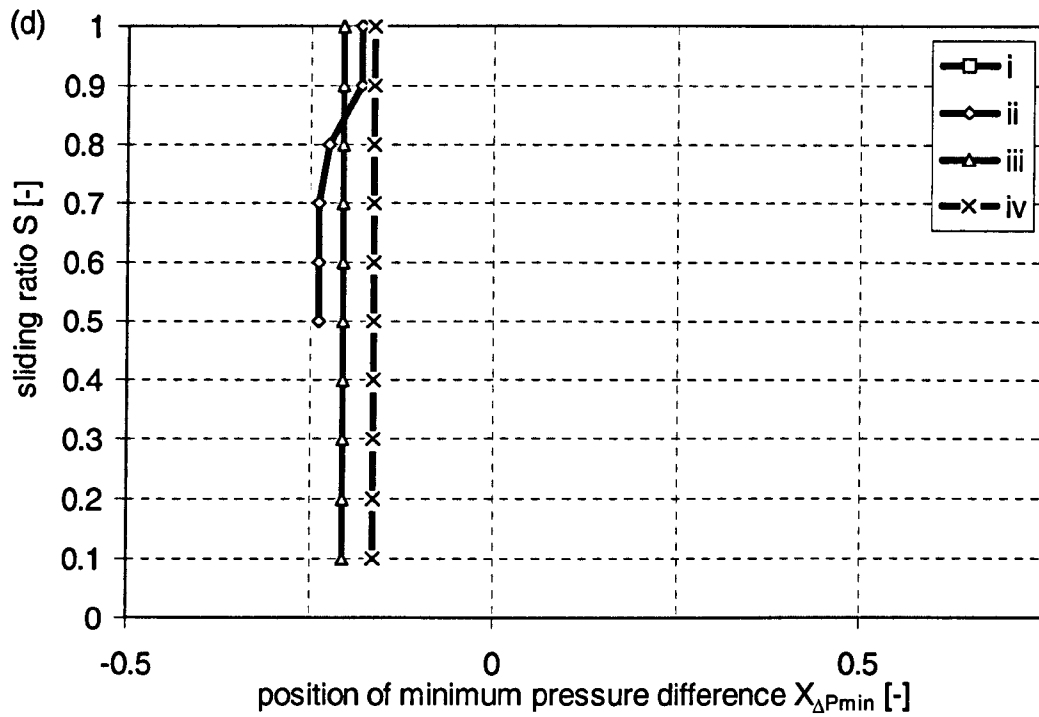
Figure 10.20: (concluded).

10.6.4   Viscosity

Only a single set of figures is presented for viscosity. Viscosity ranges more than five orders of magnitude along the gap. Graphs with a linear viscosity axis or contour plots with a linear distribution would contain a very small zone of reasonable resolution and a large zone of unsatisfactory resolution. On the other hand, introduction of a logarithmic distribution to contour plots or a logarithmic viscosity axis in x-y-plots leads to graphs identical to those presented above for pressure distribution. Hence only a set of figures showing the differences between extended and Reynolds equation based solutions, and displaying the variation of viscosity across the gap, is given.

For load case iv and three sliding ratios, $S = 0.0$, $S = 0.5$, and $S = 1.0$, relative deviation of viscosity from Reynolds equation based solution at the slow surface

$$\varepsilon_{\eta slow,Re} = \frac{\eta_{slow} - \eta_{Re}}{\eta_{Re}} \tag{10.29}$$

and at the fast surface

$$\varepsilon_{\eta fast,Re} = \frac{\eta_{fast} - \eta_{Re}}{\eta_{Re}} \tag{10.30}$$

are given in figure 10.21(a) and (b) respectively. Figure 10.21 (c) shows the relative deviation of viscosity across the gap related to the average viscosity near the surfaces

$$\varepsilon_{\Delta\eta} = \frac{\eta_{slow} - \eta_{fast}}{\frac{1}{2} \cdot (\eta_{slow} + \eta_{fast})} \tag{10.31}$$

for load case iv. The viscosity results for load case i to iii are given in appendix K, figures and K.28 to K.30.

(a)
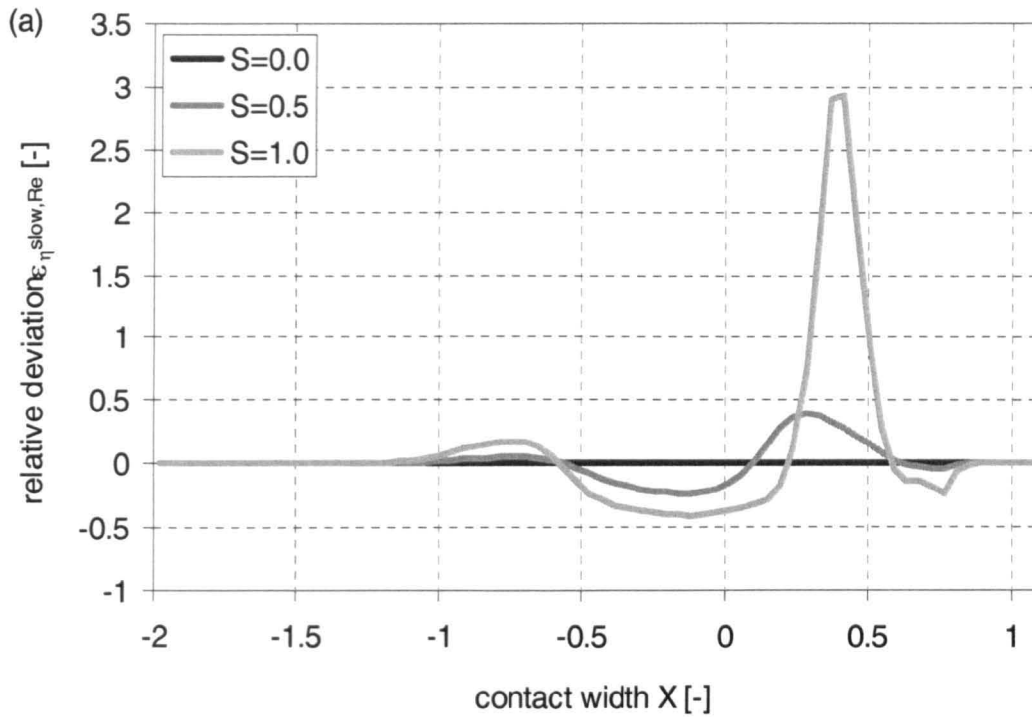
Figure 10.21: Relative deviation of viscosity from Reynolds equation based solution on the slower surface $\varepsilon_{\eta slow,Re}$ and the faster surface $\varepsilon_{\eta fast,Re}$ and relative deviation of viscosity across the gap ε_{Δ} for various sliding ratios; load case iv (table 10.1), sliding ratios S = 0.0, 0.5, and 1.0,
(a) relative deviation at slower surface $\varepsilon_{\eta slow,Re}$,
(b) relative deviation at faster surface $\varepsilon_{\eta fast,Re}$,
(c) relative deviation across the gap $\varepsilon_{\Delta \eta}$
(continued).
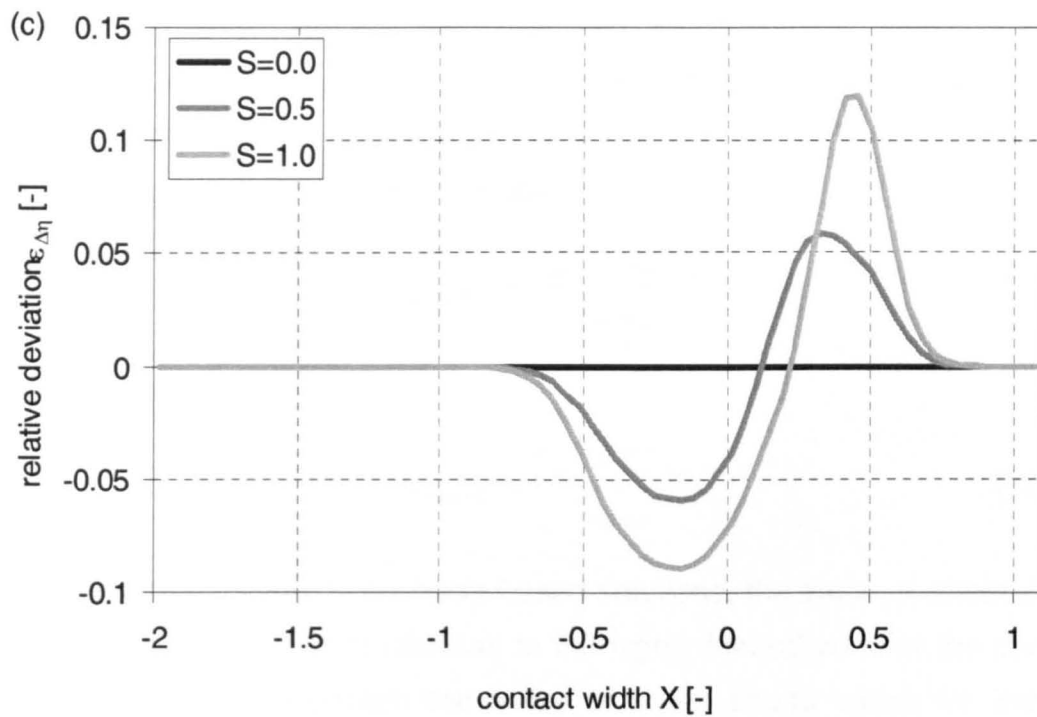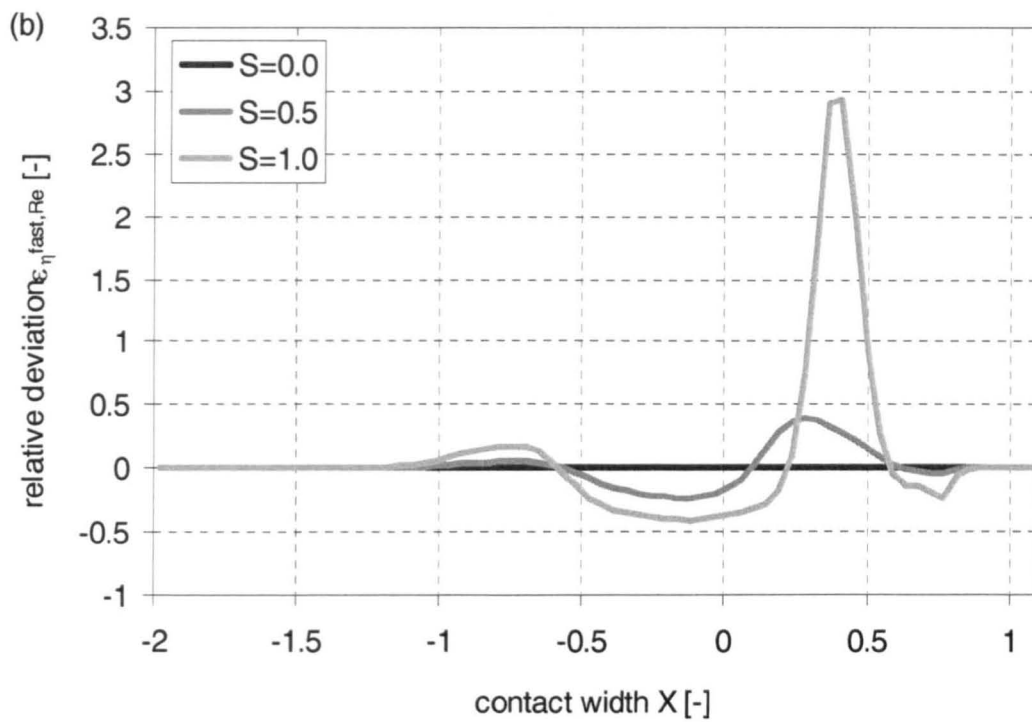
Figure 10.21: (concluded).

10.7   Shear stress and traction coefficient

In the present section, results showing the influence of the fluid film on the surfaces are presented. For load case iv, figure 10.22 shows the shear stress

$$\tau = \eta \cdot \frac{\partial v_t}{\partial n_n} \approx \eta \cdot \frac{\partial u}{\partial y} \qquad (10.32)$$

on the lubricant at the slower (a) and the faster (b) surface in the dimensionless form[*]

$$T_{slow} = \frac{\tau_{slow}}{p_{Hz}} \qquad (10.33)$$

and

$$T_{fast} = \frac{\tau_{fast}}{p_{Hz}} \qquad (10.34).$$

Results are given for the extended and the Reynolds equation based approach. In addition, comparison of these two approaches is given by displaying the relative deviation of shear stress from the Reynolds equation based approach for the slower surface

$$\varepsilon_{Tslow,Re} = \frac{T_{slow} - T_{Re,slow}}{T_{Re,slow}} \qquad (10.35)$$

and the faster surface

$$\varepsilon_{Tfast,Re} = \frac{T_{slow} - T_{Re,fast}}{T_{Re,fast}} \qquad (10.36).$$

For isothermal Reynolds equation based solutions, the value of shear stress at both surfaces is almost identical in the highly loaded zone of the contact. For the extended approach the value of shear stress varies for the two surfaces. This absolute difference between the two surfaces

$$\Delta T = T_{slow} - (-T_{fast}) \qquad (10.37)$$

is given in figure 10.23 for load case iv. Graphs for load cases i to iii are given in figures K.31 to K.33 and K.34 to K.36 of appendix K.

---

[*]   The sign for T_{slow} and T_{fast} in figures 10.22 results from the fact, that the shear stress on the lower face of a finite volume is directed towards $-x$, at the upper surface towards $+x$, cf. figures 3.1 and 3.13.

(a)
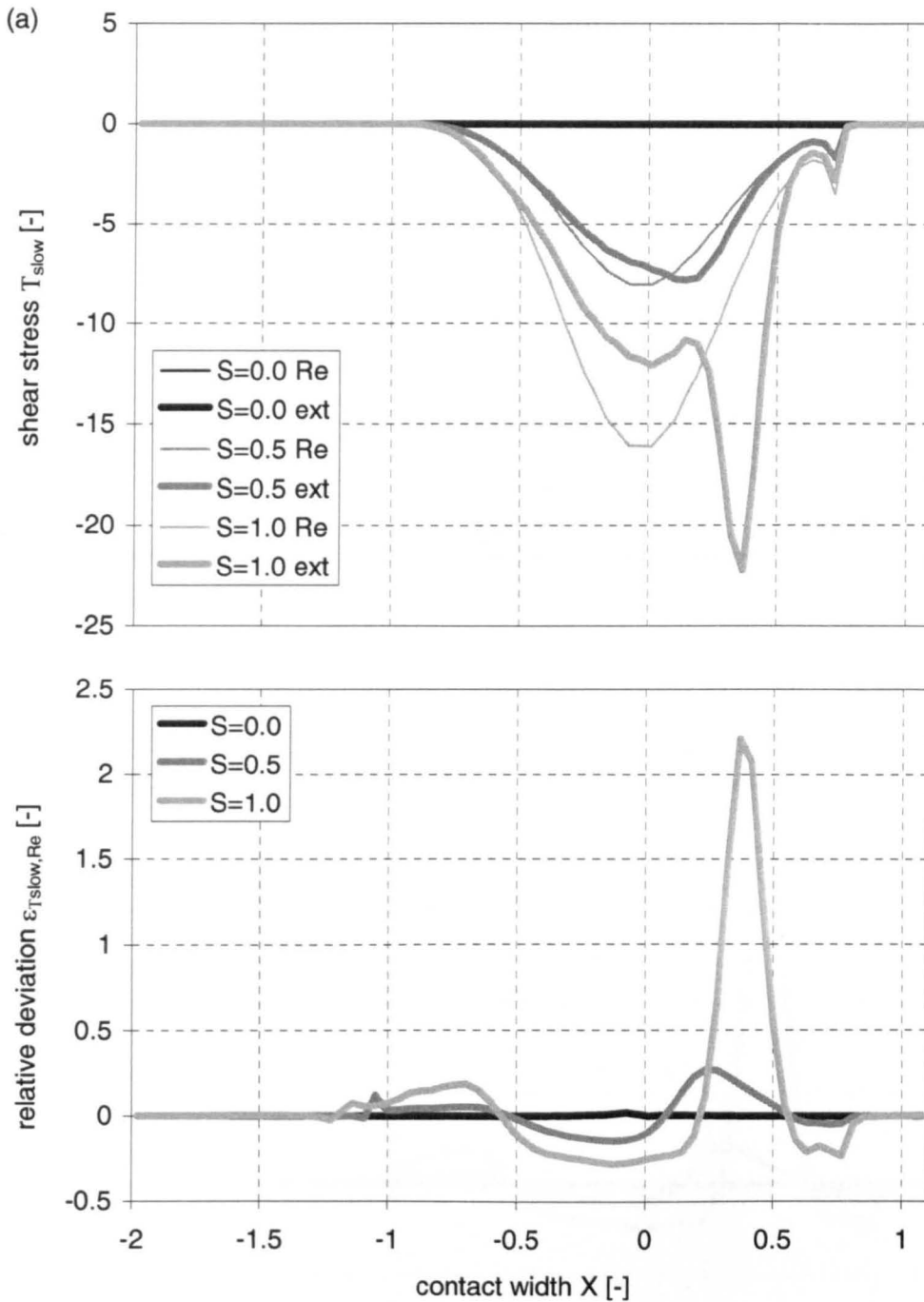
Figure 10.22: *Dimensionless shear stress on the lubricant at the slower*
surface T_{slow} and the faster surface T_{fast} and relative deviation
from Reynolds equation based solution $\varepsilon_{Tslow,Re}$ and $\varepsilon_{Tfast,Re}$ for
various sliding ratios; load case iv (table 10.1), sliding ratios
S = 0.0, 0.5, and 1.0,

(a)   shear stress on slower surface T_{slow} and relative
      deviation $\varepsilon_{Tslow,Re}$,
(b)   shear stress on faster surface T_{fast} and relative deviation
      $\varepsilon_{Tfast,Re}$
(continued).
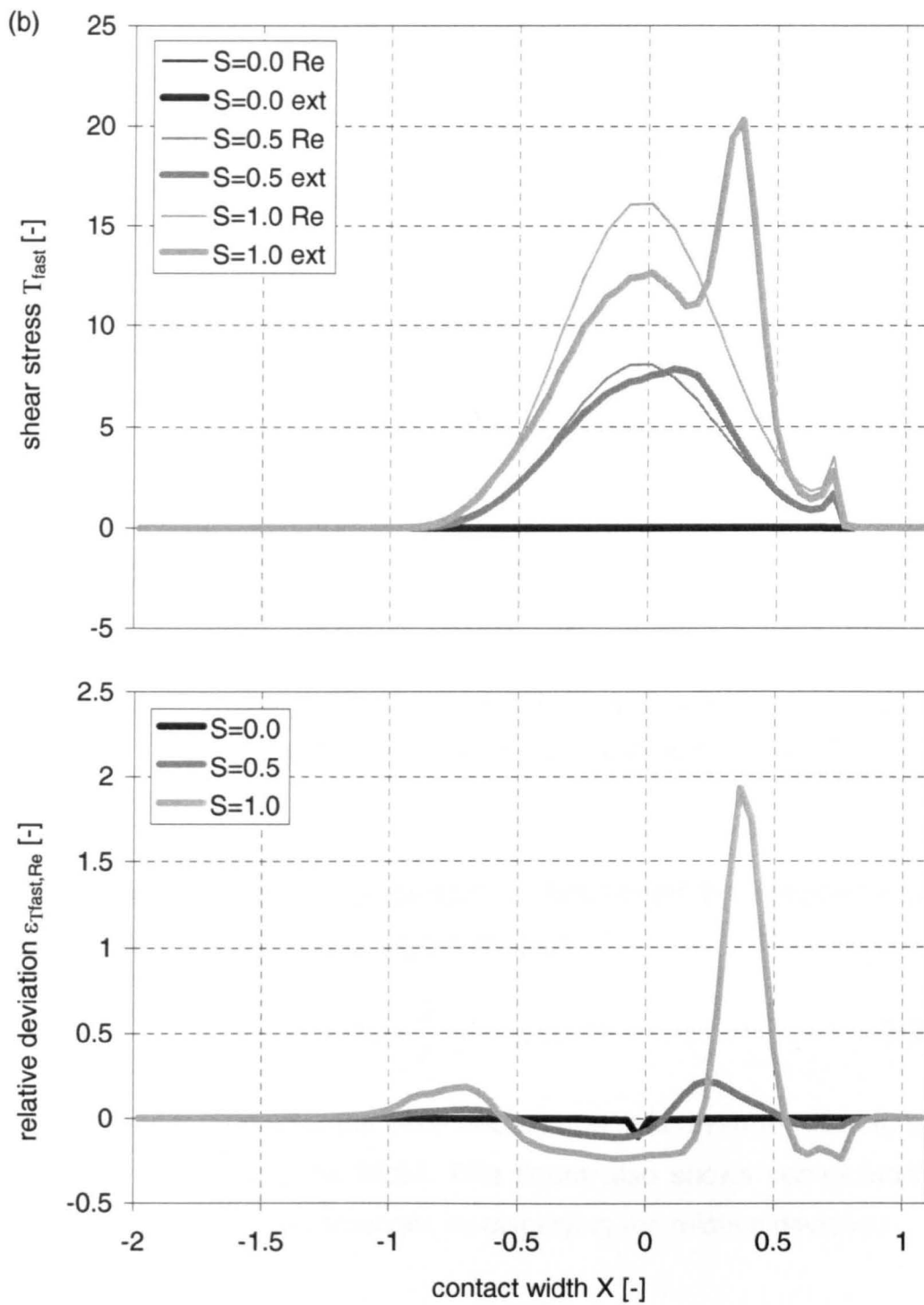
Figure 10.22: (concluded).
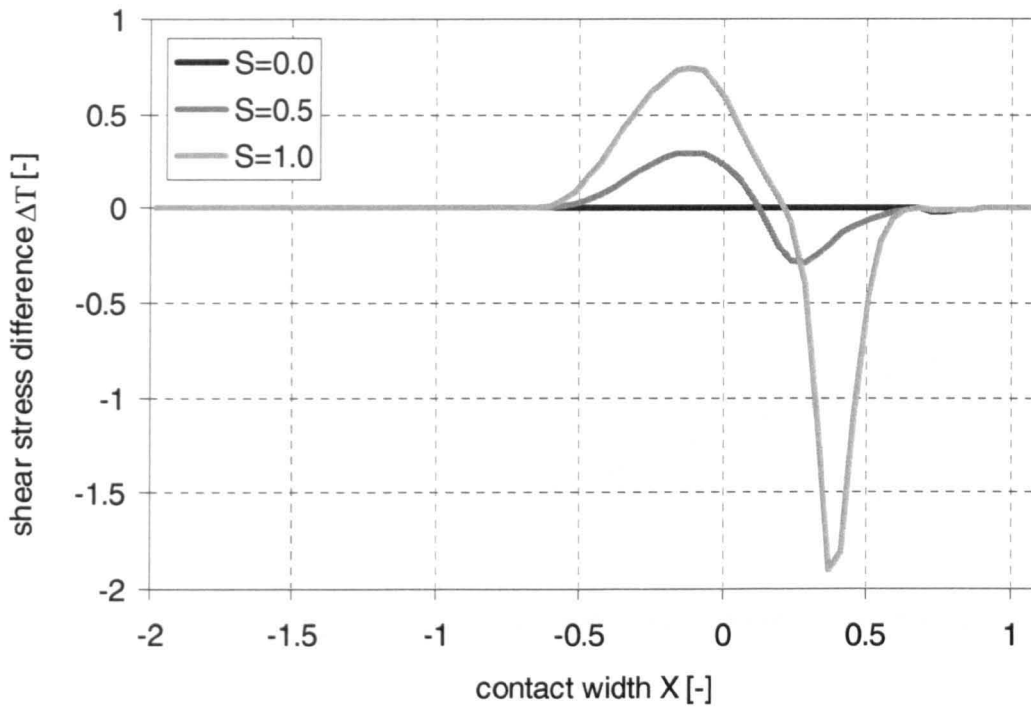
Figure 10.23: Dimensionless shear stress difference ΔT for various sliding ratios; load case iv (table 10.1), sliding ratios S = 0.0, 0.5, and 1.0.

The traction coefficient of a contact is determined by integration of the dimensionless shear stress along the contact

$$\mu_T = \frac{2}{\pi} \cdot \int \left(- T_{slow}\right) \cdot dX \qquad (10.38).$$

The traction coefficient for the extended approach is given for all load cases and sliding ratios in figure 10.24. This figure also shows comparison with Reynolds equation based solutions by displaying the relative deviation

$$\varepsilon_{\mu T,Re} = \frac{\mu_T - \mu_{T,Re}}{\mu_{T,Re}} \qquad (10.39).$$
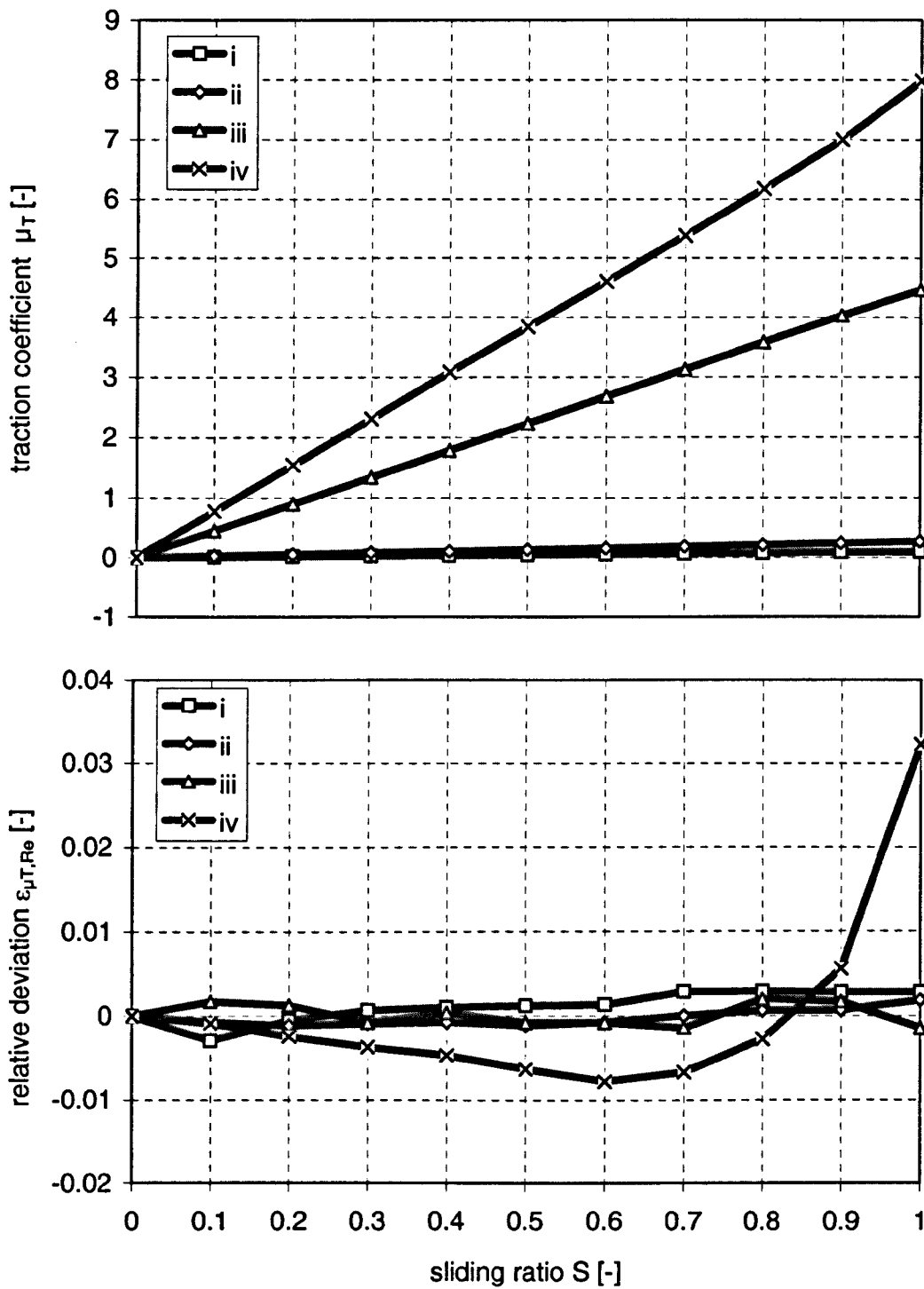
Figure 10.24: Traction coefficient μ_T and relative deviation from Reynolds equation based solution $\varepsilon_{\mu T,Re}$ for load cases i to iv (table 10.1) and various sliding ratios S.

Chapter 11

Extended approach result discussion

11.1 Introduction

Consideration of the results for the new extended approach and their comparison with the established Reynolds equation based solution, as presented in chapter 10, delivers a large number of aspects which are worthy of discussion. Because many of these aspects correlate or even interact with others and because many aspects can be of both numerical and physical relevance at the same time, the structure of the discussion is as following.

Section 11.2 discusses whether there is an influence as to which surface the deflections are applied. This is necessary to qualify the established methods of data presentation for the extended approach.

From section 11.3, the various results variables, starting with the shape of the gap, are discussed. For this discussion, initially results and their deviation from Reynolds equation based solutions are described particularly in relation to the governing equations of chapter 3 and basic fluid mechanics principles. Section 11.4 extends discussion to the velocity distribution. Beside the above aspects, correlations with the shape of the gap, already discussed at this stage, will be considered. In the same way, discussion is further broadened in section 11.5 by looking at the contact pressure and viscosity fields. Section 11.6 completes discussion of the result values by treating the traction coefficient aspects.

Subsequently, aspects of the elasto-hydrodynamic lubrication pressure spike and the relevance of the dimensionless factors are considered in section 11.7 and 11.8 respectively. The chapter is concluded by a summary of the major findings.

11.2   Influence of different load distributions on both contact surfaces

For all investigations, it is important to know whether the established method of applying all curvature and deflections to one surface can also be used for the extended approach results. The upper part of figure 10.4 suggests that it does not make any difference to the shape of the gap whether all curvature and deflection is applied to the upper, faster surface or to the lower, slower surface or whether curvature and deflections are distributed to both surfaces according to reality. The upper parts of figure 10.5 show the same result for the pressure distribution for the faster and the slower surface. However, the lower parts of figures 10.4 and 10.5 show that the curves do not perfectly agree but show minor deviations between the three configurations. For the shape of the gap and the pressure distributions, the results for curvature and deflection *"applied on lower surface"* prove to be the median and hence the reference. The deviation curves for curvature and deflections *"applied on upper surface"* tend to oscillate above the median curve, and those for curvature and deflections *"distributed to both surfaces"* below the median curve. Oscillations and deviations appear more often in the pressure distribution figure 10.5 and less in the shape of the gap, figure 10.4.

For figures 10.4 and 10.5, four-digit data material, as delivered by the CFD code, was used. Deviations of the shape of the gap or of pressure distributions can be caused by physical or numerical effects. Some of the latter effects are round-off errors. The two *"numerical accuracy"* lines in the lower parts describe the zone where deviations can appear when rounding off the data material to four digits. The deviations of the shape of the gap lie always between the two accuracy lines. The deviation lines for the pressure distributions range mostly between the accuracy lines but exceed them in the inlet zone of the contact and after the pressure spike.

Because the deviations in the high pressure zone do not exceed the accuracy, the method of distribution of curvature and deflections to the two surfaces is practically irrelevant in this zone. However this does not rule out the fact that the small tendencies mentioned above are caused by physical differences of the three configurations. The pressure deviations in the inlet zone exceeding accuracy might be caused by two effects. Firstly, the strongly converging gap causes small pressure variations across the gap, even for iso-viscous lubricants. Secondly, the pressure values themselves are small. The comparison of two small values with the method used for determining the deviations finally leads to relatively large values. The reason for the deviation is of a physical nature. However, these relatively large but absolutely still small deviations do not appear in the high pressure zone, which this study concentrates on. Hence, these deviations do not justify the presentation of the data in another manner than that established.

The reason for exceeding accuracy after the pressure spike is of a numerical nature. As above the pressure values themselves are already quite small. On the other hand, the Newton-Raphson method still delivers relatively large pressure corrections for the zone at and behind the pressure spike when convergence is reached. This idea is supported by the fact that the deviations are not wall-dependent but nearly identical for both walls. Since these deviations are neither in the interesting high pressure zone nor caused by physical effects, they also do not justify the introduction of a new presentation method.

In conclusion, the method selected to distribute curvature and deflection to the two surfaces is irrelevant for the results. As already stated in section 10.3, the traditional method of display, where all curvature and deflection is applied on the upper, normally faster, surface is also suitable and hence used for the present results from the extended approach.

11.3   Shape of the gap

11.3.1   Principal shape

For the investigated load cases, figures 10.6 and K.1 to K.3, the gap shows the well-known parallel shape with the typical constriction at the end, when pure rolling, S = 0.0, is considered. The agreement of the extended approach and Reynolds equation based solutions for pure rolling is confirmed in the lower parts of those figures 10.6 and K.1 to K.3, showing that there are no deviations between the two approaches. This agreement was expected because the governing equations 3.38 and 3.39 reduce to the basis of Reynolds equation* when the velocity gradient across the gap $\partial \overline{U}/\partial \overline{Y}$ becomes zero.

With an increase in the sliding ratio, S = 0.5 and S = 1.0, an additional constriction develops in the first half of the contact and a widening appears between that additional and the well-known, traditional ehl constriction. The shape of the gap in the inlet zone and in the traditional ehl constriction is hardly affected by the extended approach. Details regarding the traditional ehl constriction and pressure spike are discussed in section 11.7.

A zone of reduced height in the first half of the contact and a zone of extended height in the second half was also expected in the theoretical predictions, as mentioned in subsections 3.3.4.4 to 3.3.4.6. Hence, the computational results agree qualitatively with those theoretical predictions.

For load case i, figure K.1, the additional constriction can only be estimated from the deviation diagram, because accuracy of the applied data and physical effects have the same order of magnitude. This result, that extended approach phenomena are visible but overlaid by data accuracy effects, can be observed for many figures showing load case i data, but will not be discussed again in the remaining part of the present section. In conclusion, load case i represents conditions where the new approach starts to show

---

* Basic equations for Reynolds equation are $\dfrac{\partial p}{\partial x} = \eta \cdot \dfrac{\partial^2 u}{\partial y^2}$ and $\dfrac{\partial p}{\partial y} = 0$, equations 2.1 and 2.3.

physical effects but which are physically irrelevant since they are as small as the numerical accuracy.

Further consideration of figure 10.6 suggests the following phenomena for the sliding cases:

♦ The deflection rises exponentially with sliding ratio.

♦ The first additional constriction is longer and flatter in comparison to the widening which is shorter and deeper. The transition from the additional constriction to the widening appears on the outlet side of the contact centreline.

Detailed discussion of these phenomena is enabled by the consideration of figures 10.7 and 10.8.

11.3.2 Perpendicular extension of additional constriction and widening

Figure 10.7(a) and (b), the survey of minimum and maximum height H_{min}' and H_{max}' data, prove that the height of the gap changes, increasing exponentially with sliding ratio. However, for the most heavily loaded case iv, the minimum height of the gap H_{min}' varies only linearly when a sliding ratio of $S = 0.6$ is exceeded. For the maximum height H_{max}', this linearity appears when the sliding ratio exceeds $S = 0.8$. Possibly some of the interactive effects suggested in subsection 3.3.4.6, caused by the additional terms of the extended approach, are starting to have an influence. Hence, in the remaining sections of this chapter the results of load case iv at high sliding ratios will be considered particularly.

Regarding the value of the perpendicular extension of the additional constriction and of the widening, comparison of figure 10.7(a) with 10.7(b) suggests that the perpendicular extension of the additional constriction and the widening are of similar size for load cases ii and iii. This also applies to load case iv if the sliding ratio does not exceed $S = 0.5$. Only for load case iv and sliding ratios exceeding $S = 0.5$, is the perpendicular extension of the widening greater than the reduction of the additional constriction.

The minimum height for load case iv and pure sliding is approximately 6 per cent below Reynolds equation based solution values, however, the traditional ehl constriction still remains a stronger height reduction. This means that within the range of parameters considered, the extended approach should have some relevance for centreline film thickness formulae such as equation 3.26, but not on minimum film thickness formulae such as equation 3.25. Further, the extended approach would have an influence on all analyses using centreline film thickness or centreline film thickness formulae, for example advanced bearing fatigue life analyses. However, film thickness formulae are obtained by a regression process, so the actual relevance of the extended approach for film thickness formulae could only be evaluated by comparison with the accuracy of general film thickness formulae.

11.3.3   Length of additional constriction and widening

Some initial implicit information on the length of the additional constriction and the widening is given in figure 10.7(c) and its comparison with figure 10.7(a) and (b). At the contact centreline, $X = 0.0$, the additional constriction can also be observed, having still most of its maximum perpendicular reduction at this point. Since the widening is limited by the traditional constriction, the widening is shorter than the additional constriction.

Details are delivered by figure 10.8(a) and (b) which show the position of the minimum and maximum height X_{hmin} and X_{hmax}. Positions are displayed for those load case-sliding ratio combinations for which the relevant information could be determined from the CFD data.[*]

From the displayed curves for load cases ii, iii and iv, the results seem to be quite different.

---

[*] Theoretically, for all isothermal and incompressible solutions including those based on Reynolds equation, with a relative minimum in the pressure distribution between the maximum on the Hertzian pressure curve and the ehl pressure spike, there is a relative minimum and a relative maximum both shortly before the ehl pressure spike. However, they are normally so small that they cannot be detected in diagrams but only when considering very exact numerical data.

♦ For load case ii, the minimum height position moves towards the inlet for an increasing sliding ratio S, the position of maximum height maintains its position while the point of agreement of the heights from the extended and Reynolds equation based solutions moves slowly towards the inlet. This is due to the following reason as illustrated in figure 11.1(a):

Load case ii represents a load case with low load but high velocity and viscosity. It is the load case closest to the transition to hydrodynamic lubrication, as visible from figure 10.2(a)–(c). Correspondingly, pressure and height distributions, figure 10.1 show a pressure and height distribution closer to a hydrodynamic distribution than any other investigated load case.

For such cases and Reynolds equation based solutions, convergence of the so-called parallel gap* in the high pressure zone is higher than that for the other load cases. In the present case, the value and gradient of this convergence from a Reynolds equation based solution have the same order of magnitude as the value and gradient of the perpendicular change of the additional constriction by the extended approach. The addition of both effects combines both curves so that the above described movement of the characteristic points happens.

Although height variation values are relatively small, the present case ii indicates the effect, when the extended approach is applied to hydrodynamic situations. Figures 10.2(a)–(c) show that both the relevant parameters k_p and k_r, equations 3.38 and 3.39 of subsection 3.3.4.1, still have significant values when approaching the transition to hydrodynamic lubrication, so extended approach effects will also appear for hydrodynamic regimes.[†]

---

*   The "parallel" ehl gap is always very slightly converging until the transition towards the pressure spike.

[†]   Subsection 3.3.4.4 discussed that the application of the extended approach requires adaptation of the gap height so that finite pressure values appear for the singularity. Hence hydrodynamic lubrication analysis with the extended approach cannot mean an analysis assuming a rigid contour.

♦ For load case iii, the sliding ratio has no influence on any of the positions.

This is due to the fact that the order of magnitude of any changes in height due to the extended approach dominates over the convergence of a Reynolds equation based approach gap, as shown in figure 11.1(b). All positions are almost symmetrical about the contact centreline, $X = 0$, which means that the additional constriction and the widening are of similar size. Reasons for this symmetry are explained below when the pressure distribution in the contact is discussed. However, as a result of load case iii, it can be concluded that the widening is not necessarily smaller than the additional constriction.

♦ For load case iv, the minimum position is sliding ratio independent, as for load case iii. However, the maximum height position and the position where extended and Reynolds equation based approaches deliver identical height values, move towards the outlet, which means a short but extensive widening. For this case also, height changes due to the extended approach dominate over the height variation due to gap convergence. The explanation requires consideration of further aspects and will be given in section 11.5.

In conclusion, regarding the shape of the gap, all four load cases show the same development with an additional constriction in the first half of the contact and a widening between the additional and the traditional constriction. However, four different regimes are represented when considering the detailed development of this shape. The effects on the shape of the gap rise with the dimensionless speed and load parameters U and W, as well as with the factors k_p and k_r. Quantitative discussion of the variation of height values with the dimensionless factors is given in section 11.8.

(a)

$X_{hmin}(i)$

$X_{hmin}(ii)$

$X_{hmin}(iii)$

$X_{hmax}(i) \approx X_{hmax}(ii) \approx X_{hmax}(iii)$

(b)

$X_{hmin}(ii) \approx$ $X_{hmax}(ii) \approx$
$X_{hmin}(iii)$ $X_{hmax}(iii)$

———— (i)   Shape of the
for Reynolds equation approach

———— (ii)   Shape of the gap
for extended approach and small sliding ratio

———— (iii)   Shape of the gap
for extended approach and large sliding ratio
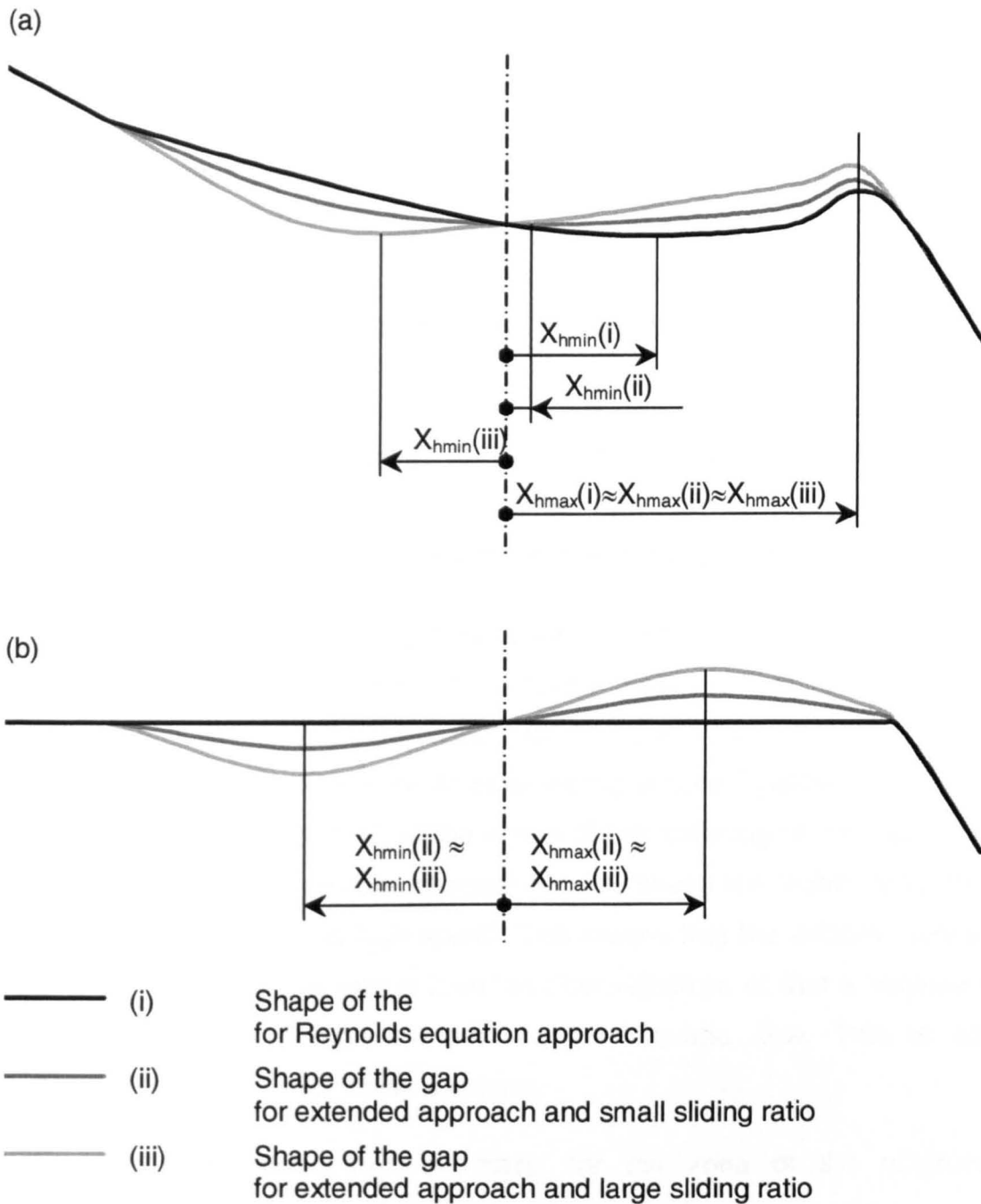
Figure 11.1: Development of characteristic points of the gap when
(a) convergence of the gap and changes due to the extended approach are of similar size,
(b) convergence of the gap is much smaller than changes due to the extended approach.

11.4   Velocity

11.4.1   Overall velocity field

The contour plots for pure rolling, figure 10.9(a), suggest for load case iv that the velocity fields are identical for the extended and Reynolds equation based approaches. This result is explained and is a requirement from the identical shapes of the gap for both approaches and the relevance of the various terms of the governing equations mentioned in the above section 11.3.1.

For increasing sliding ratios of $S = 0.5$ and $S = 1.0$, displayed in figures 10.9(b) and (c), the velocity fields differ from Reynolds equation based solutions in those zones where also the shape of the gap differs:

Best visible for the pure sliding case, figure 10.9(c), it can be observed that for the parallel gap of the Reynolds equation solution[*] the various patches between the contours are of identical width in the parallel zone, which means a regular increase in velocity or, in other words, a pure Couette flow. For the extended approach solution[t], in the zones of the widening of the gap, it can be seen, that the dark patches representing low speed are slightly wider than those bright, representing high speed. This means that the velocity increase across the height of the gap is lower at slow velocities or that a backwards directed Poiseuille component overlies the Couette flow. This is also necessary to fulfil the continuity equation.

According observations can be made for the zone of the additional constriction, indicating a forward directed Poiseuille flow component.

In the remaining parts of the contact, where the shape of the gap agrees for both approaches, the velocity field also agrees. This includes the facts that

---

[*]   The Reynolds equation based solution is shown in the lower of the two graphs of figure 10.9(c).

[t]   The extended set of equation based solution is shown in the upper of the two graphs of figure 10.9(c).

the stagnation point of the inlet flow remains at the same position as for Reynolds equation based solutions and that the traditional ehl constriction is unchanged. Identical observations can be made for load cases iii with the help of figure K.6. For load case i and ii, figures K.4 and K.5, resolution of the scalar plots is too coarse to allow even qualitative discussion.

The contour plots for load case iv, figure 10.10, showing the deviation of speed between the extended approach and a Reynolds equation based solution, confirm and quantify the results from the above contour plots. For pure rolling, $S = 0.0$, no relevant deviations can be observed. However, for partial or pure sliding, $S = 0.5$ and $S = 1.0$, considerable deviations of ±4 and ±12 per cent respectively are displayed for the additional constriction and the widening. The deviations seem to be distributed almost symmetrically about the centreline along the contact $Y^* = 0.5$. Maximum deviations appear at the centreline along the gap, reducing to zero at the solid surfaces where speed is the prescribed boundary condition. This behaviour is consistent with the idea of Poiseuille flow components proposed above.

This described symmetry is not apparent for the contour lines for the pure sliding situation, $S = 1.0$ in figure 10.10(c). Zero deviation, defined as the boundary between minimum negative and minimum positive deviation, occurs at the transition from the additional constriction to the widening. This line is not perpendicular to the axis along the gap but slightly tilted. Agreement of the extended with the Reynolds equation based approach happens closer to the contact centreline $X = 0.0$ on the upper, faster surface rather than on the lower, slower surface. This means an s-shaped flow profile which is discussed in detail later in this section.

For load cases ii and iii, the respective figures K.8 and K.9 confirm the almost symmetrical distribution of relative speed between the extended and Reynolds equation based solutions.

Forward directed Poiseuille components in the first half of the contact and backwards directed components in the second half were also expected from the theoretical considerations as to how the extended approach results will differ from Reynolds equation based solutions, subsection 3.3.4.4 to 3.3.4.6.

Theoretical predictions and computational results are thus again in qualitative agreement.

11.4.2   Flow profiles

A closer insight into the flow of load case iv can be seen from the x-y-plots of u-velocity and its deviation from Reynolds equation based solutions at the narrowest position of the additional constriction $X = X_{hmin}$, at the widest position of the widening $X = X_{hmax}$, at the position where the gap has identical height for both approaches $X = X_{cross}$ and at the contact centreline $X = 0.0$, figures 10.11(a) to (d). For sliding ratios $S = 0.5$ and $S = 1.0$, parabolic deviations, i.e. the above-mentioned forward directed Poiseuille-like flow, can be observed for the additional constriction and the contact centreline. The forward-directed Poiseuille component results in a decrease in velocity gradient at the upper, faster surface and hence a reduction of the local traction force if pressure and hence viscosity are considered unchanged. At the opposite lower and slower surface, the velocity gradient increases. This would result in an increase of the local traction force.

An exact parabolic shape of the deviation curve appears for pure one-dimensional flow if pressure, and hence viscosity, are constant across the height of the gap. However, the x-y-plots plots with forward directed Poiseuille components, figure 10.11 (a) and (d), tend to show slightly higher deviations from pure Couette flow in the lower half of the contact, $Y^* < 0.5$ [*], than in the upper half. Correspondingly, for the widening of figure 10.11(b), a slightly higher deviation can be observed for the upper part of the contact height $Y^* > 0.5$.

The observed differences from a parabolic flow profile indicate that the Poiseuille component cannot solely result from a pressure gradient purely varying along the contact; there must be other effects, such as pressure and hence viscosity variation across the gap. This viscosity variation will also

---

[*]   The differences between upper and the lower half of the deviation curves are so small that some hardly exceed the accuracy of the data used.

influence the traction coefficient which will be considered in detail in section 11.5.

Results for the position where the extended and the Reynolds equation based approaches lead to the identical height $X = X_{cross}$ show further aspects but also different behaviour for different situations. For load cases i to iii, figures K.10 to K.12, the flow shape is identical for both approaches. For load case iv and partial sliding $S = 0.5$, figure 10.11(c), a slight backwards-directed Poiseuille flow component can be observed, meaning a slightly reduced overall flow for the extended in comparison to the Reynolds equation based approach. For the pure sliding situation, $S = 1.0$ of load case iv, an s-shaped deviation from a pure Couette flow profile is obtained. Since the backwards-directed flow section exceeds that of the forward-directed, the total flow rate is also smaller for the extended approach compared with the partial sliding case. However the s-shape suggests that there must be a pressure variation across the gap with maximum pressure and hence viscosity at the centreline along the contact $Y^* = 0.5$.

11.4.3   Flow rate

The detailed summary of flow rate data for all load cases and sliding ratios, figure 10.12, shows that for load case i to iii the flow rate is independent of the sliding ratio, any deviations are likely to be of a numerical nature. This also applies to load case iv if the sliding ratio does not exceed $S = 0.4$. For sliding ratios exceeding $S = 0.4$, a small reduction in the mass flow can be observed, as expected from the previous discussion of the flow profiles. However, the relative reduction of flow rate is almost two orders of magnitude smaller than the deviations observed for other variables. Hence, it is not clear, whether it is a numerical or a physical phenomenon.

As for the height of the gap, a discussion of the dimensionless factors indicating the significance of the additional terms in the extended approach, subsections 3.3.4.1 and 3.3.4.2. is given below, in section 11.8.

11.5   Pressure and viscosity

11.5.1   Overall pressure distribution

The contour plots showing the overall pressure distribution, figure 10.13 for load case iv and figures K.13 to K.15 for load cases i to iii respectively, illustrate once more, when pure rolling, S = 0.0, is considered, that the results from the extended and Reynolds equation based approaches are identical. All other figures, which will be discussed later in the present section on pressure, show further evidence of this fact. However, none of this evidence is mentioned to avoid constant repetition.

For partial and full sliding situations, S = 0.5 and S = 1.0, the maximum isobar contour line, representing p = 0.5 GPa for load cases iii and iv are shifted and tilted in comparison to those for pure rolling S = 0.0.* In principle, shifting means a different pressure distribution along the gap while tilting means a pressure variation across the gap and hence a different pressure distribution along the gap on each surface.

While the pressure contour plots figures 10.13 and K.13, are fine enough to indicate the existence of significant pressure variation across and along the gap, the contour plots showing the differences between the extended and Reynolds equation based solutions, figure 10.15 and K.19 to K.21, gives refined information. In principle, two zones of differences can be detected, most obviously for the partial sliding case S = 0.5, figure 10.15(b):

(i)   The first zone, starting in the inlet half of the contact, approximately at the dimensionless contact width X = - 0.5, shows higher pressure for the upper, faster surface than for the lower, slower surface.

(ii)   In contrast, the second zone, starting at or just after the contact centreline X = 0.0 and ending at the traditional ehl constriction, shows higher pressure for the lower, slower surface than for the upper, faster surface.

---

*   Not only can the described phenomenon not be observed for load case i, but also for load case ii due to its smallness.

In both zones the difference values are higher at the lower, slower surface than at the faster surface. These are also the features which were predicted as the extended set of equations, in subsection 3.3.4.4 to 3.3.4.6, was derived and discussed.

The above applies to all load cases and sliding ratios S, but as before particular effects appear for the pure sliding condition of load case iv, figure 10.15(c). Pressure difference values in the second zone dominate over those of the first zone for this case.

The pressure variation across the gap and along the gap lead to different aspects of discussion, so both phenomena are treated separately in the following subsections before finally correlation effects are discussed.

11.5.2 Pressure distribution across the gap

Figure 10.14 concentrates on the pressure variation across the contact by showing the deviations of the pressure from the pressure at the centreline along the gap, $Y^* = 0.5$, at the same position X for load case iv. For non-pure-rolling conditions the above mentioned two zones of pressure variation can be detected, where in the first zone the pressure decreases from the upper, faster surface to the lower, slower surface and in the second zone the pressure increases from the upper, faster surface to the lower, slower surface. The first zone is longer than the second.

11.5.2.1 Principal relevance for the shape of the gap

For the partial sliding case $S = 0.5$ of load case iv, figure 10.14(b), in terms of its absolute values, the pressure variation across the gap is nearly symmetrical about the centreline along the gap $Y^*=0.5$ as was found in subsection 11.4.1 for the velocity deviation contour plot, figure 10.10(b). This "symmetrical" distribution thus suggests an approximately linear variation of the pressure across the height of the gap.

A pressure variation across the height of the gap means also a corresponding viscosity variation. A change to the velocity profile results as explained in the following:

The basis for any Reynolds equation allowing viscosity variation across the gap is the following simplified x-momentum equation 2.11[*]

$$\frac{\partial p}{\partial x} = \frac{\partial}{\partial y}\left(\eta \cdot \frac{\partial u}{\partial y}\right)$$

(11.1)

Assuming a negligible pressure gradient along the gap[†] $\partial p/\partial x \approx 0$, constant viscosity across the gap, and a moving and a non-moving wall, a triangular Couette velocity profile is obtained, as figure 11.2(a) shows. Introducing a variable viscosity with higher values at the moving surface, the Couette flow profile will have a forward directed Poiseuille-like profile superimposed because the velocity gradient must be smaller at the faster surface to keep the term $\eta \cdot \partial u/\partial y$ constant. A convex flow profile is generated by viscosity gradient across the gap but not by pressure gradient along the gap. Hence this flow component has previously been, and will be throughout the rest of

---

[*]   The simplified x-momentum equation

$$\frac{\partial p}{\partial x} = \frac{\partial}{\partial y}\eta \cdot \left(\frac{\partial u}{\partial y}\right)$$

is the basis for thermal ehl analysis, but also x-momentum equation 3.36 could be derived from this equation. By applying product rule

$$\frac{\partial p}{\partial x} = \frac{\partial u}{\partial y} \cdot \frac{\partial \eta}{\partial y} + \eta \cdot \frac{\partial^2 u}{\partial y^2},$$

Barus' approach for the viscosity

$$\eta = \eta_0 \cdot e^{\alpha \cdot p}$$

and resolution of the viscosity gradient as

$$\frac{\partial \eta}{\partial y} = \eta_0 \cdot \alpha \cdot e^{\alpha \cdot p} \cdot \frac{\partial p}{\partial y}$$

the following dimensional form of equation 3.36 is obtained after rearranging the terms

$$0 = -\frac{\partial p}{\partial x} + \eta_0 \cdot \alpha \cdot e^{\alpha \cdot p} \cdot \frac{\partial p}{\partial y} \cdot \frac{\partial u}{\partial y} + \eta_0 \cdot e^{\alpha \cdot p} \cdot \frac{\partial^2 u}{\partial y^2}.$$

[†]   A negligible pressure gradient appears when either the pressure gradient is zero or if viscosity values are very high. The latter is the case for flow profile description in the "parallel" section of the ehl gap.

---

this chapter, named a *"Poiseuille-like flow component"* instead of *"Poiseuille flow component"*. For the same reason, the pressure profile is logarithmic instead of parabolic, as figure 11.2(b) illustrates; this also explains the observed deviations from a parabolic Poiseuille flow component in subsection 11.4.2.

Accordingly, a backwards-directed Poiseuille-like flow component is obtained for a variable viscosity distribution with maximum viscosity at the non-moving surface, figure 11.2(c).
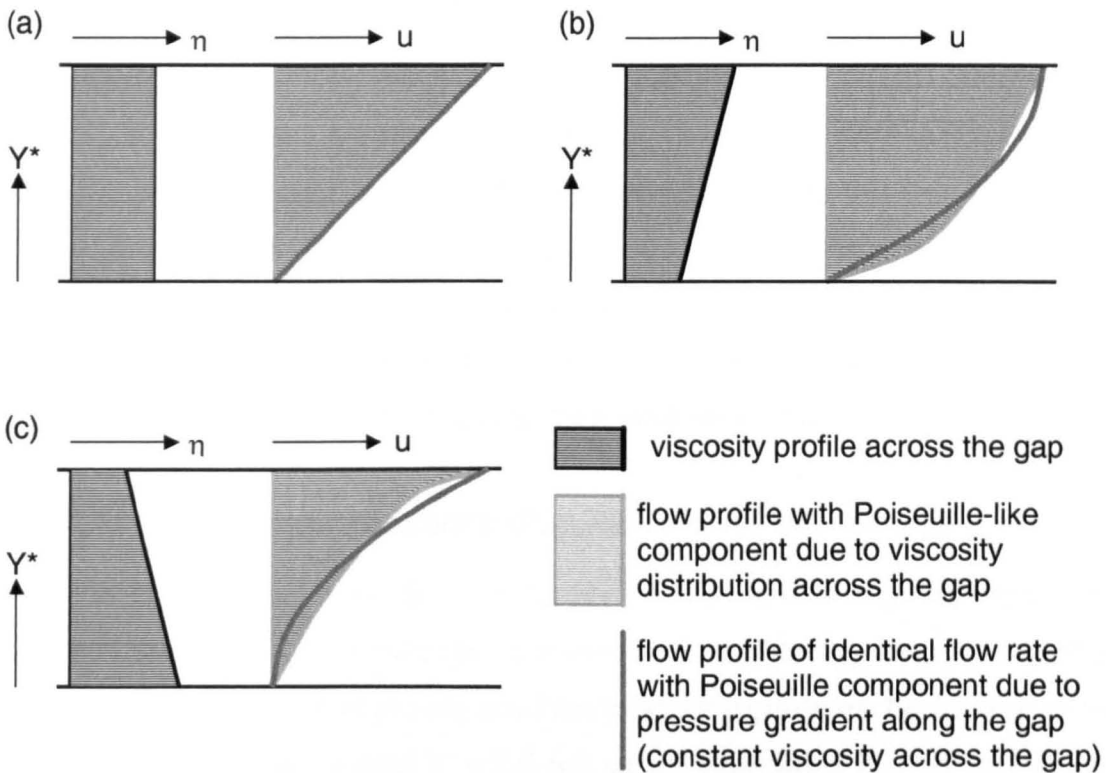
Figure 11.2:   Flow profiles for zero pressure gradient along the flow and various viscosity distribution across the height
(a)   constant viscosity across the height of the gap
(b)   linear viscosity distribution with maximum value at the faster surface.
(c)   linear viscosity distribution with minimum value at the slower surface.

Assuming an unchanged height of the gap, these flow profiles signify a higher flow rate for variable viscosity and maximum viscosity at the moving surface than for the iso-viscous case. For variable viscosity and maximum

viscosity at the non-moving surface, it means a lower flow rate than for the iso-viscous case. If a constant flow rate is desired then, in comparison with an iso-viscous case, the height of the gap must be reduced for the variable pressure and viscosity case with the maximum viscosity at the faster surface, and expanded for a variable viscosity with minimum viscosity at the faster surface. This hypothesis can be confirmed by comparison of the curve showing the deviation of height of the gap from a Reynolds equation based solution figure 10.6, and the curve showing the pressure difference across the gap in figure 10.17. Both figures show identical curve behaviour with identical minimum, cross-section and maximum position.

In conclusion, assuming the pressure gradient along the gap as negligible for the moment, the pressure and hence viscosity variation across the height of the gap not only explains and confirms the reasons why the flow distribution is not parabolic but in reality has a logarithmic Poiseuille-like flow component, shown in figures 10.11(a) to (c) and discussed in subsection 11.4.2, but also delivers an explanation as to why there must be an additional constriction at the beginning of the contact and a subsequent widening.

11.5.2.2 Non-linear pressure distribution across the gap

For the pure sliding case, $S = 1.0$, figure 10.14(c) the "symmetry" about the centreline along the gap has disappeared as it has for the velocity deviation in figure 10.10(c). The pressure patches indicating pressure below that at the centreline along the contact $Y^* < 0.5$ are wider than those indicating a higher pressure and show also higher magnitudes. That means a change from a linear towards a logarithmic pressure distribution across the height of the gap.

In principle, the above discussion made for the partial sliding case of load case iv applies also to this pure sliding case $S = 1.0$. However, the logarithmic pressure profile suggests that effects are magnified by repercussions.

Between the two major zones of pressure variation across the gap, a small zone can be detected where the pressure distribution across the gap has its

maximum at the centreline along the contact, the pressure consequently decreasing towards each surface. This pressure distribution results in a viscosity distribution with a maximum viscosity at the centreline along the contact. This distribution confirms the expectations from the flow profile discussion at the position where the height of the gap is identical for both the extended and Reynolds equation based approaches, figure 10.11(c) and subsection 11.4.2.

11.5.2.3 Correlation with governing equations

The above finding that the pressure distribution across the height of the gap and the shape of the gap are closely coupled is confirmed by the second equation of set 3.37,

$$0 = -\frac{p_{hz}}{h_0} \cdot \frac{\partial \overline{P}}{\partial \overline{Y}} \left[1 - \left(\frac{h_0 \cdot \kappa \cdot \overline{\alpha}}{p_{hz}} \cdot \frac{\partial \overline{U}}{\partial \overline{Y}}\right)^2\right] + \frac{\kappa^2 \cdot \gamma \cdot \overline{\alpha} \cdot b_{hz}}{p_{hz}} \cdot \frac{\partial \overline{U}}{\partial \overline{Y}} \cdot \frac{\partial^2 \overline{U}}{\partial \overline{Y}^2}$$

(11.2).

Isolating the pressure gradient across the gap,

$$\frac{\partial \overline{P}}{\partial \overline{Y}} = \frac{h_0^2 \cdot \kappa^2 \cdot \overline{\alpha} \cdot \frac{\partial \overline{U}}{\partial \overline{Y}}}{p_{hz}^2 \cdot \left[1 - \left(\frac{h_0 \cdot \kappa \cdot \overline{\alpha}}{p_{hz}} \cdot \frac{\partial \overline{U}}{\partial \overline{Y}}\right)^2\right]} \cdot \frac{\partial^2 \overline{U}}{\partial \overline{Y}^2}$$

(11.3)

is obtained, which is a simplified form of the equation implemented in the successive-simultaneous method for determination of the pressure variation across the gap, subsection 9.2.1.1, equation 9.12. Equation 11.3 shows, for non-pure rolling cases, that wherever there is a curvature of the flow profile there must be an according pressure gradient across the gap, which must be, due to the term $h_0 \cdot \kappa \cdot \overline{\alpha} \cdot \left(\partial \overline{U}/\partial \overline{Y}\right)/p_{hz}$ exceeding unity, of the opposite sign.

11.5.2.4 Load case features

Transferability of the above findings to the other load cases is discussed by consideration of the values for minimum and maximum pressure difference across the height of the gap, compiled in figure 10.19, and the position of these minimum and maximum pressure values, shown in figure 10.20(d) and (e) respectively.

For all load cases, a linear growth of minimum and maximum pressure variation across the height of the gap can be observed with the usual peculiarities for load case iv and high sliding ratio values. The values observed for the pressure differences are similar in magnitude to minimum and maximum pressure difference, as long as the increase is linear. The appearance of pressure difference across the height of the gap for all load cases mean that all the above described phenomena regarding pressure variation across the gap, flow profiles and the shape of the gap are present for all load cases, although they might be so small that they cannot be spotted in the respective graphs for load cases i to iii, figures K.16 to K.18 in Appendix K.

For the position of the minimum and maximum pressure difference, load cases ii and iii show slightly different behaviour, compared to that for the shape of the gap.

♦ As stated above, for load case iv, minimum and maximum pressure difference position, $X_{\Delta Pmin}$ and $X_{\Delta pmax}$, agree with minimum and maximum height deviation positions X_{hmin} and X_{hmax}: The minimum height and minimum pressure difference position maintains its position and the maximum height and maximum pressure position moves towards the outlet for increasing sliding ratio values.

♦ Load case iii also shows strong correlation between minimum height deviation and minimum pressure difference and between maximum height deviation and maximum pressure difference. Minimum and maximum values appear nearly symmetrical about the contact centreline. Consequently, the behaviour of load case iii differs from that of load case iv as it did for the height positions. Explanation of this symmetry is again provided in subsection 11.5.3.3.

♦ Consistent with the above, load case ii shows, for the maximum pressure position and the maximum height position, identical values which are independent of the sliding ratio.

For the minimum pressure and the minimum height values, however, development is different: Minimum pressure difference is approximately

at the same point as it appears for the other load cases and constant, whereas the minimum gap moves towards the inlet of the contact. For the pure sliding ratio situation, $S = 1.0$, minimum pressure difference and minimum height positions then nearly agree. As for the height of the gap, the described development is due to the similar order of magnitude of the convergence of the gap in the so-called parallel zone of the gap and the height variation due to the extended approach.

Figure 11.3 gives an example when the position of minimum height of the gap differs from that of minimum pressure difference. A negative pressure difference, figure 11.3(a), causes a corresponding forward directed Poiseuille-like pressure distribution, with a maximum for the maximum pressure difference value as given in figure 11.3(b). A converging gap, as shown in figure 11.3(c) leads to backwards directed "real" Poiseuille components as shown in figure 11.3(d), which decrease with decreasing height of the gap until the Poiseuille component becomes zero, whilst the Couette flow remains constant. Combination of both effects leads to either the dominance of the real Poiseuille component over the viscosity gradient caused Poiseuille-like component or exact compensation or dominance of the Poiseuille-like component, as figure 10.3(f) shows. Concluding from the flow profile the correlating shape of the gap gives figure 11.3(g), and comparison of part (g) with (a) shows that minimum pressure difference and minimum height of the gap appear with some distance along the gap. The dominance between real Poiseuille and Poiseuille-like pressure components will be of relevance at a later stage below.

Summarizing the three above load cases ii to iv, two zones of pressure variation across the gap are always present, however, their position and extent vary for the different load cases.
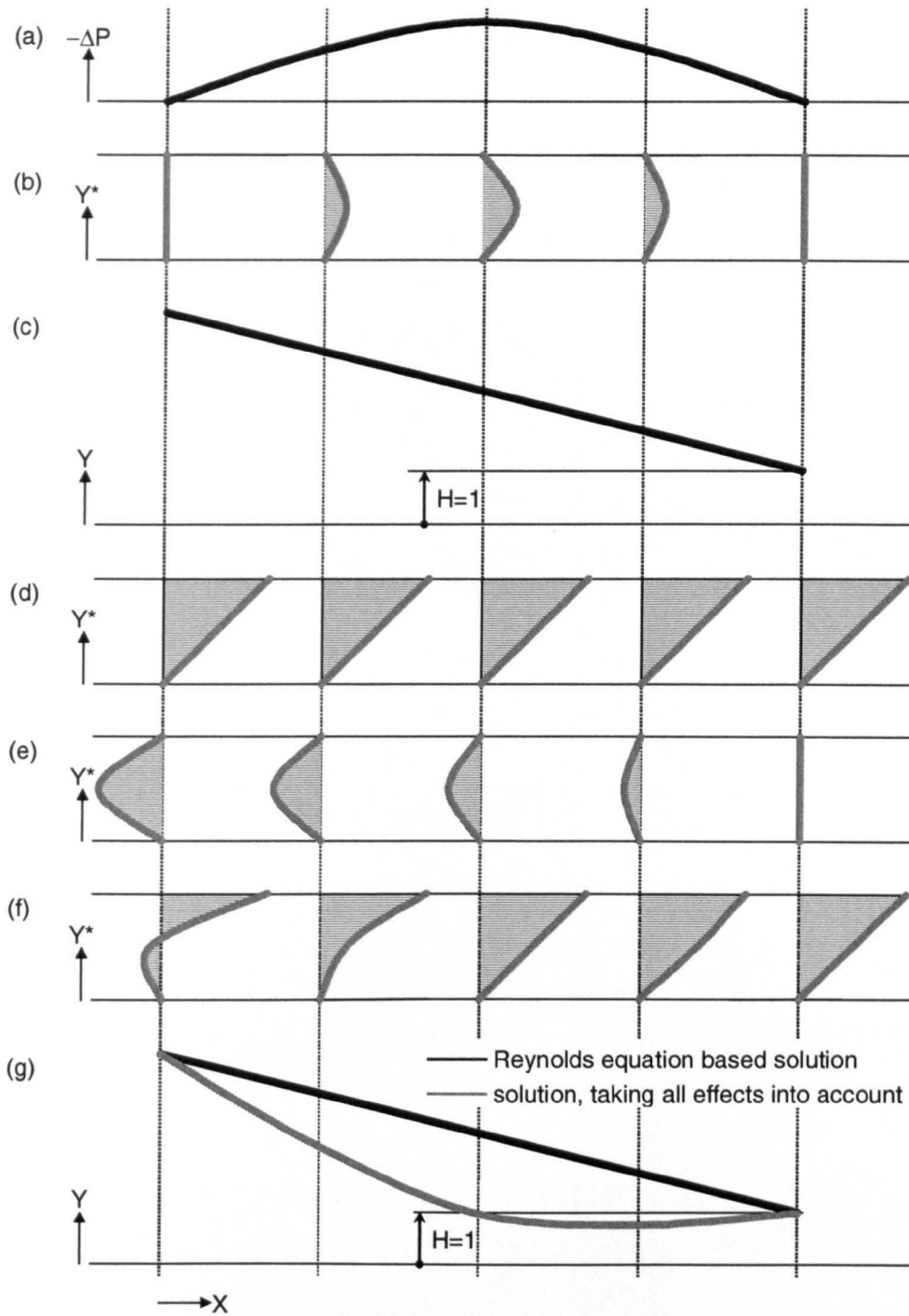
Figure 11.3: Correlation between pressure variation across the gap and shape of the gap for converging gaps:

(a) pressure, and viscosity, variation across the gap,

(b) Poiseuille-like flow component due to pressure and viscosity variation,

(c) shape of a converging gap,

(d) Couette flow component in converging gap due to moving and non-moving walls,

(e) Poiseuille flow components due to gap convergence

(f) flow profile taking components (b), (e) and (f) into account

(g) shape of the gap due to flow profile (f).

11.5.3   Pressure distribution along the gap

11.5.3.1 Typical features of pressure distribution along the gap

For load case iv, pressure variation along the contact is shown by figure 10.16 for both surfaces, (a) and (b) and the mean value (c). The mean value curve is most suitable for the discussion of pressure distribution for two reasons: Firstly, it is almost the pressure at the centreline of the contact, for which the pressure distribution along the gap is determined by the Newton-Raphson technique, section 9.2.1.2. Secondly, the mean pressure gives in a single curve that pressure distribution which is responsible for the deflection. Hence easy comparison of the extended and Reynolds equation based approach is possible whilst disregarding pressure variation across the gap.

For the mean pressure of the non-pure-rolling conditions of load case iv, figure 10.16(c) a lower pressure in the first half and also at the beginning of the second half of the contact can be observed. In the second half, a higher value is apparent. For the pure sliding case $S = 1.0$, the higher values in the second half of the contact even develop to a kind of second pressure spike.

A comparison with the Reynolds equation based solution indicates that four zones can be distinguished where Reynolds equation based solutions differ from those for the extended approach. These four zones appear for all load cases.

(i)   In the first zone, covering the inlet zone of the contact and the beginning of the high pressure zone, the pressure distribution for the extended approach exceeds that for a Reynolds equation based solution. Pressure values are small in this zone and the relative deviations displayed are at least partially due to comparison of small numbers. The total load capacity of the contact is hardly influenced.

(ii) As soon as the pressure exceeds approximately 80 per cent of Hertzian pressure, $P = 0.8$, the pressure for the extended approach falls below that for the Reynolds equation based solution. Relative deviation values are at least slightly higher than those in the first zone and are, because

of the high pressure values, relevant for load capacity and deflection considerations.

(iii) The start and end of the third zone, dependent on the load case, lies generally in the second half of the contact. In this zone the extended approach results return to exceed the Reynolds equation based solution. Values are either as big as in the second zone but rising higher when the third zone is smaller in comparison with the second zone. Deviation of pressure from Reynolds equation based values contributes to the contact load capacity and the surface deflection due to higher values. For the pure sliding situation, S = 1.0 of load case iv, this third zone is quite strongly developed.

(iv) In the fourth zone, from the pressure spike to the end of the contact, pressure falls again below Reynolds equation based values. As in the first zone, deviation values result also from the comparison of small values, so that this zone has no relevance for deflection and load capacity considerations.

The development of the mean pressure along the gap correlates with the aspects discussed for the shape of the gap in subsection 11.3.1. The reduced mean pressure in the second zone leads to the additional constriction, whilst the increased pressure in the third zone agrees with the widening between the additional and the traditional constriction. Agreement with the expectation of the theory, subsections 3.3.4.6, is also given. More detailed understanding of the pressure distribution along the gap can be provided by looking at the flow distribution again.

11.5.3.2 Pressure distribution along the gap and flow profiles

In the above subsection 11.5.2.1, it was shown that most of the flow profile curvature is due to the pressure and viscosity variation across the height of the gap and that it appears even for a constant pressure gradient across the gap. Applying the product rule to equation 11.1,

$$\frac{\partial p}{\partial x} = \frac{\partial}{\partial y}\left(\eta \cdot \frac{\partial u}{\partial y}\right) \tag{11.4},$$

leads to

$$\frac{\partial p}{\partial x} = \frac{\partial u}{\partial y} \cdot \frac{\partial \eta}{\partial y} + \eta \cdot \frac{\partial^2 u}{\partial y^2}$$ (11.5).

Assuming no pressure gradient and hence viscosity gradient across the gap, streamwise pressure gradient is responsible for all curvature of the flow profile. Assuming no pressure gradient along the gap, the total pressure curvature is caused by pressure and hence viscosity variation across the gap. Combining both considerations means that for a flow with pressure and hence viscosity variation across the gap and a pressure gradient along the gap, the total curvature of a flow profile is a combination of Poiseuille-like flow component due to pressure and hence viscosity variation across the gap and a real Poiseuille component due to a pressure gradient along the gap. Hence the same final flow profile can result from different combinations of Poiseuille-like and real Poiseuille components as figure 11.4 illustrates.

For the Reynolds equation based analyses, the real Poiseuille flow component curvature is so small that it can only be detected by particular analysis of output data and cannot be seen; however, a Poiseuille-like flow component can be clearly seen for the extended approach. The dominant contribution of the Poiseuille-like flow to the total flow profile curvature can also be seen from the dimensionless form of the simplified x-momentum equation 11.5[*],

$$0 = \frac{\partial \overline{P}}{\partial \overline{X}} \cdot \left[-\frac{p_{hz}}{b_{hz}} \right] + \frac{\partial \overline{P}}{\partial \overline{Y}} \cdot \left[\kappa \cdot \overline{\alpha} \cdot \frac{\partial \overline{U}}{\partial \overline{Y}} \right] + \left[\kappa \cdot \frac{\partial^2 \overline{U}}{\partial \overline{Y}^2} \right]$$ (11.6),

and the values of the coefficients p_{hz}/b_{hz}, $\kappa \cdot \overline{\alpha}$ and κ, which gives values of $2.3 \cdot 10^{12}$, $1.1 \cdot 10^{17}$, and $9.9 \cdot 10^{15}$ respectively for the present case iv.

---

[*]   The equation can also be obtained from the x-momentum equation for an arbitrary shape of the gap, given as the first equation of set 3.42

$$0 = \frac{\partial \overline{P}}{\partial \overline{X}} \cdot \left[-\frac{p_{hz}}{b_{hz}} + 2 \cdot \kappa \cdot \gamma^2 \cdot \overline{\alpha} \cdot \frac{\partial \overline{U}}{\partial \overline{X}} \right] + \frac{\partial \overline{P}}{\partial \overline{Y}} \cdot \left[\kappa \cdot \overline{\alpha} \cdot \frac{\partial \overline{U}}{\partial \overline{Y}} \right] + \left[\kappa \cdot \frac{\partial^2 \overline{U}}{\partial \overline{Y}^2} \right];$$

Omission of the normal tension term $2 \cdot \kappa \cdot \gamma^2 \cdot \overline{\alpha} \cdot \partial \overline{U}/\partial \overline{X}$ and rearranging the parameters gives equation 11.6.
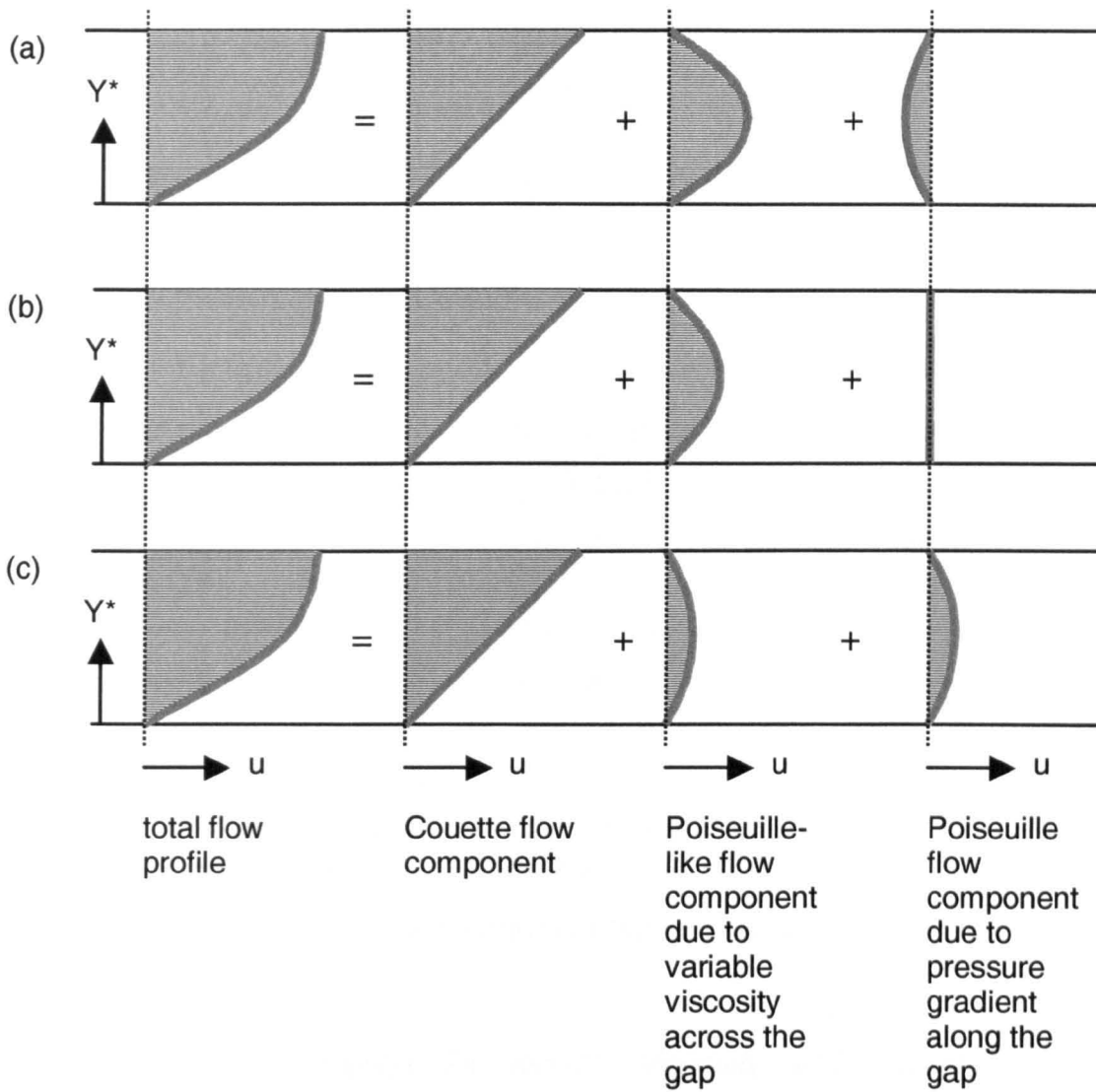
Figure 11.4:   Various combinations of Poiseuille and Poiseuille-like flow
                leading to identical flow profiles:
                (a) backwards directed (positive) Poiseuille component,
                (b) no Poiseuille component,
                (c) forward directed (negative) Poiseuille component.

Hence conclusions of the effect of the velocity profiles on the pressure
distribution are difficult. However, in the opposite direction, a positive
pressure gradient means a velocity profile slightly slower than pure
Poiseuille-like flow, figure 10.5(a) to (c) and a negative pressure gradient
means a velocity profile slightly ahead of a pure Poiseuille-like component,
figure 11.5(d) to (e).

(a)

Y*

(b)

(c)

(d)

Y*

(e)

(f)

→ u   → u   → u

total flow profile

Couette flow component and Poiseuille-like flow component
due to variable viscosity across the gap

Poiseuille flow component due to pressure gradient along
the gap
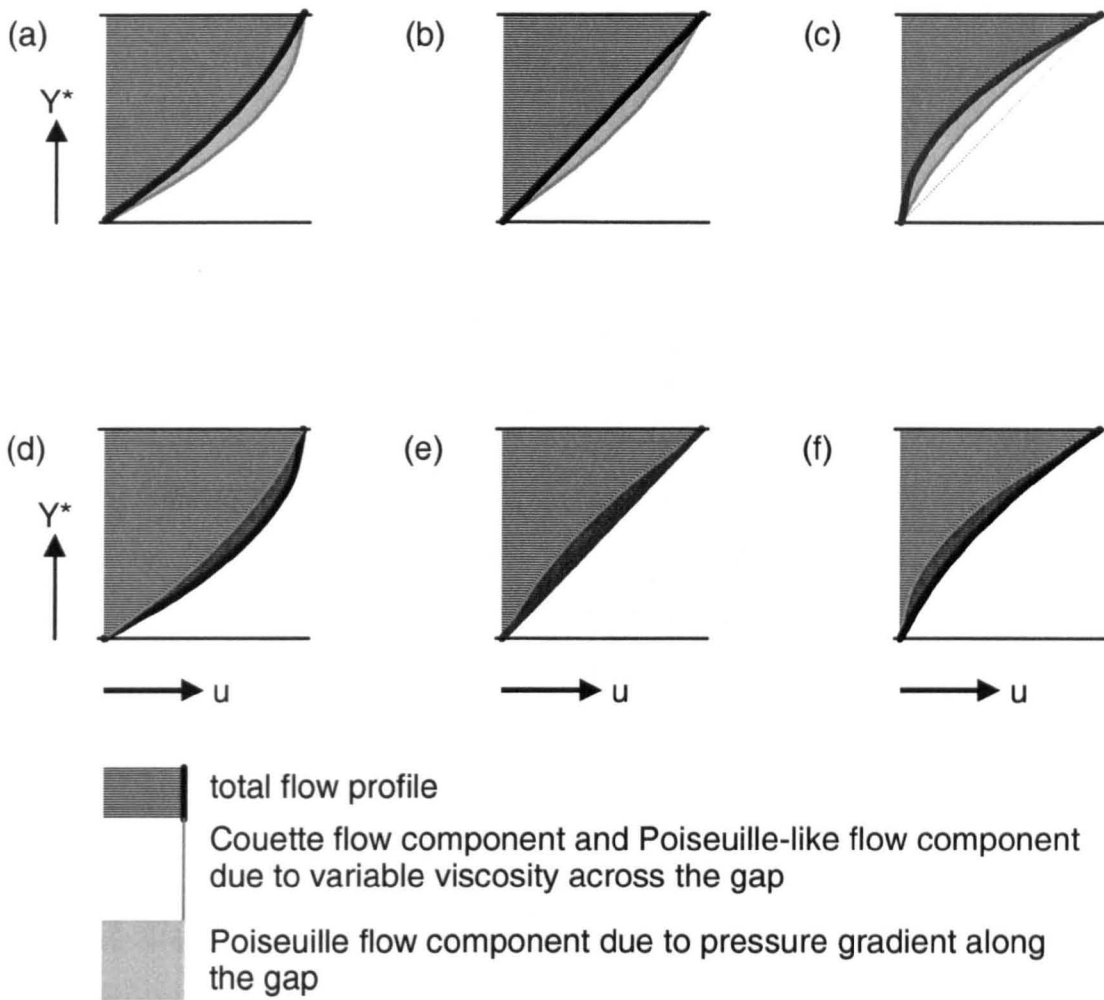
Figure 11.5:   Flow profiles for variable viscosity and various pressure
                gradients:
                (a)–(c) increasing pressure along the flow,
                (d)–(f) decreasing pressure along the flow.

11.5.3.3 Regime of the development of the pressure distribution along the gap

Understanding of the development of the pressure distribution requires the
view suggested in section 3.3.4.6.

As a result of the elimination of the pressure gradient across the gap from the
x-momentum equation, equation 11.6 becomes equation 3.39,

$$\frac{\partial \overline{P}}{\partial \overline{X}}\left[1 - \left(k_p \cdot \frac{\partial \overline{U}}{\partial \overline{Y}}\right)^2\right] = k_c \cdot \frac{\partial^2 \overline{U}}{\partial \overline{Y}^2} \qquad (11.7).$$

Assuming Hertzian pressure distribution and a parallel gap, changes to the Poiseuille flow components will appear except for the maximum pressure, with maximum values at a dimensionless contact width of $X = \pm 0.2^{*}$. In terms of their absolute value, these components will be symmetrical about the contact centreline $X = 0.0$, however they will differ with respect to their sign. Pressure distribution along the gap and shape of the gap are linked by the Boussinesq approach, which means that changes to the shape of the gap require a change to the pressure profile in the same region.

If the required pressure correction is now small enough, that the pressure variation at all points are smaller than the difference between the original elliptical Hertzian pressure value and the maximum Hertzian pressure at this point, then the maximum pressure along the contact, except for any traditional pressure spike, will remain at the original contact centreline position $X = 0.0$ as shown in figure 11.6(a). Effects from the extended approach then appear nearly independently in the first and second half of the contact only linked by some weak effects of the Boussinesq approach, with maximum pressure remaining at the contact centreline.

This development is present for all sliding ratios of load case ii and iii and for sliding ratios below $S = 0.3$ for load case iv, where the maximum pressure position, as figure 10.20(a) to (c) is not varying. When the pressure spike is now late enough so that the mean pressure distribution along the contact still follows the elliptical Hertzian distribution where the extended approach is of relevance, then a nearly symmetrical pressure variation along the contact can be observed. Figure 10.1 shows that the (degenerated) pressure spike is very late for load case iii, which explains all the symmetrical observations for this load case, for example in section 11.3.3 and 11.5.2.4.

---

*   The maximum value at X=±0.2 results from the fact that k_p varies along the Hertzian pressure distribution with an exponential pressure influence. Together with maximum elliptical Hertzian pressure distribution for the other selected analysis parameters the maximum of the term $\dfrac{\partial \overline{P}}{\partial \overline{X}} \cdot \left[1 - \left(k_p \cdot \dfrac{\partial \overline{U}}{\partial \overline{Y}} \right)^2 \right]$ is at X=±0.2 which is confirmed by the minimum height position for load cases ii to iv.

(a)

(b)

———— original, Hertzian pressure distribution

———— modified pressure distribution
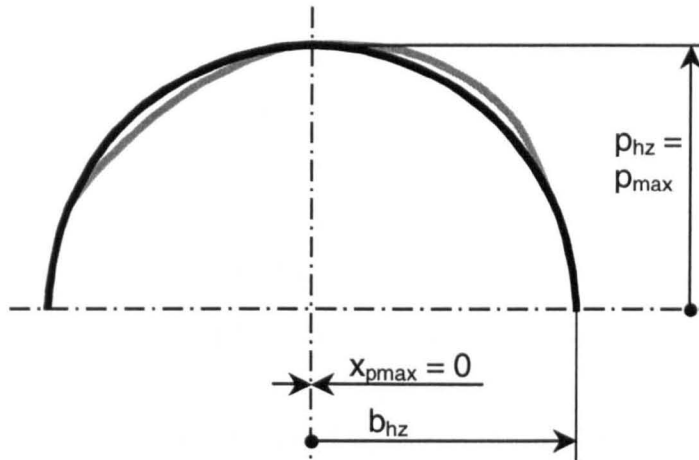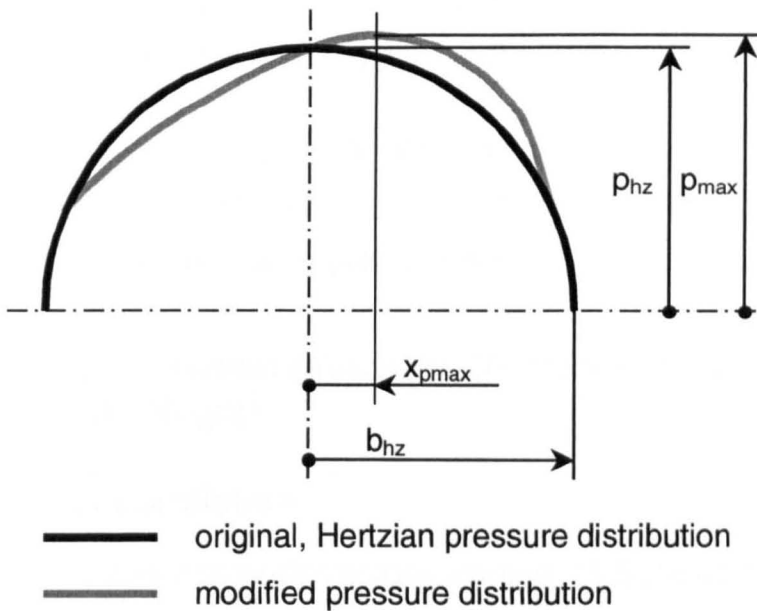
Figure 11.6:   Development of the pressure for the extended approach: (a) pressure corrections do not exceed Hertzian pressure, (b) pressure corrections exceed Hertzian pressure.

When pressure correction exceeds the difference between an originally elliptical Hertzian pressure distribution and the maximum Hertzian pressure, the maximum contact pressure will shift into the second half of the contact, as illustrated in figure 11.6(b). This means, however, that the first "half" of the contact and the additional constriction become wider, and the second "half", the widening, becomes smaller. That will cause a smaller pressure gradient in the first half and higher pressure gradient in the second half, which means

that flow profile deviation in the first half is smaller than in the second. This leads to less height reduction in the first half than height extension in the second half, causing repercussions on mean pressure distribution. This consideration explains at least the pressure distribution for the partial sliding case, S = 0.5, of load case iv and explains the movement of the maximum pressure position towards the outlet in figure 10.20(c) with increasing sliding ratio for load case iv. It explains also the movement of the position of maximum height position and position of agreement of height of the extended approach and Reynolds equation based solution, figure 10.8(b) and (c).

In conclusion, load case iii and iv represent two different regimes where repercussions do not and do play a relevant role respectively.

These repercussion effects also give an idea why load case iv behaves differently to the other load cases; however, for a full explanation, one more detail must be considered in the subsequent subsection.

11.5.4   Correlation between pressure distributions along and across the gap

11.5.4.1 Features of correlation

The section on the pressure distribution across the gap, 11.5.2 discussed two patches of pressure and hence viscosity variation across the gap and explained why the height of the gap has to differ for constant and variable viscosity distributions across the gap. However the necessary change of the gap can only be achieved by a change of the mean pressure distribution along the contact as discussed in section 11.5.3. This means that, for the extended approach, pressure variation along and across the gap have to appear simultaneously for the extended set of equations.

With the lower pressure on the lower, slower surface in the zone of the additional constriction, where the deforming mean pressure has to be below a Reynolds equation based pressure distribution, and the higher pressure on the lower, slower surface in the zone of the widening, where the deforming mean pressure is above that of a Reynolds equation based solution, the pressure at the lower, slower surface will always differ more from the

Reynolds equation based solution than at the faster surface. This is proved by the contour plots showing the deviation between the extended approach and Reynolds equation based solutions, figures 10.15(b) to (c).

11.5.4.2 Technical relevance

Pressure distribution at the contact surfaces, as a result of the pressure distribution across and along the gap, is an input parameter for stress analysis below the surface of the contact partners, which is used for fatigue life determination. So, the extended approach will lead to some changes in the stress distribution, particularly for the lower, slower surface. However, since the changes will be small and since state of the art standard fatigue analysis methods for roller bearings are based on Hertzian pressure distribution [105] the extended approach is of minor technical relevance.

11.5.4.3 Correlation with governing equations

Section 11.5.2 stated consistency of pressure variation across the gap with a view to its relevant governing equation and section 11.5.3 did the same for the pressure distribution along the gap. The pressure gradient ratio, equation 3.38,

$$\frac{\partial \overline{P}}{\partial \overline{Y}} \bigg/ \frac{\partial \overline{P}}{\partial \overline{X}} = k_r \cdot \frac{\partial \overline{U}}{\partial \overline{Y}} \tag{11.8},$$

thus provides an opportunity to compare overall pressure distribution with a single governing equation. For the partial sliding case $S = 0.5$ of load case iv, the condition is fulfilled with both pressure gradients changing sign at a dimensionless contact width of $X \approx +0.1$, figures 10.16(a) to (c) and 10.17. For the pure sliding situation $S = 1.0$, it can be seen from the same figure, that the pressure difference across the gap, and hence pressure gradient, changes sign at the contact width of $X \approx +0.2$, whilst the main maximum appears at $X \approx +0.35$, which contradicts equation 11.8.

It was stated in section 3.3.5, that there might be a need for governing equations taking also perpendicular flow components $\overline{V}$ into account, which would mean that the pressure gradient ratio equation must be rewritten.

Dividing the second equation of set 3.44 by the first and neglecting small terms as usual, leads to the following, pressure gradient ratio:

$$\frac{\dfrac{\partial \overline{P}}{\partial \overline{Y}}}{\dfrac{\partial \overline{P}}{\partial \overline{X}}} = \frac{\dfrac{\gamma \cdot \eta_0 \cdot u_h \cdot \alpha}{h_0} \cdot e^{\alpha \cdot p_{hz} \cdot \overline{P}} \cdot \left(\dfrac{\partial \overline{U}}{\partial \overline{Y}} \cdot \dfrac{\partial^2 \overline{U}}{\partial \overline{Y}^2} \right)}{\left(\dfrac{\partial^2 \overline{U}}{\partial \overline{Y}^2} \right) + \dfrac{\gamma \cdot \eta_0 \cdot u_h \cdot \alpha}{h_0} \cdot e^{\alpha \cdot p_{hz} \cdot \overline{P}} \cdot \left(\dfrac{\partial \overline{U}}{\partial \overline{Y}} \cdot \dfrac{\partial^2 \overline{V}}{\partial \overline{Y}^2} - 2 \cdot \dfrac{\partial \overline{V}}{\partial \overline{Y}} \cdot \dfrac{\partial^2 \overline{U}}{\partial \overline{Y}^2} \right)} \qquad (11.9).$$

For small values of the term $\eta_0 \cdot u_h \cdot \alpha \cdot \gamma \cdot e^{\overline{\alpha} \cdot \overline{P}}/h_0 \ll 1$ equation 11.9 returns to equation 11.8. However, for load case iv and pure sliding $S = 1.0$, term $\eta_0 \cdot u_h \cdot \alpha \cdot \gamma \cdot e^{\overline{\alpha} \cdot \overline{P}}/h_0$ becomes relevant by equalling 0.13 for a pressure of $p_{mean} = 0.50\,GPa$ and 0.24 for the maximum mean pressure of $p_{mean} = 0.52\,GPa$. Hence the results for the differentials $\left(\partial \overline{U}/\partial \overline{Y} \cdot \partial^2 \overline{V}/\partial \overline{Y}^2 - 2 \cdot \partial \overline{V}/\partial \overline{Y} \cdot \partial^2 \overline{U}/\partial \overline{Y}^2 \right)$ are of some relevance for the shape of the gap observed and must be taken into account.

For a maximum or a minimum of the height of the gap, velocity $\overline{V}$ becomes zero for both surfaces, and probably also between the two surfaces. Hence the gradients $\partial \overline{V}/\partial \overline{Y}$ and $\partial^2 \overline{V}/\partial \overline{Y}^2$ also become zero. This means that, for a dominance of term $\eta_0 \cdot u_h \cdot \alpha \cdot \gamma \cdot e^{\overline{\alpha} \cdot \overline{P}}/h_0 \gg 1$, pressure gradient will become zero near the height of the gap maximum, whilst for small terms $\eta_0 \cdot u_h \cdot \alpha \cdot \gamma \cdot e^{\overline{\alpha} \cdot \overline{P}}/h_0 \ll 1$, zero pressure gradient will occur for the case of pure triangular or trapezian flow. If the term is close to unity, $\eta_0 \cdot u_h \cdot \alpha \cdot \gamma \cdot e^{\overline{\alpha} \cdot \overline{P}}/h_0 \approx 1$, the position of pure Couette flow lies between both the described positions. This is the case for the present pure sliding situation of load case iv, where the maximum pressure position lies between $X_{cross} = +0.20$ and the height of the gap maximum $X_{hmax} = +0.45$ at $X_{Pmax} = +0.35$.

Hence load case iv represents a regime, where the extended approach not only needs the set of equations 3.38 and 3.39 but also the full Navier-Stokes equations 3.42.

In addition, the three summands of comparable magnitude in the denominator of equation 11.9 might give more locations where the sum

changes sign. Then equation 11.9 could also explain the further maximum at the contact centreline, the minimum at the position where the pressure difference across the gap changes sign at $X \approx +0.20$ and the short section of negative pressure gradient along the gap between. However, it is difficult to confirm the existence of these two extreme values, not only because values of the gradients could not be estimated with the necessary accuracy from the available results, but also because it was seen that the curvature of the flow profile across the gap showing different signs at the position $X \approx +0.20$, as shown in figure 10.11(c).

On the other hand since, for this situation, both the equations which are incorporated in the simulation method, first equation of set 3.42 and second of equation 3.44, are fulfilled and since a slightly higher pressure in the mentioned zone of negative pressure gradient would give at least qualitative fulfilment of equation 11.9, it cannot be ruled out that the applied numerical method reaches its numerical capacity although an optimum selection of parameters was attempted. Overcoming the problem is eventually possible by application of the fully simultaneous method of section 9.1. This idea originates from figure 9.13, comparing the sample results for the fully-simultaneous and the successive-simultaneous method, where a slightly flatter pressure distribution near the contact centreline $X = 0.0$ for the simultaneous-successive method might already indicate numerical phenomena which cause the concave pressure zone of the pure sliding case.

11.5.5   Viscosity

Viscosity and pressure are related by the exponential Barus' description, equation 3.18a,

$$\eta = \eta_0 \cdot e^{\alpha \cdot p} \qquad (11.10),$$

which means that both variables have identical zones of increasing and decreasing gradients and identical maximum and minimum positions. Accordingly, description of pressure variation along and across the gap also applies to viscosity. Most arguments made and conclusions drawn for velocity, section 11.4 and pressure, subsections 11.5.1 to 11.5.4, implied

pressure-viscosity dependency and hence discussed viscosity behaviour. In the remaining part of this subsection, only additional aspects are considered.

Values from the figures 10.21(a) and (b) show that differences between the extended and the Reynolds equation based approach are considerable for viscosity. For the pure sliding condition S = 1.0, viscosity reaches only 60 per cent of the value it reaches for the Reynolds equation based solution in the first half of the contact but takes on triple the value in the second half of the contact. Comparison of these values with the viscosity variation across the gap, figure 10.21(c), which is less than 15 per cent, underlines the dominance of the pressure effects along the gap.

The viscosity gradient across the height of the gap will compensate the velocity gradient and will contribute to similar shear stress at both sides of the contact. However, the significant difference in viscosity along the gap is expected to have a significant influence on the shear stress distribution along the gap. Due to the much higher viscosity at some positions along the gap, shear stress peaks are expected which will prevent any desired smaller traction coefficient values.

11.6   Shear stress and traction coefficient

Figure 10.22 shows the shear stress distribution expected from the viscosity distribution including some shear stress peaks for the pure sliding condition S = 1.0 of load case iv. Comparison of the distribution for the extended approach and the reference curves for a Reynolds equation based solution show that the average values indicate a virtually unchanged traction coefficient[*].

The dimensionless shear stress difference graph, figure 10.23 shows much smaller shear stress variations across the gap than figure 10.22 showed differences between the extended and Reynolds equation based approach. The shear stress in the first half of the contact is higher for the higher, faster surface and in the second half higher for the lower, slower surface. This

---

[*]   Traction coefficient is the integrated dimensionless shear stress.

means that pressure and hence viscosity variation across the height of the gap cause more change to the shear stress than the variation of velocity gradient across the gap. Positive and negative shear stress differences seem to balance each other along the gap, which means also that the traction coefficient of the contact with the extended approach remains unchanged.

In summary, shear stress distribution is mostly influenced by the pressure distribution along the gap, pressure variation across the gap has a smaller influence and the change to the flow profile the smallest influence on the shear stress distribution.

Finally, figure 10.24 shows the traction coefficient for all load cases versus the sliding ratio S and deviation of the traction coefficient for the extended approach from that of Reynolds equation based solutions. Except for load case iv, traction coefficient values show a linear increase with sliding ratio S and are unchanged for the extended approach in comparison with the Reynolds equation based solution. For load case iv, traction coefficient values lie increasingly but only slightly below Reynolds equation based results for a sliding ratio below S = 0.6. This trend changes for sliding ratios S above 0.6 where the full Navier-Stokes equations become relevant and numerical inaccuracies were detected.

Despite minor deviations, traction coefficient values, particularly for load case iii and iv are much above values expected from practical experience, as they are from Reynolds equation based solutions. It must be concluded that the extended approach clearly fails any expectations to contribute to an improvement of traction coefficient determination.

11.7   Pressure spike phenomena

11.7.1   Introduction

Previous sections of the present chapter discussed the effects caused by the extended approach for that region of the contact where, for Reynolds equation based solutions, the so-called parallel gap is obtained. The present section 11.7 now concentrates on the zone of the traditional ehl constriction and the corresponding pressure spike. This is also the zone where the fully

simultaneous and the combined successive-simultaneous method showed some differences.

Figure 10.1, showing the various load cases, show that for the applied, relatively coarse grid, some pressure spikes can be observed for load case ii and iv, but for load case i and iii the pressure spike degenerates to a "pressure edge". Development of the pressure spike in comparison with the Reynolds equation based solution is of particular interest when the pressure spike is in the region where the extended approach is relevant. This is determined by calculating factor k_p of equation 3.39,

$$\frac{\partial \overline{P}}{\partial \overline{X}}\left[1-\left(k_p \cdot \frac{\partial \overline{U}}{\partial \overline{Y}}\right)^2\right] = k_c \cdot \frac{\partial^2 \overline{U}}{\partial \overline{Y}^2} \qquad (11.11)$$

with

$$k_p = \frac{\eta_0 \cdot \overline{\alpha} \cdot e^{\overline{\alpha}\frac{p}{p_{hz}}} \cdot u_h}{p_{hz} \cdot h_0},$$

using the maximum *spike* pressure instead of *Hertzian* pressure. Table 11.1 gives the maximum spike pressure for the load cases and the value of k_p and shows that for load cases ii and iv pressure spike lies in the region where the extended approach is relevant.

load case number	pressure spike pressure	factor k_p	relevance for extended approach
-	GPa	-	-
i	0.24	0.16	no
ii	0.34	2.7	yes
iii	0.30	0.60	no
iv	0.42	17	yes

Table 11.1:   Factor k_p describing the relevance of the extended approach at the pressure spike for load cases i to iv (table 10.1).

Consideration of the height of the gap in figure 10.6 and of the pressure distribution in figure 10.16(a) to (c) allows the proposition that the pressure spike is not or is hardly affected by the extended approach.

11.7.2   Correlation with governing equations

The large degree of preservation of the pressure spike and the traditional constriction for the extended approach is consistent with the governing equations, when those used for the combined successive-simultaneous method are considered. These are the first equation of set 3.36 in its dimensional form,

$$\frac{\partial p}{\partial x} = \frac{\partial u}{\partial y} \cdot \frac{\partial \eta}{\partial y} + \eta \cdot \frac{\partial^2 u}{\partial y^2} \qquad (11.12),$$

and the second equation of set 3.37 in its re-arranged and dimensional form 9.13[*],

$$\frac{\partial p}{\partial y} = \frac{\eta^2 \cdot \alpha \cdot \dfrac{\partial u}{\partial y}}{1 - \left(\eta \cdot \alpha \cdot \dfrac{\partial u}{\partial y}\right)^2} \cdot \frac{\partial^2 u}{\partial y^2} \qquad (11.13).$$

As proposed in subsection 11.5.3.2, and shown by figure 11.5, a pressure increase in the first equation means that the real Poiseuille component is backwards directed in comparison to the total curvature of the flow profile; a pressure decrease means a forward directed flow profile. In the latter equation, pressure gradient across the height of the gap is determined by the total curvature.

However, as for the consideration of correlation of the pressure distribution along and across the gap, subsection 11.5.4.3, the results obtained with the combined simultaneous method contradict the pressure gradient ratio equation 3.38,

---

[*]   Equation 11.13 is equation 9.13 without that term, which was found to be irrelevant for equation 3.37. Equation 9.13 was obtained in appendix J from the second equation of set 3.44.

$$\frac{\partial \overline{P}}{\partial \overline{Y}} \bigg/ \frac{\partial \overline{P}}{\partial \overline{X}} = k_r \cdot \frac{\partial \overline{U}}{\partial \overline{Y}} \tag{11.14}.$$

This is obvious from figure 11.7, showing that there is no change in the pressure difference across the gap ΔP at the start of the ascent to the pressure spike.

Contrary to the situation in the region where a Reynolds equation based approach leads to a parallel gap, the insufficient satisfying of equation 11.14 is present not only for the pure sliding situation $S = 1.0$ but for all load cases with the presence of a pressure spike, which are load cases ii and iv.

Hence further consideration is required to understand which features mark a fully consistent pressure and height distribution in the pressure spike and constriction region. This discussion will conclude with a hypothesis in subsection 11.7.5 for the above observed not fully consistent pressure spike formation.
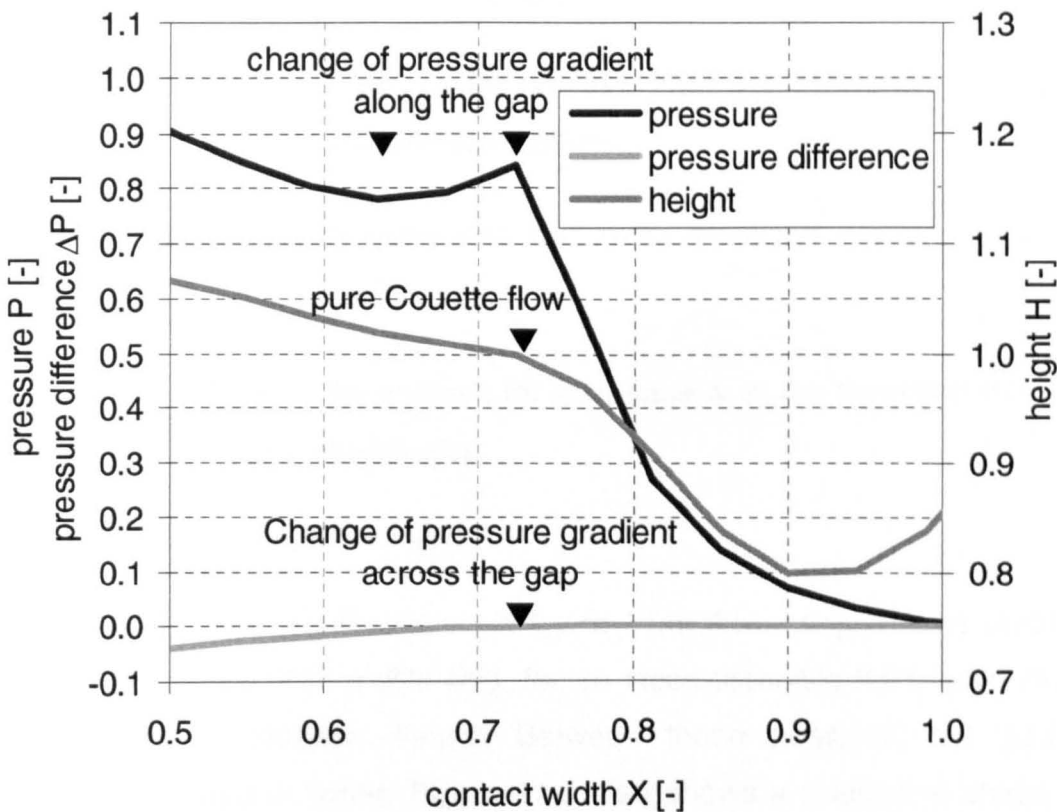
Figure 11.7:   Detail of pressure, pressure difference and height distribution for load case iv (table 10.1) and pure sliding $S = 1.0$.

11.7.3   Theoretical aspects of pressure spike existence

Combination of equation 11.13 and 11.14 lead in dimensionless form again back to equation 3.39

$$\frac{\partial \overline{P}}{\partial \overline{X}} \cdot \left[1 - \left(k_p \cdot \frac{\partial \overline{U}}{\partial \overline{Y}} \right)^2 \right] = k_c \cdot \frac{\partial^2 \overline{U}}{\partial \overline{Y}^2} \qquad (11.15),$$

which indicates that, despite the pressure and viscosity distribution, a pure linear Couette flow profile must appear when either of the factors $\partial \overline{P}/\partial \overline{X}$ or $\left[1 - \left(k_p \cdot \partial \overline{U}/\partial \overline{Y} \right)^2 \right]$ becomes zero. For a traditional ehl solution with a pressure spike, such as load case iv, four positions of flow profile change are present:

(i)   the first at the contact centreline,

(ii)   the second at the relative minimum of the pressure distribution marking the beginning of the pressure spike,

(iii)   the third at the top of the spike, and

(iv)   the last at the boundary of the analysis after the traditional constriction at the position of lubricant film rupture.

The extended approach generates two extra positions where $k_p \cdot \partial \overline{U}/\partial \overline{Y}$ becomes unity,

(v)   in the first half of the contact, for load case iv at the transition from the inlet zone to the parallel gap,

(vi)   and after the pressure spike.

These six positions are illustrated in figure 11.8. Accordingly, there must be six changes of the flow profile and, for an incompressible fluid, accordingly six positions of identical height. Between these positions, the gap is alternately smaller or wider. Figure 11.8 also shows a qualitative shape for the gap.
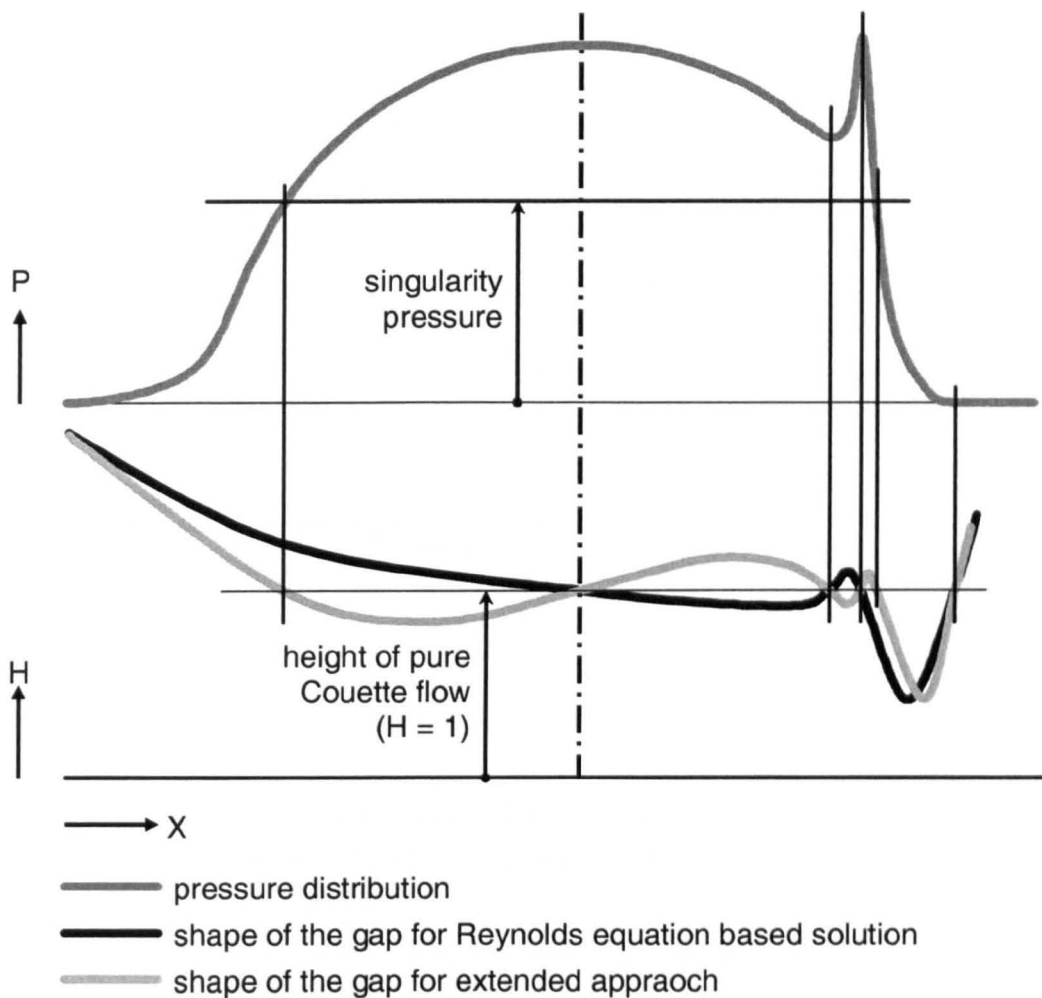
Figure 11.8: Qualitative shape of the gap resulting from a typical ehl pressure distribution with pressure spike for the Reynolds equation based and the extended approach.

However, some aspects make it difficult to imagine that such a shape of the gap can result from a qualitatively identical pressure distribution with two maximums, as for example:

♦ The extension of the additional widening of the gap due to the extended approach exceeds that of the very small widening by the pressure spike by several orders of magnitude. Accordingly, the convergence of the gap before the very small pressure spike induced widening differs also by several orders of magnitude. However, the type of dent generated by a typical pressure spike is much too small to generate a dent which allows two positions of identical height in a much stronger convergence, as figure 11.9 illustrates.

◆ Whilst for a Reynolds equation based solution the small widening before the constriction is to the left of the pressure spike which contributes to its generation, it has to change to the right side for the extended approach. Considering the pressure spike for a Reynolds equation based approach as an edge pressure, then for the extended approach this edge pressure would appear slightly inside the edge.

(a)   (b)

══════ shape of the gap (with dent)
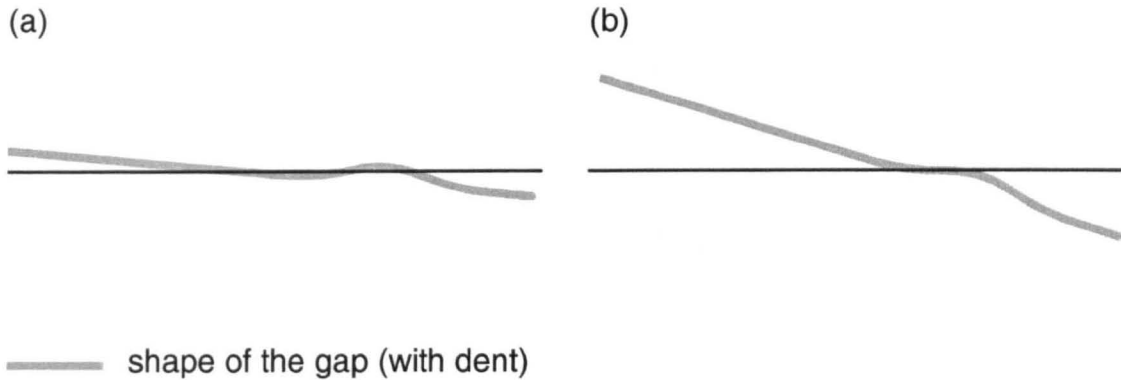
Figure 11.9:   Influence of dent depending on slope
(a)   small   slope   causing   threefold   intersection   with horizontal,
(b)   increased   slope   causing   single   intersection   with horizontal.

On the other hand, consideration of a pressure distribution along the gap as having some kind of "pressure edge" rather than a pressure spike, the number of positions, where pure Couette flow is present, is two for the Reynolds equation based approach and four for the extended approach, as shown in figure 11.10.
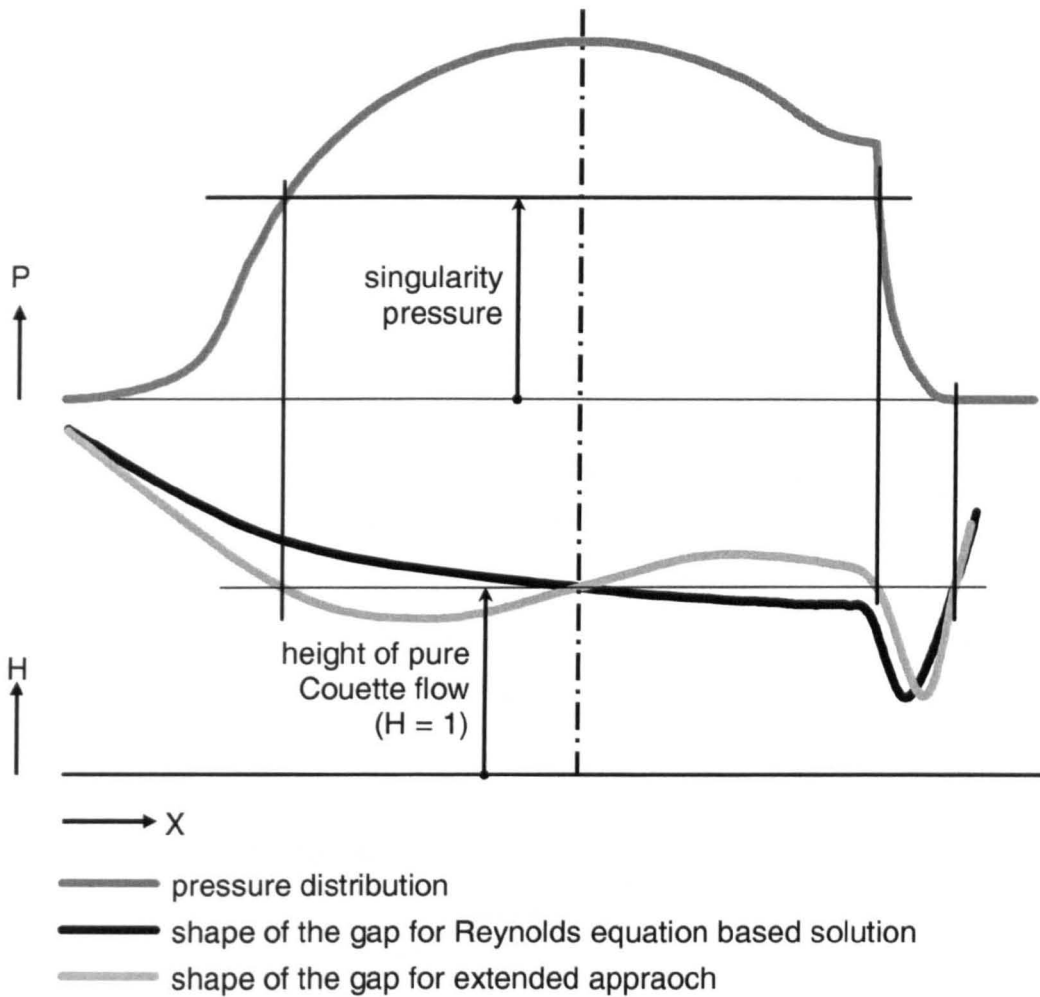
Figure 11.10: *Qualitative shape of the gap resulting from an ehl pressure distribution without pressure spike for the Reynolds equation based and the extended approach.*

For the extended approach this would lead to a direct transition from the additional widening into the traditional ehl constriction without a small extra dent. This is qualitatively the shape of the gap also shown in figure 11.10 for the computations. The pressure spike here causes a brief change in the curvature but is far from generating qualitatively the shape required for a solution with a pressure spike.

In summary, a number of theoretical arguments have been made proposing the fact that it is likely that no pressure spike should be present for the extended approach, however, there is so far no numerical evidence for the existence or non-existence of a pressure spike for the extended approach.

11.7.4   Pressure spike and the fully simultaneous method

With the above possibility, that the pressure spike might disappear for the extended approach, the sample result from the fully simultaneous method of section 9.1.2, which also misses the pressure spike, is reconsidered. According to figure 11.10, four points of linear Couette flow are expected. From figure 11.11, three points of pure linear Couette flow where the dimensionless height becomes unity, are shown, a fourth would appear for the film rupture point. Comparison with the pressure distribution shows that linear Couette flow appears for the maximum pressure and also for a dimensionless pressure $P = 0.6$ representing the pressure where the factor k_p of equations 11.15 becomes unity. The beginning of the traditional constriction appears not at the degenerated pressure spike but slightly later, causing a somewhat smaller constriction.
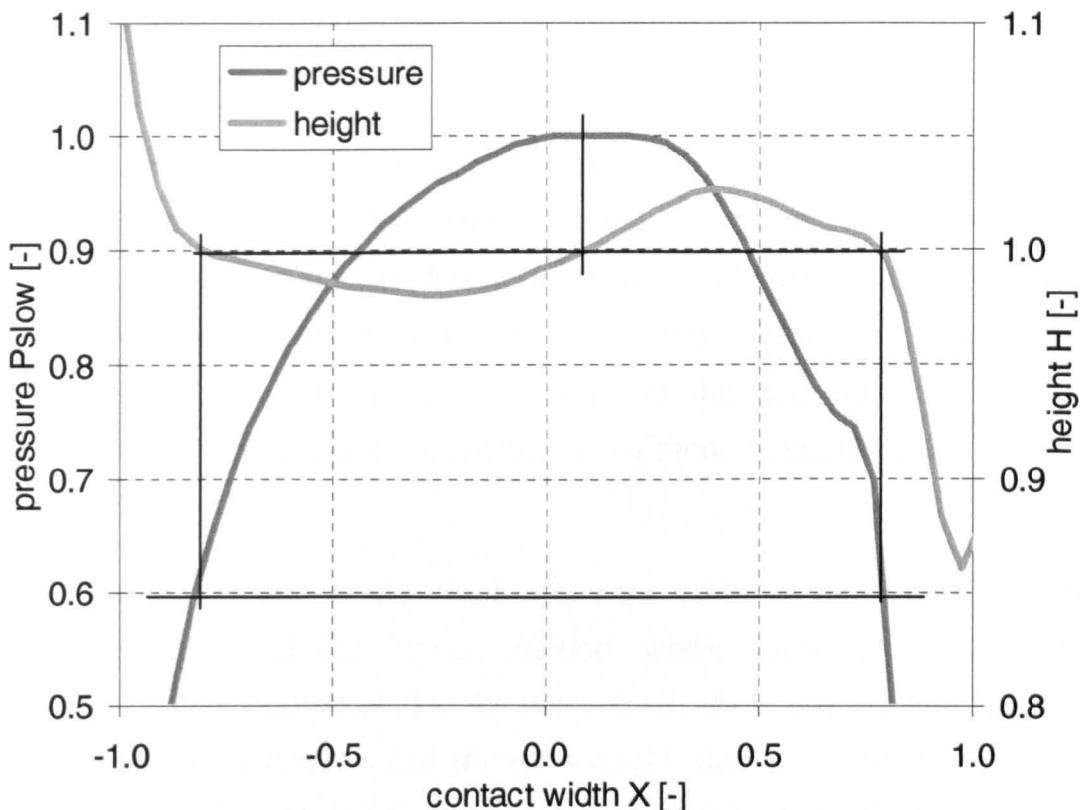
Figure 11.11: Pressure distribution along the gap and shape of the gap near the traditional constriction for load case iv (table 10.1) and partial sliding $S = 0.5$ computed by the fully simultaneous method.

In conclusion, with the result from the fully simultaneous method, it is likely that a solution of the extended approach fulfilling any combinations of governing equations, will lose the pressure spike, and will show some changes to the constriction in comparison to a Reynolds equation based solution.

11.7.5   Hypotheses for pressure spike development

Likely disappearance of the pressure spike for the fully simultaneous method and the unlikely appearance for the combined successive-simultaneous method raises the question of possible reasons. Comparison of the fully simultaneous method and the combined successive-simultaneous method in section 9.3 showed that both numerical methods show various differences with regards to the form of the governing equations finally used, the initial guess used, the residual evaluation and the values to control the analysis. These differences are subsequently discussed with regards to their possible contribution to different results.

♦   As initial guess, a fully converged ehl pressure distribution with pressure spike and the according shape of the gap was used for the fully simultaneous method in subsection 9.1.1.3 and figure 9.2(b), whilst a Hertzian pressure distribution with the successively determined pressure variation across the height of the gap was used for the combined successive-simultaneous method, subsection 9.2.1.3 and figure 9.9(b)

Physically, some of the traditional constriction is incorporated in the initial guess of the former method, whilst some of the extended approach is incorporated in the latter. Basically in any Newton-Raphson technique, different initial guesses might lead to different results, as they possibly do for the extended approach solution. However, the different initial guesses were not selected arbitrarily but were required by the respective method.

♦   Regarding the selection of the equations which were finally used, the original Navier-Stokes equations were evaluated for the fully

simultaneous method, section 9.1.1.2. For the combined successive-simultaneous method the original x-momentum equation was also used but a re-arranged equation for the determination of the pressure variation across the height of the gap

$$\frac{\partial p}{\partial x} = \frac{\partial u}{\partial y} \cdot \frac{\partial \eta}{\partial y} + \eta \cdot \frac{\partial^2 u}{\partial y^2}$$ (11.16),

and

$$\frac{\partial p}{\partial y} = \frac{\eta^2 \cdot \alpha \cdot \dfrac{\partial u}{\partial y}}{1 - \left(\eta \cdot \alpha \cdot \dfrac{\partial u}{\partial y}\right)^2} \cdot \frac{\partial^2 u}{\partial y^2}$$ (11.17).

This arrangement means that any changes in the sign of the pressure gradient along the gap in equation 11.16, does not immediately result in a change of the sign of the velocity profile curvature in equation 11.16, but slowly via changes of the pressure gradient across the gap in equation 11.17. This latter method reliably converged even for difficult convergence conditions. Application of other equations, subsection 9.2.1.1, would lead to a different behaviour as tests indicated.

♦ The differential continuity equation was used to determine the mass flow residuals for the fully simultaneous methods, subsection 9.1.1.1, and the integral continuity equation was used to determine those for the combined successive-simultaneous method, subsection 9.2.1.2. Any inconsistencies regarding other than the x-momentum equation, will be seen in the mass flow residuals determined from the differential continuity equation but not in those from the integrated continuity equation. This might be an advantage of the fully simultaneous method.

♦ Different numerical parameters to control both methods were set. Some of those had to be defined individually dependent on how the equations were coupled, which equations were applied and which residuals were used. Selection of numerical parameters can be of relevance for any solution. However, it was always attempted to set the values as tight as

possible; however, accuracy of any ehl analysis based on the CFD software is limited.

In conclusion, it appears that the generation of the pressure spike in the successive-simultaneous methods can be caused by any of the above differences. An optimisation of the method must hence consider all the above phenomena. However, a substantial increase in the accuracy of the methods would require turning away from a CFD based solution with a numerical determination of the Jacobian matrix to an analytical determination of the Jacobian.

11.8   Correlation with dimensionless factors

Consideration of the numerical results with a view to the dimensionless factors k_p, k_c and k_r of equations 3.38 and 3.39 enables a further check of the numerical method and could, vice versa, qualify such factors for application in simple design formulae which could describe the influence of the extended approach without requiring expensive numerical analysis.

11.8.1   Check of numerical method

The check of the numerical method is realised by obtaining those gradients, which are involved in the definition of the respective dimensionless factor, graphically from result plots at a selected position and a subsequent check on equality of the defining equations, 3.38 for k_r, and 3.39 for k_c and k_r, at this point.

The determination of most of the required gradients is straightforward. The pressure gradient along the gap $\partial \overline{P}/\partial \overline{X}$ can be obtained by measuring the slope in the respective plot showing the pressure distribution along the gap, as figure 10.16(c). The pressure gradient across the height of the gap $\partial \overline{P}/\partial \overline{Y}$ can be obtained from the graph showing the pressure difference across the gap $\Delta \overline{P}$, as figure 10.17, and the height of the gap at the same location, as figure 10.6. The first order velocity gradient across the gap $\partial \overline{U}/\partial \overline{Y}$ can be obtained from the sliding ratio definition, equation 3.41,

$$S = \frac{u_1 - u_2}{u_1 + u_2} \quad \Rightarrow \Delta\overline{U} = \overline{U}_1 - \overline{U}_2 = \frac{u_1 - u_2}{\frac{1}{2} \cdot (u_1 + u_2)} = 2 \cdot S \qquad (11.18),$$

and the above mentioned height of the gap. Only the determination of the second order velocity gradient $\partial^2\overline{U}/\partial\overline{Y}^2$ is difficult, since the gradient can hardly be seen in the respective graph, e.g. figure 10.11, and furthermore the graphical determination is more cumbersome. In order to overcome this problem, the second order velocity gradient of equation 3.39 was substituted by a height description of appendix L,

$$12 \cdot \frac{\overline{H} - 1}{\overline{H}^3} = \frac{\partial^2\overline{U}}{\partial\overline{Y}^2} \qquad (11.19),$$

so that equation 3.39 becomes

$$\frac{\partial\overline{P}}{\partial\overline{X}}\left[1 - \left(k_p \cdot \frac{\partial\overline{U}}{\partial\overline{Y}}\right)^2\right] = 12 \cdot k_c \cdot \frac{\overline{H} - 1}{\overline{H}^3} \qquad (11.20).$$

The applied correlation was obtained with the help of a one-dimensional, isothermal Reynolds equation as shown in Appendix L, under the assumption that the curvature due to viscosity variation is similar to that due to pressure gradient.

For the check, factors k_c, k_p and k_r are not determined with the dimensionless parameters form of equation 3.38 and 3.39,

$$k_c = 1.11 \cdot U^{-0.4} \cdot G^{-1.2} \cdot W^{0.26} \cdot e^{0.4 \cdot G \cdot W^{0.5}}$$
$$k_p = 0.53 \cdot U^{0.3} \cdot G^{0.4} \cdot W^{0.13} \cdot e^{0.4 \cdot G \cdot W^{0.5}} \qquad (11.21),$$
$$k_r = 0.63 \cdot U \cdot G \cdot W^{-0.5} \cdot e^{0.4 \cdot G \cdot W^{0.5}}$$

but from a definition, which excludes the simplifications discussed in subsection 3.3.3, and illustrated in figure 3.7, and requiring knowledge of the pressure at the investigated location[*]:

---

[*]   Details of the determination are given in Appendix D.

$$k_c = \frac{\eta_0 \cdot e^{\bar{\alpha} \cdot \bar{P}} \cdot u_h}{p_{hz} \cdot h_0 \cdot \gamma}$$

$$k_p = \frac{\eta_0 \cdot \bar{\alpha} \cdot e^{\bar{\alpha} \cdot \bar{P}} \cdot u_h}{p_{hz} \cdot h_0} \qquad (11.22).$$

$$k_r = \frac{\eta_0 \cdot \bar{\alpha} \cdot e^{\bar{\alpha} \cdot \bar{P}} \cdot u_H}{p_{hz} \cdot h_0} \cdot \gamma$$

Application of the described procedure to the partial sliding condition $S = 0.5$ of load case iv, table 10.1, as a sample case, leads to

$$k_c = 4002; \quad k_p = 68.2 \quad \text{and} \quad k_r = 0.108 \qquad (11.23)$$

and, as shown in Appendix M, to

$$\bar{H} = 0.981, \quad \frac{\partial \bar{P}}{\partial \bar{X}} = 0.190, \quad \frac{\partial \bar{P}}{\partial \bar{Y}} = 0.0213 \quad \text{and} \quad \frac{\partial \bar{U}}{\partial \bar{Y}} = 1.019 \quad (11.24)$$

so that equation 3.38,

$$\frac{\partial \bar{P}}{\partial \bar{Y}} \bigg/ \frac{\partial \bar{P}}{\partial \bar{X}} = k_r \cdot \frac{\partial \bar{U}}{\partial \bar{Y}} \qquad (11.25),$$

is reasonably fulfilled by

$$\frac{0.0217}{0.190} \approx 0.108 \cdot 1.019 \qquad (11.26)$$

$$0.114 \approx 0.110$$

and equation 3.39 modified to equation 11.20

$$\frac{\partial \bar{P}}{\partial \bar{X}} \left[1 - \left(k_p \cdot \frac{\partial \bar{U}}{\partial \bar{Y}} \right)^2 \right] = 12 \cdot k_c \cdot \frac{\bar{H} - 1}{\bar{H}^3} \qquad (11.27)$$

is reasonably fulfilled by

$$0.190 \cdot \left[1 - (68.2 \cdot 1.019)^2 \right] \approx 12 \cdot 4002 \cdot \frac{0.981 - 1}{0.981^3} \qquad (11.28)$$

$$929 \approx 966$$

The above agreement is evidence of a correct adaptation of the CFD code to the ehl problem and the correct implementation of the extended approach for the investigated set of parameters. This evidence is also obtained for other load cases and sliding ratio values. However, for those parameters, where

the applied successive-simultaneous method requires the full set of equations 3.42 and might reach its limit, subsection 11.4.4, the above agreement reduces.

11.8.2   Application to useful design formulae

The shown close consistency qualifies simple governing equations and dimensionless factors to be used to obtain some results, or even result charts as figures 3.8, 3.9, and 10.2(a) to (c), for the extended approach without expensive computations. Quantities, such as pressure variation, viscosity variation and minimum height may be described. However the factors determined for the check of the method should reasonably agree with those determined without knowing details, from the dimensionless ehl parameters G, U and W.

Table 11.2 shows these values for the situation used for the above check of the method, row (i), and for the application of the definition using the dimensionless ehl parameters, G, U and W, as in equation 11.21, row (ii). For the latter the dimensionless parameters as given in table 10.1 were used. Differences of approximately 50 per cent between the two cases can be observed for all factors, which seem to disqualify the factors k_c, k_p, and k_r for easy design formulae. The differences result from different aspects:

♦   The data of row (i) considers the real pressure at the location of pressure variation, row (ii) assumes maximum Hertzian pressure.

♦   The data of row (i) are based on the calculated centreline height of the gap, row (ii) on that estimated from the dimensionless parameters, equation 3.26.

♦   The values for the dimensionless parameters G, U and W of table 10.1, are round-off values.

♦   The derivation of the factors of form 11.22 contains also some rounding.

However, a determination of maximum pressure variation across the gap or of the shape of the gap requires the consideration of the variation with the pressure along the gap of factors k_c, k_p, and k_r. This is because if the pressure were kept constant at the Hertzian pressure the maximum values would appear at the beginning and end of a Hertzian pressure.

In order to achieve such a variable description of factors k_c, k_p, and k_r without a full ehl analysis, the result of a film thickness formulae, for example equation 3.26, must be used for the centreline film thickness h_0 in the equation of form 11.22. Alternatively, equations 11.21 are modified so that the terms considering the pressure are made variable. The exponential term is that which causes pressure dependency in equation 11.22. This can be transposed by multiplying the exponent by the normalised pressure, so the factors become:

		k_c	k_p	k_r
(i)	factors obtained from the original form 11.22, taking pressure at the position of maximum pressure variation across the gap into account	4002	68.2	0.108
(ii)	factors obtained from dimensionless speed load and material parameters equation 11.21, assuming Hertzian pressure	6018	103	0.161
(iii)	factors obtained from the original form 11.22 taking pressure at the position of maximum pressure variation across the gap into account, estimating the central film thickness from equation 3.26	4145	69.8	0.108
(iv)	factors obtained from modified dimensionless speed load and material parameters, equation 11.23, taking pressure at the position of maximum pressure variation across the gap*	4281	72.4	83.05

Table 11.2: Values of k_c, k_p and k_r for load case iv determined using various methods.

* For the present case, the accurate values for G, U and W obtained with the definitions 3.25 were used rather than the rounded values of table 10.1.

$$k_c = 1.11 \cdot U^{-0.4} \cdot G^{-1.2} \cdot W^{0.26} \cdot e^{0.4 \cdot \bar{P} \cdot G \cdot W^{0.5}}$$

$$k_p = 0.53 \cdot U^{0.3} \cdot G^{0.4} \cdot W^{0.13} \cdot e^{0.4 \cdot \bar{P} \cdot G \cdot W^{0.5}} \tag{11.23}.$$

$$k_r = 0.63 \cdot U \cdot G \cdot W^{-0.5} \cdot e^{0.4 \cdot \bar{P} \cdot G \cdot W^{0.5}}$$

Results for the former method are shown in row (iii) of table 11.2 and for the latter in row (iv): Neither the alteration of the centreline film thickness from computed 0.346 μm to estimated 0.340 μm nor application of equation 11.23 leads to significant deviations. Hence, the factors k_c, k_p and k_r can be used for easy design formulae as long as the real pressure is considered.

However, the proposed procedure becomes increasingly inaccurate when the assumptions may deviate from reality, for example, for the pressure distribution, when the point of maximum pressure starts to move into the second half of the contact. This starts to be the case when the sliding ratio of load case iv exceeds 0.5 and is almost certainly the case for load cases exceeding the investigated range of parameters. Transferability can only be proved by further investigation.

In conclusion, the limited range of validity of such formulae or charts and the minor technical relevance of the extended approach suggests not pursuing the material at this stage. The dimensionless factors k_c, k_p and k_r in its pure form 11.21 obtained from dimensionless ehl parameters G, U and W overestimate the influence of the extended approach as considered in section 3.3.

11.9   Summary

Throughout the present chapter, results have been discussed, mainly with a view to the various variables of the ehl analysis, the pressure spike and the dimensionless factors indicating the significance of additional terms defined in subsection 3.3.4.1. The present section summarises the main aspects and conclusions from the discussion by looking at the above findings from a different point of view, i.e. main features of results from the extended approach, technical relevance of the results and classification with regards to governing equations.

11.9.1   Main result features

11.9.1.1 Pure rolling

Results from the extended approach show perfect agreement with that from Reynolds equation based solution for pure rolling cases,

11.9.1.2 Partial and pure sliding

Extended approach results differ from those of a Reynolds equation based approach for non-pure-rolling conditions as follows:

♦   The shape of the gap shows an additional constriction in the first half of the contact and a widening between this first constriction and the traditional constriction. The extension of the additional constriction along the gap might exceed that of the widening. Regarding the extension across the gap, the value of gap extension in the widening zone exceeds the value of constriction in the additional constriction zone.

♦   In fulfilment of the continuity equation, a Poiseuille like logarithmic forward directed flow component, which is caused by viscosity variation across the gap, overlies the Couette flow in the constricted zone in the first half of the contact. Accordingly, a backwards directed Poiseuille like logarithmic flow component overlies a Couette flow in the zone of the additional widening. Overall flow rate is hardly affected by the extended approach.

♦   For the extended approach pressure variation across the gap is present. In the zone of the additional constriction, pressure at the faster surface exceeds that at the slower surface; in the zone of the additional widening, pressure at the slower surface exceeds that at the faster surface.

Pressure along the gap falls below values for the Reynolds equation based solutions in the first half of the contact and exceeds those in the second half.

◆ Shear forces along the contact differ considerably from that for the Reynolds equation based solution, however traction coefficient remains unchanged.

11.9.2   Technical relevance of extended approach

◆ The height outside the traditional ehl constriction is reduced in comparison to Reynolds equation based solutions in the zone of the additional constriction. The extended approach is of relevance for applications where centre line film thickness is used for further analysis as in some bearing fatigue analysis. The magnitude of height change has to be considered in comparison to the accuracy of any film thickness formulae and is hence technically irrelevant.

◆ Pressure distribution at the contact surfaces is different compared with a Reynolds equation based solution. The extended approach leads to slightly different stress distributions in the contact material, however without relevance for technical applications such as fatigue life analysis

◆ Traction coefficient values for the extended approach hardly change in comparison to Reynolds equation based solutions. Hence the extended approach cannot contribute to realistic traction coefficient values.

11.9.3   Pressure spike

The two applied numerical methods, the combined successive-simultaneous and the fully simultaneous method, show different behaviour regarding the formation of the ehl pressure spike. The fully simultaneous method proposes a disappearance of the pressure spike, which is supported by theoretical considerations. However the combined successive-simultaneous method suggests the existence of the pressure spike. Both the investigated methods show differences regarding the method of coupling, the formulation of the governing equations and initial values. Further investigations are necessary for a full understanding of the pressure spike for the presented extended approach.

11.9.4   Regimes of results for the extended approach solution

With the extended approach and the applied successive-simultaneous approach various regimes of results were observed as

♦ principal appearance of the extended approach phenomena, but with the magnitude of the numerical resolution of the result data, as in load case i,

♦ typical behaviour of the extended approach for regimes close to the hydrodynamic regime, where the additional constriction has the same order of magnitude as the hydrodynamic convergence of the gap, as load case ii,

♦ a behaviour showing a mainly independent influence of the extended approach on the first and second half of the contact without affecting centreline pressure and height, as in load case iii,

♦ a behaviour showing interference of the phenomena in the first and second half of the contact as that maximum pressure is shifted towards the second half of the contact, and the value of the additional constriction and the widening differ, as for load case iv for the partial sliding conditions S = 0.5.

♦ a behaviour showing a further development of the previous case, with a strong interaction between effects in the first and the second half of the contact, and the development of a pressure bulge in the second half of the contact, which is however not fully consistent with theoretical considerations and hence mark the border of the validity of the combined successive-simultaneous method, as for the pure sliding situation of load case iv.

Chapter 12

The extended approach with regard to other work

12.1 Introduction

The previous chapter 11 discussed the numerical and physical aspects of the results obtained from the extended approach within the assumptions made in chapter 3, such as Barus' approach and Newtonian, isothermal conditions. These assumptions were made to simplify the set of equations for theoretical and numerical analysis. The current chapter intends to broaden the discussion to a more general evaluation of the extended approach and its solution methods.

However, full quantitative validation of the extended approach cannot be applied with the current state of development of the method, because the simplifying assumptions of chapter 3 would themselves cause major deviations between theoretical and experimental results. Consequently, only some qualitative validation of pressure is considered in section 12.2.

Explanation and quantitative estimation of differences between the present study and experimental experience, is discussed in the subsequent sections 12.3 to 12.5. The consequences of dropping some simplifying assumptions of chapter 3 are considered, namely aspects due to the pressure-viscosity description, the assumption of Newtonian fluid behaviour and the assumption of isothermal conditions.

12.2   Validation using experimental pressure distribution

As stated, fully quantitative validation of the extended approach with experimental data cannot be undertaken. However, consideration of experimental pressure distributions might be useful to confirm or otherwise the existence or relevance of phenomena caused by the physical effects described by the approach. This is because pressure variation across the gap is the result feature which is most characteristic, appearing exclusively in the extended approach of the present study. If such a pressure difference is not apparent then any other physical effects reduce the extended approach features to having little significance.

However, determination of the pressure along the gap for both surfaces seems not to have been an important issue for publication so far. This might be due to the generally used assumption of constant pressure across the height of the gap and the fact that such measurements were preferably undertaken for the faster of the contact partners [106] to preserve the sensors. In addition measurement of the pressure with resistive transducers, such as those used by Baumann [106], must be temperature compensated to give the same pressure values for a sliding and a rolling contact of identical operating conditions, i.e. differences in the temperatures of the two surfaces sliding against each other can cause some apparent pressure differences. Any experimental pressure differences across the gap could also be caused by thermal phenomena, so that experimentally obtained pressures cannot be interpreted as an exclusive indication of physical pressure variation across the gap. If such experimental data were to be used for discussion of pressure variation across the height of the gap, a detailed and accurate understanding of the temperature drift would be required.

A further qualitative validation could be the search for typical features of the pressure distribution along the gap and the corresponding shape of the gap

consistent with the predictions such as a slightly reduced pressure in the first half of the contact* or the additional constriction and the widening of the gap.

Omissions due to simplifying assumptions could lead to significant changes also in the qualitative distribution of results, as, for example, thermal effects do in Hsiao and Hamrock [107]. Hence the discussion is turned towards the understanding of the omitted effects of the extended approach rather than any qualitative comparison, even though some experimentally obtained height distributions, a shape containing so-called dimples observed by Kaneta and Nishikawa [108, 109], have a qualitatively astonishing similarity to the computed results of the present study.

In conclusion, experimental evidence as to whether the additional terms of the extended approach are practically relevant, cannot be provided at present. Further consideration or even analyses are needed to overcome the simplifications made and to allow direct validation. On the other hand, extension of pressure measurements to account for both surfaces should be encouraged in the future.

12.3   Influence of other pressure-viscosity descriptions

12.3.1   Qualitative influence of Roelands' approach

In the present study, Barus' approach, equation 3.18a,

$$\eta = \eta_0 \cdot e^{\alpha \cdot p} \qquad\qquad (12.1)$$

was used, because of its compact form, in comparison to more developed descriptions such as the Roelands' equation in its isothermal form, equation 3.18b,

$$\eta = \eta_0 \cdot e^{(\ln(\eta_0)+9.67)\left[-1+\left(1+5.1\cdot10^{-9}\cdot p\right)^Z\right]} \qquad\qquad (12.2)$$

---

* Spotting this effect would be difficult anyway, because the effect is quite small for the usually experimentally investigated faster surface, but would appear to be more significant for the slower surface.

with the viscosity-pressure index

$$Z = \frac{\alpha}{5.1 \cdot 10^{-9} \cdot (\ln(\eta_0) + 9.67)}.$$

Barus' equation normally tends to overestimate the average pressure-viscosity coefficient and hence the viscosity, particularly for high pressure values.

This means that in the extended approach, the dimensionless factors k_p and k_r of equations 3.38 and 3.39 in their form of equation 11.22[*],

$$k_p = \frac{\eta_0 \cdot \alpha \cdot e^{\alpha \cdot p_{hz}} \cdot u_h}{h_0}$$

$$k_r = \frac{\eta_0 \cdot \alpha \cdot e^{\alpha \cdot p_{hz}} \cdot u_H}{h_0} \cdot \gamma$$

(12.3),

would not be as high as they are and would not change as rapidly as they do for Barus' approach in figures 3.8 and 3.9 with an increase of the dimensionless speed parameter U and the dimensionless load parameter W. This means that the importance of the additional terms is smaller when considering Roelands' rather than Barus' approach.

12.3.2 Quantitative influence of Roelands' approach

The reduced values and hence the reduction in comparison to Barus' approach can be obtained by adaptation of factors k_p and k_r to Roelands' approach. The term $e^{\alpha \cdot p_{hz}}$ in the factors represents the ratio of viscosity at Hertzian pressure over viscosity at ambient conditions and can be replaced by the respective term of Roelands' equation. The term becomes

$$\frac{\eta_{hz}}{\eta_0} = e^{\tilde{\alpha}(p_{hz})}$$

(12.4)

with

$$\tilde{\alpha}(p_{hz}) = (\ln(\eta_0) + 9.67) \cdot \left[-1 + \left(1 + 5.1 \cdot 10^{-9} \cdot p_{hz} \right)^{Z} \right].$$

---

[*] In comparison to equation 11.22, dimensionless pressure viscosity coefficient $\bar{\alpha} = \alpha \cdot p_{hz}$ was resolved into its original factors and p_{hz} cancelled for the present form.

The term α represents the derivative of the exponent of the pressure viscosity description with respect to Hertzian pressure, i.e.

$$\alpha = \frac{\partial(\alpha \cdot p_{hz})}{\partial p_{hz}} \qquad (12.5)$$

for Barus' equation and consequently becomes for Roelands' equation

$$\tilde{\alpha}'(p_{hz}) = \left(\ln(\eta_0) + 9.67\right) \cdot Z \cdot 5.1 \cdot 10^{-9} \cdot \left(1 + 5.1 \cdot 10^{-9} \cdot p\right)^{Z-1} \qquad (12.6)$$

The dimensionless factors for (isothermal) Roelands' equation hence become

$$\tilde{k}_p = \frac{\eta_0 \cdot \tilde{\alpha}'(p_{hz}) \cdot e^{\tilde{\alpha}(p_{hz})} \cdot u_h}{h_0}$$

$$\tilde{k}_r = \frac{\eta_0 \cdot \tilde{\alpha}'(p_{hz}) \cdot e^{\tilde{\alpha}(p_{hz})} \cdot u_H}{h_0} \cdot \gamma \qquad (12.7).$$

Values for the factors k_p and k_r for Barus' and $\tilde{k}_p$ and $\tilde{k}_r$ for Roelands' approach and comparisons for the load cases investigated, table 10.1, are given in table 12.1.

	dimensionless sliding influence factor		dimensionless pressure gradient ratio		comparing ratio
	using Barus' equation	using Roelands' equation	using Barus' equation	using Roelands' equation	
	k_p	$\tilde{k}_p$	k_r	$\tilde{k}_r$	$\dfrac{k_r}{\tilde{k}_r} = \dfrac{k_p}{\tilde{k}_p}$
load case i	0.604	0.207	0.0004573	0.0001572	2.90
load case ii	1.258	0.294	0.002856	0.000668	4.28
load case iii	15.747	1.683	0.021	0.002295	9.15
load case iv	98.42	4.837	0.134	0.00645	20.8

Table 12.1:   Values of factors k_p, $\tilde{k}_p$ k_r and $\tilde{k}_r$ for the load cases investigated (table 10.1).

It is apparent that a reduction factor of between 2.90 for load case i and 20.8 for load case iv exists when comparing the two equations. It is seen that, for

load case ii that factor $\tilde{k}_r$ is similar in magnitude to the value of k_r for load case i. Influence of the extended approach would hardly be evident within numerical error. For load cases iii and iv, factor $\tilde{k}_r$ also falls below the value for load cases ii and iii respectively. Accordingly, the magnitude of the changes to the results is comparable to cases ii and iii. Hence when determining the relevance of the extended approach, Barus' approach must be quoted as inaccurate even for the investigated low pressure of 0.3 GPa and 0.5 GPa, where normally Barus' approach is not considered inaccurate, Gohar [9], section 2.3.

However, the extended approach is not generally negligible but may be significant beyond the dimensionless speed and load factors U and W currently investigated. It is expected that for this range of parameters the values for dimensionless factors k_p and k_r will drop to values similar to those investigated in the current study and will not take the very high values suggested in figures 3.8 and 3.9.

For illustration of the validity of this suggestion various samples from published work, which have already been referenced earlier in this chapter, were considered, i.e.

(i)   a result of Baumann [106] including temperature measurement, for which the sensor temperature drift was considered, in the following referenced as case B1,

(ii) the maximum load case of the theoretical work by Eller [7] which complemented the experimental work of Baumann [106]; Eller's load case *"Beispiel 12"* is referenced as case E1,

(iii) two load cases used by Hsiao and Hamrock [107] as well as by Lee and Hamrock [48],referenced as H1, for their *"Oil-1"*, and H2 for their *"Oil-2"*.

Table 12.2: Parameters of selected published ehl cases.

De-signation	author and reference	Hertzian pressure p_{hz}	hydro-dynamic speed u_h	viscosity at ambient conditions η_0	pressure viscosity coefficient α	pressure viscosity index Z	reduced radius r_{red}	Hertzian width b_{hz}	centreline gap height h_0	tem-perature difference $\Delta\theta$
		[Pa]	[m s^{-1}]	[Pa s]	[Pa^{-1}]	[-]	[m]	[m]	[m]	[K]
B1	Baumann [106]	0.6×10^9	2.6	0.137 *	2.38×10^{-8} *	0.61	0.025	2.50×10^{-4}	1.86×10^{-6} **	18 ‡
E1	Eller [7]	0.9×10^9	1.0	0.114*	2.24×10^{-8} *	0.586	0.025	3.94×10^{-4}	1.07×10^{-6}	130 ‡
H1	Hsiao and Hamrock [107],	0.69×10^9	0.596	0.0411	2.28×10^{-8}	0.689	0.0111	1.35×10^{-4}	2.19×10^{-7}	2 §
H2	Lee and Hamrock [48]	0.69×10^9	1.848	0.0132	1.58×10^{-8}	0.580	0..0111	1.35×10^{-4}	1.77×10^{-7}	22 ††
K1	Kaneta and Nishikawa [108]	0.33×10^9	0.07	0.4	5.40×10^{-8}	1.20	0.0108	1.20×10^{-4}	3.00×10^{-7}	†

* values calculated from values given for other than Roelands' approach   † values not available   ‡ For sliding ratio S = 0.35   § sliding ratio S = 0.05   ** obtained using dimensionless approximation   †† for sliding ratio S = 0.5

(iv) an experimental result of Kaneta et Nishikawa [108], which showed astonishing qualitative similarity for the shape of the gap with the isothermal results of the present study, but does not give thermal parameters*; this is referenced as case K1.

The relevant parameters of these cases are listed in table 12.2[†].

Table 12.3 gives an overview of how the factors k_p, $\tilde{k}_p$, k_r and $\tilde{k}_r$ behave for these published cases under the assumption of Barus' and Roelands' description respectively.

	dimensionless sliding influence factor		dimensionless pressure gradient ratio		comparing ratio
	using Barus' equation	using Roelands' equation	using Barus' equation	using Roelands' equation	
	k_p	$\tilde{k}_p$	k_r	$\tilde{k}_r$	$\dfrac{k_r}{\tilde{k}_r}=\dfrac{k_p}{\tilde{k}_p}$
B1	7258	79.1	54.0	0.589	91.6
E1	1.36×10^6	544	3690	1.48	2801
H1	1.73×10^4	127	28.1	0.369	76.2
H2	118	2.03	0.155	2.66×10^{-3}	58.4
K1	2.76×10^5	3.42×10^6	691	8554	0.08

Table 12.3: _Values for factors k_p, $\tilde{k}_p$, k_r and $\tilde{k}_r$ using Barus' and Roelands' approach respectively for selected published results._

As expected for the first four examples, B1, E1, H1, and H2, the values of factors $\tilde{k}_p$ and $\tilde{k}_r$ for Roelands' approach are up to more than three orders of magnitude smaller than the corresponding values of k_p and k_r for Barus'

---

* Kaneta and Nishikawa [108] investigated elliptical contacts; for the present investigation, the contact with the major axis perpendicular to the motion of the surfaces and with the minor axis in the direction of motion was considered. Although it is still an elliptical contact, it was considered as a line contact for this consideration.

† The temperature column contains information relevant to section 12.5.

approach. For cases B1, E1, and H1, $\tilde{k}_r$ is approximately unity and tends to be slightly above the value of k_r for load case iv of the present study. This means that the results presented in chapter 10 and discussed in chapter 11 represent a typical magnitude of changes which can be expected for practical applications. Further, the specification for the suggested improvement of the numerical methods would not be as rigid as it seemed in chapter 11.

However, for case K1 the values of the factors $\tilde{k}_p$ and $\tilde{k}_r$ are not smaller but even greater than k_p and k_r. For factor $\tilde{k}_r$, the value is well above unity, and hence the additional terms remain of great importance. The reason for this behaviour is that the fluid used in the experiment was not a typical lubricant but the traction fluid *"santrotrac 100".* The pressure viscosity coefficient is high enough to give a viscosity-pressure index greater than unity, which leads to the observed rise in viscosity and hence values of the factors above those for Barus' approach.

12.4   Non-Newtonian effects

A Newtonian behaviour was assumed for the lubricant throughout the development and discussion of the extended approach. The influence of the application of a non-Newtonian limiting shear stress on the presented extended approach was considered by Greenwood [110] following a presentation of first sample results of the extended approach [111].

Greenwood repeated the derivation of the governing equations but in dimensional form, so that equation 3.39 was written as

$$\frac{\partial p}{\partial x}\left[1-\left(\alpha \cdot \eta \cdot \frac{\partial u}{\partial y}\right)^2\right]=\eta \cdot \frac{\partial^2 u}{\partial y^2} \tag{12.8}$$

with

$$\eta = \eta_0 \cdot e^{\alpha \cdot p}.$$

Substituting the *"usual approximation"* of the shear stress,

$$\tau_{xy} = \eta \cdot \frac{\partial u}{\partial y} \qquad (12.9),$$

into the equation gives

$$\frac{\partial p}{\partial x} \cdot \left[1 - (\alpha \cdot \tau_{xy})^2 \right] = \eta \cdot \frac{\partial^2 u}{\partial y^2} \qquad (12.10)^{*}.$$

Assuming a pressure-viscosity coefficient of $\alpha = 2.0 \cdot 10^{-8} \cdot 1/Pa$ and *"talking down"* the shear stress to $\tau_{xy} = 10 \cdot 10^6 \cdot Pa$, Greenwood suggests that the bracket term $\left[1 - (\alpha \cdot \tau_{xy})^2 \right]$ is 0.96, which is equivalent, in equation 3.39, to a value of $k_p = 0.2$. For such small values the expected change to the ehl solution due to the extended approach is smaller than that for load case i, having a k_p value of 0.6, and is hence negligible. Higher k_p values than the above cannot appear due to the limiting shear stress concept.

Consequently, Greenwood concludes that the application of the extended approach will not have to be taken into account *"provided that other essential modifications of Newtonian theory are introduced"*, as for example the limiting shear stress assumption. This statement implies that combination of the presented extended approach with established non-Newtonian approaches will not lead to further result improvement. On the other hand, it is not ruling out the fact that the extended approach of the present work could replace the non-Newtonian approach. However such a replacement is unlikely for the following two reasons:

Firstly, as stated in chapter 11, the extended approach, at least in the investigated isothermal form, cannot contribute to any relevant improvement of the traction coefficient. Secondly, in the extended approach, the fluid properties only have influence on the pressure-viscosity coefficient. High pressure-viscosity coefficient values lead to higher values for factor k_r,

---

* Although obtained in this case with the usual approximation of the shear stress, the bracket term $\left[1 - (\alpha \cdot \tau_{xy})^2 \right]$ is the exact term, even if the accurate definition of shear stress is used [110].

$$k_r = \frac{\eta_0 \cdot \alpha \cdot e^{\alpha \cdot p_{hz}} \cdot u_H}{h_0} \cdot \gamma \qquad (12.11),$$

and to a stronger change of the results in comparison with a Reynolds equation based solution. So, high pressure-viscosity coefficient values would be needed for liquids showing a strong non-Newtonian behaviour i.e. a lower limiting shear stress. In contrast, for example in [9] or [18] the highest pressure-viscosity coefficient values at ambient conditions are reported for traction liquids, which have a rather high limiting shear stress value.

Hence at the present position of this subsection, it must be stated that the extended approach using the full Navier-Stokes equations for the ehl problem, at least in its isothermal form, is not an alternative approach or additional contribution to non-Newtonian, limiting shear stress approaches, but is rather further argument for the non-Newtonian behaviour existence.

Only if the limiting shear stress is high, a co-existence of extended approach effects and non-Newtonian effects might appear. This cannot be excluded at the moment for the above described case K1 with the traction fluid and its high pressure-viscosity dependency.

For all cases considered the pressure-viscosity coefficient shows different behaviour at higher temperatures than the above described [18] so a final statement cannot be made without a thermal analysis of the extended approach.

12.5   Thermal effects

The simplifying assumption of isothermal behaviour is discussed by considering the interaction of thermal effects and the extended approach. For the pressure-viscosity dependency, initial qualitative considerations are made for both the influence of any thermal effects on the significance of the additional terms in the extended approach and vice versa, the influence of the extended approach on the thermal results. Subsequently, both aspects are combined and a proposal is made for the development of the numerical method. Finally some quantitative aspects are considered rounding off the previous findings.

12.5.1   Qualitative influence of thermal effects

12.5.1.1   Influence of thermal effects on the relevance of the additional terms

From the qualitative point of view, the introduction of thermal considerations to the extended approach will have a similar effect as the introduction of Roelands' rather than Barus' approach in section 12.3. The thermal Roelands' equation

$$\eta = \eta_0 \cdot e^{(\ln \eta_0 + 9.67)\left(-1 + \left(1 + 5.1 \cdot 10^{-9} \cdot p\right)^Z\right) - \gamma_R \cdot \Delta \vartheta}$$

(12.12)

contains an additional term in the exponent, which implies a reduction of the exponent when the temperature rises above ambient conditions. A reduction of the exponent implies a reduced viscosity, and that causes a further reduction of the relevance of the terms of the extended approach. This results in a further reduction of the range of parameters of dimensionless speed and load, U and W, where the extended approach is relevant. The range of reduction is discussed below in subsection 12.5.2.

12.5.1.2   Influence of the additional terms on the thermal results

The need for consideration of the additional terms in the extended approach resulted from the non-dimensionalisation of the Navier-Stokes equations and the subsequent evaluation of the factors accompanying the dimensionless gradients with regard to negligibility. Non-dimensionalisation and neglecting of irrelevant terms of the generally valid thermal equation according to Schlichting [55, 56],

$$\rho \cdot \frac{\partial e}{\partial t} + p \cdot \text{div } \vec{w} = \frac{\partial}{\partial x}\left(k \cdot \frac{\partial \vartheta}{\partial x}\right) + \frac{\partial}{\partial y}\left(k \cdot \frac{\partial \vartheta}{\partial y}\right) + \frac{\partial}{\partial z}\left(k \cdot \frac{\partial \vartheta}{\partial z}\right) + \eta \cdot \Phi$$

(12.13),

where Φ represents the dissipation function

$$\Phi = 2 \cdot \left[\left(\frac{\partial u}{\partial x}\right)^2 + \left(\frac{\partial v}{\partial y}\right)^2 + \left(\frac{\partial w}{\partial z}\right)^2\right]$$

$$+ \left(\frac{\partial v}{\partial x} + \frac{\partial u}{\partial y}\right)^2 + \left(\frac{\partial w}{\partial y} + \frac{\partial v}{\partial z}\right)^2 + \left(\frac{\partial u}{\partial z} + \frac{\partial w}{\partial x}\right)^2 - \frac{2}{3} \cdot \left(\frac{\partial u}{\partial x} + \frac{\partial v}{\partial y} + \frac{\partial w}{\partial z}\right)^2$$

(12.14),

leads, as shown in appendix N, to that form of the dissipation function which is also used for Reynolds equation based solutions, for example presented by Dowson and Higginson [17],

$$\Phi = \left(\frac{\partial u}{\partial y}\right)^2$$

(12.15).

The dissipation term of equation 12.13 can also be written as

$$\eta \cdot \Phi = \eta \cdot \left(\frac{\partial u}{\partial y}\right)^2 = \tau \cdot \frac{\partial u}{\partial y}$$

(12.16).

Assuming a perfectly parallel gap for the moment, so that $\partial u/\partial y$ in $\tau \cdot \partial u/\partial y$ becomes constant at all positions, a dimensionless shear stress diagram along the gap as figure 10.22 also represents the distribution of the dissipation term along the gap. Figure 12.1 shows this distribution of shear stress and dissipation for load case iv, table 10.1, partial sliding $S = 0.5$, and the Reynolds equation based and the extended approach case. Integration of the dissipation term $\eta \cdot \Phi$ along the contact leads to the dissipative heat applied to the lubricant, which is, when neglecting conductive heat transfer into the surfaces, proportional to the temperature increase. As figure 12.1 illustrates, this dissipative heat absorbed, $\int \eta \cdot \Phi \cdot dx$ up to the point of maximum shear stress $\tau = max$, is higher for the extended approach than for the Reynolds equation based solution. This means that the temperature at the maximum shear stress position will be higher for the extended approach, and hence the maximum shear stress due to the lower temperature will be smaller. This is not only expected for this single position. Generally speaking, for the extended approach, higher shear stress appears rather in the second half of the contact where the temperatures will be higher [106]. Hence a reduction of the traction coefficient in comparison to a thermal, Reynolds equation based solution might be expected.
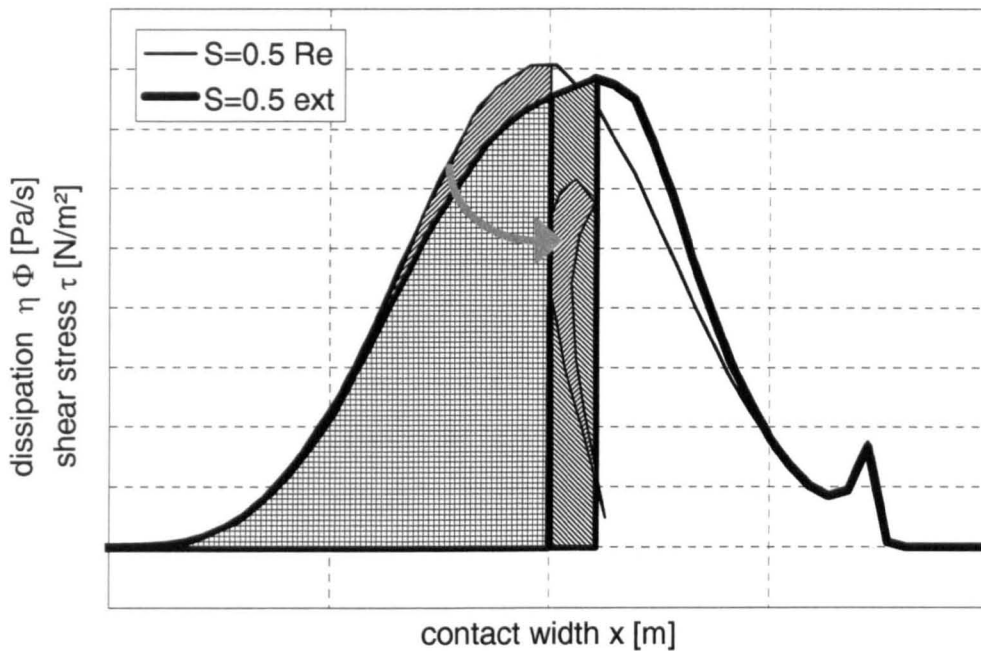
Figure 12.1:   *Qualitative dissipation and qualitative shear stress distribution for the Reynolds equation based and extended approach solution;*
load case iv (table 10.1), sliding ratio S = 0.5 .
The upwards hatched surface is shown in the downwards hatched again to simplify size comparison.

The effect described is reduced by the fact that the relevance of the extended approach is reduced by the existence of an increased temperature, and the later appearance of the maximum pressure will be smaller.

In conclusion, a thermal extended approach using the Navier-Stokes equations might have some potential to improve traction coefficient results, which were originally anticipated for the present isothermal extended approach but were not achieved.

12.5.1.3 Computational aspects of a thermal solution of the extended approach

The computation of a thermal extended approach would mean that there are two mechanisms causing a viscosity variation across the height of the gap: Firstly the extended approach with the pressure variation across the gap leads to a viscosity variation; secondly the temperature distribution across the height of the gap due to different speeds along the gap and the

consequent variation of heat conduction across the gap into the solids causes a viscosity variation across the height of the gap.

Currently, at least in Newton-Raphson techniques, the temperature distribution and hence viscosity correction across the height of the gap is mainly done in a loop superimposed on the internal loop solving the shape of the gap and the pressure distribution for a given temperature field, section 6.1.8. In contrast, pressure variation across the gap and the resulting viscosity corrections are taken into account immediately as the residuals are calculated. So the two viscosity corrections are undertaken at completely different positions of the computational procedure. This discrimination of the viscosity variation treatments requires explanation and eventual compensation.

The difference in position is because the process of finding a suitable method was driven by the idea of replacing Reynolds equation by the Navier-Stokes equations, and not by the fact that there are two potential viscosity modification features. Apparently there are two places where the viscosity variation across the gap can be unified. Incorporation of thermal aspects when analysing the flow field has already been mentioned in section 7.2, but would likely suffer from the same limitations as the method implemented.

Shifting the analyses of the pressure and viscosity variation across the gap to the superimposed loop, as is established for Newton-Raphson solutions of Reynolds equation based thermal problems, would bring the whole analysis scheme closer to established and intensively explored methods, but would still require a description of the flow which takes into account the fact that pressure varies along and across the gap. This flow equation could be a two-dimensional formulation as used for the fully simultaneous method, or perhaps a strong modification of a one-dimensional Reynolds equation going beyond Fowles' formulation [33] of a thermal Reynolds equation. Because such a method is closer to the established and better explored method, development of such a method could contribute to an expansion of the numerical borders of the present approach to a wider field of parameters and could also be used for extended isothermal analyses.

12.5.2   Quantitative influence of thermal effects

In order to quantify the relevance of the additional terms of the extended approach the development of factors k_p and k_r as used for the evaluation with Barus' and Roelands' (isothermal) pressure-viscosity description is desired. The derivation of these factors follows mainly the ideas of section 3.3 and is shown in appendix O. The thermal Roelands' equation factors, now named $\hat{k}_p$ and $\hat{k}_r$, become

$$\hat{k}_p = \frac{\eta_0 \cdot \hat{\alpha}'\left(p_{hz}, \Delta\vartheta_{max}\right) \cdot e^{\hat{\alpha}\left(p_{hz}, \Delta\vartheta_{max}\right)} \cdot u_h}{h_0}$$

$$\hat{k}_r = \frac{\eta_0 \cdot \hat{\alpha}'\left(p_{hz}, \Delta\vartheta_{max}\right) \cdot e^{\hat{\alpha}\left(p_{hz}, \Delta\vartheta_{max}\right)} \cdot u_h}{h_0} \cdot \gamma$$

$$(12.17)$$

with

$$\hat{\alpha}\left(p_{hz}, \Delta\vartheta_{max}\right) = \left(\ln\eta_0 + 9.67\right)\cdot\left[-1 + \left(1 + 5.1\cdot10^{-9}\cdot p_{hz}\right)^{Z}\right] - \gamma_R \cdot \Delta\vartheta_{max}$$ (12.18a)

and

$$\hat{\alpha}'(p_{hz}, \Delta\vartheta_{max}) = Z\cdot5.1\cdot10^{-9}\cdot\left(\ln\eta_0 + 9.67\right)\cdot\left(1 + 5.1\cdot10^{-9}\cdot p_{hz}\right)^{Z-1} - \gamma_R\frac{\Delta\vartheta_{max}}{p_{hz}}$$

$$(12.18b).$$

Equations 12.18a and b show that the relevance of the extended approach will become negligible, provided the temperature is high enough. For a realistic estimation of the relevance, knowledge of the temperature level is needed. For load cases which are required to be theoretically investigated from scratch, the temperature level is not apparent. Also for optical measurements, such as Kaneta and Nishikawa's [108] measurements for case K1 with a ball disc unit, temperature data are not available. Even for cases already investigated with regards to the temperature, such as the above-mentioned cases B1, E1, H1, and H2, it is difficult to define a correct temperature value. Considering Eller's [7] computed case E1, the temperature varies over 100 per cent between the faster surface temperature and the maximum temperature. The temperature level is overestimated since temperature reduction effects due to limiting shear stress or extended approach effects are not considered. Hence the overestimated temperature

might underestimate the significance of the extended approach. Baumann's experimental result [106] provides data for the faster surface only, and there is no information on the maximum and mean temperatures in the system, so the relevance of the extended approach might be overestimated. For Hsiao and Hamrock's [107] computed result the temperature level is again rather low because they assume limiting shear stress, which reduces dissipation and thus temperature, which leads again rather to an overestimation of the relevance. Hence a method was considered, which gives some information as to the relevance of the extended approach without knowing the contact temperature. However, it should be clear that such a method contains assumptions which will give an idea of the relevance of the extended approach. However, accurate answers can only be given by thermal numerical analysis.

The method not requiring a temperature value is based on knowledge that the traction coefficient must have realistic values, which is for simplicity assumed to be 0.1*. With the assumption that the pressure variation along the gap is a pure Hertzian elliptical distribution and that the viscosity distribution is slimmer and hence, for simplicity reasons, is assumed to be a triangular shape with maximum viscosity at the centreline and zero at the edge of the Hertzian contact, the value of the maximum viscosity, for which the given traction coefficient can be obtained, as shown in detail in appendix P[†], as

$$\eta_{max} = \frac{f \cdot p_{hz} \cdot \pi \cdot h_0}{4 \cdot S \cdot u_h} \qquad (12.19).$$

When considering this equation, it is not important as to whether this maximum viscosity value is physically existent or whether it appears for some other reason.

---

*   It is understood that real traction coefficients might differ depending on the type of the lubricant and other parameters.

†   A similar, more advanced and accurate method could be found in [112].

This value is now compared with the viscosity obtained at a certain temperature for the same Hertzian pressure, giving the viscosity ratio

$$k_\eta = \frac{\eta(p_{hz}, \Delta\vartheta_{max})}{\eta_{max}} \qquad (12.20).$$

When the viscosity ratio k_η becomes unity, viscosity due to the temperature is that which is required for a realistic traction coefficient. Figure 12.2 displays the viscosity ratio k_η versus the dimensionless pressure gradient ratio $\hat{k}_r{}^*$. Factor $\hat{k}_r$ is multiplied by the velocity gradient across the gap $\partial\overline{U}/\partial\overline{Y}$ in order to allow comparison of various sliding ratio cases. Characteristics for the selected five cases B1, E1, H1, H2, and K1, subsection 12.3.2, obtained with this method are shown.

In addition, four points are shown which can be determined for the respective cases for given temperature values, described in table 12.2.

Looking at the points, figure 12.2 shows that for case E1 and H2 the temperatures given are high enough to reduce viscosity, according to Roelands' approach, to values which are comparable with those required to give a traction coefficient estimated with equation 12.19. At the same time, pressure gradient ratio multiplied by the velocity gradient $\hat{k}_r \cdot \partial\overline{U}/\partial\overline{Y}$ is approximately 0.001, for which very small changes to the flow can be expected. Cases B1 and H1 have values of $\hat{k}_r \cdot \partial\overline{U}/\partial\overline{Y}$ close to 0.1 so changes to the flow similar to load case iv of the present study, table 10.1, can be expected. However, maximum viscosity values obtained are 10 times higher than those leading to realistic traction coefficient values.

---

* Factor $\hat{k}_r$ represents the relevance of additional terms, for the same pressure and temperature.
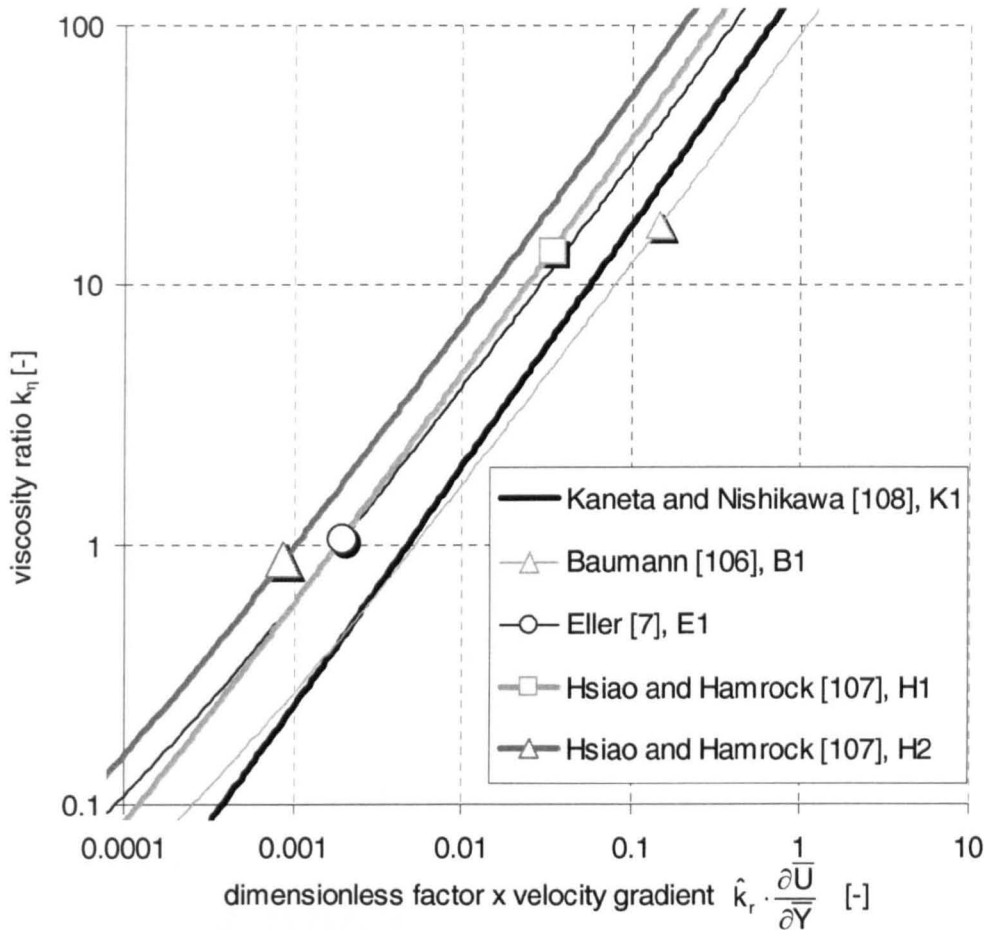
Figure 12.2:   Viscosity ratio k_η versus effective dimensionless pressure gradient ratio factor x velocity gradient $\hat{k}_r \cdot \partial\overline{U}/\partial\overline{Y}$ for various cases from published work.

With regard to the general characteristics of figure 12.2, it can be observed for all displayed cases that if viscosity ratio and hence viscosity are, for whatever reason, small enough such that realistic traction coefficients are obtained, then the pressure gradient factor multiplied by velocity gradient $\hat{k}_r \cdot \partial\overline{U}/\partial\overline{Y}$ is always smaller than 0.01. This means that the additional terms are hardly relevant and that the changes to the shape of the gap and the pressure distribution are minor. The extended approach can thus be neglected for practical applications.

On the other hand, as soon as the pressure gradient ratio (multiplied by velocity gradient) reaches values around 0.1, the dimensionless viscosity ratio has already risen to more than 10. This means that changes to the

pressure profile and the shape of the gap of the magnitude shown in chapter 10 for load case iv and partial sliding $S = 0.5$, must lead to effects which lead to a 90 per cent reduction of the traction forces on the surfaces. This is most unlikely.

The above applies to all considered cases, with also the traction liquid case K1. Here, as for E1, the required viscosity reduction is slightly milder for a given pressure gradient ratio. Hence, for the traction liquid for which a high limiting shear stress is proposed, the influence of the extended approach is slightly higher but still small and cannot contribute to the explanation of the dimple shape observed by Kaneta and Nishikawa [108].

In conclusion, not only Greenwood's statement [110], that the extended approach is negligible provided other modifications are applied to the Newtonian approach, is correct but also that modifications to the Newtonian approach are required even if the extended approach is used.

12.6 Closing remark

After theoretical discussion of the influence of some of the simplifying assumptions of chapter 3, i.e. Barus' approach, Newtonian fluid behaviour and isothermal conditions, the range of parameters computed in the present study covers, at least from the point of the dimensionless factors, most practically relevant cases. However changes to the flow in these cases are small as long as the flow is considered isothermal.

In order to achieve realistic traction coefficients, a reduction of the tangential stress acting on the surfaces of up to several orders of magnitude would be needed. This seems to be unlikely because the computed relatively small changes in flow characteristics would have to cause such a large reduction. Hence the extended approach rather underlines the need for other modifications to the Newtonian fluid assumption, such as limiting shear stress.

Chapter 13

Conclusions

13.1 Governing equations

Theoretical consideration of the Navier-Stokes equations showed that when deriving the governing equations for ehl analysis some terms are admissible, others inadmissible:

♦ Inertia forces are irrelevant for the ehl problem and hence negligible.

♦ For non pure rolling cases, additional viscous shear force terms perpendicular to the gap, appearing due to the strong viscosity gradient along the gap, must be taken into account.

→ In consequence, the pressure variation across the gap is relevant and must be taken into account for non pure rolling cases.

→ The additional viscous terms are increasingly relevant for high dimensionless load and speed parameters and high sliding ratio values.

→ The magnitude of the additionally relevant terms depends on the applied pressure-viscosity description.

→ Additional terms are irrelevant if a limiting shear stress model with a common limiting shear stress value is assumed.

13.2   Application of a general purpose software code to ehl problem

General purpose software for the solution of the Navier-Stokes equations, CFD software, was applied to the ehl problem for the first time.

◆   CFD software can be applied to solve the ehl problem.

◆   Traditional SIMPLE type pressure corrections must be replaced by e.g. a Newton-Raphson technique to achieve converged results.

◆   Analytical determination of the Jacobian matrix in the Newton-Raphson technique cannot be realised in a CFD code and hence must be substituted by numerical approximation.

   →   Numerical parameters within the CFD based solution must be carefully balanced to achieve convergence.

   →   The range of parameters, for which converging results are obtained, is reduced due to the numerical determination of the Jacobian matrix.

◆   Negative first order discretisation of the height of the gap as used in Reynolds equation cannot be realised with CFD software.

   →   Default utilisation of geometry data in CFD software is equivalent to a central discretisation scheme.

   →   A CFD based solution of the ehl problem tends to fail for the default central discretisation scheme.

   →   Grid staggering can be used to overcome fluid-structure interaction problems.

◆   Due to high analysis times, large adaptation effort and a reduced range of parameters, a CFD based solution of the ehl problem cannot compete with special purpose solutions.

13.3   Numerical techniques for an extended ehl solution

The following conclusions can be drawn for the numerical techniques and their implementation independent of the application of general purpose software or the development of special purpose software.

♦   Solution of the Navier-Stokes equations at the singularity is possible if simultaneous deflection of the shape of the gap is allowed.

♦   Newton-Raphson techniques are the most suitable to realise the solution of the extended set of equations.

♦   Various concepts are available for the solution of the extended approach: a fully simultaneous and two successive-simultaneous concepts:

  →   the fully simultaneous method requires higher computational resources but less implementation effort,

  →   the successive-simultaneous method is considerably faster but requires more implementation effort, and

  →   the successive-simultaneous method with postponed determination of the pressure variation across the gap will be of use for the thermal solution of the extended approach.

♦   Depending on the concepts, various arrangements of the governing equations can be used.

  →   The fully simultaneous method allows the solution of both momentum equations for their corresponding velocity components as implemented in standard CFD software. The continuity equation must be applied in its differential form.

  →   In the case of the successive-simultaneous method, the same integral continuity equation can be applied as for the traditional ehl problem solution. The x-momentum can be solved for the velocity along the gap but the y-momentum equation must be solved for the pressure variation across the gap.

> → Various forms of the y-momentum equations are available for the determination of the pressure variation across the gap. Depending on the form, both the implementation effort and the quality of the results can be influenced.

♦ Selection of a concept and a form of the governing equations leads to different convergence behaviour and differences with respect to the pressure spike.

♦ Additional terms of the extended approach lead to a reduction of the range of parameters, for which the ehl solution converges.

> → The iteration error of the residuals of the continuity equation increases due to the extra inner iteration of the y-momentum equation in the successive-simultaneous method.

> → The maximum pressure determining the range of parameters for which convergence is obtained, can be higher for the extended approach than for a Reynolds equation based solution of the same Hertzian pressure. Hence the range of the Hertzian pressure for which convergence is obtained is smaller.

13.4   Typical result features for an extended approach and technical relevance

Isothermal computation and discussion of the results lead to the following conclusions:

13.4.1   Pure rolling

♦ Results based on Reynolds equation and based on the extended approach are identical.

13.4.2   Partial and pure sliding

♦ The shape of the gap develops an additional constriction in the first half of the contact and develops a widening in the second half of the contact before the traditional ehl constriction.

→ If the relevance of the additional terms is small, the transition between the additional constriction and the widening is at the contact centreline and moves into the second half of the contact for increasing relevance of the terms.

→ The computed changes to the shape of the gap are too small to be of technical relevance.

♦ In the zone of the additional constriction the flow develops a forward directed Poiseuille-like component; in the zone of the widening a backward directed Poiseuille-like flow component.

♦ The mean pressure falls below Reynolds equation based solutions in the first half of the contact and rises above them in the second half of the contact.

→ The position of the maximum pressure is shifted in the second half of the contact with increasing relevance of the additional terms.

♦ A pressure difference between the slower and the faster surface of the contact develops with the pressure on the faster surface exceeding that on the slower surface in the zone of the additional constriction and vice versa in the zone of the widening.

♦ Local traction coefficient distribution changes but the integral traction coefficient shows very small changes.

→ The computed changes to the traction coefficient are to small to be of technical relevance.

♦ With the extended approach, the pressure spike is likely to disappear.

♦ A consideration of realistic pressure-viscosity approaches and incorporating thermal effects will reduce the influence of the extended approach.

♦ The extended approach cannot replace any other essential modification to a Newtonian approach, i.e. non-Newtonian behaviour.

Chapter 14

Recommendation for future work

14.1　Numerical aspects

The numerical method presented was developed to understand the influence of the extended approach on the ehl problem. It delivered results allowing many conclusions regarding the extended approach, but could not provide the numerical results for the extended approach once their influence exceeded certain limits. Hence **the re-implementation of the proposed methods in a special purpose code, and outside a general purpose CFD software** would allow **further research on the improvement of the numerical quality** of the extended approach. This would allow the obtaining of numerical results for numerical parameters beyond those which define the limit and would give a definite answer to the question of the existence of a pressure spike for the extended approach. A subsequent **extension of the method to thermal, compressible, non-Newtonian conditions** could analyse the advantage of shifting the thermal analysis into the Newton-Raphson loop as proposed in section 7 and contribute to research which is investigating the Navier-Stokes equations for rough contacts. **Application of the multigrid technique to the extended approach** would provide a further improvement of the performance of the extended approach solution, allowing a fast investigation of a wide field of parameters, fine discretisation of the contact, transient analysis and the consideration of point contacts.

14.2   Physical aspects

Although it is expected that the technical relevance of the extended approach is likely to be small for thermal conditions, once the numerical performance of the numerical methods is improved, **numerical results for the extended approach taking thermal effects and Roelands equation into account** would be an interesting completion of the present study. This is because it would give final numerical evidence for the conclusions drawn in the present study based on theoretical, one-dimensional considerations.

Chapter 15

References

[1]   Reynolds, O.:
"On the theory of lubrication and its application to Mr. Beauchamp
Tower's experiments, including an experimental determination of the
viscosity of olive oil."
Philosophical transactions of the Royal Society.
Series A, Vol. 177 (1886).
pp.157–234.

[2]   Mohrenstein-Ertel, A.:
*Die Berechnung der hydrodynamischen Schmierung gekrümmter
Oberflächen unter hoher Belastung und Relativbewegung.*
*[The analysis of the hydrodynamic lubrication of curved surfaces under
high load and relative motion.]*
VDI Fortschrittsberichte.
Series 1, No. 115.
Düsseldorf: VDI, 1984.
Originally published in Russian language by A. M. Ertel in 1945.

[3]   Grubin, A. N. and Vinogradova, J. E.:
Investigation of the contact machine components.
Book No. 30.
Moscow: Central Scientific Research Institute for Technology and
Mechanical Engineering, 1949.
D.I.S.R. Translation No. 377.

[4]   Dowson, D. and Higginson, G. R.:
"A numerical solution to the elasto-hydrodynamic problem."
Journal of mechanical engineering science.
Vol. 1 (1959).
pp. 6-15.

[5]   Bair, S., Winer, W. O., and Khonsari, M.:
        "High pressure rheology of lubricants and limitations of the Reynolds
        equation."
        New directions in tribology. Plenary and invited papers from the First
        World Tribology Congress, 8-12 September 1997.
        Edited by I. M. Hutchings.
        Bury St Edmunds: Mechanical Engineering Publications, 1997.
        pp. 21-37.

[6]   Winer, W. O. and Gwaltney, E. C.:
        "Trends and directions for tribology research and development in the
        coming years."
        Tribology 2000 plus. Conference proceedings.
        Esslingen: TAE, 2000.
        pp. 3-8.

[7]   Eller, G.:
        Ein Beitrag zur Berechnung des stationären, nichtisothermen
        elastohydrodynamischen Schmierfilms.
        [A contribution to the calculation of the steady state, non-isothermal
        elastohydrodynamic lubricating film.]
        Ph.D. thesis, TH Karlsruhe.
        Karlsruhe, 1987.

[8]   Lubrecht, A. A.:
        The numerical solution of the elastohydrodynamically lubricated line-
        and point contact problem using multigrid techniques.
        Ph.D. thesis, Universiteit Twente.
        Enschede, 1987.

[9]   Gohar, R.:
        Elastohydrodynamics.
        Chichester: Ellis Horwood, 1988.

[10]   Archard, G. D., Gair, F. C., and Hirst, W.:
        "The elastohydrodynamic lubrication of rollers."
        Proceedings of the Royal Society.
        Series A, Vol. 262 (1961).
        pp. 51-72.

[11]   Mohrenstein-Ertel, A.:
            "Hydrodynamische Theorie der Schmierung in neuen Voraussetzungen."
            ["Hydrodynamic theory of the lubrications under new conditions."]
            Zeitschrift für Angewandte Mathematik und Mechanik UdSSR.
            Vol. 3 (1939).
            Quoted in: Mohrenstein-Ertel, A.:
            *Berechnung der hydrodynamischen Schmierung gekrümmter
            Oberflächen.*
            p. 83.

[12]   Dowson, D.:
            "A generalized Reynolds equation for fluid-film lubrication."
            International journal of mechanical science.
            Vol. 4 (1962).
            pp. 159-170.

[13]   Welsch, G.:
            *Die numerische Lösung hochbelasteter, nicht-isothermer EHD-
            Linienkontakte.*
            *[The numerical solution of highly loaded, non-isothermal ehl line
            contacts.]*
            Ph.D. thesis, RWTH Aachen.
            Aachen: Shaker, 1994.

[14]   Okamura, H.:
            "A contribution to the numerical analysis of isothermal elasto-
            hydrodynamic lubrication."
            *Tribology of reciprocating engine. Proceedings of the 9th Leeds-Lyon
            symposium on tribology 1982.*
            Edited by Dowson, D. et al.
            Guildford, Surrey: Butterworths, 1983.
            pp. 313-320.

[15]   Hamrock, B. J. and Jacobson, B. O.:
            "Elastohydrodynamic lubrication of line contacts."
            ASLE Transactions.
            Vol. 27 (1984).
            pp. 275-287.

[16]   Cheng, H. S. and Sternlicht, B.:
            "A numerical solution for the pressure, temperature, and film thickness
            between two infinitely long, lubricated rolling and sliding cylinders, under
            heavy loads."
            Transactions of the ASME. Journal of basic engineering.
            Vol. 87 (1965).
            pp. 695-707.

[17]   Dowson, D. and Higginson, G. R.:
         Elasto-hydrodynamic lubrication. The fundamentals of roller and gear
         lubrication.
         Oxford: Pergamon, 1966.

[18]   Hamrock, B. J.:
         Fundamentals of fluid film lubrication.
         New York: McGraw-Hill, 1994.

[19]   Hamrock, B. J., Pan, P., and Lee, R.-T.:
         "Pressure spikes in elastohydrodynamic lubricated conjunctions."
         Transactions of the ASME. Journal of tribology.
         Vol. 110 (1988).
         pp. 279-284.

[20]   Jacobson, B. O. and Vinet, P.:
         "A model for the influence of pressure on the bulk modulus and the
         influence of temperature on the solidification pressure for liquid
         lubricants."
         Transactions of the ASME. Journal of tribology.
         Vol. 109 (1987).
         pp. 709-714.

[21]   Venner, C. H. and Bos, J.:
         "Effects of lubricant compressibility on the film thickness in ehl line and
         circular contacts."
         Wear.
         Vol. 173 (1994).
         pp. 151-165.

[22]   Barus, C.:
         "Isothermals, isopiestics and isometrics relative to viscosity."
         American journal of science.
         Series 3, Vol. 45 (1893).
         pp. 87-96.

[23]   Roelands, C. J. A.:
         Correlational aspects of the viscosity-temperature-pressure relationship
         of lubrication oils.
         Ph.D. thesis, Technische Hogeschool te Delft.
         Groningen: V. R. B., 1966.

[24]   Rodermund, H.:
         Beitrag zur elastohydrodynamischen Schmierung von Evolventen-
         zahnrädern.
         [A contribution to the elastohydrodynamic lubrication of involute gears.]
         Ph.D. thesis, TU Clausthal.
         Clausthal-Zellerfeld, 1975.

[25]   Chu, P. S. Y., and Cameron, A.:
            „Pressure-viscosity characteristics of lubrication oils."
            Journal of the Institute of Petroleum.
            Vol. 48, No. 461 (1962).
            pp. 147.

[26]   Wolff, R., Nonaka, T., Kubo, A., and Matsuo, K.:
            "Thermal elastohydrodynamic lubrication of rolling/sliding line contacts."
            Transactions of the ASME. Journal of tribology.
            Vol. 114 (1992).
            pp. 706-713.

[27]   Houpert, L. G. and Hamrock, B. J.:
            "Fast approach for calculating film thicknesses and pressures in
            elastohydrodynamically lubricated contacts at high loads."
            Transactions of the ASME. Journal of tribology.
            Vol. 108 (1986).
            pp. 411-420.

[28]   Sternlicht, B., Lewis, P., and Flynn, P.:
            "Theory of lubrication and failure of rolling contacts."
            Transactions of the ASME. Journal of basic engineering.
            Vol. 83 (1961).
            pp. 213-226.

[29]   Carslaw, H. S. and Jaeger, J. C.:
            Conduction of heat in solids.
            2nd edition.
            Oxford: Clarendon, 1959.

[30]   Lee, R.-T. and Hsu, C.-H.:
            "Advanced multilevel solution for thermal elastohydrodynamic lubrication
            of simple sliding line contacts."
            Wear.
            Vol. 171 (1994).
            pp. 227-237.

[31]   Lin, T.-R., Lin, J.-F., and Jang, J.-Y.:
            "Thermal effects in elastohydrodynamic lubrication of line contacts."
            Journal of the Chinese Society of mechanical engineers.
            Vol. 10 (1989).
            pp. 303-310.

[32]   Cheng, H. S.:
"A refined solution to the thermal-elastohydrodynamic lubrication of rolling and sliding cylinders."
ASLE Transactions.
Vol. 8 (1965).
pp.397-410.

[33]   Fowles, P. E.:
"A simpler form of the general Reynolds equation."
Transactions of the ASME. Journal of lubrication technology.
Vol. 92 (1970).
pp. 661-662.

[34]   Sui, P. C. and Sadeghi, F.:
"Non-Newtonian thermal elastohydrodynamic lubrication."
Transactions of the ASME. Journal of tribology.
Vol. 113 (1991).
pp. 390-397.

[35]   Sadeghi, F. and Dow, T. A.:
"Thermal effects in rolling/sliding contacts: Part 2 – Analysis of thermal effects in fluid film."
Transactions of the ASME. Journal of tribology. Preprints.
Paper No. 86-Trib-38 (1986).
pp. 1-6.

[36]   Liesegang, R.:
Der nichtisotherme hydrodynamische Schmierfilm zwischen hochbelasteten elastischen Walzen.
[The non-isothermal hydrodynamic lubrication film between highly loaded elastic rollers.]
Ph.D. thesis, TH Karlsruhe.
Karlsruhe, 1967.

[37]   Brüggemann, H. and Kollmann, F. G.:
"A numerical solution of the thermal elastohydrodynamic lubrication in an elliptical contact."
Transactions of the ASME. Journal of lubrication technology.
Vol. 104 (1982).
pp. 392-400.

[38]   Crook, A. W.:
"The lubrication of rollers – Part VI: Measurements of friction and effective viscosity."
Philosophical transactions of the Royal Society.
Series A, Vol. 255 (1963).
pp. 281-312.

[39]   Eyring, H.:
            "Viscosity, plasticity and diffusion as examples of absolute reaction
            rates."
            Journal of Chemical Physics.
            Vol. 4 (1936).
            pp. 283-291.

[40]   Houpert, L. G. and Hamrock, B. J.:
            "Elastohydrodynamic lubrication calculations used as a tool to study
            scuffing."
            *Mechanisms and surface distress. Global studies of mechanisms and
            local analyses of surface distress phenomena. Proceedings of the 12th
            Leeds-Lyon symposium on Tribology 1985.*
            London: Butterworths, 1986.
            pp. 1-17.

[41]   Wang, S. H., Hua, D. Y., and Zhang, H. H.:
            "A full numerical ehl solution for line contacts under pure rolling condition
            with a non-Newtonian rheological model."
            Transactions of the ASME. Journal of tribology.
            Vol. 110 (1988).
            pp. 583-586.

[42]   Lin, T.-R. and Lin, J.-F.:
            "Compressible elastohydrodynamic lubrication of rolling and sliding
            contacts with a power law fluid."
            Wear.
            Vol. 142 (1991).
            pp. 315-330.

[43]   Elsharkawy, A. A. and Hamrock, B. J.:
            "Subsurface stresses in micro-ehl line contacts."
            Transactions of the ASME. Journal of tribology.
            Vol. 113 (1991).
            pp. 645-656.

[44]   Johnson, K. L. and Tevaarwerk, J. L.:
            "Shear behaviour of ehd oil films."
            Proceedings of the Royal Society.
            Series A, Vol. 356 (1977).
            pp. 215-236.

[45]   Bair, S. and Winer, W. O.:
            "A rheological model for elastohydrodynamic contacts based on primary
            laboratory data."
            Transactions of the ASME. Journal of lubrication technology.
            Vol. 101 (1979).
            pp. 258-265.

[46]   Iivonen, H. and Hamrock, B. J.:
         "A new non-Newtonian fluid model for elastohydrodynamic lubrication of
         rectangular contacts."
         Wear.
         Vol. 143 (1991).
         pp. 297-305.

[47]   Conry, T. F., Wang, S., and Cusano, C.:
         "A Reynolds-Eyring equation for elastohydrodynamic lubrication in line
         contacts."
         Transactions of the ASME. Journal of tribology.
         Vol. 109 (1987).
         pp. 648-658.

[48]   Lee, R.-T. and Hamrock, B. J.:
         "A circular non-Newtonian fluid model: Part I – Used in
         elastohydrodynamic lubrication."
         Transactions of the ASME. Journal of tribology. Preprints.
         Paper No. 89-Trib-9 (1989).
         pp. 1-10.

[49]   Hughes, G. D. and Bush, A. W.:
         "An average Reynolds equation for non-Newtonian fluids in ehl line
         contacts."
         Transactions of the ASME. Journal of tribology.
         Vol. 115 (1993).
         pp. 666-669.

[50]   Salehizadeh, H. and Saka, N.:
         „Thermal non-Newtonian elastohydrodynamic lubrication of rolling line
         contacts."
         Transactions of the ASME. Journal of tribology.
         Vol. 113 (1991).
         pp. 481-491.

[51]   Wang, S., Cusano, C., and Conry, T. F.:
         "Thermal analysis of elastohydrodynamic lubrication of line contacts
         using the Ree-Eyring fluid model."
         Transactions of the ASME. Journal of tribology.
         Vol. 113 (1991).
         pp. 232-244.

[52]   Peiran, Y. and Shizhu, W.:
         "A generalized Reynolds equation for non-Newtonian thermal
         elastohydrodynamic lubrication."
         Transactions of the ASME. Journal of tribology.
         Vol. 112 (1990).
         pp. 631-636.

[53]   Almqvist, T. and Larsson, R.:
         "Comparison of Reynolds and Navier-Stokes approaches for solving
         isothermal ehl line contacts."
         Abstracts, papers, posters from the World Tribology Congress,
         3-7 September 2001.
         CD-Rom edition.
         Wien: ÖTG, 2001.

[54]   Almqvist, T. and Larsson, R.:
         "The Navier-Stokes approach for thermal ehl line contact solutions."
         Tribology international.
         Vol. 35 (2002).
         pp. 163-170.

[55]   Schlichting, H.:
         Grenzschicht-Theorie.
         [Boundary-layer theory.]
         5th edition.
         Karlsruhe: Braun, 1964.

[56]   Schlichting, H.:
         Boundary-layer theory.
         6th edition.
         New York: McGraw-Hill, 1968.

[57]   Zierep, J.:
         Grundzüge der Strömungslehre.
         [Fundamentals of fluid dynamics.]
         4th, revised edition.
         Karlsruhe: Braun, 1990.

[58]   Szabó, I.:
         Höhere technische Mechanik.
         [Advanced mechanical principles.]
         3rd edition.
         Berlin: Springer, 1960.

[59]   *Dubbel – Taschenbuch für den Maschinenbau.*
         [Dubbel – Mechanical engineering handbook.]
         Edited by Beitz, W. and Küttner, K.-H.
         14th, fully revised and enlarged edition.
         Berlin: Springer, 1981.

[60]   Wilson, A. R.:
         "An experimental thermal correction for predicted oil film thickness in
         elastohydrodynamic contacts".
         *Thermal effects in tribology. Proceedings of the 6th Leeds-Lyon
         symposium on tribology 1979.*
         Edited by Dowson, D. et al.
         London: Mechanical Engineering Publications, 1980.
         pp. 179-190.

[61]   Greenwood, J. A. and Kauzlarich, J. J.:
         "Inlet shear heating in elastohydrodynamic lubrication."
         Transactions of the ASME. Journal of lubrication technology.
         Vol. 95 (1973).
         pp. 417-426.

[62]   Murch, L. E. and Wilson, W. R. D.:
         "A thermal elastohydrodynamic inlet zone analysis."
         Transactions of the ASME. Journal of lubrication technology.
         Vol. 97 (1975).
         pp. 212-216.

[63]   Dowson, D. and Whitaker, A. V.:
         "A numerical procedure for the solution of the elastohydrodynamic
         problem of rolling and sliding contacts lubricated by a Newtonian fluid."
         *Elastohydrodynamic lubrication. A symposium arranged by the
         lubrication and wear group, 1965.*
         Proceedings of the Institution of Mechanical Engineers.
         Vol. 180, part 3B (1965-66).
         pp. 57-71.

[64]   Pan, P. and Hamrock, B. J.:
         "Simple formulas for performance parameters used in
         elastohydrodynamically lubricated line contacts."
         Transactions of the ASME. Journal of tribology.
         Vol. 111 (1989).
         pp. 246-251.

[65]   Hamrock, B. J. and Tripp, J. H.:
         "Numerical methods and computers used in elastohydrodynamic
         lubrication."
         *Developments in numerical and experimental methods applied to
         tribology. Proceedings of the 10th Leeds-Lyon-Symposium on tribology
         1983.*
         Edited by Dowson, D. et al.
         London: Butterworths, 1984.
         pp. 11-19.

[66]   Christensen, H.:
            "A simplified model of elastohydrodynamic lubrication of rollers – The
            central and exit solution."
            ASLE Transactions.
            Vol. 22 (1979).
            pp. 323-332.

[67]   Wallinger, M.:
            Zur Berechnung von Schmierfilmdicke und Reibung in Evolventen-
            verzahnungen mittels der elastohydrodynamischen Theorie.
            [On the analysis of the film thickness and friction in involute tooth
            systems using the elastohydrodynamic theory.]
            Ph.D. thesis, TU Clausthal.
            Clausthal-Zellerfeld: 1983.

[68]   Potthoff, H.:
            Anwendungsgrenzen vollrolliger Planetenrad-Wälzlager.
            [The limits of the application of full complementary roller bearings.]
            Ph.D. thesis, Ruhr-Universität, Bochum.
            Schriftenreihe, Heft 86.3.
            Bochum: Ruhr Universität, Fakultät für Maschinenbau, Institut für
            Konstruktionstechnik, 1986.

[69]   Weber, C. and Saalfeld, K.:
            "Schmierfilm bei Walzen mit Verformung."
            [„Lubrication film for rollers with deflection."]
            Zeitschrift für angewandte Mathematik und Mechanik.
            Vol. 34 (1954).
            pp. 54-64.

[70]   Hamrock, B. J. and Dowson, D.:
            Ball bearing lubrication. The elastohydrodynamics of elliptical contacts.
            New York: John Wiley & Sons, 1981.

[71]   Chittenden R. J., Dowson, D., Dunn, J. F. and Taylor, C.M.:
            "A theoretical analysis of the isothermal elastohydrodynamic lubrication
            of concentrated contacts. I. Direction of lubricant entrainment coincident
            with the major axis of the Hertzian contact ellipse.
            Proceedings of the Royal Society.
            Series A, Vol. 397 (1985).
            pp. 245-269.

[72]   Evans, H. P. and Snidle, R. W.:
            "The isothermal elastohydrodynamic lubrication of spheres".
            Transactions of the ASME. Journal of lubrication technology.
            Vol. 103 (1981).
            pp. 547-557.

[73]   Seabra, J. and Berthe, D.:
            "Elastohydrodynamic point contacts part I: formulation and numerical
            solution".
            Wear.
            Vol. 130 (1989).
            pp. 301-318.

[74]   Evans, H. P. and Snidle, R. W.:
            „Inverse solution of Reynolds' equation of lubrication under point-contact
            elastohydrodynamic conditions."
            Transactions of the ASME. Journal of lubrication technology.
            Vol. 103 (1981).
            pp. 539-546.

[75]   Hou, K. P., Zhu, D., and Wen, S. Z.:
            "An inverse solution to the point contact ehl problem under heavy loads."
            Transactions of the ASME. Journal of Tribology.
            Vol. 109 (1987).
            pp. 432-436.

[76]   Press, W.H., Teukolsky, S. A., Vetterling, W. T., and Flannery, B. P.:
            Numerical recipes in Fortran. The Art of Scientific Computing.
            Second Edition.
            Cambridge: Cambridge University Press, 1992.

[77]   Chang, L., Conry, T. F., and Cusano, C.:
            "An efficient, robust, multi-level computational algorithm for
            elastohydrodynamic lubrication."
            Transactions of the ASME. Journal of tribology.
            Vol. 111 (1989).
            pp. 193-199.

[78]   Kostreva, M. M.:
            „Pressure spikes and stability considerations in elastohydrodynamic
            lubrication models."
            Transactions of the ASME. Journal of tribology.
            Vol. 106 (1984).
            pp. 386-395.

[79]   Lubrecht, A. A., ten Napel, W. E., and Bosma, R.:
            „Multigrid, an alternative method for calculating film thickness and
            pressure profiles in elastohydrodynamically lubricated line contacts."
            Transactions of the ASME. Journal of tribology.
            Vol. 108 (1986).
            pp. 551-556.

[80]   Čermák, J.:
         "A control volume based discretization of the Reynolds equation for the
         numerical solution of elastohydrodynamic lubrication problems."
         International journal for numerical methods in fluids.
         Vol. 26 (1998).
         pp. 977-986.

[81]   Čermák, J.:
         "A non-symmetric discretization formula for the numerical solution of the
         ehl circular contact problem."
         Tribology international.
         Vol. 31 (1998).
         pp. 761-765.

[82]   Venner, C. H., ten Napel, W. E., and Bosma, R.:
         „Advanced multilevel solution of the ehl line contact problem."
         Transactions of the ASME. Journal of tribology.
         Vol. 112 (1990).
         pp. 426-432.

[83]   Ghosh, M. K. and Hamrock, B. J.:
         "Thermal elastohydrodynamic lubrication of line contacts."
         ASLE Transactions.
         Vol. 28 (1985).
         pp. 159-171.

[84]   Sadeghi, F. and Sui, P. C.:
         "Thermal elastohydrodynamic lubrication of rolling/sliding contacts."
         Transactions of the ASME. Journal of tribology.
         Vol. 112 (1990).
         pp. 189-195.

[85]   Roache, P. R.:
         Computational fluid dynamics.
         5th edition.
         Albuquerque, N. M.: Hermosa, 1982.

[86]   Giese, P.:
         *Untersuchungen zum hydrostatischen Käfig und zur Bordtragfähigkeit
         von Zylinderrollenlagern.*
         *[Investigations of hydrostatic cages and of the axial capacity of
         cylindrical roller bearings.]*
         Ph.D. thesis, TH Karlsruhe.
         Karlsruhe: 1985.

[87]   Steck, E., Schilling, R. and Flesch, K.O.:
            „Numerische Untersuchungen über die Genauigkeit und Schnelligkeit
            verschiedener Differenzenverfahren am Beispiel der Berechnung der
            zweidimensionalen Kanaleinlaufströmung mit Wärmeübergang."
            [„Numerical investigation of the accuracy and velocity of various finite
            difference schemes by consideration of a two-dimensional inlet flow with
            heat transfer."]
            Strömungsmechanik and Strömungsmaschinen.
            Vol. 28/80 (1980).
            pp. 1-23.

[88]   Patankar, S. V. and Spalding, D. B.:
            "A calculation procedure for heat, mass and momentum transfer in
            three-dimensional parabolic flows."
            International journal of heat and mass transfer.
            Vol. 15 (1972).
            pp. 1787-1806.

[89]   Patankar, S. V.:
            Numerical heat transfer and fluid flow.
            New York: Hemisphere, 1980.

[90]   Versteeg, H. K. and Malalasekera, W.:
            *An introduction to computational fluid dynamics. The finite volume
            method.*
            Harlow: Longman, 1995.

[91]   *CFX-4.2.*
            Software and manuals.
            Harwell: CFX International, 1997.

[92]   *CFX-5.6.*
            Software and manuals.
            Harwell: CFX, 2003.

[93]   *Fluent 6.0.*
            Software and user's guide.
            Lebanon: Fluent, 2001.

[94]   *Star CD 2.21.*
            Software and manuals.
            London: CD-adapco, 1995.

[95]   Rhie, C. M. and Chow, W. L.:
            "Numerical study of the turbulent flow past an airfoil with trailing edge
            separation."
            AIAA [American institute of aeronautics and astronautics] journal.
            Vol. 21 (1983).
            pp. 1527-1532.

[96]   Gärtner, A., Rettweiler P. and van de Sand, A.:
            „Auslegung von Fahrwerkssystemen durch Co-Simulation von MKS- und
            Fluidsimulationssoftware."
            ["Chassis design analysis using co-simulation of multi body dynamics
            and flow analysis software."]
            9. Aachener Kolloquium Fahrzeug- und Motorentechnik.
            [9th Aachen colloquium on vehicle and engine engineering.]
            Aachen: Institut für Kraftfahrtwesen, 2000.

[97]   Ramos, A.:
            2-d simulation of the motion of oil inside a shock-absorber.
            Extract of Ph.D. thesis, Ecole Nationale Supérieure d'Ingénieurs en
            Mécanique Energétique de Valenciennes ENSIMEV.
            Graz: AVL List, 1994.

[98]   Cabrera, D.:
            *An investigation into the operation of water-lubricated rubber journal
            bearings.*
            Ph.D. thesis, Liverpool John Moores University.
            Liverpool: 2003.

[99]   Penrose, J. and Kuntz, M.:
            "Fluid-structure interaction: From biomedicine to boats."
            Papers of the European CFX Conference, Strasbourg 2002.
            CD-ROM edition.
            Otterfing: CFX-Germany, 2002.

[100]   *NAG C Library, Mark 3.*
            "CLDO0203DM".
            Software and user manuals.
            Vol. 1-3.
            Oxford: NAG, 1995.

[101]   *IMSL Math/Library. Fortran subroutines for mathematical applications.*
            Software and user manuals.
            Version 2.0, September 1991.
            Houston: IMSL, 1991.

[102]   Bronstein, I. N. and Semendjajew, K. A.:
         Taschenbuch der Mathematik.
         [Mathematics handbook.]
         25th, revised edition.
         Stuttgart: Teubner, 1991.

[103]   Peric, M.:
         "Randbedingungen und Genauigkeitsfragen."
         ["Boundary conditions and accuracy issues."]
         NUMET '96 – Numerische Methoden zur Berechnung von Strömungs-
         und Wärmeübergangsproblemen.
         [NUMET '96 - Numerical methods for the calculation of fluid flow and
         heat transfer problems.]
         Edited by Franz Durst.
         Erlangen: Universität Erlangen-Nürnberg, 1996.
         pp. 1/9-34/9.

[104]   Bakolas, V. and Poulios, K.:
         TEHD 2-d. Two-dimensional simulation of lubricated contacts.
         Internal report No. A-040025-02-11-03.
         Herzogenaurach, INA-Schaeffler, 2003.
         Publically not available.

[105]   *DIN ISO 281 Beiblatt 4.*
         Rolling bearings. Dynamic load rating and rating life. Methods for
         calculation of the modified reference rating life for universally loaded
         rolling bearings.
         Berlin: DIN, 2003.

[106]   Baumann, H.:
         Druck- und Temperaturmessungen mittels aufgedampfter
         Dünnschichtaufnehmer in einem elastohydrodynamischen Linienkontakt.
         [Pressure and temperature measurement in the elastohydrodynamic line
         contact using sputtered thin layer sensors.]
         Ph.D. thesis, TU Karlsruhe.
         Karlsruhe: 1985.

[107]   Hsiao, H.-S. S. and Hamrock, B. J.:
         "A complete solution for thermal-elastohydrodynamic lubrication of line
         contacts using circular non-Newtonian fluid model."
         Transactions of the ASME. Journal of tribology.
         Vol. 114 (1992).
         pp. 540-552.

[108]   Kaneta, M. and Nishikawa, H.:
         "Formation of dimples in elliptical ehl contacts."
         Thinning films and tribological interfaces. Proceedings of the 26th Leeds-
         Lyon symposium on tribology 1999.
         Edited by Dowson, D. et al.
         Amsterdam: Elsevier, 2000.
         pp. 599-607.

[109]   *Personal discussion with Prof. M. Kaneta at the 26th Leeds-Lyon*
         symposium on tribology 1999.
         17th September 1999.
         Leeds, 1999.

[110]   Greenwood, J. A.:
         "Written discussion - contributions on 'Elastohydrodynamically lubricated
         line contact based on the Navier-Stokes equations'."
         Thinning films and tribological interfaces. Proceedings of the 26th Leeds-
         Lyon symposium on tribology 1999.
         Edited by Dowson, D. et al.
         Amsterdam: Elsevier, 2000.
         pp. 793-794.

[111]   Schäfer, C. T., Giese, P., Rowe, W. B., and Woolley, N. H.:
         "Elastohydrodynamically lubricated line contact based on the Navier-
         Stokes equations."
         Thinning films and tribological interfaces. Proceedings of the 26th Leeds-
         Lyon-Symposium on tribology 1999.
         Edited by Dowson, D. et al.
         Amsterdam: Elsevier, 2000.
         pp. 57-69.

[112]   Schouten, M. J. W. and Leeuwen van, H. J.:
         "Die Elastohydrodynamik: Geschichte und Neuentwicklungen."
         ["Elastohydrodynamics: history and current developments."]
         Gleitwälzkontakte. Grundlagen und Stand der Technik bei Wälzlagern,
         Zahnrädern und Nockenstößeln sowie stufenlos übersetzenden
         Getrieben.
         [Sliding and rolling contacts. Fundamentals and state of the art in rolling
         bearings, involute gears, cam-tappets contacts and continuously
         variable transmissions.]
         VDI-Berichte 1207.
         Düsseldorf: VDI, 1995.
         pp. 1-47.

Appendices

Appendix A

Details of Reynolds number determination

Derivation of Reynolds number written in dimensional parameters, equation 3.28b, or in dimensionless ehl parameters, equation 3.28c, follows the subsequent procedure, shown in more detail than in section 3.1.

In the definition of Reynolds number, equation 3.23c,

$$Re = \gamma \cdot \frac{\rho_0 \cdot u_h \cdot h_0}{\eta_0} \qquad (A.1)$$

the definition of the geometrical ratio, equation 3.21,

$$\gamma = \frac{h_0}{b_{hz}} \qquad (A.2)$$

is introduced and Reynolds number becomes

$$Re = \frac{\rho_0 \cdot u_h \cdot h_0{}^2}{\eta_0 \cdot b_{hz}} \qquad (A.3).$$

The introduction of the description of the Hertzian width b_{hz} by the Hertzian pressure p_{hz}, equation 3.24a,

$$b_{hz} = 4 \cdot p_{hz} \cdot \frac{r_{red}}{E'} \qquad (A.4),$$

gives for the Reynolds number

$$Re = \frac{\rho_0 \cdot u_h \cdot h_0{}^2 \cdot E'}{4 \cdot \eta_0 \cdot p_{hz} \cdot r_{red}} \qquad (A.5).$$

Replacing the central height of the gap by its definition, equation 3.26,

$$h_0 = 1.9 \cdot G^{0.6} \cdot U^{0.7} \cdot W^{-0.13} \cdot r_{red} \tag{A.7}$$

leads for the Reynolds number to

$$Re = \frac{\rho_0 \cdot u_h \cdot \left(1.9 \cdot G^{0.6} \cdot U^{0.7} \cdot W^{-0.13} \cdot r_{red}\right)^2 \cdot E'}{4 \cdot \eta_0 \cdot p_{hz} \cdot r_{red}} \tag{A.8a},$$

which can be written as

$$Re = \frac{3.61 \cdot \rho_0 \cdot u_h \cdot E' \cdot G^{1.2} \cdot U^{1.4} \cdot W^{-0.26} \cdot r_{red}}{4 \cdot \eta_0 \cdot p_{hz}} \tag{A.8b}.$$

Introduction of the definitions of the dimensionless parameters, equation 3.25,

$$W = \frac{2 \cdot \pi \cdot p_{hz}^2}{E'^2} \tag{A.9a},$$

$$U = \frac{\eta_0 \cdot u_h}{E' \cdot r_{red}} \tag{A.9b},$$

and

$$G = E' \cdot \alpha \tag{A.9c}$$

gives

$$Re = \frac{3.61 \cdot \rho_0 \cdot u_h \cdot E' \cdot \left(E' \cdot \alpha\right)^{1.2} \cdot \left(\dfrac{\eta_0 \cdot u_h}{E' \cdot r_{red}}\right)^{1.4} \cdot \left(\dfrac{2 \cdot \pi \cdot p_{hz}^2}{E'^2}\right)^{-0.26} \cdot r_{red}}{4 \cdot \eta_0 \cdot p_{hz}}$$

$$\tag{A.10a},$$

which can be reduced to equation 3.28b

$$Re = \frac{0.56 \cdot \rho_0 \cdot u_h^{2.4} \cdot E'^{1.32} \cdot \eta_0^{0.4} \cdot \alpha^{1.2}}{p_{hz}^{1.52} \cdot r_{red}^{0.4}} \tag{A.10b}.$$

Rearranging the definition of load parameter W for Hertzian pressure p_{hz} gives

$$p_{hz} = \frac{W^{0.5} \cdot E'}{\sqrt{2 \cdot \pi}} \tag{A.11a},$$

and that of the speed parameter U for the viscosity at ambient conditions η_0,

$$\eta_0 = \frac{U \cdot E' \cdot r_{red}}{u_h}$$ (A.11b).

Substitution into equation A.8b leads to

$$Re = \frac{3.61 \cdot \rho_0 \cdot u_h \cdot E' \cdot G^{1.2} \cdot U^{1.4} \cdot W^{-0.26} \cdot r_{red}}{4} \cdot \frac{u_h}{U \cdot E' \cdot r_{red}} \cdot \frac{\sqrt{2 \cdot \pi}}{W^{0.5} \cdot E' \cdot}$$

(A.12a)

which can be simplified to equation 3.28c

$$Re = 2.26 \cdot \frac{\rho_0 \cdot u_h^2}{E'} \cdot G^{1.2} \cdot U^{0.4} \cdot W^{-0.76}$$ (A.12b).

Appendix B

Determination of the maximum Reynolds number

Reynolds number is determined by the equation 3.28b

$$Re = 0.56 \cdot p_{hz}^{-1.52} \cdot r_{red}^{-0.4} \cdot u_h^{2.4} \cdot E'^{1.32} \cdot \alpha^{1.2} \cdot \eta^{0.4} \cdot \rho_0 \qquad (B.1),$$

in which the variables range between the limits shown in table B.1:

Hertzian pressure	$p_{hz} = 0.1...4.0$ GPa
reduced radius	$r_{red} = 0.0002...0.1$ m
hydrodynamic speed	$u_h = (0.0)...0.2...20$ $m \cdot s^{-1}$
reduced Young's modulus	$E' = 2.27 \cdot 10^5$ $N \cdot mm^{-2}$
pressure-viscosity coefficient	$\alpha = 2.18 \cdot 10^{-8}$ Pa^{-1}
viscosity	$\eta_0 = 0.002...0.5$ $Pa \cdot s$
density	$\rho = 870$ $kg \cdot m^{-3}$

Table B.1:   Range of parameters for Reynolds number calculation.

There are no local maxima within the domain of definition since none of the partial derivatives can become zero in the domain. Therefore, the maximum of the function must be at the edge of the domain. The maximum value is obtained if the variables with a positive exponent take their maximum value and those with negative exponents their minimum. The maximum Reynolds number is

$$Re_{max} = 6.4 \qquad (B.2)$$

However, the dimensionless parameters U and W of the above Reynolds number suggest that rigid hydrodynamic theory must be applied, whereby the definition of Reynolds number B.1 is not valid. The condition for elastohydrodynamic lubrication is

$$W \geq 0.017 \cdot U^{0.325} \qquad \text{(B.3a)}.$$

Equation B.3a can be rewritten as

$$W = k \cdot 0.017 \cdot U^{0.325} \qquad \text{(B.3b)}$$

with $\qquad\qquad\qquad k \geq 1$.

The definition of the dimensionless parameters W and U, equation 3.25, is introduced in equation B.3b, and the equation is solved for any of the variables, e.g. the Hertzian pressure p_{hz},

$$p_{hz} = k^{0.5} \cdot 0.052 \cdot \eta_0^{0.5} \cdot u_h^{0.5} \cdot r_{red}^{-0.5} \cdot E^{0.838} \qquad \text{(B.4)}$$

Substituting equation B.4 into equation B.1 leads to

$$Re = 50 \cdot \frac{u_h^{2.153} \cdot E'^{0.047} \cdot \alpha^{1.2} \cdot \eta^{0.153} \cdot \rho}{k^{0.76} \cdot r_{red}^{0.153}} \qquad \text{(B.5)}.$$

As in equation B.1, the new definition of Reynolds number does not contain any local maximum within the domain of definition. The absolute maximum appears at the border of the domain. Again, using maximum values for variables in the numerator and minimum values for those in the denominator, the maximum Reynolds number is

$$Re_{max,ehd} = 0.2 \qquad \text{(B.6)}.$$

Appendix C

Details of the derivation of the viscous terms significance

The present appendix aims to give more details of the derivation to determine the significance of the individual viscous terms of the Navier Stokes equation than is included in section 3.3.

C.1   Non-dimensional form of Navier-Stokes equations

(corresponding to section 3.3.1)

Governing equations are the incompressible, two-dimensional Navier-Stokes equations 3.15,

$$\left.\begin{array}{l} \rho \cdot \left(u \cdot \dfrac{\partial u}{\partial x} + v \cdot \dfrac{\partial u}{\partial y} \right) = -\dfrac{\partial p}{\partial x} + 2 \cdot \dfrac{\partial}{\partial x}\left[\eta \cdot \dfrac{\partial u}{\partial x} \right] + \dfrac{\partial}{\partial y}\left[\eta \cdot \left(\dfrac{\partial u}{\partial y} + \dfrac{\partial v}{\partial x} \right) \right] \\[4mm] \rho \cdot \left(u \cdot \dfrac{\partial v}{\partial x} + v \cdot \dfrac{\partial v}{\partial y} \right) = -\dfrac{\partial p}{\partial y} + 2 \cdot \dfrac{\partial}{\partial y}\left[\eta \cdot \dfrac{\partial v}{\partial y} \right] + \dfrac{\partial}{\partial x}\left[\eta \cdot \left(\dfrac{\partial u}{\partial y} + \dfrac{\partial v}{\partial x} \right) \right] \end{array}\right\} \quad \text{(C.1).}$$

Neglecting the inertia terms gives

$$\left.\begin{array}{l} 0 = -\dfrac{\partial p}{\partial x} + 2 \cdot \dfrac{\partial}{\partial x}\left[\eta \cdot \dfrac{\partial u}{\partial x} \right] + \dfrac{\partial}{\partial y}\left[\eta \cdot \left(\dfrac{\partial u}{\partial y} + \dfrac{\partial v}{\partial x} \right) \right] \\[4mm] 0 = -\dfrac{\partial p}{\partial y} + 2 \cdot \dfrac{\partial}{\partial y}\left[\eta \cdot \dfrac{\partial v}{\partial y} \right] + \dfrac{\partial}{\partial x}\left[\eta \cdot \left(\dfrac{\partial u}{\partial y} + \dfrac{\partial v}{\partial x} \right) \right] \end{array}\right\} \quad \text{(C.2).}$$

Differentiation of the products gives

$$
\left.
\begin{aligned}
0 = &-\frac{\partial p}{\partial x} + 2\cdot\eta\cdot\frac{\partial^2 u}{\partial x^2} + 2\cdot\frac{\partial\eta}{\partial x}\cdot\frac{\partial u}{\partial x} \\
&+ \eta\cdot\frac{\partial^2 u}{\partial y^2} + \frac{\partial\eta}{\partial y}\cdot\frac{\partial u}{\partial y} + \eta\cdot\frac{\partial^2 v}{\partial x\partial y} + \frac{\partial\eta}{\partial y}\cdot\frac{\partial v}{\partial x} \\
0 = &-\frac{\partial p}{\partial y} + 2\cdot\eta\cdot\frac{\partial^2 v}{\partial y^2} + 2\cdot\frac{\partial\eta}{\partial y}\cdot\frac{\partial v}{\partial y} \\
&+ \eta\cdot\frac{\partial^2 u}{\partial x\partial y} + \frac{\partial\eta}{\partial x}\cdot\frac{\partial u}{\partial y} + \eta\cdot\frac{\partial^2 v}{\partial x^2} + \frac{\partial\eta}{\partial x}\cdot\frac{\partial v}{\partial x}
\end{aligned}
\right\}
\quad\text{(C.3).}
$$

Introduction of Barus' pressure-viscosity description, equation 3.18a, gives

$$
\left.
\begin{aligned}
0 = &-\frac{\partial p}{\partial x} + 2\cdot\eta_0\cdot e^{\alpha\cdot p}\cdot\frac{\partial^2 u}{\partial x^2} + 2\cdot\frac{\partial\eta_0\cdot e^{\alpha\cdot p}}{\partial x}\cdot\frac{\partial u}{\partial x} \\
&+ \eta_0\cdot e^{\alpha\cdot p}\cdot\frac{\partial^2 u}{\partial y^2} + \frac{\partial\eta_0\cdot e^{\alpha\cdot p}}{\partial y}\cdot\frac{\partial u}{\partial y} + \eta_0\cdot e^{\alpha\cdot p}\cdot\frac{\partial^2 v}{\partial x\partial y} + \frac{\partial\eta_0\cdot e^{\alpha\cdot p}}{\partial y}\cdot\frac{\partial v}{\partial x} \\
0 = &-\frac{\partial p}{\partial y} + 2\cdot\eta_0\cdot e^{\alpha\cdot p}\cdot\frac{\partial^2 v}{\partial y^2} + 2\cdot\frac{\partial\eta_0\cdot e^{\alpha\cdot p}}{\partial y}\cdot\frac{\partial v}{\partial y} \\
&+ \eta_0\cdot e^{\alpha\cdot p}\cdot\frac{\partial^2 u}{\partial x\partial y} + \frac{\partial\eta_0\cdot e^{\alpha\cdot p}}{\partial x}\cdot\frac{\partial u}{\partial y} + \eta_0\cdot e^{\alpha\cdot p}\cdot\frac{\partial^2 v}{\partial x^2} + \frac{\partial\eta_0\cdot e^{\alpha\cdot p}}{\partial x}\cdot\frac{\partial v}{\partial x}
\end{aligned}
\right\}
\quad\text{(C.4).}
$$

Differentiation of the products introduced by Barus' equation leads to

$$
\left.
\begin{aligned}
0 = &-\frac{\partial p}{\partial x} + 2\cdot\eta_0\cdot e^{\alpha\cdot p}\cdot\frac{\partial^2 u}{\partial x^2} + 2\cdot\eta_0\cdot e^{\alpha\cdot p}\cdot\alpha\cdot\frac{\partial p}{\partial x}\cdot\frac{\partial u}{\partial x} \\
&+ \eta_0\cdot e^{\alpha\cdot p}\cdot\frac{\partial^2 u}{\partial y^2} + \eta_0\cdot e^{\alpha\cdot p}\cdot\alpha\cdot\frac{\partial p}{\partial y}\cdot\frac{\partial u}{\partial y} \\
&+ \eta_0\cdot e^{\alpha\cdot p}\cdot\frac{\partial^2 v}{\partial x\partial y} + \eta_0\cdot e^{\alpha\cdot p}\cdot\alpha\cdot\frac{\partial p}{\partial y}\cdot\frac{\partial v}{\partial x} \\
0 = &-\frac{\partial p}{\partial y} + 2\cdot\eta_0\cdot e^{\alpha\cdot p}\cdot\frac{\partial^2 v}{\partial y^2} + 2\cdot\eta_0\cdot e^{\alpha\cdot p}\cdot\alpha\cdot\frac{\partial p}{\partial y}\cdot\frac{\partial v}{\partial y} \\
&+ \eta_0\cdot e^{\alpha\cdot p}\cdot\frac{\partial^2 u}{\partial x\partial y} + \eta_0\cdot e^{\alpha\cdot p}\cdot\alpha\cdot\frac{\partial p}{\partial x}\cdot\frac{\partial u}{\partial y} \\
&+ \eta_0\cdot e^{\alpha\cdot p}\cdot\frac{\partial^2 v}{\partial x^2} + \eta_0\cdot e^{\alpha\cdot p}\cdot\alpha\cdot\frac{\partial p}{\partial x}\cdot\frac{\partial v}{\partial x}
\end{aligned}
\right\}
\quad\text{(C.5).}
$$

Non-dimensionalisation with definitions 3.19 and 3.29 results in

$$
\begin{aligned}
0 = &-\frac{p_{hz}}{b_{hz}}\frac{\partial\overline{P}}{\partial\overline{X}} + \frac{2\cdot\eta_0\cdot e^{\alpha\cdot p_{hz}\cdot\overline{P}}\cdot u_h}{b_{hz}^2}\cdot\frac{\partial^2\overline{U}}{\partial\overline{X}^2} + \frac{2\cdot\eta_0\cdot e^{\alpha\cdot p_{hz}\cdot\overline{P}}\cdot\alpha\cdot p_{hz}\cdot u_h}{b_{hz}^2}\cdot\frac{\partial\overline{P}}{\partial\overline{X}}\cdot\frac{\partial\overline{U}}{\partial\overline{X}} \\[2ex]
&+\frac{\eta_0\cdot e^{\alpha\cdot p_{hz}\cdot\overline{P}}\cdot u_h}{h_0^2}\cdot\frac{\partial^2\overline{U}}{\partial\overline{Y}^2} + \frac{\eta_0\cdot e^{\alpha\cdot p_{hz}\cdot\overline{P}}\cdot\alpha\cdot p_{hz}\cdot u_h}{h_0^2}\cdot\frac{\partial\overline{P}}{\partial\overline{Y}}\cdot\frac{\partial\overline{U}}{\partial\overline{Y}} \\[2ex]
&+\frac{\eta_0\cdot e^{\alpha\cdot p_{hz}\cdot\overline{P}}\cdot\dfrac{h_0}{b_{hz}}\cdot u_h}{b_{hz}\cdot h_0}\cdot\frac{\partial^2\overline{V}}{\partial\overline{X}\partial\overline{Y}} + \frac{\eta_0\cdot e^{\alpha\cdot p_{hz}\cdot\overline{P}}\cdot\alpha\cdot p_{hz}\cdot\dfrac{h_0}{b_{hz}}\cdot u_h}{b_{hz}\cdot h_0}\cdot\frac{\partial\overline{P}}{\partial\overline{Y}}\cdot\frac{\partial\overline{V}}{\partial\overline{X}}
\end{aligned}
$$

$$
\begin{aligned}
0 = &-\frac{p_{hz}}{h_0}\cdot\frac{\partial\overline{P}}{\partial\overline{Y}} + \frac{2\cdot\eta_0\cdot e^{\alpha\cdot p_{hz}\cdot\overline{P}}\cdot\dfrac{h_0}{b_{hz}}\cdot u_h}{h_0^2}\cdot\frac{\partial^2\overline{V}}{\partial\overline{Y}^2} + \frac{2\cdot\eta_0\cdot e^{\alpha\cdot p_{hz}\cdot\overline{P}}\cdot\alpha\cdot p_{hz}\cdot\dfrac{h_0}{b_{hz}}\cdot u_h}{h_0^2}\cdot\frac{\partial\overline{P}}{\partial\overline{Y}}\cdot\frac{\partial\overline{V}}{\partial\overline{Y}} \\[2ex]
&+\frac{\eta_0\cdot e^{\alpha\cdot p_{hz}\cdot\overline{P}}\cdot u_h}{b_{hz}\cdot h_0}\cdot\frac{\partial^2\overline{U}}{\partial\overline{X}\partial\overline{Y}} + \frac{\eta_0\cdot e^{\alpha\cdot p_{hz}\cdot\overline{P}}\cdot\alpha\cdot p_{hz}\cdot u_h}{b_{hz}\cdot h_0}\cdot\frac{\partial\overline{P}}{\partial\overline{X}}\cdot\frac{\partial\overline{U}}{\partial\overline{Y}} \\[2ex]
&+\frac{\eta_0\cdot e^{\alpha\cdot p_{hz}\cdot\overline{P}}\cdot\dfrac{h_0}{b_{hz}}\cdot u_h}{b_{hz}^2}\cdot\frac{\partial^2\overline{V}}{\partial\overline{X}^2} + \frac{\eta_0\cdot e^{\alpha\cdot p_{hz}\cdot\overline{P}}\cdot\alpha\cdot p_{hz}\cdot\dfrac{h_0}{b_{hz}}\cdot u_h}{b_{hz}^2}\cdot\frac{\partial\overline{P}}{\partial\overline{X}}\cdot\frac{\partial\overline{V}}{\partial\overline{X}}
\end{aligned}
$$

$$(C.6).$$

Introduction of the dimensionless pressure-viscosity coefficient $\overline{\alpha}=\alpha\cdot p_{hz}$, equation 3.31a, yields

$$
\begin{aligned}
0 = &-\frac{p_{hz}}{b_{hz}}\frac{\partial\overline{P}}{\partial\overline{X}} + \frac{2\cdot\eta_0\cdot e^{\overline{\alpha}\cdot\overline{P}}\cdot u_h}{b_{hz}^2}\cdot\frac{\partial^2\overline{U}}{\partial\overline{X}^2} + \frac{2\cdot\eta_0\cdot e^{\overline{\alpha}\cdot\overline{P}}\cdot\overline{\alpha}\cdot u_h}{b_{hz}^2}\cdot\frac{\partial\overline{P}}{\partial\overline{X}}\cdot\frac{\partial\overline{U}}{\partial\overline{X}} \\[2ex]
&+\frac{\eta_0\cdot e^{\overline{\alpha}\cdot\overline{P}}\cdot u_h}{h_0^2}\cdot\frac{\partial^2\overline{U}}{\partial\overline{Y}^2} + \frac{\eta_0\cdot e^{\overline{\alpha}\cdot\overline{P}}\cdot\overline{\alpha}\cdot u_h}{h_0^2}\cdot\frac{\partial\overline{P}}{\partial\overline{Y}}\cdot\frac{\partial\overline{U}}{\partial\overline{Y}} \\[2ex]
&+\frac{\eta_0\cdot e^{\overline{\alpha}\cdot\overline{P}}\cdot\dfrac{h_0}{b_{hz}}\cdot u_h}{b_{hz}\cdot h_0}\cdot\frac{\partial^2\overline{V}}{\partial\overline{X}\partial\overline{Y}} + \frac{\eta_0\cdot e^{\overline{\alpha}\cdot\overline{P}}\cdot\overline{\alpha}\cdot\dfrac{h_0}{b_{hz}}\cdot u_h}{b_{hz}\cdot h_0}\cdot\frac{\partial\overline{P}}{\partial\overline{Y}}\cdot\frac{\partial\overline{V}}{\partial\overline{X}}
\end{aligned}
$$

$$
\begin{aligned}
0 = &-\frac{p_{hz}}{h_0}\cdot\frac{\partial\overline{P}}{\partial\overline{Y}} + \frac{2\cdot\eta_0\cdot e^{\overline{\alpha}\cdot\overline{P}}\cdot\dfrac{h_0}{b_{hz}}\cdot u_h}{h_0^2}\cdot\frac{\partial^2\overline{V}}{\partial\overline{Y}^2} + \frac{2\cdot\eta_0\cdot e^{\overline{\alpha}\cdot\overline{P}}\cdot\overline{\alpha}\cdot\dfrac{h_0}{b_{hz}}\cdot u_h}{h_0^2}\cdot\frac{\partial\overline{P}}{\partial\overline{Y}}\cdot\frac{\partial\overline{V}}{\partial\overline{Y}} \\[2ex]
&+\frac{\eta_0\cdot e^{\overline{\alpha}\cdot\overline{P}}\cdot u_h}{b_{hz}\cdot h_0}\cdot\frac{\partial^2\overline{U}}{\partial\overline{X}\partial\overline{Y}} + \frac{\eta_0\cdot e^{\overline{\alpha}\cdot\overline{P}}\cdot\overline{\alpha}\cdot u_h}{b_{hz}\cdot h_0}\cdot\frac{\partial\overline{P}}{\partial\overline{X}}\cdot\frac{\partial\overline{U}}{\partial\overline{Y}} \\[2ex]
&+\frac{\eta_0\cdot e^{\overline{\alpha}\cdot\overline{P}}\cdot\dfrac{h_0}{b_{hz}}\cdot u_h}{b_{hz}^2}\cdot\frac{\partial^2\overline{V}}{\partial\overline{X}^2} + \frac{\eta_0\cdot e^{\overline{\alpha}\cdot\overline{P}}\cdot\overline{\alpha}\cdot\dfrac{h_0}{b_{hz}}\cdot u_h}{b_{hz}^2}\cdot\frac{\partial\overline{P}}{\partial\overline{X}}\cdot\frac{\partial\overline{V}}{\partial\overline{X}}
\end{aligned}
$$

$$(C.7).$$

Introducing the geometry ratio $\gamma = h_0/b_{hz}$, equation 3.21, results in

$$
0 = -\frac{p_{hz}}{b_{hz}}\frac{\partial \overline{P}}{\partial \overline{X}} + \gamma^2 \cdot \frac{2 \cdot \eta_0 \cdot e^{\overline{\alpha} \cdot \overline{P}} \cdot u_h}{h_0^2} \cdot \frac{\partial^2 \overline{U}}{\partial \overline{X}^2} + \gamma^2 \cdot \frac{2 \cdot \eta_0 \cdot e^{\overline{\alpha} \cdot \overline{P}} \cdot \overline{\alpha} \cdot u_h}{h_0^2} \cdot \frac{\partial \overline{P}}{\partial \overline{X}} \cdot \frac{\partial \overline{U}}{\partial \overline{X}}
$$

$$
+ \frac{\eta_0 \cdot e^{\overline{\alpha} \cdot \overline{P}} \cdot u_h}{h_0^2} \cdot \frac{\partial^2 \overline{U}}{\partial \overline{Y}^2} + \frac{\eta_0 \cdot e^{\overline{\alpha} \cdot \overline{P}} \cdot \overline{\alpha} \cdot u_h}{h_0^2} \cdot \frac{\partial \overline{P}}{\partial \overline{Y}} \cdot \frac{\partial \overline{U}}{\partial \overline{Y}}
$$

$$
+ \gamma^2 \cdot \frac{\eta_0 \cdot e^{\overline{\alpha} \cdot \overline{P}} \cdot u_h}{h_0^2} \cdot \frac{\partial^2 \overline{V}}{\partial \overline{X} \partial \overline{Y}} + \gamma^2 \cdot \frac{\eta_0 \cdot e^{\overline{\alpha} \cdot \overline{P}} \cdot \overline{\alpha} \cdot u_h}{h_0^2} \cdot \frac{\partial \overline{P}}{\partial \overline{Y}} \cdot \frac{\partial \overline{V}}{\partial \overline{X}}
$$

$$
0 = -\frac{p_{hz}}{h_0} \cdot \frac{\partial \overline{P}}{\partial \overline{Y}} + \gamma \cdot \frac{2 \cdot \eta_0 \cdot e^{\overline{\alpha} \cdot \overline{P}} \cdot u_h}{h_0^2} \cdot \frac{\partial^2 \overline{V}}{\partial \overline{Y}^2} + \gamma \cdot \frac{2 \cdot \eta_0 \cdot e^{\overline{\alpha} \cdot \overline{P}} \cdot \overline{\alpha} \cdot u_h}{h_0^2} \cdot \frac{\partial \overline{P}}{\partial \overline{Y}} \cdot \frac{\partial \overline{V}}{\partial \overline{Y}}
$$

$$
+ \gamma \cdot \frac{\eta_0 \cdot e^{\overline{\alpha} \cdot \overline{P}} \cdot u_h}{h_0^2} \cdot \frac{\partial^2 \overline{U}}{\partial \overline{X} \partial \overline{Y}} + \gamma \cdot \frac{\eta_0 \cdot e^{\overline{\alpha} \cdot \overline{P}} \cdot \overline{\alpha} \cdot u_h}{h_0^2} \cdot \frac{\partial \overline{P}}{\partial \overline{X}} \cdot \frac{\partial \overline{U}}{\partial \overline{Y}}
$$

$$
+ \gamma^3 \cdot \frac{\eta_0 \cdot e^{\overline{\alpha} \cdot \overline{P}} \cdot u_h}{h_0^2} \cdot \frac{\partial^2 \overline{V}}{\partial \overline{X}^2} + \gamma^3 \cdot \frac{\eta_0 \cdot e^{\overline{\alpha} \cdot \overline{P}} \cdot \overline{\alpha} \cdot u_h}{h_0^2} \cdot \frac{\partial \overline{P}}{\partial \overline{X}} \cdot \frac{\partial \overline{V}}{\partial \overline{X}}
$$

$$(C.8).$$

Finally, summarizing by defining $\kappa = \dfrac{\eta_0 \cdot e^{\overline{\alpha} \cdot \overline{P}} \cdot u_h}{h_0^{\,2}}$ gives equation 3.30

$$
0 = -\frac{p_{hz}}{b_{hz}}\frac{\partial \overline{P}}{\partial \overline{X}} + 2 \cdot \gamma^2 \cdot \kappa \cdot \frac{\partial^2 \overline{U}}{\partial \overline{X}^2} + 2 \cdot \gamma^2 \cdot \kappa \cdot \overline{\alpha} \cdot \frac{\partial \overline{P}}{\partial \overline{X}} \cdot \frac{\partial \overline{U}}{\partial \overline{X}}
$$

$$
+ \kappa \cdot \frac{\partial^2 \overline{U}}{\partial \overline{Y}^2} + \kappa \cdot \overline{\alpha} \cdot \frac{\partial \overline{P}}{\partial \overline{Y}} \cdot \frac{\partial \overline{U}}{\partial \overline{Y}}
$$

$$
+ \gamma^2 \cdot \kappa \cdot \frac{\partial^2 \overline{V}}{\partial \overline{X} \partial \overline{Y}} + \gamma^2 \cdot \kappa \cdot \overline{\alpha} \cdot \frac{\partial \overline{P}}{\partial \overline{Y}} \cdot \frac{\partial \overline{V}}{\partial \overline{X}}
$$

$$
0 = -\frac{p_{hz}}{h_0} \cdot \frac{\partial \overline{P}}{\partial \overline{Y}} + 2 \cdot \gamma \cdot \kappa \cdot \frac{\partial^2 \overline{V}}{\partial \overline{Y}^2} + 2 \cdot \gamma \cdot \kappa \cdot \overline{\alpha} \cdot \frac{\partial \overline{P}}{\partial \overline{Y}} \cdot \frac{\partial \overline{V}}{\partial \overline{Y}}
$$

$$
+ \gamma \cdot \kappa \cdot \frac{\partial^2 \overline{U}}{\partial \overline{X} \partial \overline{Y}} + \gamma \cdot \kappa \cdot \overline{\alpha} \cdot \frac{\partial \overline{P}}{\partial \overline{X}} \cdot \frac{\partial \overline{U}}{\partial \overline{Y}}
$$

$$
+ \gamma^3 \cdot \kappa \cdot \frac{\partial^2 \overline{V}}{\partial \overline{X}^2} + \gamma^3 \cdot \kappa \cdot \overline{\alpha} \cdot \frac{\partial \overline{P}}{\partial \overline{X}} \cdot \frac{\partial \overline{V}}{\partial \overline{X}}
$$

$$(C.9).$$

C.2   Simplifying the equations

(corresponding to section 3.3.2)

Equation C.9 and 3.30 respectively can be simplified by applying Schwarz' rule for mixed derivations and continuity equation to the terms containing mixed derivatives

$$\frac{\partial \overline{V}}{\partial X \partial Y} = \frac{\partial}{\partial X}\left(\frac{\partial \overline{V}}{\partial \overline{Y}}\right) = \frac{\partial}{\partial X}\left(-\frac{\partial \overline{U}}{\partial \overline{X}}\right) = -\frac{\partial^2 \overline{U}}{\partial X^2} \qquad \text{(C.10a)}$$

and

$$\frac{\partial \overline{U}}{\partial X \partial Y} = \frac{\partial}{\partial \overline{Y}}\left(\frac{\partial \overline{U}}{\partial \overline{X}}\right) = \frac{\partial}{\partial Y}\left(-\frac{\partial \overline{V}}{\partial \overline{Y}}\right) = -\frac{\partial^2 \overline{V}}{\partial Y^2} \qquad \text{(C.10b)}.$$

Equation C.9 and 3.30 respectively simplifies to

$$\left.\begin{aligned}
0 &= -\frac{p_{hz}}{b_{hz}}\frac{\partial \overline{P}}{\partial X} + \gamma^2 \cdot \kappa \cdot \frac{\partial^2 \overline{U}}{\partial \overline{X}^2} + 2 \cdot \gamma^2 \cdot \kappa \cdot \overline{\alpha} \cdot \frac{\partial \overline{P}}{\partial \overline{X}} \cdot \frac{\partial \overline{U}}{\partial \overline{X}} \\
&\quad + \kappa \cdot \frac{\partial^2 \overline{U}}{\partial Y^2} + \kappa \cdot \overline{\alpha} \cdot \frac{\partial \overline{P}}{\partial \overline{Y}} \cdot \frac{\partial \overline{U}}{\partial \overline{Y}} + \gamma^2 \cdot \kappa \cdot \overline{\alpha} \cdot \frac{\partial \overline{P}}{\partial \overline{Y}} \cdot \frac{\partial \overline{V}}{\partial \overline{X}} \\
\\
0 &= -\frac{p_{hz}}{h_0} \cdot \frac{\partial \overline{P}}{\partial \overline{Y}} + \gamma \cdot \kappa \cdot \frac{\partial^2 \overline{V}}{\partial Y^2} + 2 \cdot \gamma \cdot \kappa \cdot \overline{\alpha} \cdot \frac{\partial \overline{P}}{\partial \overline{Y}} \cdot \frac{\partial \overline{V}}{\partial \overline{Y}} \\
&\quad + \gamma \cdot \kappa \cdot \overline{\alpha} \cdot \frac{\partial P}{\partial \overline{X}} \cdot \frac{\partial \overline{U}}{\partial \overline{Y}} + \gamma^3 \cdot \kappa \cdot \frac{\partial^2 \overline{V}}{\partial X^2} + \gamma^3 \cdot \kappa \cdot \overline{\alpha} \cdot \frac{\partial \overline{P}}{\partial \overline{X}} \cdot \frac{\partial \overline{V}}{\partial \overline{X}}
\end{aligned}\right\} \text{(C.11)}.$$

Collecting with respect to the pressure gradient gives equation 3.33

$$\left.\begin{aligned}
0 &= \frac{\partial \overline{P}}{\partial \overline{X}} \cdot \left[-\frac{p_{hz}}{b_{hz}} + 2 \cdot \kappa \cdot \gamma^2 \cdot \overline{\alpha} \cdot \frac{\partial \overline{U}}{\partial \overline{X}}\right] + \\
&\quad \frac{\partial \overline{P}}{\partial \overline{Y}} \cdot \left[\kappa \cdot \overline{\alpha} \cdot \left(\frac{\partial \overline{U}}{\partial \overline{Y}} + \gamma^2 \cdot \frac{\partial \overline{V}}{\partial \overline{X}}\right)\right] + \left[\kappa \cdot \left(\gamma^2 \cdot \frac{\partial^2 \overline{U}}{\partial X^2} + \frac{\partial^2 \overline{U}}{\partial Y^2}\right)\right] \\
\\
0 &= \frac{\partial \overline{P}}{\partial \overline{Y}} \cdot \left[-\frac{p_{hz}}{h_0} + 2 \cdot \kappa \cdot \gamma \cdot \overline{\alpha} \cdot \frac{\partial \overline{V}}{\partial \overline{Y}}\right] + \\
&\quad \frac{\partial \overline{P}}{\partial \overline{X}} \cdot \left[\kappa \cdot \gamma \cdot \overline{\alpha} \cdot \left(\frac{\partial \overline{U}}{\partial \overline{Y}} + \gamma^2 \cdot \frac{\partial \overline{V}}{\partial \overline{X}}\right)\right] + \left[\kappa \cdot \gamma \cdot \left(\frac{\partial^2 \overline{V}}{\partial Y^2} + \gamma^2 \cdot \frac{\partial^2 \overline{V}}{\partial X^2}\right)\right]
\end{aligned}\right\} \text{(C.12)}.$$

The geometry ratio γ^2 can be neglected in comparison to unity, so equation C.12 simplifies to equation 3.34

$$\left.\begin{aligned}
0 &= \frac{\partial \overline{P}}{\partial \overline{X}} \cdot \left[-\frac{p_{hz}}{b_{hz}} + 2 \cdot \kappa \cdot \gamma^2 \cdot \overline{\alpha} \cdot \frac{\partial \overline{U}}{\partial \overline{X}}\right] + \frac{\partial \overline{P}}{\partial \overline{Y}} \cdot \left[\kappa \cdot \overline{\alpha} \cdot \frac{\partial \overline{U}}{\partial \overline{Y}}\right] + \left[\kappa \cdot \frac{\partial^2 \overline{U}}{\partial Y^2}\right] \\
0 &= \frac{\partial \overline{P}}{\partial \overline{Y}} \cdot \left[-\frac{p_{hz}}{h_0} + 2 \cdot \kappa \cdot \gamma \cdot \overline{\alpha} \cdot \frac{\partial \overline{V}}{\partial \overline{Y}}\right] + \frac{\partial \overline{P}}{\partial \overline{X}} \cdot \left[\kappa \cdot \gamma \cdot \overline{\alpha} \cdot \frac{\partial \overline{U}}{\partial \overline{Y}}\right] + \left[\kappa \cdot \gamma \cdot \frac{\partial^2 \overline{V}}{\partial Y^2}\right]
\end{aligned}\right\} \text{(C.13)}.$$

C.3   Consideration of parallel gap

(corresponding to section 3.3.4)

For the consideration of the parallel gap, the continuity equation is introduced to the x-momentum equation so that equation C.13 becomes

$$
\left.
\begin{aligned}
0 &= \frac{\partial \overline{P}}{\partial \overline{X}} \cdot \left[-\frac{p_{hz}}{b_{hz}} - 2 \cdot \kappa \cdot \gamma^2 \cdot \overline{\alpha} \cdot \frac{\partial \overline{V}}{\partial \overline{Y}} \right] + \frac{\partial \overline{P}}{\partial \overline{Y}} \cdot \left[\kappa \cdot \overline{\alpha} \cdot \frac{\partial \overline{U}}{\partial \overline{Y}} \right] + \left[\kappa \cdot \frac{\partial^2 \overline{U}}{\partial \overline{Y}^2} \right] \\
0 &= \frac{\partial \overline{P}}{\partial \overline{Y}} \cdot \left[-\frac{p_{hz}}{h_0} + 2 \cdot \kappa \cdot \gamma \cdot \overline{\alpha} \cdot \frac{\partial \overline{V}}{\partial \overline{Y}} \right] + \frac{\partial \overline{P}}{\partial \overline{X}} \cdot \left[\kappa \cdot \gamma \cdot \overline{\alpha} \cdot \frac{\partial \overline{U}}{\partial \overline{Y}} \right] + \left[\kappa \cdot \gamma \cdot \frac{\partial^2 \overline{V}}{\partial \overline{Y}^2} \right]
\end{aligned}
\right\} \quad \text{(C.14)}.
$$

For the consideration of the parallel contact, the velocity across the contact is defined to be zero, equation 3.35

$$ \overline{V} \equiv 0 \qquad \text{(C.15)}, $$

so that by neglecting all terms containing $\overline{V}$ equation 3.36 is obtained

$$
\left.
\begin{aligned}
0 &= -\frac{p_{hz}}{b_{hz}} \cdot \frac{\partial \overline{P}}{\partial \overline{X}} + \kappa \cdot \overline{\alpha} \cdot \frac{\partial \overline{U}}{\partial \overline{Y}} \cdot \frac{\partial \overline{P}}{\partial \overline{Y}} + \kappa \cdot \frac{\partial^2 \overline{U}}{\partial \overline{Y}^2} \\
0 &= -\frac{p_{hz}}{h_0} \cdot \frac{\partial \overline{P}}{\partial \overline{Y}} + \kappa \cdot \gamma \cdot \overline{\alpha} \cdot \frac{\partial \overline{U}}{\partial \overline{Y}} \cdot \frac{\partial \overline{P}}{\partial \overline{X}}
\end{aligned}
\right\} \quad \text{(C.16)}.
$$

For the development of equations containing only one pressure gradient, the second equation of set C.16 is solved for the two pressure gradients

$$ \frac{\partial \overline{P}}{\partial \overline{Y}} = \frac{h_0}{p_{hz}} \cdot \kappa \cdot \gamma \cdot \overline{\alpha} \cdot \frac{\partial \overline{U}}{\partial \overline{Y}} \cdot \frac{\partial \overline{P}}{\partial \overline{X}} \qquad \text{(C.17)} $$

and

$$ \frac{\partial \overline{P}}{\partial \overline{X}} = \frac{p_{hz}}{h_0} \cdot \frac{1}{\kappa \cdot \gamma \cdot \overline{\alpha} \cdot \dfrac{\partial \overline{U}}{\partial \overline{Y}}} \cdot \frac{\partial \overline{P}}{\partial \overline{Y}} \qquad \text{(C.18)}. $$

Substituting equation C.17 into the first equation of set C.16 gives an equation for the pressure gradient along the gap

$$ 0 = -\frac{p_{hz}}{b_{hz}} \cdot \frac{\partial \overline{P}}{\partial \overline{X}} + \kappa \cdot \overline{\alpha} \cdot \frac{\partial \overline{U}}{\partial \overline{Y}} \cdot \frac{h_0}{p_{hz}} \cdot \kappa \cdot \gamma \cdot \overline{\alpha} \cdot \frac{\partial \overline{U}}{\partial \overline{Y}} \cdot \frac{\partial \overline{P}}{\partial \overline{X}} + \kappa \cdot \frac{\partial^2 \overline{U}}{\partial \overline{Y}^2} \qquad \text{(C.19)}. $$

Collecting the pressure gradient terms gives

$$0 = \left[-\frac{p_{hz}}{b_{hz}} + \kappa^2 \cdot \overline{\alpha}^2 \cdot \gamma \cdot \frac{h_0}{p_{hz}} \cdot \left(\frac{\partial \overline{U}}{\partial \overline{Y}} \right)^2 \right] \cdot \frac{\partial \overline{P}}{\partial \overline{X}} + \kappa \cdot \frac{\partial^2 \overline{U}}{\partial \overline{Y}^2} \qquad (C.20).$$

Collecting the term p_{hz}/b_{hz} and resolving the geometry ratio γ yields the first equation of set 3.37

$$0 = -\frac{p_{hz}}{b_{hz}} \cdot \left[1 - \frac{h_0^2 \cdot \kappa^2 \cdot \overline{\alpha}^2}{p_{hz}^2} \cdot \left(\frac{\partial \overline{U}}{\partial \overline{Y}} \right)^2 \right] \cdot \frac{\partial \overline{P}}{\partial \overline{X}} + \kappa \cdot \frac{\partial^2 \overline{U}}{\partial \overline{Y}^2} \qquad (C.21).$$

Substituting equation C.18 into the first equation of set C.16 gives an equation for the pressure gradient across the gap

$$0 = -\frac{p_{hz}}{b_{hz}} \cdot \frac{p_{hz}}{h_0} \cdot \frac{1}{\kappa \cdot \gamma \cdot \overline{\alpha} \cdot \dfrac{\partial \overline{U}}{\partial \overline{Y}}} \cdot \frac{\partial \overline{P}}{\partial \overline{Y}} + \kappa \cdot \overline{\alpha} \cdot \frac{\partial \overline{U}}{\partial \overline{Y}} \cdot \frac{\partial \overline{P}}{\partial \overline{Y}} + \kappa \cdot \frac{\partial^2 \overline{U}}{\partial \overline{Y}^2} \qquad (C.22).$$

Multiplying by $\kappa \cdot \gamma \cdot \overline{\alpha} \cdot \dfrac{\partial \overline{U}}{\partial \overline{Y}}$ gives

$$0 = -\frac{p_{hz}}{b_{hz}} \cdot \frac{p_{hz}}{h_0} \cdot \frac{\partial \overline{P}}{\partial \overline{Y}} + \kappa \cdot \overline{\alpha} \cdot \frac{\partial \overline{U}}{\partial \overline{Y}} \cdot \kappa \cdot \gamma \cdot \overline{\alpha} \cdot \frac{\partial \overline{U}}{\partial \overline{Y}} \cdot \frac{\partial \overline{P}}{\partial \overline{Y}} + \kappa \cdot \kappa \cdot \gamma \cdot \overline{\alpha} \cdot \frac{\partial \overline{U}}{\partial \overline{Y}} \cdot \frac{\partial^2 \overline{U}}{\partial \overline{Y}^2} \qquad (C.23).$$

Dividing by p_{hz}/b_{hz} and collecting the pressure gradient terms gives

$$0 = \frac{\partial \overline{P}}{\partial \overline{Y}} \cdot \left[-\frac{p_{hz}}{h_0} + \frac{b_{hz}}{p_{hz}} \cdot \kappa^2 \cdot \overline{\alpha}^2 \cdot \gamma \cdot \left(\frac{\partial \overline{U}}{\partial \overline{Y}} \right)^2 \right] + \frac{b_{hz}}{p_{hz}} \cdot \kappa^2 \cdot \overline{\alpha} \cdot \gamma \cdot \frac{\partial \overline{U}}{\partial \overline{Y}} \cdot \frac{\partial^2 \overline{U}}{\partial \overline{Y}^2} \qquad (C.24).$$

Collecting the term p_{hz}/h_0 and resolving the geometry ratio γ yields the second equation of set 3.37

$$0 = -\frac{p_{hz}}{h_0} \cdot \frac{\partial \overline{P}}{\partial \overline{Y}} \cdot \left[1 - \frac{h_0^2 \cdot \kappa^2 \cdot \overline{\alpha}^2}{p_{hz}^2} \left(\frac{\partial \overline{U}}{\partial \overline{Y}} \right)^2 \right] + \cdot \kappa^2 \cdot \overline{\alpha} \cdot \gamma \cdot \frac{b_{hz}}{p_{hz}} \cdot \frac{\partial \overline{U}}{\partial \overline{Y}} \cdot \frac{\partial^2 \overline{U}}{\partial \overline{Y}^2} \qquad (C.25).$$

C.4   Consideration of an arbitrary shape of the gap

(corresponding to section 3.3.5)

The basis for the analysis is the governing equation 3.15

$$
\left.
\begin{aligned}
0 &= \frac{\partial \overline{P}}{\partial \overline{X}} \cdot \left[-\frac{p_{hz}}{b_{hz}} + 2 \cdot \kappa \cdot \gamma^2 \cdot \overline{\alpha} \cdot \frac{\partial \overline{U}}{\partial \overline{X}} \right] + \frac{\partial \overline{P}}{\partial \overline{Y}} \cdot \left[\kappa \cdot \overline{\alpha} \cdot \frac{\partial \overline{U}}{\partial \overline{Y}} \right] + \left[\kappa \cdot \frac{\partial^2 \overline{U}}{\partial \overline{Y}^2} \right] \\
0 &= \frac{\partial \overline{P}}{\partial \overline{Y}} \cdot \left[-\frac{p_{hz}}{h_0} + 2 \cdot \kappa \cdot \gamma \cdot \overline{\alpha} \cdot \frac{\partial \overline{V}}{\partial \overline{Y}} \right] + \frac{\partial \overline{P}}{\partial \overline{X}} \cdot \left[\kappa \cdot \gamma \cdot \overline{\alpha} \cdot \frac{\partial \overline{U}}{\partial \overline{Y}} \right] + \left[\kappa \cdot \gamma \cdot \frac{\partial^2 \overline{V}}{\partial \overline{Y}^2} \right]
\end{aligned}
\right\} \quad \text{(C.26)}.
$$

For the determination of the momentum equations containing only a single pressure gradient, equations C.26 are written in a simplified form as

$$
\left.
\begin{aligned}
0 &= \frac{\partial \overline{P}}{\partial \overline{X}} \cdot \left[x_1 + x_2 \right] + \frac{\partial \overline{P}}{\partial \overline{Y}} \cdot x_3 + x_4 \\
0 &= \frac{\partial \overline{P}}{\partial \overline{Y}} \cdot \left[y_1 + y_2 \right] + \frac{\partial \overline{P}}{\partial \overline{X}} \cdot y_3 + y_4
\end{aligned}
\right\} \quad \text{(C.27)}
$$

with

$$
x_1 = -\frac{p_{hz}}{b_{hz}} \tag{C.28a},
$$

$$
x_2 = 2 \cdot \kappa \cdot \gamma^2 \cdot \overline{\alpha} \cdot \frac{\partial \overline{U}}{\partial \overline{X}} \tag{C.28b},
$$

$$
x_3 = \kappa \cdot \overline{\alpha} \cdot \frac{\partial \overline{U}}{\partial \overline{Y}} \tag{C.28c},
$$

$$
x_4 = \kappa \cdot \frac{\partial^2 \overline{U}}{\partial \overline{Y}^2} \tag{C.28d},
$$

$$
y_1 = -\frac{p_{hz}}{h_0}, \tag{C.28e},
$$

$$
y_2 = 2 \cdot \kappa \cdot \gamma \cdot \overline{\alpha} \cdot \frac{\partial \overline{V}}{\partial \overline{Y}} \tag{C.28f},
$$

$$
y_3 = \kappa \cdot \gamma \cdot \overline{\alpha} \cdot \frac{\partial \overline{U}}{\partial \overline{Y}} \tag{C.28g},
$$

and

$$
y_4 = \kappa \cdot \gamma \cdot \frac{\partial^2 \overline{V}}{\partial \overline{Y}^2} \tag{C.28h}.
$$

In order to get an equation for the pressure gradient along the gap, the first equation of set C.27 is multiplied by (y_1+y_2) and the second is multiplied by by $-x_3$; set C.27 then becomes

$$\left.\begin{array}{l} 0 = \dfrac{\partial \overline{P}}{\partial X} \cdot [x_1 + x_2] \cdot [y_1 + y_2] + \dfrac{\partial \overline{P}}{\partial Y} \cdot x_3 \cdot [y_1 + y_2] + x_4 \cdot [y_1 + y_2] \\[3mm] 0 = -\dfrac{\partial \overline{P}}{\partial Y} \cdot [y_1 + y_2] \cdot x_3 - \dfrac{\partial \overline{P}}{\partial X} \cdot y_3 \cdot x_3 - y_4 \cdot x_3 \end{array}\right\} \quad (C.29).$$

Adding both equations gives a description of the pressure gradient along the gap

$$0 = \dfrac{\partial \overline{P}}{\partial X} \cdot [(x_1 + x_2) \cdot (y_1 + y_2) - x_3 \cdot y_3] - x_3 \cdot y_4 + x_4 \cdot (y_1 + y_2) \quad (C.30),$$

which can be simplified to

$$-\dfrac{\partial \overline{P}}{\partial X} \cdot z_1 = z_2 \quad (C.31)$$

with

$$z_1 = [(x_1 + x_2) \cdot (y_1 + y_2) - x_3 \cdot y_3] \quad (C.32a)$$

and

$$z_2 = -x_3 \cdot y_4 + x_4 \cdot (y_1 + y_2) \quad (C.32b).$$

Following the same procedure in order to get an equation for the pressure gradient across the gap, the first equation of set C.27 is multiplied by y_3 and the second by $-(x_1 + x_2)$

$$\left.\begin{array}{l} 0 = \dfrac{\partial \overline{P}}{\partial X} \cdot [x_1 + x_2] \cdot y_3 + \dfrac{\partial \overline{P}}{\partial Y} \cdot x_3 \cdot y_3 + x_4 \cdot y_3 \\[3mm] 0 = \dfrac{\partial \overline{P}}{\partial Y} \cdot [y_1 + y_2] \cdot [-(x_1 + x_2)] + \dfrac{\partial \overline{P}}{\partial X} \cdot y_3 \cdot [-(x_1 + x_2)] + y_4 \cdot [-(x_1 + x_2)] \end{array}\right\}$$

$$(C.33).$$

Adding both equations C.33 gives

$$0 = \dfrac{\partial \overline{P}}{\partial Y} \cdot [-(x_1 + x_2) \cdot (y_1 + y_2) + x_3 \cdot y_3] + x_4 \cdot y_3 - (x_1 + x_2) \cdot y_4 \quad (C.34),$$

which can be simplified to

$$z_1 \cdot \frac{\partial \overline{P}}{\partial \overline{Y}} = z_3 \qquad (C.35)$$

with z_1 as defined in equation C.32a and

$$z_3 = x_4 \cdot y_3 - (x_1 + x_2) \cdot y_4 \qquad (C.36).$$

Parameters z_1 to z_3 are determined by substituting the definitions of x_1 to x_4 and y_1 to y_4, equations C.28a–h, back into equations C.32a–b and C.36.

Parameter z_1 becomes

$$z_1 = \left(-\frac{p_{hz}}{b_{hz}} + 2 \cdot \gamma^2 \cdot \kappa \cdot \overline{\alpha} \cdot \frac{\partial \overline{U}}{\partial \overline{X}} \right) \cdot \left(-\frac{p_{hz}}{h_0} + 2 \cdot \gamma \cdot \kappa \cdot \overline{\alpha} \cdot \frac{\partial \overline{V}}{\partial \overline{Y}} \right)$$
$$-\kappa \cdot \overline{\alpha} \cdot \frac{\partial \overline{U}}{\partial \overline{Y}} \cdot \gamma \cdot \kappa \cdot \overline{\alpha} \cdot \frac{\partial \overline{U}}{\partial \overline{Y}} \qquad (C.37).$$

The second bracket is modified by adapting the denominator of the term $-p_{hz}/h_0$ to the same form used for the corresponding term in the first bracket using geometry ratio γ

$$z_1 = \left(-\frac{p_{hz}}{b_{hz}} + 2 \cdot \gamma^2 \cdot \kappa \cdot \overline{\alpha} \cdot \frac{\partial \overline{U}}{\partial \overline{X}} \right) \cdot \left(-\frac{p_{hz}}{b_{hz}} + 2 \cdot \gamma^2 \cdot \kappa \cdot \overline{\alpha} \cdot \frac{\partial \overline{V}}{\partial \overline{Y}} \right) \cdot \frac{1}{\gamma}$$
$$-\kappa \cdot \overline{\alpha} \cdot \frac{\partial \overline{U}}{\partial \overline{Y}} \cdot \gamma \cdot \kappa \cdot \overline{\alpha} \cdot \frac{\partial \overline{U}}{\partial \overline{Y}} \qquad (C.38).$$

The velocity gradient term in the second bracket is replaced by using the continuity equation $\partial \overline{V}/\partial \overline{Y} = -\partial \overline{U}/\partial \overline{X}$ so that

$$z_1 = \left(-\frac{p_{hz}}{b_{hz}} + 2 \cdot \gamma^2 \cdot \kappa \cdot \overline{\alpha} \cdot \frac{\partial \overline{U}}{\partial \overline{X}} \right) \cdot \left(-\frac{p_{hz}}{b_{hz}} - 2 \cdot \gamma^2 \cdot \kappa \cdot \overline{\alpha} \cdot \frac{\partial \overline{U}}{\partial \overline{X}} \right) \cdot \frac{1}{\gamma}$$
$$-\kappa \cdot \overline{\alpha} \cdot \frac{\partial \overline{U}}{\partial \overline{Y}} \cdot \gamma \cdot \kappa \cdot \overline{\alpha} \cdot \frac{\partial \overline{U}}{\partial \overline{Y}} \qquad (C.39).$$

This equation can be summarized to

$$z_1 = \frac{1}{\gamma} \cdot \left[\left(\frac{p_{hz}}{b_{hz}} \right)^2 - \left(2 \cdot \gamma^2 \cdot \kappa \cdot \overline{\alpha} \cdot \frac{\partial \overline{U}}{\partial \overline{X}} \right)^2 - \left(\gamma \cdot \kappa \cdot \overline{\alpha} \cdot \frac{\partial \overline{U}}{\partial \overline{Y}} \right)^2 \right] \qquad (C.40).$$

The geometry ratio γ is small in comparison with unity, and hence the second summand, which is γ^2 smaller than the third, can be neglected, and hence equation C.40 simplifies to

$$z_1 = \frac{1}{\gamma} \cdot \left[\left(\frac{p_{hz}}{b_{hz}} \right)^2 - \left(\gamma \cdot \kappa \cdot \overline{\alpha} \cdot \frac{\partial \overline{U}}{\partial \overline{Y}} \right)^2 \right] \tag{C.41}.$$

Parameter z_2 is

$$z_2 = -\kappa \cdot \overline{\alpha} \cdot \frac{\partial \overline{U}}{\partial \overline{Y}} \cdot \kappa \cdot \gamma \cdot \frac{\partial^2 \overline{V}}{\partial \overline{Y}^2} + \kappa \cdot \frac{\partial^2 \overline{U}}{\partial \overline{Y}^2} \cdot \left(-\frac{p_{hz}}{h_0} + 2 \cdot \gamma \cdot \kappa \cdot \overline{\alpha} \cdot \frac{\partial \overline{V}}{\partial \overline{Y}} \right) \tag{C.42}.$$

Multiplication and rearranging gives

$$z_2 = -\kappa \cdot \frac{p_{hz}}{h_0} \cdot \frac{\partial^2 \overline{U}}{\partial \overline{Y}^2} - \kappa^2 \cdot \gamma \cdot \overline{\alpha} \cdot \frac{\partial \overline{U}}{\partial \overline{Y}} \cdot \frac{\partial^2 \overline{V}}{\partial \overline{Y}^2} + 2 \cdot \gamma \cdot \kappa^2 \cdot \overline{\alpha} \cdot \frac{\partial \overline{V}}{\partial \overline{Y}} \cdot \frac{\partial^2 \overline{U}}{\partial \overline{Y}^2} \tag{C.43},$$

which can be simplified to

$$z_2 = -\kappa \cdot \frac{p_{hz}}{h_0} \cdot \frac{\partial^2 \overline{U}}{\partial \overline{Y}^2} - \kappa^2 \cdot \gamma \cdot \overline{\alpha} \cdot \left(\frac{\partial \overline{U}}{\partial \overline{Y}} \cdot \frac{\partial^2 \overline{V}}{\partial \overline{Y}^2} - 2 \cdot \frac{\partial \overline{V}}{\partial \overline{Y}} \cdot \frac{\partial^2 \overline{U}}{\partial \overline{Y}^2} \right) \tag{C.44}.$$

Parameter z_3 is

$$z_3 = \kappa \cdot \frac{\partial^2 \overline{U}}{\partial \overline{Y}^2} \cdot \kappa \cdot \gamma \cdot \overline{\alpha} \cdot \frac{\partial \overline{U}}{\partial \overline{Y}} - \left(-\frac{p_{hz}}{b_{hz}} + 2 \cdot \kappa \cdot \gamma^2 \cdot \overline{\alpha} \cdot \frac{\partial \overline{U}}{\partial \overline{X}} \right) \cdot \kappa \cdot \gamma \cdot \frac{\partial^2 \overline{V}}{\partial \overline{Y}^2} \tag{C.45}.$$

Multiplying and re-arranging gives

$$z_3 = \kappa \cdot \gamma \cdot \frac{p_{hz}}{b_{hz}} \cdot \frac{\partial^2 \overline{V}}{\partial \overline{Y}^2} - 2 \cdot \kappa^2 \cdot \gamma^3 \cdot \overline{\alpha} \cdot \frac{\partial \overline{U}}{\partial \overline{X}} \cdot \frac{\partial^2 \overline{V}}{\partial \overline{Y}^2} + \kappa^2 \cdot \gamma \cdot \overline{\alpha} \cdot \frac{\partial \overline{U}}{\partial \overline{Y}} \cdot \frac{\partial^2 \overline{U}}{\partial \overline{Y}^2} \tag{C.46},$$

which can be summarised to

$$z_3 = \kappa \cdot \gamma \cdot \frac{p_{hz}}{b_{hz}} \cdot \frac{\partial^2 \overline{V}}{\partial \overline{Y}^2} + \kappa^2 \cdot \gamma \cdot \overline{\alpha} \cdot \left(\frac{\partial \overline{U}}{\partial \overline{Y}} \cdot \frac{\partial^2 \overline{U}}{\partial \overline{Y}^2} - 2 \cdot \gamma^2 \cdot \frac{\partial \overline{U}}{\partial \overline{X}} \cdot \frac{\partial^2 \overline{V}}{\partial \overline{Y}^2} \right) \tag{C.47}.$$

The second term in the bracket is negligible since the geometry ration γ^2 is small, and hence equation C.47 reduces to

$$z_3 = \kappa \cdot \gamma \cdot \left(\frac{p_{hz}}{b_{hz}} \cdot \frac{\partial^2 \overline{V}}{\partial \overline{Y}^2} + \kappa \cdot \overline{\alpha} \cdot \frac{\partial \overline{U}}{\partial \overline{Y}} \cdot \frac{\partial^2 \overline{U}}{\partial \overline{Y}^2} \right) \tag{C.48}.$$

Substituting the definitions of z_1 to z_3, equations C.41, C.44, and C.48, into the equation for the pressure variation along the gap, equation C.31, gives

$$\frac{\partial \overline{P}}{\partial X} \cdot \frac{1}{\gamma} \cdot \left[\left(\frac{p_{hz}}{b_{hz}} \right)^2 - \left(\gamma \cdot \kappa \cdot \overline{\alpha} \cdot \frac{\partial \overline{U}}{\partial Y} \right)^2 \right] =$$

$$\kappa \cdot \frac{p_{hz}}{h_0} \cdot \frac{\partial^2 \overline{U}}{\partial \overline{Y}^2} + \kappa^2 \cdot \gamma \cdot \overline{\alpha} \cdot \left(\frac{\partial \overline{U}}{\partial \overline{Y}} \cdot \frac{\partial^2 \overline{V}}{\partial \overline{Y}^2} - 2 \cdot \frac{\partial \overline{V}}{\partial \overline{Y}} \cdot \frac{\partial^2 \overline{U}}{\partial \overline{Y}^2} \right)$$

(C.49)

and, with the resolution of the geometry ratio γ and further re-arrangements, the first equation of set 3.43 is obtained

$$\frac{\partial \overline{P}}{\partial X} \cdot \left[\left(\frac{p_{hz}}{b_{hz}} \right)^2 - \left(\gamma \cdot \kappa \cdot \overline{\alpha} \cdot \frac{\partial \overline{U}}{\partial \overline{Y}} \right)^2 \right] =$$

$$\kappa \cdot \left(\frac{p_{hz}}{b_{hz}} \cdot \frac{\partial^2 \overline{U}}{\partial \overline{Y}^2} + \kappa \cdot \gamma^2 \cdot \overline{\alpha} \cdot \left(\frac{\partial \overline{U}}{\partial \overline{Y}} \cdot \frac{\partial^2 \overline{V}}{\partial \overline{Y}^2} - 2 \cdot \frac{\partial \overline{V}}{\partial \overline{Y}} \cdot \frac{\partial^2 \overline{U}}{\partial \overline{Y}^2} \right) \right)$$

(C.50).

Substituting the definitions of z_1 to z_3, equations C.41, C.44, and C.48, into the equation for the pressure variation across the gap, equation C.35, gives

$$\frac{1}{\gamma} \cdot \left[\left(\frac{p_{hz}}{b_{hz}} \right)^2 - \left(\gamma \cdot \kappa \cdot \overline{\alpha} \cdot \frac{\partial \overline{U}}{\partial Y} \right)^2 \right] \cdot \frac{\partial \overline{P}}{\partial \overline{Y}} = \kappa \cdot \gamma \cdot \left(\frac{p_{hz}}{b_{hz}} \cdot \frac{\partial^2 \overline{V}}{\partial \overline{Y}^2} + \kappa \cdot \overline{\alpha} \cdot \frac{\partial \overline{U}}{\partial \overline{Y}} \cdot \frac{\partial^2 \overline{U}}{\partial \overline{Y}^2} \right)$$

(C.51)

and, with further re-arrangements, the second equation of set 3.43 is obtained

$$\frac{\partial \overline{P}}{\partial \overline{Y}} \cdot \left[\left(\frac{p_{hz}}{b_{hz}} \right)^2 - \left(\gamma \cdot \kappa \cdot \overline{\alpha} \cdot \frac{\partial \overline{U}}{\partial \overline{Y}} \right)^2 \right] = \kappa \cdot \gamma^2 \cdot \left(\frac{p_{hz}}{b_{hz}} \cdot \frac{\partial^2 \overline{V}}{\partial \overline{Y}^2} + \kappa \cdot \overline{\alpha} \cdot \frac{\partial \overline{U}}{\partial \overline{Y}} \cdot \frac{\partial^2 \overline{U}}{\partial \overline{Y}^2} \right)$$

(C.52).

Expanding the abbreviations defined in equations 3.31a–c,

$$\kappa = \frac{\eta_0 \cdot u_h \cdot e^{\alpha \cdot p_{hz} \cdot \overline{P}}}{h_0^2}$$

(C.53a),

$$\gamma = \frac{h_0}{b_{hz}}$$

(C.53b),

and

$$\overline{\alpha} = \alpha \cdot p_{hz}$$

(C.53c),

equations C.50 and C.52 become

$$\frac{\partial \overline{P}}{\partial \overline{X}} \cdot \left[\left(\frac{p_{hz}}{b_{hz}} \right)^2 - \left(\frac{h_0}{b_{hz}} \cdot \frac{\eta_0 \cdot u_h \cdot e^{\alpha \cdot p_{hz} \cdot \overline{P}}}{h_0^2} \cdot \alpha \cdot p_{hz} \cdot \frac{\partial \overline{U}}{\partial \overline{Y}} \right)^2 \right] =$$

$$\frac{\eta_0 \cdot u_h \cdot e^{\alpha \cdot p_{hz} \cdot \overline{P}}}{h_0^2} \cdot \left(\frac{p_{hz}}{b_{hz}} \cdot \frac{\partial^2 \overline{U}}{\partial \overline{Y}^2} + \frac{\eta_0 \cdot u_h \cdot e^{\alpha \cdot p_{hz} \cdot \overline{P}}}{h_0^2} \cdot \frac{h_0^2}{b_{hz}^2} \cdot \alpha \cdot p_{hz} \cdot \left(\frac{\partial \overline{U}}{\partial \overline{Y}} \cdot \frac{\partial^2 \overline{V}}{\partial \overline{Y}^2} - 2 \cdot \frac{\partial \overline{V}}{\partial \overline{Y}} \cdot \frac{\partial^2 \overline{U}}{\partial \overline{Y}^2} \right) \right)$$

$$(C.54a)$$

and

$$\frac{\partial \overline{P}}{\partial \overline{Y}} \cdot \left[\left(\frac{p_{hz}}{b_{hz}} \right)^2 - \left(\frac{h_0}{b_{hz}} \cdot \frac{\eta_0 \cdot u_h \cdot e^{\alpha \cdot p_{hz} \cdot \overline{P}}}{h_0^2} \cdot \alpha \cdot p_{hz} \cdot \frac{\partial \overline{U}}{\partial \overline{Y}} \right)^2 \right] =$$

$$\frac{\eta_0 \cdot u_h \cdot e^{\alpha \cdot p_{hz} \cdot \overline{P}}}{h_0^2} \cdot \frac{h_0^2}{b_{hz}^2} \cdot \left(\frac{p_{hz}}{b_{hz}} \cdot \frac{\partial^2 \overline{V}}{\partial \overline{Y}^2} + \frac{\eta_0 \cdot u_h \cdot e^{\alpha \cdot p_{hz} \cdot \overline{P}}}{h_0^2} \cdot \alpha \cdot p_{hz} \cdot \frac{\partial \overline{U}}{\partial \overline{Y}} \cdot \frac{\partial^2 \overline{U}}{\partial \overline{Y}^2} \right)$$

$$(C.54b).$$

Dividing the equation by p_{hz}/b_{hz} and collecting these terms on the left hand side gives

$$\frac{p_{hz}}{b_{hz}} \cdot \frac{\partial \overline{P}}{\partial \overline{X}} \cdot \left[1 - \left(\frac{h_0}{b_{hz}} \cdot \frac{\eta_0 \cdot u_h \cdot e^{\alpha \cdot p_{hz} \cdot \overline{P}}}{h_0^2} \cdot \frac{b_{hz}}{p_{hz}} \cdot \alpha \cdot p_{hz} \cdot \frac{\partial \overline{U}}{\partial \overline{Y}} \right)^2 \right] =$$

$$\frac{\eta_0 \cdot u_h \cdot e^{\alpha \cdot p_{hz} \cdot \overline{P}}}{h_0^2} \cdot \left(\frac{\partial^2 \overline{U}}{\partial \overline{Y}^2} + \frac{\eta_0 \cdot u_h \cdot e^{\alpha \cdot p_{hz} \cdot \overline{P}}}{h_0^2} \cdot \frac{h_0^2}{b_{hz}^2} \cdot \frac{b_{hz}}{p_{hz}} \cdot \alpha \cdot p_{hz} \cdot \left(\frac{\partial \overline{U}}{\partial \overline{Y}} \cdot \frac{\partial^2 \overline{V}}{\partial \overline{Y}^2} - 2 \cdot \frac{\partial \overline{V}}{\partial \overline{Y}} \cdot \frac{\partial^2 \overline{U}}{\partial \overline{Y}^2} \right) \right)$$

$$(C.55a)$$

and

$$\frac{p_{hz}}{b_{hz}} \cdot \frac{\partial \overline{P}}{\partial \overline{Y}} \cdot \left[\left(\frac{b_{hz}}{p_{hz}} \right)^2 - \left(\frac{h_0}{b_{hz}} \cdot \frac{\eta_0 \cdot u_h \cdot e^{\alpha \cdot p_{hz} \cdot \overline{P}}}{h_0^2} \cdot \alpha \cdot p_{hz} \cdot \frac{b_{hz}}{p_{hz}} \cdot \frac{\partial \overline{U}}{\partial \overline{Y}} \right)^2 \right] =$$

$$\frac{\eta_0 \cdot u_h \cdot e^{\alpha \cdot p_{hz} \cdot \overline{P}}}{h_0^2} \cdot \frac{h_0^2}{b_{hz}^2} \cdot \left(\frac{\partial^2 \overline{V}}{\partial \overline{Y}^2} + \frac{\eta_0 \cdot u_h \cdot e^{\alpha \cdot p_{hz} \cdot \overline{P}}}{h_0^2} \cdot \alpha \cdot p_{hz} \cdot \frac{b_{hz}}{p_{hz}} \cdot \frac{\partial \overline{U}}{\partial \overline{Y}} \cdot \frac{\partial^2 \overline{U}}{\partial \overline{Y}^2} \right)$$

$$(C.55b),$$

which simplifies to equation 3.44

$$\frac{p_{hz}}{b_{hz}} \cdot \frac{\partial \overline{P}}{\partial \overline{X}} \cdot \left[1 - \left(\frac{\eta_0 \cdot u_h \cdot \alpha}{h_0} \cdot e^{\alpha \cdot p_{hz} \cdot \overline{P}} \cdot \frac{\partial \overline{U}}{\partial \overline{Y}} \right)^2 \right] =$$

$$\frac{\eta_0 \cdot u_h}{h_0^2} \cdot e^{\alpha \cdot p_{hz} \cdot \overline{P}} \cdot \left(\frac{\partial^2 \overline{U}}{\partial \overline{Y}^2} + \gamma \cdot \frac{\eta_0 \cdot u_h \cdot \alpha}{h_0} \cdot e^{\alpha \cdot p_{hz} \cdot \overline{P}} \cdot \left(\frac{\partial \overline{U}}{\partial \overline{Y}} \cdot \frac{\partial^2 \overline{V}}{\partial \overline{Y}^2} - 2 \cdot \frac{\partial \overline{V}}{\partial \overline{Y}} \cdot \frac{\partial^2 \overline{U}}{\partial \overline{Y}^2} \right) \right)$$

$$(C.56a)$$

and

$$\frac{p_{hz}}{b_{hz}} \cdot \frac{\partial \overline{P}}{\partial \overline{Y}} \cdot \left[1 - \left(\frac{\eta_0 \cdot u_h \cdot \alpha}{h_0} \cdot e^{\alpha \cdot p_{hz} \cdot \overline{P}} \cdot \frac{\partial \overline{U}}{\partial \overline{Y}} \right)^2 \right] =$$

$$\frac{\eta_0 \cdot u_h}{b_{hz}^2} \cdot e^{\alpha \cdot p_{hz} \cdot \overline{P}} \cdot \left(\frac{\partial^2 \overline{V}}{\partial \overline{Y}^2} + \frac{\eta_0 \cdot u_h \cdot \alpha}{h_0 \cdot \gamma} \cdot e^{\alpha \cdot p_{hz} \cdot \overline{P}} \cdot \frac{\partial \overline{U}}{\partial \overline{Y}} \cdot \frac{\partial^2 \overline{U}}{\partial \overline{Y}^2} \right)$$

(C.56b).

Appendix D

Details of dimensionless factor determination

The determination of the dimensionless factors k_c, k_p, and k_r follows a similar procedure as the determination of Reynolds number in Appendix A.

By comparison of equations 3.36 and 3.37 with 3.38 and 3.39, it can be seen that

$$k_c = \kappa \cdot \frac{b_{hz}}{p_{hz}} \qquad \text{(D.1a)},$$

$$k_p = \kappa \cdot \overline{\alpha} \cdot \frac{h_0}{p_{hz}} \qquad \text{(D.1b)},$$

and

$$k_r = \kappa \cdot \gamma \cdot \overline{\alpha} \cdot \frac{h_0}{p_{hz}} \qquad \text{(D.1c)}.$$

Expanding the abbreviations defined in equation 3.31a–c,

$$\kappa = \frac{\eta_0 \cdot u_h \cdot e^{\alpha \cdot p_{hz} \cdot \overline{P}}}{h_0^2} \qquad \text{(D.2a)},$$

$$\gamma = \frac{h_0}{b_{hz}} \qquad \text{(D.2b)},$$

and

$$\overline{\alpha} = \alpha \cdot p_{hz} \qquad \text{(D.2c)},$$

and assuming unity for the dimensionless pressure $\overline{P}$ factors k_c, k_p, and k_r become

$$k_c = \frac{\eta_0 \cdot u_h \cdot e^{\alpha \cdot p_{hz}}}{h_0^2} \cdot \frac{b_{hz}}{p_{hz}} \qquad (D.3a),$$

$$k_p = \frac{\eta_0 \cdot u_h \cdot e^{\alpha \cdot p_{hz}}}{h_0^2} \cdot \alpha \cdot p_{hz} \cdot \frac{h_0}{p_{hz}} = \frac{\eta_0 \cdot u_h \cdot \alpha}{h_0} \cdot e^{\alpha \cdot p_{hz}} \qquad (D.3b),$$

and

$$k_r = \frac{\eta_0 \cdot u_h \cdot e^{\alpha \cdot p_{hz}}}{h_0^2} \cdot \frac{h_0}{b_{hz}} \cdot \alpha \cdot p_{hz} \cdot \frac{h_0}{p_{hz}} = \frac{\eta_0 \cdot u_h \cdot \alpha}{b_{hz}} \cdot e^{\alpha \cdot p_{hz}} \qquad (D.3c).$$

Introducing, where applicable, the description of the Hertzian width b_{hz} by the Hertzian pressure p_{hz}, equation 3.24a,

$$b_{hz} = 4 \cdot p_{hz} \cdot \frac{r_{red}}{E'} \qquad (D.4)$$

gives

$$k_c = \frac{\eta_0 \cdot u_h \cdot e^{\alpha \cdot p_{hz}}}{h_0^2} \cdot \frac{4 \cdot p_{hz} \cdot \frac{r_{red}}{E'}}{p_{hz}} = \frac{4 \cdot \eta_0 \cdot u_h \cdot r_{red}}{h_0^2 \cdot E'} \cdot e^{\alpha \cdot p_{hz}} \qquad (D.5a),$$

$$k_p = \frac{\eta_0 \cdot u_h \cdot \alpha}{h_0} \cdot e^{\alpha \cdot p_{hz}} \qquad (D.5b),$$

and

$$k_r = \frac{\eta_0 \cdot u_h \cdot \alpha}{4 \cdot p_{hz} \cdot \frac{r_{red}}{E'}} \cdot e^{\alpha \cdot p_{hz}} = \frac{\eta_0 \cdot u_h \cdot \alpha \cdot E'}{4 \cdot p_{hz} \cdot r_{red}} \cdot e^{\alpha \cdot p_{hz}} \qquad (D.5c).$$

Introducing the definitions of the dimensionless ehl parameters G, U, and W, equation 3.25, where the dimensionless material parameter G is rearranged for the pressure-viscosity coefficient

$$\alpha = \frac{G}{E'} \qquad (D.6a),$$

the dimensionless velocity parameter U is rearranged for the product of viscosity at ambient conditions and the hydrodynamic speed

$$\eta_0 \cdot u_h = U \cdot E' \cdot r_{red} \qquad (D.6b),$$

and the dimensionless load parameter W is rearranged for the Hertzian pressure,

$$p_{hz} = \frac{W^{0.5} \cdot E'}{\sqrt{2 \cdot \pi}}$$ (D.6c).

Introducing the film thickness formula 3.26,

$$h_0 = 1.9 \cdot G^{0.6} \cdot U^{0.7} \cdot W^{-0.13} \cdot r_{red}$$ (D.7),

equations D.5a–c become

$$k_c = \frac{4 \cdot U \cdot E' \cdot r_{red} \cdot r_{red}}{\left(1.9 \cdot G^{0.6} \cdot U^{0.7} \cdot W^{-0.13} \cdot r_{red}\right)^2 \cdot E'} \cdot e^{\frac{G}{E'} \cdot \frac{W^{0.5} \cdot E'}{\sqrt{2 \cdot \pi}}}$$ (D.8a),

$$k_p = \frac{U \cdot E' \cdot r_{red} \cdot \dfrac{G}{E'}}{1.9 \cdot G^{0.6} \cdot U^{0.7} \cdot W^{-0.13} \cdot r_{red}} \cdot e^{\frac{G}{E'} \cdot \frac{W^{0.5} \cdot E'}{\sqrt{2 \cdot \pi}}}$$ (D.8b),

and

$$k_r = \frac{U \cdot E' \cdot r_{red} \cdot \dfrac{G}{E'} \cdot E'}{4 \cdot \dfrac{W^{0.5} \cdot E'}{\sqrt{2 \cdot \pi}} \cdot r_{red}} \cdot e^{\frac{G}{E'} \cdot \frac{W^{0.5} \cdot E'}{\sqrt{2 \cdot \pi}}}$$ (D.8c).

Simplification of the above leads to

$$k_c = 1.11 \cdot G^{-1.2} \cdot U^{-0.4} \cdot W^{0.26} \cdot e^{0.4 \cdot G \cdot W^{0.5}}$$ (D.9a),

$$k_p = 0.53 \cdot G^{0.4} \cdot U^{0.3} \cdot W^{0.13} \cdot e^{0.4 \cdot G \cdot W^{0.5}}$$ (D.9b),

and

$$k_r = 0.63 \cdot G \cdot U \cdot W^{-0.5} \cdot e^{0.4 \cdot G \cdot W^{0.5}}$$ (D.9c).

Appendix E

Values for the geometrical ratio γ

For the determination of values of the geometrical ratio γ, equation 3.21,

$$\gamma = \frac{h_0}{b_{hz}} \tag{E.1},$$

initially the description of the Hertzian width b_{hz} in terms of the Hertzian pressure p_{hz}, equation 3.24a,

$$b_{hz} = 4 \cdot p_{hz} \cdot \frac{r_{red}}{E'} \tag{E.2}$$

is introduced into equation E.1 so that it becomes

$$\gamma = \frac{h_0 \cdot E'}{4 \cdot p_{hz} \cdot r_{red}} \tag{E.3}.$$

With the definition of the dimensionless load parameter W, equation 3.25, resolved for the Hertzian pressure p_{hz},

$$p_{hz} = \frac{W^{0.5}}{\sqrt{2 \cdot \pi}} \cdot E' \tag{E.4},$$

and the definition for the height of the gap, equation 3.26,

$$h_0 = 1.9 \cdot G^{0.6} \cdot U^{0.7} \cdot W^{-0.13} \cdot r_{red} \tag{E.5},$$

the geometrical ratio γ can be written in the dimensionless ehl parameters G, U, and W as

$$\gamma = \frac{1.9 \cdot G^{0.6} \cdot U^{0.7} \cdot W^{-0.13} \cdot r_{red} \cdot E'}{4 \cdot \dfrac{W^{0.5}}{\sqrt{2 \cdot \pi}} \cdot E' \cdot r_{red}} \approx 1.19 \cdot G^{0.6} \cdot U^{0.7} \cdot W^{-0.63} \qquad (E.6).$$

With the definition of the transition between the elastohydrodynamic regime and the hydrodynamic regime, equation 3.27,

$$W \geq 0.017 \cdot U^{0.325} \qquad (E.7)$$

the geometrical ratio at the transition line to the hydrodynamic regime becomes

$$\gamma \approx 15 \cdot G^{0.6} \cdot U^{0.5} \qquad (E.8)$$

The maximum value for γ in the borders shown in figure 3.8 and 3.9 is obtained at the transition to the hydrodynamic lubrication regime for the maximum dimensionless velocity parameter $U = 10^{-9}$

as

$$\gamma_{max} = 0.078 \qquad (E.9).$$

The minimum value for γ is obtained for minimum dimensionless velocity parameter $U = 10^{-13}$ and maximum load parameter $W = 10^{-3}$ as

$$\gamma_{min} = 1.2 \times 10^{-5} \qquad (E.10).$$

Appendix F

Tangential and normal wall forces

The tangential wall force on an infinitesimal small element can be seen in figure 3.1. Considering a wall normal to the y-direction and assuming line contact conditions, the wall force in the x-direction is

$$dF_t = \sigma_{xy} \cdot dA_y \qquad (F.1).$$

Introducing the definition of the stress terms, equation 3.3, gives

$$dF_t = \eta \cdot \left(\frac{\partial u}{\partial y} + \frac{\partial v}{\partial x} \right) \cdot dA_y \qquad (F.2).$$

Together with Barus' equation 3.9, equation F.2 becomes

$$dF_t = \eta_0 \cdot e^{\alpha \cdot p} \cdot \left(\frac{\partial u}{\partial y} + \frac{\partial v}{\partial x} \right) \cdot dA_y \qquad (F.3).$$

Non-dimensionalisation, using the definitions of equations 3.18 and 3.29, gives

$$dF_t = \eta_0 \cdot e^{\alpha \cdot p_{hz} \cdot P} \cdot \left(\frac{u_h}{h_0} \cdot \frac{\partial \overline{U}}{\partial \overline{Y}} + \frac{u_h \cdot \frac{h_0}{b_{hz}}}{b_{hz}} \cdot \frac{\partial \overline{V}}{\partial \overline{X}} \right) \cdot dA_y \qquad (F.4).$$

Application of the geometry ratio $\gamma = h_0 / b_{hz}$ leads to

$$dF_t = \frac{\eta_0 \cdot u_h}{h_0} \cdot e^{\alpha \cdot p_{hz} \cdot P} \cdot \left(\frac{\partial \overline{U}}{\partial \overline{Y}} + \gamma^2 \cdot \frac{\partial \overline{V}}{\partial \overline{X}} \right) \cdot dA_y , \qquad (F.5),$$

where the second term can be neglected, because γ^2 is much smaller than unity. The tangential wall force hence is

$$dF_t = \frac{\eta_0 \cdot u_h}{h_0} \cdot e^{\alpha \cdot p_{hz} \cdot P} \cdot \frac{\partial \overline{U}}{\partial \overline{Y}} \cdot dA_y \qquad \text{(F.6).}$$

The normal wall force on an infinitesimal wall element consists of a pressure component and a tensile stress component

$$dF_n = \left(-p + \sigma_{yy}\right) \cdot dA_y \qquad \text{(F.7).}$$

With the definition of stress terms, equation 3.3, and the assumption of an incompressible fluid, normal force becomes

$$dF_n = \left(-p + 2 \cdot \eta \cdot \frac{\partial v}{\partial y}\right) \cdot dA_y \qquad \text{(F.8).}$$

With Barus' equation 3.9, equation F.8 becomes

$$dF_n = \left(-p + 2 \cdot \eta_0 \cdot e^{\alpha \cdot p} \cdot \frac{\partial v}{\partial y}\right) \cdot dA_y \qquad \text{(F.9).}$$

Non-dimensionalisation, using the definitions of equations 3.18 and 3.29, gives

$$dF_n = \left(-p_{hz} \cdot \overline{P} + 2 \cdot \frac{\eta_0 \cdot u_h \cdot \dfrac{h_0}{b_{hz}}}{h_0} \cdot e^{\alpha \cdot p_{hz} \cdot \overline{P}} \cdot \frac{\partial \overline{V}}{\partial \overline{Y}}\right) \cdot dA_y \qquad \text{(F.10),}$$

which can be simplified to

$$dF_n = \left(-p_{hz} \cdot \overline{P} + 2 \cdot \frac{\eta_0 \cdot u_h}{b_{hz}} \cdot e^{\alpha \cdot p_{hz} \cdot \overline{P}} \cdot \frac{\partial \overline{V}}{\partial \overline{Y}}\right) \cdot dA_y \qquad \text{(F.11).}$$

Taking p_{hz} out of the brackets and understanding the parameters accompanying the velocity gradient in terms of k_r, e.g. equation D.3c of appendix D, gives

$$dF_n = p_{hz} \cdot \left(-\overline{P} + \frac{2 \cdot k_r}{p_{hz} \cdot \alpha} \cdot \frac{\partial \overline{V}}{\partial \overline{Y}}\right) \cdot dA_y \qquad \text{(F.12).}$$

With the definitions of the dimensionless ehl parameters G, U and W, equation 3.25, pressure viscosity coefficient α can be replaced by

$$\alpha = \frac{G}{E'} \quad\quad\quad \text{(F.13),}$$

and Hertzian pressure can be replaced by

$$p_{hz} = \frac{W^{0.5} \cdot E'}{\sqrt{2 \cdot \pi}} \quad\quad\quad \text{(F.15).}$$

Equation F.12 changes to

$$dF_n = p_{hz} \cdot \left(-\overline{P} + \frac{2 \cdot k_r}{\dfrac{W^{0.5} \cdot E'}{\sqrt{2 \cdot \pi}} \cdot \dfrac{G}{E'}} \cdot \frac{\partial \overline{V}}{\partial \overline{Y}} \right) \cdot dA_y \approx p_{hz} \cdot \left(-\overline{P} + \frac{5 \cdot k_r}{G \cdot W^{0.5}} \cdot \frac{\partial \overline{V}}{\partial \overline{Y}} \right) \cdot dA \quad \text{(F.16).}$$

For the parameters displayed in figures 3.8 and 3.9, i.e the dimensionless material parameter of $G = 5000$ and a dimensionless load parameter from $W = 10^{-6}$ to 10^{-3}, the factor $5/(G \cdot W^{0.5})$ ranges between unity and 0.03. This means that the factor accompanying the velocity gradient becomes significant if k_r becomes also relevant. However, that is only the case for a significant velocity gradient, i.e. when the gap is not parallel.

The force components of a fluid element onto the wall are of identical absolute value but of different sign.

Appendix G

Grid calculation in the CFD code

CFX-4.2 allows the user-defined determination of the grid by Cartesian co-ordinates. As illustrated in figure G.1, the user has to determine the co-ordinates of the nodes representing the corners of the finite volumes; the co-ordinates of the centre points are calculated by the program. The CFD code uses dimensional values during its calculation and hence all user-defined data must be provided in SI dimensions.
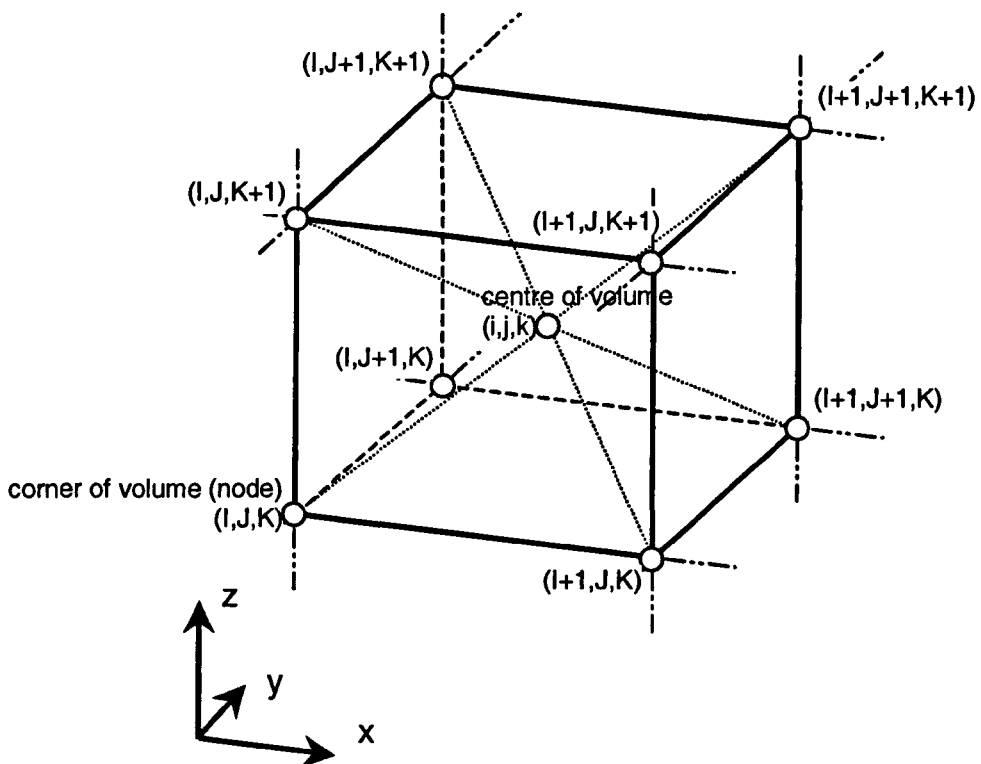
Figure G.1:   Finite volume; centre of volume and corners of volume; nomenclature.

For the ehl problem, an equidistant grid was chosen along the gap because areas requiring improved resolution are still unknown for the extended approach. The co-ordinates in the x-direction of all the corners can be determined from the location of the inlet and outlet boundaries and from the number of cells along this distance by

$$x_{I,J} = x_{inlet} + \frac{I-1}{N-1} \cdot (x_{outlet} - x_{inlet})$$ (G.1),

where N and M   is the total number of corners along and across the domain or the number of volumes n and m plus one,

        I and J   run from zero to N and M respectively, and

        x_{outlet} and x_{inlet} are the positions of the inlet and outlet respectively.

All variables are illustrated in figure G.2.
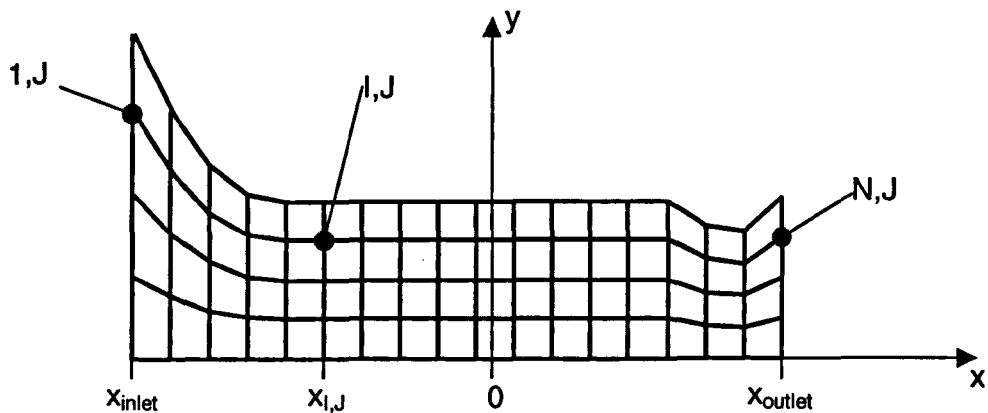
Figure G.2:   *Calculation of co-ordinates of the corners in x-direction.*

The co-ordinates in the y-direction are calculated in a similar way taking the local minimum and maximum edge of the gap into account, compare figure G.3

$$y_{I,J} = y_{I,min} + \frac{J-1}{M-1} \cdot (y_{I,max} - y_{I,min})$$ (G.2),

where I, J, N and M   are as above,

        $y_{I,min}$ is the position of the lower surface in y-direction, which is zero when employing the widely used method of presentation, and

        $y_{I,max}$ is the position of the upper surface in y-direction.
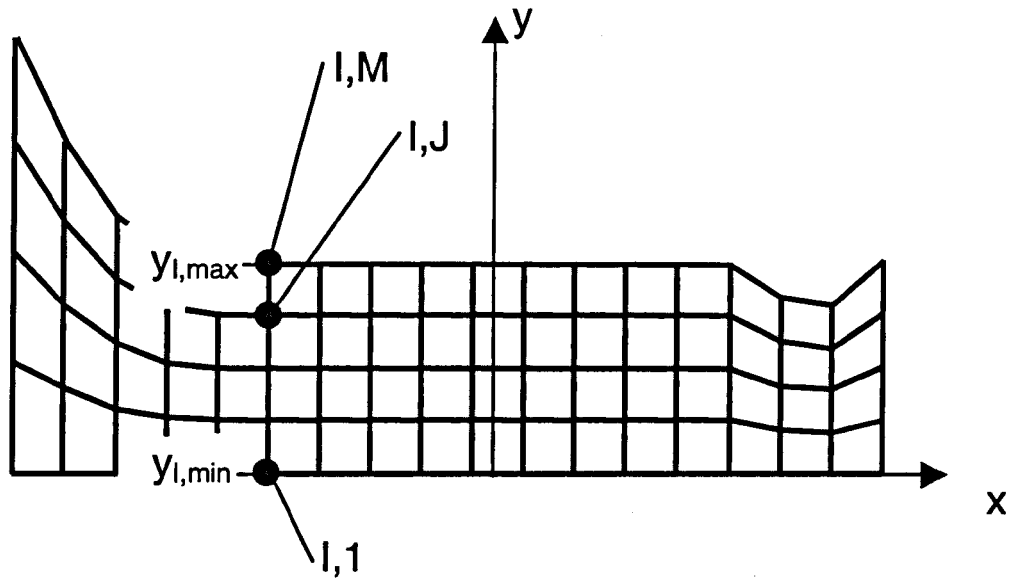
Figure G.3:   Calculation of co-ordinates of the corners in y-direction.

For the established Reynolds equation based solutions, $y_{I,min}$ is normally assumed to be zero along the gap, and all changes in height due to deformation and curvature are applied to the upper surface as shown in figure G.4(a). However, a practical application normally consists of two elastic and curved surfaces and agrees with figure G.4(b), where, as an example, identical material properties and radii are assumed for both surfaces.
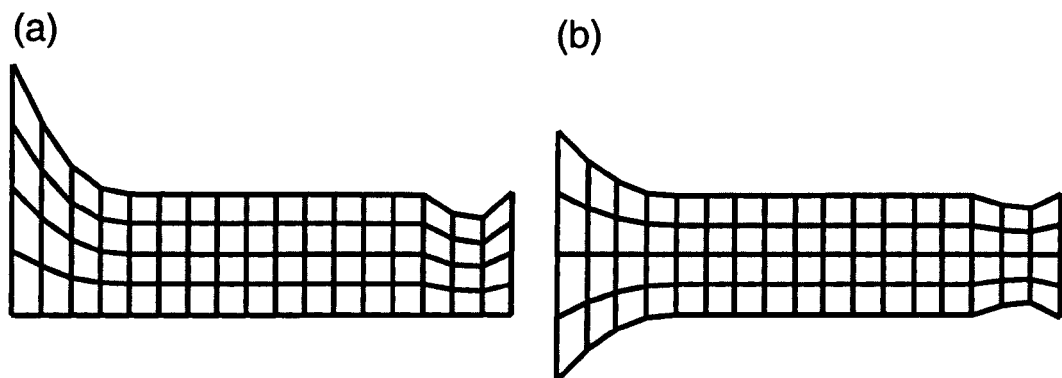
Figure G.4:   Established geometry distribution assuming all contributions to one surface (a) and real geometry distribution assuming identical surface curvatures and material properties (b).

For the established isothermal Reynolds equation based solutions the two above considerations do not lead to any difference. This is because all the variables appearing in Reynolds equation are assumed to vary in one direction only, pressure and viscosity in longitudinal direction, velocity in perpendicular direction. This can also be shown mathematically by applying co-ordinate transformation on those simplified Navier-Stokes equations from which Reynolds equation is derived. Details are shown by Liesegang [36].

However, for the extended set of governing equations 3.42 as well as for thermal equations, the solution is influenced by the position of the centreline of the gap. Co-ordinate transformation shows that the coefficients in the transformed and discretised governing equations can change with different definitions of the centreline. However, these changed coefficients and the boundary values are expected to cancel out and hence practical influence on the solution is expected to be small [36].

The positions of the lower and upper surface in y-direction are

$$y_{l,min} = 0.0 \, [m] \quad \text{and} \quad y_{l,max} = h_0 + h_{r1} + h_{r2} + v_{d1} + v_{d2} \qquad (G.3)$$

when all curvatures and deformations are applied to one surface and

$$y_{l,min} = -h_{r1} - v_{d1} \quad \text{and} \quad y_{l,max} = h_0 + h_{r2} + v_{d2} \qquad (G.4)$$

when the curvatures and deformations are applied to the corresponding surface, with the variables explained below.

The value of the height of the gap at the contact centreline h_0 must be determined during the calculation. As an initial value for h_0 equation 3.26 is used

$$h_0 = 1.9 \cdot G^{0.6} \cdot U^{0.7} \cdot W^{-0.13} \cdot r_{red} \qquad (G.5).$$

The height of the gap due to curvature was calculated using Pythagoras' law

$$h_{r1} = r_1 - \sqrt{r_1^2 - x^2} \qquad (G.6a)$$

and

$$h_{r2} = r_2 - \sqrt{r_2^2 - x^2} \qquad (G.6b)$$

for the lower and the upper surface respectively. The deflection is calculated from the Boussinesq equation 3.11,

$$v(x) - v(x_{ref}) = -2 \cdot \frac{1 - v^2}{E \cdot \pi} \cdot \int_{-\infty}^{+\infty} p(s) \cdot \ln\left(\frac{x - s}{x_{ref} - s}\right) \cdot ds \qquad (G.7).$$

For the present calculation, the centre of the contact $x_{ref} = 0.0$ [m], was chosen as the reference point. The employment of CFD software based on the finite volume method leads to the fact, that the pressure is given at the volume centres and at the centres of the boundary faces, while deformation must be calculated for the nodes, determining the corners of the volumes. Hence, the discretisation of the deformation is slightly different as, for example, for the finite difference method (FDM). A zeroth order and a first order discretisation scheme were considered, both illustrated in figure G.5.
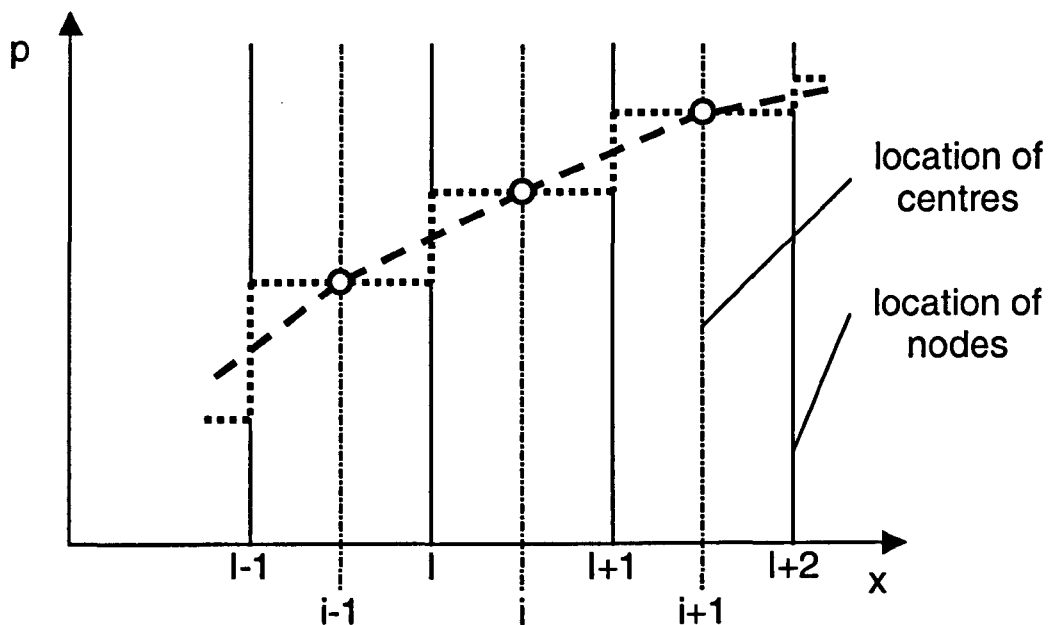
O   boundary pressure from CFD code

••••••• zeroth order pressure distribution for
        deformation calculation

— —   first order pressure distribution for
        deformation calculation

Figure G.5:   *Zeroth and first order discretisation of pressure for deformation*
               calculation.

Zeroth order approximation assumes constant pressure over the complete volume surface. Zero order approximation agrees with the standard method

implemented in the CFD code for determination of surface forces and would provide full consistency with data available from the CFD code. For the lower surface Boussinesq' equation becomes discretised

$$v_{d1l} = -\frac{2 \cdot (1-v^2)}{\pi \cdot E} \cdot \sum_{i=1}^{i=n} \int_{s=s_i-\frac{\Delta x}{2}}^{s=s_i+\frac{\Delta x}{2}} p_i \cdot \ln\left|\frac{x_i - s}{x_{ref} - s}\right| \cdot ds \qquad (G.8),$$

and, with the integral solved,

$$v_{d1l} = -\frac{2 \cdot (1-v^2)}{\pi \cdot E} \cdot \sum_{i=1}^{i=n} \left[p_i \cdot \left[(\ln|x_i - s| - 1) \cdot (x_i - s) - (\ln|x_{ref} - s| - 1) \cdot (x_{ref} - s)\right]_{s=s_i-\frac{\Delta x}{2}}^{s=s_i+\frac{\Delta x}{2}} \right.$$

$$(G.9)$$

where

$$\lim_{x_i \to s}(\ln|x_i - s| - 1) \cdot (x_i - s) = 0 \qquad (G.10a)$$

and

$$\lim_{x_{ref} \to s}(\ln|x_{ref} - s| - 1) \cdot (x_{ref} - s) = 0 \qquad (G.10b).$$

For the upper surface the values are obtained in the same manner.

First order discretisation assumes linear pressure distribution between the centre points of the boundary faces. The method is more accurate than the previous but not consistent with force determination of the CFD software. Neglecting those half volumes at the edges of the system, i.e. between x_i and x_i and x_n and x_N, discretisation of Boussinesq's equation gives, again for the lower surface,

$$v_{d1l} = -\frac{2 \cdot (1-v^2)}{\pi \cdot E} \cdot \sum_{i=2}^{i=n} \int_{s=s_{i-1}}^{s=s_i} \left(p_{i-1} + (p_i - p_{i-1}) \cdot \frac{s - s_{i-1}}{s_i - s_{i-1}} \right) \cdot \ln\left|\frac{x_i - s}{x_{ref} - s}\right| \cdot ds \qquad (G.11)$$

and, with the integral solved,

$$
v_{d1l} = -\frac{2 \cdot \left(1 - v^2\right)}{\pi \cdot E} \cdot \sum_{i=2}^{i=n} \Bigg[
$$

$$
\left(p_{i-1} - \frac{s_{i-1}}{s_i - s_{i-1}} \cdot \left(p_i - p_{i-1}\right) \right)
$$

$$
\cdot \left[\left(\ln|x_1 - s| - 1\right) \cdot \left(x_1 - s\right) - \left(\ln|x_{ref} - s| - 1\right) \cdot \left(x_{ref} - s\right) \right] +
$$

$$
\left(\frac{s}{s_i - s_{i-1}} \cdot \left(p_i - p_{i-1}\right) \right) \cdot
$$

$$
\left[\left(-\frac{x_1 + s}{2} \cdot \ln|x_1 - s| + \frac{3 \cdot x_1 + s}{4} \right) \cdot \left(x_1 - s\right) - \left(-\frac{x_{ref} + s}{2} \cdot \ln|x_{ref} - s| + \frac{3 \cdot x_{ref} + s}{4} \right) \cdot \left(x_{ref} - s\right) \right] \Bigg]_{s_{i-1}}^{s_i}
$$

$$
(G.12)
$$

With respect to the location of the deflection x_l, the pressure distribution is of second order accuracy, because the pressure gradient approximation defined by positions i and i-1 is the second order approximation with respect to the position I. Because the discretisation of the CFD software is of second order, the above approximation is sufficiently accurate.

Appendix H

Details of dominance factor determination

The determination of the factor D follows a similar procedure as the determination of Reynolds number in appendix A.

The dominance factor D is defined in equation 8.24 as

$$D = \frac{b_{hz} \cdot \eta_0 \cdot e^{\alpha \cdot p_{hz} \cdot \overline{P}} \cdot u_h}{h_0^2 \cdot p_{hz}} \cdot \frac{m^2}{n} \qquad (H.1).$$

Assuming unity for the dimensionless pressure $\overline{P}$ and introducing the description of the Hertzian width b_{hz} by the Hertzian pressure p_{hz}, equation 3.24a,

$$b_{hz} = 4 \cdot p_{hz} \cdot \frac{r_{red}}{E'} \qquad (H.2),$$

the dominance factor becomes

$$D = \frac{4 \cdot \frac{r_{red}}{E'} \cdot \eta_0 \cdot e^{\alpha \cdot p_{hz}} \cdot u_h}{h_0^2} \cdot \frac{m^2}{n} \qquad (H.3).$$

Introducing the definitions of the dimensionless ehl parameters G, U, and W, equation 3.25, where the dimensionless material parameter G is rearranged for the pressure-viscosity coefficient

$$\alpha = \frac{G}{E'} \qquad (H.4a),$$

- 404 -

the dimensionless velocity parameter U is rearranged for the product of viscosity at ambient conditions and the hydrodynamic speed

$$\eta_0 \cdot u_h = U \cdot E' \cdot r_{red} \tag{H.4b},$$

and the dimensionless load parameter W is rearranged for the Hertzian pressure,

$$p_{hz} = \frac{W^{0.5} \cdot E'}{\sqrt{2 \cdot \pi}} \tag{H.4c},$$

and introducing the film thickness formula 3.26,

$$h_0 = 1.9 \cdot G^{0.6} \cdot U^{0.7} \cdot W^{-0.13} \cdot r_{red} \tag{H.5},$$

equation H.3 becomes

$$D = \frac{4 \cdot \frac{r_{red}}{E'} \cdot U \cdot E' \cdot r_{red} \cdot e^{\frac{G}{E'} \cdot \frac{W^{0.5} \cdot E'}{\sqrt{2 \cdot \pi}}}}{1.9^2 \cdot G^{1.2} \cdot U^{1.4} \cdot W^{-0.26} \cdot r_{red}^2} \cdot \frac{m^2}{n} \tag{H.6}.$$

Simplification of the above leads to equation 8.30,

$$D = 1.11 \cdot \frac{m^2}{n} \cdot G^{-1.2} \cdot U^{-0.4} \cdot W^{0.26} \cdot e^{0.4 \cdot G \cdot W^{0.5}} \tag{H.7}.$$

Appendix I

Estimation of the residuals of the extended x-momentum equation

Basis for the calculation is the simplified Navier-Stokes equation 3.15 without inertia terms:

$$0 = -\frac{\partial p}{\partial x} + 2 \cdot \frac{\partial}{\partial x}\left[\eta \cdot \frac{\partial u}{\partial x}\right] + \frac{\partial}{\partial y}\left[\eta \cdot \left(\frac{\partial u}{\partial y} + \frac{\partial v}{\partial x}\right)\right] \qquad (I.1).$$

Non-dimensionalisation of the bracket $(\partial u/\partial y + \partial v/\partial x)$ shows that the second summand* is much smaller than the first one and hence negligible. Other terms would also be negligible but complicate the later discretisation. Equation I.1 becomes

$$0 = -\frac{\partial p}{\partial x} + 2 \cdot \frac{\partial}{\partial x}\left(\eta \cdot \frac{\partial u}{\partial x}\right) + \frac{\partial}{\partial y}\left(\eta \cdot \frac{\partial u}{\partial y}\right) \qquad (I.2).$$

Assuming a rectangular volume for simplicity and applying finite volume discretisation according to Patankar and Spalding [88] or Versteeg and

---

* Compare section 3.2, non-dimensionalising by assuming

$$\overline{X} = \frac{x}{b_{hz}}, \ \overline{Y} = \frac{y}{h_0}, \ \overline{U} = \frac{u}{u_h} = \frac{u}{\frac{1}{2} \cdot (u_1 + u_2)} \text{ and } \overline{V} = \frac{v}{v_m} = \frac{v}{u_h \cdot (h_0/b_{hz})}$$

the bracket term becomes

$$\frac{u_h}{h_0} \cdot \left(\frac{\partial \overline{U}}{\partial \overline{Y}} + \gamma^2 \cdot \frac{\partial \overline{V}}{\partial \overline{X}}\right)$$

where $\gamma = h_0/b_{hz} \ll 1$ and hence the second term of the sum is negligible.

Malalasekera [90] with the nomenclature of figure I.1, the discretised momentum equation is

$$\int_{\Delta V} \frac{d}{dx}\left(\eta \cdot \frac{du}{dx}\right) \cdot dV + \int_{\Delta V} \frac{d}{dy}\left(\eta \cdot \frac{du}{dy}\right) \cdot dV - \int_{\Delta V}\left(\frac{dp}{dx}\right) \cdot dV =$$

$$= \left(\eta \cdot A_x \cdot \frac{du}{dx}\right)_{I+1} - \left(\eta \cdot A_x \cdot \frac{du}{dx}\right)_{I} + \left(\eta \cdot A_y \cdot \frac{du}{dy}\right)_{J+1} - \left(\eta \cdot A_y \cdot \frac{du}{dy}\right)_{J} - \hat{S} \cdot \Delta V =$$

$$= 0$$

(I.3)

where

$$\int_{\Delta V}\left(\frac{dp}{dx}\right) \cdot dV = \hat{S} \cdot \Delta V \qquad (I.4).$$
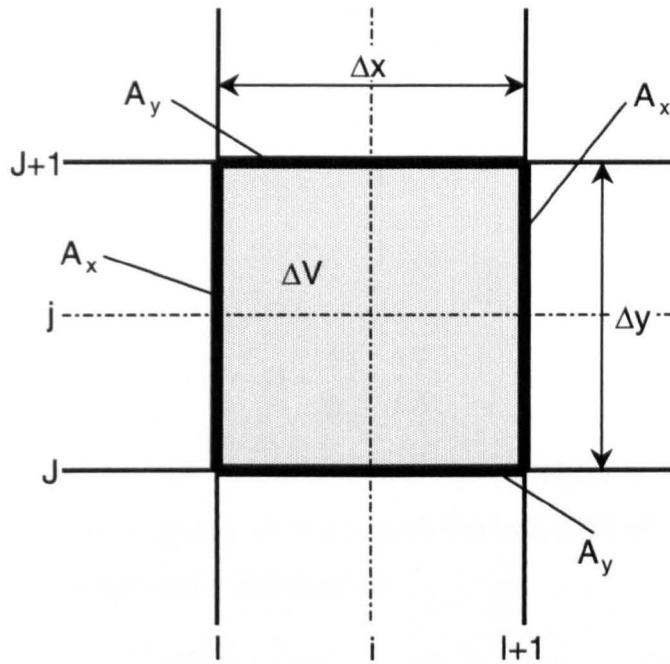
Figure I.1:   Nomenclature of finite volume discretisation.

Approximating the velocity gradients by second order central approximation and taking into account that volume is a cuboid and hence facing surfaces are equal, equation I.3 becomes

$$\frac{\eta_{I+1} \cdot A_x}{\Delta x} \cdot \left(u_{i+1} - u_i\right) - \frac{\eta_I \cdot A_x}{\Delta x} \cdot \left(u_i - u_{i-1}\right) +$$

$$\frac{\eta_{J+1} \cdot A_x}{\Delta y} \cdot \left(u_{j+1} - u_j\right) - \frac{\eta_J \cdot A_x}{\Delta y} \cdot \left(u_j - u_{j+1}\right) - \hat{S} \cdot \Delta V = 0 \tag{I.5}.$$

Introducing non-dimensionalisation as in section 3.3[*] and Barus' equation[†], equation I.5 becomes

$$\frac{\eta_0 \cdot e^{\overline{\alpha} \cdot \overline{P}_{i+1,j}} \cdot u_h \cdot h_0 \cdot l_c}{b_{hz}} \cdot \frac{\Delta Y \cdot \Delta Z}{\Delta X} \cdot \overline{U}_{i+1,j} +$$

$$\frac{\eta_0 \cdot e^{\overline{\alpha} \cdot \overline{P}_{i,j+1}} \cdot u_h \cdot b_{hz} \cdot l_c}{h_0} \cdot \frac{\Delta X \cdot \Delta Z}{\Delta Y} \cdot \overline{U}_{i,j+1} -$$

$$\frac{\eta_0 \cdot u_h \cdot b_{hz} \cdot l_c}{h_0} \cdot \frac{\Delta X \cdot \Delta Z}{\Delta Y} \left[\beta^2 \cdot \left(e^{\overline{\alpha} \cdot \overline{P}_{i,j+1}} + e^{\overline{\alpha} \cdot \overline{P}_{i,j-1}} \right) + e^{\overline{\alpha} \cdot \overline{P}_{i+1,j}} + e^{\overline{\alpha} \cdot \overline{P}_{i-1,j}} \right] \cdot \overline{U}_{i,j} +$$

$$\frac{\eta_0 \cdot e^{\overline{\alpha} \cdot \overline{P}_{i-1,j}} \cdot u_h \cdot h_0 \cdot l_c}{b_{hz}} \cdot \frac{\Delta Y \cdot \Delta Z}{\Delta X} \cdot \overline{U}_{i-1,j} +$$

$$\frac{\eta_0 \cdot e^{\overline{\alpha} \cdot \overline{P}_{i,j-1}} \cdot u_h \cdot b_{hz} \cdot l_c}{h_0} \cdot \frac{\Delta X \cdot \Delta Z}{\Delta Y} \cdot \overline{U}_{i,j-1} = \hat{S} \cdot \Delta V \tag{I.6},$$

where

$$\beta = \frac{h_0}{b_{hz}} \cdot \frac{\Delta Y}{\Delta X} \tag{I.7}.$$

When calculating the above equation, the computation is not exact due to limited computational accuracy. A change of the last digit of the central speed component i,j hence causes a residual of

$$f_{i,j} = \frac{\eta_0 \cdot u_h \cdot b_{hz} \cdot l_c}{h_0} \cdot \frac{\Delta X \cdot \Delta Z}{\Delta Y} \left[\beta^2 \cdot \left(e^{\overline{\alpha} \cdot \overline{P}_{i,j+1}} + e^{\overline{\alpha} \cdot \overline{P}_{i,j-1}} \right) + e^{\overline{\alpha} \cdot \overline{P}_{i+1,j}} + e^{\overline{\alpha} \cdot \overline{P}_{i-1,j}} \right] \cdot E_{computational} \tag{I.8}$$

or, with the assumptions that the pressure is constant in the volume and that the geometry ratio β is small,

---

[*] $\overline{X} = \dfrac{x}{b_{hz}}$, $\overline{Y} = \dfrac{y}{h_0}$, $\overline{U} = \dfrac{u}{u_h} = \dfrac{u}{\frac{1}{2} \cdot (u_1 + u_2)}$, $\overline{V} = \dfrac{v}{v_m} = \dfrac{v}{u_h \cdot (h_0/b_{hz})}$, $\overline{P} = \dfrac{p}{p_{hz}}$

[†] $\eta = \eta_0 \cdot e^{\alpha_{p_m} \cdot \overline{P}}$

$$f_{x-mom,i,j} = 2 \cdot \frac{\eta_0 \cdot u_h \cdot b_{hz} \cdot l_c}{h_0} \cdot \frac{\Delta X \cdot \Delta Z}{\Delta Y} \cdot e^{\overline{\alpha \cdot \overline{P}_{i,j}}} \cdot E_{computational} \qquad (I.9),$$

where $E_{computational}$ is the error due to the limited accuracy of the computation, which is 10^{-16} for double precision, and

$\Delta X, \Delta Y$ and ΔZ is the dimensionless volume width in x-, y-, and z-direction,

$$\Delta X = \frac{1}{n}, \ \Delta Y = \frac{1}{m} \ \text{and} \ \Delta Z = \frac{1}{l}.$$

The sum of the residuals is obtained by summing up the residuals of all volumes

$$f_{x-mom,sum} = \sum_{\substack{i=1 \\ j=1}}^{\substack{i=n \\ j=m}} f_{i,j} \qquad (I.10).$$

Assuming the residuals of all individual volumes having the same value of $f_{i,j}$, the minimum sum residual becomes

$$f_{x-mom,sum} = f_{i,j} \cdot n \cdot m \cdot l = 2 \cdot \frac{\eta_0 \cdot e^{\alpha \cdot P_{hz} \cdot P} \cdot u_h \cdot b_{hz} \cdot l_c \cdot m^2}{h_0} \cdot E_{computational} \qquad (I.11).$$

Hence, the residual value agrees with the value obtained for the solution with constant pressure across the height of the gap.

Appendix J

Re-dimensionalisation of the y-momentum equation

Basis for the re-dimensionalisation is the secod equation of set 3.44, repeated as equation 9.12,

$$
\frac{\partial \overline{P}}{\partial \overline{Y}} = \frac{b_{hz}}{p_{hz}} \cdot \left[1 - \left(\frac{\eta_0 \cdot u_h \cdot \alpha}{h_0} \cdot e^{\alpha \cdot p_{hz} \cdot \overline{P}} \cdot \frac{\partial \overline{U}}{\partial \overline{Y}} \right)^2 \right]^{-1} \cdot
$$
$$
\left\{ \frac{\eta_0 \cdot u_h}{b_{hz}^2} \cdot e^{\alpha \cdot p_{hz} \cdot \overline{P}} \cdot \left[\frac{\partial^2 \overline{V}}{\partial \overline{Y}^2} + \frac{\eta_0 \cdot u_h \cdot \alpha}{h_0 \cdot \gamma} \cdot e^{\alpha \cdot p_{hz} \cdot \overline{P}} \cdot \left(\frac{\partial \overline{U}}{\partial \overline{Y}} \cdot \frac{\partial^2 \overline{U}}{\partial \overline{Y}^2} \right) \right] \right\}
$$

(J.1).

Equation J.1 is re-arranged by multiplication by p_{hz}/b_{hz} and expansion of the last bracket,

$$
\frac{p_{hz}}{b_{hz}} \cdot \frac{\partial \overline{P}}{\partial \overline{Y}} = \left[1 - \left(\frac{\eta_0 \cdot u_h \cdot \alpha}{h_0} \cdot e^{\alpha \cdot p_{hz} \cdot \overline{P}} \cdot \frac{\partial \overline{U}}{\partial \overline{Y}} \right)^2 \right]^{-1} \cdot
$$
$$
\left\{ \frac{\eta_0 \cdot u_h}{b_{hz}^2} \cdot e^{\alpha \cdot p_{hz} \cdot \overline{P}} \cdot \frac{\partial^2 \overline{V}}{\partial \overline{Y}^2} + \frac{\eta_0^2 \cdot u_0^2 \cdot \alpha}{b_{hz}^2 \cdot h_0 \cdot \gamma} \cdot \left(e^{\alpha \cdot p_{hz} \cdot \overline{P}} \right)^2 \cdot \left(\frac{\partial \overline{U}}{\partial \overline{Y}} \cdot \frac{\partial^2 \overline{U}}{\partial \overline{Y}^2} \right) \right\}
$$

(J.2).

Hertzian width b_{hz} is written in terms of h_0 and the geometry ratio $\gamma = h_0/b_{hz}$,

$$
\frac{p_{hz}}{h_0} \cdot \frac{\partial \overline{P}}{\partial \overline{Y}} = \left[1 - \left(\frac{\eta_0 \cdot u_h \cdot \alpha}{h_0} \cdot e^{\alpha \cdot p_{hz} \cdot \overline{P}} \cdot \frac{\partial \overline{U}}{\partial \overline{Y}} \right)^2 \right]^{-1} \cdot
$$
$$
\left\{ \frac{\gamma \cdot \eta_0 \cdot u_h}{h_0^2} \cdot e^{\alpha \cdot p_{hz} \cdot \overline{P}} \cdot \frac{\partial^2 \overline{V}}{\partial \overline{Y}^2} + \frac{\eta_0^2 \cdot u_0^2 \cdot \alpha}{h_0^3} \cdot \left(e^{\alpha \cdot p_{hz} \cdot \overline{P}} \right)^2 \cdot \left(\frac{\partial \overline{U}}{\partial \overline{Y}} \cdot \frac{\partial^2 \overline{U}}{\partial \overline{Y}^2} \right) \right\}
$$

(J.3).

Re-introducing the definition of viscosity,

$$\eta_0 \cdot e^{\alpha \cdot p_{hz} \cdot \overline{P}} = \eta \qquad \text{(J.4)},$$

reduces equation J.3 to

$$\frac{p_{hz}}{h_0} \cdot \frac{\partial \overline{P}}{\partial \overline{Y}} = \left[1 - \left(\eta \cdot \frac{u_h \cdot \alpha}{h_0} \cdot \frac{\partial \overline{U}}{\partial \overline{Y}} \right)^2 \right]^{-1} \cdot \left\{ \eta \cdot \frac{\gamma \cdot u_h}{h_0^2} \cdot \frac{\partial^2 \overline{V}}{\partial \overline{Y}^2} + \eta^2 \cdot \frac{u_0^2 \cdot \alpha}{h_0^3} \cdot \left(\frac{\partial \overline{U}}{\partial \overline{Y}} \cdot \frac{\partial^2 \overline{U}}{\partial \overline{Y}^2} \right) \right\}$$

$$\text{(J.5)}.$$

Application of the definition of dimensionless variables, equation 3.19,

$$\frac{p}{p_{hz}} = \overline{P} \qquad \text{(J.6a)},$$

$$\frac{u}{u_0} = \overline{U} \qquad \text{(J.6b)},$$

$$\frac{v}{u_h \cdot \gamma} = \overline{V} \qquad \text{(J.6c)},$$

and

$$\frac{y}{h_0} = \overline{Y} \qquad \text{(J.6d)},$$

simplifies equation J.5 to equation 9.13,

$$\frac{\partial p}{\partial y} = \left[1 - \left(\eta \cdot \alpha \cdot \frac{\partial u}{\partial y} \right)^2 \right]^{-1} \cdot \left\{ \eta \cdot \frac{\partial^2 v}{\partial y^2} + \eta^2 \cdot \alpha \cdot \left(\frac{\partial u}{\partial y} \cdot \frac{\partial^2 u}{\partial y^2} \right) \right\} \qquad \text{(J.7)}.$$

Employment of the continuity equation 3.14

$$\frac{\partial u}{\partial x} + \frac{\partial v}{\partial y} = 0$$

allows the exclusion of the v-velocity component of equation J.7 (9.13), so that equation 9.14 is obtained,

$$\frac{\partial p}{\partial y} = \left[1 - \left(\eta \cdot \alpha \cdot \frac{\partial u}{\partial y} \right)^2 \right]^{-1} \cdot \left\{ -\eta \cdot \frac{\partial^2 u}{\partial x \, \partial y} + \eta^2 \cdot \alpha \cdot \left(\frac{\partial u}{\partial y} \cdot \frac{\partial^2 u}{\partial y^2} \right) \right\} \qquad \text{(J.8)}.$$

Appendix K

Further result graphs

The graphs are displayed on the following pages.
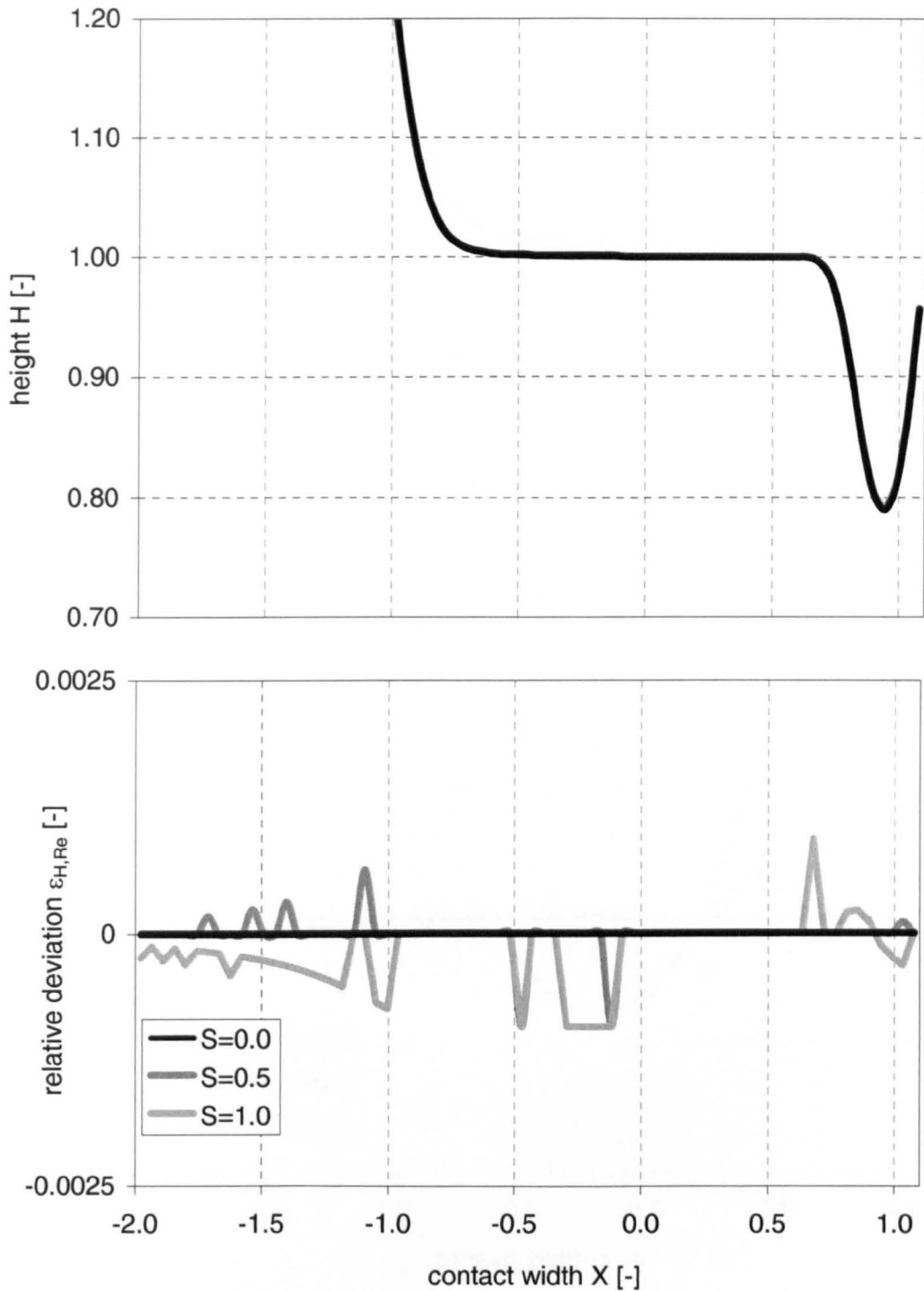
Figure K.1:   Height of the gap H and relative deviation from Reynolds equation based solution $\varepsilon_{H,Re}$ for various sliding ratios; load case i (table 10.1), sliding ratios S = 0.0, 0.5, and 1.0.
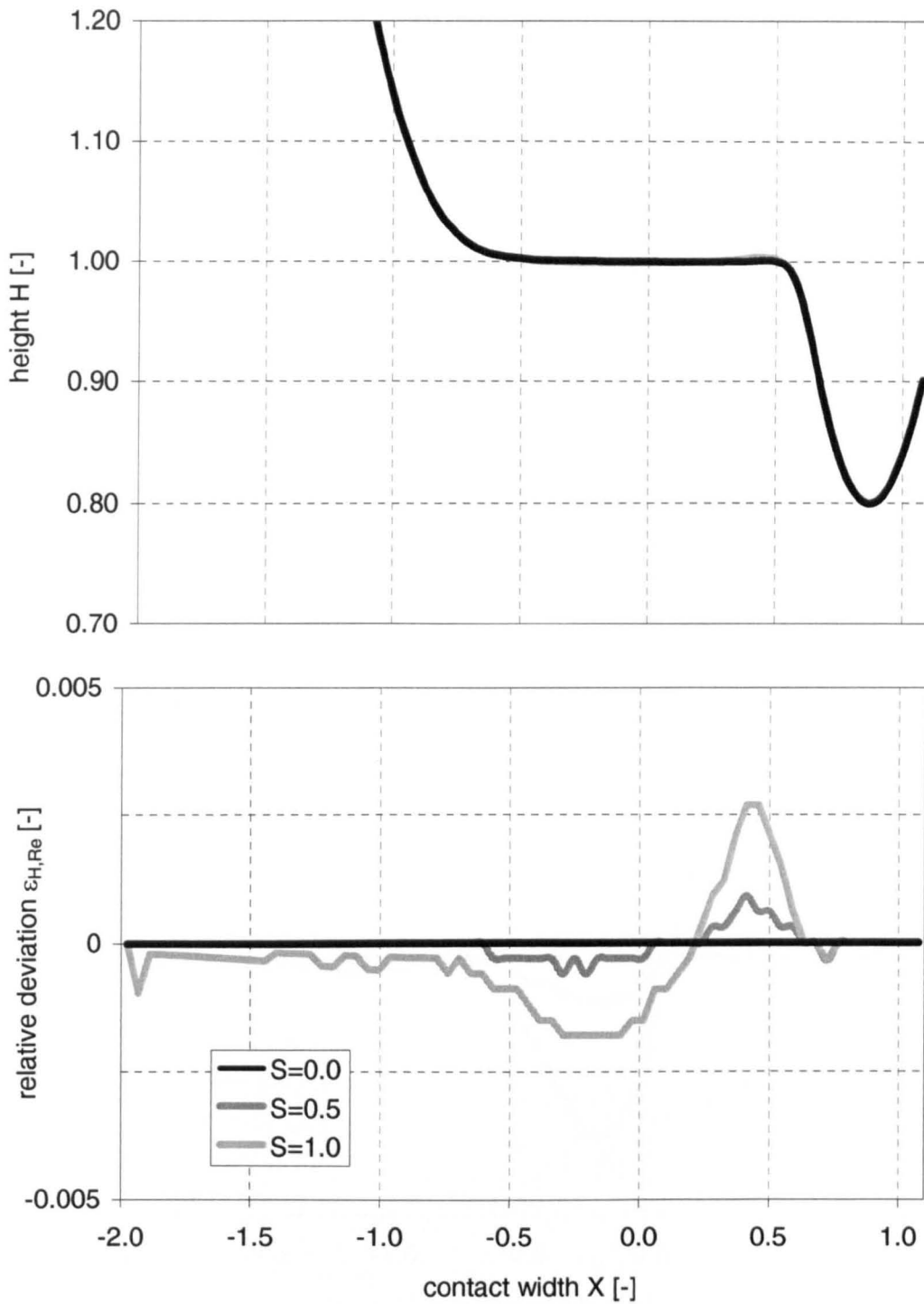
Figure K.2:   *Height of the gap H and relative deviation from Reynolds equation based solution $\varepsilon_{H,Re}$ for various sliding ratios; load case ii (table 10.1), sliding ratios S = 0.0, 0.5, and 1.0.*
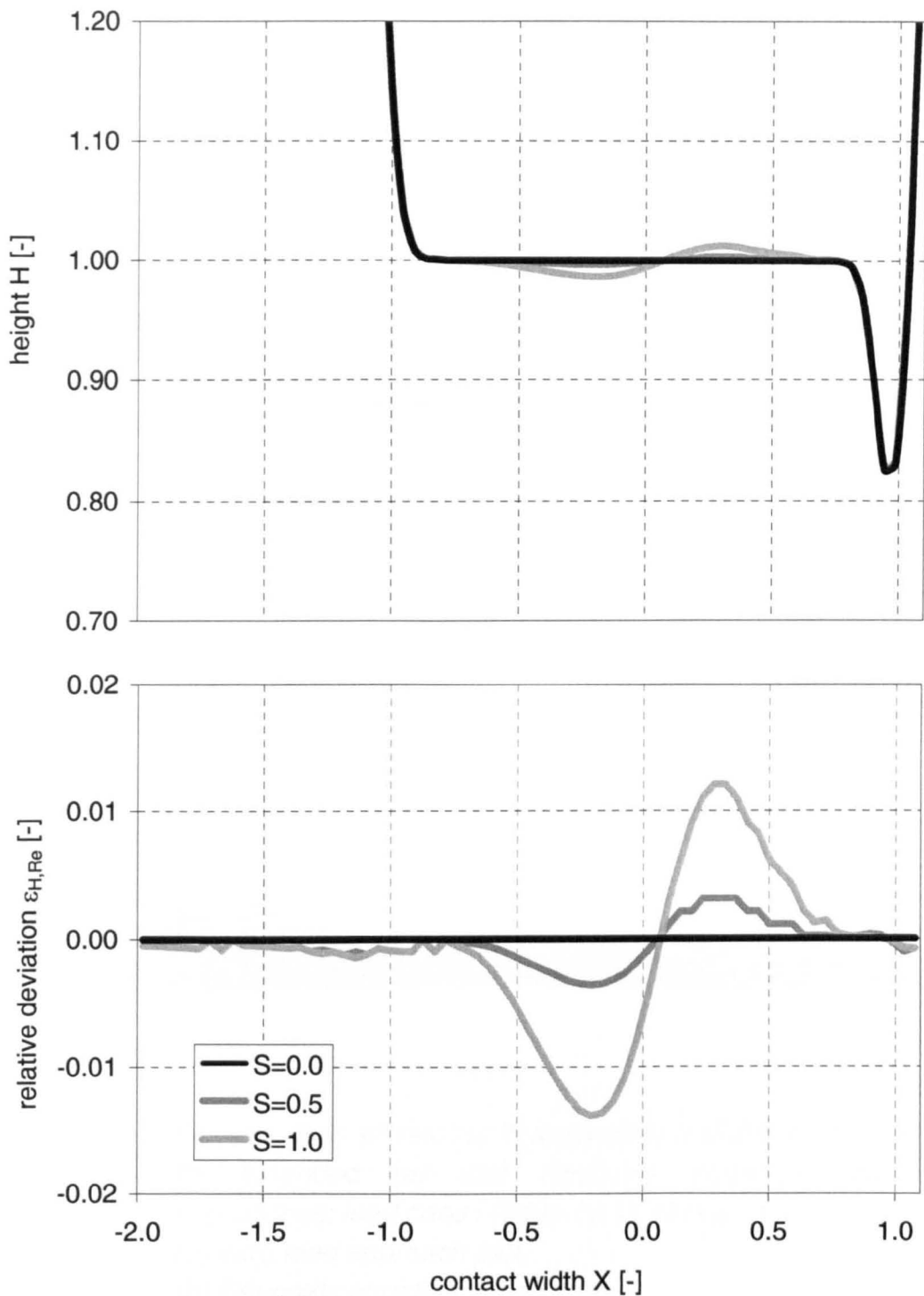
Figure K.3:   Height of the gap H and relative deviation from Reynolds equation based solution $\varepsilon_{H,Re}$ for various sliding ratios; load case iii (table 10.1), sliding ratios S = 0.0, 0.5, and 1.0.
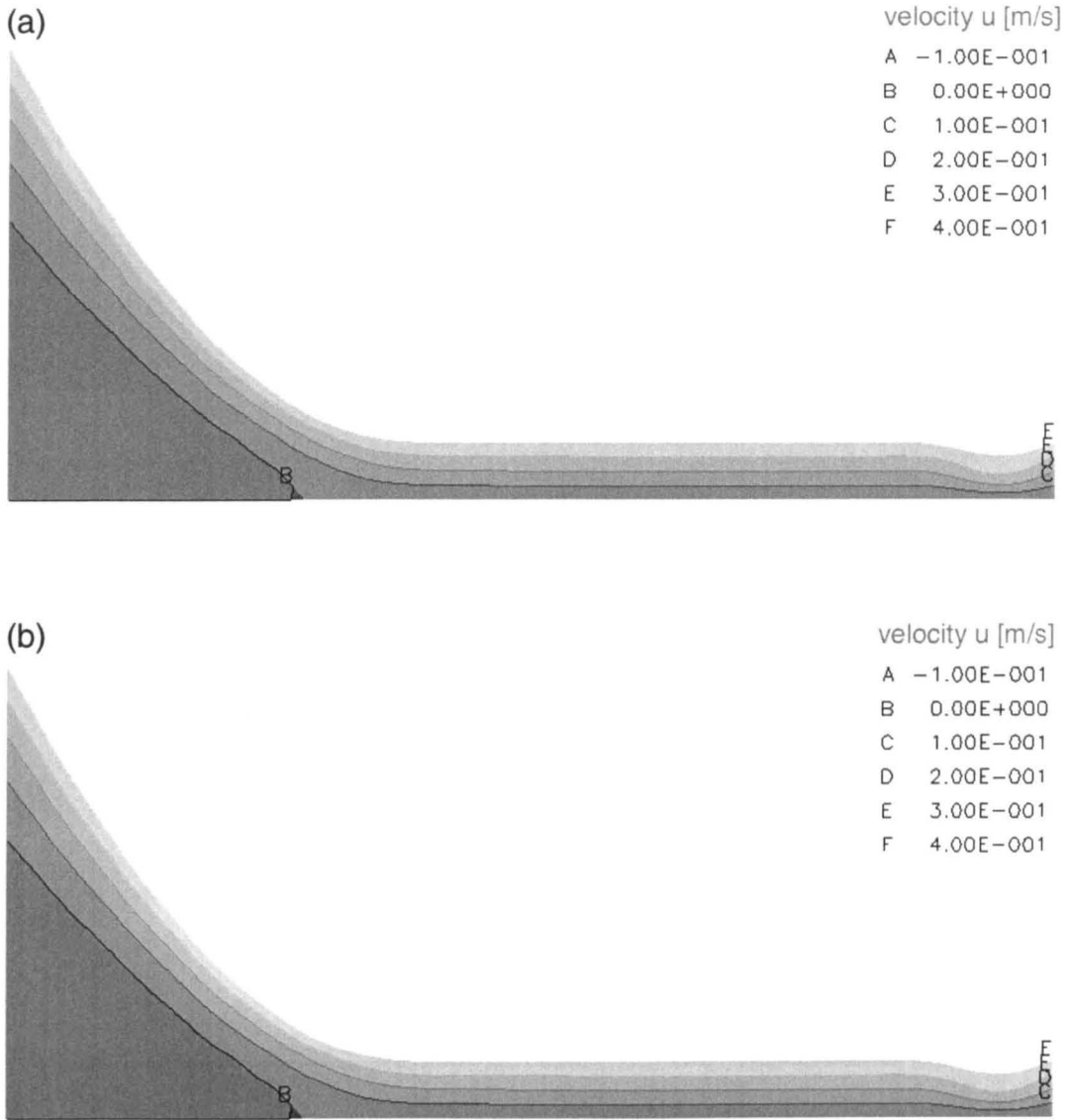
Figure K.4:   Contour plots of velocity in x-direction u distribution in the gap
              for extended (a) and Reynolds equation based (b)
              approaches; load case i (table 10.1), sliding ratio S = 1.0,
              (a) extended approach plot,
              (b) Reynolds equation based plot.

(a)

velocity u [m/s]
A $-2.00E-001$
B $-2.48E-009$
C $2.00E-001$
D $4.00E-001$
E $6.00E-001$
F $8.00E-001$
G $1.00E+000$

(b)

velocity u [m/s]
A $-2.00E-001$
B $-2.48E-009$
C $2.00E-001$
D $4.00E-001$
E $6.00E-001$
F $8.00E-001$
G $1.00E+000$
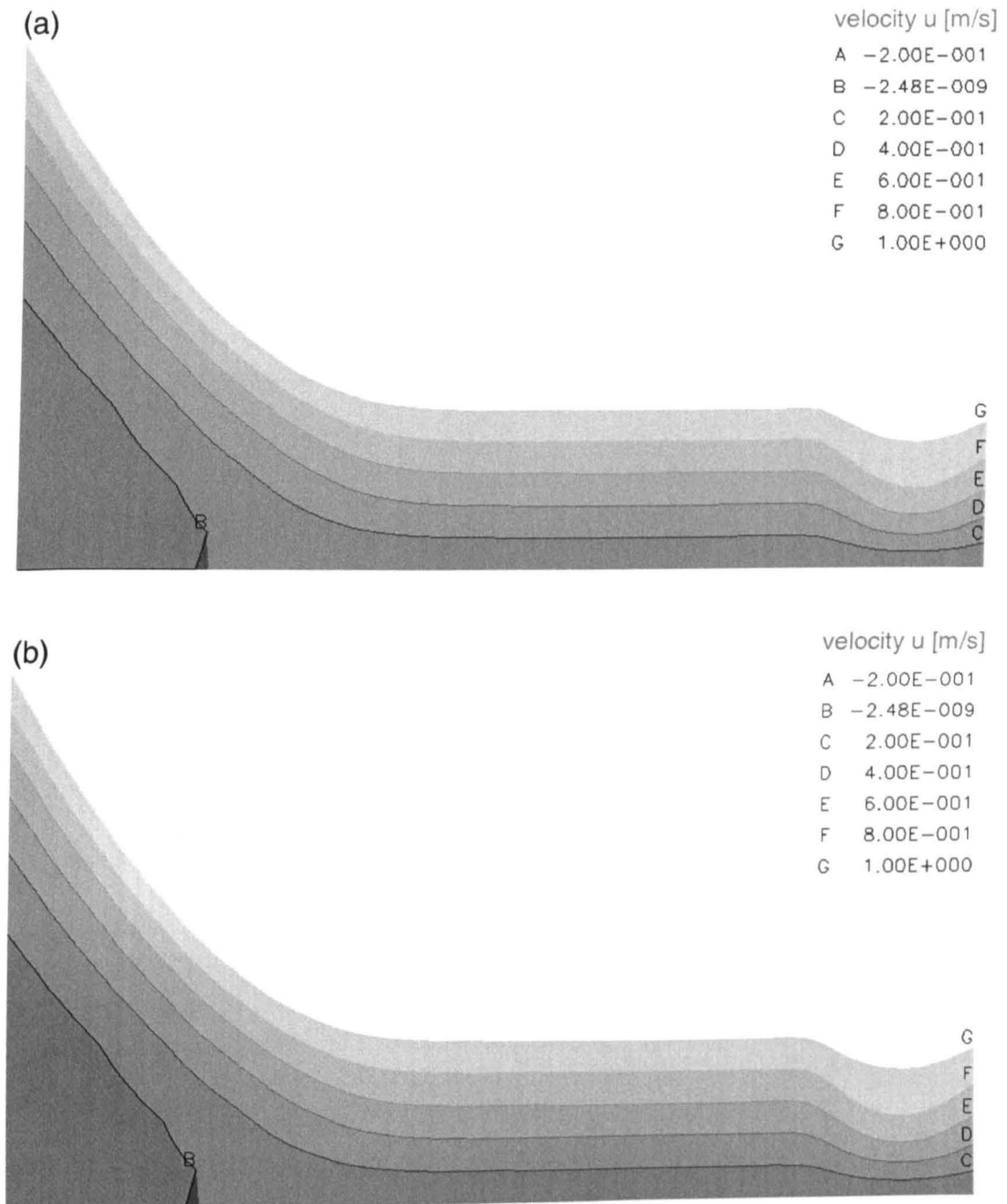
Figure K.5:   *Contour plots of velocity in x-direction u distribution in the gap*
for extended (a) and Reynolds equation based (b) approaches;
load case ii (table 10.1) sliding ratio S = 1.0,
(a) extended approach plot,
(b) Reynolds equation based plot.
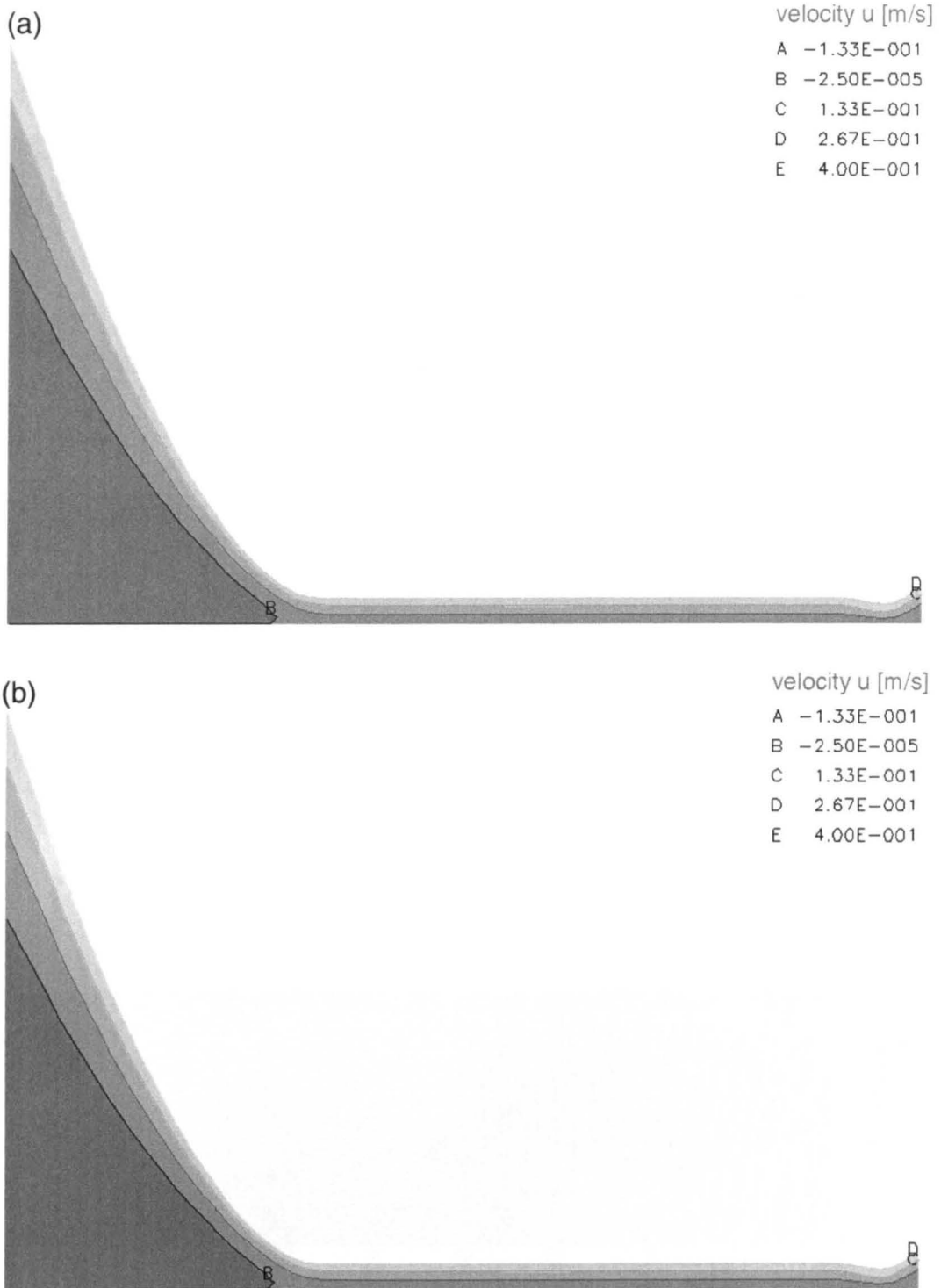
Figure K.6:   *Contour plots of velocity in x-direction u distribution in the gap for extended (a) and Reynolds equation based (b) approaches; load case iii (table 10.1) sliding ratio S = 1.0,*
          (a) extended approach plot,
          (b) Reynolds equation based plot.
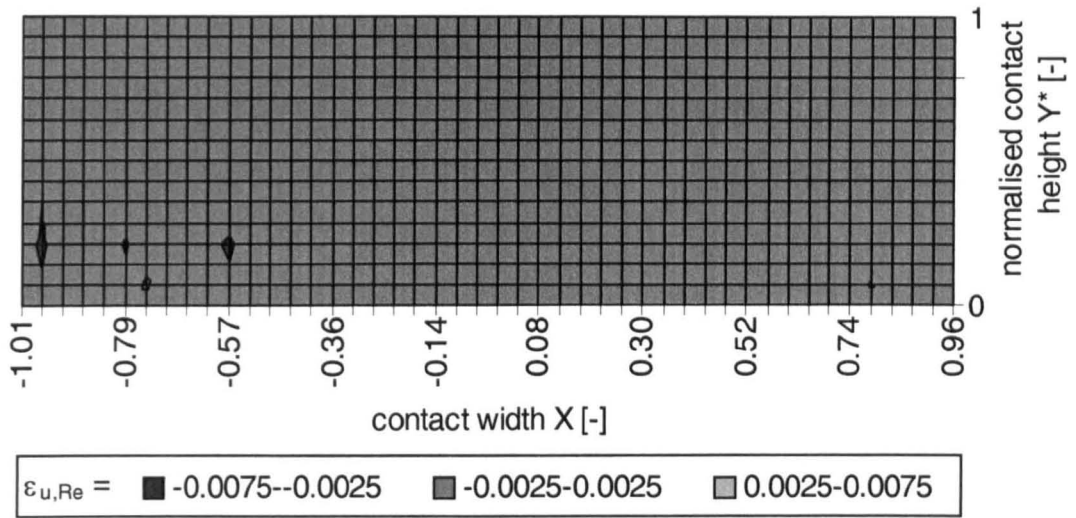
Figure K.7:   Relative deviation of velocity in x-direction u of extended from Reynolds equation based approach $\varepsilon_{u,Re}$; load case i (table 10.1), sliding ratio 1.0.
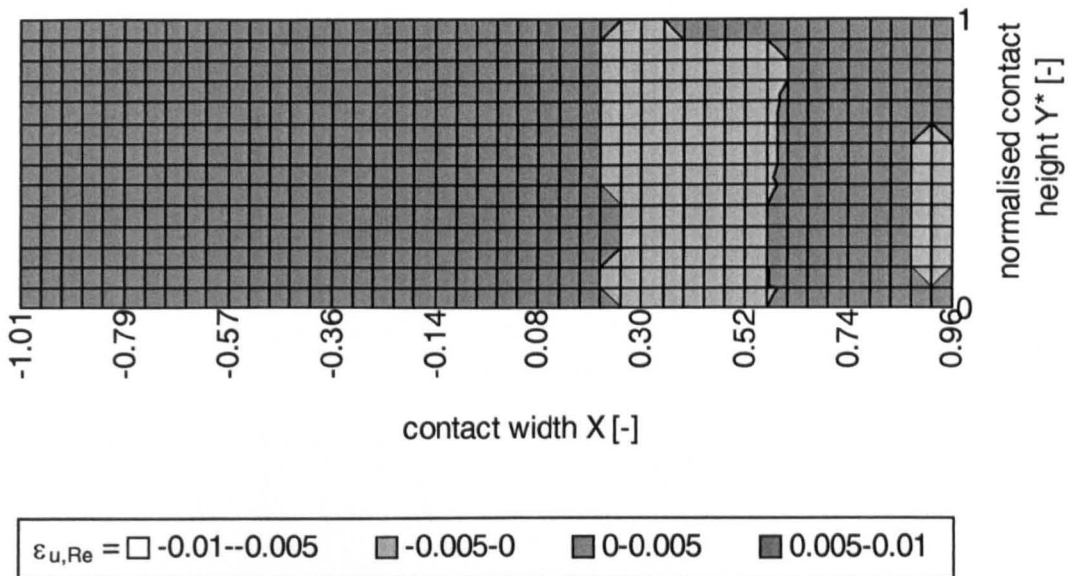
Figure K.8:   Relative deviation of velocity in x-direction u of extended from Reynolds equation based approach $\varepsilon_{u,Re}$; load case ii (table 10.1), sliding ratio 1.0.
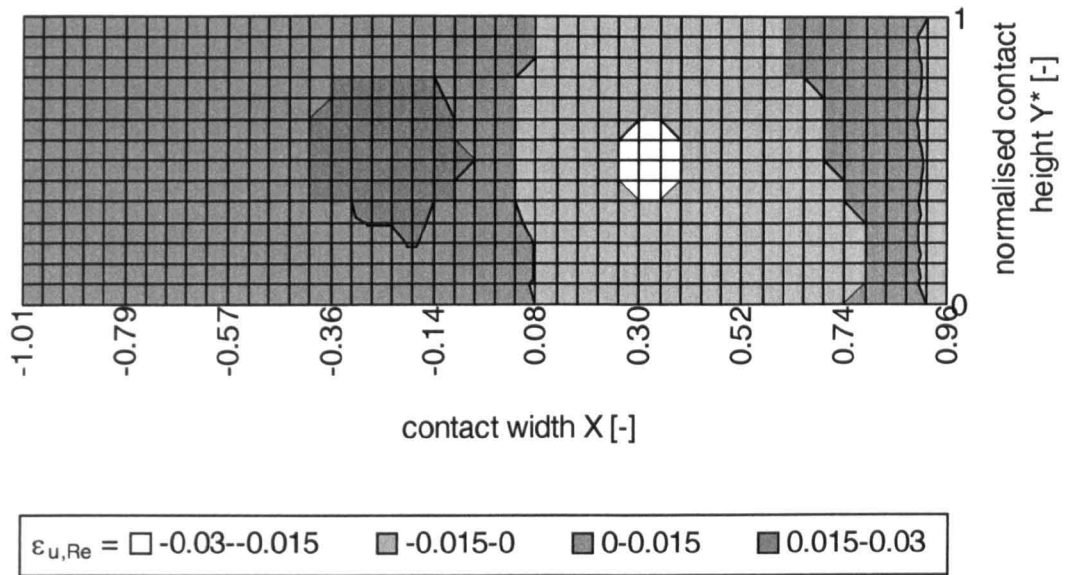
Figure K.9:   *Relative deviation of velocity in x-direction u of extended from Reynolds equation based approach $\varepsilon_{u,Re}$; load case iii (table 10.1), sliding ratio 1.0.*
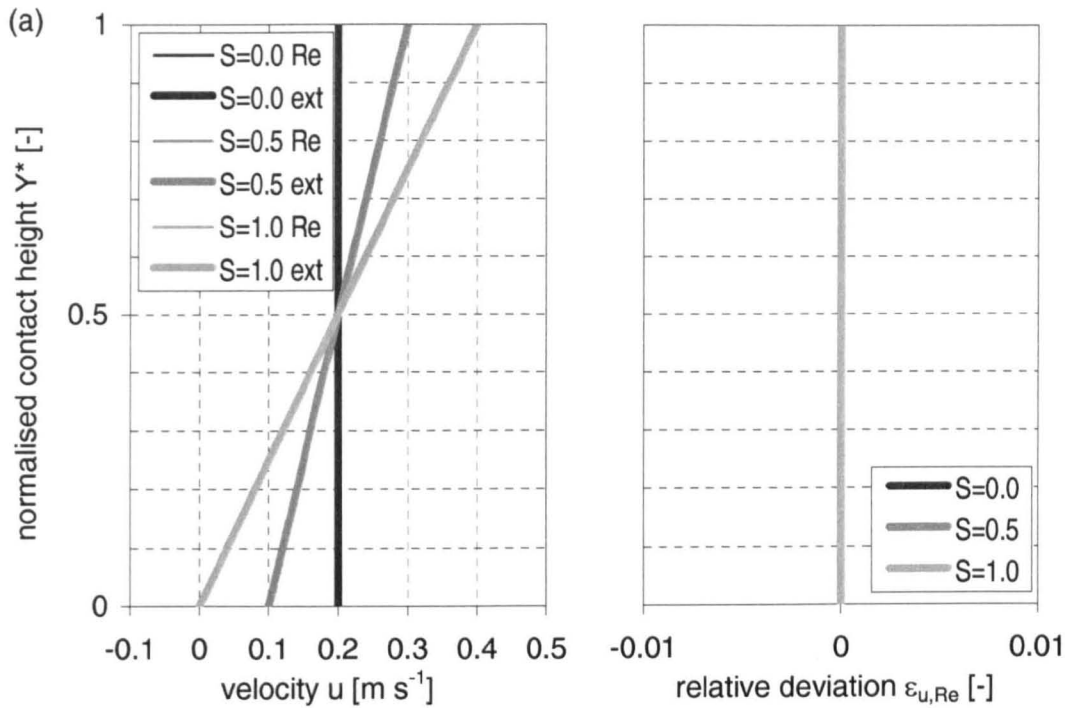
Figure K.10:   *Velocity in x-direction u and relative deviation from Reynolds equation based solution $\varepsilon_{u,Re}$ at selected positions X for various sliding ratios; load case i (table 10.1), sliding ratios $S = 0.0$, 0.5, and 1.0,*
   (a)   at the position of minimum height of the gap X_{hmin},
   (b)   at the position of maximum height of the gap X_{hmax},
   (c)   at the position of agreement of Reynolds equation and extended approach based solution X_{cross},
   (d)   at the contact centreline $X = 0.0$
   (continued).
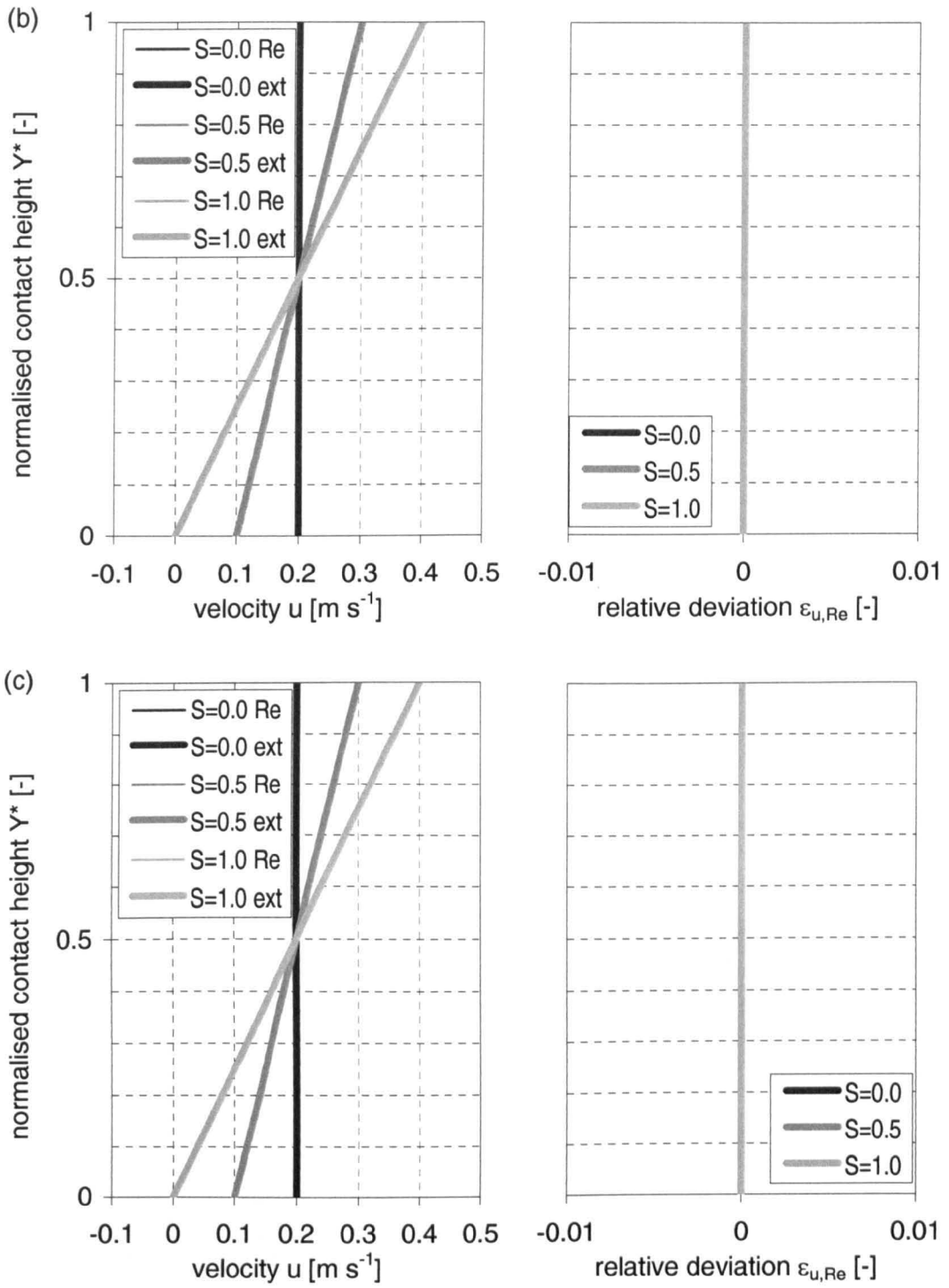
Figure K.10:   *(continued).*
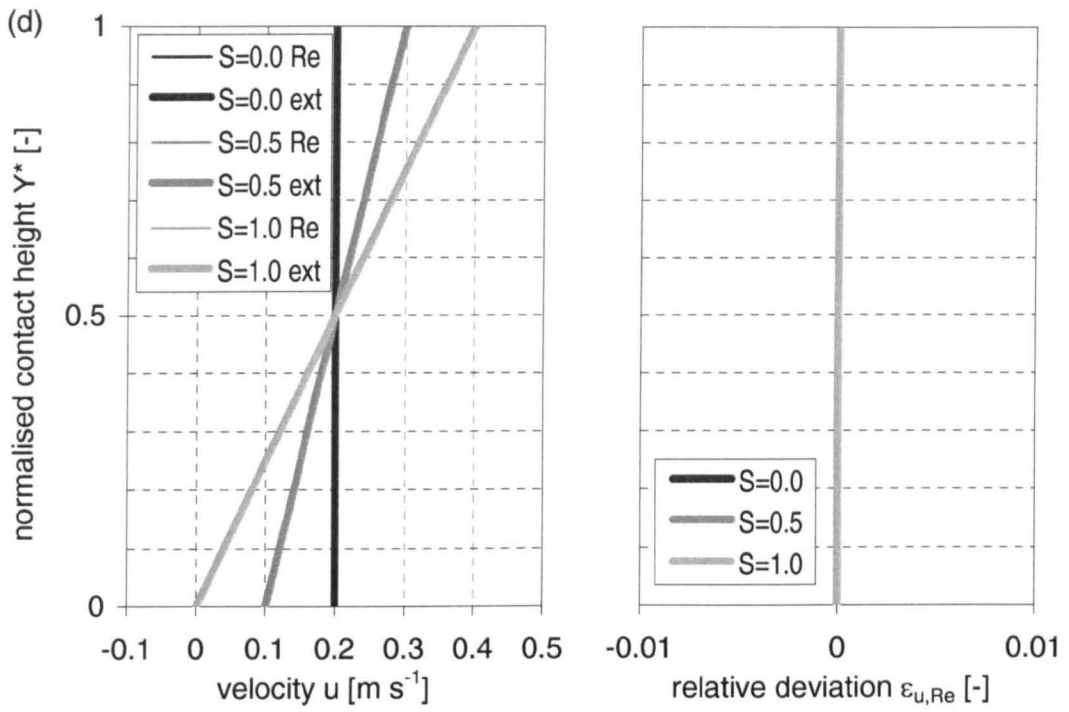
Figure K.10:   (concluded).
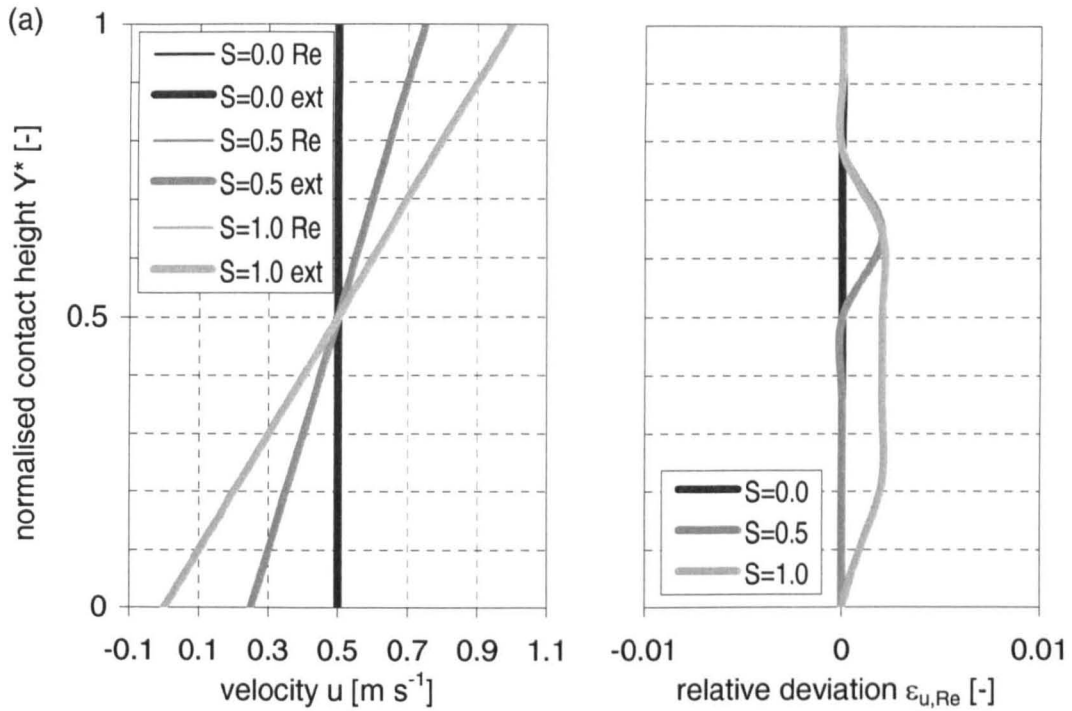
Figure K.11: Velocity in x-direction u and relative deviation from Reynolds equation based solution $\varepsilon_{u,Re}$ at selected positions X for various sliding ratios; load case ii (table 10.1), sliding ratios S = 0.0, 0.5, and 1.0,

(a)   at the position of minimum height of the gap X_{hmin},

(b)   at the position of maximum height of the gap X_{hmax},

(c)   at the position of agreement of Reynolds equation and extended approach based solution X_{cross},

(d)   at the contact centreline X = 0.0
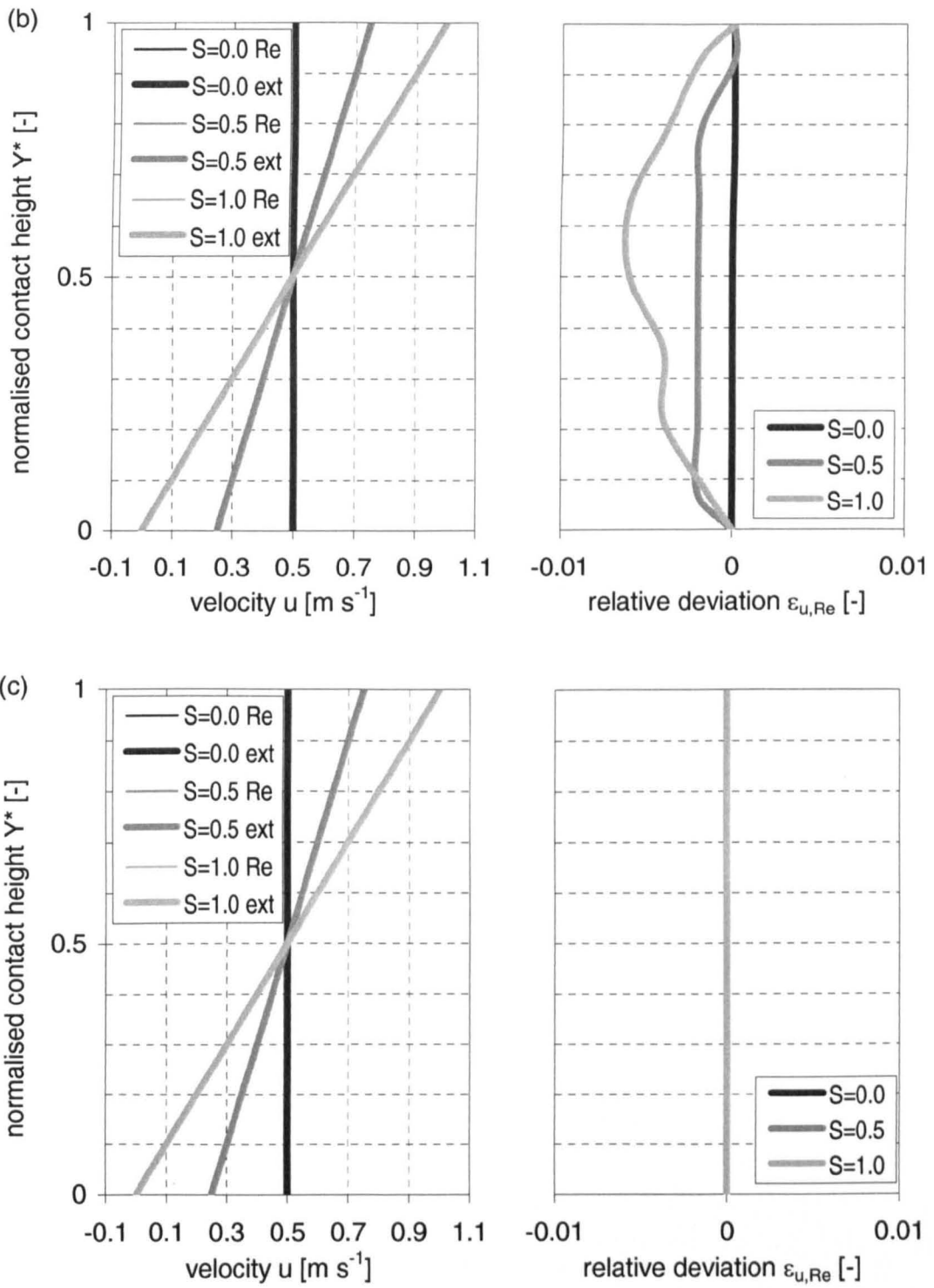
(continued).

Figure K.11:   (continued).
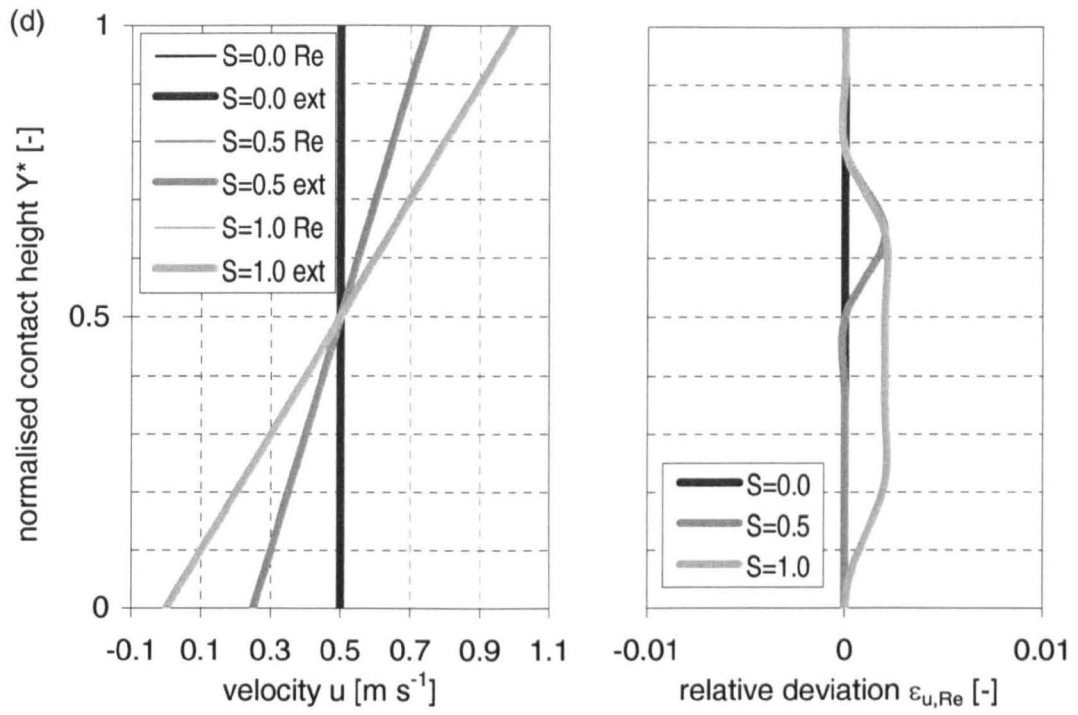
Figure K.11:   (concluded).
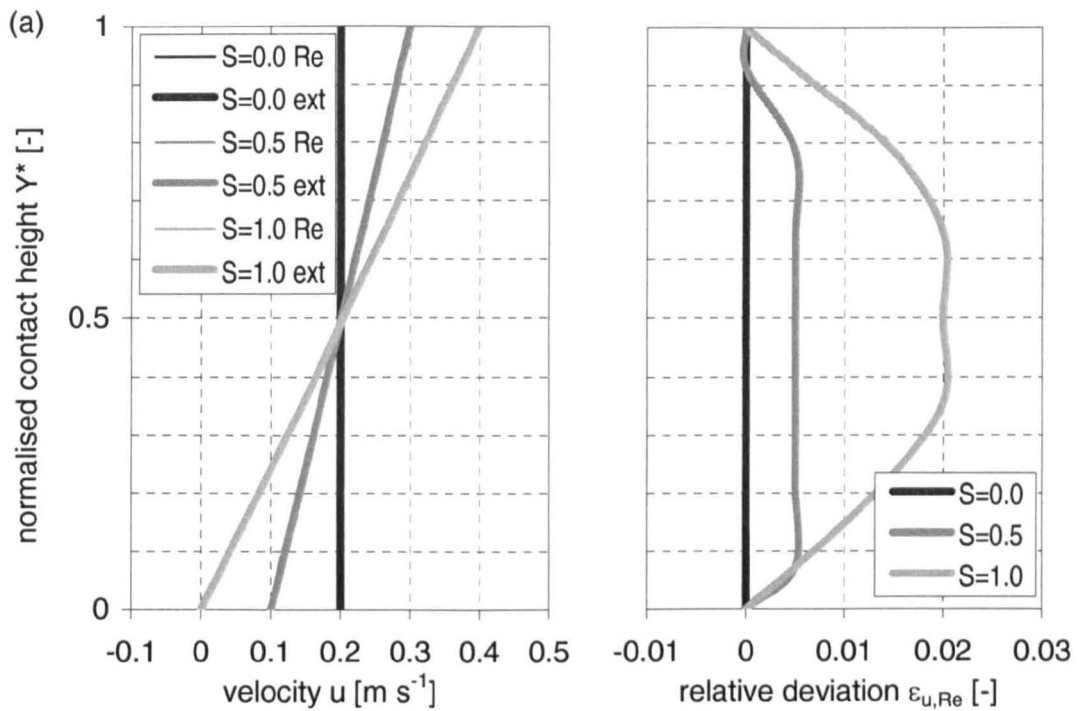
Figure K.12:   Velocity in x-direction u and relative deviation from Reynolds equation based solution $\varepsilon_{u,Re}$ at selected positions X for various sliding ratios; load case iii (table 10.1), sliding ratios S = 0.0, 0.5, and 1.0,
(a)   at the position of minimum height of the gap X_{hmin},
(b)   at the position of maximum height of the gap X_{hmax},
(c)   at the position of agreement of Reynolds equation and extended approach based solution X_{cross},
(d)   at the contact centreline X = 0.0
(continued).
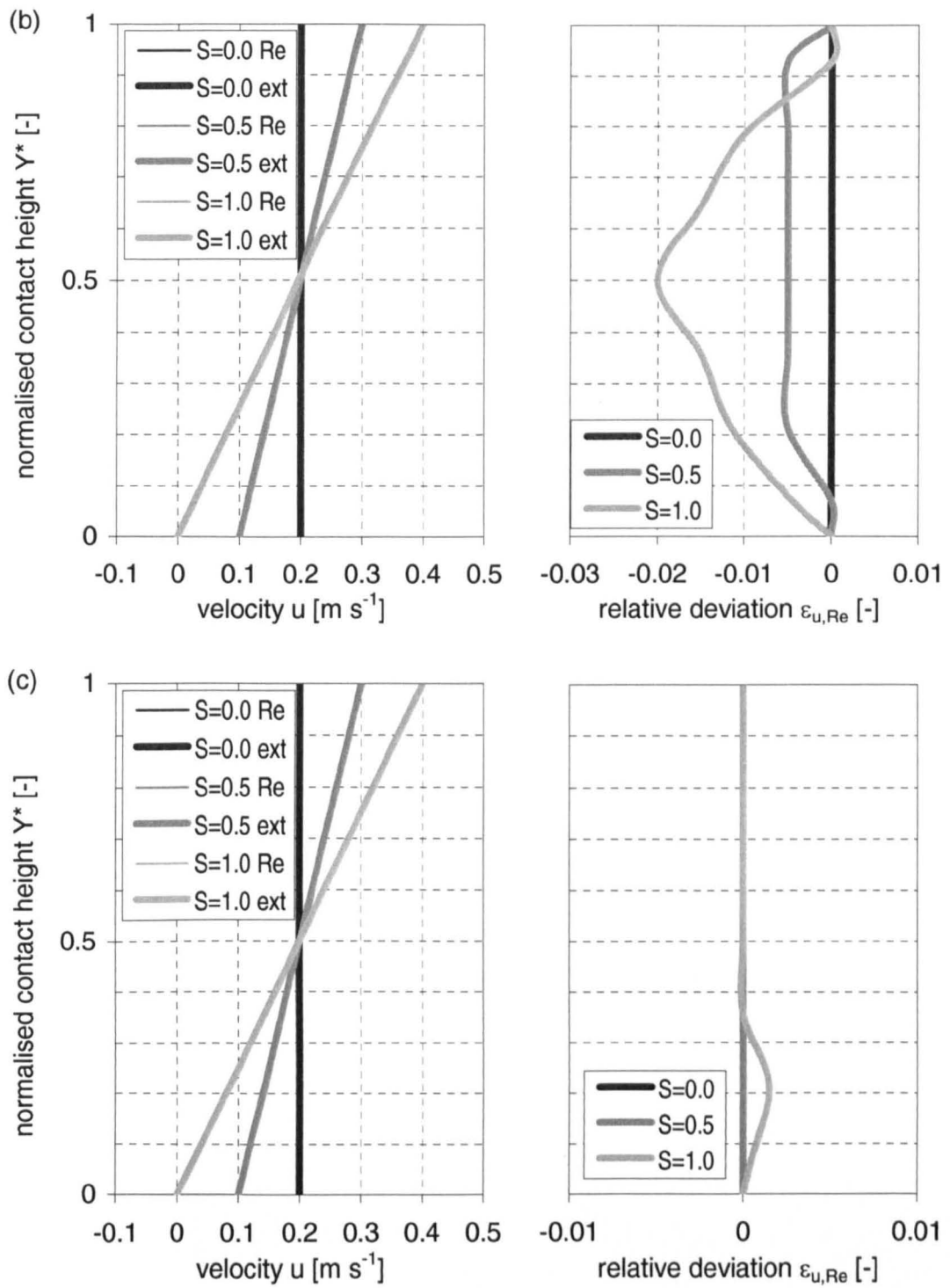
Figure K.12:   (continued).

Figure K.12:   (concluded).

(a)

pressure p [Pa]

A   0.00E+000
B   5.00E+007
C   1.00E+008
D   1.50E+008
E   2.00E+008
F   2.50E+008
G   3.00E+008

(b)

pressure p [Pa]

A   0.00E+000
B   5.00E+007
C   1.00E+008
D   1.50E+008
E   2.00E+008
F   2.50E+008
G   3.00E+008
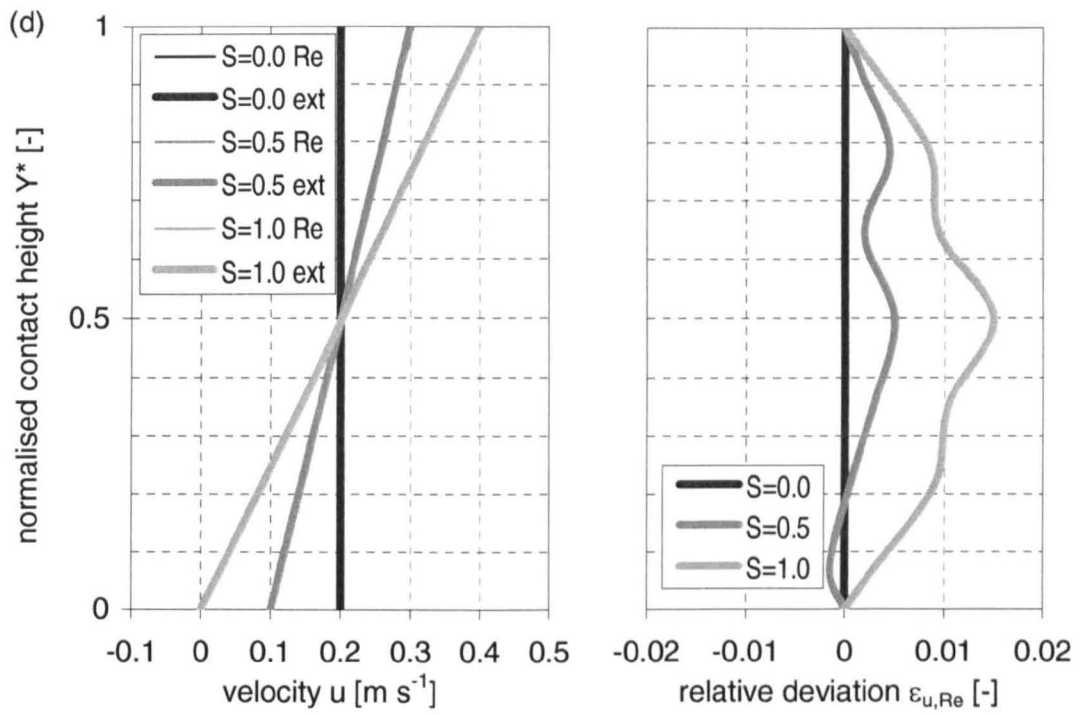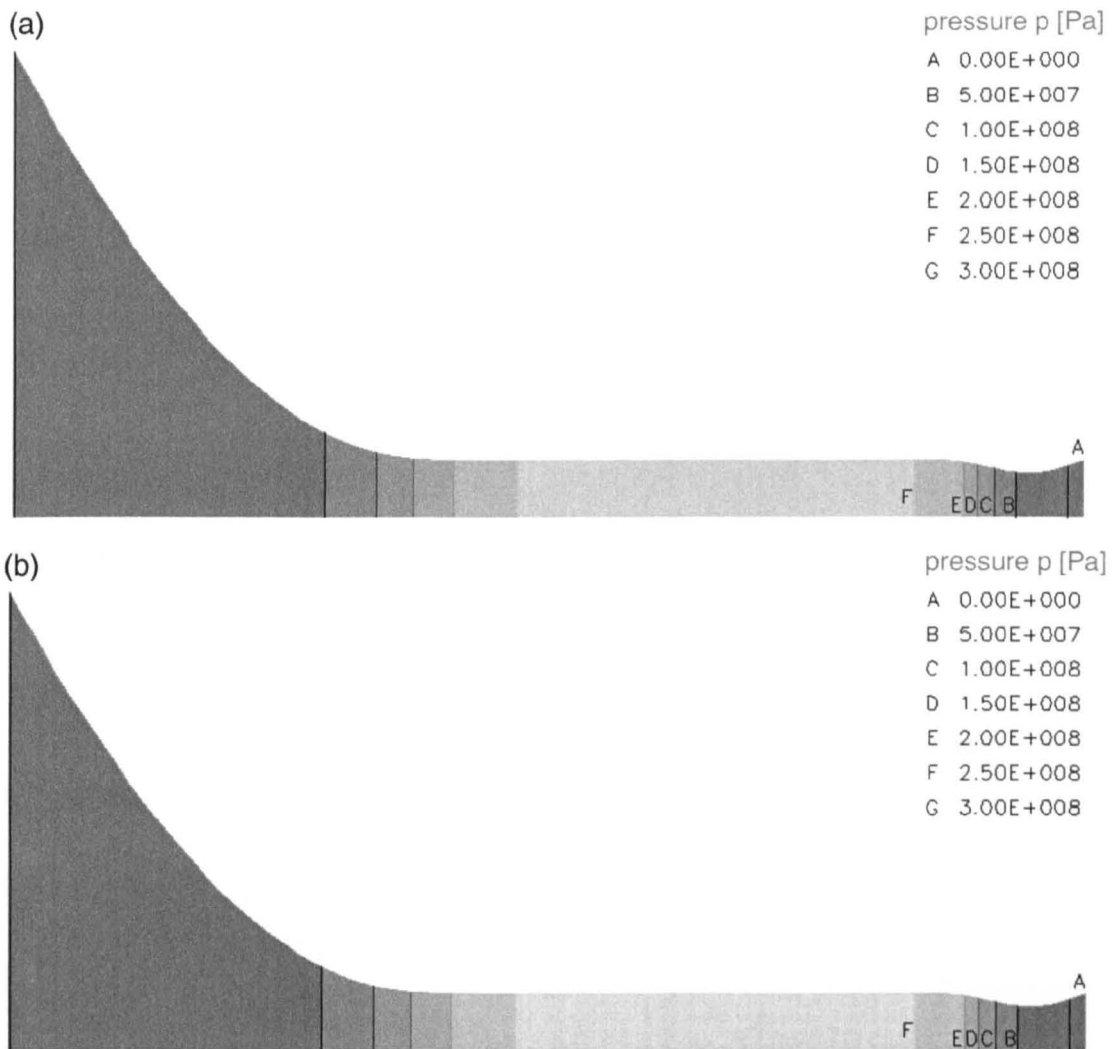
Figure K.13:   *Contour plots of pressure distribution p in the gap for extended and Reynolds equation based approaches; load case i (table 10.1), sliding ratios S = 0.0, 0.5, and 1.0,*
(a) sliding ratio S = 0.0,
(b) sliding ratio S = 0.5,
(c) sliding ratio S = 1.0,
(d) Reynolds equation based solution
(continued).

(c)

pressure p [Pa]

A 0.00E+000
B 5.00E+007
C 1.00E+008
D 1.50E+008
E 2.00E+008
F 2.50E+008
G 3.00E+008

(d)

pressure p [Pa]

A 0.00E+000
B 5.00E+007
C 1.00E+008
D 1.50E+008
E 2.00E+008
F 2.50E+008
G 3.00E+008
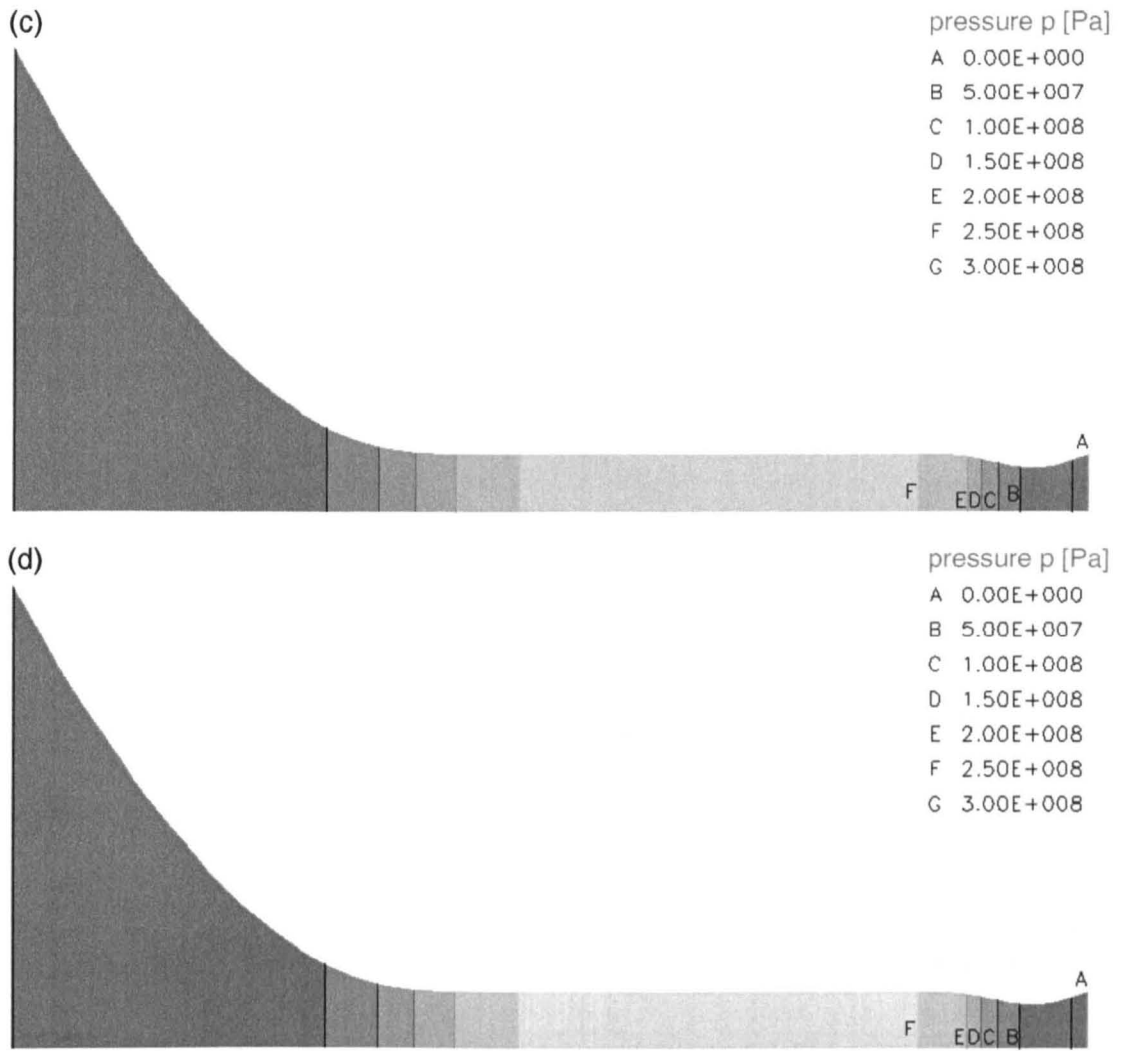
Figure K.13:   (concluded).
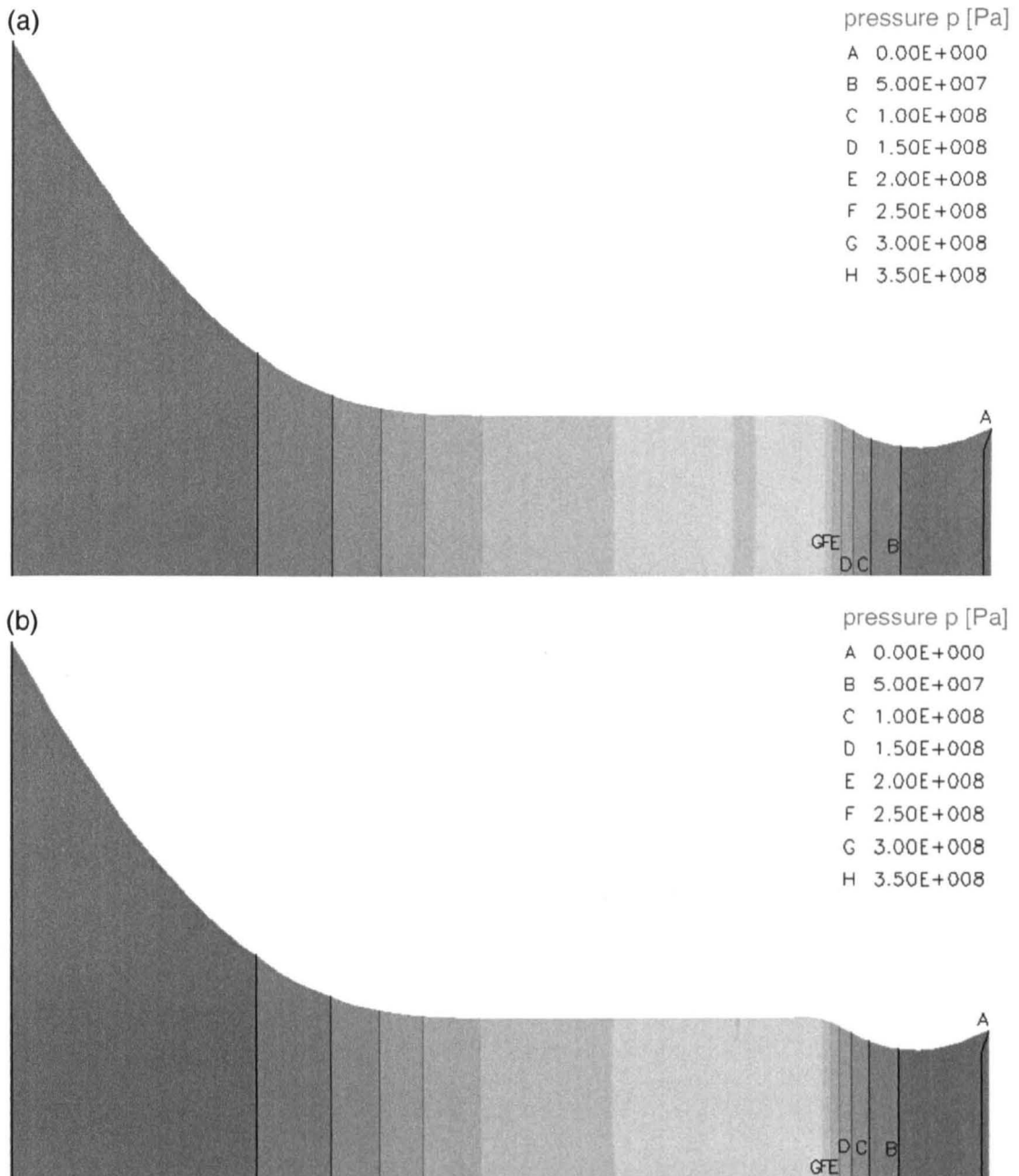
Figure K.14:   Contour plots of pressure distribution p in the gap for extended and Reynolds equation based approaches; load case ii (table 10.1), sliding ratios S = 0.0, 0.5, and 1.0,
(a) sliding ratio S = 0.0,
(b) sliding ratio S = 0.5,
(c) sliding ratio S = 1.0,
(d) Reynolds equation based solution
(continued).

(c)

pressure p [Pa]
A 0.00E+000
B 5.00E+007
C 1.00E+008
D 1.50E+008
E 2.00E+008
F 2.50E+008
G 3.00E+008
H 3.50E+008

(d)

pressure p [Pa]
A 0.00E+000
B 5.00E+007
C 1.00E+008
D 1.50E+008
E 2.00E+008
F 2.50E+008
G 3.00E+008
H 3.50E+008

Figure K.14:   (concluded).

(a)

pressure p [Pa]
A 0.00E+000
B 1.00E+008
C 2.00E+008
D 3.00E+008
E 4.00E+008
F 5.00E+008
G 6.00E+008

(b)

pressure p [Pa]
A 0.00E+000
B 1.00E+008
C 2.00E+008
D 3.00E+008
E 4.00E+008
F 5.00E+008
G 6.00E+008
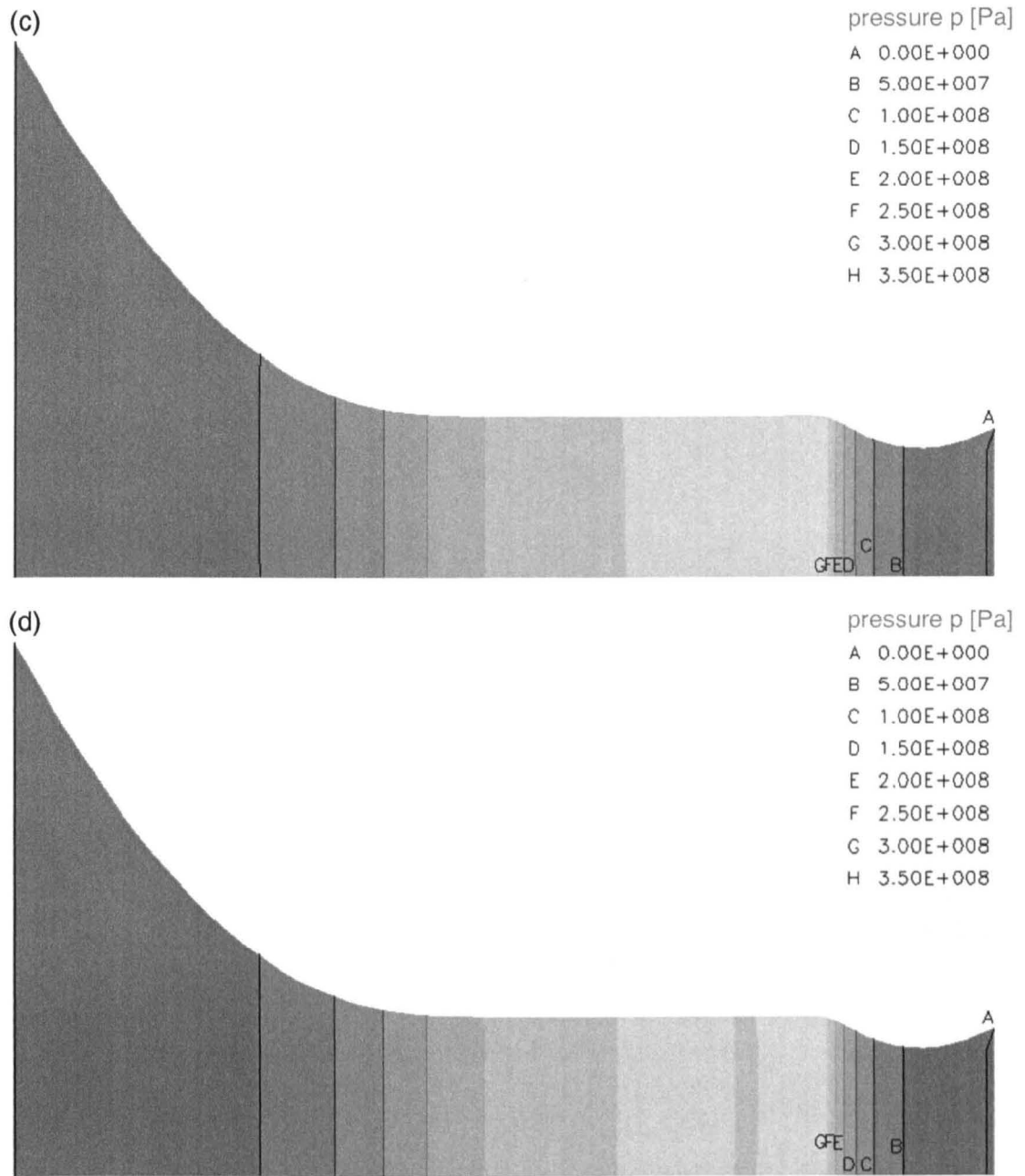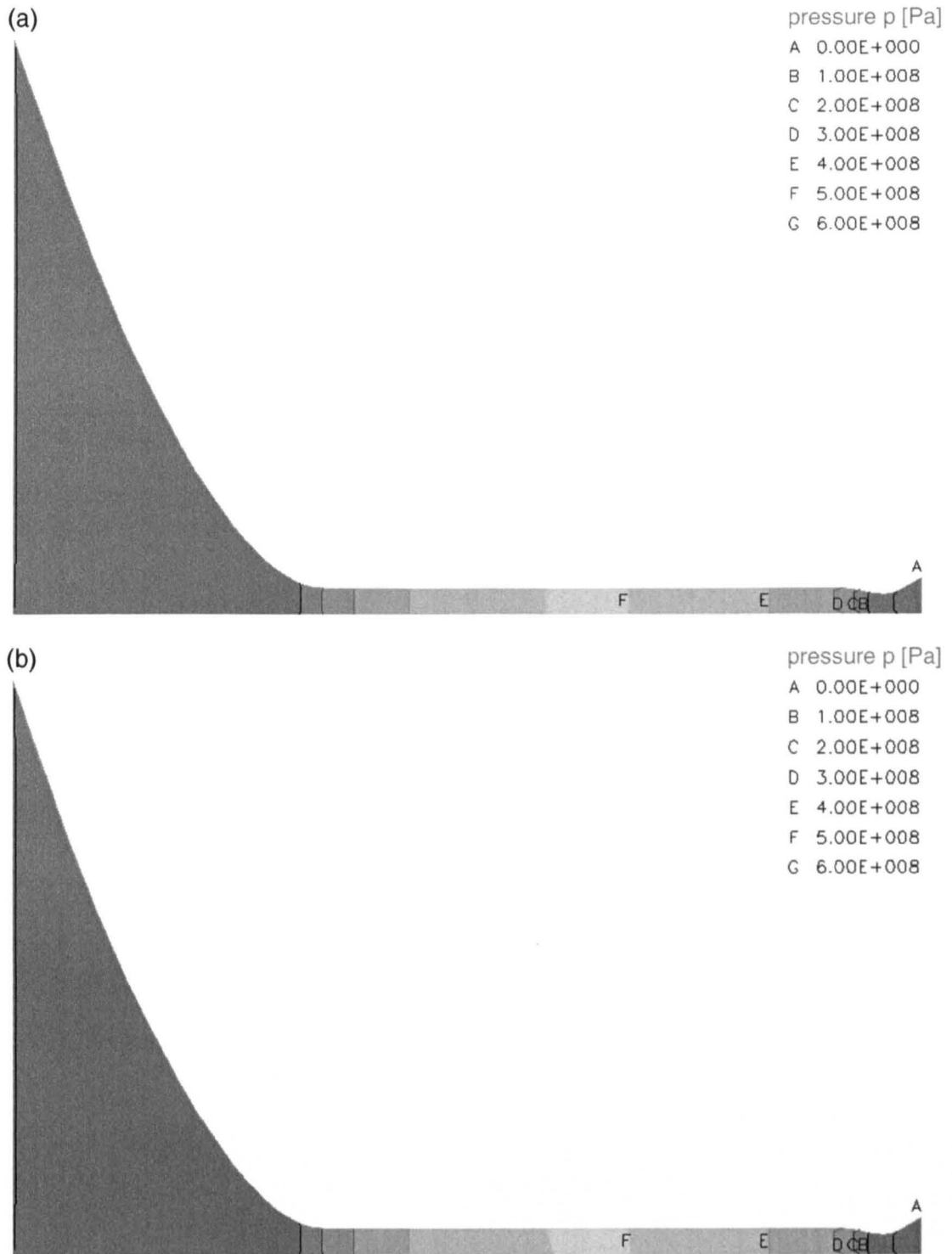
Figure K.15:   Contour plots of pressure distribution p in the gap for extended
               and Reynolds equation based approaches; load case iii (table
               10.1), sliding ratios S = 0.0, 0.5, and 1.0,
               (a) sliding ratio S = 0.0,
               (b) sliding ratio S = 0.5,
               (c) sliding ratio S = 1.0,
               (d) Reynolds equation based solution
               (continued).

(c)

	pressure p [Pa]
A	0.00E+000
B	1.00E+008
C	2.00E+008
D	3.00E+008
E	4.00E+008
F	5.00E+008
G	6.00E+008

(d)

	pressure p [Pa]
A	0.00E+000
B	1.00E+008
C	2.00E+008
D	3.00E+008
E	4.00E+008
F	5.00E+008
G	6.00E+008

Figure K.15:   (concluded).

(a)

absolute pressure deviation $\varepsilon_{p,abs}$ [Pa]
A $-6.00E+005$
B $-2.00E+005$
C $2.00E+005$
D $6.00E+005$

(b)

absolute pressure deviation $\varepsilon_{p,abs}$ [Pa]
A $-6.00E+005$
B $-2.00E+005$
C $2.00E+005$
D $6.00E+005$
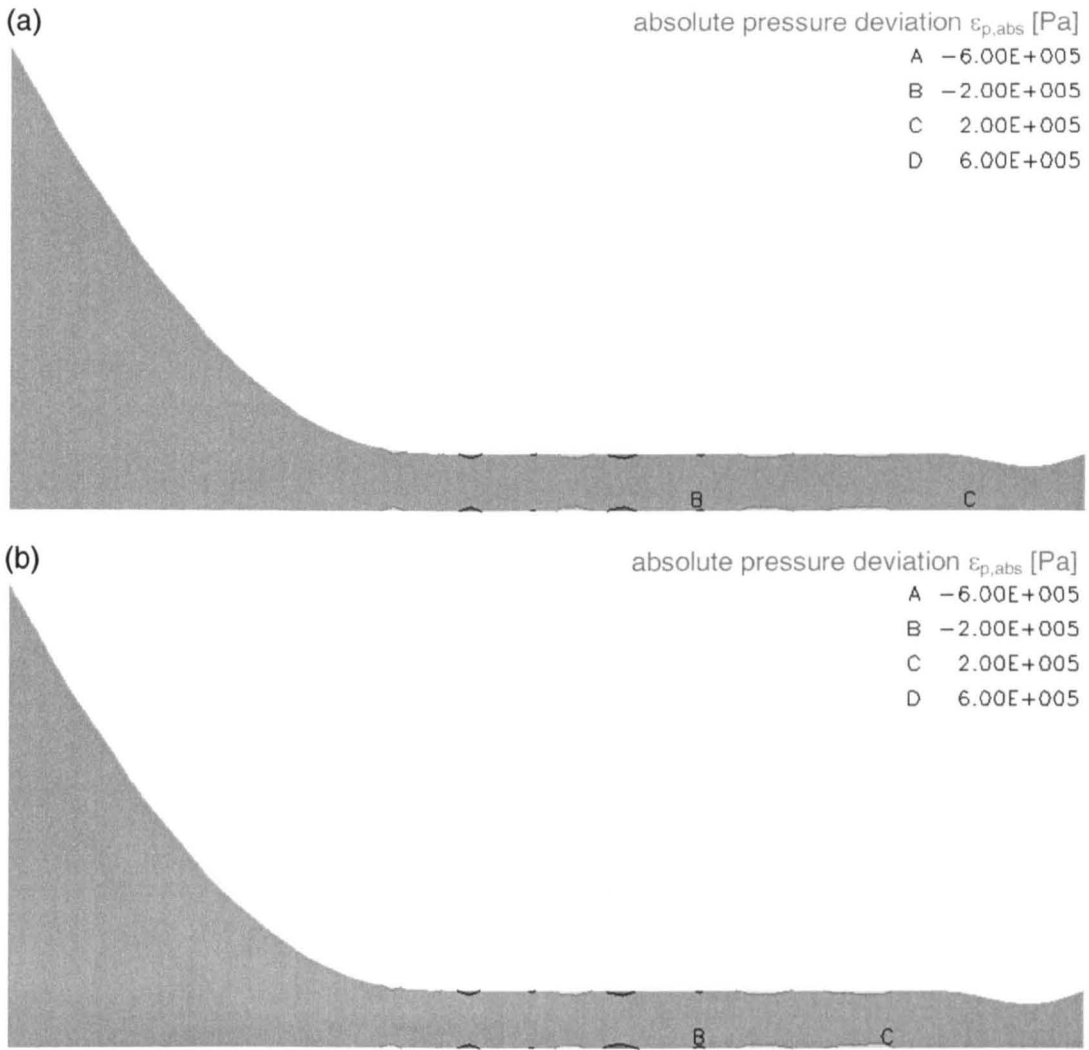
Figure K.16:   Contour plots of absolute pressure deviation from the centreline pressure $\varepsilon_{p,abs}$ in the gap for extended approach; load case i (table 10.1), sliding ratios $S = 0.0$, 0.5, and 1.0,
(a) $S = 0.0$,
(b) $S = 0.5$,
(c) $S = 1.0$
(continued).

(c)

absolute pressure deviation $\varepsilon_{p,abs}$ [Pa]

A	−6.00E+005
B	−2.00E+005
C	2.00E+005
D	6.00E+005

Figure K.16: *(concluded).*

(a)

absolute pressure deviation $\varepsilon_{p,abs}$ [Pa]

A	−6.00E+005
B	−2.00E+005
C	2.00E+005
D	6.00E+005
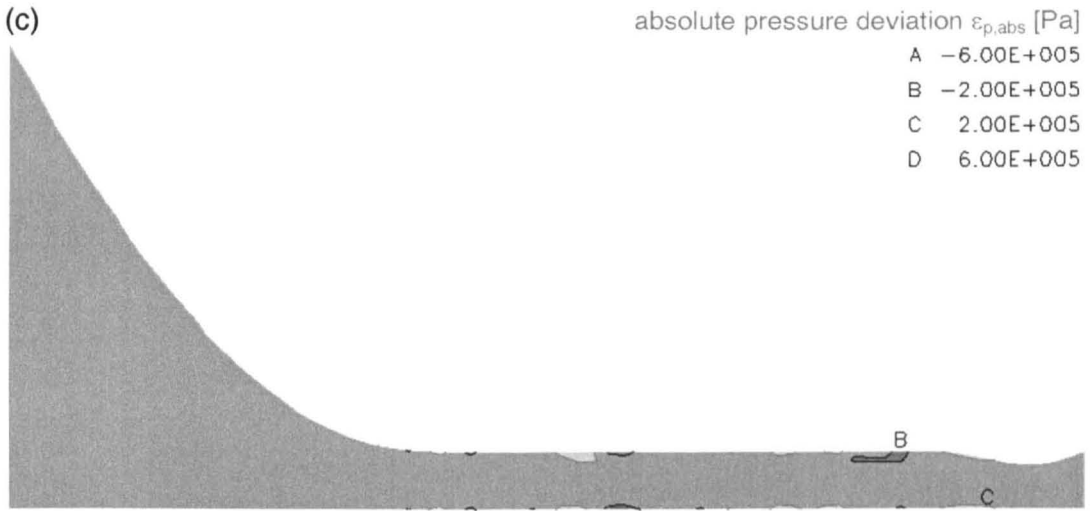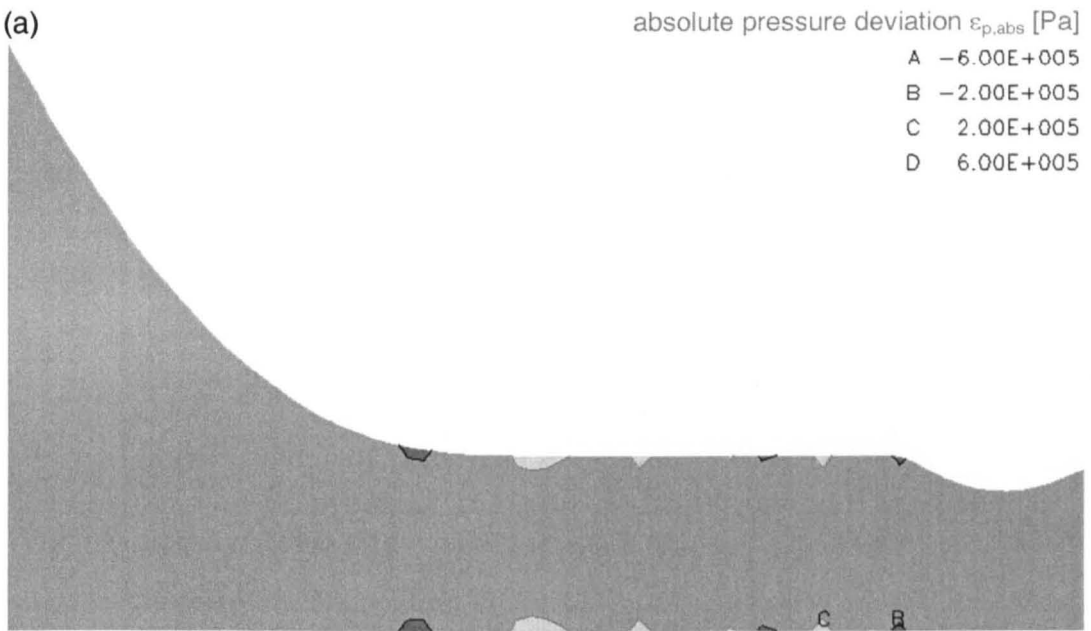
Figure K.17: *Contour plots of absolute pressure deviation from the centreline pressure $\varepsilon_{p,abs}$ in the gap for extended approach; load case ii (table 10.1), sliding ratios S = 0.0, 0.5, and 1.0,*
(a) S = 0.0,
(b) S = 0.5,
(c) S = 1.0
(continued).

(b)

absolute pressure deviation $\varepsilon_{p,abs}$ [Pa]

A	−6.00E+005
B	−2.00E+005
C	2.00E+005
D	6.00E+005
E	1.00E+006

(c)

absolute pressure deviation $\varepsilon_{p,abs}$ [Pa]

A	−1.00E+006
B	−6.00E+005
C	−2.00E+005
D	2.00E+005
E	6.00E+005

Figure K.17:   (concluded).

(a)

absolute pressure deviation $\varepsilon_{p,abs}$ [Pa]

A	$-1.00E+007$
B	$-3.33E+006$
C	$3.33E+006$
D	$1.00E+007$

(b)

absolute pressure deviation $\varepsilon_{p,abs}$ [Pa]

A	$-5.00E+006$
B	$-1.67E+006$
C	$1.67E+006$
D	$5.00E+006$
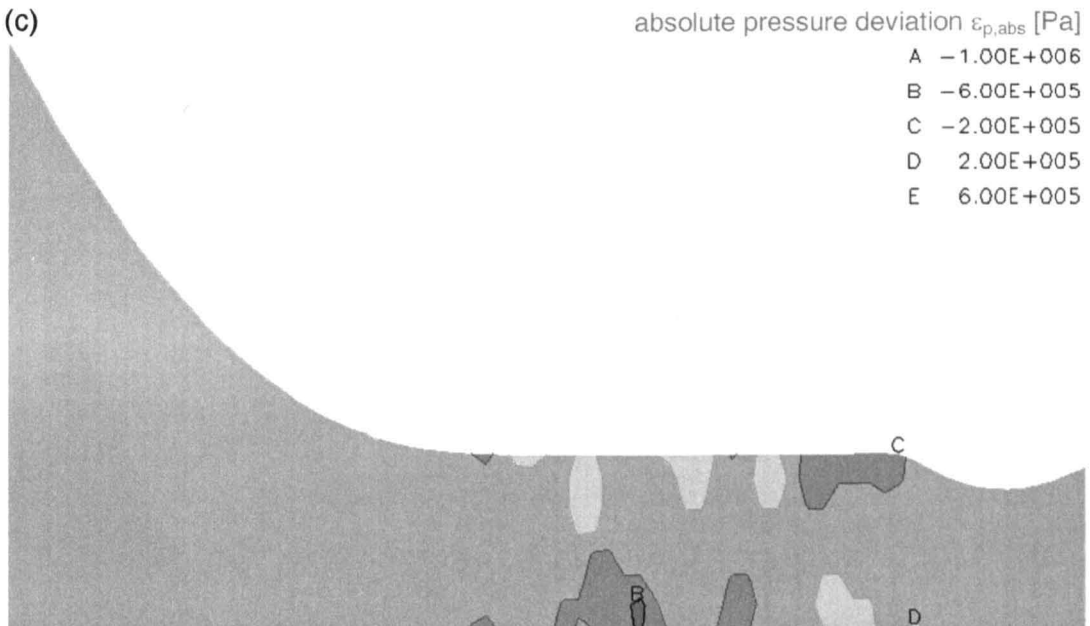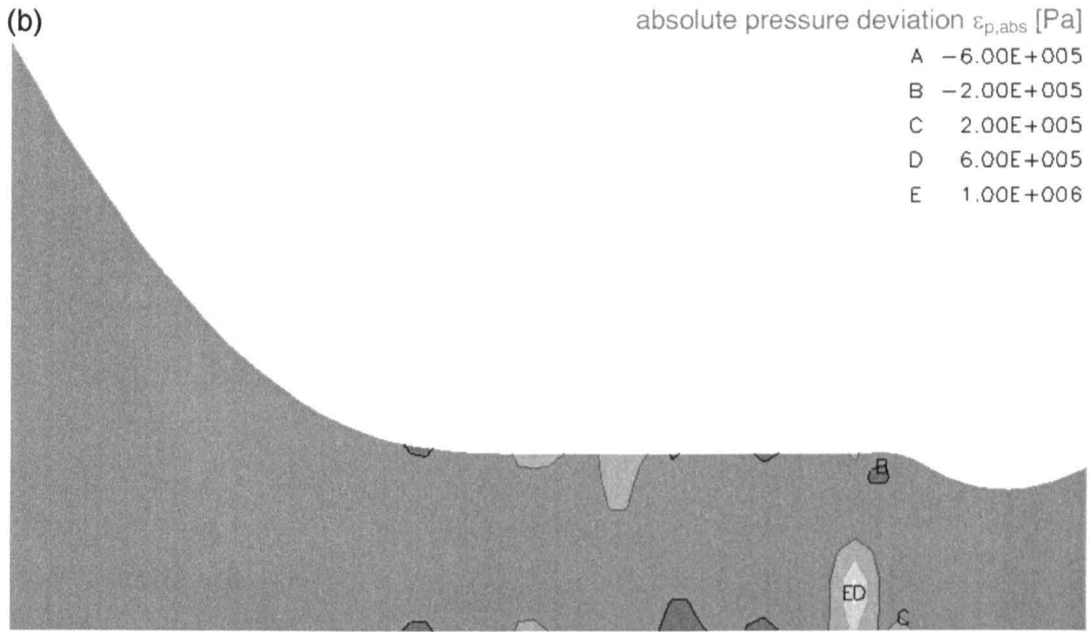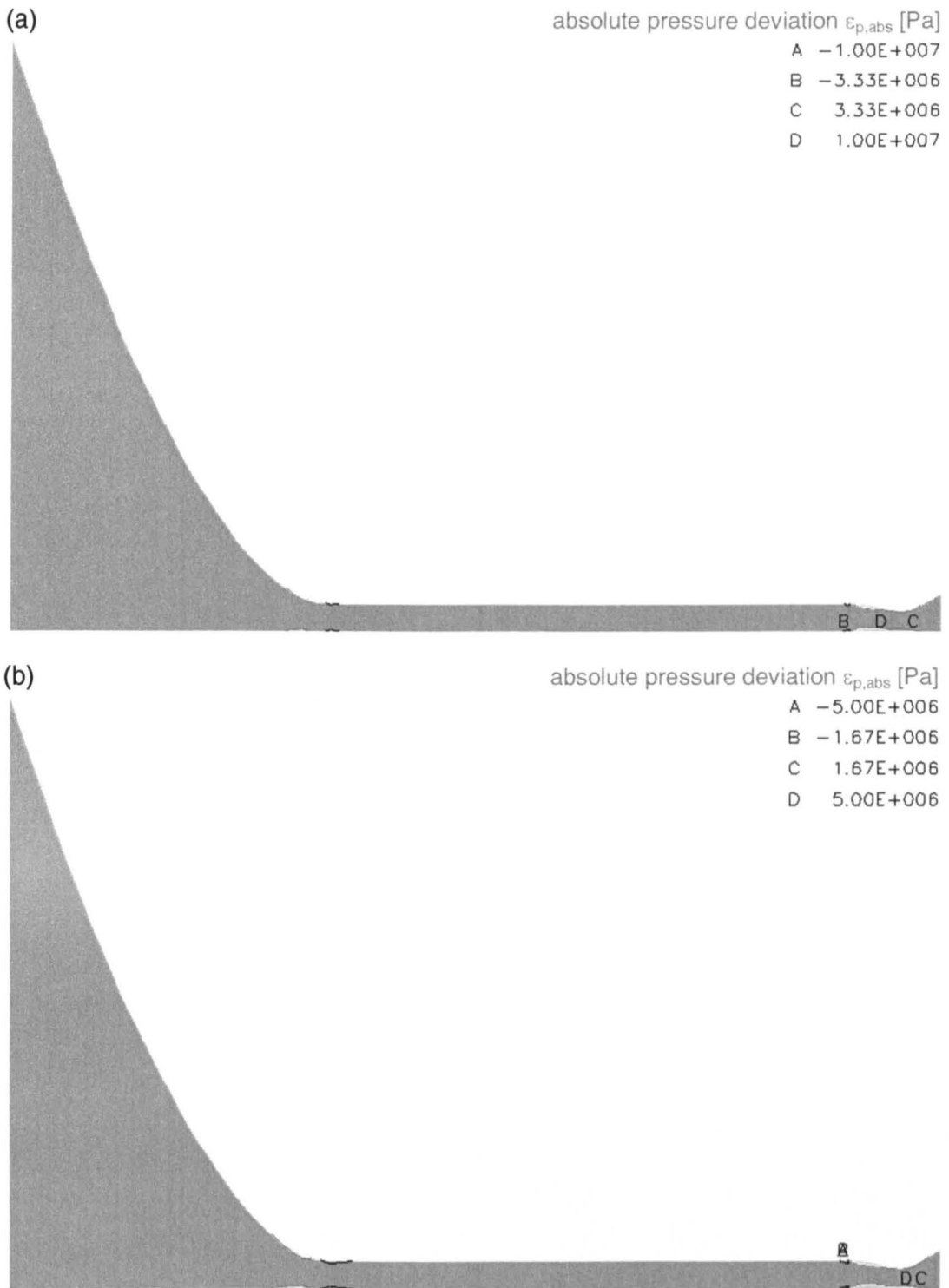
Figure K.18: Contour plots of absolute pressure deviation from the centreline pressure $\varepsilon_{p,abs}$ in the gap for extended approach; load case iii (table 10.1), sliding ratios $S = 0.0$, 0.5, and 1.0,
(a) $S = 0.0$,
(b) $S = 0.5$,
(c) $S = 1.0$
(continued).

(c)

absolute pressure deviation $\varepsilon_{p,abs}$ [Pa]

A	$-5.00E+006$
B	$-1.67E+006$
C	$1.67E+006$
D	$5.00E+006$
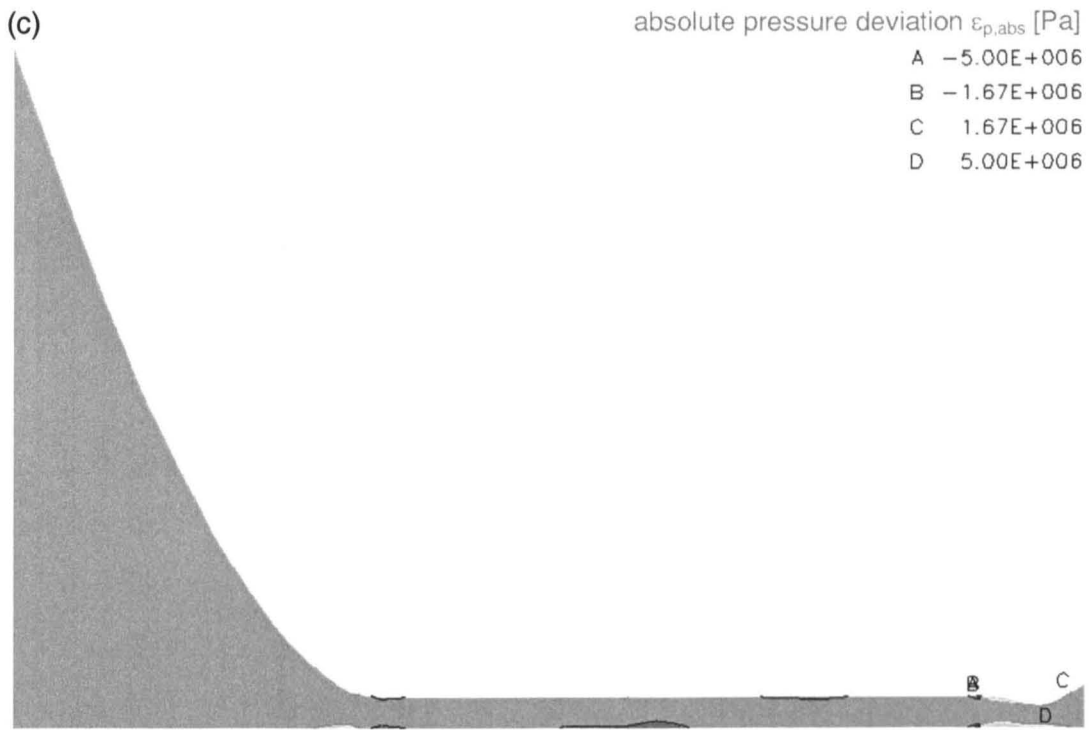
Figure K.18:   (concluded).

(a)
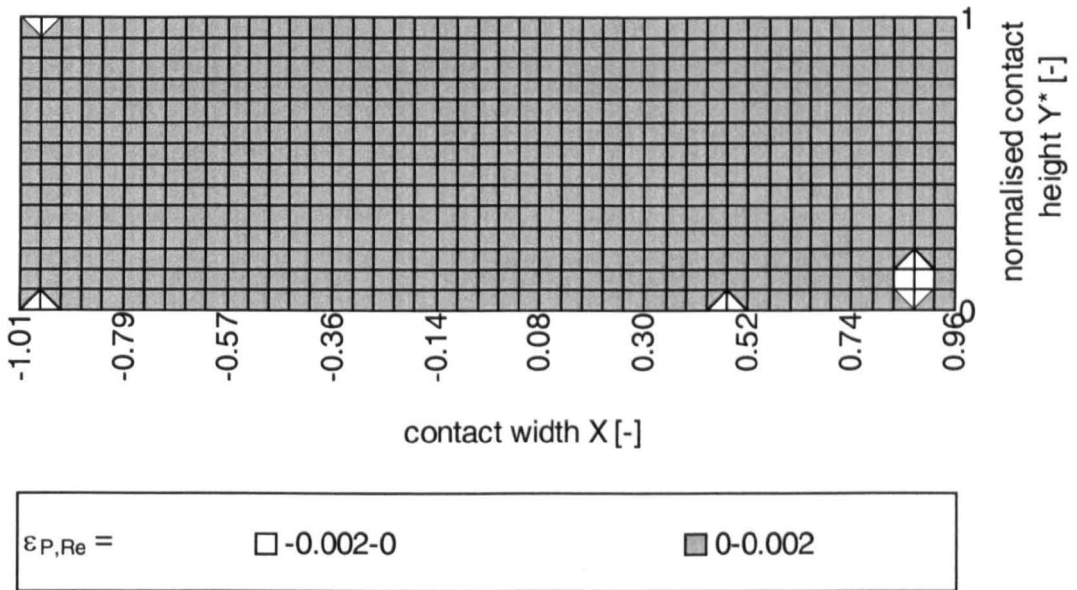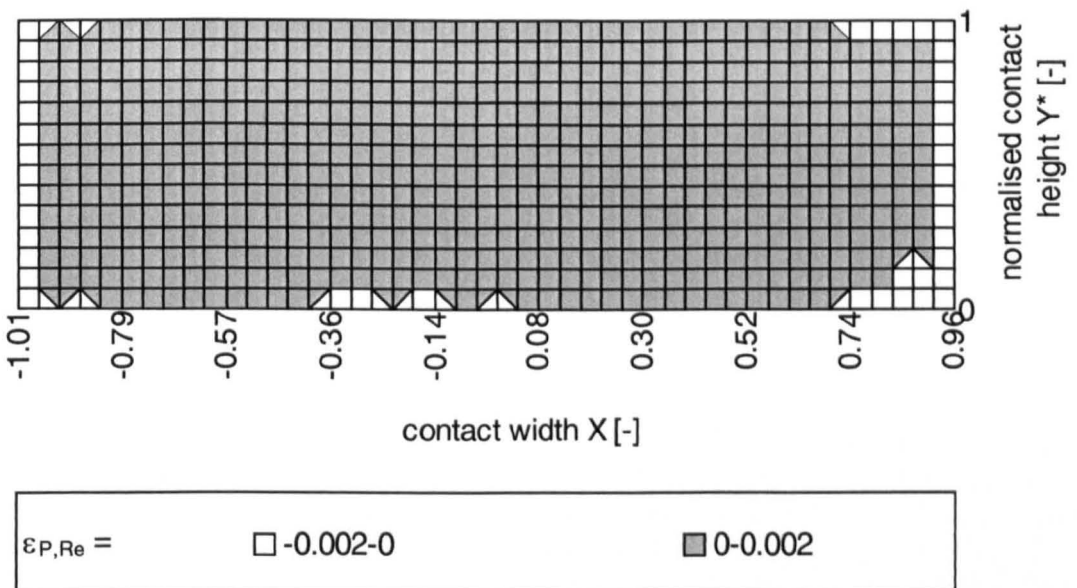
Figure K.19:   Relative deviation of pressure of extended from Reynolds
equation based approach $\varepsilon_{P,Re}$; load case i (table 10.1), sliding
ratios $S = 0.0$, 0.5, and 1.0,
(a) $S = 0.0$,
(b) $S = 0.5$,
(c) $S = 1.0$
(continued).

(c)
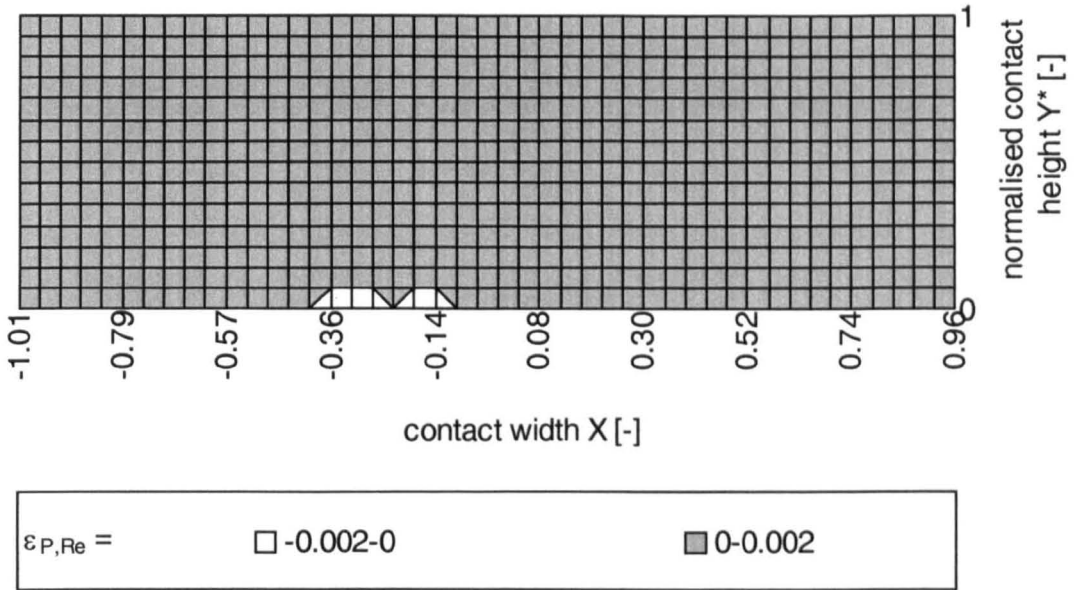
Figure K.19:   (concluded).

(a)
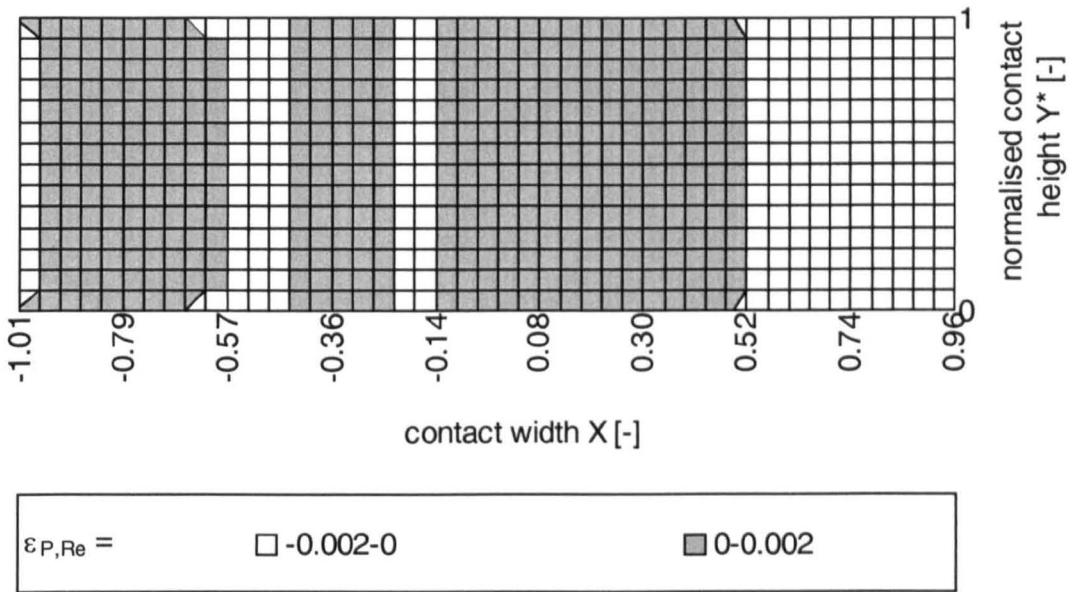
Figure K.20: *Relative deviation of pressure of extended from Reynolds equation based approach $\varepsilon_{P,Re}$; load case ii (table 10.1), sliding ratios S = 0.0, 0.5, and 1.0,*
(a) S = 0.0,
(b) S = 0.5,
(c) S = 1.0
(continued).

(b)

$\varepsilon_{P,Re} =$ □ -0.002-0   ▨ 0-0.002

(c)

$\varepsilon_{P,Re} =$ □ -0.01--0.005   ▨ -0.005-0   ▨ 0-0.005   ■ 0.005-0.01
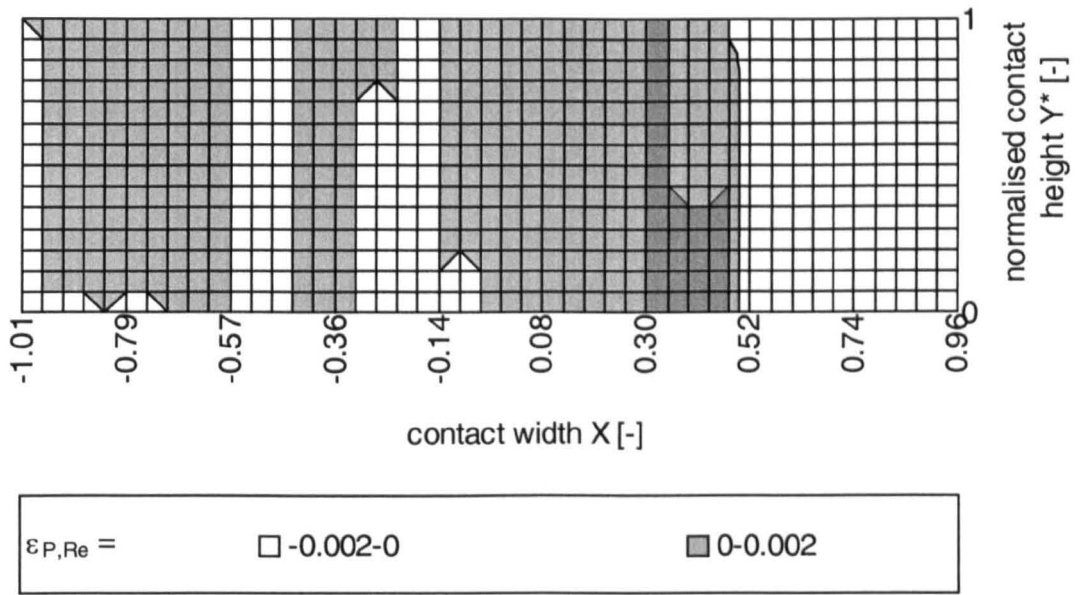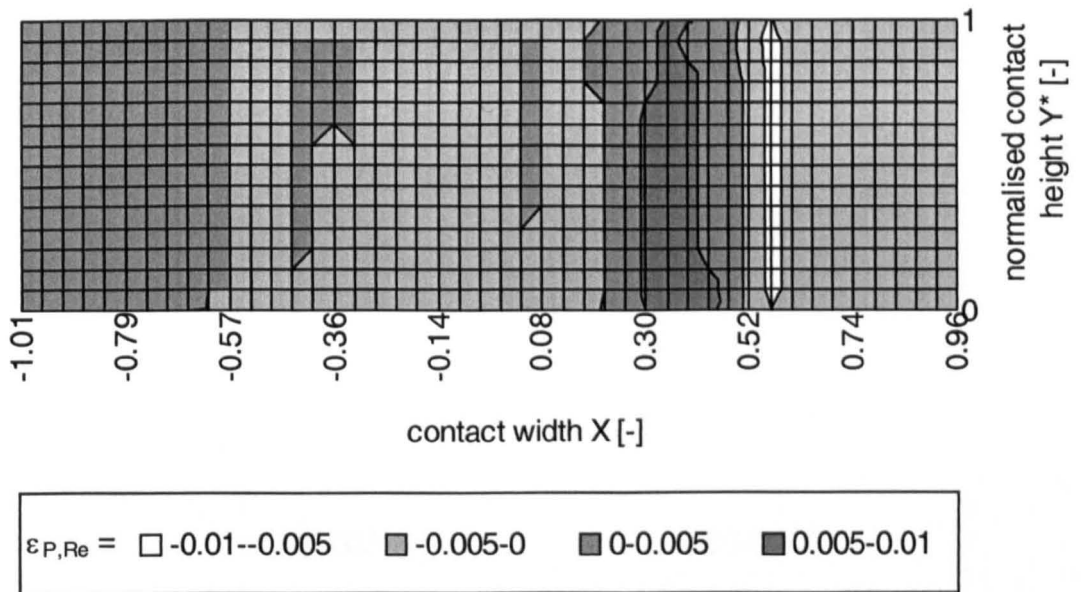
Figure K.20:   (concluded).

(a)
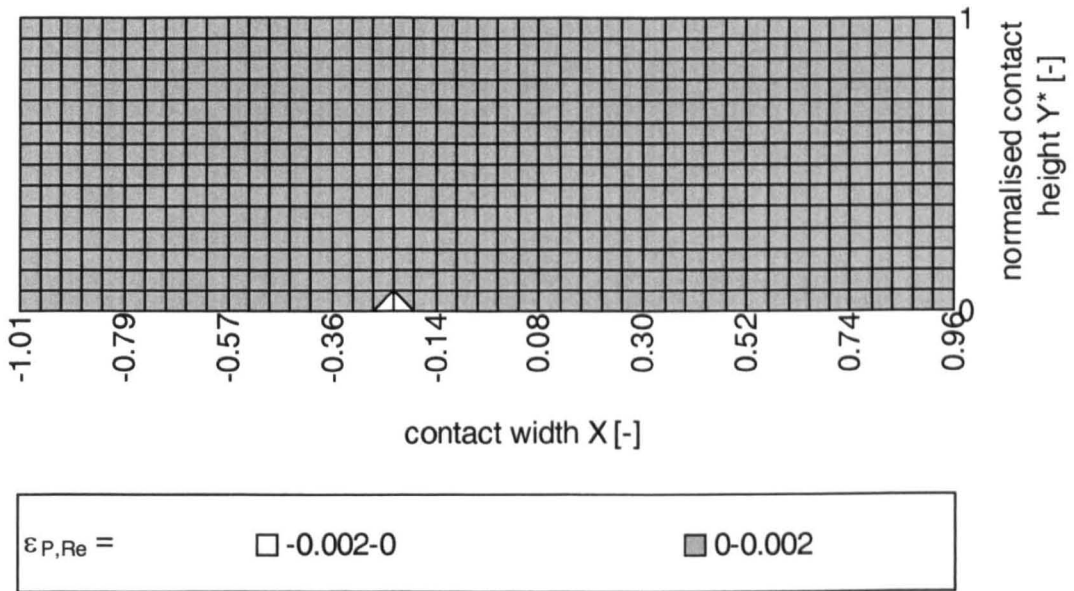
(b)
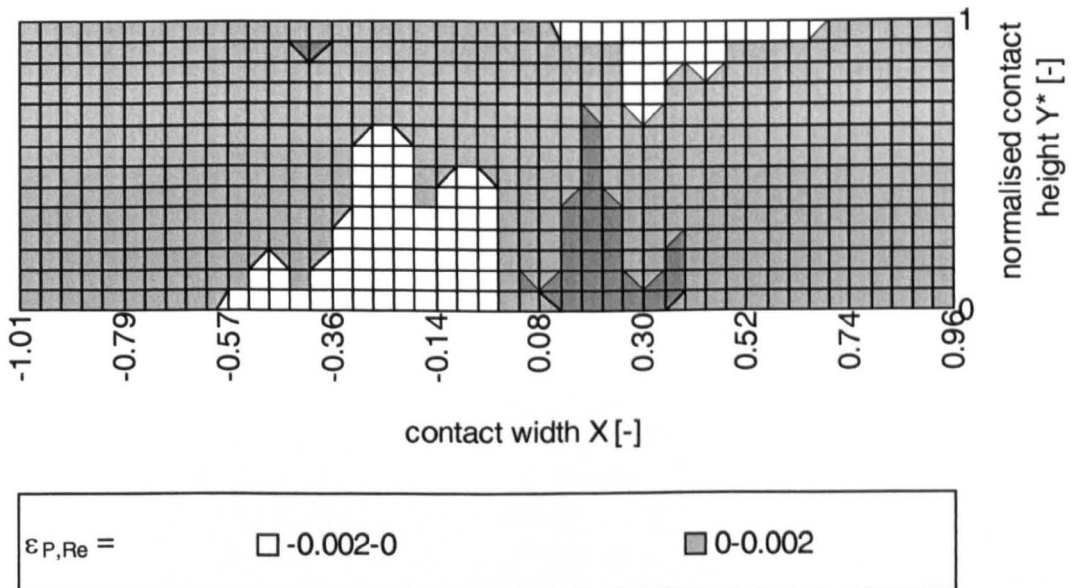
Figure K.21:   Relative deviation of pressure of extended from Reynolds
equation based approach $\varepsilon_{P,Re}$; load case iii (table 10.1),
sliding ratios $S = 0.0$, 0.5, and 1.0,
(a) $S = 0.0$,
(b) $S = 0.5$,
(c) $S = 1.0$
(continued).

(c)
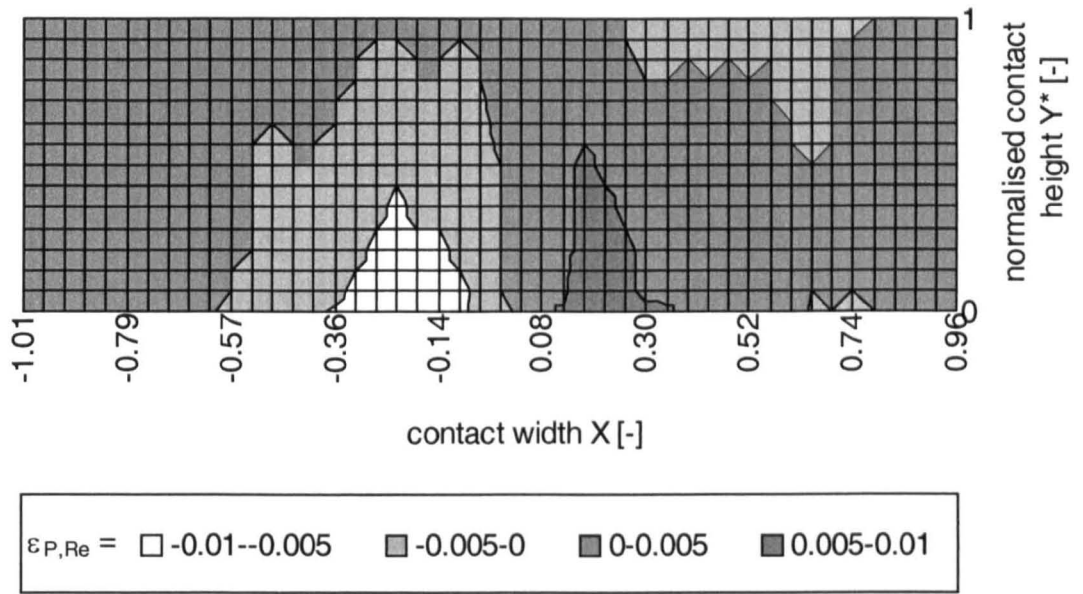
Figure K.21: (concluded).
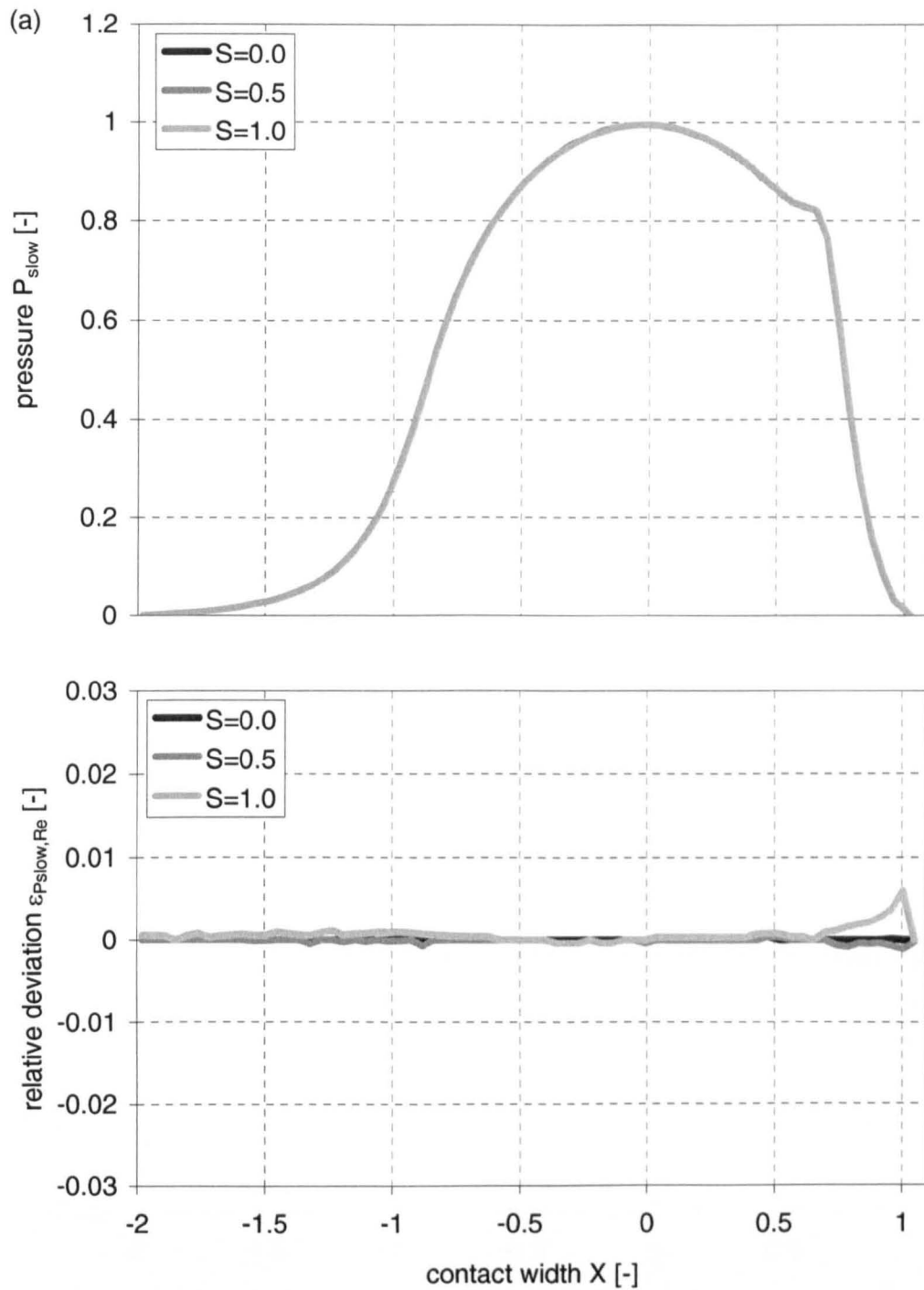
Figure K.22:   *Pressure on the slower surface P_{slow} and the faster surface P_{fast} and mean pressure P_{mean} and relative deviation of these values from Reynolds equation based solution $\varepsilon_{Pslow,Re}$, $\varepsilon_{Pfast,Re}$ and $\varepsilon_{Pmean,Re}$ for various sliding ratios; load case i (table 10.1), sliding ratios $S = 0.0$, 0.5, and 1.0,*
(a) pressure on slower surface P_{slow} and relative deviation $\varepsilon_{Pslow,Re}$,
(b) pressure on faster surface P_{fast} and relative deviation $\varepsilon_{Pfast,Re}$,
(c) mean pressure P_{mean} and relative deviation $\varepsilon_{Pmean,Re}$
*(continued).*

Figure K.22:   *(continued).*
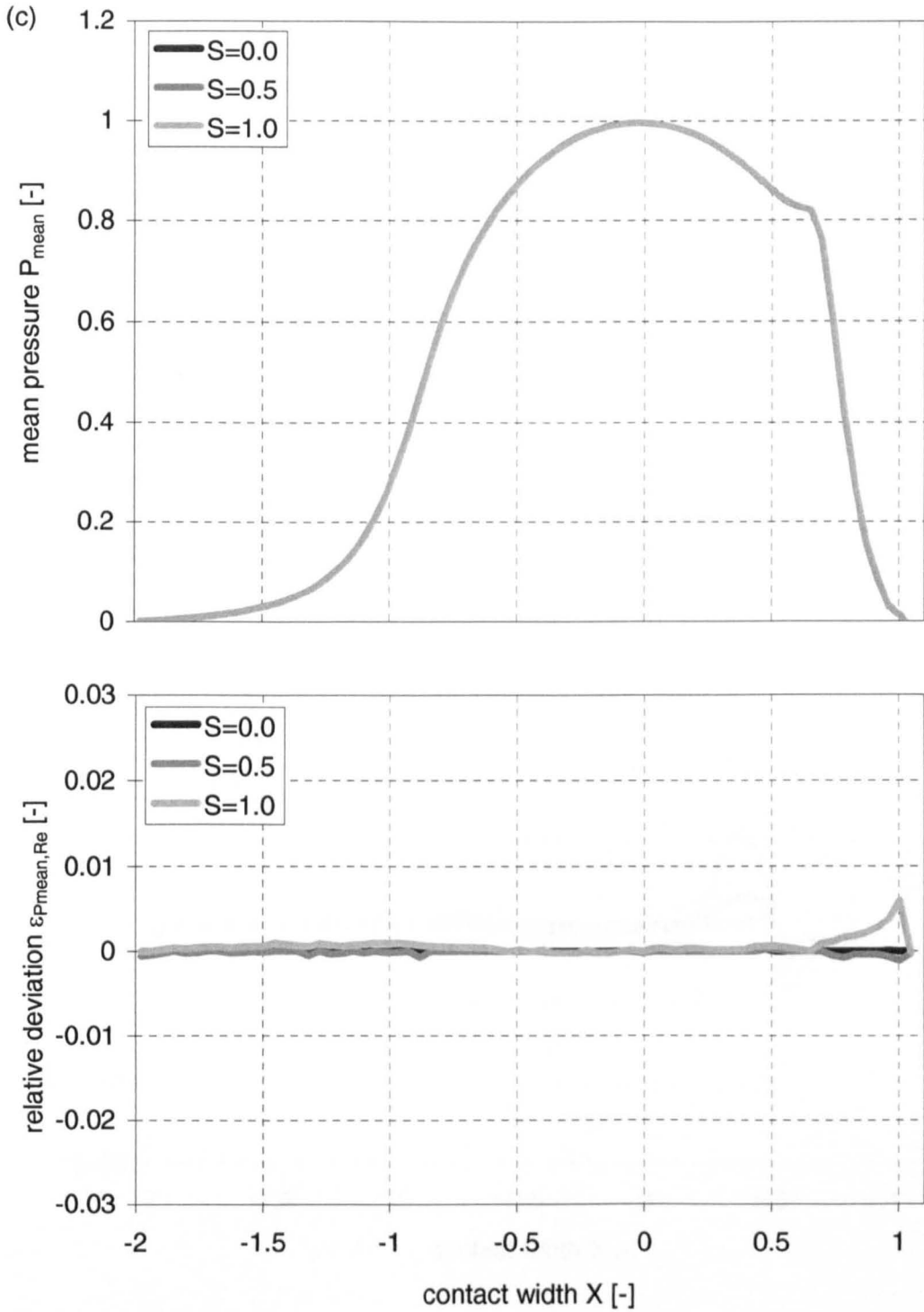
Figure K.22:   (concluded).
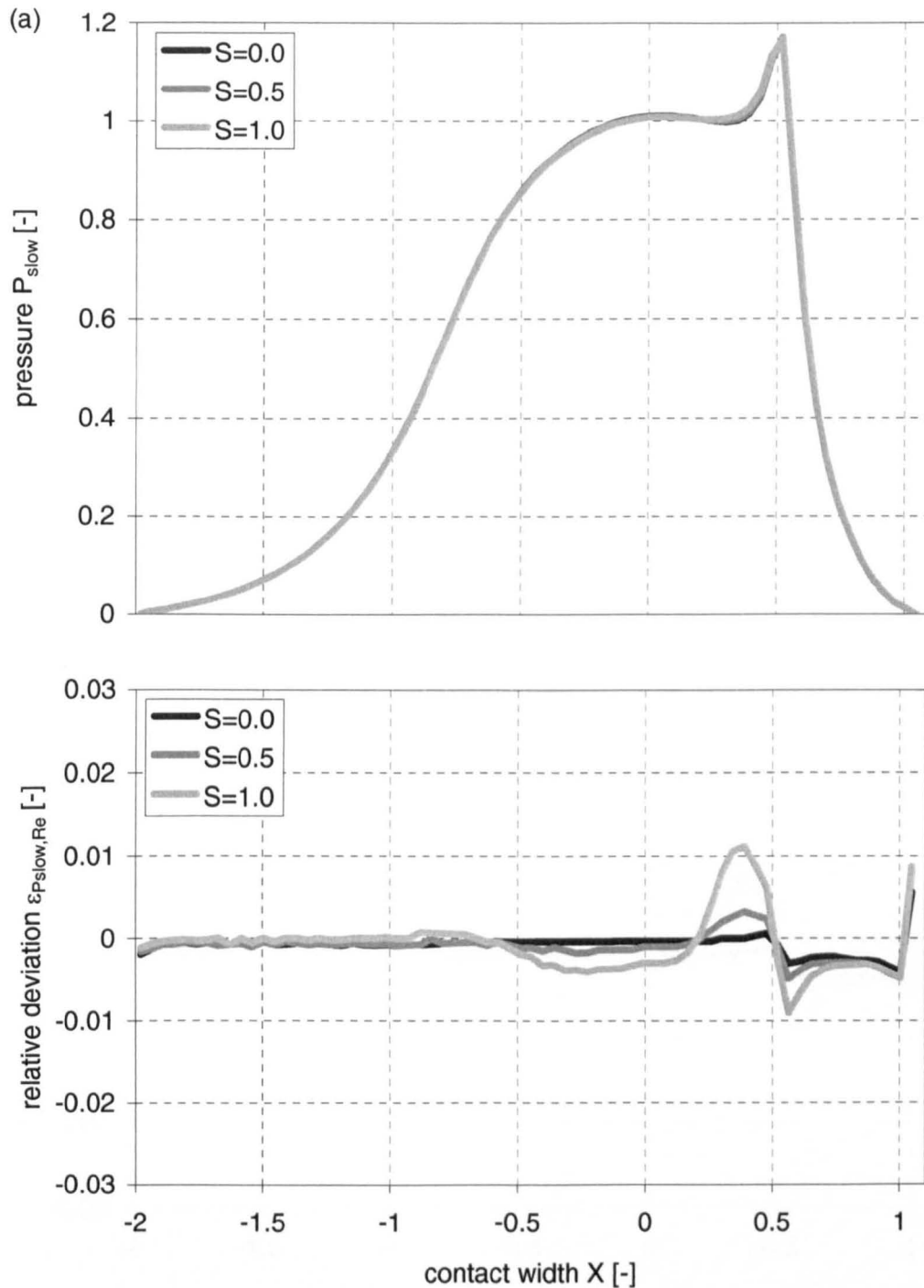
Figure K.23: Pressure on the slower surface P_{slow} and the faster surface P_{fast} and mean pressure P_{mean} and relative deviation of these values from Reynolds equation based solution $\varepsilon_{Pslow,Re}$, $\varepsilon_{Pfast,Re}$ and $\varepsilon_{Pmean,Re}$ for various sliding ratios; load case ii (table 10.1), sliding ratios $S = 0.0$, 0.5, and 1.0,
(a) pressure on slower surface P_{slow} and relative deviation $\varepsilon_{Pslow,Re}$,
(b) pressure on faster surface P_{fast} and relative deviation $\varepsilon_{Pfast,Re}$,
(c) mean pressure P_{mean} and relative deviation $\varepsilon_{Pmean,Re}$
(continued).

Figure K.23: (continued).
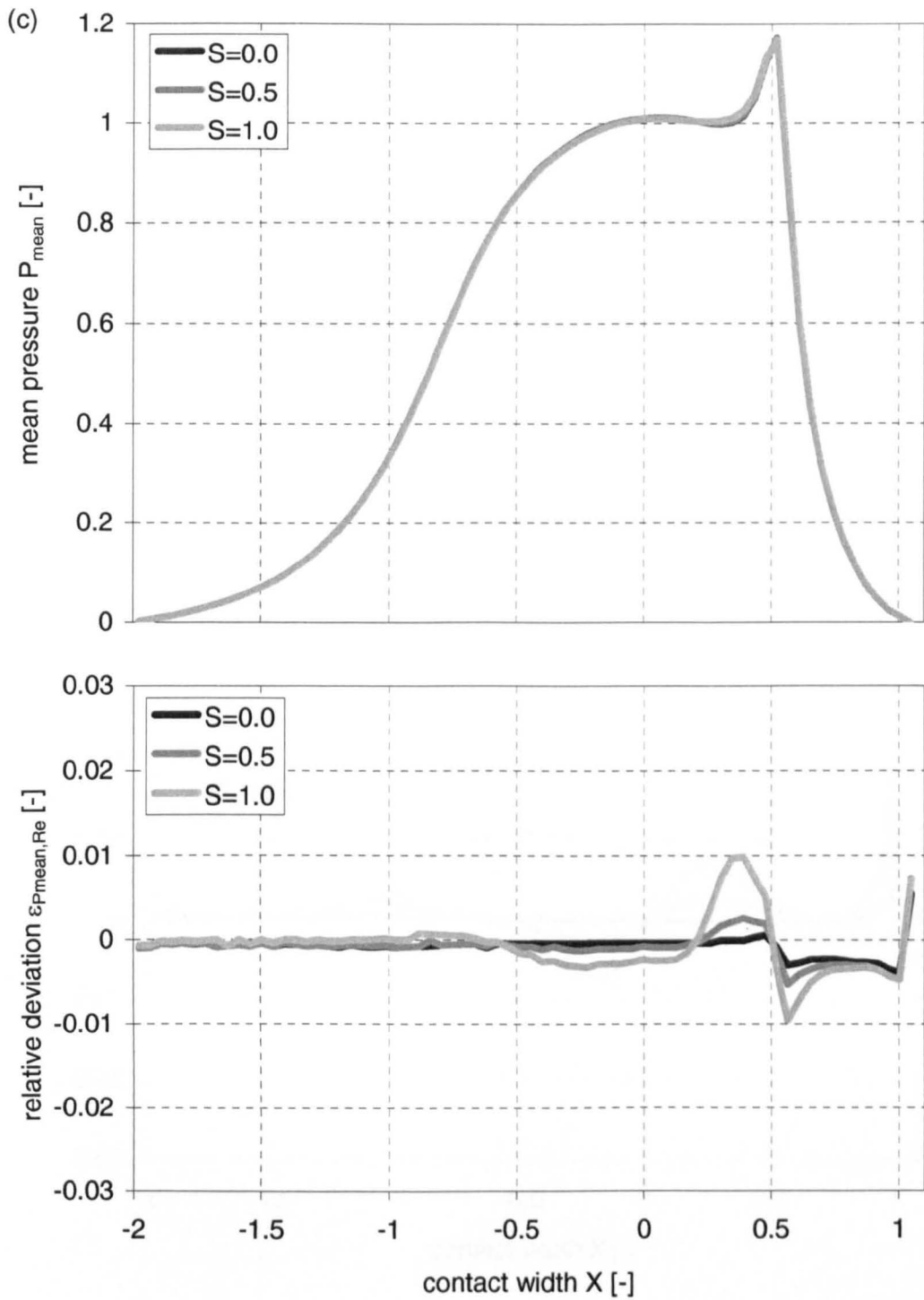
Figure K.23:   (concluded).
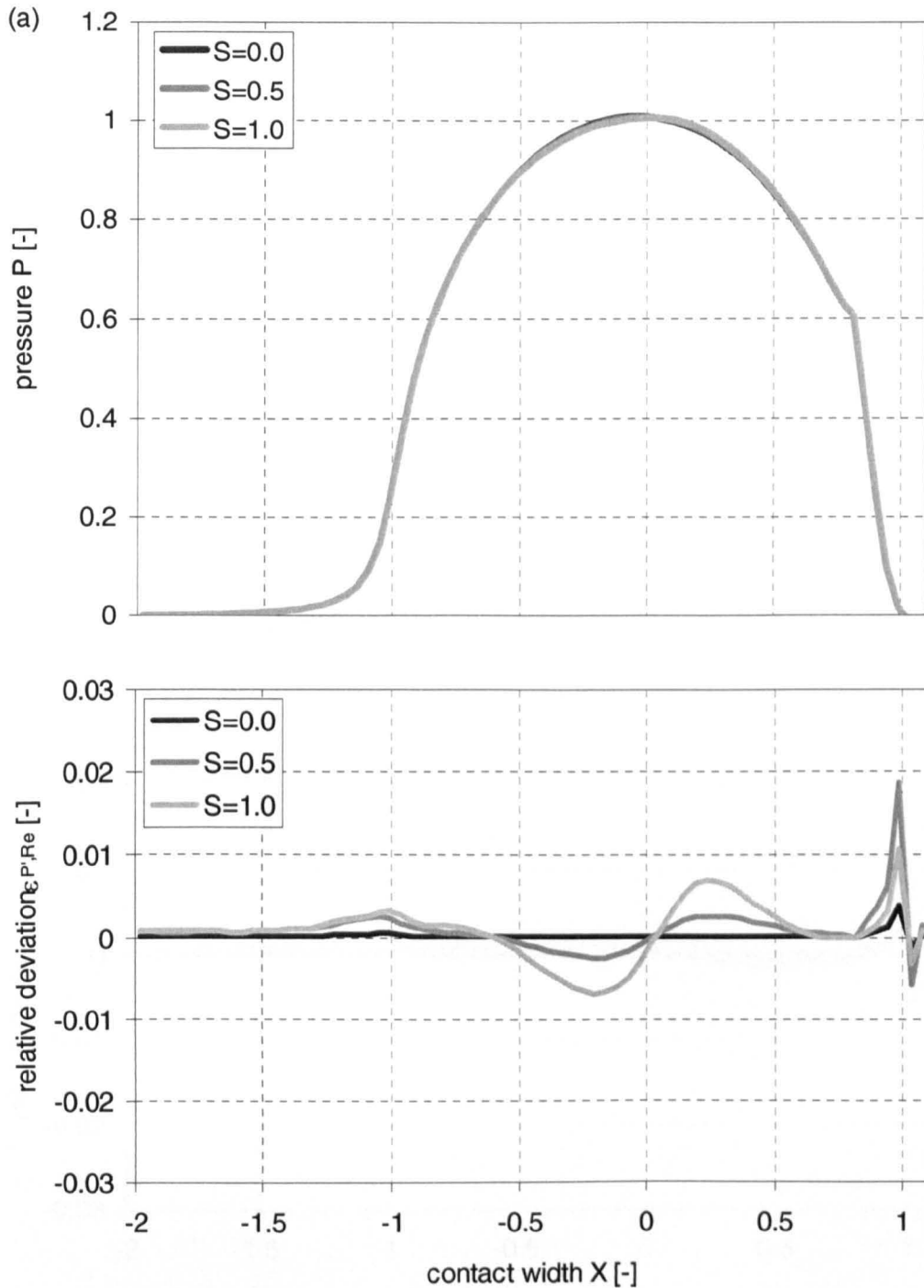
Figure K.24:   *Pressure on the slower surface P_{slow} and the faster surface P_{fast} and mean pressure P_{mean} and relative deviation of these values from Reynolds equation based solution $\varepsilon_{Pslow,Re}$, $\varepsilon_{Pfast,Re}$ and $\varepsilon_{Pmean,Re}$ for various sliding ratios; load case iii (table 10.1), sliding ratios $S = 0.0$, 0.5, and 1.0,*
(a) pressure on slower surface P_{slow} and relative deviation $\varepsilon_{Pslow,Re}$,
(b) pressure on faster surface P_{fast} and relative deviation $\varepsilon_{Pfast,Re}$,
(c) mean pressure P_{mean} and relative deviation $\varepsilon_{Pmean,Re}$
(continued).
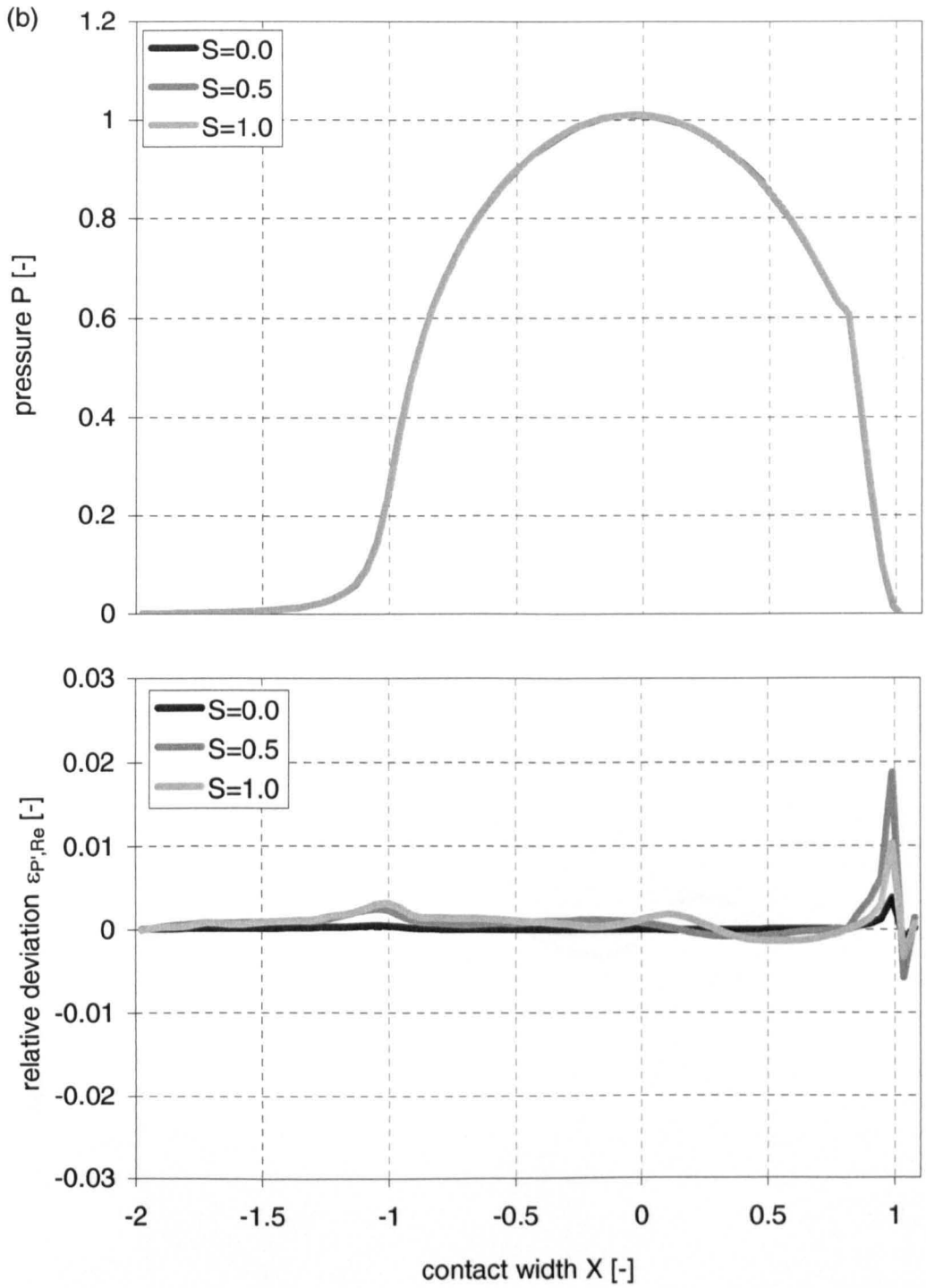
Figure K.24:   (continued).
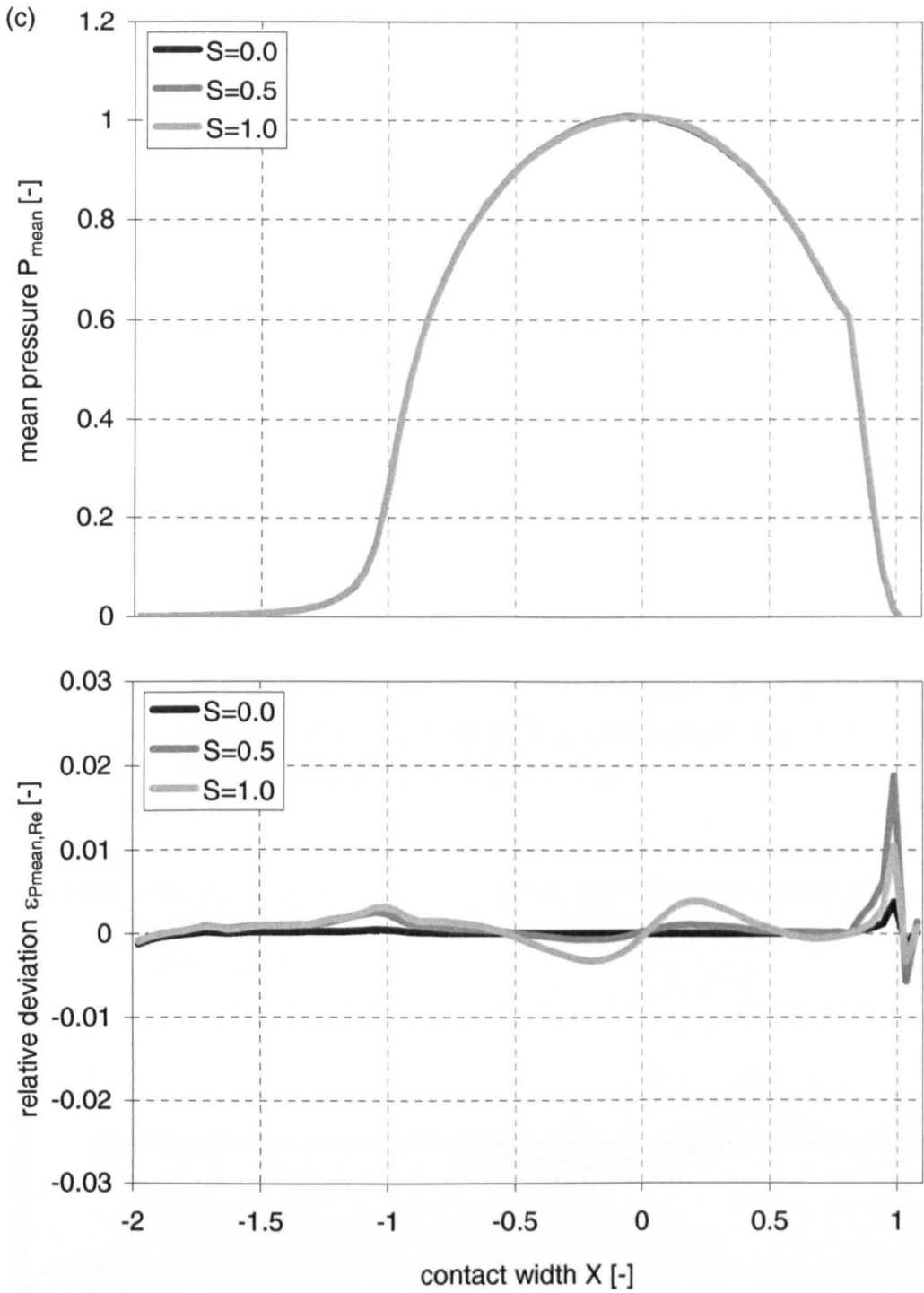
Figure K.24:   (concluded).
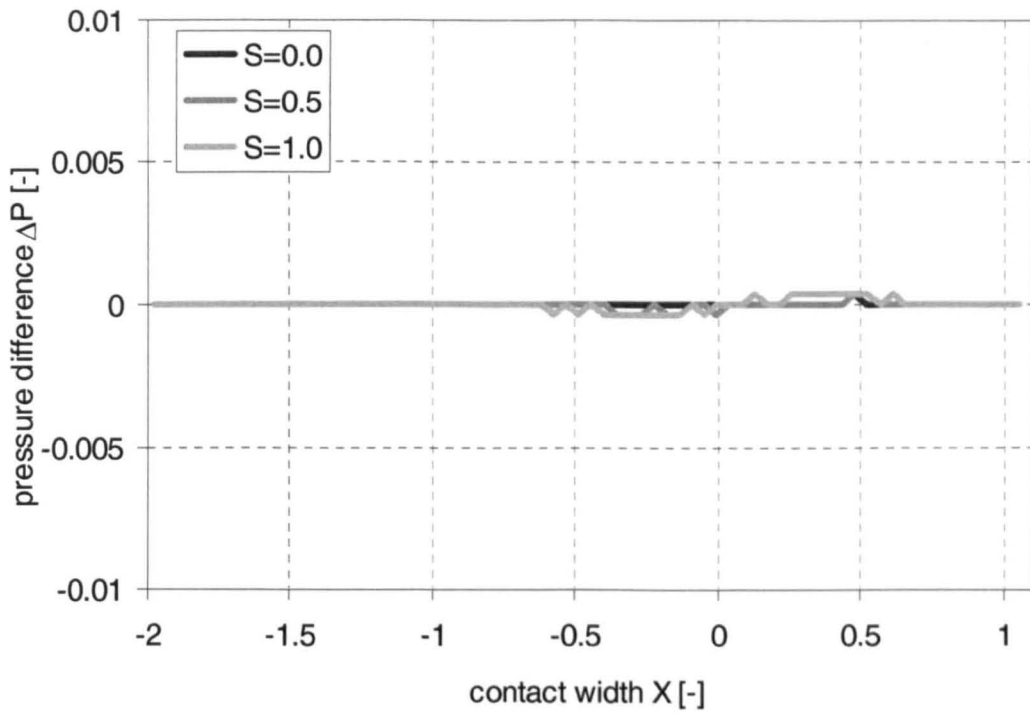
Figure K.25:   Dimensionless pressure difference between faster and slower surface ΔP for various sliding ratios; load case i (table 10.1), sliding ratios S = 0.0, 0.5, and 1.0.
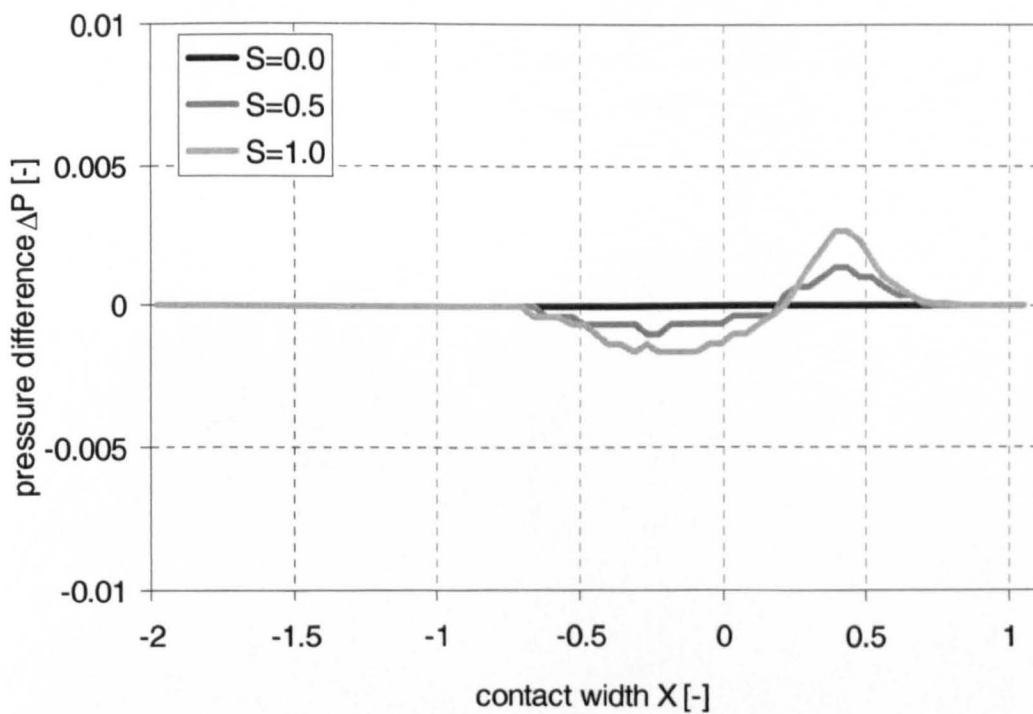
Figure K.26:   Dimensionless pressure difference between faster and slower surface ΔP for various sliding ratios; load case ii (table 10.1), sliding ratios S = 0.0, 0.5, and 1.0.
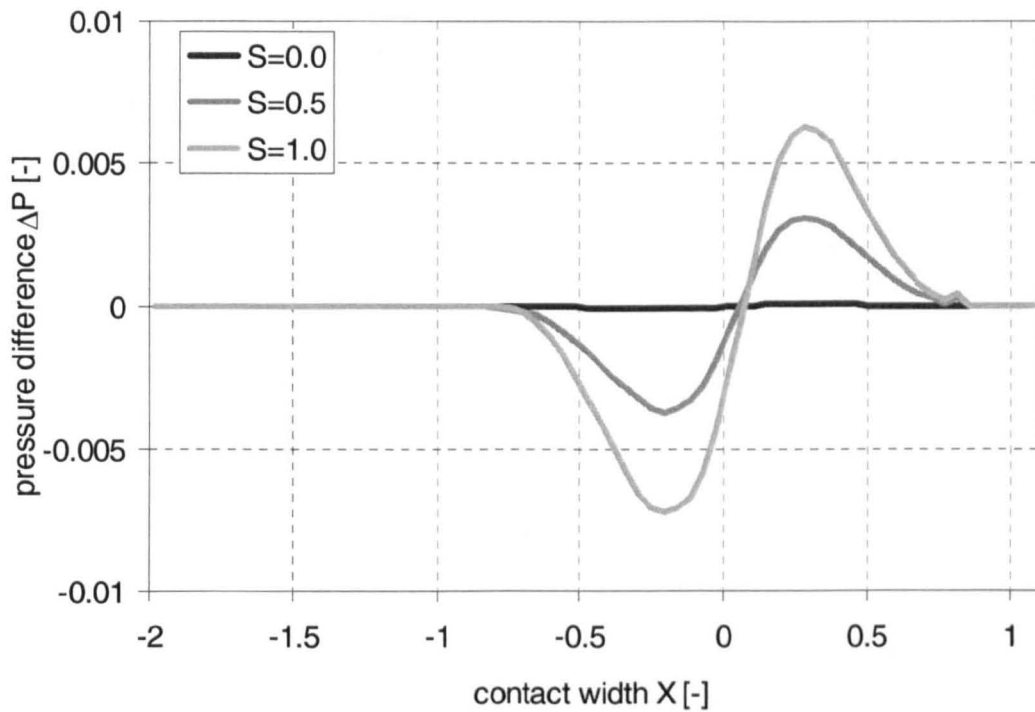
Figure K.27:   *Dimensionless pressure difference between faster and slower surface ΔP for various sliding ratios; load case iii (table 10.1), sliding ratios $S = 0.0$, 0.5, and 1.0.*
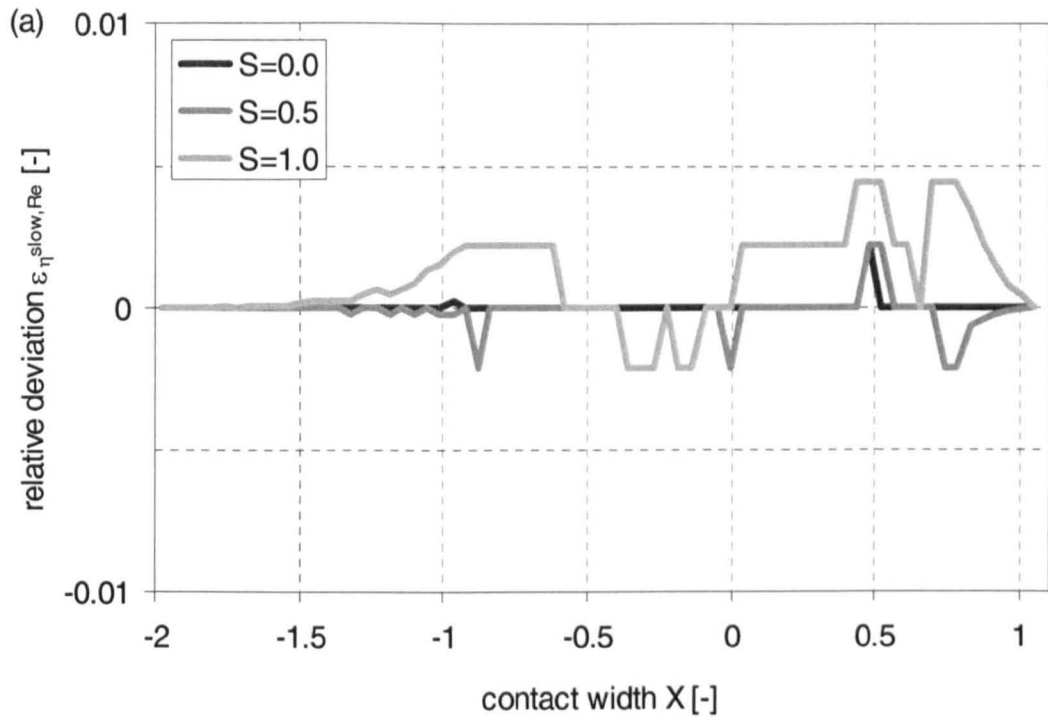
Figure K.28:   Relative deviation of viscosity from Reynolds equation based
               solution on the lubricant at the slower surface $\varepsilon_{\eta slow,Re}$ and the
               faster surface $\varepsilon_{\eta fast,Re}$ and relative deviation of viscosity across
               the gap $\varepsilon_{\Delta\eta}$ for various sliding ratios; load case i (table 10.1),
               sliding ratios S = 0.0, 0.5, and 1.0,
               (a) relative deviation at slower surface $\varepsilon_{\eta slow,Re}$,
               (b) relative deviation at faster surface $\varepsilon_{\eta fast,Re}$,
               (c) relative deviation across the gap $\varepsilon_{\Delta\eta}$
   (continued).
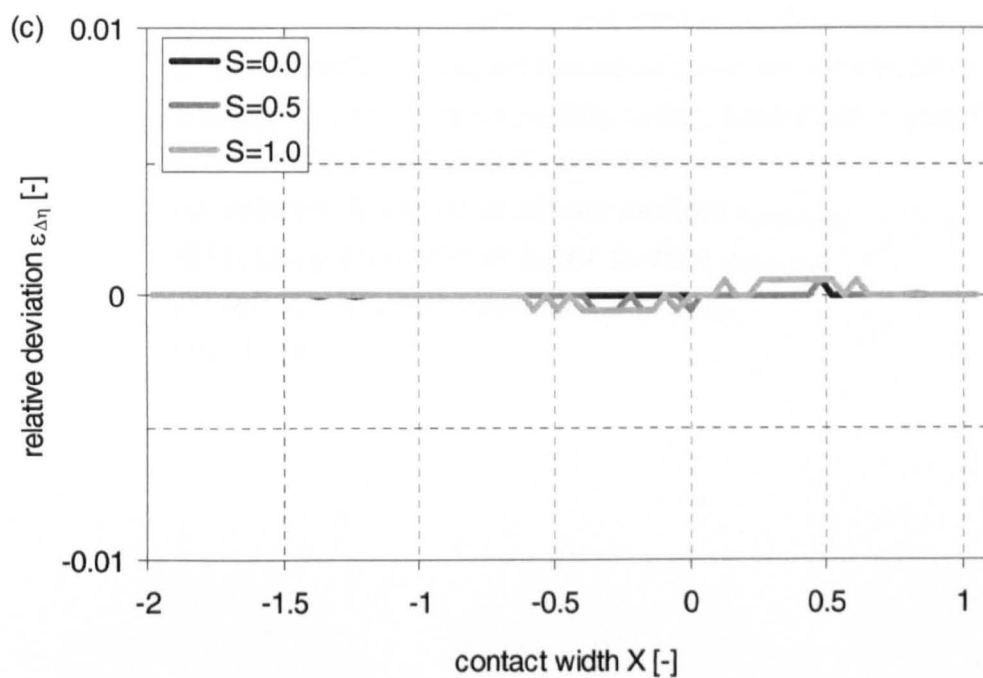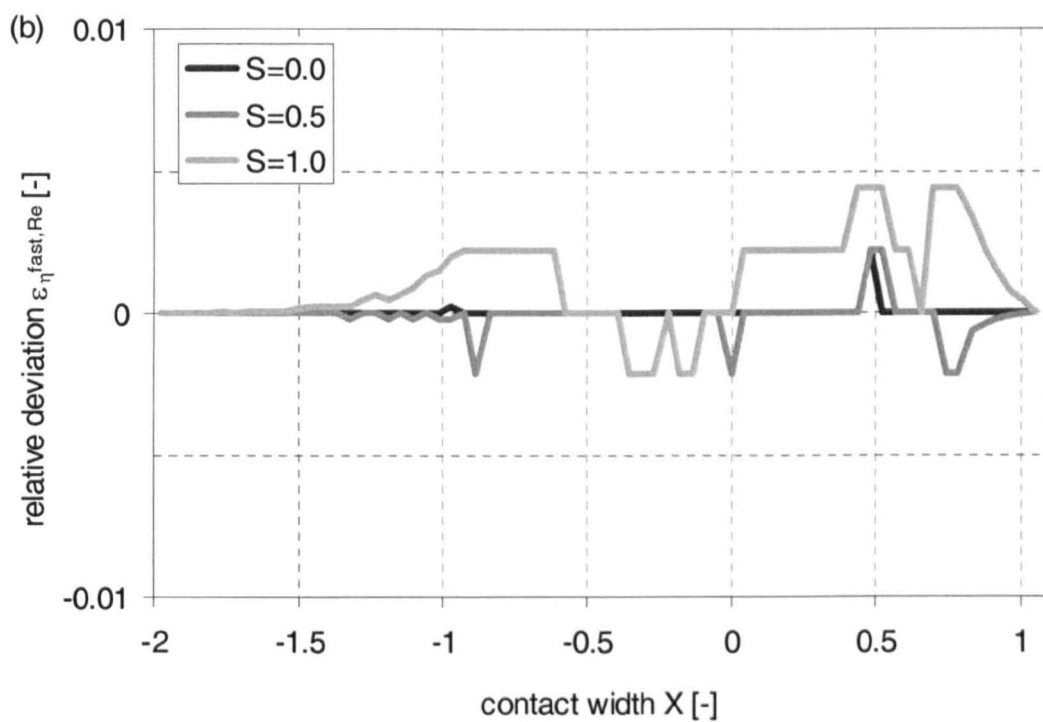
Figure K.28:   (concluded).
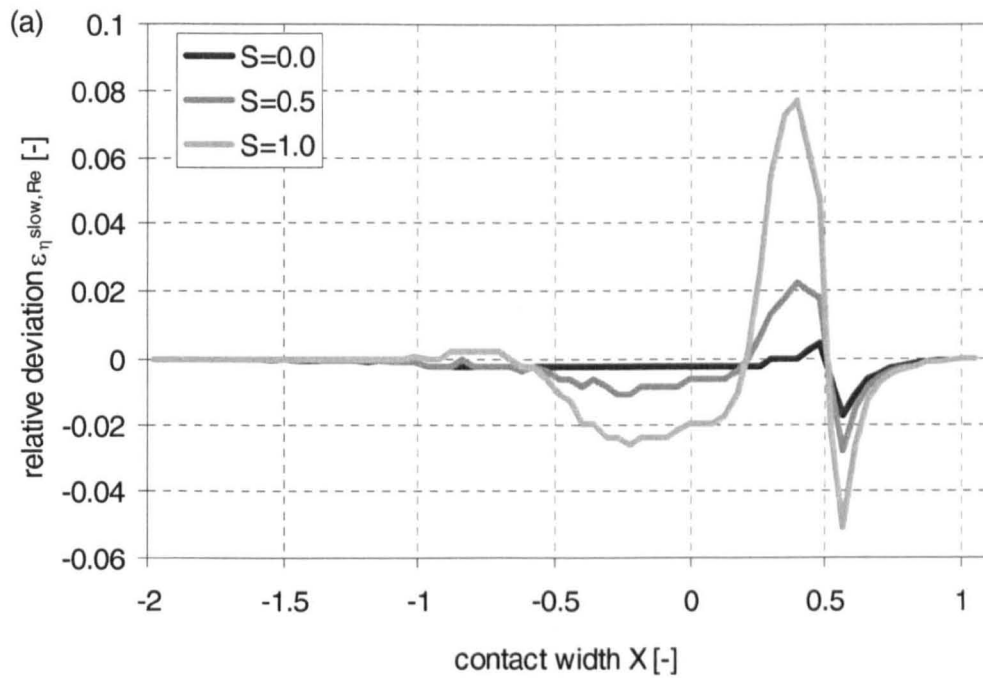
Figure K.29:   *Relative deviation of viscosity from Reynolds equation based solution on the lubricant at the slower surface $\varepsilon_{\eta slow,Re}$ and the faster surface $\varepsilon_{\eta fast,Re}$ and relative deviation of viscosity across the gap $\varepsilon_{\Delta\eta}$ for various sliding ratios; load case ii (table 10.1), sliding ratios S = 0.0, 0.5, and 1.0,*
(a) relative deviation at slower surface $\varepsilon_{\eta slow,Re}$,
(b) relative deviation at faster surface $\varepsilon_{\eta fast,Re}$,
(c) relative deviation across the gap $\varepsilon_{\Delta\eta}$
(continued).
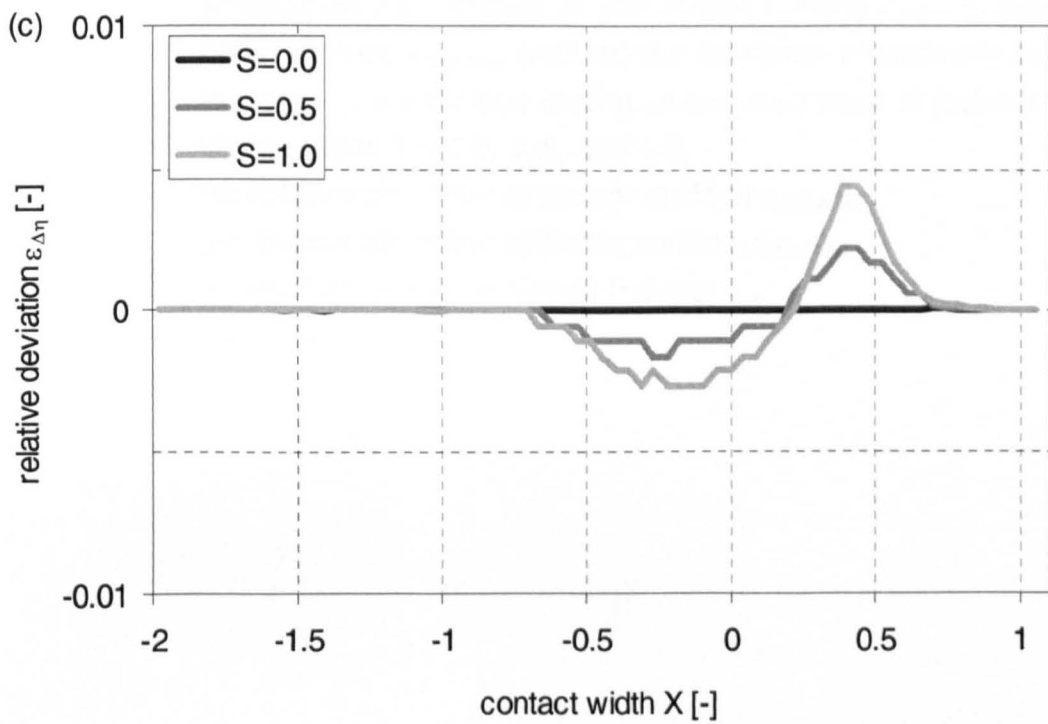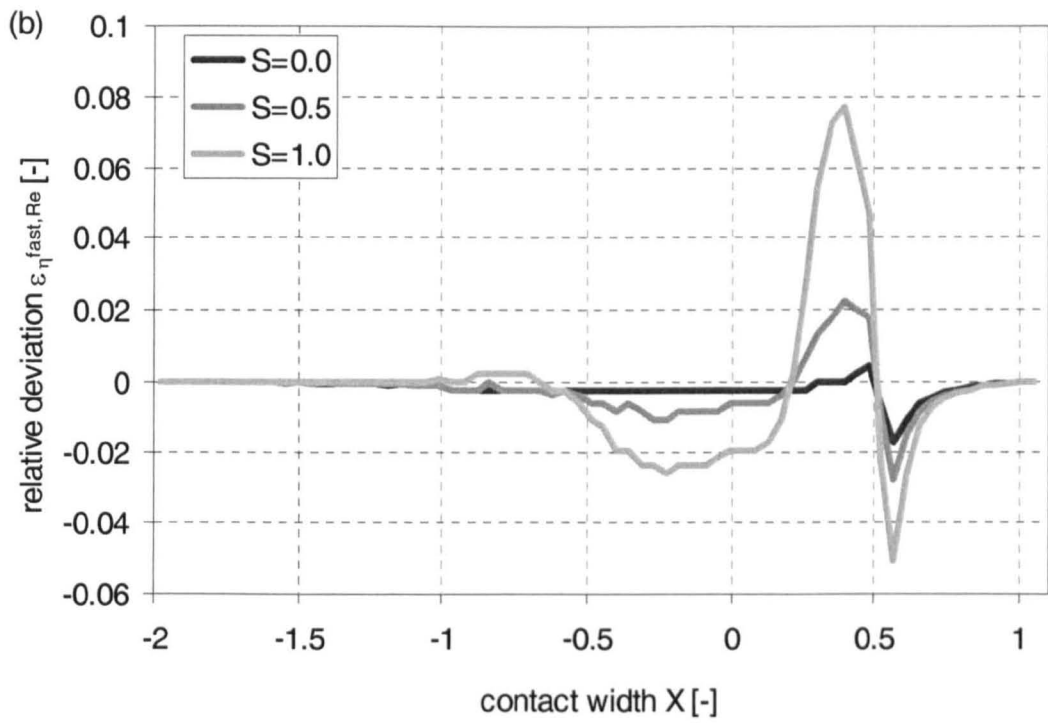
Figure K.29:   *(concluded).*
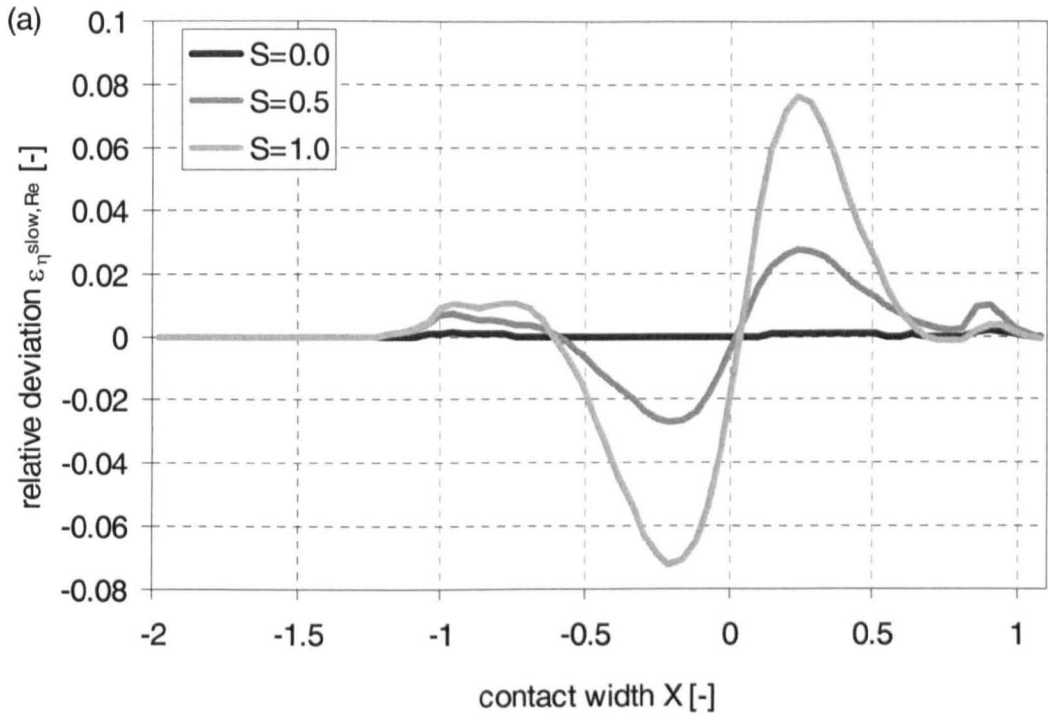
Figure K.30:   *Relative deviation of viscosity from Reynolds equation based solution on the lubricant at the slower surface $\varepsilon_{\eta slow,Re}$ and the faster surface $\varepsilon_{\eta fast,Re}$ and relative deviation of viscosity across the gap $\varepsilon_{\Delta\eta}$ for various sliding ratios; load case iii (table 10.1), sliding ratios $S = 0.0$, 0.5, and 1.0,*
(a) relative deviation at slower surface $\varepsilon_{\eta slow,Re}$,
(b) relative deviation at faster surface $\varepsilon_{\eta fast,Re}$,
*(c) relative deviation across the gap $\varepsilon_{\Delta\eta}$*
*(continued).*
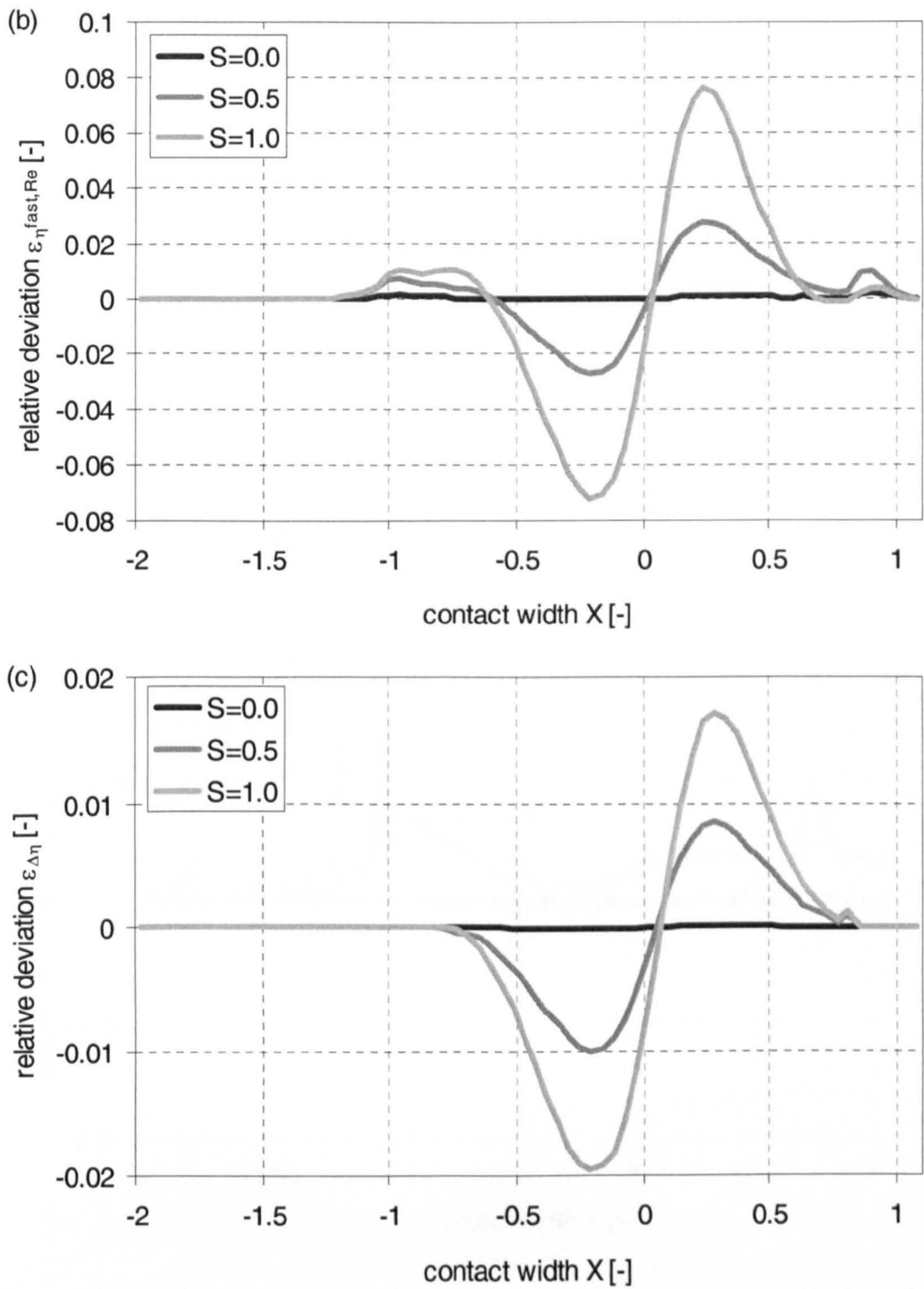
Figure K.30:   (concluded).
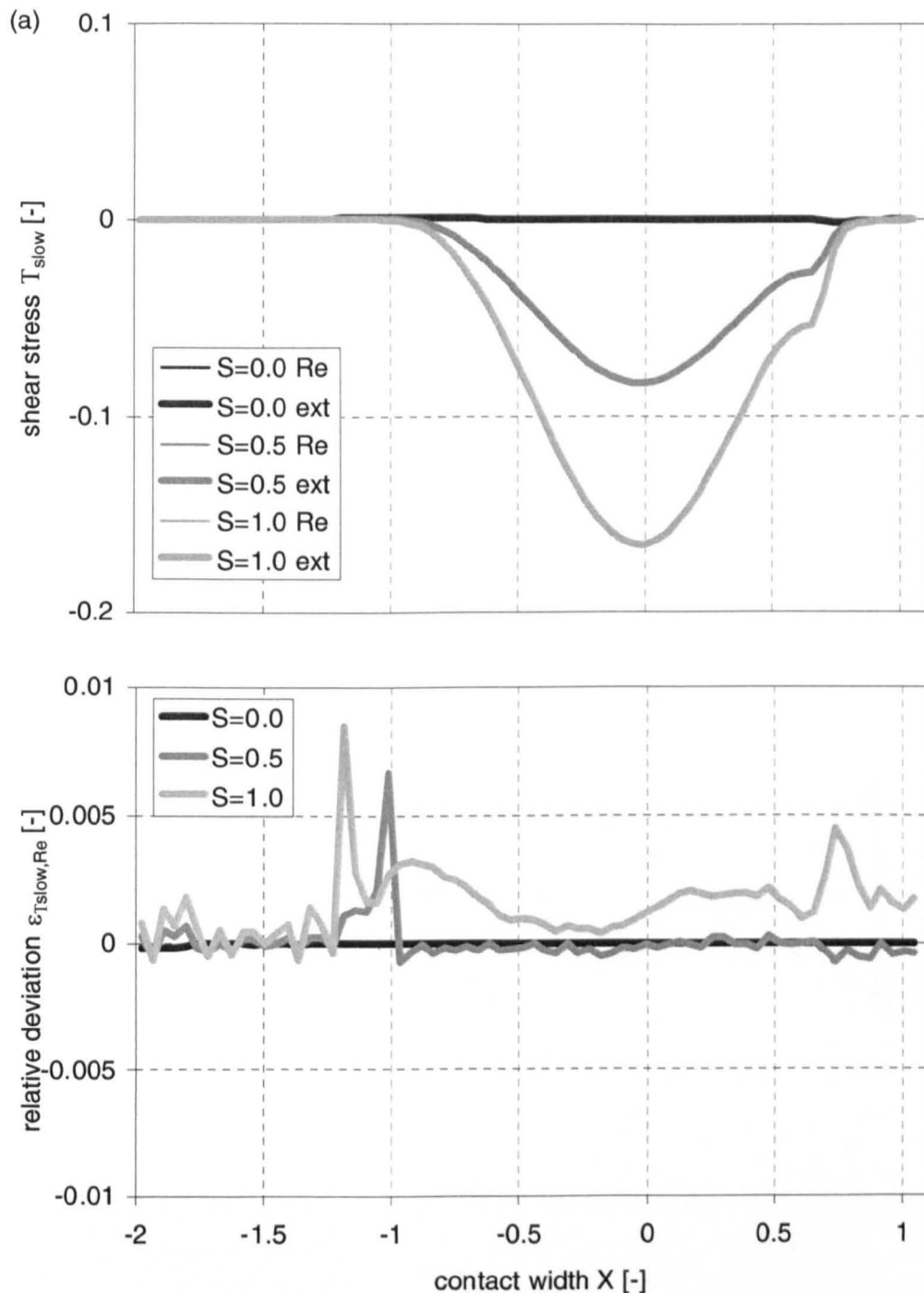
Figure K.31: *Dimensionless shear stress on the lubricant at the slower surface T_{slow} and the faster surface T_{fast} and relative deviation from Reynolds equation based solution $\varepsilon_{Tslow,Re}$ and $\varepsilon_{Tfast,Re}$ for various sliding ratios; load case i (table 10.1), sliding ratios $S = 0.0$, 0.5, and 1.0,*

(a)   shear stress on slower surface T_{slow} and relative deviation $\varepsilon_{Tslow,Re}$,

(b)   shear stress on faster surface T_{fast} and relative deviation $\varepsilon_{Tfast,Re}$

*(continued).*
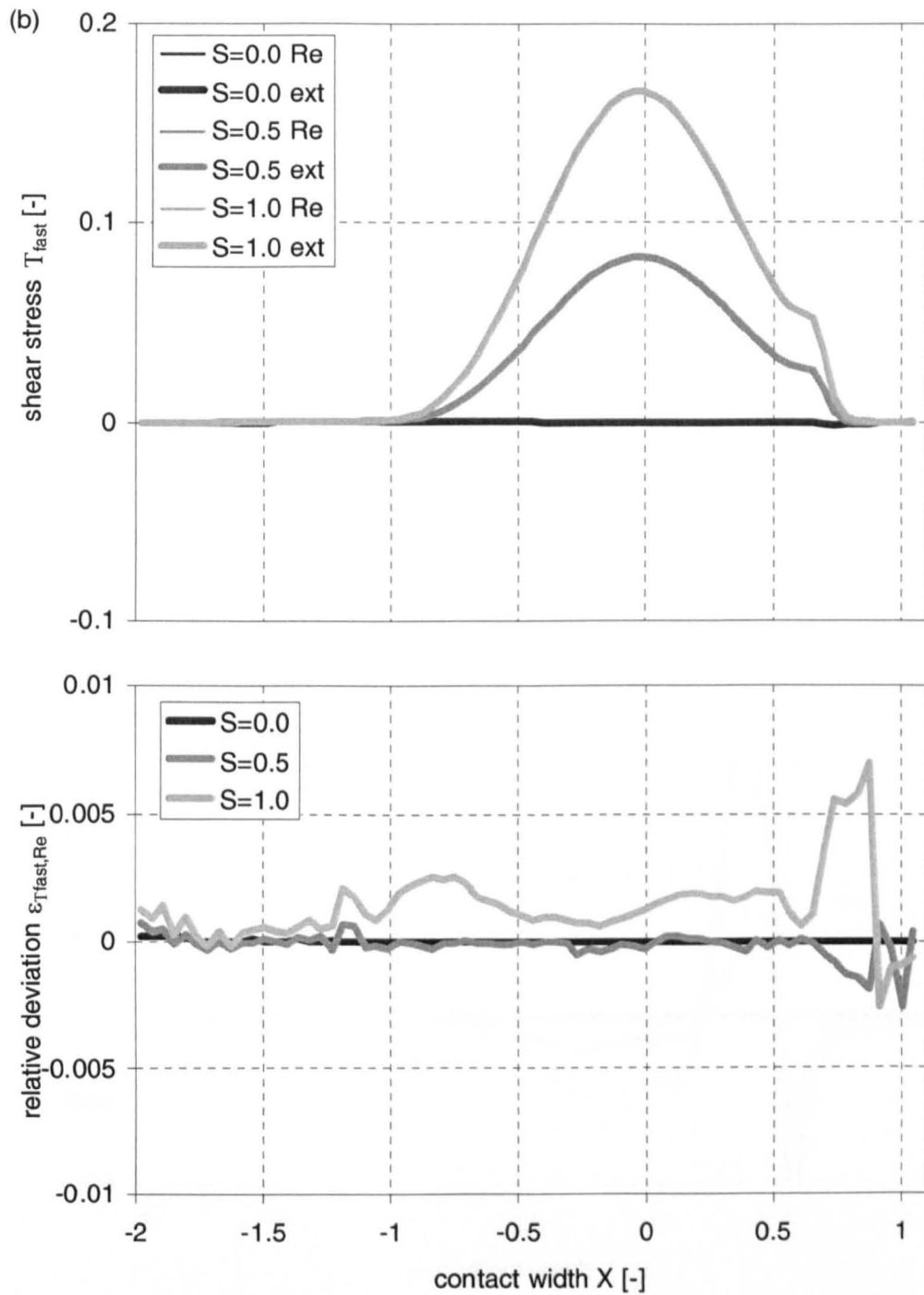
Figure K.31:   (concluded).
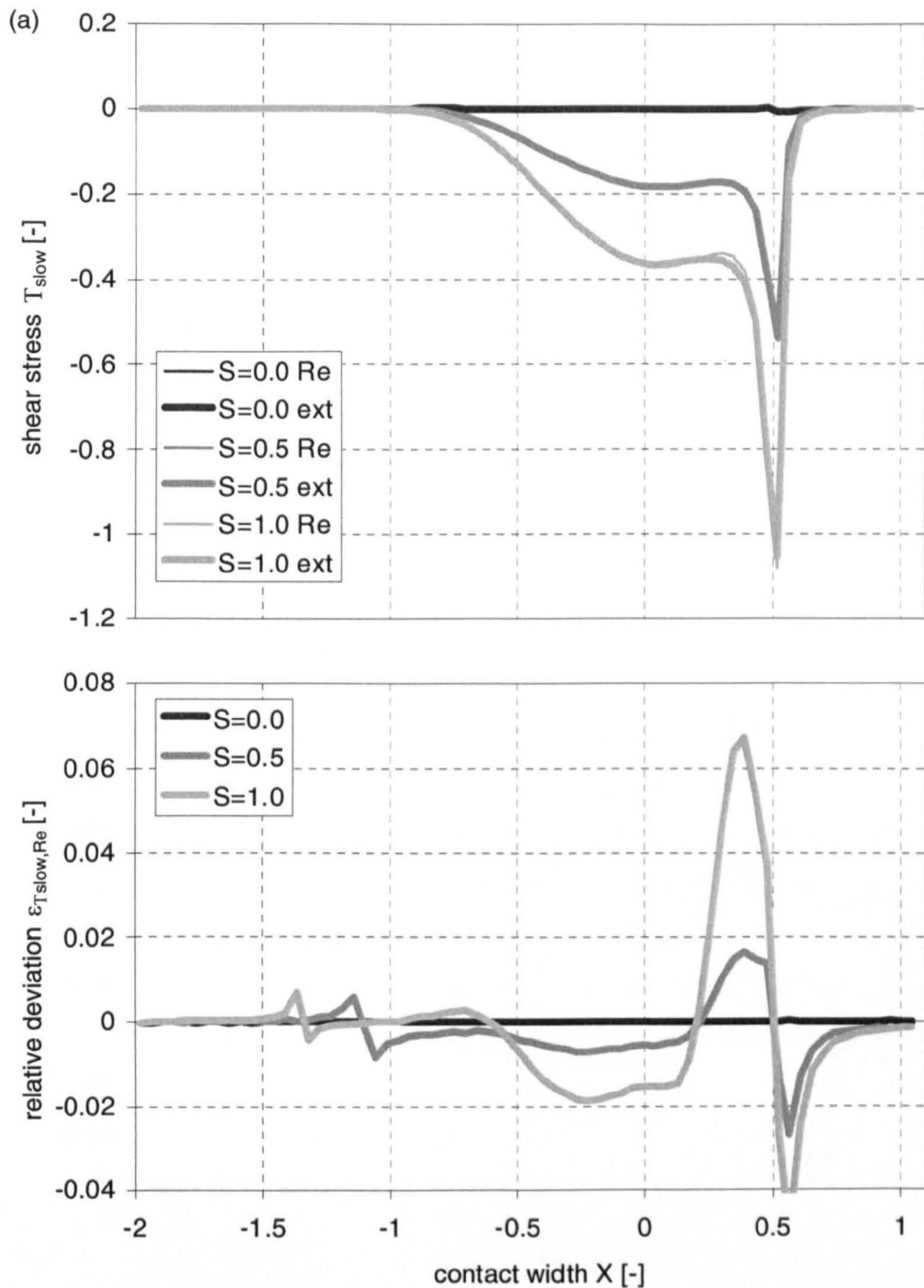
Figure K.32: *Dimensionless shear stress on the lubricant at the slower surface T_{slow} and the faster surface T_{fast} and relative deviation from Reynolds equation based solution $\varepsilon_{Tslow,Re}$ and $\varepsilon_{Tfast,Re}$ for various sliding ratios; load case ii (table 10.1), sliding ratios $S = 0.0$, 0.5, and 1.0,*

(a)   shear stress on slower surface T_{slow} and relative deviation $\varepsilon_{Tslow,Re}$,

(b)   shear stress on faster surface T_{fast} and relative deviation $\varepsilon_{Tfast,Re}$

(continued).
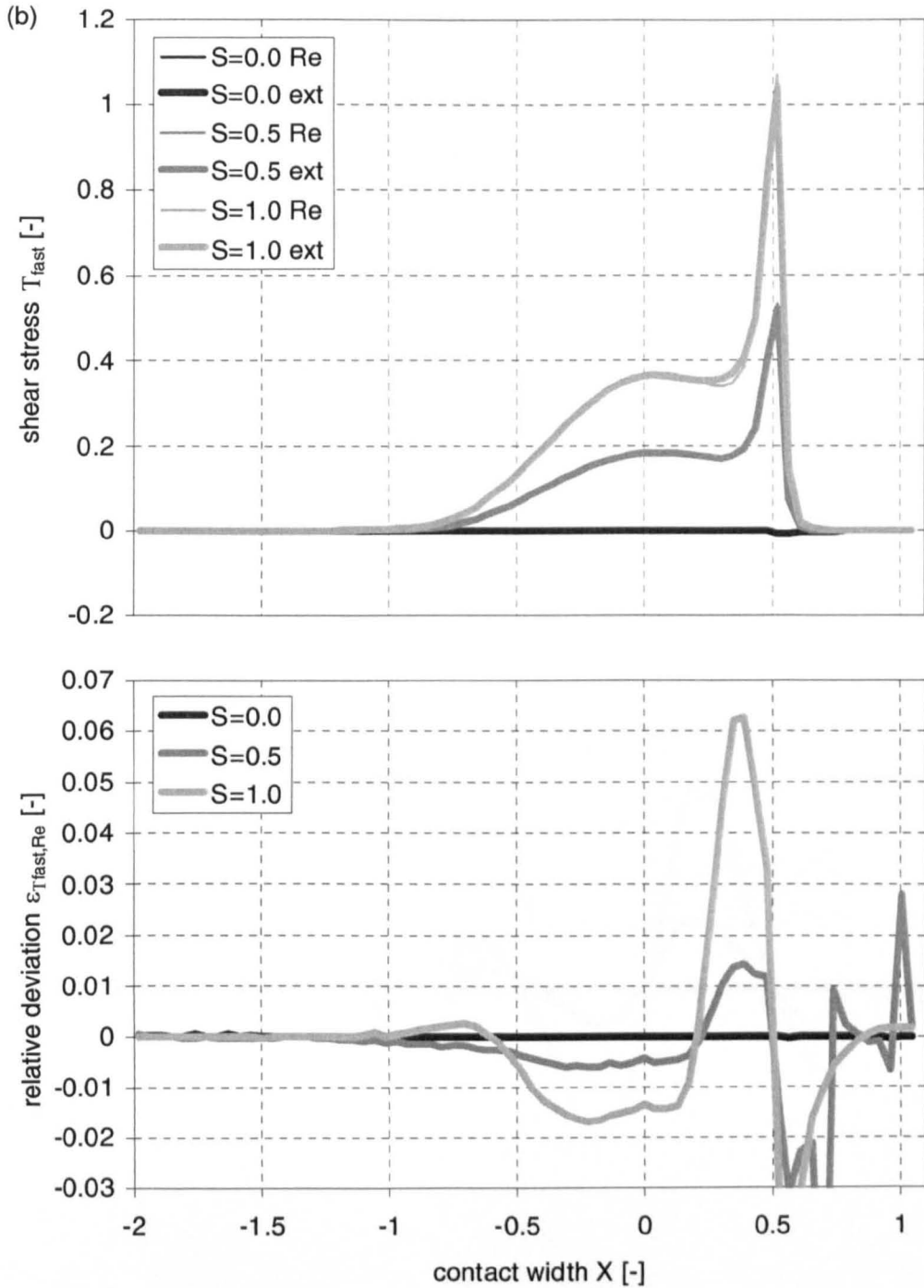
Figure K.32:   (concluded).
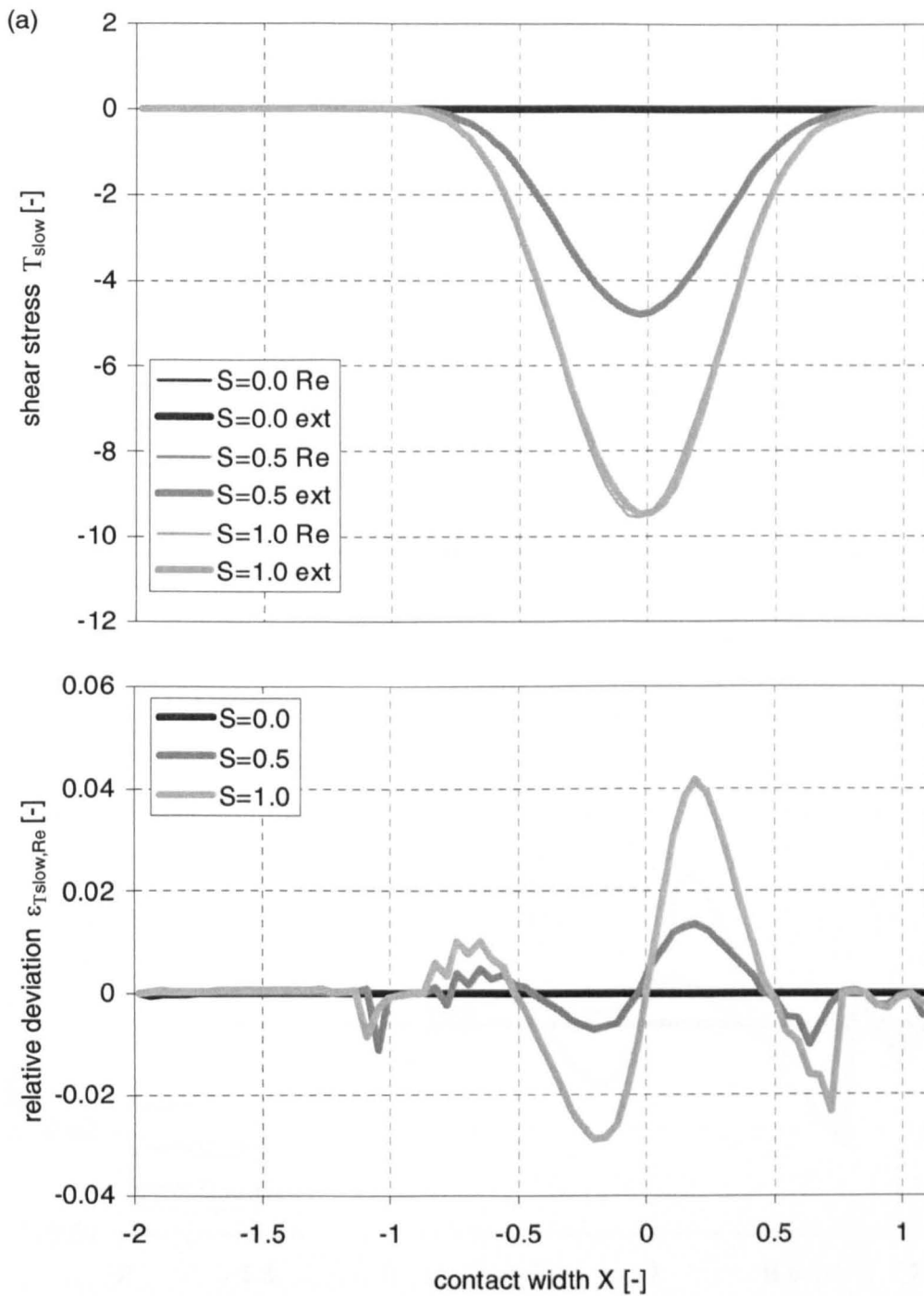
Figure K.33: Dimensionless shear stress on the lubricant at the slower surface T_{slow} and the faster surface T_{fast} and relative deviation from Reynolds equation based solution $\varepsilon_{Tslow,Re}$ and $\varepsilon_{Tfast,Re}$ for various sliding ratios; load case iii (table 10.1), sliding ratios $S = 0.0, 0.5,$ and 1.0,

    (a)   shear stress on slower surface T_{slow} and relative deviation $\varepsilon_{Tslow,Re}$,

    (b)   shear stress on faster surface T_{fast} and relative deviation $\varepsilon_{Tfast,Re}$

(continued).
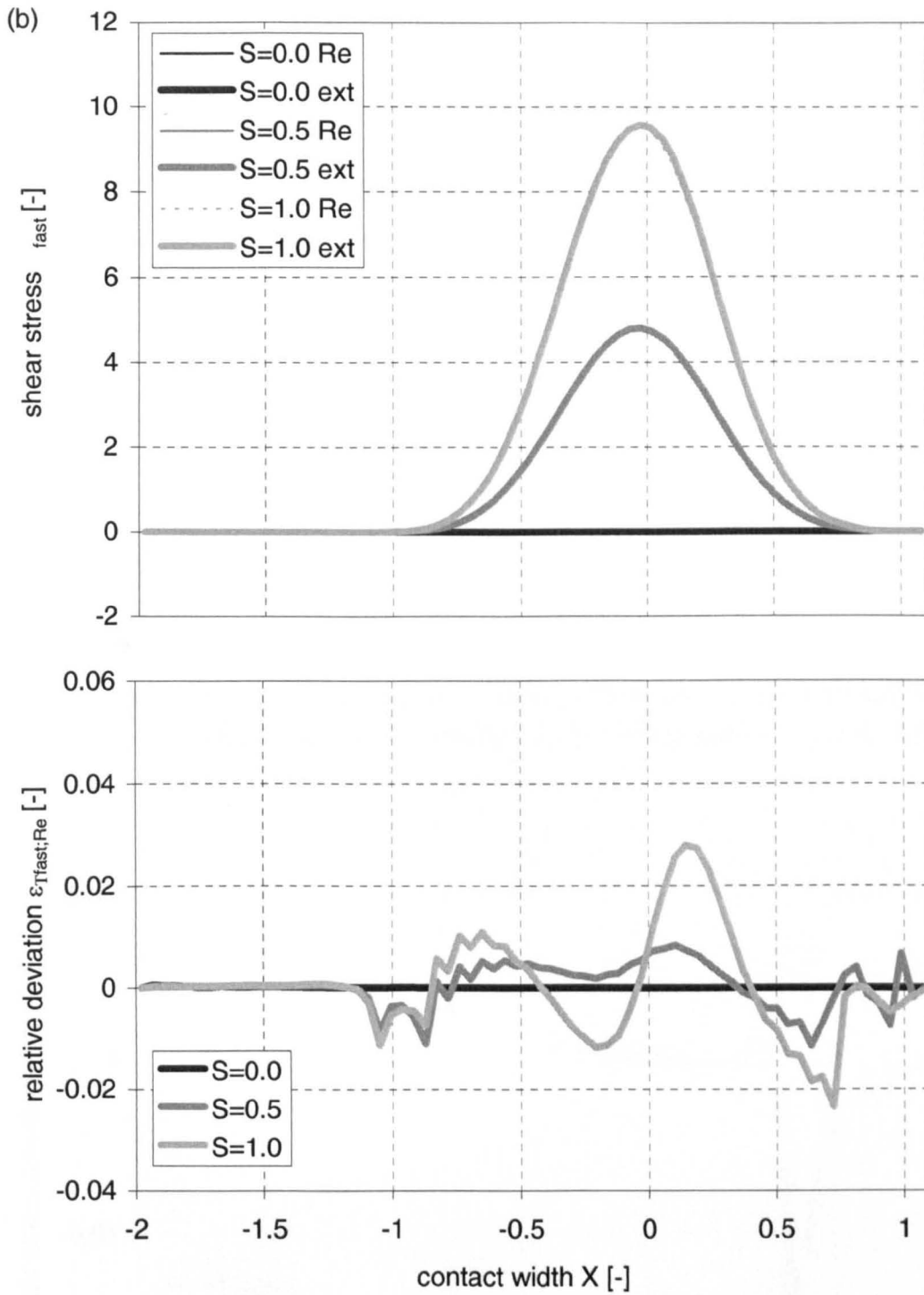
Figure K.33:   (concluded).
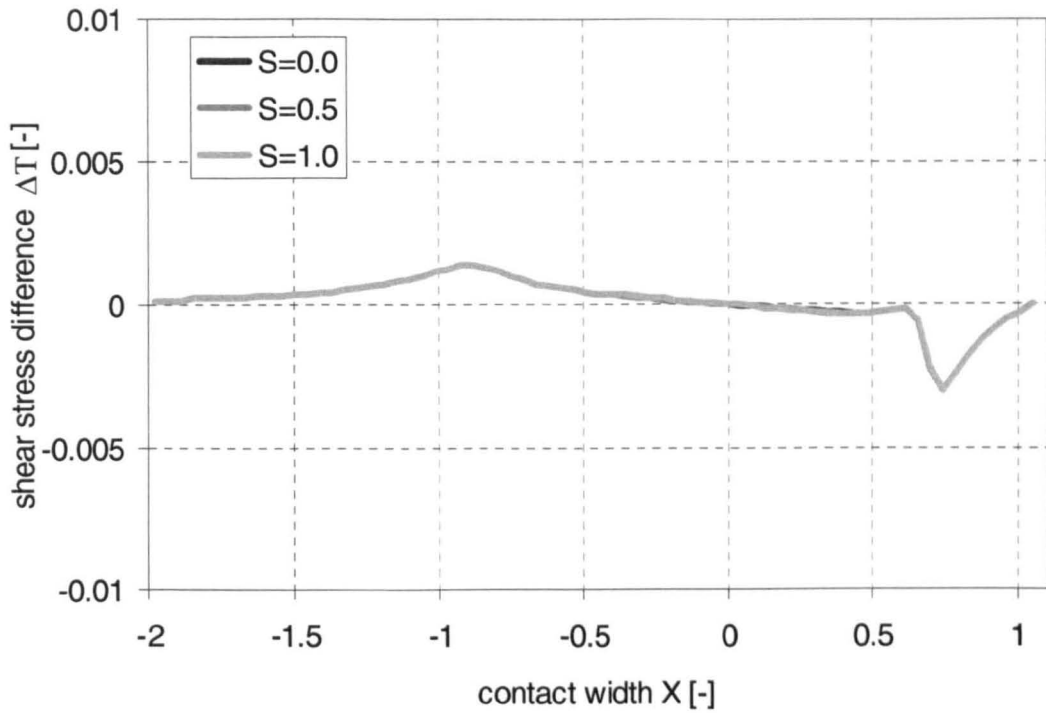
Figure K.34:   *Dimensionless shear stress difference ΔT for various sliding ratios; load case i (table 10.1), sliding ratios $S = 0.0$, 0.5, and 1.0.*
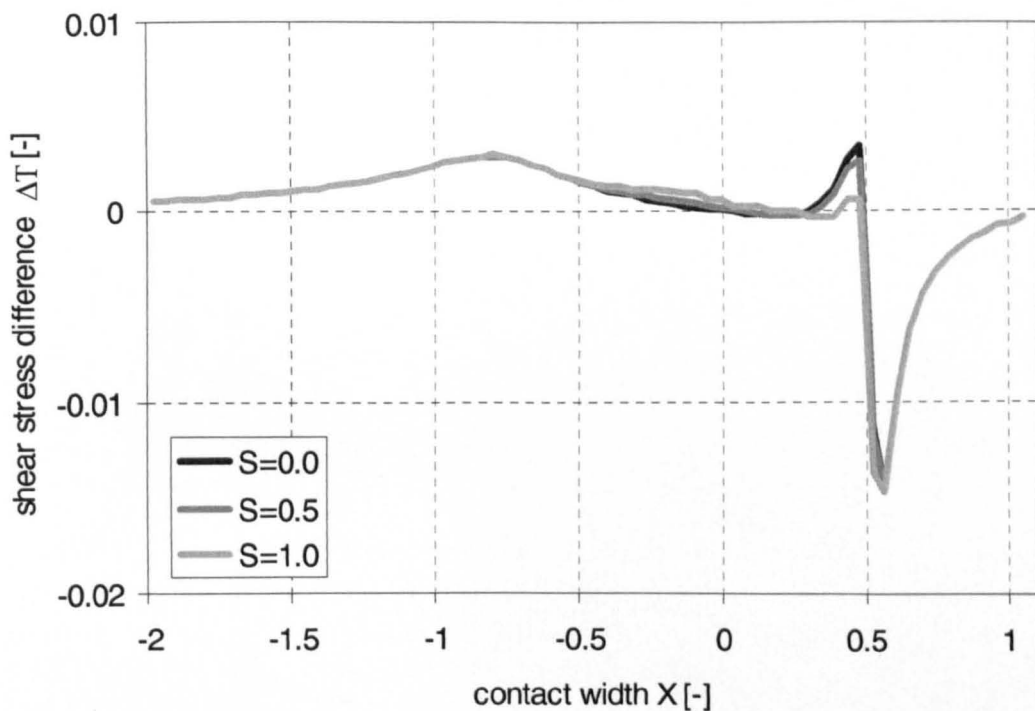
Figure K.35:   *Dimensionless shear stress difference ΔT for various sliding ratios; load case ii (table 10.1), sliding ratios $S = 0.0$, 0.5, and 1.0.*
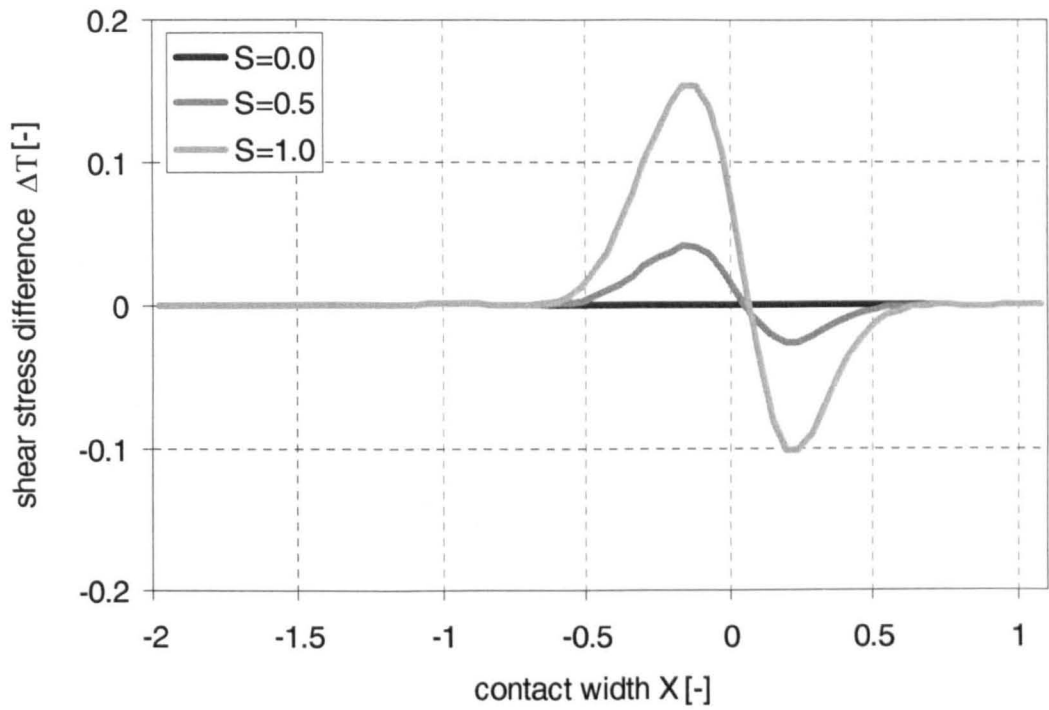
Figure K.36: Dimensionless shear stress difference ΔT for various sliding ratios; load case iii (table 10.1), sliding ratios $S = 0.0$, 0.5, and 1.0.

Appendix L

Derivation of a dependency of height and second order velocity gradient

Governing equation for the derivation of a height-second order velocity gradient dependency is the governing equation for a one-dimensional, iso-viscous Reynolds equation 2.1:

$$\frac{1}{\eta} \cdot \frac{\partial p}{\partial x} = \frac{\partial^2 u}{\partial y^2} \qquad \text{(L.1)}.$$

Twofold integration with respect to the velocity leads to

$$\frac{1}{\eta} \cdot \frac{\partial p}{\partial x} \cdot y + C_1 = \frac{\partial u}{\partial y} \qquad \text{(L.2)}$$

and

$$\frac{1}{\eta} \cdot \frac{\partial p}{\partial x} \cdot \frac{y^2}{2} + C_1 \cdot y + C_2 = u \qquad \text{(L.3)}.$$

With the boundary conditions, that each wall has its velocity,

$$u(y = 0) = u_1,$$

$$u(y = h) = u_2 \qquad \text{(L.4a, b)},$$

the equation describing the velocity profile becomes

$$u = \frac{1}{2 \cdot \eta} \cdot \frac{\partial p}{\partial x} \cdot \left(y^2 - h \cdot y\right) + \left(u_2 - u_1\right) \cdot \frac{y}{h} + u_1 \qquad \text{(L.5)}.$$

Integration of equation L.5 across the height of the gap gives the flow rate in the gap, which is constant along the gap,

$$\int_0^h u \cdot dy = \dot{V} = -\frac{1}{12 \cdot \eta} \cdot \frac{\partial p}{\partial x} \cdot h^3 + (u_2 - u_1) \cdot \frac{h}{2} + u_1 \cdot h \qquad \text{(L.6)}.$$

Defining h_0 as the height where pure Couette flow is obtained, flow rate becomes at this point

$$\dot{V} = (u_2 - u_1) \cdot \frac{h_0}{2} + u_1 \cdot h_0 \qquad \text{(L.7)}$$

and equation L.6 can be rewritten with the help of equation L.7 as

$$(u_2 - u_1) \cdot \frac{h - h_0}{2} + u_1 \cdot (h - h_0) = \frac{1}{12 \cdot \eta} \cdot \frac{\partial p}{\partial x} \cdot h^3 \qquad \text{(L.8)},$$

which can be solved for the pressure gradient

$$\frac{\partial p}{\partial x} = 6 \cdot \eta \cdot (u_2 + u_1) \cdot \frac{h - h_0}{h^3} \qquad \text{(L.9)}.$$

With substitution of the pressure gradient into the original equation L.1, a description for the height-second order velocity gradient description is obtained

$$6 \cdot (u_2 + u_1) \cdot \frac{h - h_0}{h^3} = \frac{\partial^2 u}{\partial y^2} \qquad \text{(L.10)},$$

rewritten in dimensionless form as

$$6 \cdot (\overline{U}_2 + \overline{U}_1) \cdot \frac{\overline{H} - 1}{\overline{H}^3} = \frac{\partial^2 \overline{U}}{\partial \overline{Y}^2} \qquad \text{(L.11)},$$

which reduces to

$$12 \cdot \frac{\overline{H} - 1}{\overline{H}^3} = \frac{\partial^2 \overline{U}}{\partial \overline{Y}^2} \qquad \text{(L.12)}$$

when considering that

$$\overline{U}_2 + \overline{U}_1 = \frac{2 \cdot \left(\dfrac{u_1 + u_2}{2} \right)}{u_h} = \frac{2 \cdot u_h}{u_h} = 2 \qquad \text{(L.13)}.$$

Appendix M

Graphical determination of gradients

For partial sliding $S = 0.5$ of load case iv, table 10.1, various values and gradients are determined graphically within this appendix for a check of the developed numerical method by using the dimensionless factors.

The dimensionless height $\overline{H}$ at the position $\overline{X} = -0.2$ can determined from the shape distribution, figure M.1, as

$$\overline{H}(\overline{X} = -0.2) = H(X = -0.2) = 0.981 \tag{M.1}.$$

The pressure gradient along the gap $\partial \overline{P} / \partial \overline{X}$ can be approximated from figure M.2 as

$$\frac{\partial \overline{P}}{\partial \overline{X}}(\overline{X} = -0.2) \approx \frac{\Delta P}{\Delta X}(X = -0.2) = \frac{0.2}{1.05} = 0.190 \tag{M.2}.$$

The pressure $\overline{P}$ itself can also be obtained from figure M.2 as

$$\overline{P}(\overline{X} = -0.2) = P(X = -0.2) = 0.98 \tag{M.3}.$$

The pressure gradient can be obtained with help of the dimensionless pressure difference across the gap, figure M.3, wherein the pressure difference across the height of the gap is

$$\Delta P(X = -0.2) = 0.0213 \tag{M.4},$$

which leads, together with the dimensionless height of the gap, to
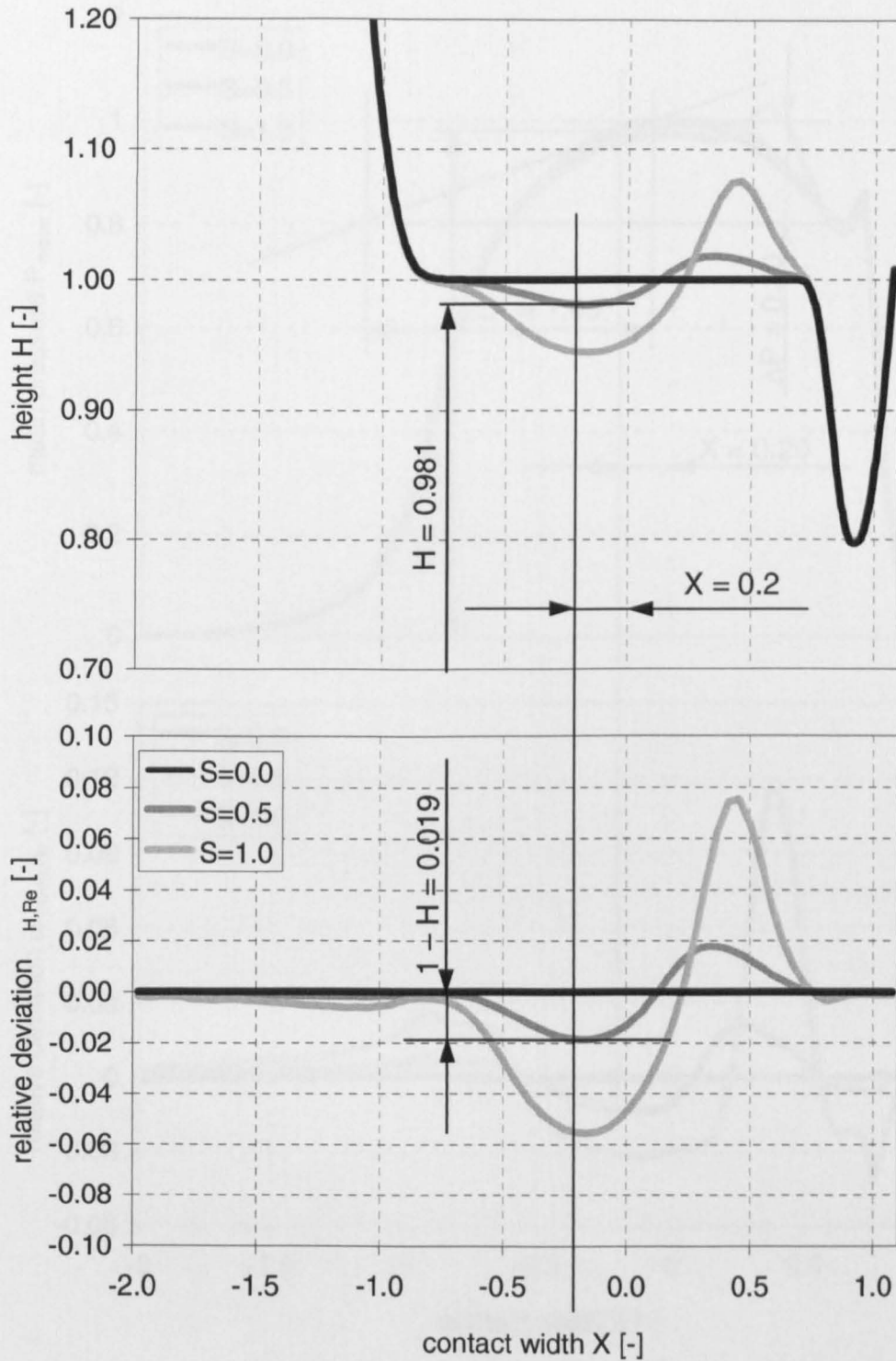
Figure M.1: Determination of the dimensionless height $\overline{H}$ from the shape of the gap figure 10.5.
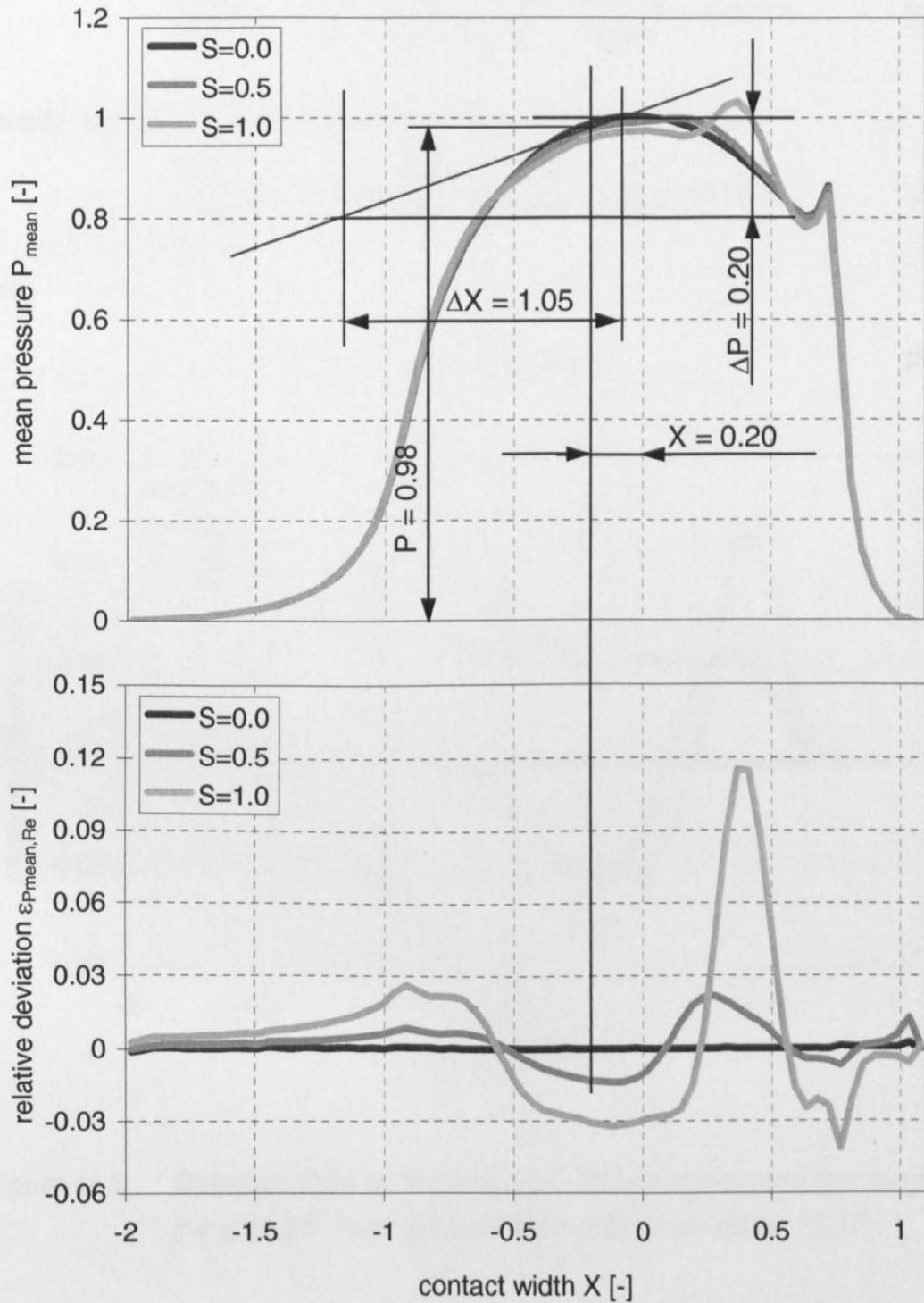
Figure M.2:   Determination of the pressure $\overline{P}_{mean}$ and the pressure gradient $\partial \overline{P} / \partial \overline{X}$ from the centreline pressure distribution figure 10.16(c).

$$\frac{\partial \overline{P}}{\partial \overline{Y}}\left(\overline{X}=-0.2\right) \approx \frac{\Delta P(X=-0.2)}{H(X=-0.2)} = \frac{0.0213}{0.981} = 0.0217 \qquad (M.5).$$

Finally, the velocity gradient across the height of the gap is

$$\frac{\partial \overline{U}}{\partial \overline{Y}}\left(\overline{X}=-0.2\right) \approx \frac{\Delta \overline{U}(X=-0.2)}{H(X=-0.2)} = \frac{1}{0.981} = 1.019 \qquad (M.6)$$

with

$$\Delta \overline{U} = 2 \cdot S = 2 \cdot 0.5 = 1 \qquad (M.7).$$
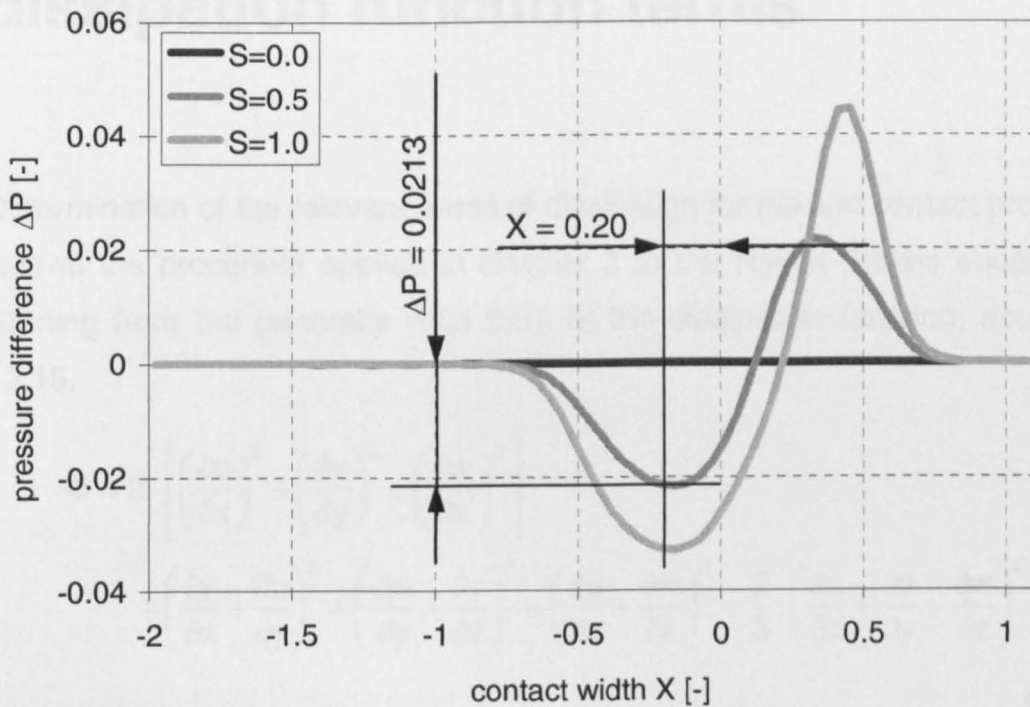

Figure M.3:   *Determination of the pressure difference across the height of the gap* $\Delta \overline{P}$ *from the pressure difference figure 10.17.*

Appendix N

Determination of relevant dissipation function terms

Determination of the relevant terms of dissipation for the line contact problem follows the procedure applied in chapter 3 to the Navier-Stokes equations. Starting from the generally valid form of the dissipation function, equation 12.15,

$$\Phi = 2 \cdot \left[\left(\frac{\partial u}{\partial x} \right)^2 + \left(\frac{\partial v}{\partial y} \right)^2 + \left(\frac{\partial w}{\partial z} \right)^2 \right]$$
$$+ \left(\frac{\partial v}{\partial x} + \frac{\partial u}{\partial y} \right)^2 + \left(\frac{\partial w}{\partial y} + \frac{\partial v}{\partial z} \right)^2 + \left(\frac{\partial u}{\partial z} + \frac{\partial w}{\partial x} \right)^2 - \frac{2}{3} \cdot \left(\frac{\partial u}{\partial x} + \frac{\partial v}{\partial y} + \frac{\partial w}{\partial z} \right)^2$$

$$(N.1),$$

this equation simplifies by the assumption of a infinitely wide gap, equation 3.12a,

$$\frac{\partial}{\partial z} = 0 \text{ and } w = 0 \qquad (N.2),$$

to the two-dimensional form

$$\Phi = 2 \cdot \left[\left(\frac{\partial u}{\partial x} \right)^2 + \left(\frac{\partial v}{\partial y} \right)^2 \right] + \left(\frac{\partial v}{\partial x} + \frac{\partial u}{\partial y} \right)^2 - \frac{2}{3} \cdot \left(\frac{\partial u}{\partial x} + \frac{\partial v}{\partial y} \right)^2 \qquad (N.3).$$

By introducing the continuity equation 3.14, which is already written in the two-dimensional form

$$\frac{\partial u}{\partial x} + \frac{\partial v}{\partial y} = 0 \qquad \text{(N.4)},$$

dissipation function of equation N.3 simplifies to

$$\Phi = 2 \cdot \left[\left(\frac{\partial u}{\partial x} \right)^2 + \left(\frac{\partial v}{\partial y} \right)^2 \right] + \left(\frac{\partial v}{\partial x} + \frac{\partial u}{\partial y} \right)^2 \qquad \text{(N.5)}.$$

Non-dimensionalisation following the definitions of equation 3.19a–d,

$$\overline{X} = \frac{x}{b_{hz}} \qquad \text{(N.6a)},$$

$$\overline{Y} = \frac{y}{h_o} \qquad \text{(N.6b)},$$

$$\overline{U} = \frac{u}{u_h} = \frac{u}{\frac{1}{2} \cdot (u_1 + u_2)} \qquad \text{(N.6c)},$$

and

$$\overline{V} = \frac{v}{v_m} = \frac{v}{u_h \cdot (h_o / b_{hz})} \qquad \text{(N.6d)},$$

leads to

$$\Phi = 2 \cdot \left[\left(\frac{u_h}{b_{hz}} \cdot \frac{\partial \overline{U}}{\partial \overline{X}} \right)^2 + \left(\frac{u_h}{h_o} \cdot \frac{h_o}{b_{hz}} \cdot \frac{\partial \overline{V}}{\partial \overline{Y}} \right)^2 \right] + \left(\frac{u_h}{b_{hz}} \cdot \frac{h_9}{b_{hz}} \cdot \frac{\partial \overline{V}}{\partial \overline{X}} + \frac{u_h}{h_o} \cdot \frac{\partial \overline{U}}{\partial \overline{Y}} \right)^2$$

$$\text{(N.7)}$$

and, with the geometry ratio γ, equation 3.21,

$$\gamma = \frac{h_o}{b_{hz}} \qquad \text{(N.8)},$$

to

$$\Phi = 2 \cdot \left[\left(\gamma \cdot \frac{u_h}{h_o} \cdot \frac{\partial \overline{U}}{\partial \overline{X}} \right)^2 + \left(\gamma \cdot \frac{u_h}{h_o} \cdot \frac{\partial \overline{V}}{\partial \overline{Y}} \right)^2 \right] + \left(\gamma^2 \cdot \frac{u_h}{h_o} \cdot \frac{\partial \overline{V}}{\partial \overline{X}} + \frac{u_h}{h_o} \cdot \frac{\partial \overline{U}}{\partial \overline{Y}} \right)^2 \quad \text{(N.9a)}$$

and

$$\Phi = \left(\frac{u_h}{h_0}\right)^2 \cdot \left[2 \cdot \gamma^2 \left(\frac{\partial \overline{U}}{\partial \overline{X}}\right)^2 + 2 \cdot \gamma^2 \left(\frac{\partial \overline{V}}{\partial \overline{Y}}\right)^2 + \gamma^4 \cdot \left(\frac{\partial \overline{V}}{\partial \overline{X}}\right)^2 + 2 \cdot \gamma^2 \cdot \left(\frac{\partial \overline{V}}{\partial \overline{X}} \cdot \frac{\partial \overline{U}}{\partial \overline{Y}}\right) + \left(\frac{\partial \overline{U}}{\partial \overline{Y}}\right)^2 \right]$$

(N.9b).

The geometry ratio γ is much smaller than zero. Hence, all gradients accompanied by γ^2 or γ^4 can be neglected and equation N.9b simplifies to

$$\Phi = \left(\frac{u_h}{h_0}\right)^2 \cdot \left(\frac{\partial \overline{U}}{\partial \overline{Y}}\right)^2$$

(N.10),

which can be re-transformed into its dimensional form with the help of equations N.6a–d to

$$\Phi = \left(\frac{\partial u}{\partial y}\right)^2$$

(N.11)

as presented by Dowson and Higginson [4].

Appendix O

Determination of dimensionless factors for thermal Roelands' approach

Instead of using the method, which was used in section 12.3 to determine factors k_p and k_r, by adaptation, the dimensionless factors are derived from the re-dimensionalised form of the governing equations for the isothermal system, equation 3.36

$$\frac{\partial p}{\partial x} = \frac{\partial \eta}{\partial y} \cdot \frac{\partial u}{\partial y} + \eta \cdot \frac{\partial^2 u}{\partial y^2}$$

$$\frac{\partial p}{\partial y} = \frac{\partial \eta}{\partial x} \cdot \frac{\partial u}{\partial y}$$

(O.1).

Following the procedure used in section 3.3 to obtain compact equations, the viscosity gradient along the contact is determined by differentiation from Roelands' equation

$$\eta = \eta_0 \cdot e^{(\ln \eta_0 + 9.67) \cdot \left(-1 + \left(1 + 5.1 \cdot 10^{-9} \cdot p \right)^Z \right) - \gamma_R \cdot \Delta \vartheta}$$

(O.2)

as

$$\frac{\partial \eta}{\partial x} = \eta_0 \cdot \left[Z \cdot 5.1 \cdot 10^{-9} \cdot (\ln \eta_0 + 9.67) \cdot \left(1 + 5.1 \cdot 10^{-9} \cdot p \right)^{Z-1} \cdot \frac{\partial p}{\partial x} - \gamma_R \cdot \frac{\partial \Delta \vartheta}{\partial x} \right] \cdot$$

$$\cdot e^{(\ln \eta_0 + 9.67) \cdot \left[-1 + \left(1 + 5.1 \cdot 10^{-9} \cdot p \right)^Z \right] - \gamma_R \cdot \Delta \vartheta}$$

(O.3),

and hence

$$\frac{\partial \eta}{\partial x} = \eta_0 \cdot \frac{\partial p}{\partial x} \cdot \left[Z \cdot 5.1 \cdot 10^{-9} \cdot (\ln \eta_0 + 9.67) \cdot (1 + 5.1 \cdot 10^{-9} \cdot p)^{Z-1} - \gamma_R \cdot \frac{\dfrac{\partial \Delta \vartheta}{\partial x}}{\dfrac{\partial p}{\partial x}} \right] \cdot$$

$$\cdot e^{(\ln \eta_0 + 9.67)\left[-1+(1+5.1\cdot10^{-9}\cdot p)^Z\right] - \gamma_R \cdot \Delta \vartheta}$$

$$(O.4).$$

Non-dimensionalisation as before 3.19a and 3.29a with

$$\overline{X} = \frac{x}{b_{hz}} \text{ and } \overline{P} = \frac{p}{p_{hz}} \qquad (O.5a, b)$$

and introduction of dimensionless temperature defined with the maximum temperature, which is not yet known for new analysis but known when considering experiments

$$\overline{\Delta \vartheta} = \frac{\Delta \vartheta}{\Delta \vartheta_{max}} \qquad (O.5c)$$

gives

$$\frac{\partial \eta}{\partial x} = \eta_0 \cdot \frac{p_{hz}}{b_{hz}} \cdot \frac{\partial \overline{P}}{\partial \overline{X}} \cdot$$

$$\cdot \left[Z \cdot 5.1 \cdot 10^{-9} \cdot (\ln \eta_0 + 9.67) \cdot (1 + 5.1 \cdot 10^{-9} \cdot \overline{P} \cdot p_{hz})^{Z-1} - \gamma_R \frac{\Delta \vartheta_{max}}{p_{hz}} \cdot \frac{\dfrac{\partial \overline{\Delta \vartheta}}{\partial \overline{X}}}{\dfrac{\partial \overline{P}}{\partial \overline{X}}} \right] \cdot$$

$$\cdot e^{(\ln \eta_0 + 9.67)\cdot\left[-1+(1+5.1\cdot10^{-9}\cdot\overline{P}\cdot p_{hz})^Z\right] - \gamma_R \cdot \Delta \vartheta_{max} \cdot \overline{\Delta \vartheta}}$$

$$(O.6)$$

As in subsection 3.3.3, for the further determination of factors k_p and k_r, $\overline{P}$ and $\overline{\Delta \vartheta}$ are considered as unity. The gradient ratio can take on arbitrary signs and values. Furthermore, it is assumed that the pressure and temperature distributions have identical shape and thus the ratio becomes unity due to its non-dimensional form, so that equation O.6 can be re-written as

$$\frac{\partial \eta}{\partial x} = \eta_0 \cdot \frac{p_{hz}}{b_{hz}} \cdot \frac{\partial \overline{P}}{\partial \overline{X}} \cdot \hat{\alpha}'(p_{hz}, \Delta \vartheta_{max}) \cdot e^{\hat{\alpha}(p_{hz}, \Delta \vartheta_{max})} \qquad (O.7a)$$

with

$$\hat{\alpha}'(p_{hz}, \Delta\vartheta_{max}) = Z \cdot 5.1 \cdot 10^{-9} \cdot (\ln \eta_0 + 9.67) \cdot$$

$$\cdot \left(1 + 5.1 \cdot 10^{-9} \cdot \overline{P} \cdot p_{hz}\right)^{Z-1} - \gamma_R \frac{\Delta\vartheta_{max}}{p_{hz}} \cdot \frac{\dfrac{\partial\overline{\Delta\vartheta}}{\partial\overline{X}}}{\dfrac{\partial\overline{P}}{\partial\overline{X}}} \qquad (O.7b)$$

and

$$\hat{\alpha}(p_{hz}, \Delta\vartheta_{max}) = (\ln \eta_0 + 9.67) \cdot \left[-1 + \left(1 + 5.1 \cdot 10^{-9} \cdot \overline{P} \cdot p_{hz}\right)^Z\right] - \gamma_R \cdot \Delta\vartheta_{max} \cdot \overline{\Delta\vartheta}$$

$$(O.7c).$$

Substituting into the second equation of set O.1 and non-dimensionalisation of the other terms leads to the well-known form

$$\frac{\partial\overline{P}}{\partial\overline{Y}} \bigg/ \frac{\partial\overline{P}}{\partial\overline{X}} = \hat{k}_r \cdot \frac{\partial\overline{U}}{\partial\overline{Y}} \qquad (O.8)$$

with

$$\hat{k}_r = \frac{\eta_0 \cdot \hat{\alpha}'(p_{hz}, \Delta\vartheta_{max}) \cdot e^{\hat{\alpha}(p_{hz}, \Delta\vartheta_{max})} \cdot u_h}{h_0} \cdot \gamma \qquad (O.9a)$$

and correspondingly

$$\hat{k}_p = \frac{\eta_0 \cdot \hat{\alpha}'(p_{hz}, \Delta\vartheta_{max}) \cdot e^{\hat{\alpha}(p_{hz}, \Delta\vartheta_{max})} \cdot u_h}{h_0} \qquad (O.9b)$$

and

$$\hat{k}_c = \frac{\eta_0 \cdot e^{\hat{\alpha}(p_{hz}, \Delta\vartheta_{max})} \cdot u_h}{p_{hz} \cdot h_0 \cdot \gamma} \qquad (O.9c).$$

Appendix P

Maximum viscosity determination

The maximum viscosity which could be expected in an ehl contact can be estimated as following. The traction coefficient is defined as the ratio of tangential force to normal force,

$$\mu_T = \frac{F_t}{F_n}$$ (P.1).

Assuming a triangular viscosity distribution with its maximum at the centreline, zero viscosity at the edges and a parallel gap, the tangential force can be estimated as

$$F_t = \frac{1}{2} \cdot \eta_{max} \cdot \frac{\partial u}{\partial y} \cdot 2 \cdot b_{hz} \cdot w' = \frac{1}{2} \cdot \eta_{max} \cdot \frac{2 \cdot S \cdot u_h}{h_0} \cdot 2 \cdot b_{hz} \cdot w'$$ (P.2)

and the latter normal force, with the assumption of an elliptical Hertzian pressure distribution as

$$F_n = \frac{1}{2} \cdot p_{hz} \cdot b_{hz} \cdot w' \cdot \pi$$ (P.3).

The effective viscosity is then

$$\eta_{max} = \frac{\mu_T \cdot p_{hz} \cdot \pi \cdot h_0}{4 \cdot S \cdot u_h}$$ (P.4).

Appendix Q

Published work

Schäfer, C. T., Giese, P., Rowe, W. B., and Woolley, N. H.:
"Elastohydrodynamically lubricated line contact based on the Navier-Stokes equations."
Thinning films and tribological interfaces. Proceedings of the 26th Leeds-Lyon Symposium on tribology, 14th–17th September 1999.
Edited by Dowson, D. et al.
Amsterdam: Elsevier, 2000.
pp. 57-69.

Schäfer, C. T. and Woolley, N. H.:
"Elastohydrodynamic lubrication – a particular fluid-structure-interaction problem."
Proceedings of the 2002 European CFX conference. Strasbourg, 16th–18th September 2002.
CD-Rom edition.
Otterfing: CFX, 2002.